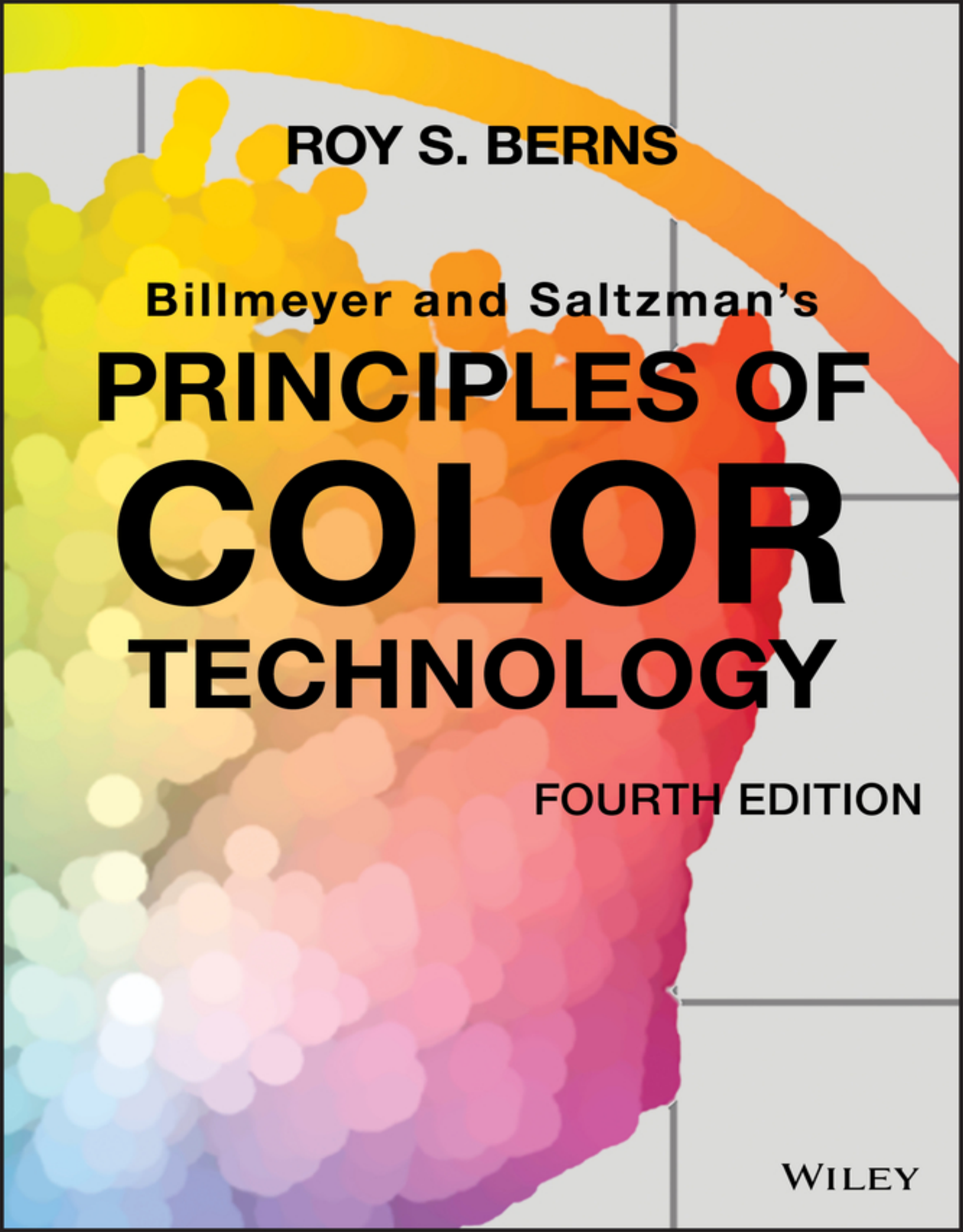

ROY S. BERNS

Billmeyer and Saltzman's

PRINCIPLES OF COLOR TECHNOLOGY

FOURTH EDITION

WILEY

Billmeyer and Saltzman's

Principles of Color Technology

Billmeyer and Saltzman's

PRINCIPLES OF COLOR TECHNOLOGY

Fourth Edition

Roy S. Berns

R. S. Hunter Professor in Color Science, Appearance, and Technology
Program of Color Science
Munsell Color Science Laboratory
Rochester Institute of Technology

WILEY

This edition first published 2019

Edition History
John Wiley & Sons Inc. (3e, 2000)

Registered Office
John Wiley & Sons, Inc., 111 River Street, Hoboken, NJ 07030, USA

Editorial Office
111 River Street, Hoboken, NJ 07030, USA

For details of our global editorial offices, customer services, and more information about Wiley products visit us at www.wiley.com.

Wiley also publishes its books in a variety of electronic formats and by print-on-demand. Some content that appears in standard print versions of this book may not be available in other formats.

Library of Congress Cataloging-in-Publication Data

Names: Berns, Roy S., 1954- author. | Billmeyer, Fred W. | Saltzman, Max.
Title: Billmeyer and Saltzman's principles of color technology / Roy S. Berns (R.S. Hunter Professor in Color Science, Appearance, and Technology, Munsell Color Science Laboratory, Rochester Institute of Technology).
Other titles: Principles of color technology
Description: Fourth edition. | Hoboken, NJ : Wiley, [2019] | Includes bibliographical references and index. |
Identifiers: LCCN 2018056449 (print) | LCCN 2018060654 (ebook) | ISBN 9781119367192 (AdobePDF) | ISBN 9781119366683 (ePub) | ISBN 9781119367222 (hardcover)
Subjects: LCSH: Color. | Colorimetry.
Classification: LCC QC495 (ebook) | LCC QC495 .B398 2019 (print) | DDC 667–dc23
LC record available at https://lccn.loc.gov/2018056449

Cover Design: Wiley
Cover Image: Courtesy of Roy S. Berns

Set in 10/12pt TimesLTStd by SPi Global, Chennai, India

Printed in the United States of America

10 9 8 7 6 5 4 3 2 1

This edition is dedicated to the most important person in my life—Susan Stanger.
Susan, you bring out the best in me and I love you for it.

Contents

Preface

This is the second time I have revised and updated *Billmeyer and Saltzman's Principles of Color Technology*. The four editions span 50 years, beginning in 1966. The first edition focused on *how* to measure color and correctly interpreting the data. Billmeyer and Saltzman encouraged readers to use common sense, to measure enough samples for a good mean estimate, to always be on the lookout for metamerism, and to *think and look*.

In their preface to the second edition, they wrote, "We have been gratified to see the unexpectedly wide use of *Principles of Color Technology* as a textbook. We found, however, very little need to change the text to accommodate this use: a few numerical examples have been added to assist both the instructor and the student." They did add a chapter *Problems and Future Directions in Color Technology*, where material that was research oriented and not introductory was included.

When I began to revise the book for a third edition in 1998, the text was 30 years old. The field had matured considerably. An understanding of colorimetry was necessary for the new application—digital imaging. The majority of the text was rewritten and color imaging was added to the chapter *Producing Colors*. I added an appendix, *Mathematics of Color Technology*, principally to support color imaging and for use in graduate courses in color science. I retained the style of the first edition to the best of my abilities.

Two years ago, I began the fourth edition. The third edition was 20 years old. I sent out a questionnaire to colleagues to ask about content and the appropriate mathematical level. I included both industrial scientists and educators. The respondents split into two groups. One group wanted the book to be simpler, having less historical background and returning the book to the first edition. The argument was that instrument manufacturers were not providing adequate industrial education and this book should fill the gap. The mathematical level of the book should remain at an algebra level. The other group wanted the book expanded to include color-appearance models, multivariate analyses of colorimetric data, and measurements of visual texture. This group also wanted less historical background and assumed that any scientist or engineer with a college degree would have some experience with matrix algebra. My experiences, both industrial and academic, were more aligned with the second group.

This edition, as was the third, is another rewrite. The content has been reorganized from 6 to 10 chapters. Color imaging has its own chapter. Metamerism, still of utmost importance, has its own chapter along with color inconstancy. Color measurement has been expanded to include measuring color and material appearance using conventional spectrophotometers and spectroradiometers and imaging devices that characterize surface topography and visual texture. I used the simplest mathematics I could, which in many cases, is matrix algebra. At its first introduction, I provide both algebra and matrix algebra. I have removed a lot of history and formulas no longer in use. I have increased the number of numerical examples. The mathematics appendix was removed. The annotated bibliography has returned from the first and second editions and I added a section of recommended books for those who want a color science library. I have endeavored to keep the voice of Billmeyer and Saltzman and their informal writing style. Although I am the sole author, "we" is used liberally. In each case, I imagined the three of us discussing the particular point. If we were not unanimous, the point was removed.

I learned very early in my career to ask for help. I still do and I sincerely thank the following for their help: Paula Alessi, David Alman, Yuta Asano, Paul Beymore, Janet Bridgland, Ellen Carter, Robert Chung, Guihua Cui, Maxim Derhak, Christopher Edwards, Patrick Emmel, Mark Fairchild, Susan Farnand, James Ferwerda, Edmond and Susan Gilbert, Nick Harkness, Luke Hellwig, Sean Herman, Robert Hirschler, Kurt Huemiller, Emmett Ientilucci, Fu Jiang, Eric Kirschner, Andeas Kraushaar, Rolf Kuehni, Hideyasu Kuniba, Jennifer Kruschwitz, Ann Laidlow, M. Ronnier Luo, Manuel Melgosa, Michael Murdoch, Francis O'Donnell, Yongmin Park, Jonathan Phillips, Daniella Pinna, Michael Pointer, Mark Rea, Danny Rich, Javier Romero, Renzo Shamey, M. James Shyu, Susan Stanger, Philipp Urban, Stephen Viggiano, Joseph Voelkel, Stephen Westland, David Wyble, Hao Xie, and Joanne Zwinkels.

Finally, I would like to acknowledge the generosity of the late Richard and Elizabeth Hunter for establishing the Hunter Professorship in Color Science, Appearance, and Technology at Rochester Institute of Technology. As the Hunter Professor, I have the freedom to engage in intellectual pursuits of my choosing. This book is tangible evidence of this freedom.

Rochester, New York
August 2018

ROY S. BERNS

Chapter 1

Physical Properties of Colors

A. WHAT THIS BOOK IS ABOUT?

This is a book about *color*, *colorants*, the *coloring* of materials including measurement and control, and *reproducing the color* of materials through imaging.

Color can mean many things. In this book, color may mean a certain kind of light, its effect on the human eye, or — most important of all — the result of this effect in the mind of the viewer. We describe each of these aspects of color, and relate them to one another.

Colorants, on the other hand, are purely physical things. They are the dyes and pigments used in the process of coloring materials.

Coloring is a physical process: that of applying dyes to textiles or incorporating, by dispersion, pigments into paints, inks, and plastics. A part of this book is devoted to describing these physical substances and processes.

But color is much more than something physical. Color is what we see—and we repeat this many times—it is the result of the physical modification of light by colorants as detected by the human eye (called a response process) and interpreted in the brain (called a perceptual process, which introduces psychology). This is an enormously complicated train of events. To describe color and coloring, we must understand something of each aspect of it. A large portion of the book deals with this problem.

With an understanding of color in this broad sense, we can approach some commercial problems involving color. These problems are concerned with answering such questions as, Does this sample have the same color as the one I made yesterday, or last week, or last year? Does this batch of material have the same color as a standard? Does this reproduced image match the original? How much of what colorants do I use to produce a color just like this one? How can I choose colorants that will perform satisfactorily in a certain application?

Historically, most of these questions have had only subjective answers, based on the skill and memory of the trained color matcher or press operator. Fortunately, through the application of the principles of color technology and the use of color measurement, we can provide objective answers. We consider the industrial application of color technology largely in this objective vein.

In summary, we provide a brief résumé of the present state of the art of color, color control, coloring, color reproduction, and colorants—a very complex field. To simplify, we have omitted much. Among our omissions are conflicting points of view: we tend to present our best current opinion rather than a studied evaluation of all sides of any question. Some topics that are important to include are still evolving; for these cases, we will present the general concepts rather than focus on a particular solution. We hope our readers will be stimulated to seek more detailed and more varied information on many of the subjects we touch upon only briefly.

To this end we provide—and consider of major importance—an annotated bibliography in which we identify those citations among all of our references that we consider key to the body of knowledge comprising color technology. We also provide an annotated list of recom-

Billmeyer and Saltzman's Principles of Color Technology, Fourth Edition. Roy S. Berns.

mended books to establish a color-science library. We hope that our readers will recognize with us that this book can be no more than a beginning and that they will make use of its bibliography and book recommendations as a guide to the extensive and often complex literature on color.

This book is *not* a "how to" manual for any process or industry. It does not tell you the best way to make a beige shade in vinyl plastic at the lowest cost. Nor does it provide a detailed study of what ink amounts in a multi-ink printer are necessary to reproduce the beige plastic. It *does* tell you in principle how to avoid having that beige go off-shade in tungsten light; it *does* tell why different combinations of inks can match the beige.

This book is *not* an instrument manual or a catalog of instruments; it does not tell you how to operate any specific color-measuring instrument—designed for a single color or many colors simultaneously—to measure samples of a given material. It *does* tell you what types of instruments are available and for what purposes they can or cannot be used. It *does* tell you how to make the best use of these instruments.

This book does *not* attempt to give the "best" ways to use color, the "best" ways to use colorants, or the "best" colorants to use for any application. These are important practical questions, but to answer them would require much more detail than can be put into this book. For these subjects, as for others we do not discuss, there are references to the literature.

B. THE SPECTRUM AND WAVE THEORY

To describe *color*, we must talk about physical actions, such as producing a stimulus in the form of light, both directly and indirectly by interacting with a material, and subjective results, such as receiving and interpreting this stimulus in the eye and the brain or *visual system*. (Throughout the book, important terms will be set in italics the first time they are introduced.) This is depicted in Figure 1.1, a figure we will show throughout this book. Since color exists only in the mind of the viewer, these latter effects are the more important to us. To aid in understanding them, we first consider the *visible spectrum*.

Visible radiation is a form of energy, part of the family that includes radio waves and X-rays, as well as ultraviolet and infrared radiation. Radiation we can see is called *light*. Light can be described by its *wavelength*, for which the *nanometer* (nm) is a convenient unit of length, shown in Figure 1.2. One nanometer is 1/1 000 000 000 m.

The relation of light to the other members of its family is shown in Figure 1.3. The relative insensitivity of the eye limits the visible part of the spectrum to a narrow band of wavelengths between about 380 and 780 nm. The hue we recognize as blue lies below about 480 nm; green, roughly between 480 and 560 nm; yellow, between 560 and 590 nm; orange, between 590 and 630 nm; and red at wavelengths

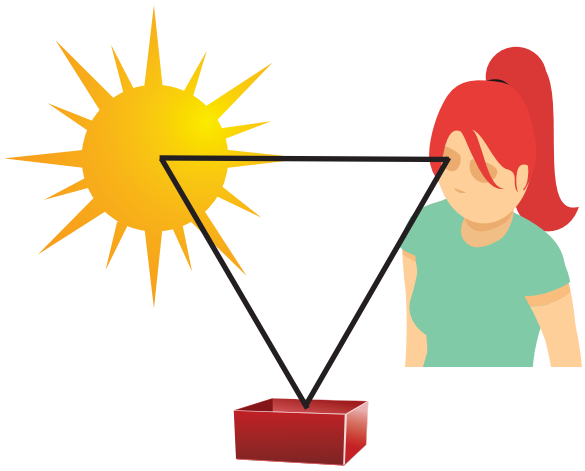

Figure 1.1 *Color* results from the interaction of a light source, an object, and the eye and brain, or visual system.

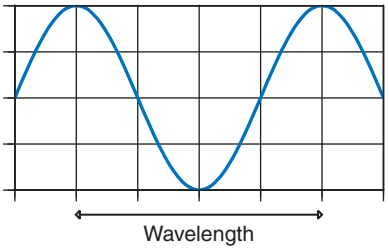

Figure 1.2 Radiation can be described as a wave. The distance from peak to peak is called its *wavelength*.

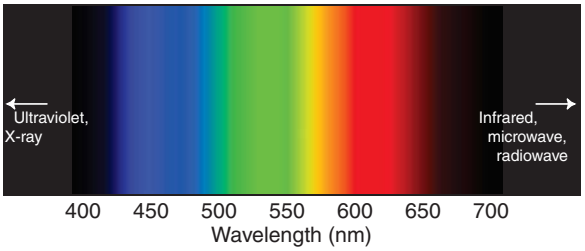

Figure 1.3 A rendition of the visible spectrum and its relationship to other kinds of radiation (not to scale).

longer than 630 nm. Magenta, which is produced by mixing red and blue light from the extremes of the spectrum, is one common hue not found in the spectrum.

The vast majority of colored stimuli are composed of many wavelengths, shown as graphs where radiation, in the case of lighting, or reflection, in the case of an opaque material, is plotted as a function of wavelength. Such graphs are shown in Figures 1.4 and 1.5. Newton (1730) and others (see Hunt 2000) showed many years ago, by using a prism to disperse light into a spectrum, that white light is normally made up of all the visible wavelengths, shown in Figure 1.6.

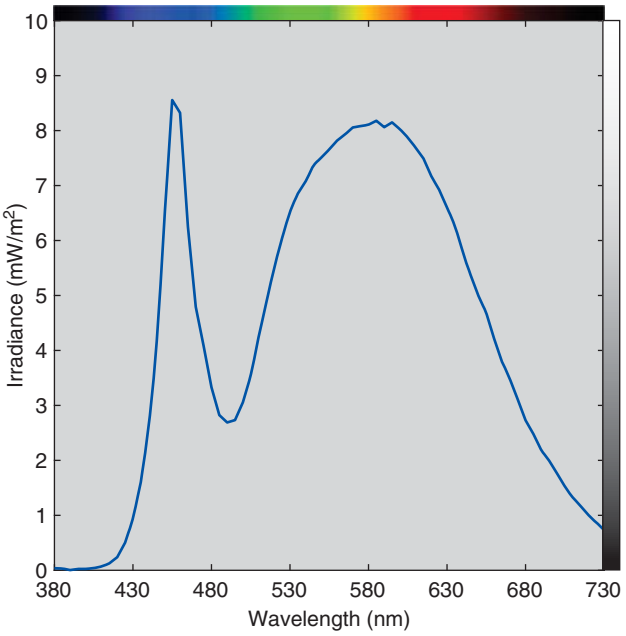

Figure 1.4 The *spectral irradiance* (defined in Chapter 6) of a solid-state white light.

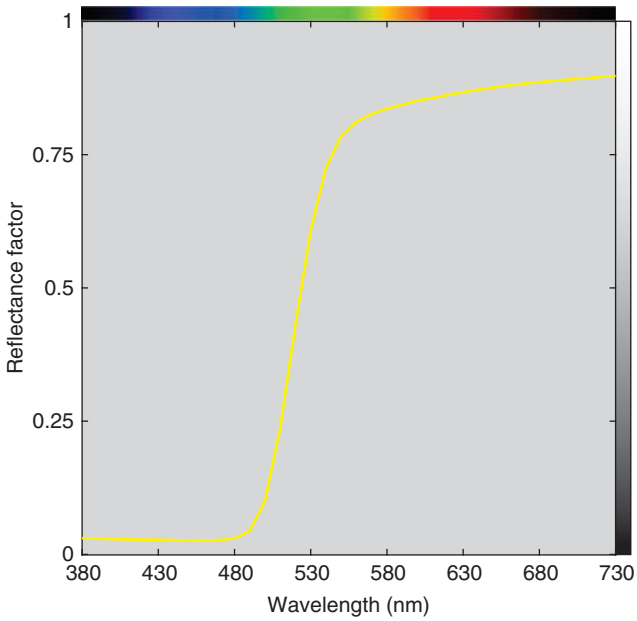

Figure 1.5 The *spectral reflectance factor* (defined in Chapter 6) of a yellow paint.

C. LIGHT SOURCES

Many of the objects we think of as sources of light emit light that is white or nearly white—the sun, hot metals like the filaments of light bulbs, and solid-state lamps, among others. The light from any source can be described in four ways.

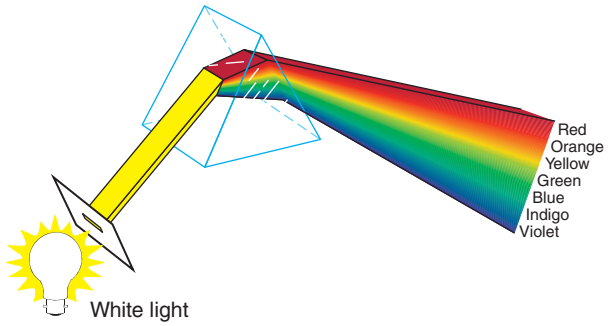

Figure 1.6 Dispersing white light into a spectrum. The color names are somewhat arbitrary; these were used by Newton (1730).

The first is *irradiance*, the amount of light received on a surface per unit area, often defined by watts per unit area expressed in meters squared (W/m^2) and the letter "E."

The second is *radiance*, the amount of light emanating from or falling on a surface per unit projected area, often defined by watts per unit area per *solid angle* expressed in meters squared steradians (W/m^2 Sr) and the letter "L." We can think of solid angle as a measure of the size of an object relative to a fixed position. An object that is close to us subtends a larger solid angle than the same object viewed from a distance. Instruments that measure irradiance have diffusers while instruments that measure radiance have lenses, described in more detail in Chapter 6.

The third is to normalize the spectrum relative to a specific wavelength, and the fourth is to normalize to the same intensity ("brightness"). Daylight and a solid-state light are plotted the last three ways in Figure 1.7. Because solid-state lights can be narrow-band, such as shown in Figure 1.7, plotting multiple sources normalized to the same intensity is the most descriptive way to compare spectra.

Definitions

Throughout the book, we will be defining various terms. Unless otherwise noted, definitions are based on the CIE International Lighting Vocabulary (CIE 2011) or the ASTM Standard Terminology of Appearance (2013a).

- *Radiant flux:* The time rate of flow of radiant energy. "Power" and "flux" are synonymous.
- *Irradiance:* The radiant flux incident per unit area.
- *Radiance:* Radiant flux in a beam, emanating from a surface, or falling on a surface, in a given direction, per unit of projected area of the surface as viewed from that direction, per unit of solid angle.

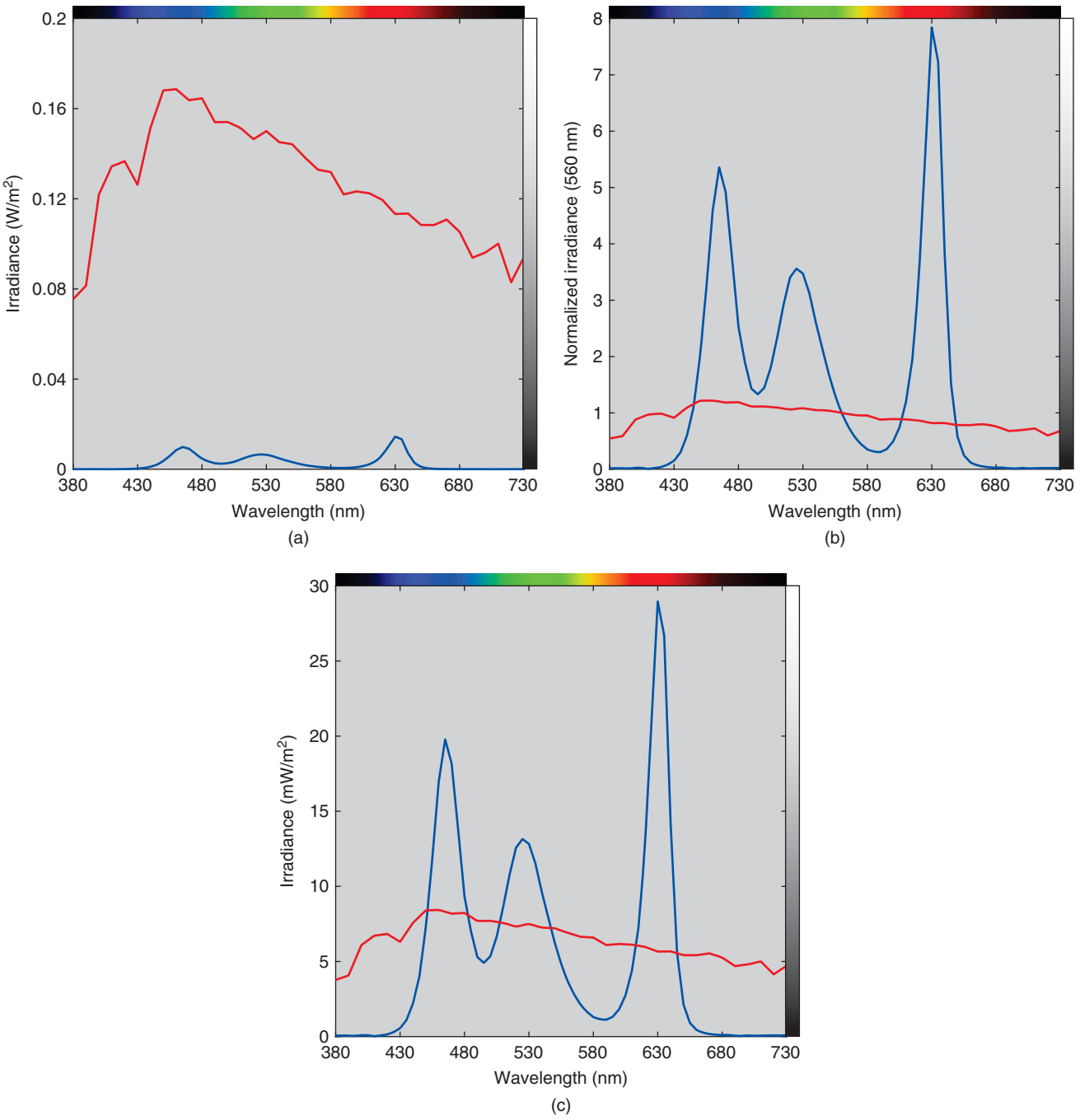

Figure 1.7 Daylight (red lines) and a solid-state light (bllue lines) are plotted as (a) irradiance, (b) normalized at 560 nm, and (c) normalized to equal illuminance ("intensity"), all as a function of wavelength. Both sources have the same *correlated color temperature* (defined in Chapter 7).

A number of light sources have been defined by the *International Commission on Illumination* (Commission Internationale de l'Éclairage, or *CIE*) for use in describing color (ISO 2007a; CIE 2018). These distributions are known, in CIE terminology, as *illuminants*. They are based on physical standards or on statistical representations of measured light. There are illuminants for incandescent, fluorescent, outdoor daylight, indoor daylight, solid state, and high-pressure (e.g. sodium and metal halide) lighting. Different industries have standardized specific illuminants for color specification. In manufacturing, two common CIE illuminants are *D65*, corresponding to indirect outdoor daylight (e.g. from a north-facing window in the northern hemisphere or under cloudy conditions), and *A*, corresponding to incandescent

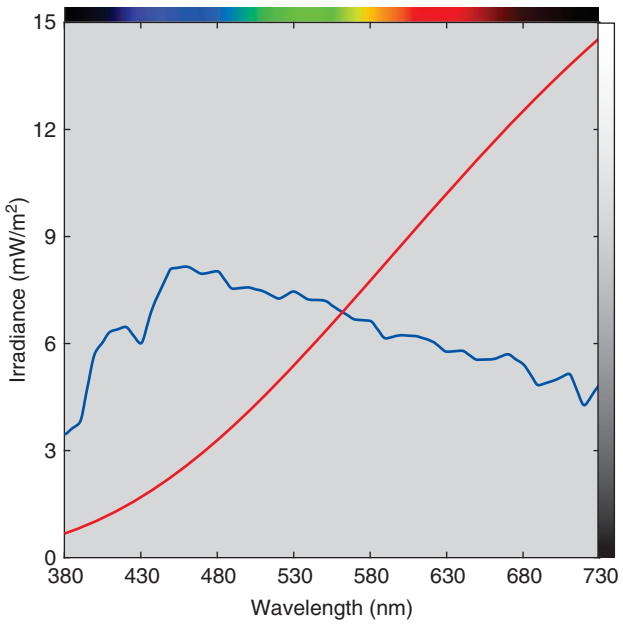

Figure 1.8 *CIE illuminants D*65 (blue line) and *A* (red line) plotted at equal illuminance as a function of wavelength.

lighting; these illuminants are plotted in Figure 1.8. We will have much more to say about lighting in Chapter 7.

D. CONVENTIONAL MATERIALS

When light strikes an object, one or more things pertinent to color can happen:

Transmission

The light can go through essentially unchanged. It is said to be *transmitted* through the material, which is described as *transparent*. If the material is colorless, all the light is transmitted except for a small amount that is *reflected* from the two surfaces of the object, shown in Figure 1.9 for a smooth surface.

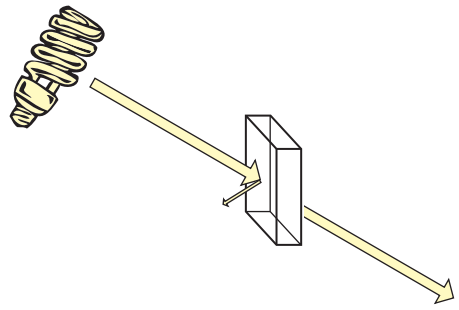

Figure 1.9 Light interacting with a smooth, transparent, colorless object. A small amount of light is reflected in the specular, or mirror-like, direction (drawn only at the front surface).

The small amount of reflected light results from light slowing down inside the material. The reduction in speed relative to a vacuum (the speed in air is almost identical) is defined by a quantity called the *refractive index*, notated by *n*. Water has a refractive index of 1.33. Since the speed of light in air is about 300 000 km/s, dividing by 1.33 calculates the speed of light in water, about 225 000 km/s. The term "refracted" is used because in addition to the change in speed, the light is bent or refracted. Putting a spoon halfway into a glass of water and looking from the side, the spoon appears bent.

We might perform an experiment where a ray of *monochromatic* light (one wavelength) strikes a piece of glass at various angles. In this experiment, we can measure how the light changes both its direction and intensity, depicted in Figure 1.10 when the ray of light strikes at 45° from straight on—that is, at *normal incidence*. At a refractive index change, such as the front surface of the material, the specular angle is in the direction such that equal angles are made by the incident and reflected light beams with the normal to the surface. The intensity of the specular light depends on the light's incident angle, wavelength, and *polarization* state, calculated using the *Fresnel equations*, described in a nearby sidebar. The wavelength dependency explains how light is dispersed into a spectrum by a prism.

As light of a specific wavelength travels toward you, the wave oscillates along one or more planes. When the oscillation is restricted to a single plane, it is said to be polarized, otherwise unpolarized. A polarizing filter will only pass

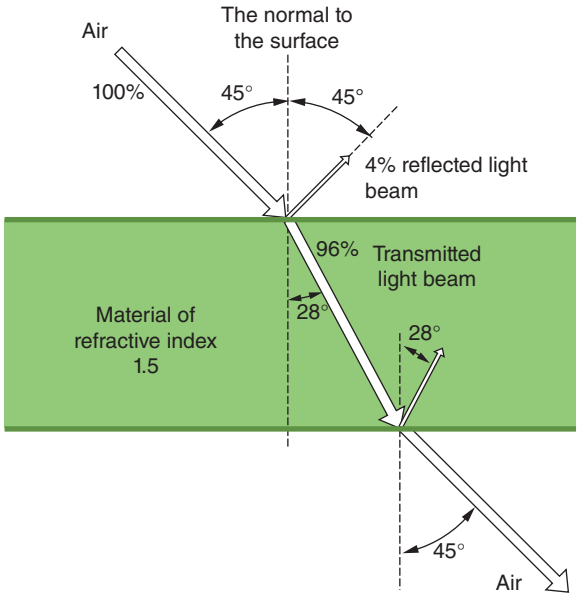

Figure 1.10 At every boundary where there is a change in *refractive index*, some of the light is reflected. The direction of the light beam is changed by an amount that depends on the change in refractive index and the original direction of the beam.

light along a single plane. First-surface reflections tend to have polarization parallel to a surface. Polarizing lenses on sunglasses block parallel polarization thereby reducing glare from streets, water, and ice.

As light is refracted through a material of dissimilar refractive index, the specific angle is calculated using *Snell's law* (Tilley 2011). The intensity of this light is the difference between the incident and reflected light. For window glass, typically with a refractive index around 1.5, only about 90% of the light passes through the glass for normal incidence.

Absorption

In addition to being transmitted, light may be *absorbed*, or lost as visible light. (If a very large amount of light is absorbed, we can sense that at least part of it is converted into heat.) If the material absorbs part of the light, it appears colored but is still transparent Figure 1.11; if all the light is absorbed, the material is black and is said to be *opaque* Figure 1.12.

For transparent materials, knowledge about their absorption properties as a function of wavelength can be used

First-Surface Reflections

The light reflected at the interface of two media with dissimilar refractive indices is often referred to as *first-surface reflection*. When the surface is smooth, this reflection occurs at the specular angle. Determining the percentage of the incident light reflected is attributed to Fresnel and for the case shown in Figure 1.10, Eqs. (1.1) and (1.2) are used (Wyszecki and Stiles 1982):

$$R_{\text{parallel}} = \left\{ \frac{\cos(\theta) - \left[\left({}^{n_{\text{material}}}/_{n_{\text{air}}} \right)^2 - \sin(\theta)^2 \right]^{1/2}}{\cos(\theta) + \left[\left({}^{n_{\text{material}}}/_{n_{\text{air}}} \right)^2 - \sin(\theta)^2 \right]^{1/2}} \right\}^2 \tag{1.1}$$

$$R_{\text{perpendicular}} = \left\{ \frac{\left({}^{n_{\text{material}}}/_{n_{\text{air}}} \right)^2 \cos(\theta) - \left[\left({}^{n_{\text{material}}}/_{n_{\text{air}}} \right)^2 - \sin(\theta)^2 \right]^{1/2}}{\left({}^{n_{\text{material}}}/_{n_{\text{air}}} \right)^2 \cos(\theta) + \left[\left({}^{n_{\text{material}}}/_{n_{\text{air}}} \right)^2 - \sin(\theta)^2 \right]^{1/2}} \right\}^2 \tag{1.2}$$

where θ is the incident angle and n is refractive index. The amount of reflected light depends on the polarization of the incident light, either parallel or perpendicular to the plane of the material. In many cases, the light is unpolarized and the two polarization states are averaged, as in Eq. (1.3)

$$R_{\text{unpolarized}} = \frac{(R_{\text{parallel}} + R_{\text{perpendicular}})}{2} \tag{1.3}$$

For glass with a refractive index of 1.5, the first-surface reflectance varies between 4% at normal incidence and 100% at the angle perpendicular to the normal angle (90°).

The remaining light enters the material, Eq. (1.4)

$$T = 1 - R_{\text{unpolarized}} \tag{1.4}$$

The light changes direction as it refracts, the angle defined using *Snell's law*, shown in Eq. (1.5)

$$\theta_{\text{transmitted}} = \arcsin\left\{ {}^{n_{\text{air}}}/_{n_{\text{material}}} \sin(\theta_{\text{incident}}) \right\} \tag{1.5}$$

Quite often, the spectral transmittance of glass or plastic is measured using spectrophotometers where the angle of incidence is along the normal (0°) and the light is unpolarized. In this case, the Fresnel equations reduce to Eq. (1.6) and the reflected light is notated as K_1 (Saunderson 1942)

$$K_1 = \left(\frac{n_{\text{material}} - n_{\text{air}}}{n_{\text{material}} + n_{\text{air}}} \right) \tag{1.6}$$

The light travels through the material and again encounters a refractive-index change and the same formulas are used to calculate the amount of first-surface reflection, the amount of light entering air, and its refracted angle. The first-surface reflected light continues to inter-reflect inside the material, and as a consequence, less light transmits than when assuming just the two surfaces of the material. For normal incidence, the transmitted light depends on K_1 and the inherent transmittance properties of the material, that is, its internal transmittance, T_{internal}, shown in Eq. (1.7) (Allen 1980)

$$T_{\text{measured}} = \frac{(1 - K_1)^2 T_{\text{internal}}}{1 - K_1^2 T_{\text{internal}}^2} \tag{1.7}$$

Because the change in first-surface reflection is nearly constant for incident light angles found in spectrophotometers used for color measurement, Eq. (1.7) is used to calculate transmitted light, irrespective of the spectrophotometer geometry.

Light transmitting through a material as shown in Figure 1.10, that is, at 45° incidence relative to the normal angle of a material with a refractive index of 1.5, results in the following values: $R_{\text{parallel}} = 0.080$, $R_{\text{perpendicular}} = 0.013$, $R_{\text{unpolarized}} = 0.047$, $T_{\text{inside top surface}} = 0.953$, $\theta_{\text{transmitted}} = 28.1$, and $T_{\text{measured}} = 0.092$.

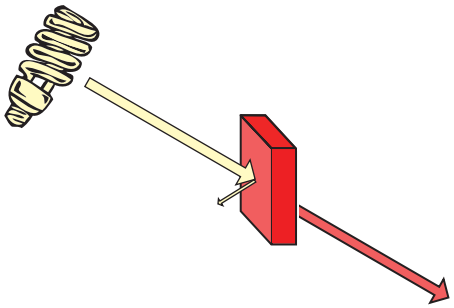

Figure 1.11 Light interacting with a smooth, *transparent* colored object.

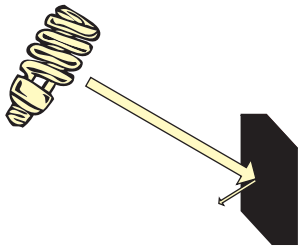

Figure 1.12 Light interacting with a smooth, *opaque* colored object.

to estimate their color. *Bouguer* or *Lambert's law* is used to predict changes in color with changes in a material's thickness (Bouguer 1729; Lambert 1760). *Beer's law* is used to predict changes in color with changes in concentration (Beer 1852, 1854). These laws and their use in predicting color mixtures are described in detail in Chapter 9.

Surface Scattering

Many materials do not produce specular reflections; rather they appear *matte*, *satin*, or *semi-glossy* to borrow terms from the paint industry. The first-surface reflections are *scattered*, caused by a rough surface, shown in Figure 1.13. Surfaces will vary between perfect mirrors and *perfect reflecting diffusers* where light is scattered in all directions equally. (The scattering of a perfect reflecting diffuser is a combination of surface and internal scattering, described below; in addition, light is not absorbed.)

The specific light scattering about the specular angle is called *bidirectional reflectance distribution function* or *BRDF* (Nicodemus et al. 1977), and numerous models have been derived that predict the BRDF of various materials (Dorsey, Rushmeier, and Sillion 2008). Simpler models have two adjustable parameters, similar to a normal distribution where the mean and standard deviation are changed, shown in Figure 1.14 for the Ward model (Ward 1992; Pellacini, Ferwerda, and Greenberg 2000). There are changes in the distinctness of image of the checkerboard background and the shape, sharpness, and intensity of the specular highlight. Hunter (1937) identified six types of gloss: (i) specular gloss, identified by shininess; (ii) sheen, identified by surface shininess at grazing angles; (iii) contrast gloss, identified by contrasts between specularly reflecting areas of surfaces and other areas; (iv) absence-of-bloom gloss, identified by the absence of reflection haze or smear adjacent to reflected highlights; (v) distinctness-of-reflected-image gloss, identified by the distinctness of images reflected in surfaces; and (vi) absence-of-surface-texture gloss, identified by the lack of surface texture and surface blemishes. These rendered cue balls encompass the first five.

The surface roughness of a transparent coating, such as a polyurethane finish or automotive clear coat, affects the material appearance beneath, shown in Figure 1.15 where a painting becomes nearly unrecognizable when the surface is very rough.

Internal Scattering

Light may be scattered when it interacts with matter. Some light is absorbed and re-emitted at the same wavelength, but now part of the light travels in one direction, part in another, until ultimately some light travels in many different directions. The effects of light scattering are both common and important. Light scattering by the molecules of the air accounts for the blue color of the sky, and scattering from larger particles accounts for the white color of clouds, smoke, milk, and most white pigments.

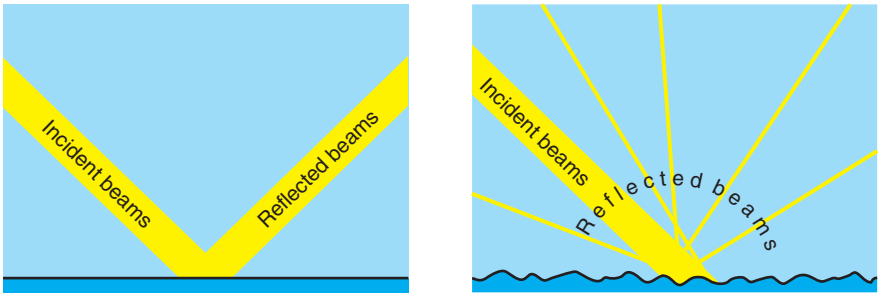

Figure 1.13 Incident light reflecting from smooth and rough surfaces. (a) Specular reflection of light from a mirror-like surface. (b) Diffuse reflection of light from a rough surface.

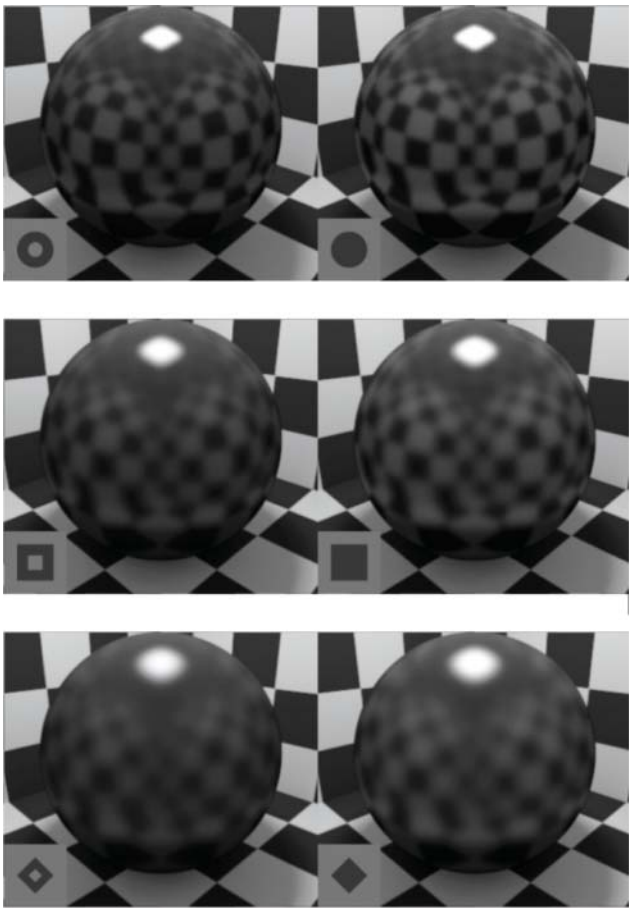

Figure 1.14 Rendered black cue ball using the Ward BRDF model where specular lobe energy is increased going from left to right and specular lobe width is increased going from top to bottom. Source: From Pellacini, Ferwerda, and Greenberg (2000).

When there is enough scattering, we say that light is *diffusely reflected* from a material. If only part of the light passing through the material is scattered, and part is transmitted, the material is said to be *translucent* or *turbid*, shown in Figure 1.16. If the scattering is so intense that no light passes through the material (some absorption is often present), it is said to be *opaque*, shown in Figure 1.17. The color of the material depends on the amount and kind of scattering and absorption present: if there is no absorption and the same amount of scattering at each wavelength, the material looks white, otherwise colored.

Scattering results when light falls on small particles with a refractive index different from that of the surrounding *medium*. The amount of light that is scattered depends strongly on the difference in refractive index between the two materials. When the two have the same refractive index, no light is scattered and the boundary between them, as every microscopist knows, cannot be seen, depicted in Figure 1.18.

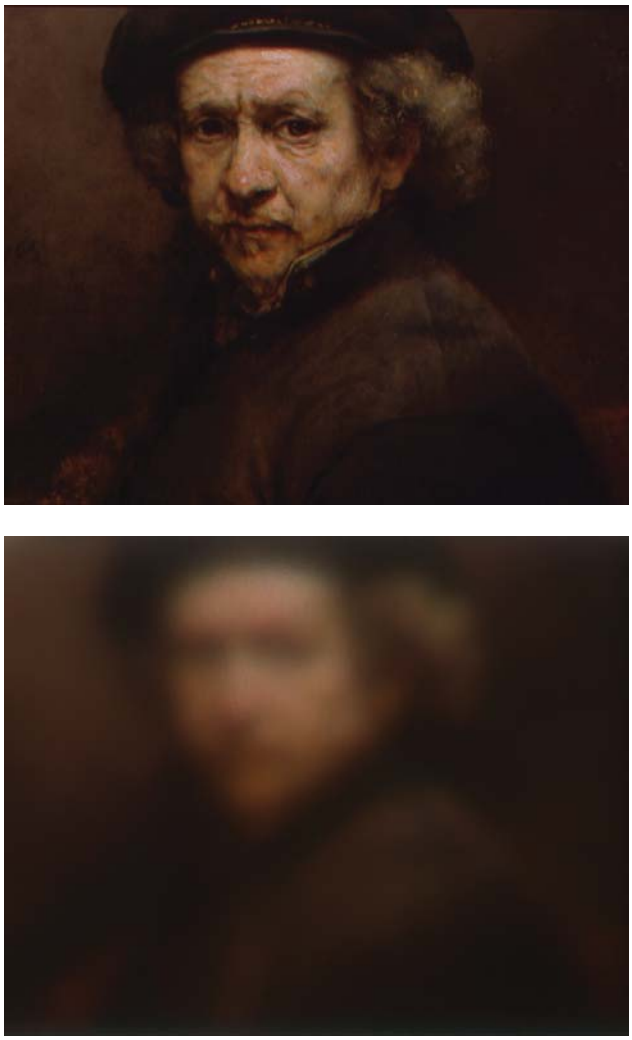

Figure 1.15 Detail of Rembrandt van Rijn (Dutch, 1606–1669), *Self-Portrait*, 1659. Oil on canvas, 83.8 cm × 66 cm (33¼ in. × 26 in.). Washington, National Gallery of Art, 1937.1.72. For these images, a photograph of the painting is viewed through (top) clear and (bottom) sandblasted glass. Source: Adapted from Berns and de la Rie (2003).

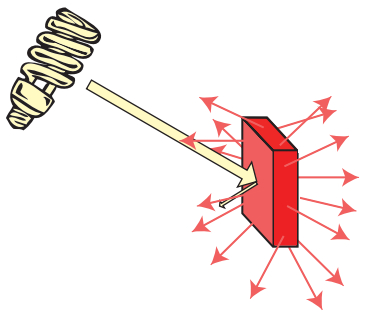

Figure 1.16 The scattering of light by a turbid or translucent material. In such a material, some light is transmitted and some is diffusely reflected by scattering.

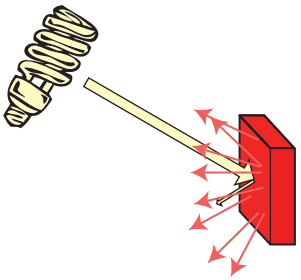

Figure 1.17 With an opaque material, no light is transmitted, but some is diffusely reflected by scattering.

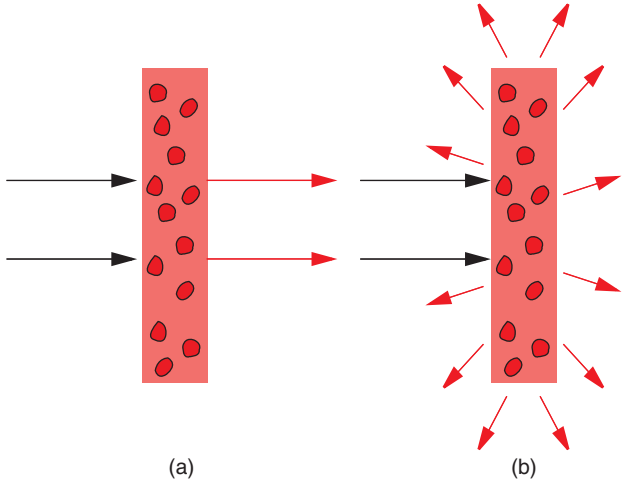

Figure 1.18 (a) If particles are placed in a medium of the same refractive index, there is no scattering, but (b) if there is a difference in refractive indices, scattering results.

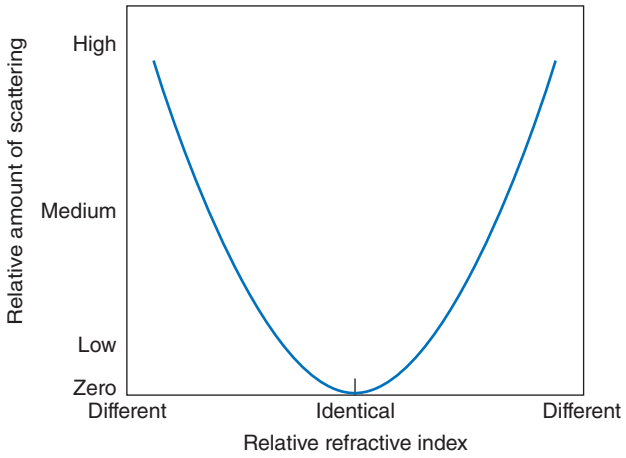

Figure 1.19 Scattering increases as the difference in refractive index between particles and their surrounding medium increases.

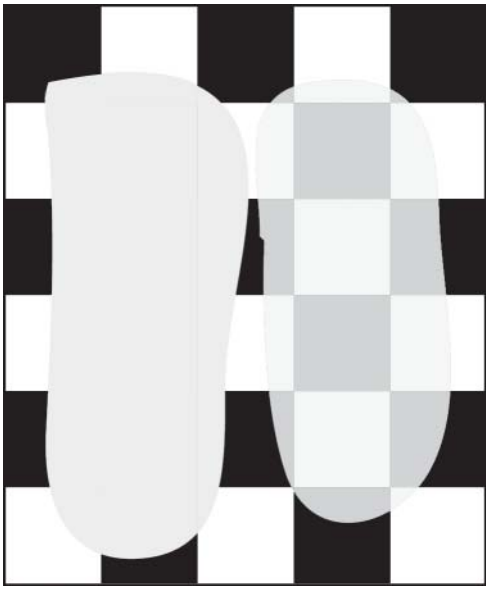

Figure 1.20 Two white paints applied at identical thickness to a checkerboard substrate. The difference in refractive index between the colorant and its medium determines opacity. The paint on the left has a larger difference than that on the right.

As the difference increases, scattering increases, shown in Figures 1.19 and 1.20. The amount of light scattering also depends strongly on the size of the scattering particles (Gueli et al. 2017), shown in Figures 1.21 and 1.22. Very small particles scatter very little light. Scattering increases with increasing *particle size* until the particles are about the same size as the wavelength of light and then decreases for still larger particles.

For these reasons, pigments are most efficient as light scatterers when their refractive index is quite different from that of the medium, for example, resin, plastic, or linseed oil, with which they are to be used, and their particle diameter is about equal to the wavelength of light. When pigments are of very small particle size and have about the same refractive index as the medium with which they are used, they scatter so little light that they look transparent. Scattering can therefore be controlled by selection of pigments with appropriate differences in refractive index or by control of particle size. One can get transparent coatings with very small particle iron-oxide pigments in spite of the difference in refractive index between the medium and the pigment. By control of the particle size, one can get scattering with organic pigments in spite of a relatively close match for refractive index. Depending on a pigment's particle size, small changes, due to process variability, can have a large effect on scattering power and, in turn, color.

Knowledge of the absorption and scattering properties of colorants as functions of the wavelength allows us to predict their colors. This is discussed in Chapter 9.

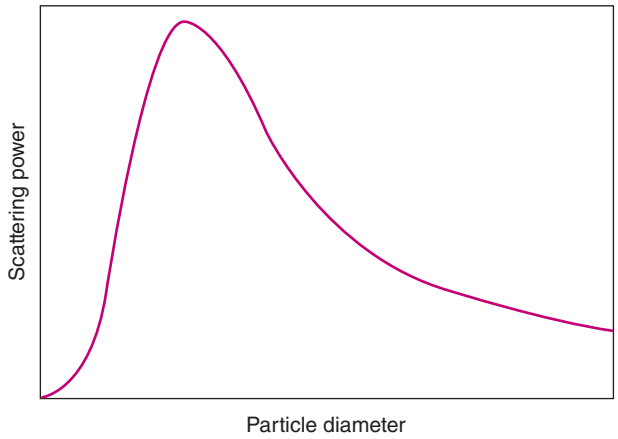

Figure 1.21 Scattering as a function of particle size for a typical pigment.

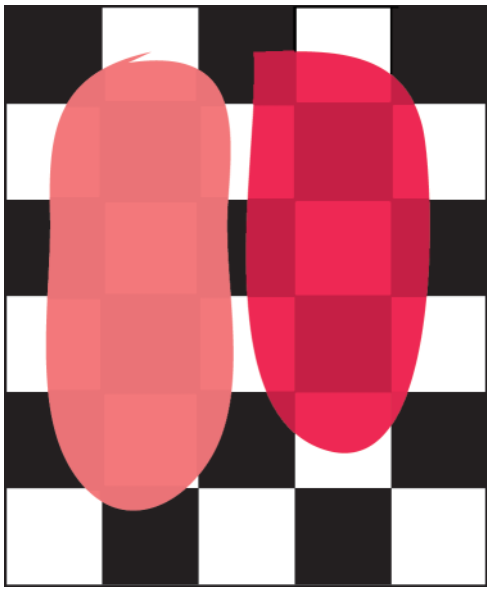

Figure 1.22 Although transparency or the lack of it is sometimes used to tell a dye from a pigment, this distinction does not always hold. Here, the same colorant is shown to have different transparency depending on its particle size and degree of dispersion. The sample on the right has smaller particle size.

Terminology – Dyes Versus Pigments

While *colorant* is the correct term for describing the materials used to impart color to objects, the word is still somewhat unfamiliar. Most people prefer to speak of dyes or pigments instead of using the more general term. But the need to use two words to include all colorants, as well the confusion existing between dyes and pigments, is a strong argument for changing to the word colorant. Even more confusing to those seeking precise definitions is the use of the word *color* in place of *colorant*. Sometimes, the use of the word "color" is due to familiarity and legacy. The most notable example is the *Colour Index*™, first printed in 1924 (http://colour-index.com/). Its name belies an extensive usage of the word "colorant" and, to a lesser extent, the word "substance." As it is used in this book, color means an effect perceived by an observer and determined by the interaction of the three components of light source, object, and observer (or two components when considering colored lights or displays).

In the past, it was easy to distinguish between a dye and a pigment. A dye was a soluble substance used to color material from a solvent. A pigment was an insoluble, particulate material that was dispersed in the medium it colored and produced scattering. While this simple distinction still holds in most cases, there are many exceptions so that additional criteria must be sought to make a distinction between these two types of colorants. No single definition is completely satisfactory since a given chemical compound can be either a dye or a pigment depending on how it is used.

For many years it has been commonly stated that "dyes are soluble; pigments, insoluble." This is generally true: most dyes are water-soluble at some stage in their application to a fiber or fabric. But there are some exceptions, or at least borderline cases. Vat dyes, for example, indigo used to color blue jeans, are normally insoluble in water but are "solubilized" chemically during the dyeing operation. In contrast to dyes, pigments are always insoluble in the medium in which they are used: any degree of solubility (called *bleed* in pigment-using industries) is considered a defect. We know of no exceptions to this. To put it another way, however, whenever a colorant normally used as the insoluble pigment is utilized in solution, it is simply called a dye!

Another traditional distinction between dyes and pigments is that dyes are organic and pigments are inorganic substances. The number of inorganic dyes is almost zero, but the number of organic pigments has grown steadily since the rise of the organic chemical industry. Today the distinction works only one way: most dyes are still organic, but it is not true that most chromatic pigments are inorganic. Until recently, all white pigments were inorganic, for example, titanium dioxide or zinc oxide, but now plastic microspheres are used as efficient lightweight scattering pigments.

A third distinction arose from the use of dyes and pigments to color materials such as paints or plastics. Colorants that dissolved in the medium and thus gave transparent mixtures were called dyes, in contrast to pigments, which did not dissolve but scattered light and gave translucent or opaque formulations. If opacity is desired, pigments are used, whereas if one wants to color a transparent medium without spoiling its transparency, dyes soluble in the medium (generally classed as solvent-soluble or oil-soluble dyes) are used. Another method to achieve transparency is to use pigments with very small particle sizes, and if possible of similar refractive index to the medium. When well

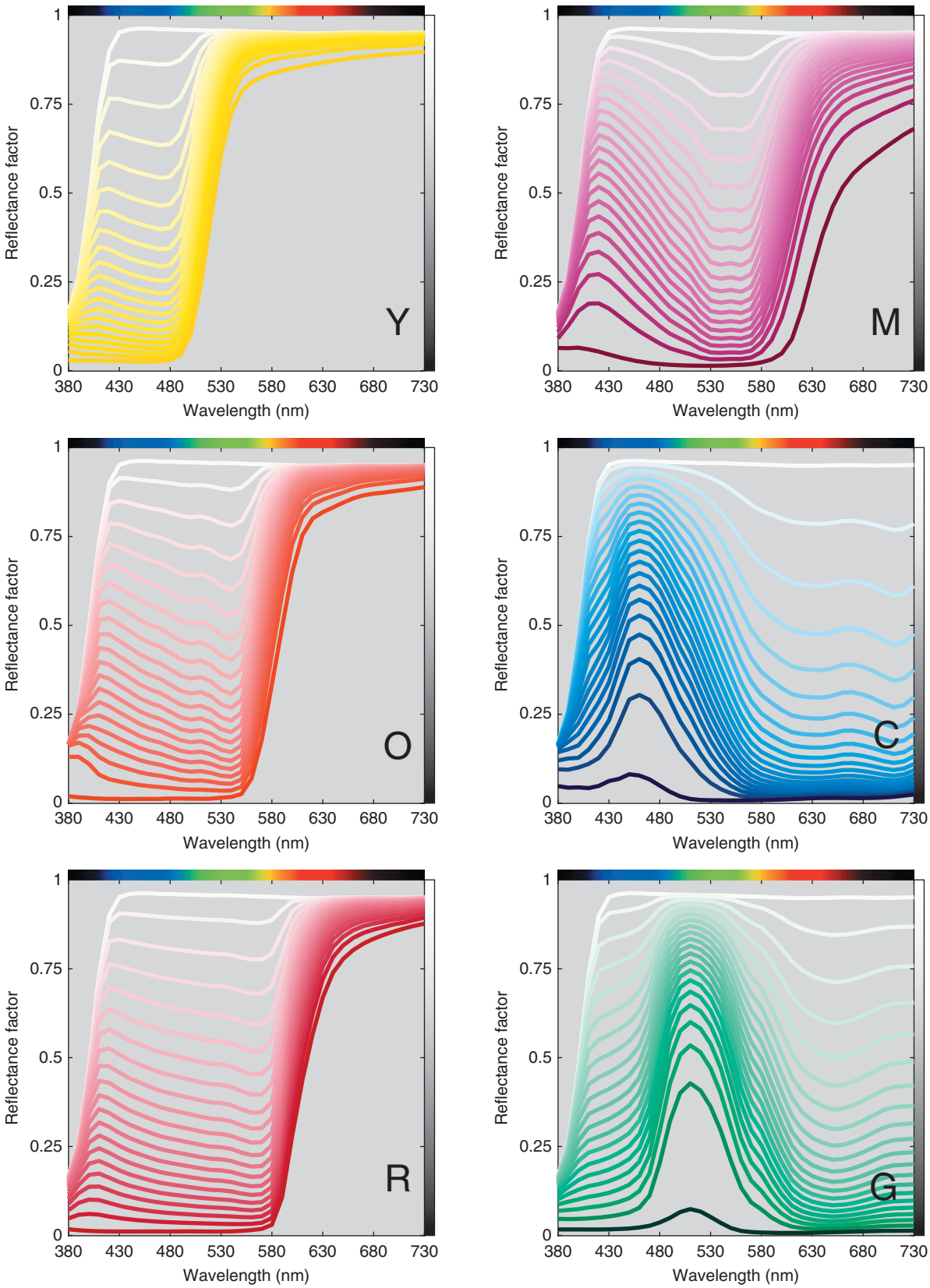

Figure 1.23 Spectral reflectance curves of the following acrylic dispersion paints, each mixed with titanium white (PW 6) at varying ratios: arylide yellow (PY 74), pyrrole orange (PO 73), pyrrole red (PR 254), quinacridone magenta (PR 122), phthalocyanine blue (PB 15), and phthalocyanine green (PG 36).

dispersed, the resulting colored materials are effectively transparent.

A final distinction, to us the one with greatest validity and fewest exceptions, is based on the mechanism by which the colorant is bound to the substrate. If the colorant has an affinity for the substrate (textile, paper, etc.) and will become a part of the colored material without the need for an intermediate binder, we consider such a colorant to be a dye. This substantivity or affinity for the substrate clearly distinguishes dyes from pigments. Pigments have no affinity to the substrate and require a binder so that the pigment is fixed to the substrate. A pigment applied to a surface without a binder will not adhere to the surface.

The Colour Index (C.I.) has become the arbiter of how a coloring material is classified. Available only online, it describes 27 000 individual products. A generic name and a five-digit number that gives the chemical constitution when disclosed (the exact chemical nature of many colorants is still a trade secret) define a colorant, for example, C.I. Pigment Yellow 74 No. 11741. We will define a colorant by its common name based on its chemical composition or historical name with the color-index generic name in parentheses, for example, arylide yellow (PY 74).

- *Radiant flux:* Power emitted, transmitted, or received in the form of radiation.
- *Incident radiant flux:* Radiant flux falling on or striking a material.
- *Transmission:* The process whereby radiant energy passes through a material or object.
- *Transmittance:* The ratio of the transmitted radiant flux to the incident radiant flux under specified geometric and spectral conditions.
- *Absorption:* The transformation of radiant energy to a different form of energy by interaction with matter.
- *Absorptance:* The ratio of the absorbed radiant flux to the incident radiant flux.
- *Reflection:* The process by which radiant energy is returned from a material or object.
- *Reflectance:* Ratio of the reflected radiant flux to the incident radiant flux in the given conditions.
- *Reflectance factor:* Ratio of the radiant flux reflected from the specimen to the radiant flux reflected from the perfect reflecting diffuser under the same geometric and spectral conditions of measurement.
- *Specular reflection:* Reflection that excludes diffuse reflection, as in a mirror.
- *Diffuse reflection:* Reflection that excludes specular (mirror) reflection.

Spectral Characteristics of Conventional Materials

From the standpoint of color, the effect of an object on light can be described by its *spectral transmittance* or *reflectance curve* (for transparent or opaque materials, respectively; both are needed for translucent objects). These curves show the fraction of the light reflected at each wavelength from the material (compared to that reflected from a suitable white reflecting standard, usually the perfect reflecting diffuser) or transmitted through it (compared to that transmitted by a suitable standard, usually air). These curves describe the object just as the spectral power distribution curve describes a source of light. The spectral reflectance curves of several common colorants are plotted in Figure 1.23. In each plot, the colorant is in *masstone* form in which the colorant is dispersed in a medium at high concentration, for example, tube paint, and intermixed with a white colorant in masstone form, resulting in a tint series (*tint ladder*). The white determines the maximum reflectance at each wavelength. Yellow, orange, and red colorants absorb light at shorter wavelengths and reflect light at longer wavelengths. The transition wavelength region from short to long wavelengths differentiates the three colorants. Magenta and purple colorants absorb light in the middle wavelengths. Cyan colorants absorb light at longer wavelengths. Green colorants absorb light at short and long wavelengths. Each colorant has a unique spectral "signature" that sometimes can be used for identification. For example, the secondary reflectance at longer wavelengths identifies the cyan as phthalocyanine blue. However, the clarity of the signature depends on concentration, and as a consequence, reflectance is transformed nonlinearly such that spectra are invariant with changes in concentration (Derby 1952; Johnston-Feller 2001).

E. FLUORESCENT MATERIALS

Most dyes and pigments dissipate absorbed light in the form of heat. However, *luminescent* materials emit light without heat, a process known as *photoluminescence*. This occurs by absorbing light over a range of wavelengths and *emitting* them, most often, at longer wavelengths. When the emitted light continues after *excitation* ceases, it is called *phosphorescence*. When the emission ceases when excitation ceases, it is called *fluorescence*. The emitted light is always diffuse.

Fluorescent whitening agents (*FWAs*) absorb *ultraviolet radiation* between about 300 and 400 nm and re-emit this radiation as light between 400 and 500 nm. FWAs are used commonly to whiten paper and textiles to make materials look "whiter than white." What happens is that such a material radiates more *visible* light than is incident on it, making it look brighter than a nonfluorescent material that, at best, can only reflect all the visible light that falls on it.

- *Luminescence:* Emission of light ascribable to nonthermal excitation.
- *Photoluminescence:* Luminescence produced by the absorption of light (excitation); distinguished from ordinary reflection by a time delay and, usually, a shift toward longer wavelengths.
- *Phosphorescence:* Photoluminescence that continues after excitation ceases.
- *Fluorescence:* Photoluminescence that ceases when excitation ceases.
- *Total radiance factor:* The sum of fluorescent and nonfluorescent reflected light from a specimen in comparison to the reflected light from a perfect reflecting diffuser under identical specified geometric conditions.

To obtain this effect, the light source must contain energy at the appropriate wavelengths in the ultraviolet range to produce the emission in the blue region of the visible spectrum. Since soiled textiles are usually yellowish, the emitted blue light replaces the amount of blue light absorbed by the yellow. In a similar fashion, FWAs are used to counteract the yellow appearance of many resins and papers. FWAs are also used to produce "bright white" paper, shown in Figure 1.24.

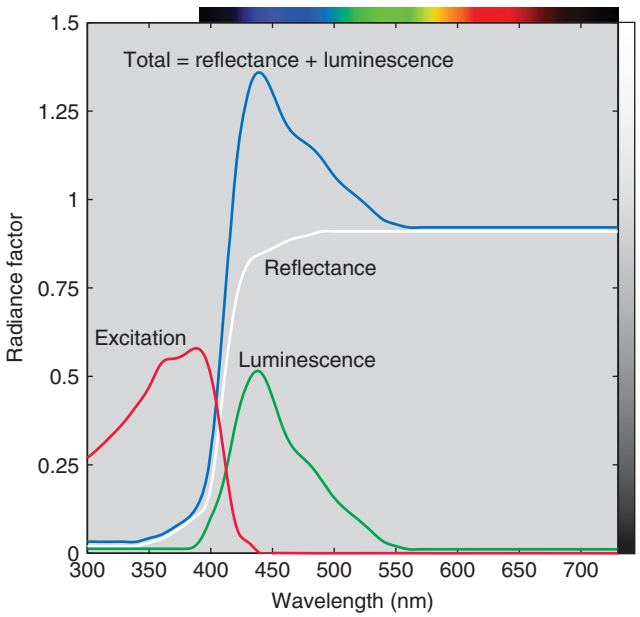

Figure 1.24 Spectral properties of "bright white" paper illuminated by skylight. (Note the wavelength scale extending from 300 to 730 nm.) Any absorbed radiation within the excitation region leads to luminescence that occurs across a range of wavelengths. The reflectance spectrum is the property of the paper without the FWA. The paper's appearance is determined by its *total radiance factor*, the luminescent and nonluminescent components added together.

Fluorescent colorants both absorb and emit light within the visible spectrum and are used in many products. As shown in Figure 1.25, the green light causes excitation of a fluorescent colorant, which emits diffuse light that is orange in color. As with FWAs, the combined fluorescent emission and nonfluorescent reflection produce spectra that exceed the reflection of a perfect reflecting diffuser, seen in Figure 1.26. The emission of both fluorescent colorants and FWAs depends on the spectral properties of the light source, making standardized measurements that correlate with appearance difficult. Ideally, the light source in an instrument used to measure fluorescent materials should have the same spectral properties as the viewing environment used to illuminate them. Several measurement techniques are described in Chapter 6.

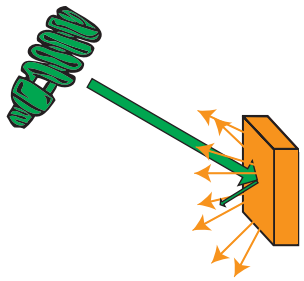

Figure 1.25 The emission of light by an opaque, fluorescent object. The green light is re-emitted diffusely at longer wavelengths, leading to an orange color.

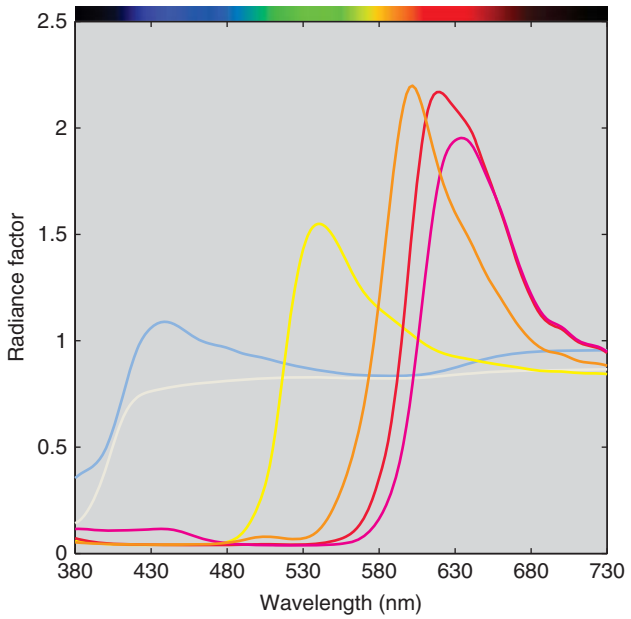

Figure 1.26 Spectral radiance factor of nonfluorescent paper (white line), paper containing FWAs (blue line), fluorescent yellow (yellow line), orange (orange line), red (red line), and magenta (magenta line) paints. The illumination is daylight.

F. GONIOAPPARENT MATERIALS

Thus far, we have described opaque materials having internal reflections (ignoring surface reflections) that are diffuse, and as a consequence, their appearance is largely independent of illuminating and viewing geometries. Such materials are often referred to as *isotropic* and *Lambertian* materials. Coatings containing *metal flakes*, *pearlescent* pigments, *interference* pigments, and *diffraction* pigments have appearances that can change with changes in illumination or viewing angle. These materials are known as *gonioapparent* materials. The terms *effect pigment* and *goniochromatic* pigments are also used. Quite often, these changes are most dramatic near the specular angle, irrespective of the incident angle. Thus, geometries are defined relative to the specular angle, known as the *aspecular angle*, shown in Figure 1.27.

Anisotropic is another common term associated with gonioapparent materials. However, not all coatings containing effect pigments are anisotropic. For example, a coating containing metal flakes can appear isotropic if the flakes have a small particle size and are dispersed with a random orientation within the coating.

Metallic Materials

Since the Egyptians' first use of gold overlays in decorative arts, metals have been used to alter the reflectance properties of man-made objects. One of the distinct characteristics of metals is that their specular reflections are the color of the metal rather than the color of the light source. Because of adhesion problems with thin beaten metal overlays, powdered metals were mixed with vehicles and applied as paints. Today, commonly used metals include gold, bronze, copper, zinc, stainless steel, nickel, graphite, and aluminum.

- *Isotropic:* Having an appearance that is independent of illuminating and viewing geometry.
- *Anisotropic:* Having an appearance that is dependent on illuminating and viewing geometry.

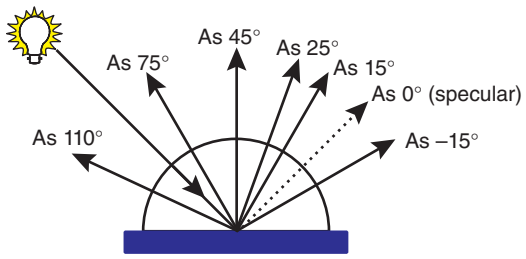

Figure 1.27 Common angles when measuring opaque gonioapparent materials. All the listed angles are *aspecular* angles. The light source is defined as 45° from the normal angle.

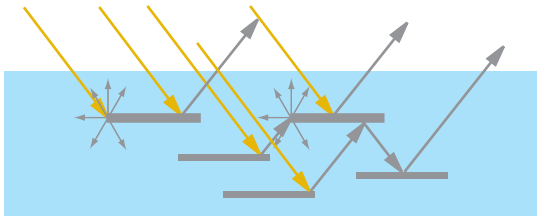

Figure 1.28 Aluminum flakes are oriented within a vehicle. Incident light is specularly reflected. At the edge of a flake, the light is reflected diffusely. Thus, smaller flake diameter increases the amount of diffuse reflection.

Aluminum flake is widely used in the automotive industry to create paint finishes with a metallic appearance. Under a microscope, the pigment particles can look like corn flakes, hence their name. It is also possible to produce metallic pigments that resemble thin disks (Maile, Pfaff, and Reynders 2005). The aluminum flakes tend to be between 0.1 and 2 μm in thickness with diameters ranging between 0.5 and 200 μm. Flake diameter affects both the diffuse and specular properties of the coating, shown in Figure 1.28. Large diameters produce a narrower specular distribution. Decreasing diameter increases the amount of diffuse reflection, resulting in a widening of the specular distribution and a "whitening" of the finish. These can be used in combination to increase or decrease the difference between the mid-aspecular and either the near-aspecular or far-aspecular properties. (Colloquially, mid- and far-aspecular are known as face and flop colors, respectively.)

The addition of metallic flake to paint produces large changes in color with changes in viewing angle, simulated (Kirchner and Houweling 2009) in Figure 1.29. These large changes accentuate contours. The orientation of the flakes within the paint is another parameter affecting appearance. For quality control, multiangle measurements are required when aluminum or other metal flakes are added to coatings. Imaging techniques may also be required. These topics are described in Chapter 6.

Pearlescent Materials

Pearlescent colorants are commonly used to impart the appearance resembling that of natural pearls and mother-of-pearl. Pearlescent flakes are thin, transparent platelets of high refractive index, which partially reflect and partially transmit light (Greenstein 1988; Pfaff and Reynders 1999). Their interaction with incident light is shown in Figure 1.30. Unlike metallic flakes that only reflect light, pearlescent colorants both reflect and transmit. The specular reflection resulting from many layers of similarly oriented

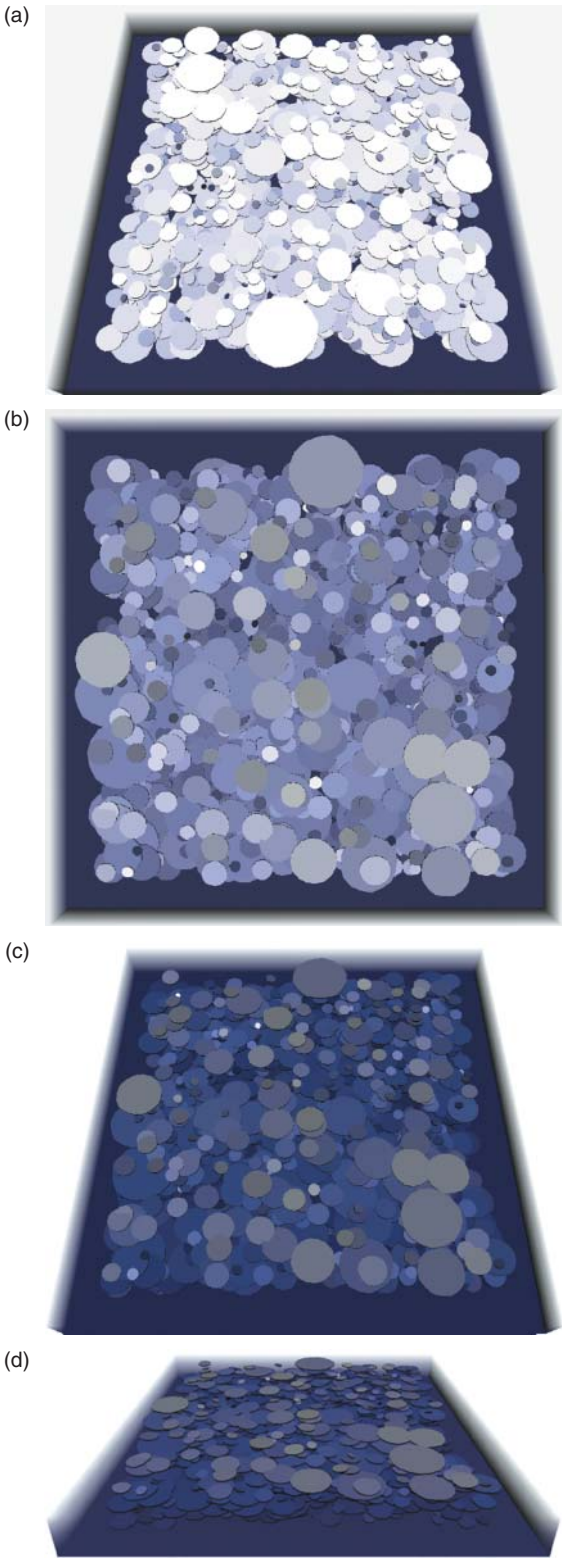

Figure 1.29 Simulating the change in appearance of a metallic coating at different viewing angles: (a) 15° aspecular, (b) 45° aspecular ("face"), (c) 75° aspecular, and (d) 110° aspecular ("flop"). Source: Courtesy of AkzoNobel.

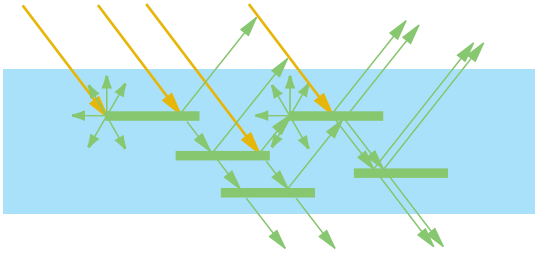

Figure 1.30 Pearlescent flakes are also oriented within a vehicle. Unlike metallic flakes, pearlescent flakes both reflect and transmit light.

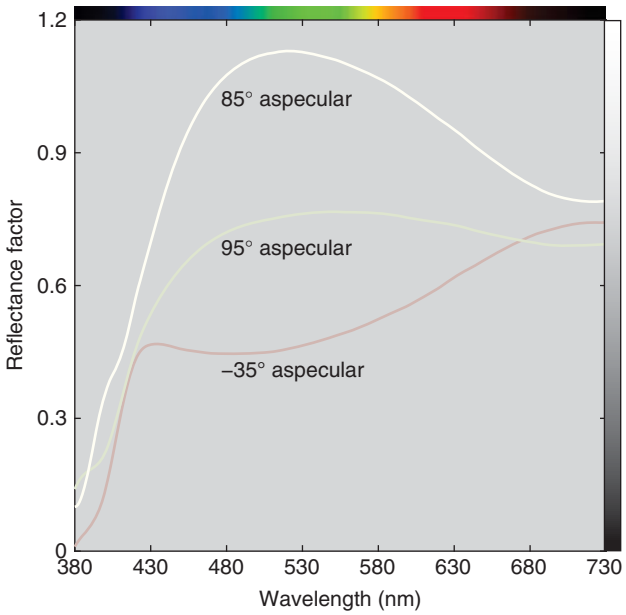

Figure 1.31 Spectral reflectance factor of a green pearlescent mica and white artist paint at each listed aspecular angle.

flakes creates a pearlescent luster. The term *nacreous* is sometimes used in place of pearlescent. During the 1950s and 1960s, basic lead carbonate was used in various plastics to create pearlescent luster (e.g. in buttons). Similar to metallic colorants, their color also varies appreciably with changes in viewing angle. The reflectance factor of a green pearlescent mica and white artist paint at three angles is shown in Figure 1.31. For large aspecular angles, the color is black.

Interference Materials

Certain platelet thicknesses of pearlescent flakes produce color due to light interference. They are known as *interference flakes* or *interference pigments*. Interference occurs through the interaction of light rays of the upper and lower surfaces of the transparent platelet (see Bolomey and Greenstein 1972; Greenstein 1988; Pfaff and Reynders 1999; Nassau 2001; Tilley 2011). Changes in the

Figure 1.32 Simulation of an interference pigment coating. Source: From Musbach (2016).

platelet thickness change the interference color. The transmission and reflection interference colors are different. Fish scales are an organic example of an interference pigment. Titanium-dioxide-coated mica is the most common pearlescent and interference flake pigment. Normal pigments can also be coated onto the mica along with titanium dioxide, resulting in combination pigments.

Recently, thin-film vapor-deposition technology has been used to create interference pigments with high-chromatic-intensity and metallic characteristics. A multilayer structure is produced that consists of a central opaque aluminum layer surrounded by a glass-like layer that is finally surrounded by a semitransparent absorber layer. Controlling the thicknesses of each layer results in a wide range of colors. Because the color results from interference alone, the change in color with change in geometry is dramatic, shown in Figure 1.32. The central aluminum layer creates a colored metallic appearance rather than a colored pearlescent appearance.

Depending on the properties of the pearlescent flake and the color of conventional pigments, very dramatic gonioapparent effects can be achieved in coatings. Modern automotive finishes and nail polishes have very interesting changes in hue and chroma with changes in illumination and viewing geometry. In order to maximize the pearlescent effects, the pearlescent flakes should have a high refractive index (often close to 3.0), optimal platelet thickness and diameter, transparency, and a smooth surface. As with metallics, varying the diameter affects the goniophotometric characteristics of the coatings. Unlike metallics (because they do not produce light interference), varying thickness changes the color of the specular reflection.

Diffraction Materials

Diffraction materials have a metal substrate embossed with parallel grooves that is coated with an inorganic substance (Ferrero et al. 2016). They are essentially tiny diffraction gratings and their colors change at all angles. When added to a coating, a rainbow effect is achieved. The particle size and its orientation within a coating affect the strength of the spectrum.

G. PHOTOCHROMIC AND THERMOCHROMIC COLORANTS

In the past, photochromism and thermochromism were viewed as engineering "defects," limiting the usage of certain colorants (van Beek 1983). Today, these properties have been exploited. Thermochromic colorants are used in textiles in which changes in body temperature change the color of the fabric (Aitken et al. 1996). Photochromic colorants are used to darken eyeglasses and change the color of nail polishes; ultraviolet radiation activates the chemical change (Viková and Vik 2006; Exelby 2008; Corns, Partington, and Towns 2009).

- *Photochromism:* A reversible change in color of a specimen due to exposure to light (or other radiation) without appreciable heating of the specimen.
- *Thermochromism:* A change in color with temperature change.

H. SUMMARY

Light is radiant flux (power) that we sense. The first step in defining color is understanding the interaction between incident light and a material. Incident light can only be reflected, transmitted, or absorbed. Materials that only reflect or absorb light are opaque. When the light transmits through the material without changing its direction, it is transparent. Translucent materials both reflect and transmit incident light. The geometric distribution of reflected and transmitted light depends on both surface and internal scattering. The surface roughness affects appearance parameters such as gloss and distinctness of image, quantified by a bidirectional reflection distribution function. Internal scattering depends on the size, orientation, and refractive index of the colorants compared with their surrounding medium. Traditional colorants produce colors that do not change with changes in illumination and viewing geometry (viewed away from specular angles). Gonioapparent colorants produce colors that do change with changes in illumination and viewing geometry. Metal, pearlescent, interference, and diffraction colorants are examples. Fluorescent colorants absorb light in one wavelength region and emit the light at longer wavelengths. Thermochromic colorants change color with changes in their temperature. Photochromic colorants change color with changes in the amount of UV radiation. The next step in understanding color is how we respond to this light, the subject of Chapter 2.

Chapter 2
Color and Spatial Vision

So far, we have limited our discussion about *color* to the physical stimulus, producing light which, when detected and interpreted through our visual system, results in the stimulus having a particular *color*. The conversion from light energy to color names such as red, green, and brown is exceedingly complex. It requires an understanding of physiology, optics, detectors, neural processing, and cognition. Every year, vision scientists fill in more pieces of the puzzle. The comprehensive textbooks of Backhaus, Kliegl, and Werner (1998), Gegenfurtner and Sharpe (1999), Palmer (1999), Valberg (2005), Daw (2012), and Livingstone (2014) are suggested for more in-depth study. Fortunately, it is not essential for our purposes in this book to know in detail how the visual system works; knowledge of a few basic principles will suffice.

A. TRICHROMACY

A cross section of the eye is shown in Figure 2.1. Light entering our eyes is imaged onto the back of the eyeball, the *retina*. The *cornea* and *lens* focus the image by changing their shape. The *iris* modulates how much light enters the eye. The retina contains *photoreceptors* that absorb a portion of the incident light and generate a signal that is eventually interpreted by the brain. In many respects, the image formation is similar to that in a camera. The quality of the retinal image depends on the absorption, scattering, and focusing properties of the *cornea*, *lens*, and fluids filling the eyeball (*aqueous* and *vitreous humor*). These optical elements influence the spectral and spatial properties of the photoreceptors, or simply, receptors.

There are two classes of receptors, *rods* and *cones*, named according to their shape. They reside within the retina, forming a *retinal mosaic*. Their placement varies throughout the retina and from person to person. In the center of the eye, there is a depression in the retina called the *fovea* or the *foveal pit*. This region contains only cones. Foveal vision is used for distinguishing very fine detail, such as for reading and seeing objects at a distance. A yellowish pigment, *macular pigment*, is also present in the fovea. The macular pigment helps protect the foveal receptors from damage from the sun. Outside the fovea, the number of cones is greatly reduced and they are situated quite far apart from one another. The remainder of the mosaic consists of rods. Since the retina is spherical, the total number of rods far exceeds the total number of cones.

A schematic of the retina in the foveal region is shown in Figure 2.2. Each individual cone does not have a separate connection to the brain; rather, there are interconnections between the horizontal, bipolar, amacrine, and ganglion cells, forming *receptive fields* (Wiesel and Hubel 1966). Thus *resolution*, the ability to resolve fine detail, depends ultimately on both the spatial mosaic of the photoreceptors and how they interconnect.

Rods detect very small amounts of light, such as starlight. A single photon of light can produce a signal. The light-sensitive material in a receptor is called a *photopigment*. Because rods have only a single photopigment, the signal results in an achromatic response where we only see objects as shades of gray. As the amount of light increases, the rods cease sending signals to the brain. During the day or in a well-lit room, the rod signals are inactive.

Cones, the second class of receptors, have much lower sensitivity to incident light. As the amount of light increases,

Billmeyer and Saltzman's Principles of Color Technology, Fourth Edition. Roy S. Berns.

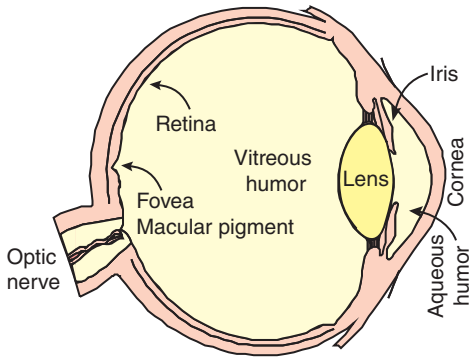

Figure 2.1 The cross section of the human eye.

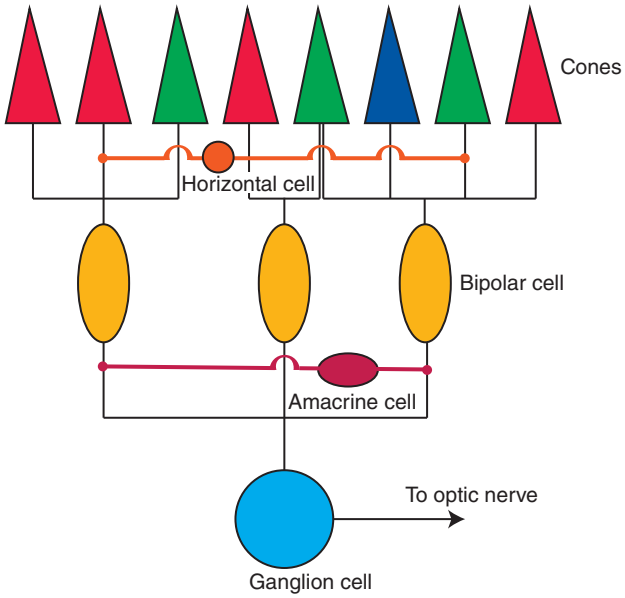

Figure 2.2 Simplified model of the retina (excluding rods).

the cones start sending neural signals. The cones are our color receptors. As the sun begins to rise in the morning, the gray world becomes colored. Our sensations of color are a result of having three types of photopigments that respond differently to light of various wavelengths. Different colored stimuli result from different cone signals. The letters L, M, and S are used to represent the three cone types with their peak sensitivities in the long, middle, and short wavelength regions, respectively. As shown in Figure 2.3, their *spectral sensitivities* overlap quite a bit, particularly those of the L and M cones. This improves color discrimination. Notice also the gap between the S and M cones. Because the spectrum is not sampled uniformly, spectral differences are only rarely used to predict visual differences.

Two stimuli—whether colored lights or illuminated materials—match in color when they produce the same cone signals. Color matches can be calculated by knowing the cones' spectral sensitivities and the stimuli's spectra. As

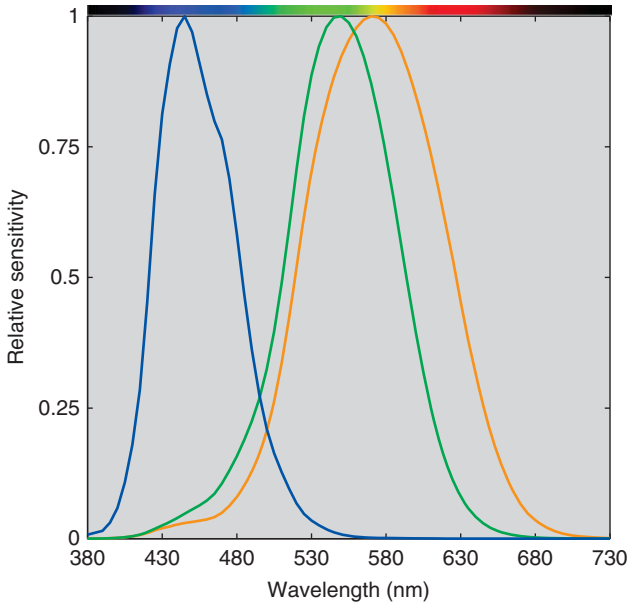

Figure 2.3 Spectral sensitivities of the human visual system cone fundamentals where the orange, green, and blue lines correspond to the L, M, and S cones, respectively.
Source: Adapted from Smith and Pokorny 1975.

do any detectors of radiation, the cones integrate—that is, sum up—the light at all wavelengths incident on them. Each such integration of all the incident wavelengths reduces the entire spectrum of incident light to three signals, one for each type of cone, resulting in what is called *trichromacy*. Trichromatic theory is usually associated with Young (1802) and von Helmholtz (1866), although there is evidence that a number of scientists and technologists theorized the existence of trichromacy during the eighteenth century, notably Palmer in 1777 (Weale 1957).

The reduction from spectra to trichromatic signals is shown in Eqs. (2.1)–(2.3):

$$L = \int_{\lambda} S_{\lambda} R_{\lambda} l_{\lambda} \, d\lambda \tag{2.1}$$

$$M = \int_{\lambda} S_{\lambda} R_{\lambda} m_{\lambda} \, d\lambda \tag{2.2}$$

$$S = \int_{\lambda} S_{\lambda} R_{\lambda} s_{\lambda} \, d\lambda \tag{2.3}$$

where S_{λ} is an illuminant's spectral power distribution, R_{λ} is an object's spectral reflectance factor, and l_{λ}, m_{λ}, and s_{λ} are the spectral sensitivities of the human visual system. These formulas are depicted in Figure 2.4. The spectra of the illuminant and object are plotted in the top row. The light reflecting from the object is plotted in the second row. The spectral sensitivities of the L, M, and S cones are plotted in the third row. The spectra of the product of the light entering our eyes and our cones' spectral sensitivities are shown in the fourth row.

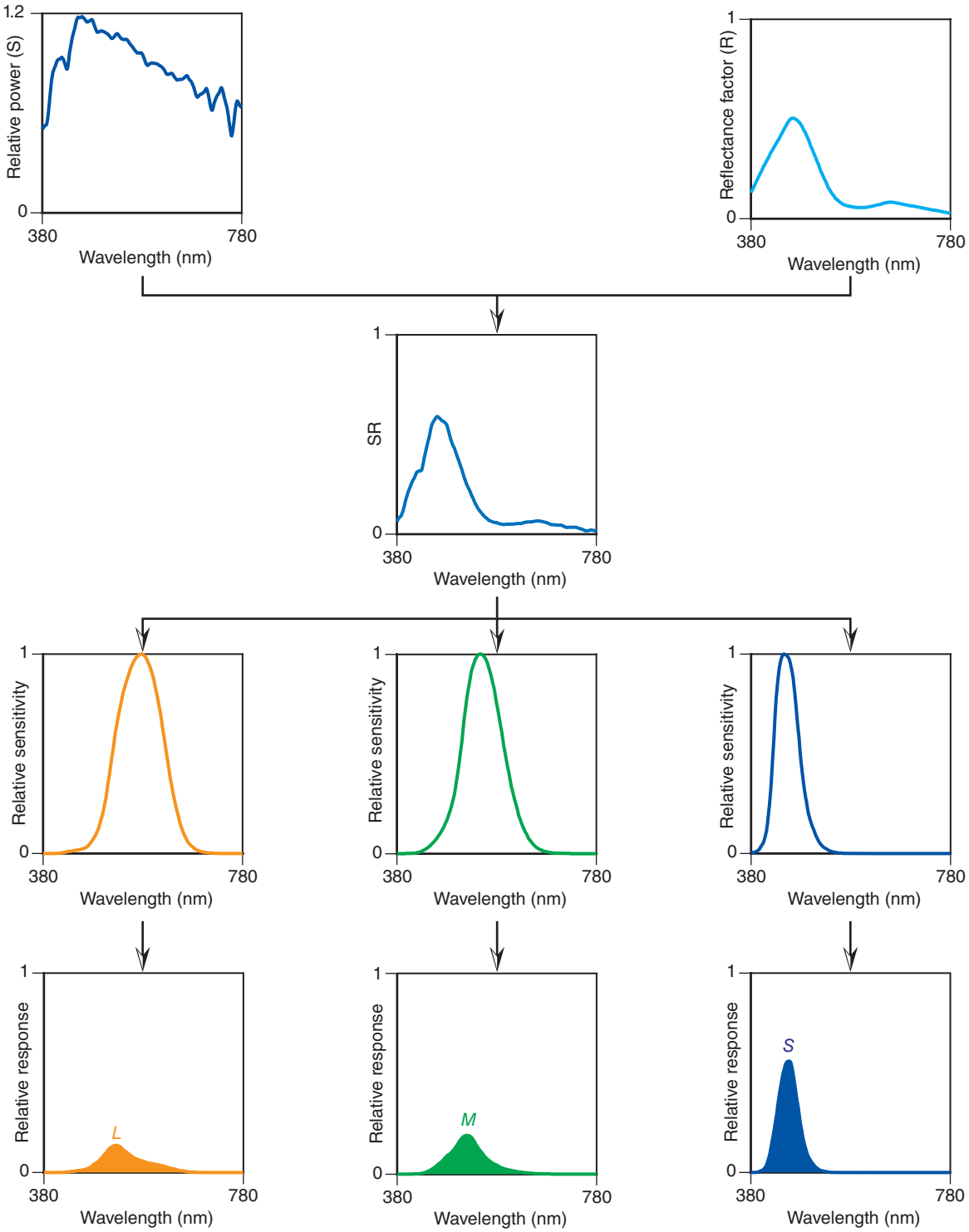

Figure 2.4 The integrated *L*, *M*, and *S* responses that result from the light entering the eye from an illuminated object. This can be calculated as the product of the spectral properties of the light source, the object, and the observer's sensitivities, followed by integration over wavelength, essentially, calculating the areas under the last row of curves.

Approximating Integration Using Summation and Matrix Algebra

Throughout this book, we will show mathematical formulas in the most straightforward way possible. In some cases, this will be in the form of matrix algebra. Integrating incident light to three trichromatic signals is commonly approximated by summation, shown in Eqs. (2.4)–(2.6)

$$L = \sum_{\lambda} S_\lambda R_\lambda l_\lambda \Delta\lambda \tag{2.4}$$

$$M = \sum_{\lambda} S_\lambda R_\lambda m_\lambda \Delta\lambda \tag{2.5}$$

$$S = \sum_{\lambda} S_\lambda R_\lambda s_\lambda \Delta\lambda \tag{2.6}$$

Matrix algebra is very useful when calculating *LMS* signals for several objects, particularly images where there are millions of "objects." For such cases, Eqs. (2.4)–(2.6) become Eq. (2.7), shown for two objects:

$$\mathbf{t} = \mathbf{TSR} \tag{2.7}$$

where

$$\mathbf{T} = \begin{pmatrix} l_\lambda & \dots & l_\lambda \\ m_\lambda & \dots & m_\lambda \\ s_\lambda & \dots & s_\lambda \end{pmatrix} \tag{2.8}$$

$$\mathbf{S} = \begin{pmatrix} S_\lambda & 0 & 0 \\ 0 & \ddots & 0 \\ 0 & 0 & S_\lambda \end{pmatrix} \tag{2.9}$$

$$\mathbf{R} = \begin{pmatrix} R_{\lambda,1} & R_{\lambda,2} \\ \vdots & \vdots \\ R_{\lambda,1} & R_{\lambda,2} \end{pmatrix} \tag{2.10}$$

$$\mathbf{t} = \begin{pmatrix} L_1 & L_2 \\ M_1 & M_2 \\ S_1 & S_2 \end{pmatrix} \tag{2.11}$$

The areas under the curve are the cone responses. Because the light entering the visual system in this example has power mainly in the short wavelength region, the area under the curve for the S cones is greatest.

We have shown plots of the spectral sensitivities of the L, M, and S cones in Figures 2.3 and 2.4. Looking at the cross section of the eye in Figure 2.1, we see that the light entering our eyes is modified by the absorption and scattering properties of the cornea, aqueous humor, lens, vitreous humor, and in the fovea, macular pigment. How are we accounting for these properties? The L, M, and S "cone responses" and "spectral sensitivities" are based on measurements that include *prereceptor absorption and scattering*. These are different than measuring the spectral absorption of the light-sensitive material in a cone, called a *photopigment*. The term *cone fundamental* is used to represent measurements made in front of the eye. When we refer to L, M, and S "cones," we mean to say "cone fundamentals."

Metamerism: Phenomenon in which spectrally different stimuli appear to match to a given observer.

The conversion from spectra to three signals, that is the process of trichromacy, is one of the most important properties of the visual system. This means that different spectra can produce the same trichromatic response. This property is called *metamerism* (Grassmann 1853) and there are many examples, notably images. Color printing reproduces much of our chromatic world with just four inks—cyan, magenta, yellow, and black. Color displays combine red, green, and blue lights. This is shown in Figure 2.5 where the light produced by a display matches the sunlight reflecting from light skin. Color imaging is ubiquitous because our vision is trichromatic.

The example of metamerism shown in Figure 2.5 is defined by Eqs. (2.12)–(2.14):

$$\int_\lambda S_\lambda R_\lambda l_\lambda \, d\lambda = \int_\lambda L_\lambda l_\lambda \, d\lambda \tag{2.12}$$

$$\int_\lambda S_\lambda R_\lambda m_\lambda \, d\lambda = \int_\lambda L_\lambda m_\lambda \, d\lambda \tag{2.13}$$

$$\int_\lambda S_\lambda R_\lambda s_\lambda \, d\lambda = \int_\lambda L_\lambda s_\lambda \, d\lambda \tag{2.14}$$

where S_λ is the spectral power distribution of sunlight, R_λ is the skin's spectral reflectance factor, L_λ is the display's spectral radiance, and l_λ, m_λ, and s_λ are the spectral sensitivities of the L, M, and S cones. Following the integration, the match can be defined by Eq. (2.15)

$$\begin{pmatrix} L \\ M \\ S \end{pmatrix}_{\text{illuminated skin}} = \begin{pmatrix} L \\ M \\ S \end{pmatrix}_{\text{liquid crystal display}} \tag{2.15}$$

Metamerism also occurs in ways that are detrimental to our experience of color. Different materials often require different colorants. If the colorants are not carefully selected, metameric matches can be made in which the materials match only for one set of viewing and illuminating conditions. Imagine an automotive interior in which all of the colored parts match only in the showroom! We consider issues surrounding metamerism throughout this book, including a chapter devoted to this topic, Chapter 8.

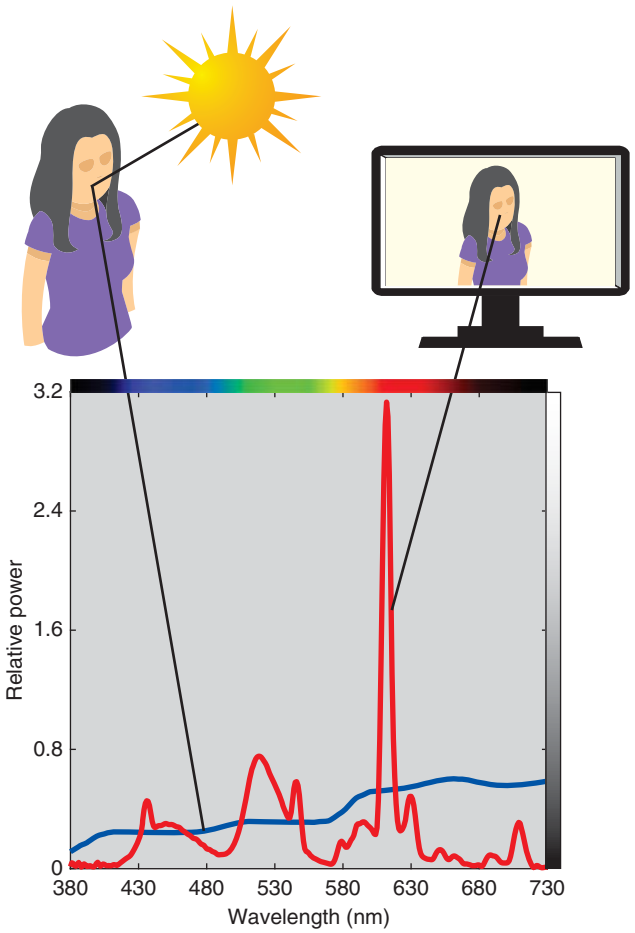

Figure 2.5 The sunlight reflecting from skin (blue line) and the light emitting from a liquid crystal display (LCD) (red line) result in a metameric match.

B. LIGHT AND CHROMATIC ADAPTATION

Going about our daily lives, we encounter a range of illumination including sunrise, a cloudy day, a sunny day, incandescent lighting, fluorescent lighting, LED lighting, and so on. These vary in both intensity and color. Yet, the colors of our clothing and our skin, to name a few, seem constant. *Color constancy* is another fundamental property of human vision. This occurs because we adapt to changes in our environment. Compensating for intensity is known as *light adaptation* and compensating for color is known as *chromatic adaptation*. Physiologically there are changes in pupil diameter, cone sensitivities, and the number of cones whose signals are pooled, all of which increase as intensity decreases.

We adapt fully over a wide range of levels and colors. For example, the paper of this book appears white as lighting conditions vary. von Kries (1902) hypothesized that adaptation is a simple gain adjustment in which our receptors increase or decrease their sensitivities such that "white"

- *Chromatic adaptation*: Changes in the visual system that approximately compensate for changes in the spectral quality of illumination.
- *Light adaptation*: Changes in the visual system that approximately compensate for changes in the intensity of illumination.
- *Color constancy*: General tendency of the color of an object to remain approximately constant when the intensity and color of the illumination are changed.
- *Corresponding colors*: A pair of stimuli that match in color when each stimulus is illuminated with light of a different color.

lighting appears without hue. This is shown mathematically in Eqs. (2.16)–(2.18) for two lighting conditions:

$$\frac{L_1}{L_{n,1}} = \frac{L_2}{L_{n,2}} \tag{2.16}$$

$$\frac{M_1}{M_{n,1}} = \frac{M_2}{M_{n,2}} \tag{2.17}$$

$$\frac{S_1}{S_{n,1}} = \frac{S_2}{S_{n,2}} \tag{2.18}$$

where L_n, M_n, and S_n are the signals of a stimulus that appears white, and subscripts 1 and 2 refer to illuminating conditions 1 and 2.

The von Kries model predicts that neutral colors and specular highlights appear neutral and white under all lighting conditions. Although this occurs for many conditions, there are also many conditions where we are aware of the color of the lighting. An incandescent light bulb of sufficient wattage appears white. As the light is dimmed, it takes on an orange hue. The orange hue will persist no matter how long we look at the light. We are experiencing *incomplete chromatic adaptation*. When objects appear color constant under such conditions, we are *cognitively discounting the color of the illumination*. This is demonstrated in Figure 2.6 where a painting of a bowl of fruit was imaged with white light and bluish light. Although the lighting is colored, observed by looking at the color of the rinds, the fruit is color constant. By using the blue-light-lit lemon in place of the daylight-lit lemon, we see the effect of chromatic adaptation in determining a stimulus's color appearance. The lemon has turned into a lime!

We want to point out that color constancy is only approximate. Very few materials are truly invariant to changes in lighting. We will consider this in more detail in Chapter 8.

(a)

(b)

(c)

Figure 2.6 Jacob van Hulsdonck (Dutch, 1582–1647), *Still Life with Lemons, Oranges and a Pomegranate*, c. 1620–1640. Oil on panel, 41.9 cm × 49.5 cm (16½ in. × 19½ in.). Los Angeles, J. Paul Getty Museum, 86.PB.538. The painting was imaged with (a) white and (b) colored light. When the central lemon from the colored-light image is overlaid on the white-light image (c), it becomes a lime, revealing our strong propensity to see fruit as color constant, even under colored light.
Source: Digital image courtesy of the Getty's Open Content Program.

Chromatic Adaptation and Corresponding Colors

Chromatic adaptation transformations (*CATs*) are often used to predict the *LMS* signals for a different object viewed under a second light such that the two objects will match in their respective lighting conditions. This is defined as a pair of *corresponding colors*. Suppose that there are two lighting conditions, notated by subscripts 1 and 2. An object is illuminated by light 1. The von Kries model can be used to predict the corresponding color when viewed under light 2, shown in Eqs. (2.19)–(2.22)

$$L_2 = L_1 \frac{L_{n,2}}{L_{n,1}} \tag{2.19}$$

$$M_2 = M_1 \frac{M_{n,2}}{M_{n,1}} \tag{2.20}$$

$$S_2 = S_1 \frac{S_{n,2}}{S_{n,1}} \tag{2.21}$$

$$\begin{pmatrix} L_2 \\ M_2 \\ S_2 \end{pmatrix} = \begin{pmatrix} \frac{L_{n,2}}{L_{n,1}} & 0 & 0 \\ 0 & \frac{M_{n,2}}{M_{n,1}} & 0 \\ 0 & 0 & \frac{S_{n,2}}{S_{n,1}} \end{pmatrix} \begin{pmatrix} L_1 \\ M_1 \\ S_1 \end{pmatrix} \tag{2.22}$$

A D factor for *degree of adaptation* has been developed to expand the von Kries model to account for incomplete chromatic adaptation (Fairchild 2013), shown in Eq. (2.23)

$$\begin{pmatrix} L_2 \\ M_2 \\ S_2 \end{pmatrix} = \begin{pmatrix} \frac{DL_{n,2}+(1-D)L_{n,1}}{L_{n,1}} & 0 & 0 \\ 0 & \frac{DM_{n,2}+(1-D)M_{n,1}}{M_{n,1}} & 0 \\ 0 & 0 & \frac{DS_{n,2}+(1-D)S_{n,1}}{S_{n,1}} \end{pmatrix} \begin{pmatrix} L_1 \\ M_1 \\ S_1 \end{pmatrix} \tag{2.23}$$

The corresponding color is calculated for a light that is intermediate between the two lights. The D factor is largely a function of the light's intensity.

As a worked example, a light gray sample has a reflectance factor of 0.7. It is illuminated by incandescent light. Its corresponding color is calculated for daylight with about twice the level of illumination and D factors ranging between 1.0 and 0.0, listed in Table 2.1 and visualized in Figure 2.7. With complete adaptation, $D = 1.0$, the sample appears gray. As adaptation becomes less complete, the gray takes on an orangish appearance. When $D = 0.0$, we are adapted to daylight and looking into a room lit by incandescent lighting; the sample appears orange.

Table 2.1 *LMS* responses for corresponding color calculations using Eq. (2.23) between incandescent light and daylight.

	L	*M*	*S*
Incandescent			
Lighting	11.0	7.6	2.1
Stimulus	7.7	5.3	1.4
Daylight corresponding colors			
Lighting	18.6	15.9	11.6
Stimulus, $D = 1.0$	13.0	11.1	8.1
Stimulus, $D = 0.8$	11.9	10.0	6.8
Stimulus, $D = 0.6$	10.9	8.8	5.5
Stimulus, $D = 0.4$	9.8	7.6	4.1
Stimulus, $D = 0.2$	8.8	6.5	2.8
Stimulus, $D = 0.0$	7.7	5.3	1.4

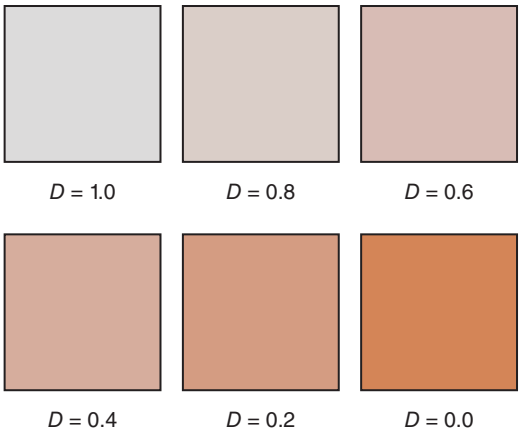

Figure 2.7 Visualization of the corresponding color calculations listed in Table 2.1.

Other changes occur as illumination level is reduced: colored objects become dimmer and less chromatic, discrimination reduces, and blurriness increases. This is simulated (Pattanaik et al. 1998) in Figure 2.8.

C. COMPRESSION

We might perform an experiment where an observer is shown a series of neutral colors one at a time and asked to assign a lightness value where 0 is black and 100 is white. This type of experiment is known as a *psychophysical experiment*, that is, quantifying the psychological response to a physical stimulus (Fechner 1860). The resulting *psychometric function* is plotted in Figure 2.9: For dark colors, lightness has an increasing rate of change; for light colors, lightness has a decreasing rate of change. This is a *compressive response* and many of our senses share this nonlinear relationship (Stevens 1957; Gescheider 1997). The function has been modeled both logarithmically (Weber 1834; Fechner 1860) and exponentially (Plateau 1872). The exponential model is shown in Eq. (2.24):

$$\Psi = kI^{1/\gamma} \tag{2.24}$$

where Ψ is the psychometric response, k is a normalizing constant to account for differences in units, I is the stimulus scaled between zero and unity, and $1/\gamma$ is an exponent. When scaling lightness, γ is between two and three.

This nonlinear relationship can also occur when mixing colored materials. Red and black artist acrylic paints were intermixed in even and cube-root increments by weight, shown in Figure 2.10. The cube-root increments produced a more visually uniform scale.

D. OPPONENCY

It seems logical that our trichromatic signals, following chromatic adaptation and compression, finally send their individual signals to our brain. A red color has a large *L* and small *M* and *S*; a blue color has a large *S* and small *M* and *L*; and so on. The signals are all positive, as is typical for sensors. But there are many visual phenomena that cannot be explained using trichromatic theory. For one thing, a color cannot appear simultaneously red and green or yellow and blue; that is, there is no such color as reddish green or bluish yellow. For another, people with color-vision deficiencies often confuse reds and greens.

Such observations led to a different theory of color vision, first postulated by Hering (1878). Rather than cone signals that are all positive, the three signals sent to the brain are positive and negative: white opposed by black, red opposed by green, and yellow opposed by blue. The difficulty in accepting opponency over trichromacy is envisioning a sensor that could produce both positive and negative signals. Several vision scientists of the late nineteenth and early twentieth century proposed a two-stage theory of color vision, the first trichromatic and the second opponent (von Kries 1882; Schrödinger 1920; Müller 1930; Judd 1951), which was verified experimentally during the 1950s (Svaetichin 1956; Hurvich and Jameson 1957; De Valois et al. 1958). These experiments, among others, revealed that visual signals are modulated temporally. A neutral color produces a nominal pulse rate. A red stimulus will increase the rate, while a green stimulus will decrease it; thus, relative to the nominal rate, signals are positive and negative. Although two-stage theory is

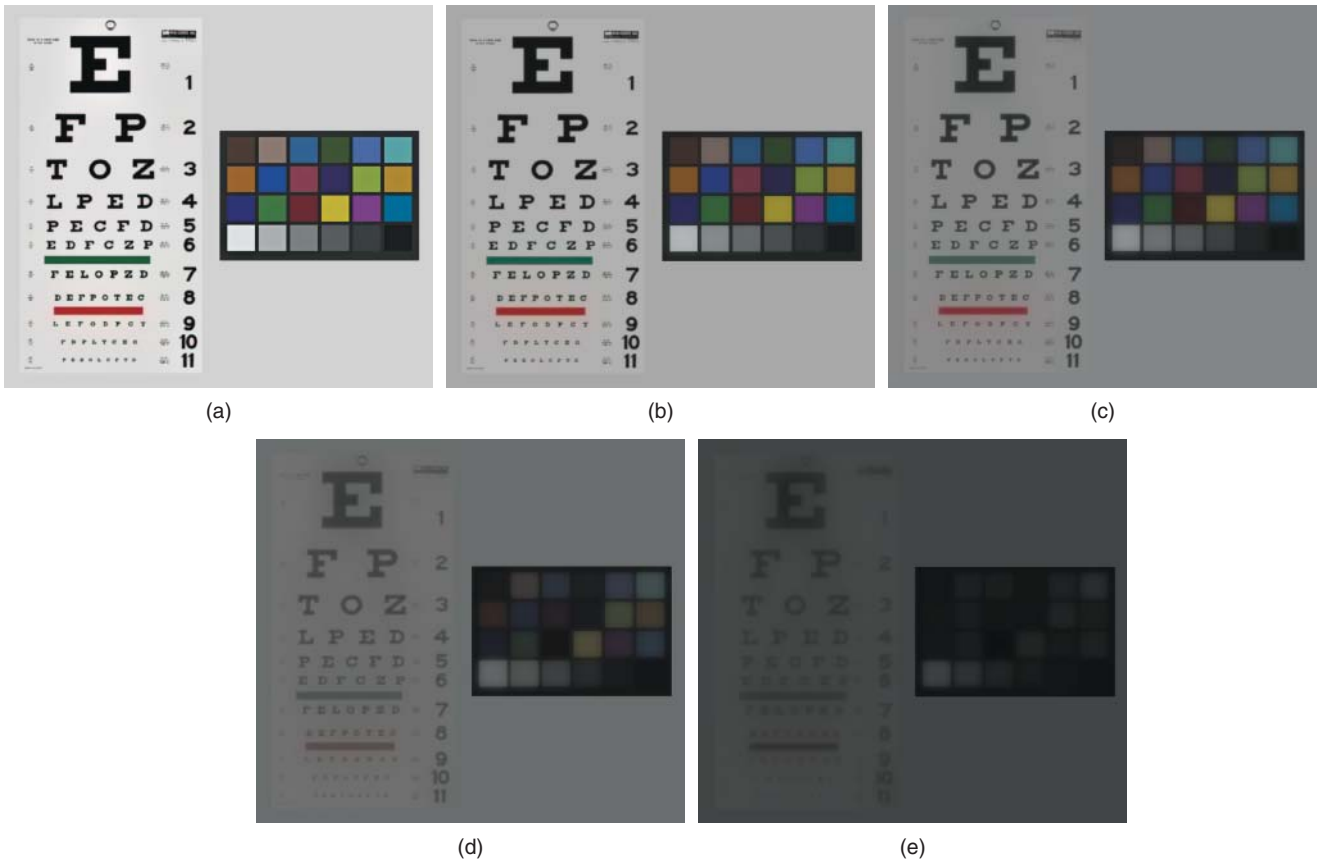

Figure 2.8 Simulation of the effect of level of illumination on visual perception: (a) 1000, (b) 100, (c) 10, (d) 1, and (e) 0.1 cd/m^2.
Source: From Pattanaik et al. 1998.

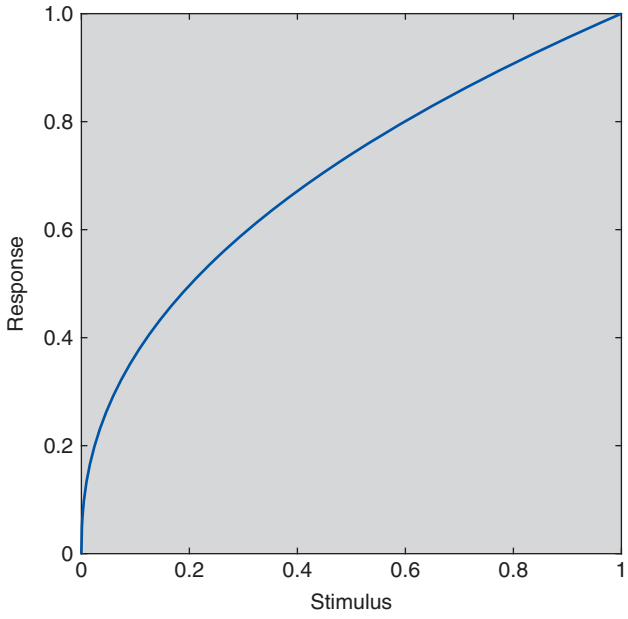

Figure 2.9 Psychometric function based on Eq. (2.24) where $k = 1$ and $\gamma = 2.3$.

a simplification, its use is reasonable as it explains many visual phenomena, and it serves as the basis for numerical color specification. See Shevell and Martin (2017) for more details.

Opponent signals result from the interaction of groups of cones that combine to form *receptive fields*. L and M cones combine, forming the white opposed by black signal. The red opposed by green channel is mainly a result of the M cones being subtracted from the L cones. The yellow opposed by blue channel results mainly from the addition of L and M and subtraction of S cone signals. These simple additions and subtractions are shown—in concept only—in Eq. (2.25)

$$\begin{pmatrix} \text{white} \Longleftrightarrow \text{black} \\ \text{red} \Longleftrightarrow \text{green} \\ \text{yellow} \Longleftrightarrow \text{blue} \end{pmatrix} = \underbrace{\begin{pmatrix} 0.5 & 0.5 & 0 \\ 1 & -1 & 0 \\ 0.5 & 0.5 & -1 \end{pmatrix}}_{\text{conceptual opponency}} \begin{pmatrix} L \\ M \\ S \end{pmatrix} \tag{2.25}$$

However, this does not result in the red opposed by green channel having a positive red response in short wavelengths, leading to these wavelengths appearing violet. A matrix based on a plausible set of opponent primaries

Figure 2.10 Mixtures of red and black paints in either even (top) or cube-root (bottom) increments by weight. The uneven increments result in a more uniform perceptual scale.

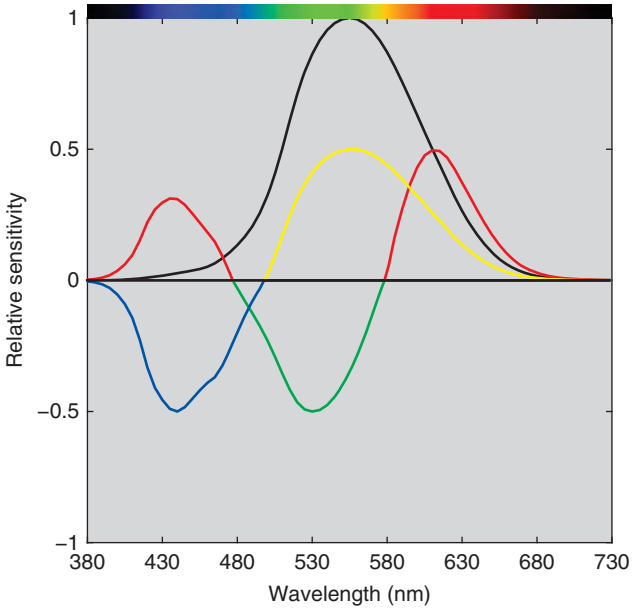

Figure 2.11 Relative spectral sensitivities of the human visual system's opponent channels.

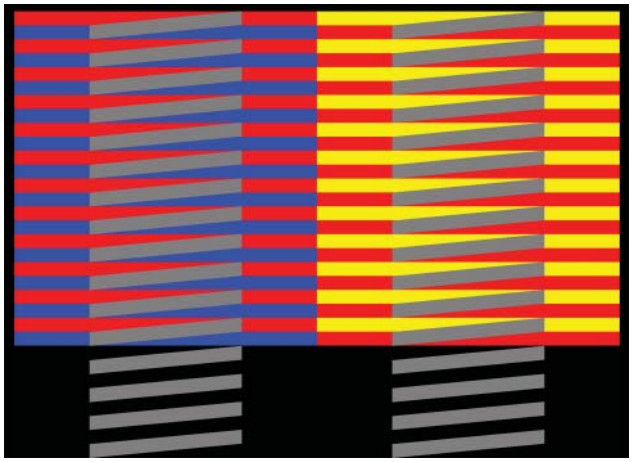

Figure 2.12 Based on "Just GREY" example.
Source: From Gianni A. Sarcone, 1997 – present, www.giannisarcone.com, shown on the Archimedes Lab website: http://www.archimedes-lab.org/color_optical_illusions.html.

(Hurvich 1981) is shown in Eq. (2.26) where the LMS spectra are normalized at peak height, as plotted in Figure 2.3

$$\begin{pmatrix} \text{white} \Longleftrightarrow \text{black} \\ \text{red} \Longleftrightarrow \text{green} \\ \text{yellow} \Longleftrightarrow \text{blue} \end{pmatrix} = \begin{pmatrix} 0.64 & 1.12 & 0.35 \\ 0.39 & -1.50 & 0.15 \\ -0.01 & 0.34 & -0.53 \end{pmatrix}_{\text{opponency}} \begin{pmatrix} L \\ M \\ S \end{pmatrix} \tag{2.26}$$

Transforming from trichromatic to opponent signals and rescaling peak heights results in the spectra shown in Figure 2.11. There are a number of opponent-channel color spaces that have been derived to have good performance when used for industrial applications such as setting tolerances; in these cases, the matrix elements are optimized based on visual color-discrimination data (Ebner and Fairchild 1998; Berns 2008a).

There is very strong evidence for spatial interactions between cone receptors. During the ninteenth century, Chevreul (1854) made systematic studies of how thread changed its color depending on the colors of neighboring threads in the manufacture of tapestries. These studies led to his law of simultaneous contrast and his seminal book, *De la loi du contraste simultané des couleurs et de l'assortiment des objets colorés* (The Principles of Harmony and Contrast of Colors). Another groundbreaking book demonstrating simultaneous contrast is Albers's *Interaction of Color* (1963); based on student work, the effects of surround color are exquisitely explored.

An interesting example demonstrating spatial interactions is shown in Figure 2.12. The gray stripes are all the same physical color, as are the red stripes, but because they are surrounded by different colors, they do not appear to be the same. The gray stripes appear shaded; the hue of the red stripes changes dramatically depending on the blue or yellow stripes surrounding them. Depending on the size of the image, the effects are either complementary (meaning that, for instance, the red stripes appear more yellowish when surrounded by the blue stripes viewed normally) or additive (the red stripes appear more bluish when surrounded by the blue stripes either viewed from a distance or when the size is reduced). These effects are often referred to as *simultaneous contrast* and *assimilation*, respectively.

The opponent signals leave the retina via the optic nerve and eventually arrive at the back of the brain. The brain signals are interpreted through a cognitive process that results in *color*. We again show that color results from the interaction of a light source, an object, and our visual system in Figure 2.13. The line joining the light source and the observer represents chromatic adaptation.

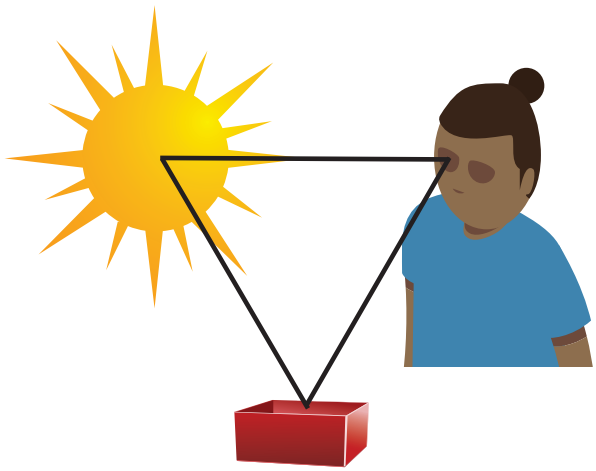

Figure 2.13 "Color" results from the interaction of a light source, an object, and the eye and brain, or visual system. The connection between the light source and eye represents chromatic adaptation.

A General Color Vision Model

Our visual system has been modeled using Eqs. (2.1)–(2.26) defining four processes: trichromacy, chromatic adaptation, compression, and opponency. These steps can be generalized

$$\begin{pmatrix} L \\ M \\ S \end{pmatrix}_{\text{reference illuminant}} = \mathbf{M}_{\text{von Kries } D \text{ factor}}\,\mathbf{TSR} \qquad (2.27)$$

$$\begin{pmatrix} \text{white} \Longleftrightarrow \text{black} \\ \text{red} \Longleftrightarrow \text{green} \\ \text{yellow} \Longleftrightarrow \text{blue} \end{pmatrix} = \mathbf{M}_{\text{opponency}} \begin{pmatrix} L^{1/\gamma} \\ M^{1/\gamma} \\ S^{1/\gamma} \end{pmatrix}_{\text{reference illuminant}} \qquad (2.28)$$

Such spaces have a reference illuminant, often daylight or the equal-energy spectrum—a curve shape that is spectrally flat.

E. SPATIAL VISION

People with trichromatic vision have three classes of cone receptors, as we have described—L, M, and S. Given the similarity among us in how we see fine detail, that is our visual *acuity*, it was assumed that we have similar retinal mosaics and similar numbers of each cone type. (The third edition of this book defined the ratio of L to M to S cones as 6:3:1.) Research during the beginning of the twenty-first century revealed that the ratio of L and M cones varies dramatically from person to person, where some have many more cones of one type than the other (Roorda et al. 2001; Hofer et al. 2005). This is yet further evidence of opponent vision and the concept of receptive fields. The number of S cones is about 10% of the total number of L and M cones, consistent with scattering of short wavelength light caused by limitations in the optical quality of our cornea, lens, and aqueous and vitreous humors. Because short wavelength light is quite blurry by the time it reaches the retina, having increased numbers of S cones is unnecessary.

Each opponent channel's receptive field is formed based on different arithmetic operations, and therefore, each has a different acuity, that is, different *spatial resolution*. Our white opposed by black channel has the highest acuity because the L and M cones add together, that is, the receptive fields cover a small area. Our red opposed by green channel has reduced acuity because a greater area of the retina is used for subtraction. Our yellow opposed by blue channel has low acuity because of the additional limiting factor of few S cones.

We have quantified our receptors' color response by plotting sensitivity data as a function of wavelength. We quantify spatial response by plotting sensitivity data as a function of *spatial frequency*. Spatial frequency is visualized by producing *sinusoidal gratings* varying between two colors whose widths become narrower from left to right, shown in the top panels of Figure 2.14 for white and black and for cyan and magenta colors of similar lightness. The number of stripes over a defined distance is known as *spatial frequency*. The wide stripes have low spatial frequency, while the narrow stripes have high spatial frequency. Moving from bottom to top, each of the two colors is intermixed with the average of the two colors. Thus, the difference between the two colors decreases from bottom to top. This difference is defined as *contrast*, that is, contrast reduces from bottom to top. Looking at the top panels, our ability to discern the stripes with changes in both spatial frequency and contrast is different when comparing the achromatic and chromatic gratings. It is possible to trace a curve that envelops the stripes, producing a *contrast sensitivity function*, or *csf*. In general, achromatic functions are *band-pass* in nature where response has a maximum in the middle spatial frequencies and drops off at shorter and longer spatial frequencies; chromatic functions are *short-pass* in nature where short and middle spatial frequencies are constant and response drops off at longer spatial frequencies (Mullen 1985). Typical csfs for our three opponent channels are plotted in Figure 2.15.

Spatial filtering was performed on the two gratings, also shown in Figure 2.14, in order to clarify differences between

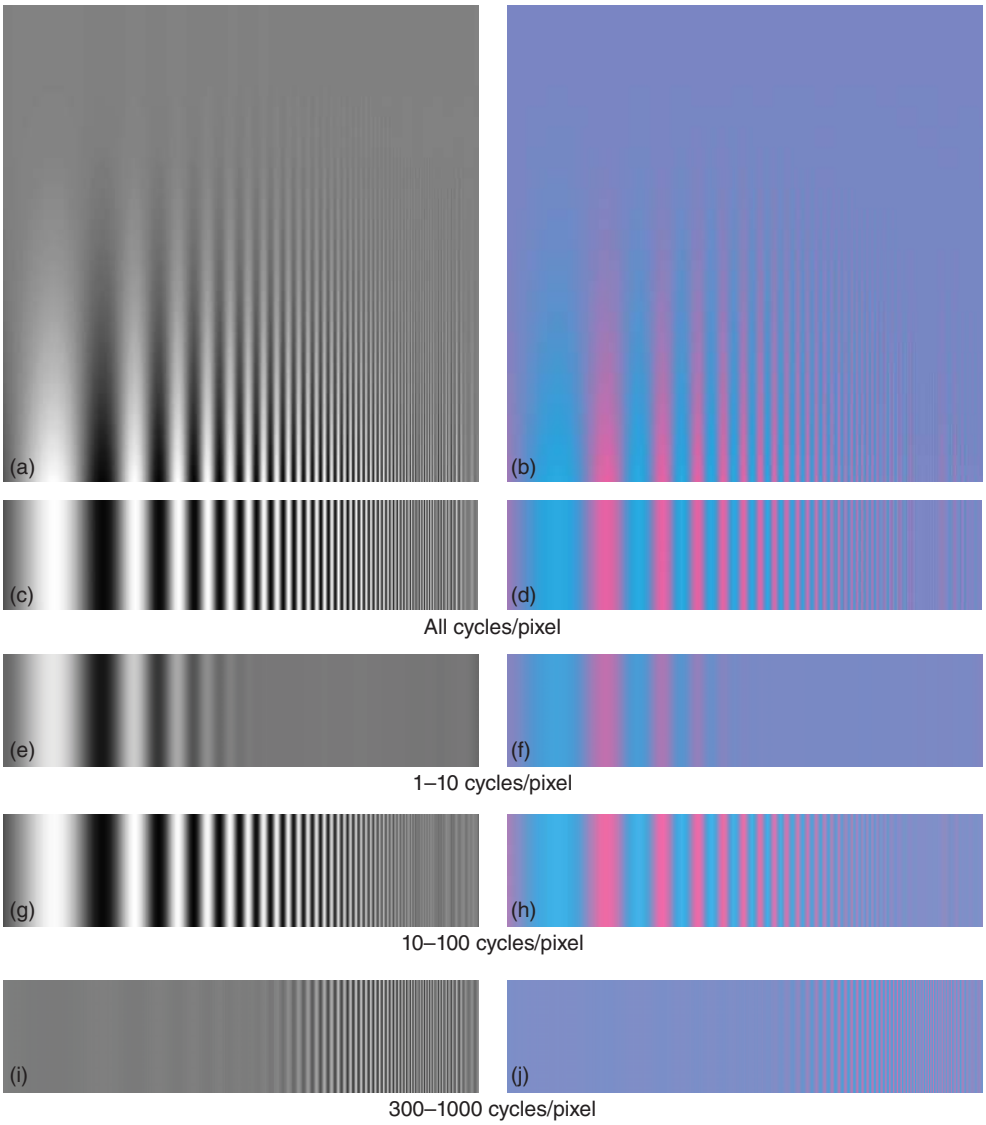

Figure 2.14 (a) Achromatic and (b) chromatic sinusoidal gratings where spatial frequency increases from left to right and contrast reduces from bottom to top. (c and d) The gratings at maximum contrast are divided into (e) and (f) low (1–10 cycles/pixel), (g) and (h) medium (10–100 cycles/pixel), and (i) and (j) high (300–1000 cycles/pixel) spatial frequencies.

low, medium, and high spatial frequencies. The same spatial filters were applied to a painting by Vincent van Gogh, shown in Figure 2.16. The low spatial frequency image is very blurry, revealing the average colors without any detail. The medium spatial frequency image has much more detail, but appears a bit blurry. The high spatial frequency image contains only detail. The greenish color is the average color of the entire image.

When defining spatial properties of a visual system, field of view is used rather than physical length. An object seen up close extends across a larger field of view than the same object viewed from a distance. Moving away from the object increases its spatial frequency. Objects appearing sharp or blurry give us clues to distance. A portrait by Manet, Figure 2.17, was segmented into foreground (Jeanne) and background, followed by blurring the background using a low-pass spatial filter, known as bokeh. The resulting effect gives the impression that Jeanne is separated in space from the background, increasing the three-dimensional quality of the image.

The differences in spatial resolution among the three opponent channels have been used to commercial advantage in broadcast television and digital imaging. Television signals are encoded for transmission using signals that are

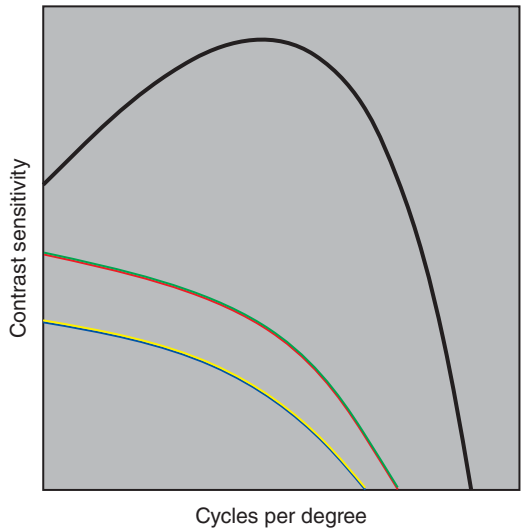

Figure 2.15 Plot of typical contrast sensitivity functions of our white opposed by black (black line), red opposed by green (red and green lines), and yellow opposed by blue (yellow and blue lines) channels.

similar to those of the visual system's opponent channels. The spatial resolutions of the color signals are reduced before transmission, yielding a great savings in signal content. Because of the limitations of the visual system's spatial (and temporal) resolution, we do not notice the loss of resolution when we watch television. This technique is also used when digital color images are compressed using JPEG or similar image-compression schemes. Essentially, the color image is transformed into two opponent chromatic channels and one achromatic channel. The chromatic channels are reduced in spatial resolution and then recombined with the full-resolution black-white image. This is shown in Figure 2.18 using the Manet portrait and blurring each opponent channel the same amount. The image degradation is pronounced when the white opposed by black image is blurred but hardly seen when the chromatic channels are blurred.

In summary, the visual system images the world onto the retina. The retina is composed of rods and cones, arranged in a mosaic. In very low light, the rods send signals to the brain resulting in monochrome perception. With an increase

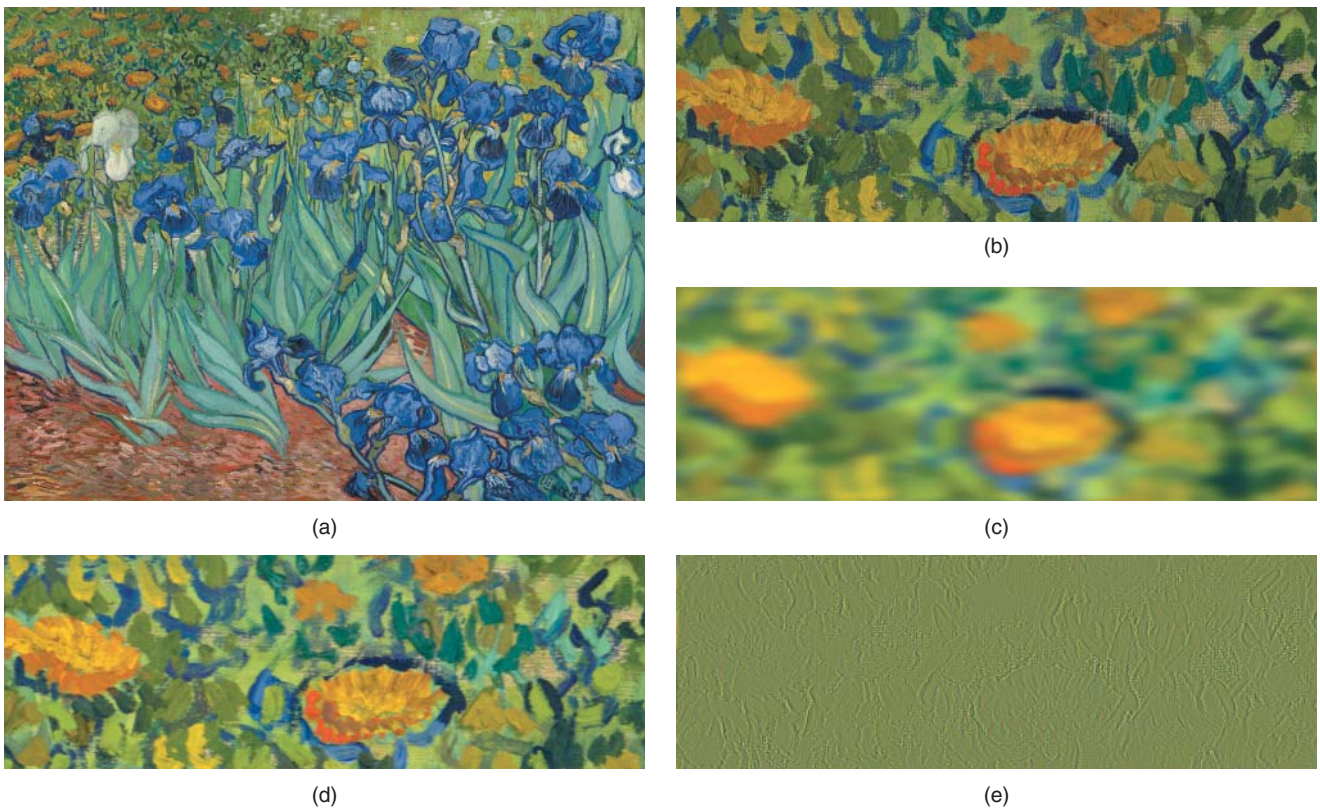

Figure 2.16 (a) Vincent van Gogh (Dutch, 1853–1890), *Irises*, 1889. Oil on canvas, 71.1 cm × 93 cm (28 in. × 36⅝ in.). Los Angeles, J. Paul Getty Museum, 90.PA.20, (b) detail, divided into (c) low (1–10 cycles/pixel), (d) medium (10–100 cycles/pixel), and (e) high (300–1000 cycles/pixel) spatial frequencies.
Source: (a) Digital image courtesy of the Getty's Open Content Program.

(a) (b)

Figure 2.17 (a) Édouard Manet (French, 1832–1883), *Le Printemps (Jeanne Demarsy)*, 1881. Oil on canvas, 74 cm × 51.4 cm (29⅛ in. × 20¼ in.). (b) The background has been blurred, resulting in a three-dimensional quality.
Source: Digital image courtesy of the Getty's Open Content Program.

of light, the cones start responding. There are three cone types, L, M, and S, each with unique spectral and spatial properties. The cones combine, forming opponent signals: white opposed by black, red opposed by green, and yellow opposed by blue. The three opponent channels have different spatial resolution. By matching cone responses (or the equivalent opponent responses), it is possible for stimuli to match that do not have identical physical properties. These metameric stimuli are the basis for color reproduction and the matching of materials using very different colorants.

F. OBSERVER VARIABILITY

Unsurprisingly, there is a range of color vision in the human race. A large source of variability is caused by the "yellowing" of the lens from exposure to ultraviolet (UV) radiation, eventually leading to cataracts (Young 1991). As exposure to UV increases, overall transmittance decreases, scattering increases, and transmittance reduces in short wavelengths (Marmor 2006). Although our visual system will adapt to the yellow light to a large extent, the significant amount of blurring makes reading and other visual tasks difficult, if not impossible; that is, acuity becomes quite poor. This is simulated for a painted color target in Figure 2.19. Because of cataracts, the canvas texture cannot be seen, the text is nearly unreadable, there is a yellow caste and a loss of color intensity, and differences in hue are less discernible.

There are additional sources of observer variability. The chemical compounds that form photopigments vary among the population. Each retinal mosaic is unique. The physical shapes of the receptors vary within the retina. The amount of macular pigment varies from person to person and throughout the retina. Thus, color vision varies significantly among observers with *normal color vision*. Asano, Fairchild, and Blondé (2016) have summarized the many experiments quantifying observer variability.

We can think of changes in the amount of macular pigment and the yellowing of the lens as a pair of colored filters in front of our receptors, as shown in

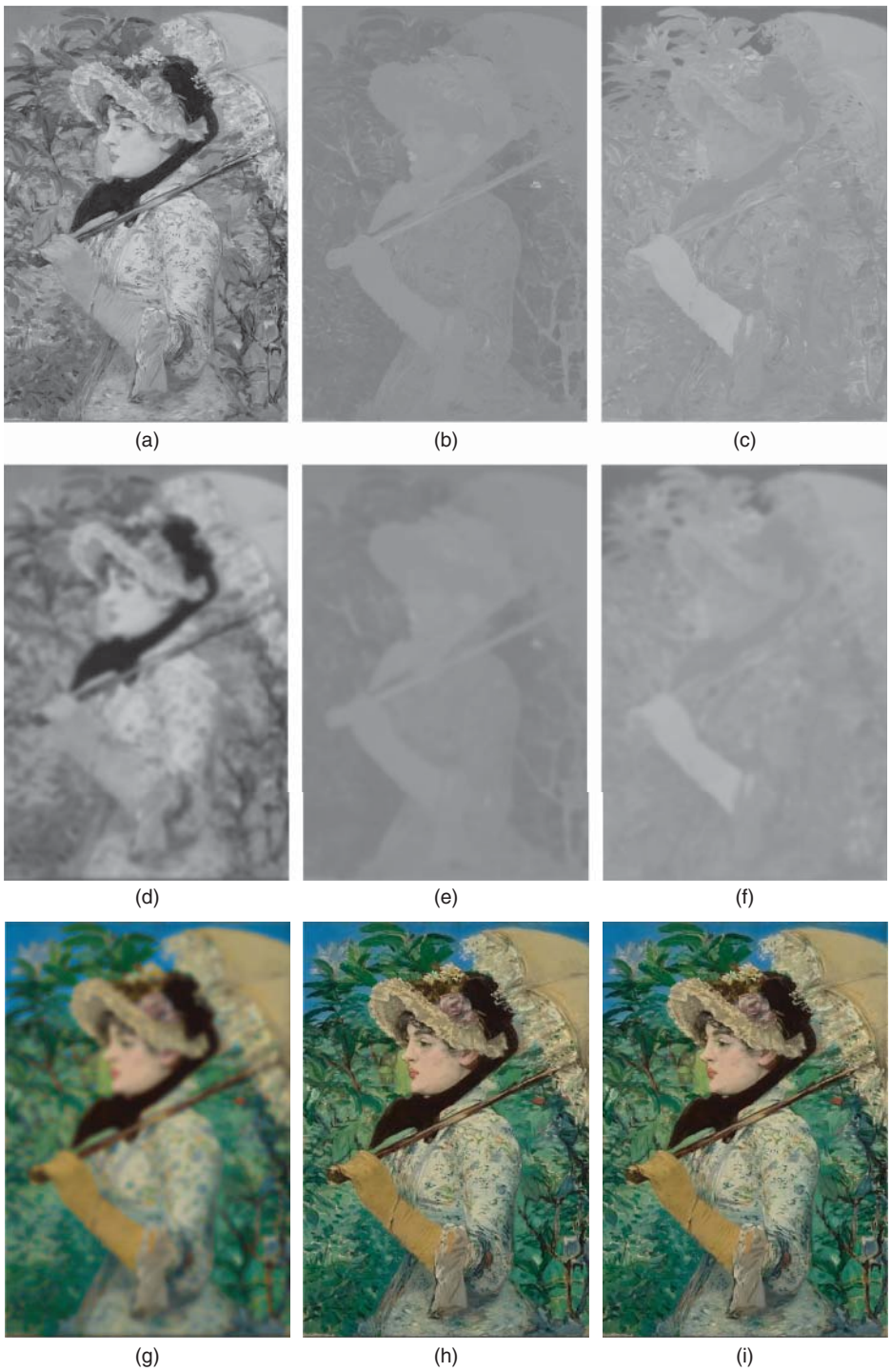

Figure 2.18 *Le Printemps (Jeanne Demarsy)*: (a) white opposed by black image, (b) red opposed by green image mapped to gray scale, (c) yellow opposed by blue image mapped to gray scale, (d) white opposed by black image blurred, (e) red opposed by green image blurred, (f) yellow opposed by blue image blurred, (g) recombined image using blurred white opposed by black channel, (h) recombined image using blurred red opposed by green channel, and (i) recombined image using blurred yellow opposed by blue channel. Although the amount of blurring is the same in each altered image, we notice the reduced sharpness only when the black-white channel is blurred. This demonstrates that we have reduced spatial resolution—that is, acuity—in our chromatic visual channels in comparison to our white opposed by black channel.

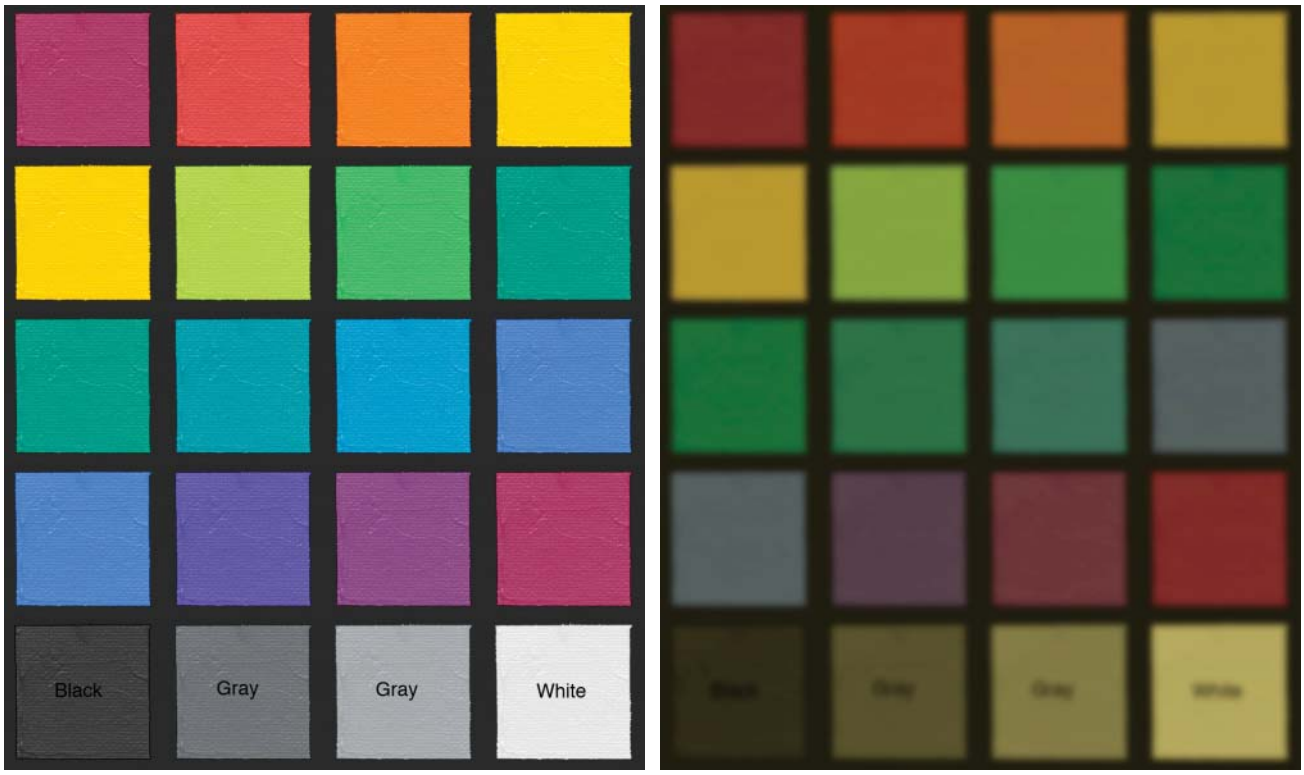

Figure 2.19 Simulation of how (a) a painted target would appear to (b) someone requiring cataract surgery.

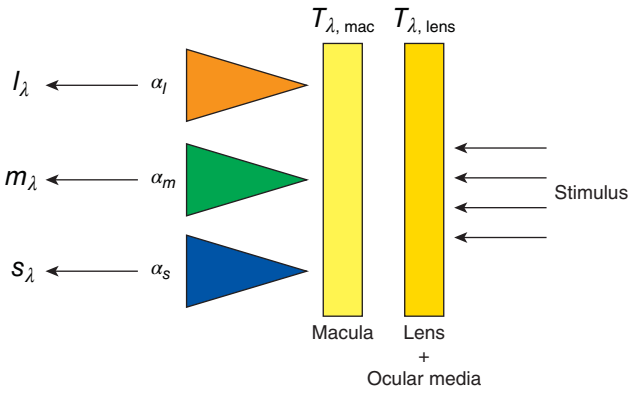

Figure 2.20 Schematic of the eye. Cone fundamentals depend on the spectral sensitivities of the L, M, and S photopigments, the transmittance of the macula, and the transmittance of the lens and other ocular media.

Figure 2.20. The thickness of each filter modulates the incoming light, leading to differences in cone fundamental spectral sensitivities, shown mathematically in Eqs. (2.29)–(2.31):

$$l_\lambda = \alpha_{\lambda,l} \cdot T_{\lambda,\text{macula}} \cdot T_{\lambda,\text{lens}} \tag{2.29}$$

$$m_\lambda = \alpha_{\lambda,m} \cdot T_{\lambda,\text{macula}} \cdot T_{\lambda,\text{lens}} \tag{2.30}$$

$$s_\lambda = \alpha_{\lambda,s} \cdot T_{\lambda,\text{macula}} \cdot T_{\lambda,\text{lens}} \tag{2.31}$$

where l_λ, m_λ, and s_λ are cone fundamentals, $\alpha_{\lambda,\,l}$, $\alpha_{\lambda,\,m}$, and $\alpha_{\lambda,\,s}$ are photopigment spectral sensitivities; $T_{\lambda,\text{ macula}}$ is the transmittance of the macular pigment; and $T_{\lambda,\text{ lens}}$ is the transmittance of the lens and other ocular media, all as a function of wavelength, λ. Each color-normal observer would have a specific set of sensitivities and transmittances.

In 2006, the CIE published a technical report where cone fundamentals for a population average can be calculated as a function of age ranging between 20 and 80 years old and of field of view ranging between 1° and 10° (CIE 2006a). The model, with simplified nomenclature, is shown in Eqs. (2.32)–(2.34)

$$\bar{l}_{\lambda,f,a} = \alpha_{\lambda,l,f} \cdot 10^{[-D_{\text{max,macula},f} \cdot D_{\lambda,\text{macula,relative}} - D_{\lambda,\text{lens},a}]} \tag{2.32}$$

$$\overline{m}_{\lambda,f,a} = \alpha_{\lambda,m,f} \cdot 10^{[-D_{\text{max,macula},f} \cdot D_{\lambda,\text{macula,relative}} - D_{\lambda,\text{lens},a}]} \tag{2.33}$$

$$\bar{s}_{\lambda,f,a} = \alpha_{\lambda,s,f} \cdot 10^{[-D_{\text{max,macula},f} \cdot D_{\lambda,\text{macula,relative}} - D_{\lambda,\text{lens},a}]} \tag{2.34}$$

Variables with λ subscripts are a function of wavelength; variables with f subscripts are a function of field of view;

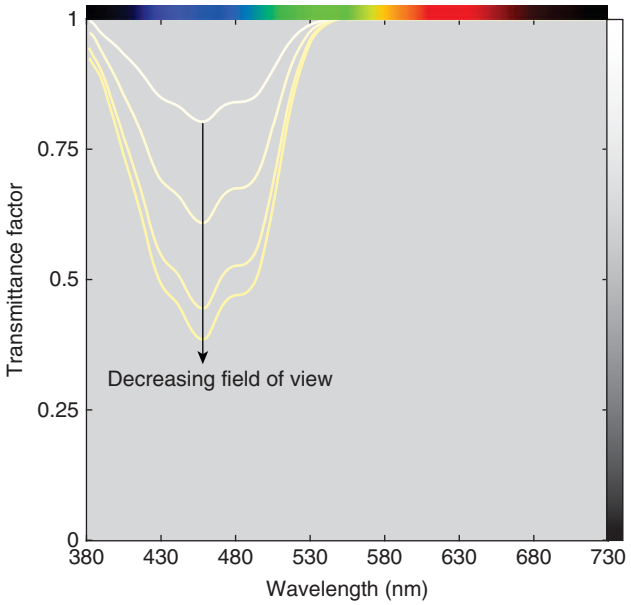

Figure 2.21 Changes in spectral transmittance of macular pigment as a function of field of view.

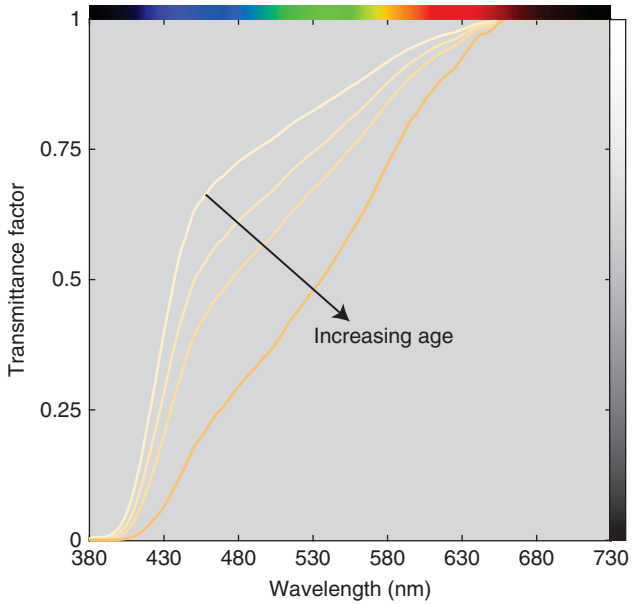

Figure 2.22 Changes in spectral transmittance of the lens and other ocular media as a function of age.

variables with a subscripts are a function of age. D stands for optical density, calculated as shown in Eqs. (2.35) and (2.36)

$$D_\lambda = -\log(T_\lambda) \tag{2.35}$$

$$T_\lambda = 10^{-D_\lambda} \tag{2.36}$$

The specific model parameters and optical densities are based on published experimental data. Changes in the macular pigment transmittance as a function of field of view are plotted in Figure 2.21. Light is absorbed only in the blue region of the visible spectrum. The shapes are very similar and when plotted in optical density, they scale to a single spectrum. Accordingly, the spectrum is defined as a relative spectrum, $D_{\lambda,\,\text{macula, relative}}$, and scaled as a function of field size, $D_{\text{max, macula},f}$. Changes in the lens and other ocular media as a function of aging are plotted in Figure 2.22. With aging, less short-wavelength light is transmitted. Light is absorbed (and scattered) throughout a large range of the visible spectrum until 660 nm, revealing why changes in lens transmittance are a large factor in observer variability. The curve shapes are quite different from one another and cannot be scaled from a single relative spectrum as done for the macular pigment. (Two different optical-density spectra are required to model changes in the lens transmittance.) Changes in photopigment spectral sensitivity are plotted in Figure 2.23. The changes are very small and are observed only for the L cone photopigments.

The CIE 2006 model was enumerated for changes in age from 21 through 80 and in field size from 1° through 10°. The resulting 600 cone fundamentals are plotted in

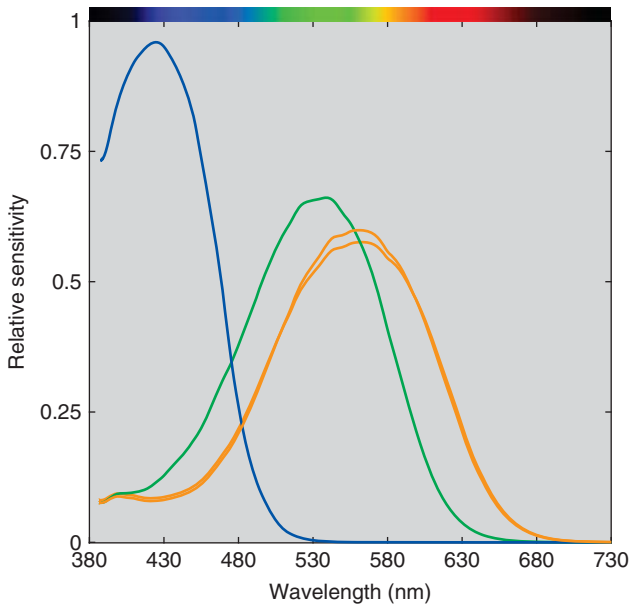

Figure 2.23 Changes in spectral sensitivity of the photopigments, normalized to equal area, as a function of field of view. (The published data range from 390 to 780 nm.)

Figure 2.24. The differences in macula and lens transmittances lead to a range of fundamentals for all of the three cone types.

The consequence of having a range of cone fundamentals depends on the particular stimulus. This is demonstrated for the metameric pair plotted in Figure 2.5 along with a third stimulus, generated by a laser projector. All three

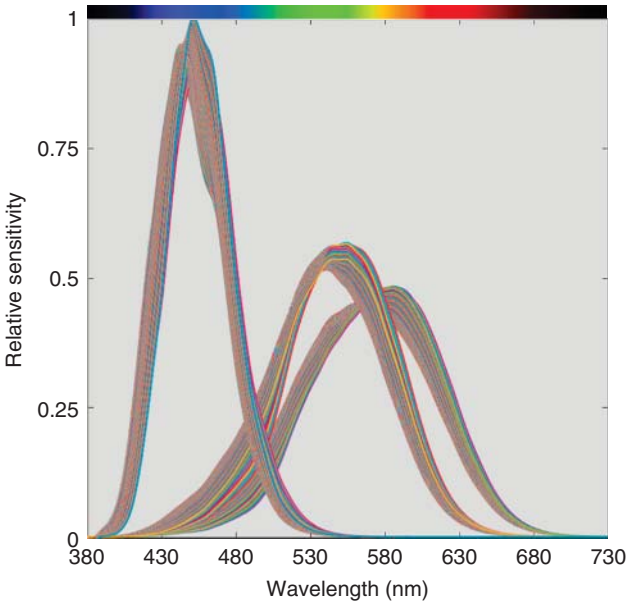

Figure 2.24 L, M, and S cone fundamentals normalized to equal area based on enumerating the CIE 2006 model for changes in age 21–80 and in field size 1°–10°. Color coding is arbitrary.

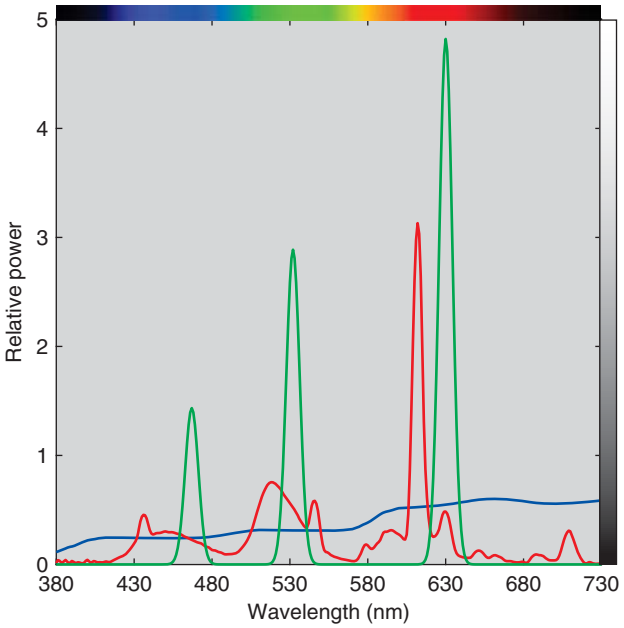

Figure 2.25 Three metameric stimuli: light skin illuminated by sunlight (blue line), an LCD (red line), and a laser display (green line).

stimuli are plotted in Figure 2.25. Sunlight-illuminated light skin has a smoothly varying spectrum. The liquid crystal display (LCD) is jagged. The laser projector has a spectrum with three spikes. The *LMS* responses for the 600 cone fundamentals were calculated for each stimulus using Eqs. (2.4)–(2.6). The average cone fundamentals were calculated and used to derive a transformation to *RGB* display values. (The transformation mathematics are described in detail in Chapter 4.) Using this transformation, all the *LMS* responses can be visualized as an image, shown in Figure 2.26. For both sunlight-illuminated light skin and the LCD, the range of colors is small. For the laser projector there is a much bigger range of colors. A stimulus seen as tan by one observer could be seen as green by another observer. Fairchild and Wyble (2007) have published similar results.

The CIE 2006 model predicts average responses for a specific age and field of view. The CIE model has been extended to account for individual differences (Asano, Fairchild, and Blondé 2016; Fairchild and Heckaman 2016). In particular, these models include changes in the peak location of the photoreceptor spectral sensitivities. The Asano model has 10 parameters, 2 of which (age and field size) are the CIE model parameters plus deviation from the average optical density of the lens and other ocular media, deviation from the average optical density of macular pigment, deviations from the maximum optical density of the L, M, and S photopigments, and deviations from the average wavelength of maximum optical density of

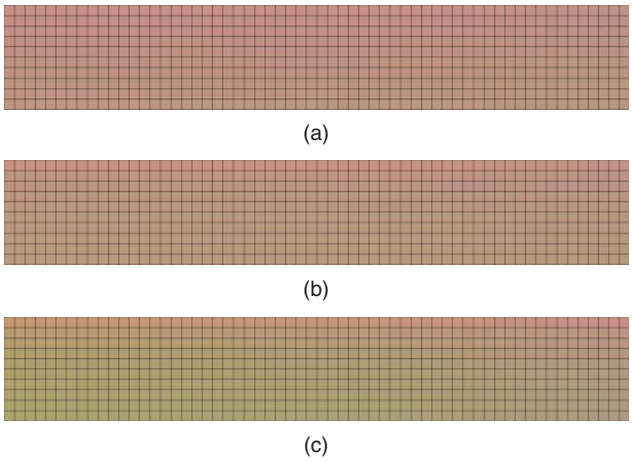

Figure 2.26 Rendered colors for (a) light skin illuminated by sunlight, (b) an LCD, and (c) a laser display for the 600 cone fundamentals calculated using the CIE 2006 model. In each row, field size increases from top to bottom while in each column age increases from left to right.

the L, M, and S photopigments. Another set of 600 cone fundamentals was generated. There were 60 fundamentals calculated for each of the 10 fields of view. The remaining nine physiological parameters were selected randomly. Age was constrained to match the 2010 United States consensus data and the age range limited from 21 through 80 years old. The cone fundamentals are plotted in Figure 2.27. As expected, there is much more variability than with the cone

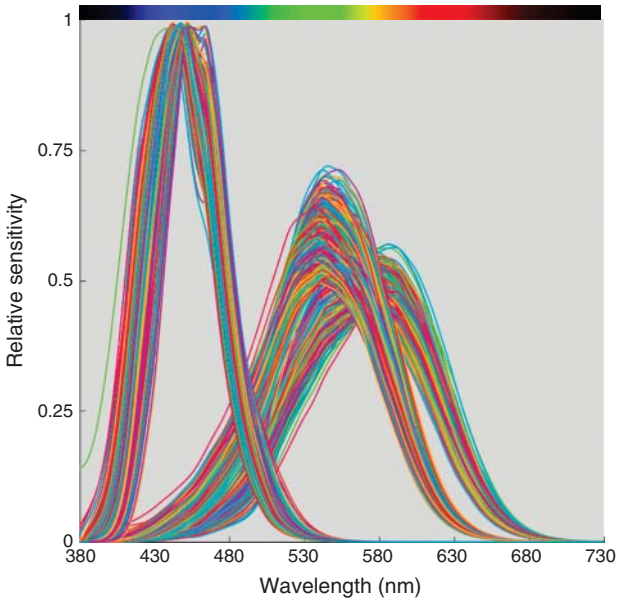

Figure 2.27 L, M, and S cone fundamentals normalized to equal area based on enumerating the Asano model for changes in age 20–80 and in field size 1°–10°. Color coding is arbitrary.

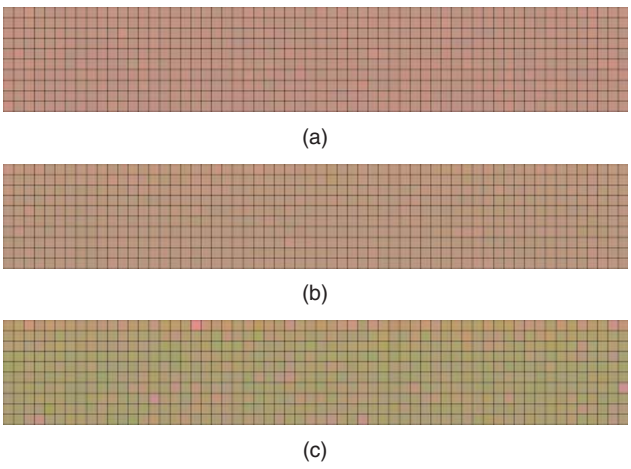

Figure 2.28 Rendered colors for (a) light skin illuminated by sunlight, (b) an LCD, and (c) a laser display for the 600 cone fundamentals calculated using the Asano, Fairchild, and Blondé model. In each row, field size increases from top to bottom.

fundamentals plotted in Figure 2.24 for the CIE model. The image renderings for these cone fundamentals are plotted in Figure 2.28. There is a corresponding increase in the range of colors. In the case of the laser projector, color varied from a vivid pink to green. Asano et al. (2014) and Fairchild and Heckaman (2016) have performed similar calculations and visualizations.

When the wavelength shifts are large, people are considered to have anomalous trichromatism, known as protanomaly and deuteranomaly for anomalies in the L and M cones, respectively. One percent and 5% of males have protanomaly and deuteranomaly, respectively. Because of the specific underlying genetic defects, predominantly males are affected. These people have color vision, but their ability to discriminate differences in hue for red and green colors is reduced. In others, one cone type is absent, resulting in dichromatic vision. People missing the L or M cones have protanopia and deuteranopia, respectively, each affecting one percent of males. Colloquially, this is "red-green color blindness." Protanopia and deuteranopia are simulated (Brettel, Viénot, and Mollon 1997) for the painted color target in Figure 2.29. Having low functionality or missing S cones is extremely rare, affecting males and females equally, and is known as tritanomaly and tritanopia, respectively. This is also simulated in Figure 2.29.

The most common screening test for color vision deficiencies was developed by Ishihara (1962) where observers identify a number or a pattern within a random dot pattern. An example is shown in Figure 2.30. The test is available in both printed form and online. Devices with greater precision include the Farnsworth–Munsell 100 Hue Test, shown in Figure 2.31, and the Nagel anomaloscope. Obviously, anyone involved in visual color assessments should have their color vision tested (Committee on Vision, N. R. C. 1981; Birch 1993; ASTM 2016a).

The most important consequence of color vision variability, both color normal and color defective, is that metameric matches often mismatch when viewed by a different observer or in a different spatial location within the retina. The degree of mismatch can be severe. For this reason, much of color technology is based on using observers with average color vision properties in which light is imaged on a particular location of the retina. These observers are known as *standard observers*. Furthermore, because of color vision variability, successful color technologists work very hard to produce color matches that are not metameric. We will have much more to say about both standard observers and producing nonmetameric matches.

G. SUMMARY

Color perception is complex. In the simplest case, we think of color perception as the result of interaction between a light source, object, and observer. We have shown how various aspects of the source (e.g. spectral properties and the intensity of light), object (e.g. size and texture), observer (e.g. spectral sensitivities, lens properties, macular pigment,

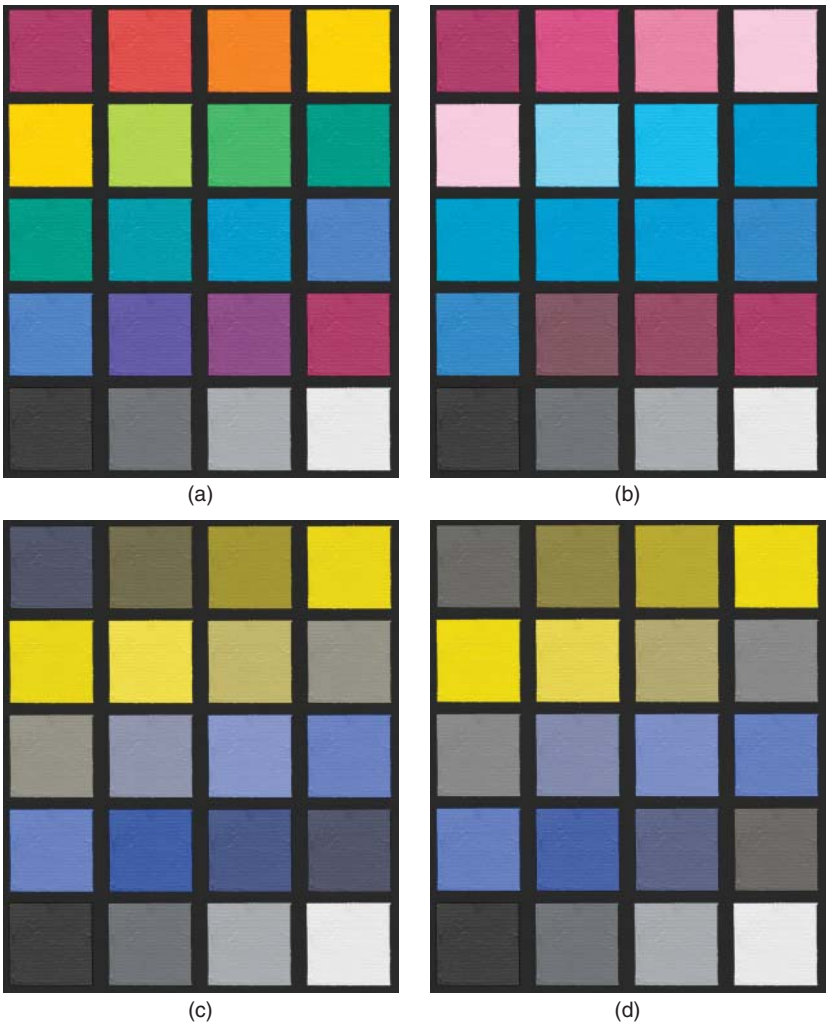

Figure 2.29 Simulation of (a) a painted color target as seen by an observer missing either (b) S, (c) L, or (d) M cones.

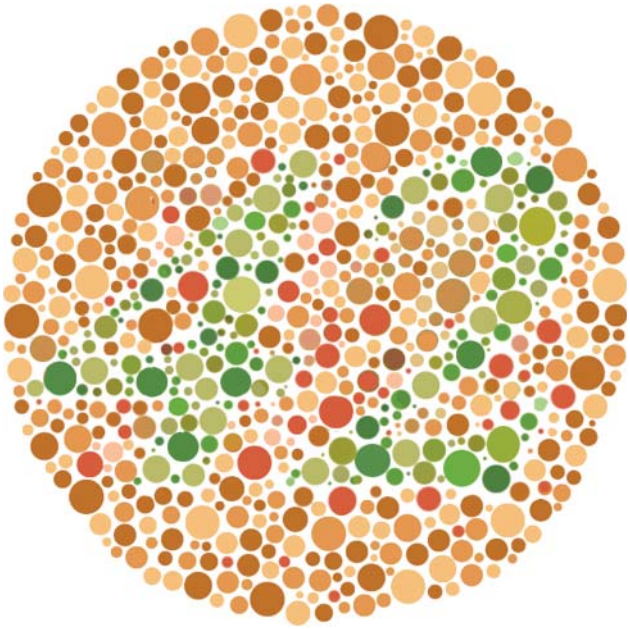

Figure 2.30 Pseudoisochromatic plates are random dots embedded with numbers. An observer missing either L or M cones will see this image only as a field of random dots.

Figure 2.31 Farnsworth–Munsell 100 hue test. Observers are instructed to order the colored caps by hue. Observers with color-vision deficiencies will make systematic errors, enabling diagnoses.

light, and chromatic adaptation), and their interrelationships (e.g. adjacent colors) transform our simple case into a very complex science. Fortunately, in order to solve many problems associated with color technology, we only have to understand the *principles* of vision. Developing these understandings and learning to solve these problems are among the major objectives of this book.

Chapter 3
Visual Color Specification

At this point, we invite the reader to approach the subject of color with us from an entirely different point of view. Rather than describing the physics of materials and light, or the physiology of the eye, we want to provide a vocabulary for describing color as we see it. We seek nouns and adjectives that have universal meaning and whose meanings are intuitive. Color names such as orange and gray conjure up reasonably consistent perceptions. In fact, 11 *basic color names* (mono-lexemic) have been identified (Berlin and Kay 1969; Kay and Regier 2006; Kay et al. 2010): white, gray, black, red, yellow, green, blue, orange, purple, pink, and brown. (See the review by Hardin 1998.) There have also been suggestions for a basic name between green and blue, such as "grue" or "turquoise" (Jameson 2005; Mylonas and MacDonald 2016). However, two samples may both be red, yet differ widely from one another. We need additional descriptions with greater precision within a basic color name. Finally, it is also useful to organize colors to facilitate visual color specification.

A. ONE-DIMENSIONAL SCALES

Kuehni and Schwarz (2008) have defined three independent psychological attributes that are used to describe colors viewed under a single set of illuminating and viewing conditions: hue, lightness, and chromatic intensity.

Hue

Describing an object's hue is an intuitive and straightforward task. The colors red, yellow, green, blue, orange, and purple differ in hue. A set of colors varying in hue is shown in Figure 3.1. An important aspect of hue is a lack of starting or ending point; hence, colors varying in hue are usually organized into a closed ring, shown in Figure 3.2. As we described in Chapter 2, there are two chromatic opponent channels: red opposed by green and yellow opposed by blue. The implication is that the color names red, green, yellow, and blue are fundamental, that is, each is a *unique hue*. A unique red is a red without yellowness or blueness. A unique yellow is a yellow without redness or greenness. And so on. These unique hues locate on a hue circle as shown in Figure 3.3. The set of colors can be placed on the hue circle according to their similarity to the unique hues, creating a hue scale.

Not every person perceives the same unique hues. As an example (R. Shamey, M. Zubair, and H. Cheema, personal communication) found that unique green was the least consistent while unique red and yellow were the most consistent for 25 observers. The range of hues from their experiment is shown in Figure 3.4.

- *Hue:* Attribute of a visual perception according to which an area appears to be similar to one of the colors, red, yellow, green, and blue, or to a combination of adjacent pairs of these colors considered in a closed ring.
- *Lightness:* Attribute by which a perceived color is judged to be equivalent to one of a series of neutrals ranging from black to white.
- *Chromatic intensity:* Attribute of a visual perception according to which the color of an area appears to be more or less chromatic.

Billmeyer and Saltzman's Principles of Color Technology, Fourth Edition. Roy S. Berns.

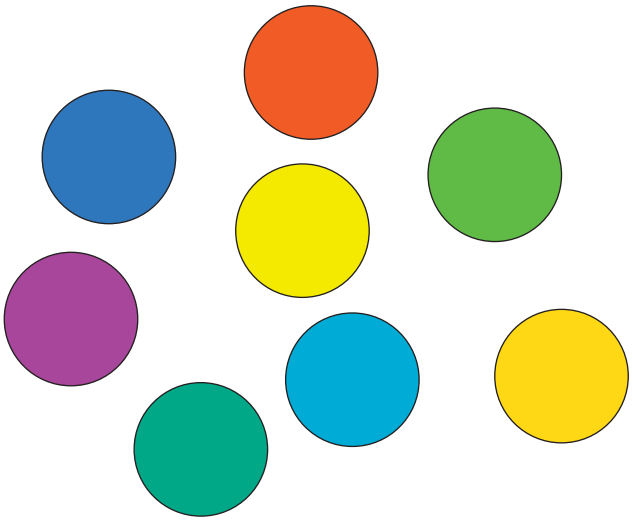

Figure 3.1 A set of colors varying principally in hue.

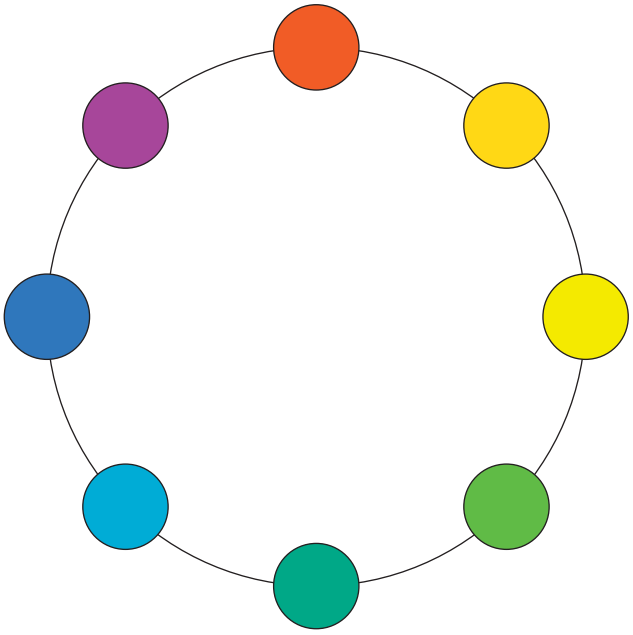

Figure 3.2 Colors shown in Figure 3.1 organized into a hue circle.

Lightness

The second psychological attribute is lightness, defined as a color's similarity to a neutral color ranging from black to white (ASTM 2013a). Ideally, the neutral colors are *spectrally nonselective*, that is, have spectra that are constant with respect to wavelength. For reflecting materials, black does not reflect any incident light while white reflects all the incident light. Another common name for this quality, used by artists, is *value*. Examples of colors varying in lightness are shown in Figure 3.5.

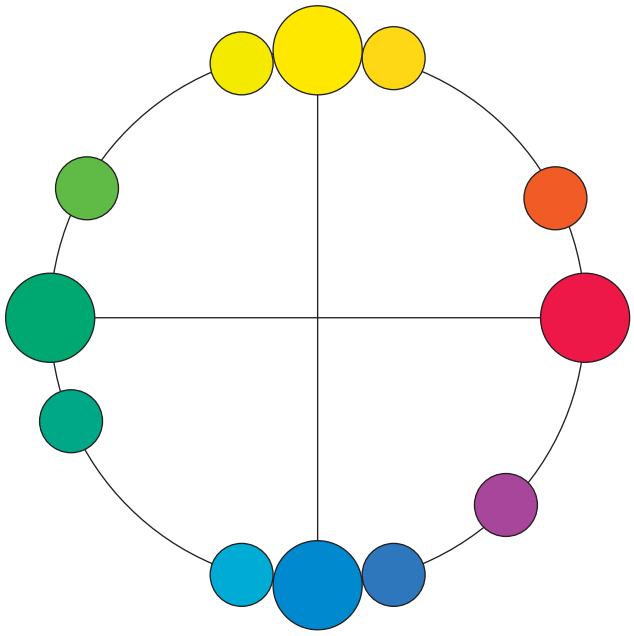

Figure 3.3 Colors shown in Figure 3.1 arranged according to their similarity to unique red, yellow, green, and blue. The unique hues are shown as large colored circles.

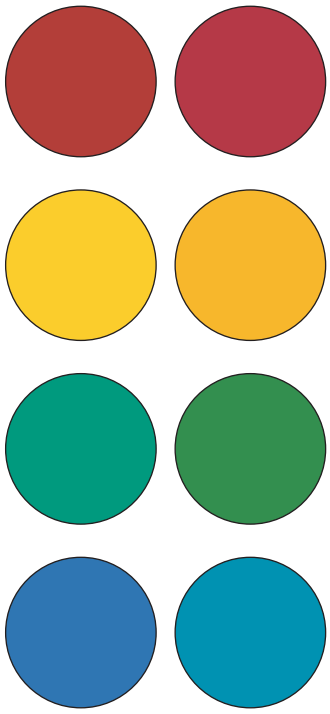

Figure 3.4 Range of unique hues for 25 observers. Source: Adapted from R. Shamey, M. Zubair, and H. Cheema, personal communication.

As we described in Chapter 2, opponent theory has the achromatic channel of white opposed by black. Thus, colors can be described by their *whiteness* or *blackness* with gray as the null position. This results in *six elementary colors*, also

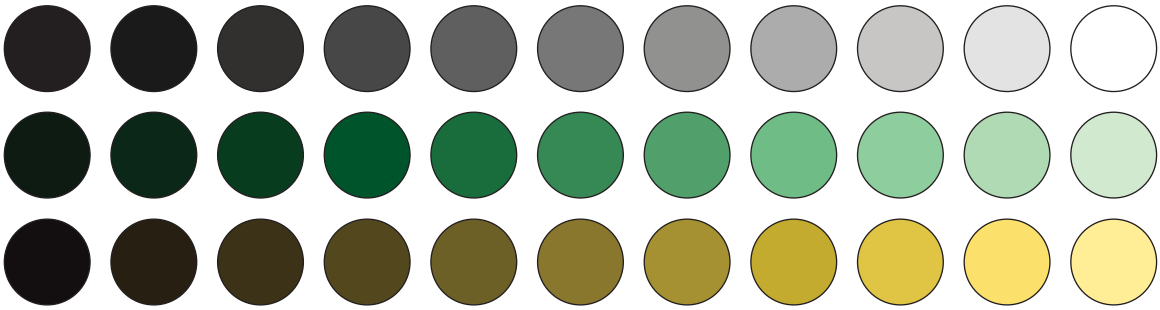

Figure 3.5 Neutral, green, and yellow colors increasing in lightness from left to right.

known as the *Hering primaries*. Whiteness is also important for near-white materials such as paper and teeth.

Chromatic Intensity

The third psychological attribute is *chromatic intensity*, defined as the amount of color. Chromatic intensity is shown in Figure 3.6 for a magenta color when mixed with white, gray, or black. Moving from left to right, chromatic intensity increases. The mixtures with white and black also vary in lightness, while the mixture with gray has a constant lightness.

B. THREE-DIMENSIONAL SYSTEMS

Given a large number of colors, we might choose to organize them along perceptual axes. The arrangement depends on the number of dimensions, the attributes of each dimension, and their geometric interrelationships. When these colors are viewed under identical conditions, three dimensions are sufficient. The evolution of color-order systems is fascinating, particularly the transition from two to three dimensions (Kuehni 2003; Kuehni and Schwarz 2008).

Geometries

We have established that hue is arranged logically as a closed ring. In most systems, the hue circle is without tilt and the

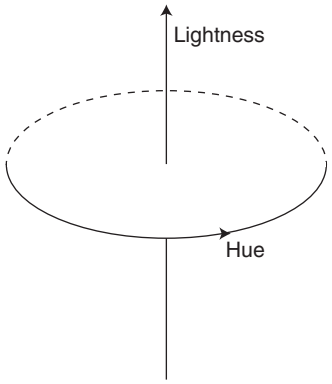

Figure 3.7 Geometric relationship between hue and lightness.

achromatic scale is perpendicular to the hue circle, shown in Figure 3.7. Several configurations with this constraint are shown in Figure 3.8. One configuration is a sphere with white at the top, black at the bottom, and medium gray in the center; spherical coordinates define position (Figure 3.8a). Position can also be defined with polar-cylindrical coordinates (Figure 3.8b). A conical arrangement is also possible with corresponding coordinates (Figure 3.8c,d). The cone's vertex can be at either end of the achromatic dimension. A cylinder is another possibility with position defined by polar-cylindrical coordinates (Figure 3.8e). Finally, two cones can be placed base to base forming a double cone (Figure 3.8e). For a given hue, two of the three sides define coordinates as in an isosceles triangle.

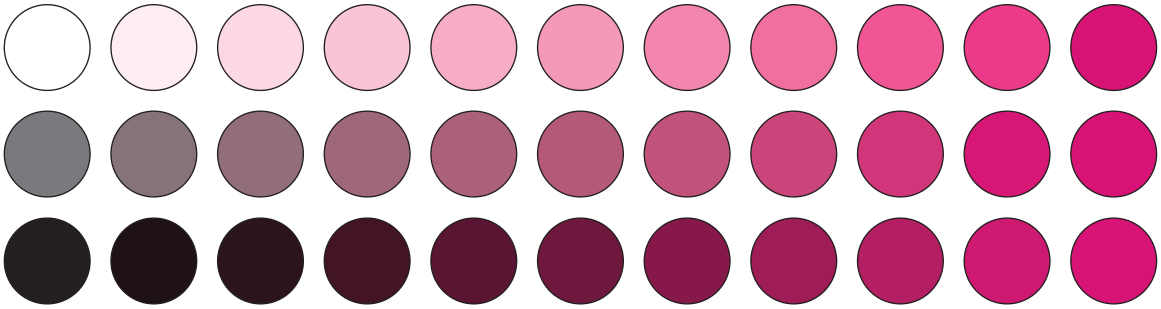

Figure 3.6 Chromatic intensity of a magenta color increasing from left to right.

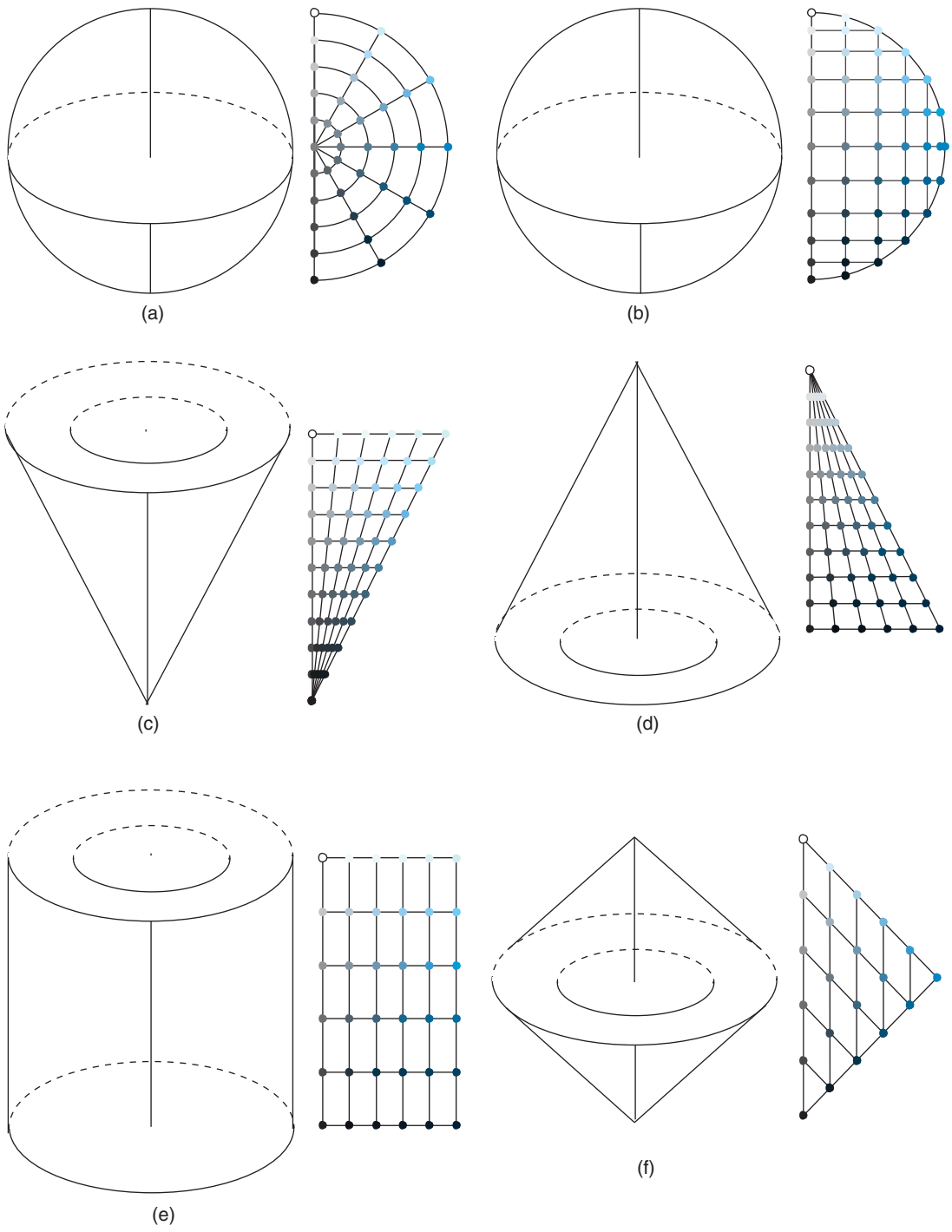

Figure 3.8 Three-dimensional arrangements of color: sphere with either (a) spherical or (b) polar-cylindrical coordinates, cone with (c) black at the apex or (d) white at the apex, (e) cylinder, and (f) double cone.

Natural Color System

We describe in Chapter 2 how the eye's physiology leads to opponent channels of white opposed by black, red opposed by green, and yellow opposed by blue. This can lead to six elementary colors: white (W), black (swarthy) (S), yellow (Y), red (R), blue (B), and green (G). Hering (1878) considered these elementary colors "natural." Hering's ideas were interpreted by Johansson (1937) during the 1930s, leading to a his "natural color system." Hesselgren

(1952) performed extensive visual experiments in order to produce an exemplification of Johansson's systems, the *Hesselgren color atlas*. However, the atlas had visual irregularities, likely a result of limitations in the visual experiments, aging of the samples, and the use of only visual judgments in the atlas's manufacture. The Swedish Color Center Foundation, founded in 1964, undertook a revision of Hesselgren's atlas by performing new visual experiments and incorporating instrumental measurements and colorimetric specifications. Their initial experiments and a careful study of the English translation of Hering's *Outlines of a Theory of the Light Sense* revealed that Johansson's interpretation could be greatly improved upon. Following 15 years of research and development, the *Swedish Standard Colour Atlas* was released in 1979 (Swedish Standards Institute 1979; Hård and Sivik 1981; Sivik 1994; Hård, Sivik, and Tonnquist 1996a,b). The system is referred to as NCS®©.

The guiding principle of NCS is defining a color by its resemblance to Hering's elementary colors, expressed as percentages. The elementary colors can be arranged into a hexagon as seen in Figure 3.9, showing possible combinations allowable according to Hering's opponent theories. For example, elemental blue connects with green, red, white, and black. Blue does not connect with yellow and in similar fashion red does not connect with green. As opponent elemental colors, it is not possible to have yellowish blues, bluish yellows, and so on.

The NCS system is arranged as a double cone with *NCS whiteness* at the top, *NCS blackness* at the bottom, and *NCS chromaticness* radiating outward from the central achromatic axis, shown in Figure 3.10. Each hue has the same maximum chromaticness, which can be thought of as a normalization of each hue's inherent *chromatic strength* (Nayatani 2005). Slicing through the three-dimensional space at constant blackness (or whiteness) results in a hue circle. A stimulus's hue is defined as a percentage between adjacent elementary chromatic colors. For example, hues between elementary yellow (100Y) and red (100R) are denoted as Y10R, Y20R, . . . , Y90R, and in similar fashion for the other three hue quadrants. The designation Y10R is equivalent to 90%Y and 10%R.

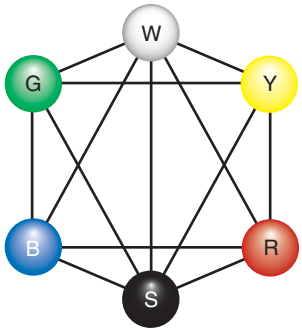

Figure 3.9 The connecting lines in the NCS hexagon indicate the elementary color pairs between which one can envision continuous color changes. Note that there are no lines connecting R and G or Y and B.
Source: Hård, Sivik, and Tonnquist (1996a,b). Reproduced with permission of John Wiley & Sons.

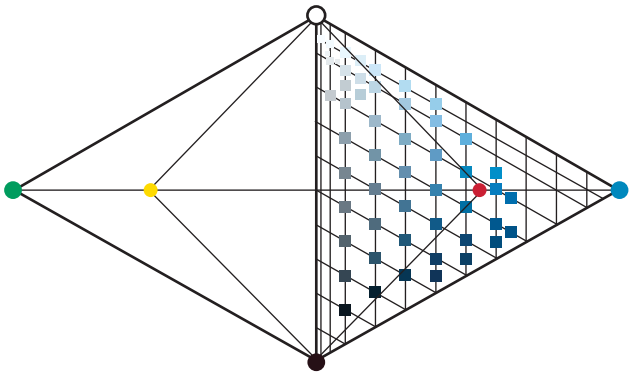

Figure 3.10 The NCS color space.
Source: Courtesy of NCS Colour AB.

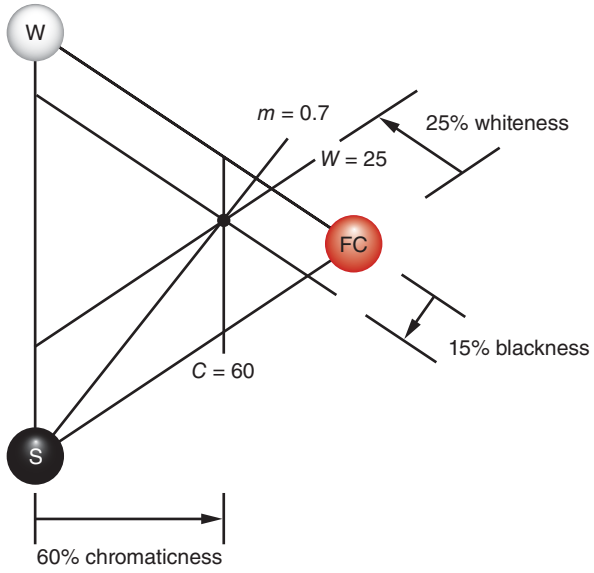

Figure 3.11 NCS color triangle. A point on the color triangle denotes *NCS nuance*. The distance from the line joining white (W) and black (S) toward a given hue at full color (FC) defines chromaticness, C. The distance from the line joining white and a given hue toward black defines blackness, S. The distance from the line joining black and a given hue toward white defines whiteness, W. It is also possible to calculate *NCS saturation*, *m* (from Swedish *mättnad*), equal to $C/(C + W)$.

The color space can be sliced along planes of constant *NCS nuance* resulting in an NCS color triangle, shown in Figure 3.11. From a stimulus's position in the triangle, chromaticness (c), blackness (s), and whiteness (w) are calculated, also expressed as percentages. Since these three

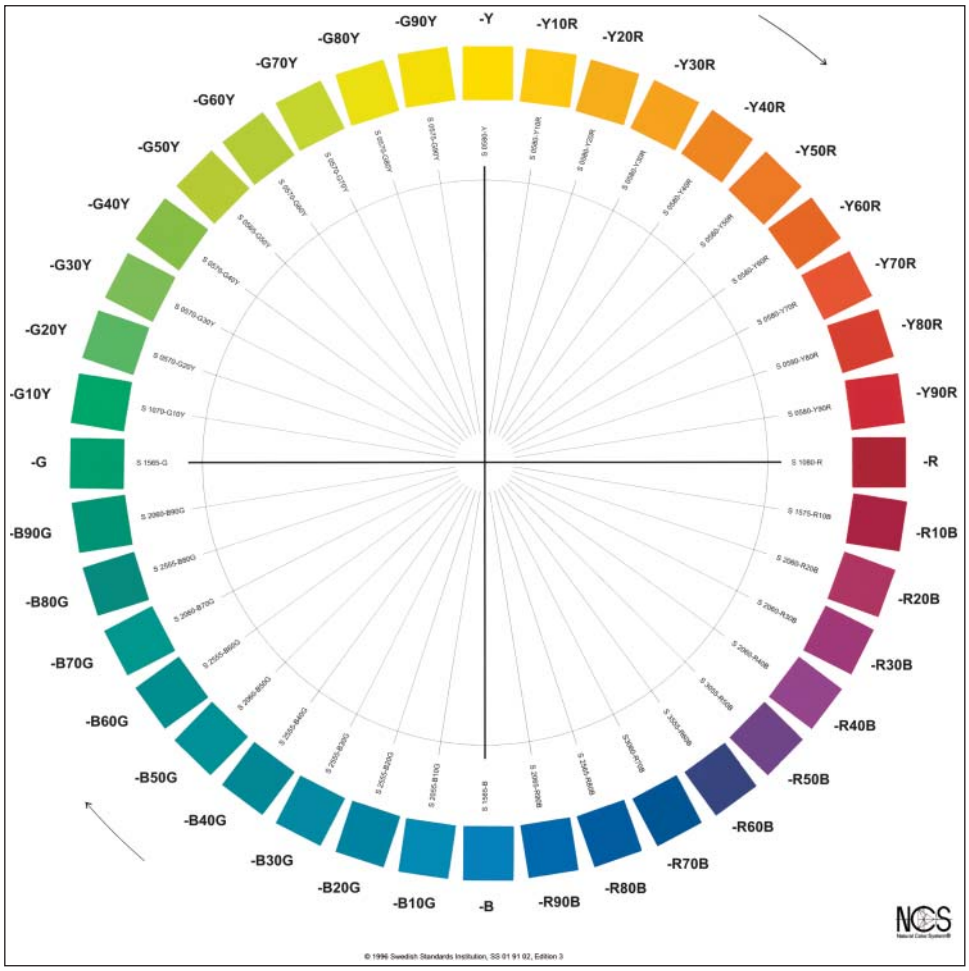

Figure 3.12 Bisecting the NCS color space at constant blackness reveals the NCS color circle. The distance from the center to the circle represents chromaticness.
Source: Courtesy of Swedish Standard Institution.

attributes always sum to 100, only chromaticness and blackness, by convention, are recorded. Thus, in the NCS system, a stimulus is defined by its blackness, chromaticness, and hue. For example, a chromatic green color would have a designation 1080-G20Y where the first two digits define blackness, the third and fourth digits define chromaticness, and hue follows the hyphen.

An observer wanting to assign an NCS notation first answers the question, "To what degree do you consider the color of this sample to characteristically resemble, or remind you of, your own conception of pure black (S), pure white (W), and the most chromatic (full) color (FC) you can imagine?" This can be expressed as a set of values summing to 100 or as a position on the NCS color triangle. Next the observer answers the question, "To what degree do you consider the color of this sample to characteristically resemble, or remind you of, your own conception of any of the chromatic colors: pure yellow (Y), pure red (R), pure blue (B), and pure green (G)?" This can be expressed as a percentage between adjacent hue in the NCS hue circle or as a position on the NCS hue circle (Hård, Sivik, and Tonnquist 1996a,b).

The NCS is produced in glossy and matte books, fan decks, and individual samples. Furthermore, as it is a Swedish and Norwegian standard, many materials such as house paint, building materials, and art supplies have their colors specified using NCS designations. Example pages from the atlas are shown in Figures 3.12 and 3.13.

Munsell Color System

The Munsell color system was developed by Munsell in 1905 as a teaching aid for art students and for color specification (Munsell 1905; Landa and Fairchild 2005). His goal was to have both a numerical system and an atlas, realized via the *Atlas of the Munsell Colors* (Munsell 1915). His guiding principles were equality of visual spacing and using physical measurements to define the system and validate

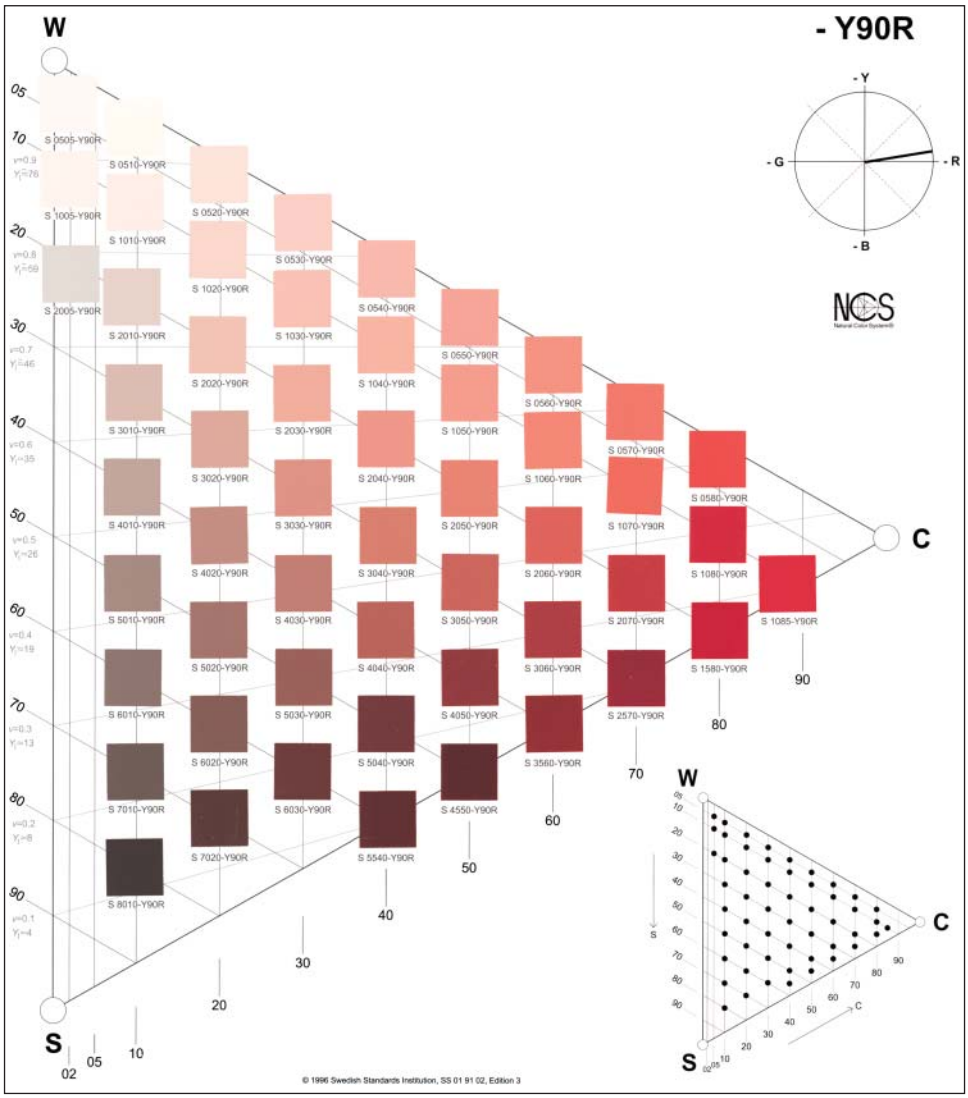

Figure 3.13 Page from the *NCS Colour Atlas*.
Source: Courtesy of Swedish Standard Institution.

its manufacture. Kuehni (2002) has chronicled the early development of the Munsell system from his diaries (Munsell 1899) as a primary reference while Nickerson (1940, 1963) and Berns and Billmeyer (1985) chronicled later developments.

Munsell was well versed in the psychometric functions of Fechner (1860) and Plateau (1872), described in Chapter 2, and used the latter to define a lightness scale called value. This required a measurement of reflectance. Munsell designed and patented a visual photometer (1901) that enabled measurements of reflectance weighted by the eye's response to visibility, known as luminous reflectance (defined in Chapter 4). This enabled any color's value to be determined instrumentally.

His interest in the decimal system led to 10 hues: red (R), yellow–red (YR), yellow (Y), green–yellow (GY), green (G), blue–green (BG), blue (B), purple–blue (PB), purple (P), and red–purple (RP), arranged in a circle. Each principal hue can be further divided into 10 subhues: 1R, 2R, . . . , 9R, and 10R. Having hue divided into 100 steps (or the lowest common principal number of hues, five) led to much greater visual equality between neighboring hues than systems based on three or four principal hues. The specific colors of the five principal hues were determined visually; Munsell reasoned that these five hues should form a neutral when mixed using a spinning disk. He built a device that spun a globe painted with the five principal hues at different values to demonstrate this principle, a sketch of which is shown in Figure 3.14.

The ability to measure value meant that chromatic intensity was sampled at constant value. Munsell coined the term chroma for such scales.

Figure 3.14 The painted globe of Munsell, used to define the specific colors of the five principal hues red, yellow, green, blue, and purple.
Source: From Munsell (1905).

Figure 3.15 The *Munsell Color Tree*, showing the three-dimensional relationships between hue, value, and chroma.
Source: Courtesy of X-Rite Pantone, Inc.

His first three-dimensional representation of hue, value, and chroma was spherical with polar-cylindrical coordinates. He quickly realized that sampling constrained to a sphere would result in an atlas with a small range of colors. The sphere needed to be pushed out for different hues. A yellow at maximum chroma is considerably lighter than a purple at maximum chroma. This changed the arrangement from a sphere to a spheroid, known as the *Munsell color solid*, shown in Figure 3.15. Without a specific shape, chroma is unbounded. The maximum chroma for a yellow is higher than the maximum for purple. As a result, chromatic strength is not normalized between hues.

It is remarkable that a painter devised such a system because paint mixtures rarely have constant lightness, reinforcing his guiding principles of physical measurement and visual uniformity.

A Munsell notation is defined as H V/C where H represents hue, V represents value, and C represents chroma. A red brick might have the notation 5R 4/6. Achromatic colors are notated with the Prefix "N" – for example, N0, N1, . . . , N10.

The original atlas has undergone considerable refinement and development based on extensive visual experimentation. The first refinement included a more perceptually uniform value scale (Godlove 1933; Munsell, Sloan, and Godlove 1933) and improvements in spacing of hue and chroma (Berns and Billmeyer 1985). To avoid confusion, the revised atlas was retitled the *Munsell Book of Color* (Munsell 1929). During the late 1930s, it became evident that the visual spacing could be further improved. A subcommittee of the Optical Society of America performed further visual experiments totaling over 300 000 observations using more sophisticated experimental techniques (Newhall 1940). Rather than producing an atlas, colorimetry was used to define the Munsell system and the data were published in the Journal of the Optical Society of America (Newhall, Nickerson, and Judd 1943). (We describe colorimetry and its use in color specification in Chapter 4.) It is possible to make an atlas using different materials and versions have been made using matte and glossy paints, textiles, and inkjet printing. An example page from the matte collection is shown in Figure 3.16.

Despite these improvements, one defect remains. Colors with constant value are assumed to have constant lightness. This is well known to be false, the effect known as the Helmholtz–Kohlrausch phenomenon (Fairchild 2013). An example is shown in Figure 3.17.

In the past, we have heard that describing colors using lightness, redness opposed by greenness, and yellowness opposed by blueness is more intuitive than lightness, chroma,

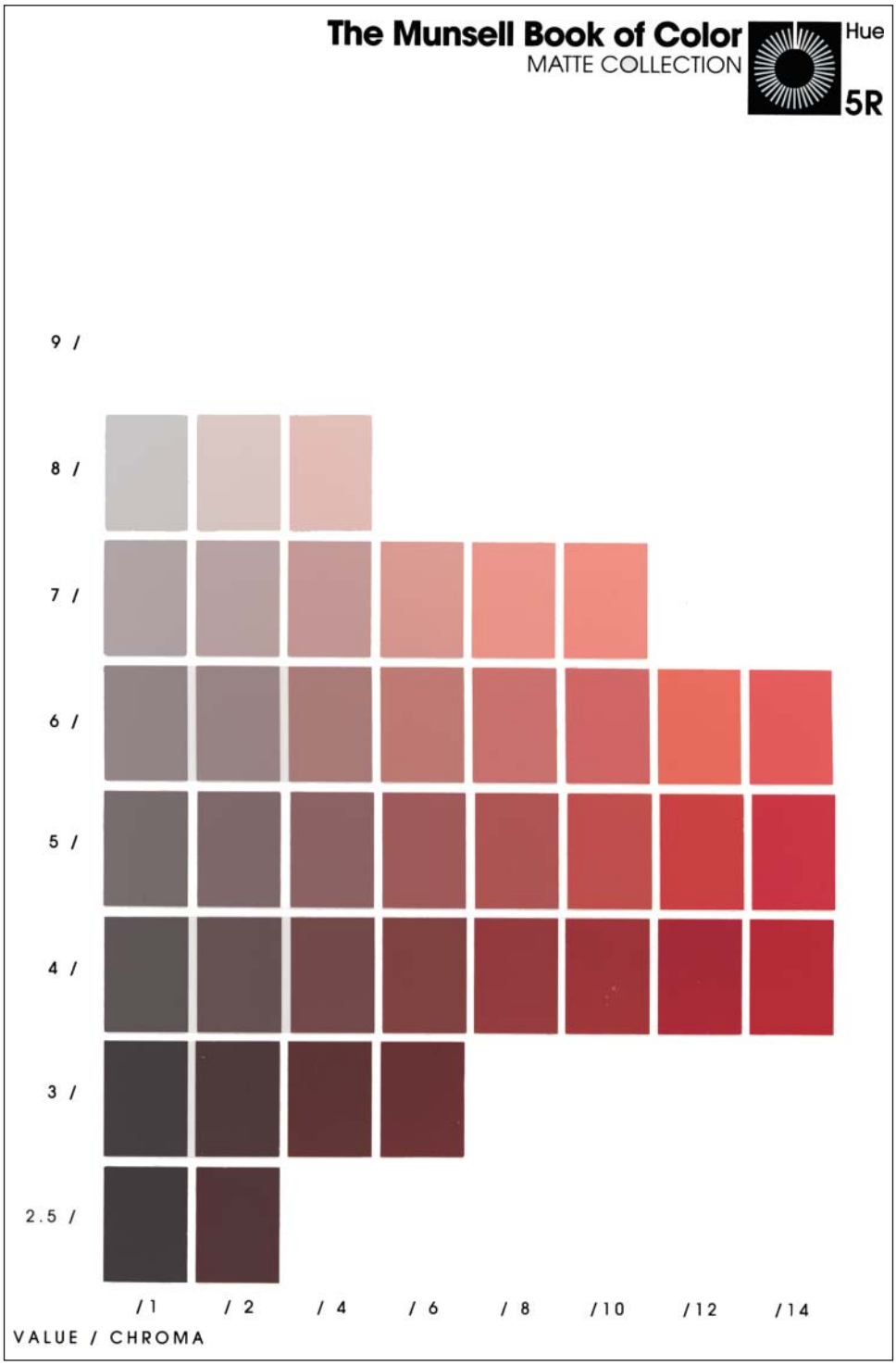

Figure 3.16 A page from the *Munsell Book of Color*, Matte Collection.

and hue because of the physiological connection with opponent color vision. Zhang and Montag (2006) found that both descriptions were equivalent when used as observer controls for color matching and color discrimination experiments. In experiments where observers scale hue, lightness, and chromatic intensity (e.g. chromaticness, chroma, colorfulness, etc.), chromatic intensity is the least reliable, indicating the difficulty in understanding this dimension of color. Using a color order system for visual specification is always more effective with training.

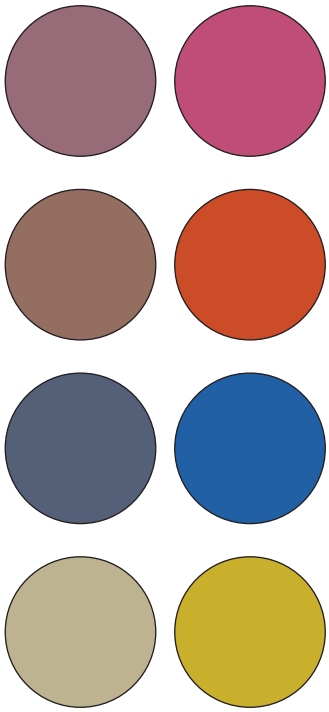

Figure 3.17 Each color pair has constant Munsell value and dissimilar Munsell chroma. Differences in perceived lightness are caused by the Helmholtz–Kohlrausch phenomenon.

Other Color-Order Systems

Other systems used for color specification include the OSA Uniform Color Scales (OSA-UCS) (MacAdam 1974, 1978; Nickerson 1978, 1981), the DIN system developed by Richter and produced by the Deutsches Institut für Normung (German Standardization Institute, DIN) (Richter 1952, 1955; Richter and Witt 1986), the Coloroid system (Nemcsics 1980, 1987), the RAL (Reichs-Ausschuss für Lieferbedingungen) Design System (www.ral-farben.de), the Universal Color Language (Kelly 1965; Kelly and Judd 1976), and the ISCC-NBS Method of Designating Colors (Kelly and Judd 1955, 1976; Kelly 1958, 1965). Reviews of color order systems have been published by Simon (1980, 1997), Billmeyer (1987), Derefeldt (1991), and Nemcsics and Caivano (2016). See also Kuehni (2003), Kuehni and Schwarz (2008), and Koenderink (2010).

C. COLOR APPEARANCE: MULTIDIMENSIONAL SYSTEMS

Three-dimensional systems are sufficient when colors are viewed under a single set of conditions. However, there are many cases when we are comparing colors viewed under different conditions. This is common in color imaging where images taken outdoors are viewed indoors. Television images look different during the day than when viewed at night with either dim lighting or the lights turned off. We have entered the world of *color appearance* (Fairchild 2013) where color is defined with five dimensions! The additional two dimensions differentiate between *absolute* and *relative color appearances*. Suppose that we are inside studying a page from the Munsell Book of Color, for example, Figure 3.16. The relationships between Munsell value and chroma are evident. Taking the page outside, the relationships are unchanged, but all the colors appear brighter and more colorful. We perceive color on both an absolute level—hue, brightness, and colorfulness—and a relative level—hue, lightness, and chroma. Both inside and outside, we are conscious of the appearance of white whether it is observed or inferred. This is known as the *scene white*. Lightness is the brightness of a color relative to the brightness of the scene white. Chroma is the colorfulness of a color relative to the brightness of the scene white. We experience this distinction when an object is partially in shadow, shown in Figure 3.18. In shadow, brightness and colorfulness have reduced, yet we continue to perceive Munsell value and chroma as if the page was lit uniformly.

What about saturation? It is the colorfulness of an object relative to its brightness, which is equivalent to chroma relative to lightness. This is a conical arrangement with black at the apex.

- *Color appearance:* (i) Aspect of visual perception by which things are recognized by their color. (ii) *In psychophysical studies:* Visual perception in which the spectral aspects of a visual stimulus are integrated with its illuminating and viewing environment.
- *Hue:* Attribute of a visual perception according to which an area appears to be similar to one of the colors red, yellow, green, and blue, or to a combination of adjacent pairs of these colors considered in a closed ring.
- *Brightness:* Attribute of a visual sensation according to which an area appears to emit, or reflect, more or less light.
- *Colorfulness:* Attribute of a visual sensation according to which the perceived color of an area appears to be more or less chromatic.
- *Lightness:* The brightness of an area judged relative to the brightness of a similarly illuminated area that appears to be white or highly transmitting.
- *Chroma:* Colorfulness of an area judged as a proportion of the brightness of a similarly illuminated area that appears white or highly transmitting.
- *Saturation:* Colorfulness of an area judged in proportion to its brightness.

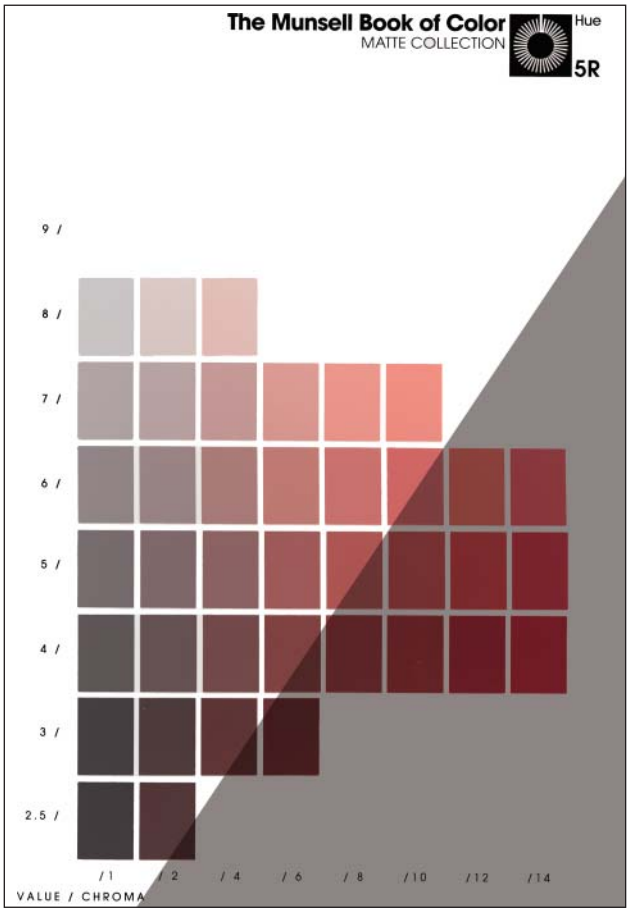

Figure 3.18 A page from the *Munsell Book of Color* partially in shadow.

D. COLOR-MIXING SYSTEMS

A color-mixing system exemplifies relationships between *color primaries* and their intermixtures. A color is defined by the amount of each primary. For example, in printing, colors are most often produced from four primary inks: cyan, magenta, yellow, and black. The Pantone system uses 14 inks for spot color printing, that is, premixing one or more inks to produce a single color. Color displays use three lights: red, green, and blue. Point of sales paint-dispensing systems use about a dozen pigment concentrates. Even when names are used, there is an underlying recipe. In general, a particular color is made from a mixture of four colorants or fewer. Several systems warrant further description.

RGB and *HSB*

The simplest system, perhaps, is the mixing of colored light, easily exemplified with a color display. When the amounts of the three primaries are at their minimum, black results; when the amounts of the three are at their maximum, white results. Increasing or decreasing amounts of individual primaries or their various combinations produces a systematic arrangement of colors. An *RGB color cube*, shown in Figure 3.19, has each primary (i.e. red, green, and blue), secondary (magenta—composed of red plus blue, yellow—composed of red plus green, cyan—composed of green and blue), white (composed of red plus green plus blue), and black at its vertices.

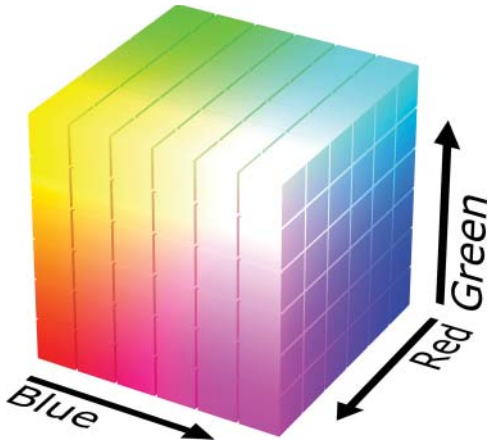

Figure 3.19 *RGB* color cube. .
Source: https://commons.wikimedia.org/wiki/File:RGB_color_solid_cube.png

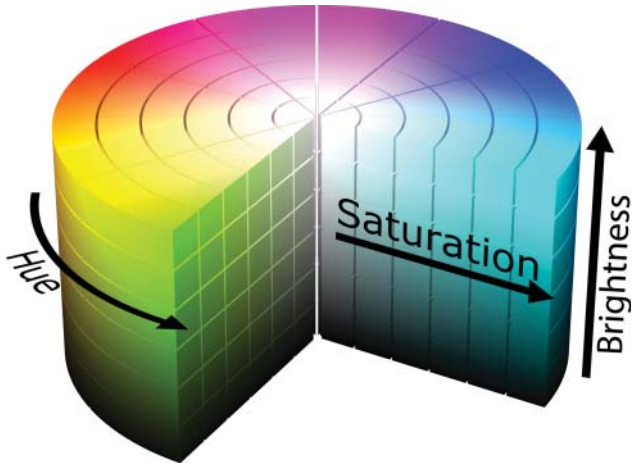

Figure 3.20 *HSB* cylindrical system.
Source: Modified from https://upload.wikimedia.org/wikipedia/commons/4/4e/HSV_color_solid_cylinder.png.

Choosing a color with red, green, and blue controls is not intuitive and takes practice. This is remedied by transforming *RGB* to a system with familiar terms; the most common are hue, saturation, and brightness: *HSB*. Colors are arranged in a cylinder with polar-cylindrical coordinates, shown in Figure 3.20. Although "brightness" and "saturation" bear little resemblance to their true definitions above, the system is very easy to use.

RGB to HSB Formulas

The formulas to calculate *HSB* from *RGB* are shown in Eqs. (3.1)–(3.6).

$$H = \begin{cases} \text{ATAN2}(\beta, \alpha)\frac{180}{\pi} & \text{ATAN2}(\beta, \alpha) \geq 0 \\ \text{ATAN2}(\beta, \alpha)\frac{180}{\pi} + 360 & \text{ATAN2}(\beta, \alpha) < 0 \end{cases} \tag{3.1}$$

$$S = 100\frac{\Delta}{\max(R, G, B)} \tag{3.2}$$

$$B = 100\frac{\max(R, G, B)}{255} \tag{3.3}$$

where

$$\alpha = \frac{2R - G - B}{2} \tag{3.4}$$

$$\beta = \frac{\sqrt{3}(G - B)}{2} \tag{3.5}$$

$$\Delta = \max(R, G, B) - \min(R, G, B) \tag{3.6}$$

Test data are given in Table 3.1.

Table 3.1 Test data for calculating *HSB* from *RGB* where *R*, *G*, and *B* vary between 0 and 255.

R	*G*	*B*	*H* (°)	*S* (%)	*B* (%)
255	0	0	0	100	100
0	255	0	120	100	100
0	0	255	240	100	100
255	255	0	60	100	100
255	0	255	300	100	100
0	255	255	180	100	100
20	60	81	200	75	32
200	150	100	30	50	78
102	200	50	100	75	78

HSB is used in Adobe Photoshop as a *color picker*, shown in Figure 3.21. In addition to *RGB* and *HSB*, colors are defined by LAB—defined in Chapter 4—and CMYK. Transforming to these descriptors requires what is known as *color management*, described in Chapter 10.

The Pantone Matching System

Often in package printing, a desired color, known as a *spot color*, is produced by premixing several inks. This color is applied to the paper using a separate printing unit. Fan decks of spot colors organized by hue along with their recipes of ink amounts are used to communicate color between designers and printers. The most common set of ink mixtures is the *Pantone matching system* or *PMS*. The Pantone system is based on 14 primary inks. The range of colors obtainable using the Pantone system is much greater than that achieved using cyan, magenta, yellow, and black inks. Several pages from a Pantone fan deck are shown in Figure 3.22. Each color has a numerical designation and an ink recipe. The popularity of the PMS has led to

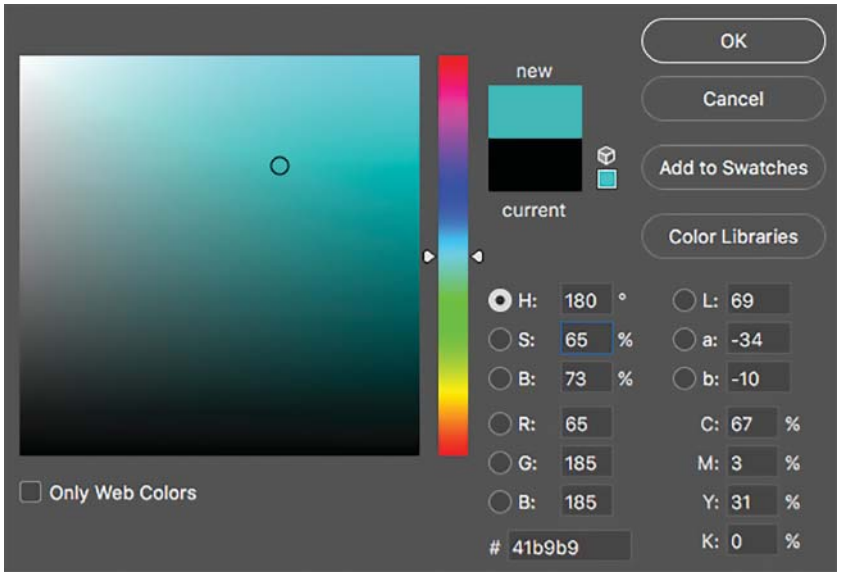

Figure 3.21 Screenshot of the Adobe color picker used in Photoshop.

Figure 3.22 Pantone examples.

additional products made from four-color process printing, fluorescent and metallic inks, dyed textiles, and pigmented plastics.

There are other systems in addition to Pantone including DIC, FOCOLTONE, HKS, TOYO, and TRUMATCH. These systems are also used in color pickers to select and define color, shown in Figure 3.23.

Limitations of Color-Mixing Systems for Color Specification

There are several critical issues to be aware of when any color-mixing system is used for color specification, essentially as a link between designers or consumers and technologists, and between suppliers and purchasers. By definition, the primary amounts define the specification, not the resulting color. If every aspect of producing visual examples is not highly consistent and standardized, large variations in perceived color can result from the identical specification. Excellent consistency is extremely difficult to achieve, particularly for printing systems in which the inks, papers, and printing processes are can be variable. Lack of consistency leads to additional problems when the material is changed (e.g. when Pantone specifications are produced for dyed textiles). Since the specification is defined as an ink recipe, a representative sample must first be produced and used as a standard to be matched in the new material. If the printing system has poor consistency, what ensures that these "standards" are representative? Furthermore, the new material is usually metameric to the originals, further reducing consistency since viewing and illuminating conditions are rarely controlled. As a consequence, visual examples should be used only as a guide, despite claims of high consistency. (This can easily be tested by purchasing or producing several examples made to the same specification.) When a designer wants to use a color-mixing system for specification, the particular visual examples used by the designer must be made available to the color technologist for color matching.

E. SUMMARY

For a single condition of illumination and viewing, three attributes are sufficient to describe a color: hue, lightness, and chromatic intensity. Differences in both the three-dimensional arrangement and the interpretation of chromatic intensity result in different color-order systems. The NCS and Munsell System are fundamentally different systems, easily verified when one system is defined using the other's coordinate system (Billmeyer and Bencuya 1987). Both are useful. Color-mixing systems can also be used for color specification, though great care

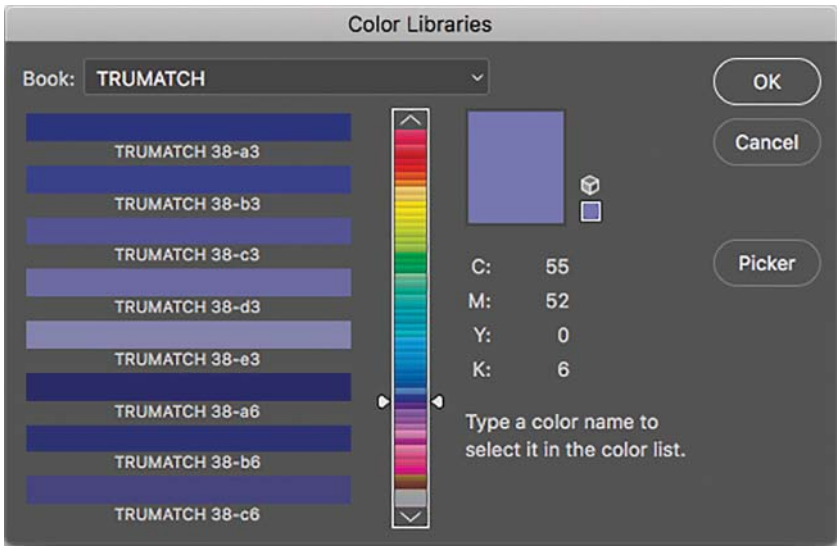

Figure 3.23 Screenshot from Adobe Photoshop of the TRUMATCH system.

is required in their proper use. The need to differentiate colors seen in multiple conditions of illumination and viewing has led to the absolute color-appearance terms of brightness and colorfulness. In Chapter 4, color-appearance models will be introduced where a sample's hue, brightness, lightness, colorfulness, chroma, and saturation can be calculated.

Chapter 4

Numerical Color Specification: Colorimetry

We have learned that color is quite complex and can be described in many ways. We can describe physical properties that lead to color, such as colorant concentration or an object's spectral properties. We can describe physiological properties such as receptor responses and opponent signals. We can describe color perceptions using color names such as red and pink, or with color-order systems. If a manufacturer and customer both have the same system, they can specify colors numerically and validate a material's color visually using the system's atlas. Physical standards and visual matching have been practiced, likely, for hundreds of years including today. For many applications, visual matching is inadequate because of a lack of control of illuminating and viewing geometries and variability in color vision. The solution to this problem is threefold and occurred during the early twentieth century. First, spectrophotometers were used to measure a sample's spectral-reflectance factor. The spectrophotometers' geometries were standardized to include only two choices. Second, lighting was standardized to include only three choices. (Today, there are a large number of standardized illuminants.) Third, only two observers were standardized. The standard observers and lights were tables of data. By calculation, an object's color was defined numerically. This numerical system is the subject of this chapter.

A. COLOR MATCHING

One of the ways to simplify color specification greatly is to reduce the problem to one of color matching. The color to be reproduced must match the color of a sample viewed and illuminated under a specified set of conditions. If the standard and its reproduction are both materials, we would place the samples adjacent to one another under the specified set of conditions. If we are comparing colored lights with material samples, for example, comparing a color display to a color print, we further simplify the viewing conditions so that the light emitted from the display matches the light reflected off of the paper. The problem in its simplest form, shown in Figure 4.1, is answering the question, "Do two colored lights match one another?"

Color-matching experiments with light were first performed by Newton (1730) in the early 1700s. He found that combining only blue and yellow wavelengths could reproduce white light, shown in Figure 4.2. This experiment produced a metameric match: different stimuli, one being all of the wavelengths and the other, only yellow and blue wavelengths, produced identical visual responses. Either stimulus could be used to specify other white lights.

Imagine that we have a portable device that generates light varying in hue, lightness, and chromatic intensity,

Billmeyer and Saltzman's Principles of Color Technology, Fourth Edition. Roy S. Berns.

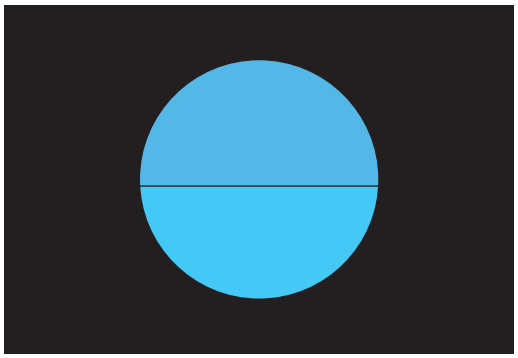

Figure 4.1 A color specification can be reduced to a color-matching problem: Do the two fields match in color?

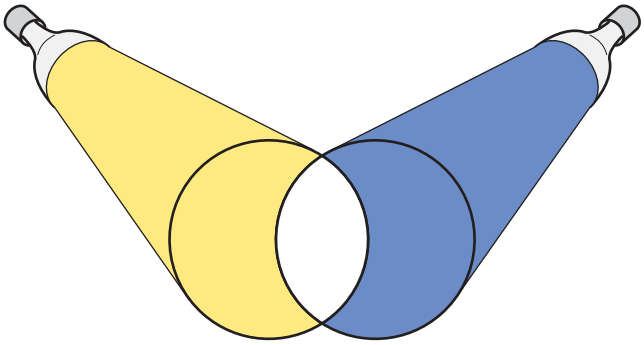

Figure 4.2 Newton found that when blue and yellow lights were mixed together, white resulted.

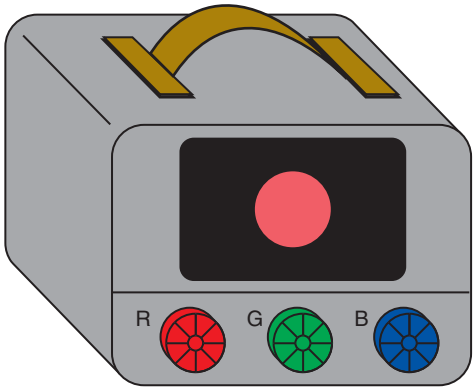

Figure 4.3 A portable visual colorimeter using red, green, and blue lights.

shown in Figure 4.3. Mixing red, green, and blue lights produces a large range of colors, that is, a large *color gamut*. We have controls that enable us to vary the color of the light continuously. If we want to specify a color, we dial in the color on the device. We can take the device to our supplier and show him the color. His job is to produce his product with color identical to that displayed on the device. Eventually, we realize that it would be more efficient to have two identical devices. If the devices had digital controls, we could text numerical specifications to our supplier. We have designed a visual color-matching system, a process often called *visual colorimetry*.

■ *Colorimetry:* A synthesis of two words, color and *metrein* (Greek, meaning "to measure"). It is the science of color measurement.

Visual colorimetry dates back to the late nineteenth century. Lovibond (1887), a brewer, developed a device with which he could specify the color of beer visually, using sets of colored glasses. The *Lovibond Tintometer* generated a gamut of colors encompassing the color range of beer and other liquids including oils, paint vehicles, and sugar solutions. In another early example, the first production of the 1929 *Munsell Book of Color* was based on a spinning disk, with which a set of colored papers and their percentage area coverage were used to specify each Munsell designation (Berns and Billmeyer 1985). The disk is spun at a sufficient rate so that only a single color is observed. This is known as *disk colorimetry*.

All of these visual colorimeters, by definition, are based on the principle of metamerism. As a consequence, a match for one person will probably not remain a match when viewed by another person. The greater the differences in spectral properties between the output of the visual colorimeter and the manufactured material, the more likely that problems will arise when several observers are involved in the specification process. Use of a visual colorimeter that is not designed for a specific application will often result in significant metamerism. If we could replace any particular observer with an average observer, this limitation would be reduced slightly, based solely on the principles of statistics. If this average observer were standardized, the *standard observer*, then all specifications would be consistent, and not dependent on any particular observer's visual properties.

This concept, using visual colorimetry with a standard observer and a standardized device as a method of color specification, dates to the 1920s (Troland 1922). The *International Commission on Illumination* (Commission Internationale de l'Éclairage, or *CIE*) wanted a method of specifying red, green, and yellow colored lights used in railroad and, shortly thereafter, highway traffic control (Holmes 1981). The concept quickly evolved into a measurement-based system in which stimuli requiring specification were first measured spectrally. The spectral information was used to calculate the standardized device controls such that when the standard observer viewed the stimulus and device, they matched in color, a *colorimetric match*. This system was first standardized by the CIE in 1931 (CIE 1931; Judd 1933; Wright 1981b; Fairman, Brill,

and Hemmendinger 1997; Schanda 2007). It is the "heart" of all modern color-measurement systems.

We learn in Chapter 2 that two stimuli match in color when they lead to equal cone responses. It seems that specifying color matches should be very straightforward: cone responses would provide the numerical system. These are directly calculated from the average observer's cone spectral sensitivities (cone fundamentals) and spectral measurements of the stimuli. During the early twentieth century when colorimetry was developed, accurate measurements had yet to be made of the eye's spectral sensitivities. A standardized color-matching system was the only viable approach. MacAdam (1993) and Schanda (2007) have compiled a number of historical publications that form the framework for modern colorimetry. Richter (1984) has summarized the contributions of the "founding fathers and mothers" of colorimetry.

The CIE technical report, "Colorimetry," CIE Publication 15:2018 describes the current recommendations (CIE 2018).

B. DERIVATION OF THE STANDARD OBSERVERS

Theoretical Considerations

Let's imagine an ideal observer—with respect to visual colorimetry—with cone fundamentals as shown in Figure 4.4.

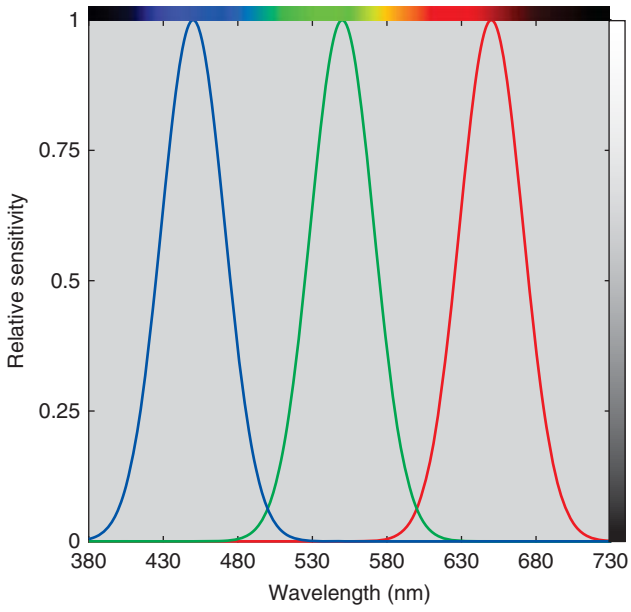

Figure 4.4 The spectral sensitivities of an *ideal observer* when building a visual colorimeter with three lights. At 450, 550, and 650 nm, one of the three receptors has its maximum sensitivity while the others have none.

For any stimulus, the cone responses can be calculated via integration, shown in Eqs. (4.1)–(4.3):

$$L = \int_{\lambda} S_{\lambda} R_{\lambda} l_{\lambda} \, d\lambda \tag{4.1}$$

$$M = \int_{\lambda} S_{\lambda} R_{\lambda} m_{\lambda} \, d\lambda \tag{4.2}$$

$$S = \int_{\lambda} S_{\lambda} R_{\lambda} s_{\lambda} \, d\lambda \tag{4.3}$$

where S_{λ} is an illuminant's spectral power distribution, R_{λ} is an object's spectral-reflectance factor, and l_{λ}, m_{λ}, and s_{λ} are the cone fundamentals of the ideal observer. We need to build a visual colorimeter that can display a color that matches any stimulus the ideal observer encounters. The easiest way to build the colorimeter is by using three lights. Suppose that the lights are *monochromatic* (a single wavelength) with wavelengths of 450, 550, and 650 nm. As shown in Figure 4.5, varying the radiance of the 450 nm light results in changing the response of only the ideal observer's short-wavelength receptor. The long- and middle-wavelength receptors cannot "see" light at 450 nm, having no response at this wavelength. In a similar fashion, varying the 550 nm light only causes responses in the ideal observer's middle-wavelength receptor; varying the 650 nm light only causes responses in the ideal observer's long-wavelength receptor. Thus, any stimulus can be matched by varying the amounts of the 450, 550, and 650 nm lights. It is possible to "dial in" any response for

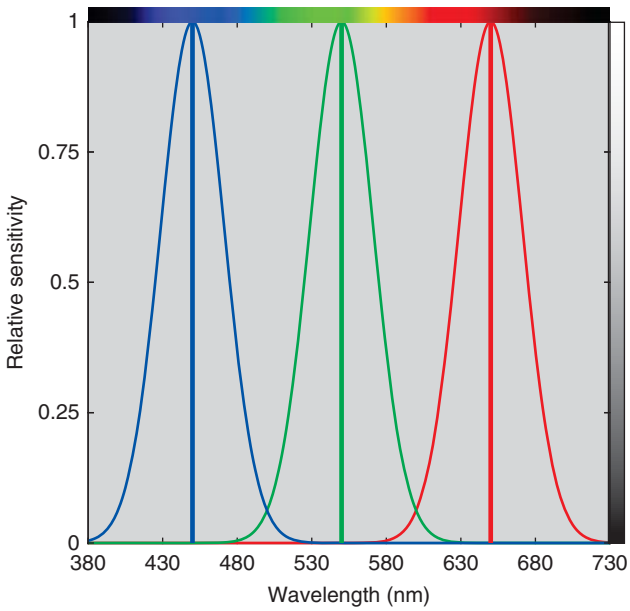

Figure 4.5 When building a visual colorimeter, the optimal primaries for this ideal observer are 450, 550, and 650 nm. Each primary stimulates only a single receptor type. The primaries coincide with the receptor spectral-sensitivity maxima, yielding optimal efficiency.

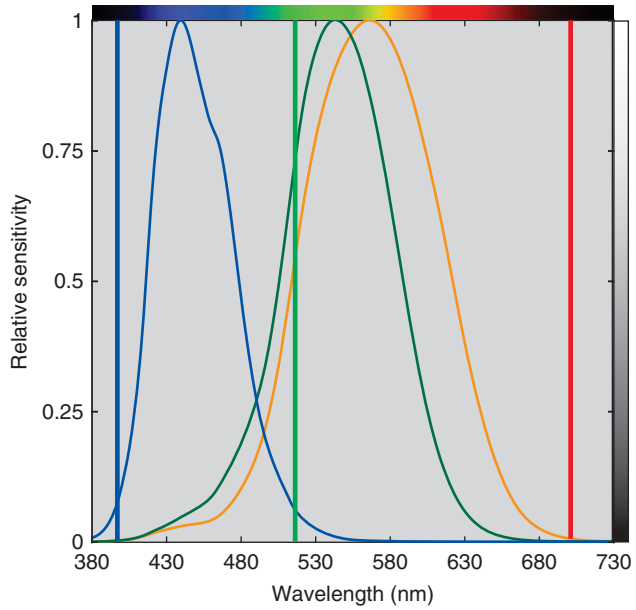

Figure 4.6 Primaries of 400, 520, and 700 nm maximize the independent stimulation of the eye's cone responses and, in turn, maximize the visual colorimeter's color gamut.

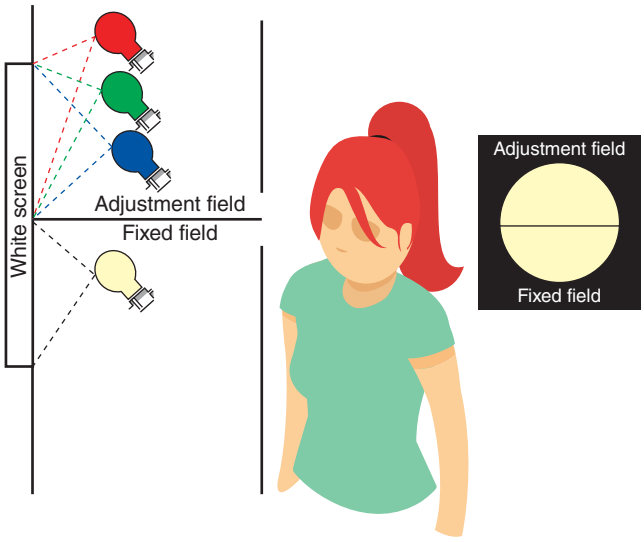

Figure 4.7 A visual colorimeter and the bipartite field as seen by the summer intern.

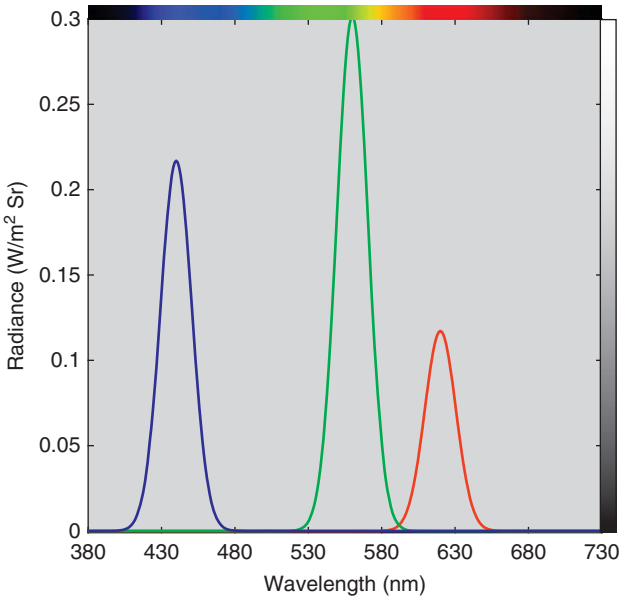

Figure 4.8 Spectral radiance of each primary at unit amount. When combined, a color equal to the color of the equal-energy spectrum results.

this ideal observer. A visual colorimeter with *primaries* of 450, 550, and 650 nm could be used to standardize the color of any stimulus of interest for this ideal observer.

What happens when we apply this reasoning using a real observer? We would like to find three primaries that enable each cone response to be independently controlled. Evaluating a real observer's cone spectral sensitivities reveals that it is not possible to achieve this aim. About the best that can be achieved uses wavelengths of 400, 520, and 700 nm, shown in Figure 4.6. Although it is straightforward to choose wavelengths that stimulate only the short-wavelength and long-wavelength receptors, it is impossible to select a wavelength that stimulates only the middle-wavelength receptor because of the large amount of overlap between it and the long-wavelength receptor. As a consequence, any visual colorimeter that contains only three primaries cannot produce matches to every possible stimulus. (By extension, any three-primary-color system has the same limitation.)

The Color-Matching Experiment

Let's suppose that a student has an interest in color science. She secures funding from the university and is hired as a summer intern to learn firsthand about colorimetry. Having knowledge of the theoretical considerations just described, she designs and builds a visual colorimeter, such as shown in Figure 4.7. The colorimeter produces two fields of light, forming a *bipartite field*. In the adjustment field, light results from the admixture of three primaries: 440, 560, and 620 nm. (Though not shown in the drawing, the radiance of each light is adjustable.) Unit amounts of each primary when combined produce a white equal to the color of the equal-energy spectrum. The spectra are plotted in Figure 4.8. In the fixed field, a number of different lights can be used. A masking screen is used to control the size of the bipartite field, expressed as a *field of view* in degrees.

In the first experiment, the three lights are adjusted until a match is made to an incandescent light. Our intern has verified the principle of *metamerism*: that colors can be matched despite their differences in spectral properties. In her second

experiment, she doubles the amount of light in both fields. She finds that although the two fields look brighter, they still match. She doubles them again with the same result. Next, she reduces the amount of light in both fields. Even though the two fields get dimmer, they continue to match. This matching property is known as *proportionality*.

In a third experiment, shown in Figure 4.9, the fixed field contains a combination of greenish-blue light and the red primary at a moderate intensity. The resulting color has lower chromatic intensity than the greenish-blue light alone. Again, she adjusts the primary radiances in the adjustment field until it and the fixed field are indistinguishable. If she *increases* the red primary by the same amount in both fields, the two fields continue to match, although their color changes. If she *decreases* the red primary by the same amount in both fields, the two fields continue to match. This matching property is known as *additivity*. She also notices that as she decreases the amount of red light in the adjustment field, chromatic intensity increases. The red primary modulates color between greenish-blue and white, shown in Figure 4.10.

Our budding scientist has verified what are known as *Grassmann's laws of additive color matching* (Grassmann 1853; Wyszecki and Stiles 1982). Essentially, color matching

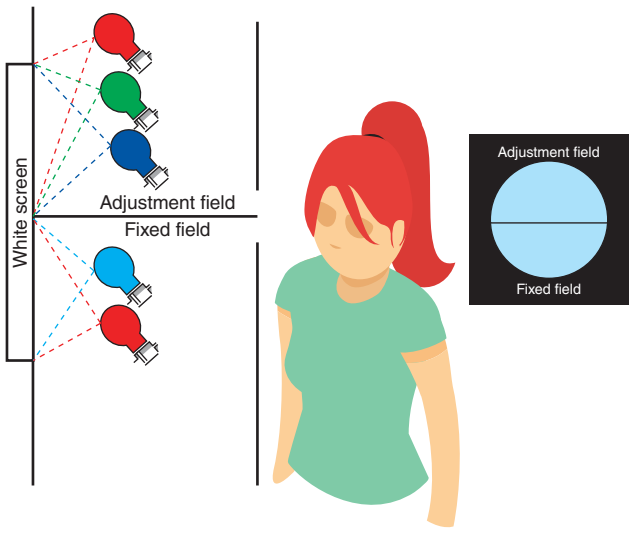

Figure 4.9 Visual colorimetric match of a greenish-blue light mixed with a moderate amount of the red primary.

Figure 4.10 Colors that result from adding red light to a greenish-blue light. Increasing the amount of red (moving left to right) reduces the chromatic intensity of the greenish-blue light.

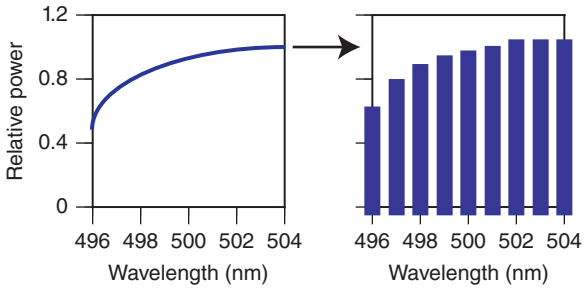

Figure 4.11 A continuous spectrum (on the left) can be thought of as a additive mixture of 1 nm lights.

follows the principles of algebra. She has also discovered a "trick" that can help her overcome the inability to select primaries that control each of the cone responses separately. Can you guess what it is?

When one is performing a color-matching experiment, the question arises as to what colors to match. Rather than thinking about a test light as a spectral power distribution with power that is continuous over the entire wavelength range, it is helpful to think of it as a combination of monochromatic (or nearly so) lights, each suitably weighted, shown in Figure 4.11. If 301 sources, each of equal radiance and of 1 nm width and centered at 400, 401 nm, and so on through 700 nm were simultaneously projected into the fixed field, they would produce a color that matches a continuous spectrum with equal radiance at each wavelength. Using this reasoning, every color stimulus can be thought of as a combination of light at individual wavelengths. Thus, it is sufficient to perform a color-matching experiment in which an observer matches the two fields at each wavelength. In practice, the experiment is performed at every 10 nm throughout the visible spectrum. Interpolation is used to estimate the 1 nm data.

Our industrious intern next builds a device that produces variable monochromatic light at constant spectral radiance, shown in Figure 4.12. As she varies its wavelength, she notices a large change in the brightness of each individual wavelength: green wavelengths appear much brighter than the other visible wavelengths. She decides to perform a brightness experiment in which the monochromatic light is set to 555 nm. Next, the blue primary in the adjustable field is varied (while the other primaries are turned off) until a brightness match is made. This is repeated for the green and red primaries. This type of experiment is called *heterochromatic brightness matching* and despite how difficult this visual task is to perform consistently, our intern found that about 50 times more radiance for the blue primary and about three times more radiance for the red primary were required to match the brightness at 555 nm. The green primary had similar radiance to 555 nm. That is, if all four lamps were adjusted to the same radiance and displayed next to one

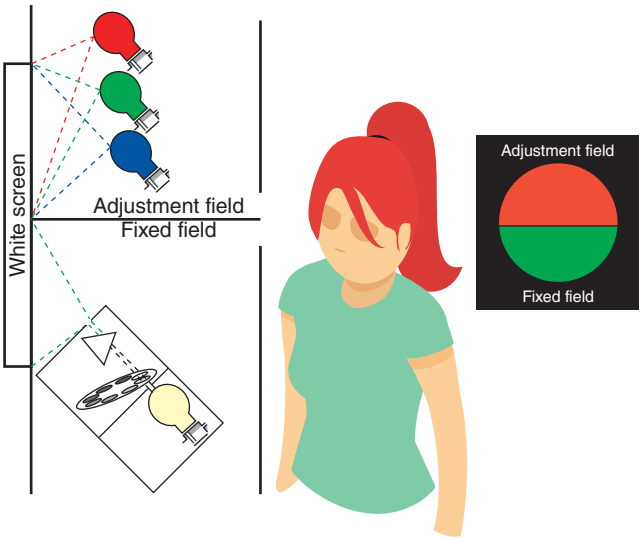

Figure 4.12 Visual colorimeter where the fixed field is a monochromatic light at constant radiance (achieved by using neutral-density filters). A heterochromatic match is made between the red primary and 555 nm.

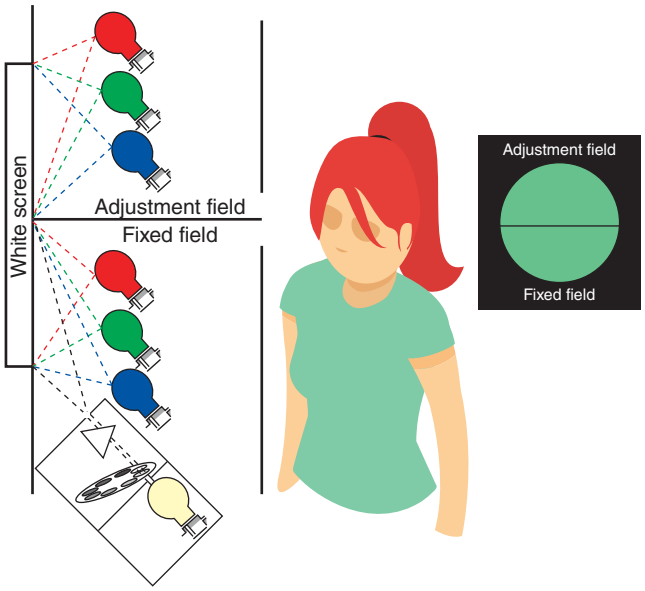

Figure 4.13 Visual colorimeter capable of measuring the amounts of the three primaries necessary to match the visible spectrum presented wavelength by wavelength.

another, the blue primary would appear the dimmest and 555 nm would appear the brightest. Recalling that our cone receptors reduce in sensitivity toward each end of the visible spectrum, these results are reasonable.

Having completed a number of experiments, including verifying Grassmann's laws and brightness matching, the student is ready to perform a color-matching experiment. The experimental task is determining the amounts of each primary necessary to match monochromatic light presented in succession throughout the visible spectrum. From her experiments verifying Grassmann's laws and a realization that monochromatic light has very high chromatic intensity, it is clear that she will have to use one or more of the primaries in the fixed field in order to reduce the chromatic intensity of the monochromatic light such that the two fields can be matched, shown in Figure 4.13. This "trick" enables the experiment to be completed.

Having to keep track of the amounts of each of the six primaries would be cumbersome. Instead, Grassmann's laws are used to define color matches with positive and negative quantities, essentially rearranging an algebraic equation. The results of the color-matching experiment performed by our intern are shown in Figure 4.14 as a plot in which the amounts of each primary are functions of wavelength. These curves are called *color-matching functions*. Notice that they have both positive and negative lobes. The negative lobes indicate the amounts of a given primary added to the fixed field. The net amounts of each primary required to match a color are called *tristimulus values*. Tristimulus values can be both positive and negative. At the end of the summer, the student is encouraged to apply for a PhD in color science.

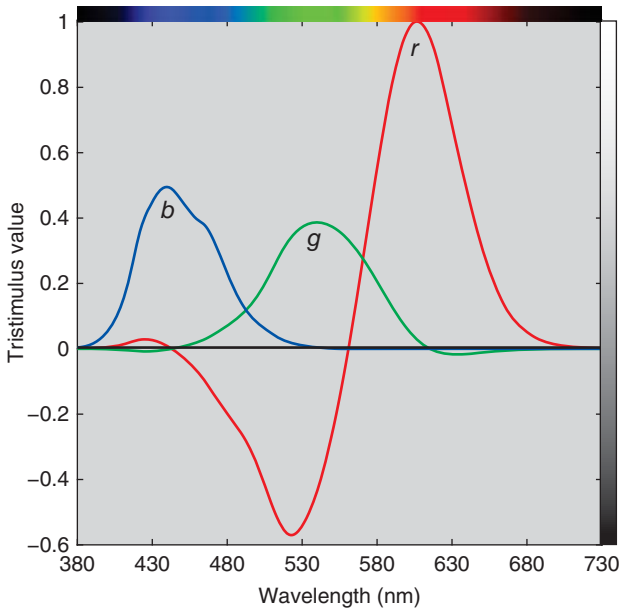

Figure 4.14 Color-matching functions that might result from using 440 nm (blue), 560 nm (green), and 620 nm (red). The amounts of each primary are called *tristimulus values*. The tristimulus values are scaled so the maximum tristimulus value is unity. Notice that the primaries are located where two of the color-matching functions have values of 0, not their peak values.

- *Tristimulus values:* The amounts of three specified stimuli required to match a color.

Intern's Color-Matching Functions

The summer intern is an invention of the author. Therefore, her color-matching functions were produced computationally. Her cone fundamentals were assumed to match the Smith and Pokorny data (1975), plotted in Figure 4.6. The first step was calculating a matrix containing the L, M, and S integrated responses for each primary displayed individually at unit amount, shown in Eq. (4.4):

$$\begin{pmatrix} L_R & L_G & L_B \\ M_R & M_G & M_B \\ S_R & S_G & S_B \end{pmatrix} = \begin{pmatrix} l_\lambda & \dots & l_\lambda \\ m_\lambda & \dots & m_\lambda \\ s_\lambda & \dots & s_\lambda \end{pmatrix} \begin{pmatrix} L_{\lambda,r} & \dots & L_{\lambda,r} \\ L_{\lambda,g} & \dots & L_{\lambda,g} \\ L_{\lambda,b} & \dots & L_{\lambda,b} \end{pmatrix}' \quad (4.4)$$

where L defines radiance and the prime superscript, $'$, denotes a matrix transpose.

The color-matching functions, r_λ, g_λ, and b_λ, are calculated as shown in Eq. (4.5)

$$\begin{pmatrix} r_\lambda & \cdots & r_\lambda \\ g_\lambda & \cdots & g_\lambda \\ b_\lambda & \cdots & b_\lambda \end{pmatrix} = \begin{pmatrix} L_R & L_G & L_B \\ M_R & M_G & M_B \\ S_R & S_G & S_B \end{pmatrix}^{-1} \begin{pmatrix} l_\lambda & \cdots & l_\lambda \\ m_\lambda & \cdots & m_\lambda \\ s_\lambda & \cdots & s_\lambda \end{pmatrix} \quad (4.5)$$

These calculations are a linear transformation between two coordinate systems, *LMS* and *RGB*, known as a *transformation of primaries*. This is considered in more detail in Section F.

The 1924 CIE Standard Photopic Observer

During the beginning of the twentieth century, it was noticed that physical measurements of the power of a light source (i.e. radiance or irradiance) correlated poorly with the source's visibility. Two lights that produced equal radiance often had very different brightnesses. Our intern found this out as well when comparing the brightness of each of her primaries (440, 560, and 620 nm) with 555 nm. Rather than perform heterochromatic brightness-matching experiments, known to be difficult and imprecise, a technique known as *flicker photometry* was used. In flicker photometry, the two lights are displayed alternately rather than simultaneously. The rate of flicker is set such that only the visual system's white opposed by black opponent channel is stimulated. (The opponent channels' temporal responses are similar to their spatial responses, described in Chapter 2.) The radiance of the test lamp is varied until flicker is minimized. Based on performing flicker photometry or heterochromatic brightness matching for each wavelength of the spectrum in comparison to results at a reference wavelength (such as 555 nm), a brightness-sensitivity function is derived. In 1923, Gibson and Tyndall compiled the results from a number of studies, about 200 observers in total. They calculated a weighted

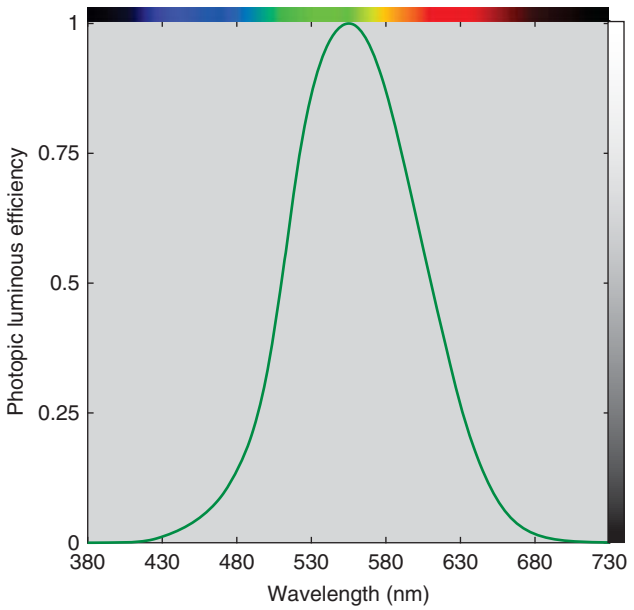

Figure 4.15 The 1924 CIE standard photometric observer. Observers are less *efficient* in converting radiance to visibility at each end of the visible spectrum in comparison to 555 nm.

average based on several criteria (see Kaiser 1981). In 1924, the CIE adopted Gibson and Tyndall's "visibility curve," known today as the *CIE standard photometric observer* or *luminous efficiency function*, plotted in Figure 4.15 and denoted by V_λ (CIE 1926, 2018).

The "brightness" of a source is calculated by multiplying its spectral properties by the V_λ function, wavelength by wavelength, followed by integration, and finally multiplying by a normalization constant, K_m, shown in Figure 4.16 and Eqs. (4.6) and (4.7)

$$L = K_m \int_\lambda L_\lambda V_\lambda \, d\lambda \quad (4.6)$$

$$E = K_m \int_\lambda E_\lambda V_\lambda \, d\lambda \quad (4.7)$$

The normalizing constant, K_m, equals 683 lm/W, known as the *maximum luminous efficacy*. A *lumen* is a quantity that weights light by the luminous efficiency function, V_λ. When a light source's spectral irradiance, E_λ, is measured, illuminance, E, has units of lux (lx, lumens per square meter). When spectral radiance, L_λ, is measured, luminance, L, has units of candelas per square meter (cd/m^2, or lumens per square meter per steradian). A candela is a unit of luminous intensity defined as 1/683 W/Sr. Illuminance is used to define the amount of light falling on a surface expressed as lux or *foot-candles* (fc, lumens per square foot). Foot-candles multiplied by 10.76 equals lux. Luminance is used to define the amount of light generated by a source. Essentially, luminance measurements are not dependent on distance; illuminance measurements are. See Wyszecki and

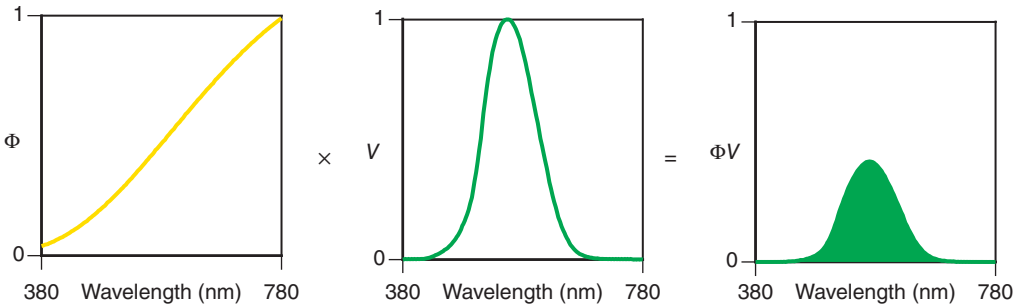

Figure 4.16 Photometric quantities are calculated by multiplying the stimulus, Φ_λ (generally expressed by irradiance or radiance), and the luminous efficiency function, V_λ, wavelength by wavelength, to give the curve $(\Phi V)_\lambda$. The area under this curve, suitably normalized, is the photometric quantity.

Stiles (1982) and McCluney (2014) for greater details on photometry and radiometry.

We have referred to brightness in quotations because of the large body of experimental evidence that indicates that a source's photometric measurement does not correlate with its perceived brightness (Kaiser 1981; Wyszecki and Stiles 1982; CIE 1988). A computer display appears much brighter in a darkened room than in one that is fully lit. If two lights are adjusted to have the same photometric quantity but one is highly chromatic while the other appears white, the chromatic source appears brighter. Despite the known limitations of photometry, it is still used extensively to define the level of illumination, and in other industrial applications as diverse as gloss and photographic film speed.

The 1931 CIE Standard Colorimetric Observer

Two experiments were performed during the 1920s in England that measured the color-matching functions of a small number of color-normal observers. Guild (1931) measured seven observers and Wright (1928, 1929) measured 10 observers. Both experiments employed the same viewing conditions, a bipartite field subtending a 2° field of view that was surrounded by darkness. In 1931 at a meeting of the Colorimetry Committee of the CIE, delegates representing a number of countries agreed to adopt a color-matching system based on the Guild and Wright experimental results. The committee concluded that the agreement was sufficiently close to provide both independent validation and reasonable population estimation. The average data were calculated based on a set of primaries that would provide excellent repeatability when building laboratory visual colorimeters. The primaries selected were 435.8, 546.1, and 700 nm. (In imaging, these are known as the *CIERGB primaries*.) The first two wavelengths correspond to two of the mercury emission lines. It was reasoned that 700 nm would stimulate only the long-wavelength receptor and therefore, small errors in setting this wavelength accurately would have a negligible effect on color matching. Another requirement

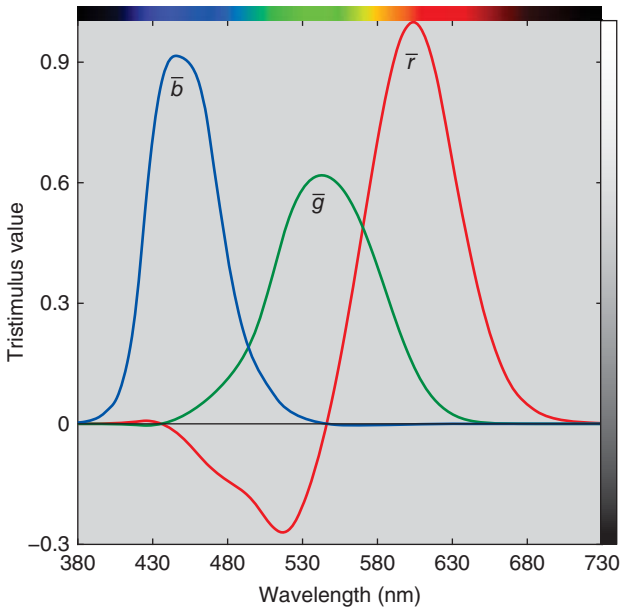

Figure 4.17 These curves are the *RGB color-matching functions* for the *CIE* 1931 *standard observer*, the average results of 17 color-normal observers matching each wavelength of the equal-energy spectrum with primaries of 435.8, 546.1, and 700 nm normalized to produce the color of the equal-energy spectrum at unit amounts.

when calibrating a colorimeter is defining the white that results from the admixture of the three primaries, each set to a unit amount. The white produced by an equal-energy light source was selected. This set of color-matching functions, shown in Figure 4.17 is known as $\bar{r}_\lambda$, $\bar{g}_\lambda$, and $\bar{b}_\lambda$. They define the *tristimulus values of the spectrum colors* for this particular set of primaries. The bar over each variable implies average, as in $\bar{x}$.

At this time period, the General Electric-Hardy Recording Spectrophotometer (Hardy 1929; Oil 1929) was near completion and soon to be marketed. This instrument produced an analog signal that traced an object's spectral

reflectance or transmittance. It was envisioned, correctly, that this signal could be interfaced with mechanical or electrical devices that would be used to perform tristimulus integrations. This would allow colorimetry to evolve from a visual system to a computational system. However, since the $\bar{r}_\lambda$, $\bar{g}_\lambda$, and $\bar{b}_\lambda$ color-matching functions all have both positive and negative tristimulus values, such devices would have to have six channels, greatly increasing their complexity and cost. If a second set of primaries was defined that resulted in all-positive color-matching functions, these devices could be built practically since only three channels would be required.

A second concern about $\bar{r}_\lambda$, $\bar{g}_\lambda$, and $\bar{b}_\lambda$ was also raised. Photometry using the visibility curve was already in use by the lighting industry. Since this system was based on different experimental techniques and a different set of observers, it was possible that two colors having the same tristimulus values could have different photometric values. Furthermore, for some applications, it might be necessary to calculate both colorimetric and photometric values — four integrations.

These two major concerns were alleviated by deriving an approximately linear transformation such that the color-matching functions were all positive and that one of the color-matching functions would be the 1924 CIE standard photometric observer function, V_λ. Having all-positive color-matching functions meant that the corresponding primaries would be physically nonrealizable. Variables *X*, *Y*, and *Z* were used for the new system to clarify that the primaries were not actual lights, resulting in color-matching functions labeled as $\bar{x}_\lambda$, $\bar{y}_\lambda$, and $\bar{z}_\lambda$, plotted in Figure 4.18.

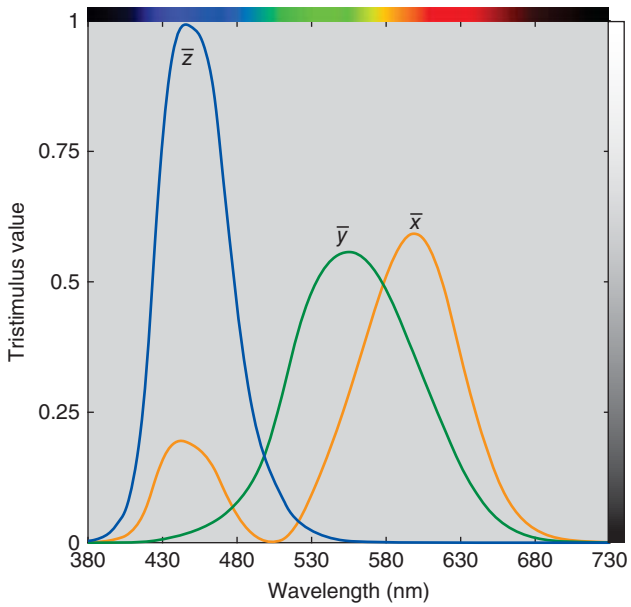

Figure 4.18 The *CIE XYZ 1931 standard colorimetric observer*.

These color-matching functions are known as the *CIE 1931 standard colorimetric observer*, or simply, the *standard observer*.

The details of how the transformation from $\bar{r}_\lambda$, $\bar{g}_\lambda$, $\bar{b}_\lambda$ to $\bar{x}_\lambda$, $\bar{y}_\lambda$, $\bar{z}_\lambda$ was derived can be found in Fairman, Brill, and Hemmendinger (1997, 1998). We will focus on several of them. First, $\bar{r}_\lambda$, $\bar{g}_\lambda$, and $\bar{b}_\lambda$, and V_λ were normalized to unit area as shown in Eq. (4.10)

$$\int_\lambda V_\lambda \, d\lambda = \int_\lambda \bar{r}_\lambda \, d\lambda = \int_\lambda \bar{g}_\lambda \, d\lambda = \int_\lambda \bar{b}_\lambda \, d\lambda = 1 \tag{4.10}$$

The $\bar{y}_\lambda$ color-matching function was arbitrarily defined to equal V_λ

$$\bar{y}_\lambda = V_\lambda \tag{4.11}$$

Ideally, $\bar{y}_\lambda$ is a linear combination of $\bar{r}_\lambda$, $\bar{g}_\lambda$, and $\bar{b}_\lambda$. Least squares (i.e. pseudo-inverse) was used to calculate the scalars of each color-matching function, shown in Eq. (4.12):

$$(0.176\,90 \;\; 0.812\,40 \;\; 0.010\,63) = \begin{pmatrix} V_\lambda & \dots & V_\lambda \end{pmatrix} \begin{pmatrix} \bar{r}_\lambda & \dots & \bar{r}_\lambda \\ \bar{g}_\lambda & \dots & \bar{g}_\lambda \\ \bar{b}_\lambda & \dots & \bar{b}_\lambda \end{pmatrix}^+ \tag{4.12}$$

where superscript + denotes pseudo-inverse. These scalars define the position of primary *Y*.

Because *Y* defines luminance, the other primaries are without luminance. This constrained the locations of primaries *X* and *Z* along a specific line. Two additional constraints were imposed to locate *X* and *Z* on this line. The first was to define the volume of the new *XYZ* space to just encompass the gamut of real colors. The second was to maximize the number of wavelengths where $\bar{z}_\lambda$ equaled zeroes. This resulted in the transformation matrix shown in Eq. (4.13)

$$M = \begin{pmatrix} 0.49 & 0.31 & 0.20 \\ 0.176\,97 & 0.812\,40 & 0.010\,63 \\ 0.00 & 0.01 & 0.99 \end{pmatrix} \tag{4.13}$$

Because there was a small amount of residual error in estimating $\bar{y}_\lambda$, color-matching functions $\bar{r}_\lambda$, $\bar{g}_\lambda$, and $\bar{b}_\lambda$ were first normalized by multiplying by n_λ such that $\bar{y}_\lambda$ was identical with V_λ. The final transformation is shown in Eqs. (4.14) and (4.15):

$$\begin{pmatrix} \bar{x}_\lambda & \dots & \bar{x}_\lambda \\ \bar{y}_\lambda & \dots & \bar{y}_\lambda \\ \bar{z}_\lambda & \dots & \bar{z}_\lambda \end{pmatrix} = \begin{pmatrix} 0.49 & 0.31 & 0.20 \\ 0.176\,97 & 0.812\,40 & 0.010\,63 \\ 0.00 & 0.01 & 0.99 \end{pmatrix} \bullet \begin{pmatrix} \bar{r}_\lambda & \dots & \bar{r}_\lambda \\ \bar{g}_\lambda & \dots & \bar{g}_\lambda \\ \bar{b}_\lambda & \dots & \bar{b}_\lambda \end{pmatrix} \begin{pmatrix} n_\lambda & & \\ & \ddots & \\ & & n_\lambda \end{pmatrix} \tag{4.14}$$

What is a Linear Transformation?

A linear transformation of primaries is a conversion from one set of coordinates to another set. This is done by rotating the axes from one set to another. We encounter this when using a GPS or mapping software to help direct us. The map is constantly rotating so that the direction we are driving is always upward. If we take a picture of something stationary, and then rotate the camera and reshoot, shown in Figure 4.19, the spatial relationships do not change, just how a specific position is defined.

One way to determine the required rotation is to locate the positions of each axis defined in the other coordinate system. Positions are defined at unit amounts, which are the locations of each primary. These positions are the coefficients of a matrix, the *transformation matrix*, shown in Eqs. (4.8) and (4.9) for two spaces: *ABC* and *DEF*

$$\begin{pmatrix} D \\ E \\ F \end{pmatrix} = \begin{pmatrix} D_{A=1,B=0,C=0} & D_{A=0,B=1,C=0} & D_{A=0,B=0,C=1} \\ E_{A=1,B=0,C=0} & E_{A=0,B=1,C=0} & E_{A=0,B=0,C=1} \\ F_{A=1,B=0,C=0} & F_{A=0,B=1,C=0} & F_{A=0,B=0,C=1} \end{pmatrix} \begin{pmatrix} A \\ B \\ C \end{pmatrix} \tag{4.8}$$

$$\begin{pmatrix} A \\ B \\ C \end{pmatrix} = \begin{pmatrix} D_{A=1,B=0,C=0} & D_{A=0,B=1,C=0} & D_{A=0,B=0,C=1} \\ E_{A=1,B=0,C=0} & E_{A=0,B=1,C=0} & E_{A=0,B=0,C=1} \\ F_{A=1,B=0,C=0} & F_{A=0,B=1,C=0} & F_{A=0,B=0,C=1} \end{pmatrix}^{-1} \begin{pmatrix} D \\ E \\ F \end{pmatrix} \tag{4.9}$$

(a) (b) (c)

Figure 4.19 Detail of Édouard Manet (French, 1832–1883), *Le Printemps (Jeanne Demarsy)*, 1881. Oil on canvas, 74 cm × 51.4 cm (29 1/8 in. × 20 1/4 in.). Los Angeles, J. Paul Getty Museum, 2014.62. The camera had two different orientations, the images shown in (a) and (b). Rotating image (b) counterclockwise, the images are aligned, shown in (c). The rotation is a linear transformation in two dimensions.

where

$$n_\lambda = V_\lambda/(0.176\,90\bar{r}_\lambda + 0.812\,40\bar{g}_\lambda + 0.010\,63\bar{b}_\lambda) \quad (4.15)$$

The *CIEXYZ system* with color-matching functions of $\bar{x}_\lambda$, $\bar{y}_\lambda$, and $\bar{z}_\lambda$ is often referred to as the 1931 *standard observer* or the 2° *observer* and is assumed to represent the color-matching results of the average of the human population having normal color vision and viewing stimuli with a 2° field of view. When we compare color-matching functions with cone fundamentals (e.g. Figure 4.6), it is clear that color-matching functions should not be referred to as the eye's spectral sensitivities. As we will show below, they can be referred to as linear transformations of the eye's spectral sensitivities.

The 1964 CIE Standard Colorimetric Observer

We describe in Chapter 2 how the structure of the eye is different in the central region of the retina, the fovea, than in the surrounding regions. The experiments leading to the 1931 CIE standard observer were performed using only the fovea, which covers about a 2° angle of view. Because of experimental limitations during the 1920s, it was much easier to produce uniform bipartite fields if they were kept small. Also, the light that could be generated by visual colorimetry was somewhat dim. Since the fovea does not contain rods, the resulting color-matching functions should be equally applicable for colors viewed at typical levels of illumination. That is, Grassmann's law of proportionality should be upheld.

However, there are a number of applications in which stimuli subtend a much larger field of view. The CIE encouraged experiments that would both determine whether the 2° observer would accurately predict matches for larger fields of view and validate the continued use of the 1931 standard observer.

During the 1950s Stiles, at the National Physical Laboratory in England, performed a pilot experiment in which 10 observers' color-matching functions were determined for both 2° and 10° fields of view. The two fields of view are compared in Figure 4.20. The CIE Colorimetry Committee concluded that for practical colorimetry, the 1931 standard observer was valid for small-field color matching; however, for large-field color matching, research should continue (Wyszecki and Stiles 1982).

Stiles and Burch (1959) measured the color-matching functions of 49 observers with a 10° field of view. Very high levels of illumination were used to minimize *rod intrusion* and further computations eliminated these nearly negligible rod effects. Speranskaya (1959) measured the color-matching functions of 27 observers, also with a 10° field of view, but at considerably lower levels of illumination. The CIE removed the effects of rod intrusion in Speranskaya's data and weight averaged the two data sets,

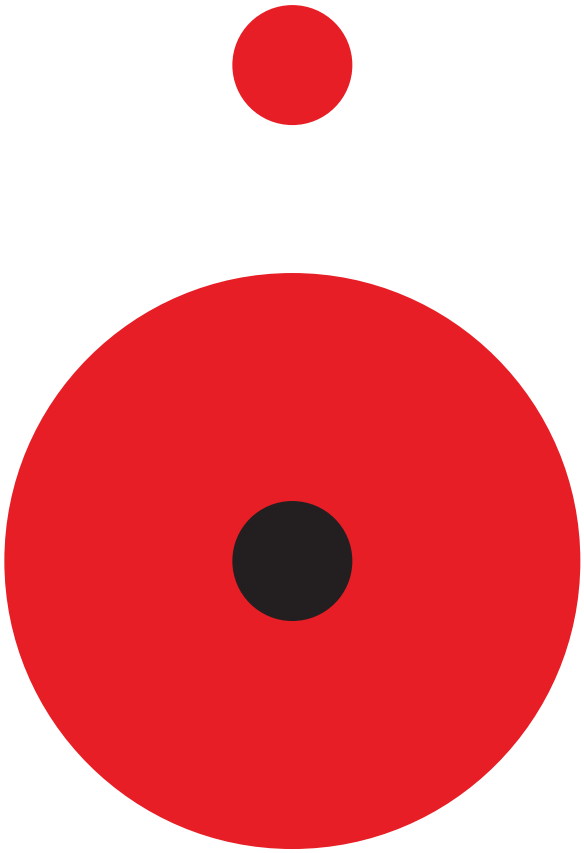

Figure 4.20 At a normal viewing distance of 0.5 m (19.7 in.), the circle on the top represents the 2° field on which the 1931 CIE standard observer is based. The figure on the bottom is the 10° field on which the 1964 CIE standard observer is based. The center of the 10° field is black to remind us that the 2° field was ignored (Stiles and Burch 1959) or masked (Speranskaya 1959) so that the central 2° was not included in the visual data.

resulting in the 1964 *CIE standard colorimetric observer* (Wyszecki and Stiles 1982; Trezona and Parkins 1998; CIE 2018). It is usually referred to as the *1964 standard observer* or the 10° *observer*. Its color-matching functions are notated as $\bar{x}_{\lambda,10}$, $\bar{y}_{\lambda,10}$, $\bar{z}_{\lambda,10}$ and compared with the 1931 standard observer in Figure 4.21. A word of warning: $\bar{y}_{\lambda,10}$ is not the same as $\bar{y}_\lambda$, or V_λ, and the corresponding tristimulus value Y_{10} does *not* directly represent a color's luminance. Its use is recommended whenever color-matching conditions exceed a 4° field of view.

- *Rod intrusion:* At low levels of illumination, rod receptors may not be fully desensitized, resulting in signals that *intrude* upon the cone signals. When this occurs, Grassmann's laws fail and a calculated match may not be a visual match.

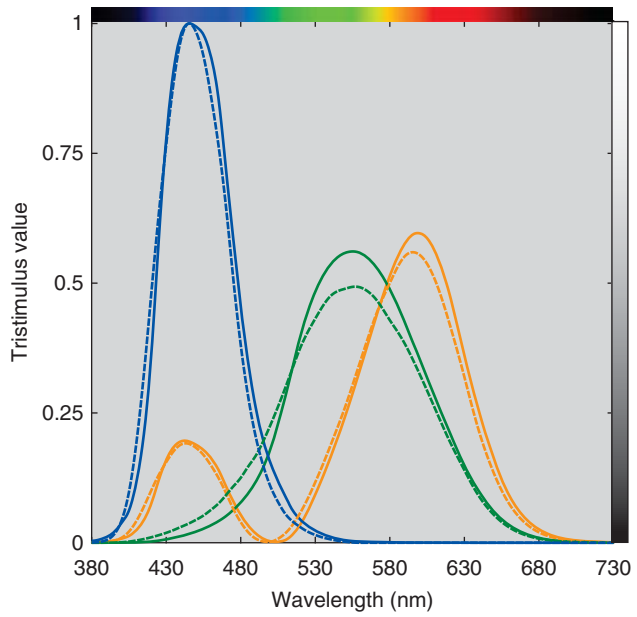

Figure 4.21 The color-matching functions $\bar{x}_\lambda$, $\bar{y}_\lambda$, and $\bar{z}_\lambda$ of the 1931 CIE standard colorimetric observer (solid lines) and $\bar{x}_{\lambda,10}$, $\bar{y}_{\lambda,10}$, and $\bar{z}_{\lambda,10}$ of the 1964 CIE standard colorimetric observer (dashed lines) are compared here.

Clearly, the 10° observer has a firmer statistical foundation since it is based on many more observers. Furthermore, large-field color matching has higher precision (Wyszecki and Stiles 1982). Anecdotally, it is often believed that the 10° observer correlates more closely with visual evaluations when judging the color difference within metameric pairs. However, this is likely observer dependent. Most industries that manufacture colored products use the 1964 standard observer. For imaging applications, the 1931 standard observer is used.

Cone-Fundamental-Based Colorimetric Observers

In Chapter 2, we describe that there is a range of color vision among color-normal observers. In 2006, the CIE published a model in which cone fundamentals can be calculated for average observers ranging in age from 21 to 80 years old and from a 1° to a 10° field of view (CIE 2006a). However, cone fundamentals are not all-positive color-matching functions. Work is underway by the CIE to provide a standard practice to convert cone fundamentals to the *XYZ* system, enabling the practical use of the 2006 CIE model. Thus far, matrices have been published that convert cone fundamentals for 32 years of age and either a 2° or 10° field of view, notated as $\bar{x}_{\lambda,F}$, $\bar{y}_{\lambda,F}$, $\bar{z}_{\lambda,F}$ and $\bar{x}_{\lambda,F,10}$, $\bar{y}_{\lambda,F,10}$, $\bar{z}_{\lambda,F,10}$, respectively. Both standard observers have color vision equivalent to the average population of 32-year-old color-normal observers. The transformations are shown in Eqs. (4.16) and (4.17), respectively (CIE 2018)

$$\begin{pmatrix} \bar{x}_{\lambda,F} & \cdots & \bar{x}_{\lambda,F} \\ \bar{y}_{\lambda,F} & \cdots & \bar{y}_{\lambda,F} \\ \bar{z}_{\lambda,F} & \cdots & \bar{z}_{\lambda,F} \end{pmatrix} = \begin{pmatrix} 1.947\,354\,69 & -1.414\,451\,23 & 0.364\,763\,27 \\ 0.689\,902\,72 & 0.348\,321\,89 & 0 \\ 0 & 0 & 1.934\,853\,43 \end{pmatrix} \bullet \begin{pmatrix} \bar{l}_{\lambda,2,32} & \cdots & \bar{l}_{\lambda,2,32} \\ \bar{m}_{\lambda,2,32} & \cdots & \bar{m}_{\lambda,2,32} \\ \bar{s}_{\lambda,2,32} & \cdots & \bar{s}_{\lambda,2,32} \end{pmatrix} \tag{4.16}$$

$$\begin{pmatrix} \bar{x}_{\lambda,F,10} & \cdots & \bar{x}_{\lambda,F,10} \\ \bar{y}_{\lambda,F,10} & \cdots & \bar{y}_{\lambda,F,10} \\ \bar{z}_{\lambda,F,10} & \cdots & \bar{z}_{\lambda,F,10} \end{pmatrix} = \begin{pmatrix} 1.939\,864\,43 & -1.346\,643\,59 & 0.430\,449\,35 \\ 0.692\,839\,32 & 0.349\,675\,67 & 0 \\ 0 & 0 & 2.146\,879\,45 \end{pmatrix} \bullet \begin{pmatrix} \bar{l}_{\lambda,10,32} & \cdots & \bar{l}_{\lambda,10,32} \\ \bar{m}_{\lambda,10,32} & \cdots & \bar{m}_{\lambda,10,32} \\ \bar{s}_{\lambda,10,32} & \cdots & \bar{s}_{\lambda,10,32} \end{pmatrix} \tag{4.17}$$

The 2° standard observer is based on the 1924 CIE standard photometric observer, as we described above. With time, it became clear that the weighting used by Gibson and Tyndall when deriving V_λ was in error, particularly in the short-wavelength region where visibility was underestimated. For full-spectrum lights, ignoring this error is inconsequential. Today, where stimuli can be narrow band such as LED lighting and laser primary digital projection, this error cannot be ignored. The 1931 standard observer and the 32 years of age and 2° field of view cone-fundamental observer are compared in Figure 4.22, showing the magnitude of error. When accurate photometric quantities are required, either the cone-fundamental or 1964 standard observer should be used.

C. CALCULATING TRISTIMULUS VALUES FOR MATERIALS

Tristimulus values for materials are calculated in a similar fashion to the *L*, *M*, and *S* integrated signals described in Chapter 2. The $\bar{x}_\lambda$, $\bar{y}_\lambda$, and $\bar{z}_\lambda$ color-matching functions replace cone fundamentals, the new formulas shown in Eqs. (4.18)–(4.21):

$$X = k \int_\lambda S_\lambda R_\lambda \bar{x}_\lambda \, d\lambda \tag{4.18}$$

$$Y = k \int_\lambda S_\lambda R_\lambda \bar{y}_\lambda \, d\lambda \tag{4.19}$$

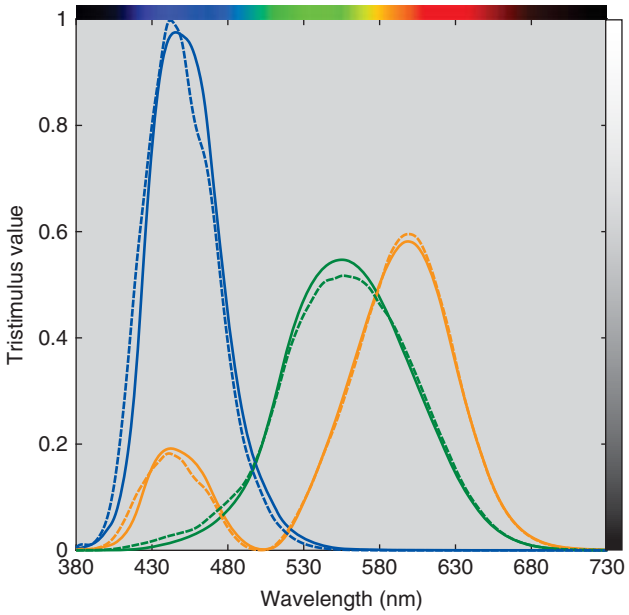

Figure 4.22 Comparison between the CIE 1931 standard colorimetric observer (solid lines) and the cone-fundamental-based colorimetric observer for 32 years of age and a 2° field of view (dashed lines).

$$Z = k \int_{\lambda} S_{\lambda} R_{\lambda} \bar{z}_{\lambda} \, d\lambda \tag{4.20}$$

$$k = {100} \Big/ \int_{\lambda} S_{\lambda} \bar{y}_{\lambda} \, d\lambda \tag{4.21}$$

where S_λ is a CIE standard illuminant, R_λ is an object's spectral-reflectance factor, and k is a normalizing constant such that Y for the perfect reflecting diffuser is 100. Tristimulus integration is visualized in Figure 4.23.

The CIE color-matching function data are an ISO standard and defined from 360 to 830 nm in 1 nm increments (ISO 2007a). The CIE has determined that a wavelength sampling of 380 to 780 nm with a 5 nm increment has sufficient accuracy when approximating integration with summation. For instruments sampling at larger increments, it is necessary to interpolate and extrapolate the missing values. The ASTM has published a method of calculating tristimulus values that incorporates both interpolation and extrapolation (ASTM 2015a). This method precalculates *tristimulus weights* for different instrument characteristics and is used by most instrument manufacturers. Weights are published for the most common instrument characteristics, CIE illuminants, and the 1931 and 1964 standard observers. A CIE technical committee is developing a recommendation and method for calculating tristimulus values in a similar fashion to ASTM. At the time of this writing, a CIE method has not been published.

The practice of normalizing tristimulus values to Y or $Y_{10} = 100$ for reflecting (and transmitting) materials is not universal. In many imaging applications, Y or $Y_{10} = 1$. In both cases, these are relative units and absolute appearance attributes of brightness and colorfulness cannot be determined. When using the 1931 system, the tristimulus value Y of an object is known as the *luminance factor*, or the *luminous reflectance* or the *luminous transmittance*, whichever is appropriate, and is expected to be related to the material's lightness.

> *Luminance factor:* Ratio of the luminance of an object, in the given direction, to that of the perfect reflecting or transmitting diffuser identically illuminated and viewed (CIE 2011). By definition, tristimulus value Y for objects is luminance factor. Sometimes, the ratio, Y/Y_n, is used to denote luminance factor in order to avoid ambiguity of the range of values.

The value $Y = 100$ (or 1), assigned to a perfect white object reflecting 100% at all wavelengths, or to the perfect colorless sample transmitting 100% at all wavelengths, is the maximum value that Y can have for nonfluorescent samples. There is no similar restriction to a maximum value of X or Z. Their values may be greater or less than *100* (or *1*). For example, when illuminant D65 and the 1931 standard observer are used, the values for the perfect white or colorless sample are approximately $X = 95$ and $Z = 109$. The exact values depend slightly on factors such as the choice of wavelength interval and method of tristimulus integration.

Fluorescent samples can have higher values of X, Y, and Z than those for the perfect white if what is measured is the total radiance factor.

D. CHROMATICITY COORDINATES AND THE CHROMATICITY DIAGRAM

Tristimulus values, as three variables, can be thought of as a three-dimensional space in which each axis is a primary $\mathscr{X}$, $\mathscr{Y}$, and $\mathscr{Z}$, and a sample's tristimulus values define a position within the three-dimensional space, shown in Figure 4.24. Recall that color-matching functions define the tristimulus values necessary to match each wavelength forming the equal-energy spectrum. When these tristimulus values are plotted three-dimensionally, they begin and end nearly at the origin, forming an unusual shape. A plane can be drawn through the three-space at a unit distance from the origin. Limiting this *unit plane* to the three axes results in an equilateral triangle. A line can be drawn beginning at the origin, passing through one of these tristimulus values, and ending on the triangular unit plane. Repeating for all the wavelengths of the color-matching functions results in a

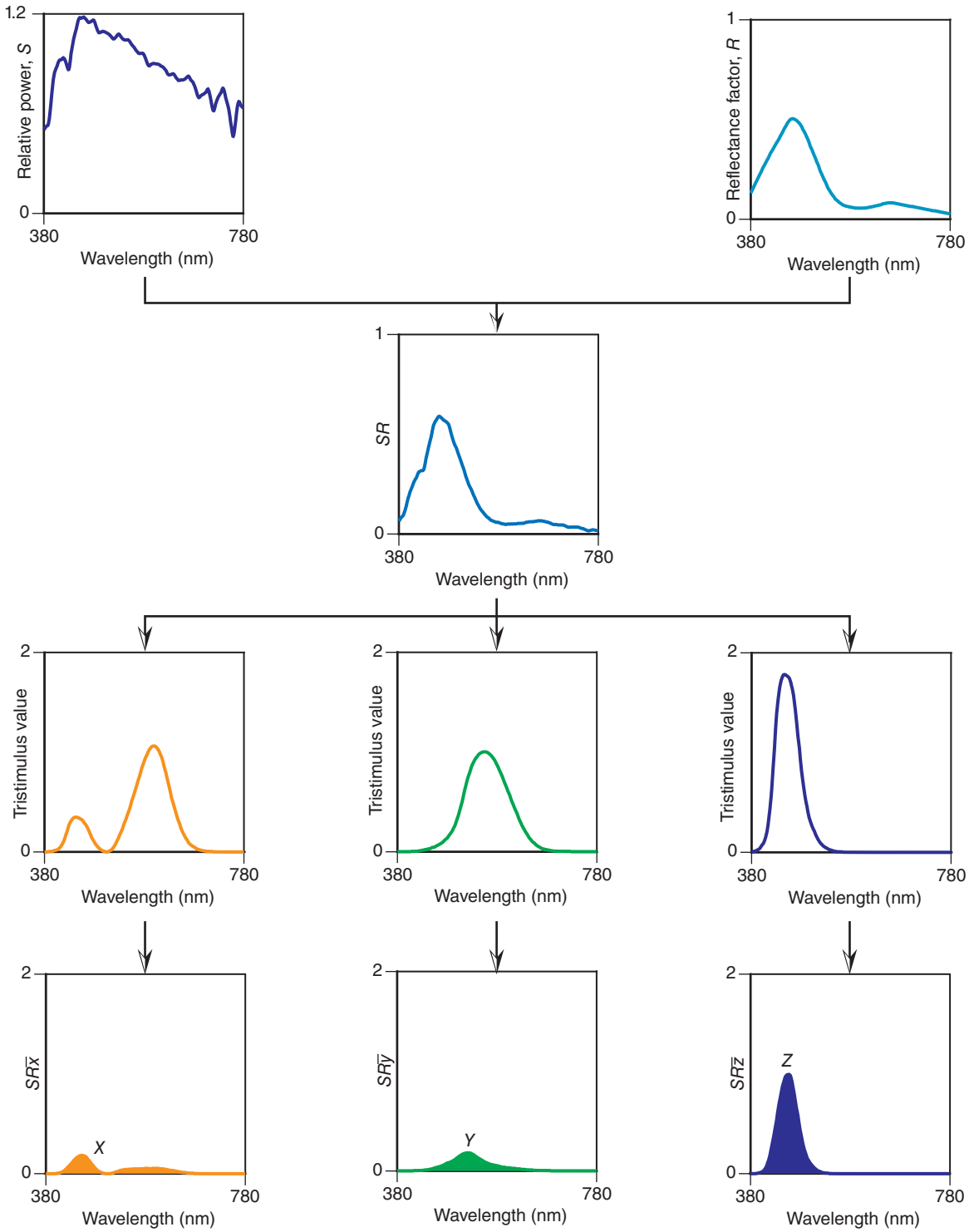

Figure 4.23 Here are all the spectral curves needed to calculate CIE tristimulus values *X, Y*, and *Z*. Wavelength by wavelength, the values of the curves of S_λ and R_λ are multiplied together to give the curve, $(SR)_\lambda$. Then this curve is multiplied, in turn, by $\bar{x}_\lambda$, by $\bar{y}_\lambda$, and by $\bar{z}_\lambda$ to obtain the curves $(SR\bar{x})_\lambda$, $(SR\bar{y})_\lambda$, and $(SR\bar{z})_\lambda$. The areas under these curves, followed by a normalization (not shown) are the tristimulus values *X*, *Y*, and *Z*.

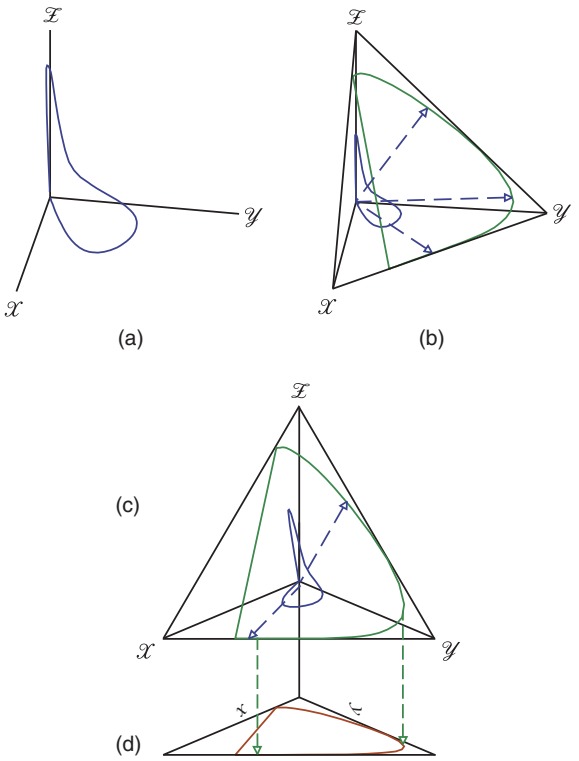

Figure 4.24 (a) CIE tristimulus space can be thought of as a three-dimensional space with axes, $\mathcal{X}$, $\mathcal{Y}$, and $\mathcal{Z}$ and coordinates X, Y, and Z. The tristimulus values of a set of color-matching functions plot as an unusual shape (blue line). (b) A unit plane is added to the three-space. Lines beginning at the origin, passing through each coordinate forming the color-matching function, and ending on the surface of the unit plane form a horseshoe shape (green line). A line is added between the shortest and longest wavelengths (also a green line). (c) A rotation of (b). (d) A projection of the unit plane looking down the Z-axis results in a *chromaticity diagram* with coordinates of lower-case x and y.

horseshoe shape. It is customary to add a line between the shortest and longest wavelengths. This is a projection from three dimensions onto a two-dimensional plane. A second projection is performed resulting in a right triangle. Again, a horseshoe shape emerges, known as the *spectrum locus*. The straight line is known as the *purple line*. The final projection is defined as a *chromaticity diagram*, having coordinates of lowercase x and y.

The formulas for projecting from X, Y, and Z to x, y, and z are shown in Eqs. (4.22)–(4.24)

$$x = \frac{X}{X+Y+Z} \tag{4.22}$$

$$y = \frac{Y}{X+Y+Z} \tag{4.23}$$

$$z = \frac{Z}{X+Y+Z} = 1 - x - y \tag{4.24}$$

Notice that chromaticity z can be calculated directly from x and y. Thus, there are only two independent variables. The projective transformation has transformed three variables into two variables. Looking at Eqs. (4.22)–(4.24), *magnitudes* of the tristimulus values are transformed into *ratios* of tristimulus values. Historically, color information that was independent of luminance (or luminance factor) was called chromaticness, hence the chromaticity diagram. *Chromaticities* should correlate to some extent with a stimulus's hue and chromatic intensity.

The *chromaticity coordinates* x, y, and z are obtained by taking the ratios of the tristimulus values to their sum, $(X+Y+Z)$. Since the sum of the chromaticity coordinates is 1 for any stimulus, they provide only two of the three coordinates needed to describe a color. One of the tristimulus values, usually Y, must also be specified. Notice that calculating tristimulus values from chromaticity coordinates, shown in Eqs. (4.25) and (4.26), requires knowing Y

$$X = \frac{x}{y}Y \tag{4.25}$$

$$Z = \frac{z}{y}Y = \frac{1-x-y}{y}Y \tag{4.26}$$

An alternative set of coordinates in the CIE system, sometimes called the *Helmholtz coordinates* of *dominant wavelength*, λ_d, and *excitation purity*, p_c, somewhat correlate with the visual aspects of hue and chromatic intensity, respectively, shown in Figure 4.25, although their steps and spacing are not visually uniform. The dominant wavelength of a color is the wavelength of the spectrum color whose

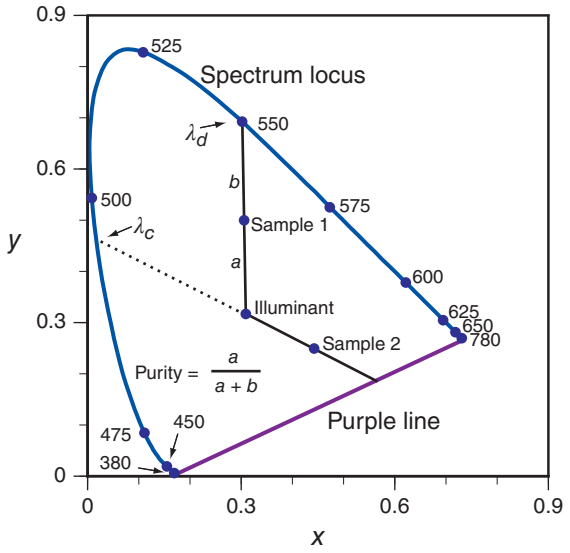

Figure 4.25 The definitions of dominant wavelength, complementary dominant wavelength, and purity are shown on this chromaticity diagram. These are also known as the Helmholtz coordinates.

chromaticity is on the same straight line as the sample point and the illuminant point. Excitation purity is the distance from illuminant point to sample point, divided by that from illuminant point to the spectrum locus. If the sample point lies between the illuminant point and the purple boundary connecting the ends of the spectrum locus, the construction is made between the illuminant point and the purple line and the wavelength is known as the *complementary dominant wavelength*, designated λ_c.

We are often asked where the $\mathcal{X}$, $\mathcal{Y}$, and $\mathcal{Z}$ primaries lie on the chromaticity diagram: the answer is at $x = 1$, $y = 0$; $x = 0$, $y = 1$; and $x = 0$, $y = 0$ (where $z = 1$), respectively. Like all other points outside the area bounded by the spectrum locus and the purple boundary, they do not represent real colors.

It is important to note that the CIE tristimulus system is not based on steps of equal visual perception in any sense, although many modifications have been proposed as approaches to equal perception. Indeed, the CIE tristimulus system is intended to do no more than tell whether two colors match (they match if they have the same tristimulus values, otherwise not). The CIE chromaticity diagram, likewise, is properly used only to tell whether two colors have the same chromaticities, not what they look like, or how they differ if they do not match. In fact, a given chromaticity can have a wide range of appearances depending on adaptation and viewing conditions. For example, Hunt (1976) has demonstrated how a chromaticity can appear sky blue or pink. In the demonstration of chromatic adaptation in Figure 2.6, the lemon has constant chromaticities although it appears yellowish or greenish. Coordinates of *XYZ*, or *xyY* should never be used as direct estimates of a color's appearance.

The lack of uniformity is often demonstrated by plotting Munsell colors in *xyY* as a rectangular three-space, shown in Figure 4.26 for the renotation colorimetric coordinates (Newhall, Nickerson, and Judd 1943) at Munsell value 3, 5, and 8. The hue loci are curved, the chroma contours are oblong, and the area encompassed reduces as value increases.

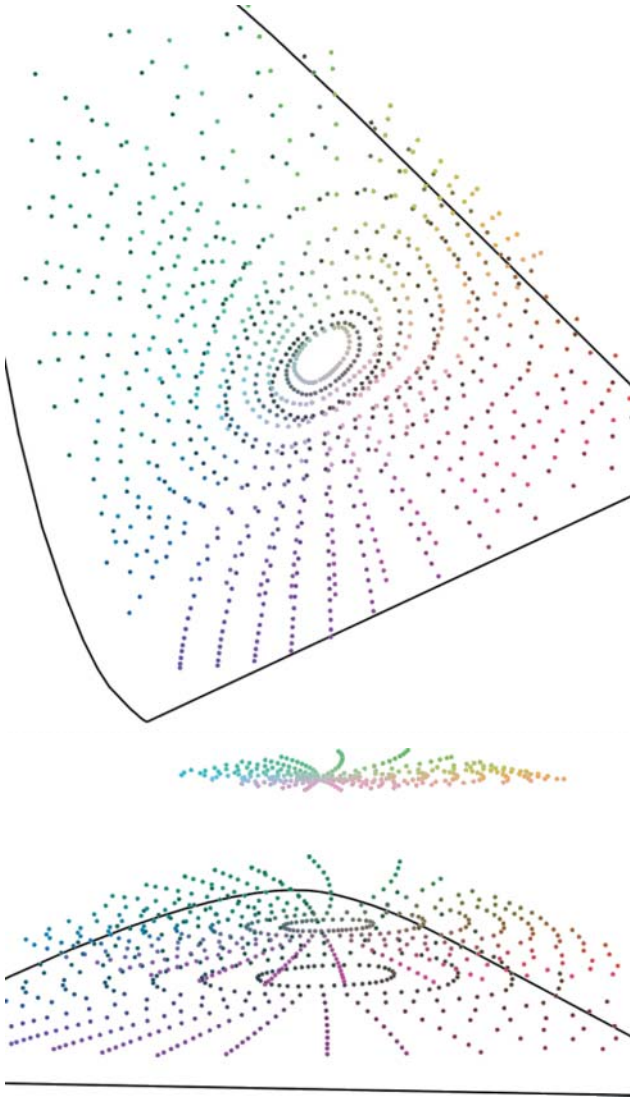

Figure 4.26 Munsell colors at value 3, 5, and 8 plotted in *xyY* at different orientations.

It is common to find chromaticity diagrams that have been colored, for example, in Figure 4.27. However, any set of inks used to produce the chart will not fully encompass the diagram. The same is true for a color display. The location of white is static; it should change with changes in the illuminant used when calculating tristimulus values. Furthermore, the third dimension of color, lightness, is not shown. Where is black, gray, or brown? In the third edition of this book, we suggested tearing up such diagrams. Because this is difficult to do when the colored chromaticity diagram is a displayed image, we urge our readers to remember the limitations of this diagram.

Only two of the three dimensions of color can be shown on a chromaticity diagram. Often, a three-dimensional CIE color space is made by plotting an axis of luminance factor, rising from the illuminant point of the chromaticity diagram. Only colors of very low luminance factor, such as spectrum colors, can lie as far away from the illuminant axis as the spectrum locus; all other colors have lower purity. The limits within which all nonfluorescent reflecting colors must lie have been calculated (Rösch 1929; MacAdam 1935) and are shown projected onto the plane of the chromaticity diagram in Figure 4.28. They serve to outline the volume within which all real nonfluorescent colors lie. Although Rösch predates MacAdam, these limits are known as the *MacAdam limits*.

Note that there is a significant difference in concept as well as in shape between the three-dimensional *xyY* space and color-order systems with uniform perceptual spacing. Both have white located at a single point on the top of an achromatic axis (e.g. Munsell value or NCS blackness).

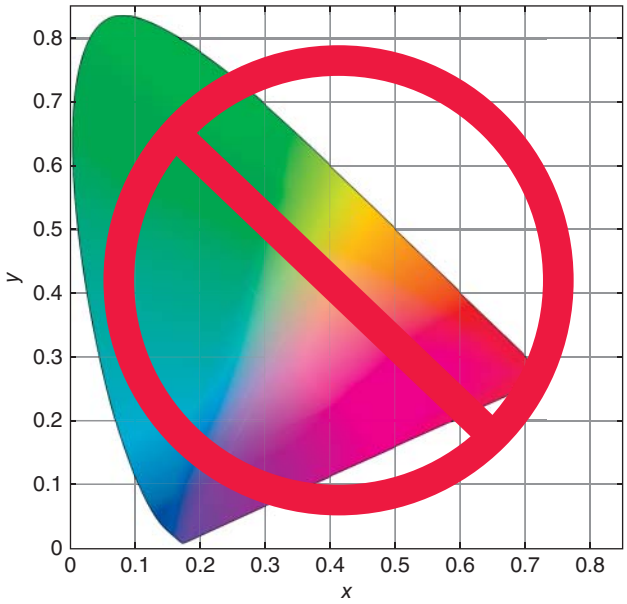

Figure 4.27 It is common to find chromaticity diagrams that have been colored. However, any set of inks used to produce the chart will not fully encompass the diagram. Furthermore, the third dimension of color, lightness, is not shown. Where is black, gray, or brown?

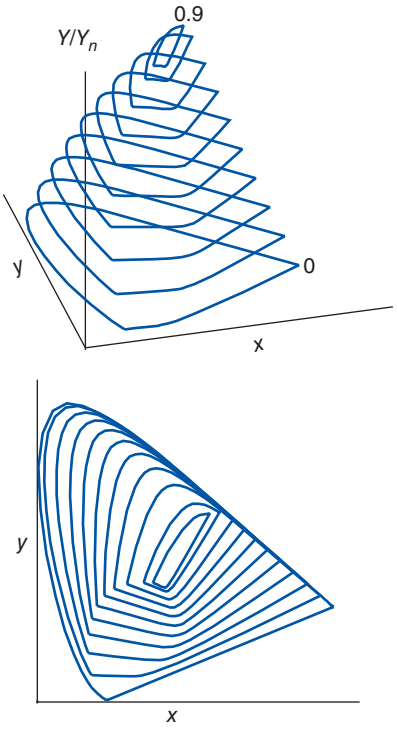

Figure 4.28 The MacAdam limits of surface colors calculated using the 1931 standard observer and CIE illuminant D65.

In a perceptual space, black is located at a single point at the bottom of the achromatic axis, as our perceptual senses tell us it should be. But in *xyY* space the location of black is not well defined, for it corresponds to all three tristimulus values *X*, *Y*, and *Z* equal to zero, and by the mathematical definitions of *x* and *y*, black can lie anywhere on the chromaticity diagram. This is but one of many examples supporting our earlier warning that one should not associate the appearance of colors with locations on the *x*, *y* diagram!

By this point you might feel that letters "*X*," "*Y*," and "*Z*" are overused and it is difficult to keep track of the differences. We agree! Here is a summary.

- $\mathcal{X}$, $\mathcal{Y}$, *and* $\mathcal{Z}$*:* Axes of a three-dimensional space with physically nonrealizable primaries.
- *X, Y, and Z:* Coordinates of each axis. These are tristimulus values representing the amounts of their respective primaries.
- $\bar{x}_\lambda$, $\bar{y}_\lambda$, *and* $\bar{z}_\lambda$*:* Tristimulus values of each wavelength defining the equal energy spectrum. These are known as color-matching functions.
- *x, y, and z:* Chromaticity coordinates. Normally only *x* and *y* are recorded. They are ratios of the amounts of the three tristimulus values.
- *x, y, and Y:* Defining a color of a reflecting or transmitting material by a combination of chromaticities and luminance factor.
- *x, y, and L:* Defining a colored light by a combination of chromaticities and luminance.

E. CALCULATING TRISTIMULUS VALUES AND CHROMATICITY COORDINATES FOR SOURCES

We have shown that calculating the tristimulus values of a color requires knowledge of the source, object, and observer. This is true for materials that reflect or transmit light interacting with them.

There are many colors that are not materials, such as lights and displays. When calculating their tristimulus values, the spectral-reflectance factor is not included in the tristimulus-integration equations. Furthermore, the convention of normalizing *Y* such that it equals 100 or 1 is generally not used. Instead, photometric units are used, for which the normalizing constant in the tristimulus equations, *k*, equals 683 lm/W, known as the *maximum luminous efficacy* with K_m replacing *k*, shown in Eqs. (4.27)–(4.29):

$$X = K_m \int_\lambda \Phi_\lambda \bar{x}_\lambda \, d\lambda \tag{4.27}$$

$$Y = K_m \int_\lambda \Phi_\lambda \bar{y}_\lambda \, d\lambda \tag{4.28}$$

$$Z = K_m \int_\lambda \Phi_\lambda \bar{z}_\lambda \, d\lambda \tag{4.29}$$

where Φ_λ is either spectral irradiance, E_λ, or spectral radiance, L_λ.

Devices that measure the colorimetric values of sources, such as spectroradiometers and colorimeters, do not report *X*, *Y*, *Z,* rather they report *x, y, Y*. This separates the chromatic and achromatic information, since these two parameters can easily be varied independently. Tristimulus value *Y* has units of either lx (from irradiance) or cd/m^2 (from radiance).

- *Luminous:* Weighted according to the spectral luminous efficiency function, V_λ of the CIE.
- *Luminance:* Luminous flux in a beam, emanating from a surface, or falling on a surface, in a given direction, per unit of projected area of the surface as viewed from that direction, per unit solid angle.
- *Illuminance:* Luminous flux incident per unit of area.
- *Lumen:* Luminous flux emitted within one steradian by a point source having a spatially uniform luminous intensity of 1 cd.

F. TRANSFORMATION OF PRIMARIES

Displays

The spectral radiance measurements of each primary of an LED backlight liquid-crystal display, each at six different levels, are shown in Figure 4.29. Each primary has similar spectral characteristics. The relationship between these spectra is defined in Eqs. (4.30)–(4.32):

$$L_{\lambda,r} = RL_{\lambda,r\,\max} \tag{4.30}$$

$$L_{\lambda,g} = GL_{\lambda,g\,\max} \tag{4.31}$$

$$L_{\lambda,b} = BL_{\lambda,b\,\max} \tag{4.32}$$

where *R, G*, and *B* are scalars modulating the intensity of each primary between zero and maximum. This property is known as *scalability*.

The relationship between spectral radiance and tristimulus values is linear, shown in Eqs. (4.33)–(4.35) for the red primary. Similar equations can be written for the green and blue primaries

$$X_r = K_m \int_\lambda RL_{\lambda,r\,\max} \bar{x}_\lambda \, d\lambda \tag{4.33}$$

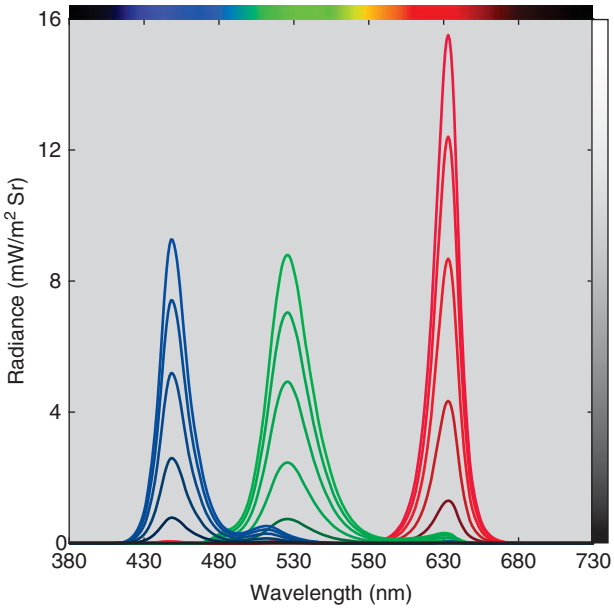

Figure 4.29 Spectral radiance of each primary of an LED backlight liquid-crystal display, each at six different intensities between zero and maximum.

$$Y_r = K_m \int_\lambda RL_{\lambda,r\,\max} \bar{y}_\lambda \, d\lambda \tag{4.34}$$

$$Z_r = K_m \int_\lambda RL_{\lambda,r\,\max} \bar{z}_\lambda \, d\lambda \tag{4.35}$$

Linearity between *R* and *XYZ*, *G* and *XYZ*, and *B* and *XYZ*, where *RGB* is defined using Eqs. (4.30)–(4.32), means that the tristimulus values of each primary define a line in the $\mathcal{X}\,\mathcal{Y}\,\mathcal{Z}$ three-space, shown in Figure 4.30.

A second aspect to explore is whether the sum of individual measurements of the three primaries is identical to a measurement of the three primaries displayed simultaneously, shown in Eq. (4.36)

$$L_\lambda = L_{\lambda,r} + L_{\lambda,g} + L_{\lambda,b} \tag{4.36}$$

This is verified experimentally, sampling the display's color gamut. This property is known as *additivity*.

A simple way to analyze scalability and additivity is to plot the chromaticities based on measurements of each primary at several intensities and their sum, producing a gray scale. There should be four points, one for each primary and one for the neutral. This is shown for two displays in Figure 4.31, one that is scalable and additive and one that is not.

For the display that is scalable and additive, also known as having *stable primaries*, we can predict tristimulus values for any color combination from measuring the spectral radiance of each primary, that is, three measurements. This

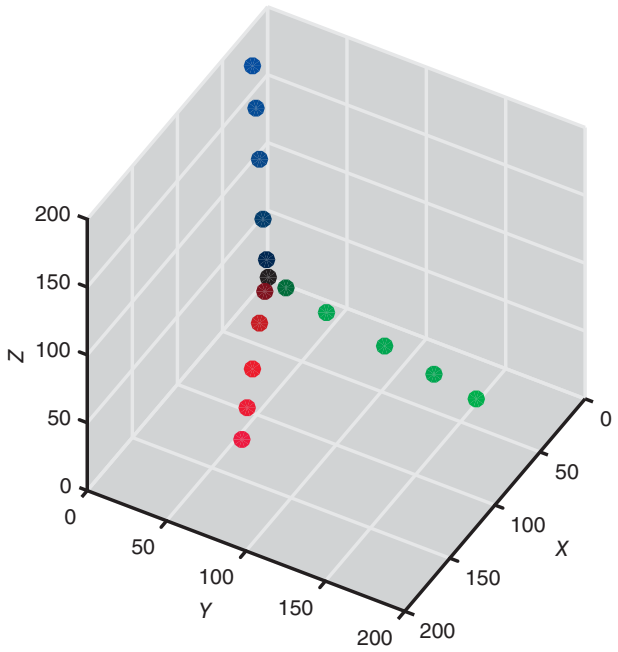

Figure 4.30 Tristimulus values of the spectra plotted in Figure 4.29 plotted in *XYZ* three-space. *XYZ* have units of cd/m^2.

is shown in Eq. (4.37)

$$\begin{pmatrix} X \\ Y \\ Z \end{pmatrix} = \begin{pmatrix} X_{r\,\max} & X_{g\,\max} & X_{b\,\max} \\ Y_{r\,\max} & Y_{g\,\max} & Y_{b\,\max} \\ Z_{r\,\max} & Z_{g\,\max} & Z_{b\,\max} \end{pmatrix} \begin{pmatrix} R \\ G \\ B \end{pmatrix} \tag{4.37}$$

The white point of the display, X_n, Y_n, and Z_n, is calculated by setting the display to $R = G = B = 1$, shown in Eq. (4.38)

$$\begin{pmatrix} X_n \\ Y_n \\ Z_n \end{pmatrix} = \begin{pmatrix} X_{r\,\max} & X_{g\,\max} & X_{b\,\max} \\ Y_{r\,\max} & Y_{g\,\max} & Y_{b\,\max} \\ Z_{r\,\max} & Z_{g\,\max} & Z_{b\,\max} \end{pmatrix} \begin{pmatrix} 1 \\ 1 \\ 1 \end{pmatrix} \tag{4.38}$$

Each primary's chromaticities remain stable for any setting. Accordingly, the primary tristimulus matrix can be expanded into a product of a chromaticity matrix and a luminance matrix, shown in Eq. (4.39) for a display's white point, expressed by chromaticities and peak luminance

$$\begin{pmatrix} (x_n/y_n)L_n \\ L_n \\ (z_n/y_n)L_n \end{pmatrix} = \begin{pmatrix} (x_r/y_r) & (x_g/y_g) & (x_b/y_b) \\ 1 & 1 & 1 \\ (z_r/y_r) & (z_g/y_g) & (z_b/y_b) \end{pmatrix} \bullet \begin{pmatrix} L_{r\,\max} & 0 & 0 \\ 0 & L_{g\,\max} & 0 \\ 0 & 0 & L_{b\,\max} \end{pmatrix} \begin{pmatrix} 1 \\ 1 \\ 1 \end{pmatrix} \tag{4.39}$$

By rearranging Eq. (4.39), the luminance of each channel can be calculated for any desired white point, shown in Eq. (4.40)

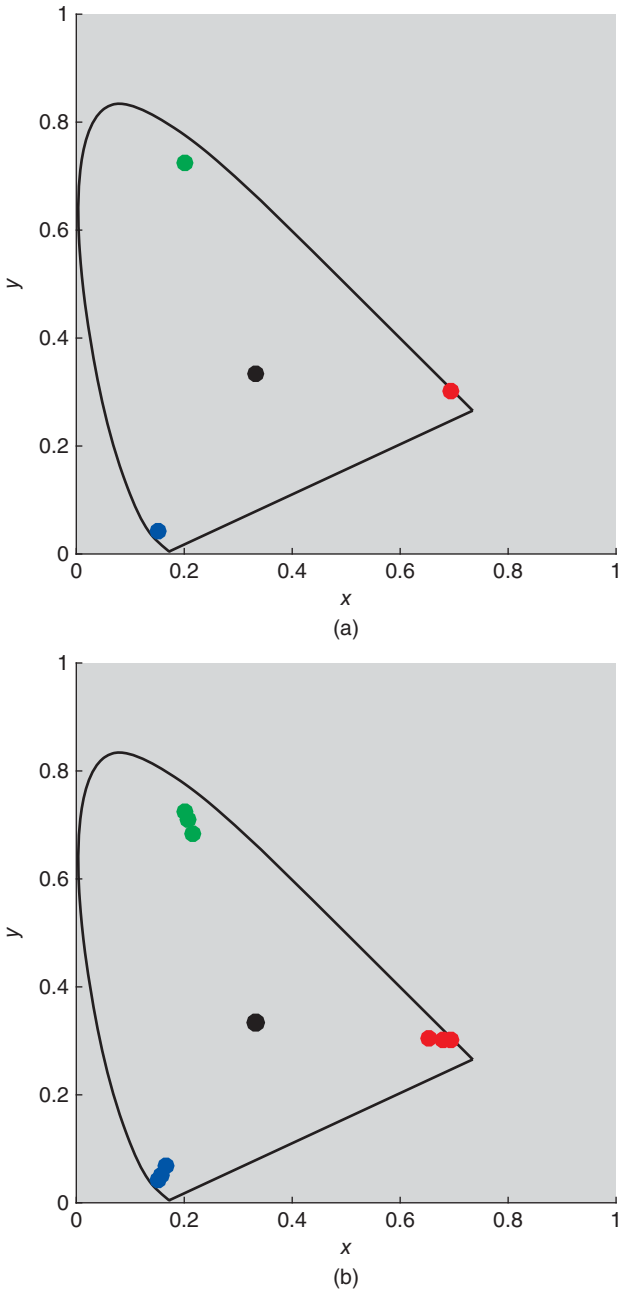

Figure 4.31 LED backlight liquid-crystal display with either (a) stable primaries, or (b) unstable primaries. The instability was caused by backlight leakage.

$$\begin{pmatrix} L_{r\,\max} & 0 & 0 \\ 0 & L_{g\,\max} & 0 \\ 0 & 0 & L_{b\,\max} \end{pmatrix} \begin{pmatrix} 1 \\ 1 \\ 1 \end{pmatrix} = \begin{pmatrix} (x_r/y_r) & (x_g/y_g) & (x_b/y_b) \\ 1 & 1 & 1 \\ (z_r/y_r) & (z_g/y_g) & (z_b/y_b) \end{pmatrix}^{-1} \begin{pmatrix} (x_n/y_n)L_n \\ L_n \\ (z_n/y_n)L_n \end{pmatrix} \tag{4.40}$$

Usually, the luminance ratio is specified. By defining $L_n = 1$ and performing the multiplication on the left-hand

side of Eq. (4.40), the luminances of each channel are calculated, shown in Eq. (4.41)

$$\begin{pmatrix} L_{r\,\max} \\ L_{g\,\max} \\ L_{b\,\max} \end{pmatrix} = \begin{pmatrix} (x_r/y_r) & (x_g/y_g) & (x_b/y_b) \\ 1 & 1 & 1 \\ (z_r/y_r) & (z_g/y_g) & (z_b/y_b) \end{pmatrix}^{-1} \begin{pmatrix} (x_n/y_n) \\ 1 \\ (z_n/y_n) \end{pmatrix} \quad (4.41)$$

Finally, the tristimulus matrix is calculated as shown in Eq. (4.42)

$$\begin{pmatrix} X_{r\,\max} & X_{g\,\max} & X_{b\,\max} \\ Y_{r\,\max} & Y_{g\,\max} & Y_{b\,\max} \\ Z_{r\,\max} & Z_{g\,\max} & Z_{b\,\max} \end{pmatrix} = \begin{pmatrix} (x_r/y_r) & (x_g/y_g) & (x_b/y_b) \\ 1 & 1 & 1 \\ (z_r/y_r) & (z_g/y_g) & (z_b/y_b) \end{pmatrix} \begin{pmatrix} L_{r\,\max} & 0 & 0 \\ 0 & L_{g\,\max} & 0 \\ 0 & 0 & L_{b\,\max} \end{pmatrix} \quad (4.42)$$

Calculating Color-Matching Functions for a Display

Suppose that we are interested in performing a color-matching experiment using the display described above. We want to set up the display to have a white point of illuminant E. The chromaticities of this display and illuminant E are listed in Table 4.1.

The first step is to calculate the chromaticity matrix, shown in Eq. (4.43)

$$\begin{pmatrix} (x_r/y_r) & (x_g/y_g) & (x_b/y_b) \\ 1 & 1 & 1 \\ (z_r/y_r) & (z_g/y_g) & (z_b/y_b) \end{pmatrix} = \begin{pmatrix} 2.31 & 0.28 & 3.52 \\ 1.00 & 1.00 & 1.00 \\ 0.02 & 0.10 & 18.79 \end{pmatrix} \quad (4.43)$$

Next, the chromaticity matrix is inverted, shown in Eq. (4.44)

$$\begin{pmatrix} (x_r/y_r) & (x_g/y_g) & (x_b/y_b) \\ 1 & 1 & 1 \\ (z_r/y_r) & (z_g/y_g) & (z_b/y_b) \end{pmatrix}^{-1} = \begin{pmatrix} 0.49 & -0.13 & -0.09 \\ -0.49 & 1.13 & 0.03 \\ 0.00 & -0.01 & 0.05 \end{pmatrix} \quad (4.44)$$

Equation (4.39) is used to calculate the luminances of each channel, shown in Eq. (4.45)

$$\begin{pmatrix} 0.28 \\ 0.67 \\ 0.05 \end{pmatrix} = \begin{pmatrix} 0.49 & -0.13 & -0.09 \\ -0.49 & 1.13 & 0.03 \\ 0.00 & -0.01 & 0.05 \end{pmatrix} \begin{pmatrix} (0.33/0.33)1 \\ 1 \\ (0.33/0.33)1 \end{pmatrix} \quad (4.45)$$

Table 4.1 Chromaticities of the LED backlight LCD display and illuminant E.

	x	y
Red	0.6934	0.3004
Green	0.2021	0.7255
Blue	0.1512	0.0429
White	0.3333	0.3333

Equation (4.40) is used to calculate the tristimulus matrix, shown in Eq. (4.46)

$$\begin{pmatrix} X_{r\,\max} & X_{g\,\max} & X_{b\,\max} \\ Y_{r\,\max} & Y_{g\,\max} & Y_{b\,\max} \\ Z_{r\,\max} & Z_{g\,\max} & Z_{b\,\max} \end{pmatrix} = \begin{pmatrix} 0.64 & 0.19 & 0.17 \\ 0.28 & 0.67 & 0.05 \\ 0.01 & 0.07 & 0.93 \end{pmatrix} \quad (4.46)$$

Color-matching functions for this display are calculated using Eqs. (4.47) and (4.48). The normalization results in the maximum luminance achievable by this display. The color-matching functions for this display are plotted in Figure 4.32. Comparing this set of color-matching functions with those shown in Figures 4.14 and 4.17 reveals that the choice of primaries has a large effect on the corresponding color-matching functions

$$\begin{pmatrix} r_\lambda & \dots & r_\lambda \\ g_\lambda & \dots & g_\lambda \\ b_\lambda & \dots & b_\lambda \end{pmatrix} = \begin{pmatrix} 0.64 & 0.19 & 0.17 \\ 0.28 & 0.67 & 0.05 \\ 0.01 & 0.07 & 0.93 \end{pmatrix}^{-1} \begin{pmatrix} \bar{x}_\lambda & \dots & \bar{x}_\lambda \\ \bar{y}_\lambda & \dots & \bar{y}_\lambda \\ \bar{z}_\lambda & \dots & \bar{z}_\lambda \end{pmatrix} \quad (4.47)$$

$$\begin{pmatrix} r_{\lambda,\text{norm}} & \cdots & r_{\lambda,\text{norm}} \\ g_{\lambda,\text{norm}} & \cdots & g_{\lambda,\text{norm}} \\ b_{\lambda,\text{norm}} & \cdots & b_{\lambda,\text{norm}} \end{pmatrix} = \begin{pmatrix} r_\lambda & \cdots & r_\lambda \\ g_\lambda & \cdots & g_\lambda \\ b_\lambda & \cdots & b_\lambda \end{pmatrix} \cdot$$

$$\begin{pmatrix} 1/\max(r_\lambda, g_\lambda, b_\lambda) & 0 & 0 \\ 0 & 1/\max(r_\lambda, g_\lambda, b_\lambda) & 0 \\ 0 & 0 & 1/\max(r_\lambda, g_\lambda, b_\lambda) \end{pmatrix} \quad (4.48)$$

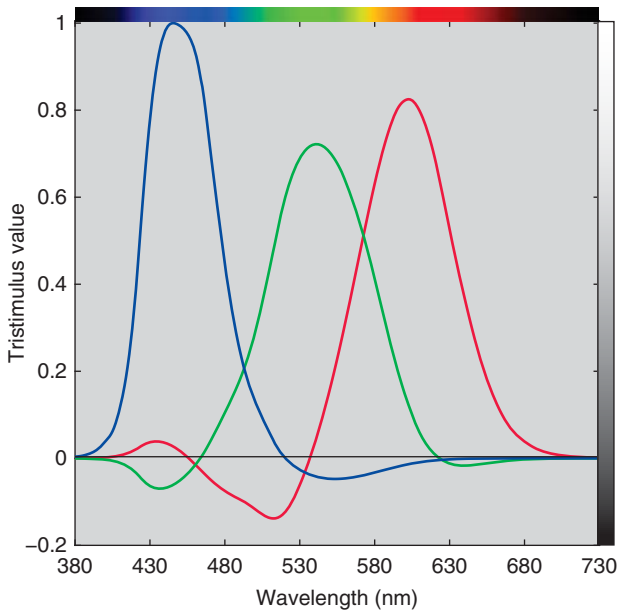

Figure 4.32 Color-matching functions for LED backlight liquid-crystal display with colorimetric properties listed in Table 4.1. The tristimulus values are normalized such that the maximum of all three primaries is defined as unity.

Cone Fundamentals

Thus far, we have used the well-established (Smith and Pokorny 1975) cone fundamentals when plotting the eye's spectral sensitivities. However, these fundamentals are not linear transformations of CIE color-matching functions as shown above in Figure 4.22 and there are a number of applications where LMS functions that are linear transformations of CIE color-matching functions are useful. The set derived by Hunt and Pointer (1985) based on research by Estevez on color-defective vision is in most common use, known as the *HPE cone fundamentals*. The transformation matrix is given in Eq. (4.49) and the cone fundamentals compared with the Smith and Pokorny set are plotted in Figure 4.33

$$\begin{pmatrix} l_{\lambda\text{HPE}} & \dots & l_{\lambda\text{HPE}} \\ m_{\lambda\text{HPE}} & \dots & m_{\lambda\text{HPE}} \\ s_{\lambda\text{HPE}} & \dots & s_{\lambda\text{HPE}} \end{pmatrix} = \begin{pmatrix} 0.38971 & 0.68898 & -0.07868 \\ -0.22981 & 1.18340 & 0.04641 \\ 0 & 0 & 1 \end{pmatrix} \bullet \begin{pmatrix} \bar{x}_\lambda & \dots & \bar{x}_\lambda \\ \bar{y}_\lambda & \dots & \bar{y}_\lambda \\ \bar{z}_\lambda & \dots & \bar{z}_\lambda \end{pmatrix} \tag{4.49}$$

G. APPROXIMATELY UNIFORMLY SPACED SYSTEMS

It has often been said that one of the greatest disadvantages of the CIE tristimulus or chromaticity systems is that they are far from equally visually spaced. But why should they be, since neither is meant to give any information about the appearance of colors? In fact, we would be shocked if tristimulus space or the *xy* projection were equally visually spaced given that the primaries were arbitrary, having been defined to overcome engineering limitations during 1931. If the tristimulus values recorded cone responses, it would be reasonable to expect better visual correlation.

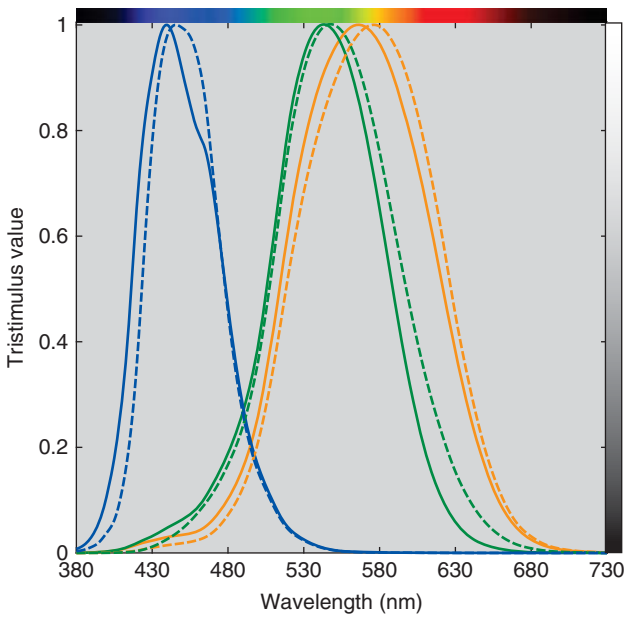

Figure 4.33 The Smith and Pokorny (solid lines) and HPE (dashed lines) cone fundamentals.

Between 1931 and today (we feel confident that whenever this book is read, this statement will still be valid), color scientists and engineers have developed and continue to develop new color spaces with the goal of providing uniform visual spacing and correlation with color perception.

Why is this task so difficult? Given the computational tools at our disposal today, it should be possible to find a new color space that achieves these goals. However, several factors work against us. First, visual data are inherently highly variable, that is, noisy. It is often difficult to separate consistent trends from random noise. Second, color perception is very complex with many factors affecting judgments. In order to develop a color space with general applicability to all industries, experiments must be performed in which each factor is studied separately and analyzed in comparison to a set of baseline factors. Despite the importance of this step, there has been insufficient effort to generate this knowledge.

Despite these difficulties, progress has been made. During the twentieth century, the problem was reduced in complexity by focusing on developing color spaces that had reasonable performance for quantifying color differences between pairs of samples not too different in color. That is, the difference in color coordinates for the sample pair correlated with their perceived difference in color. All the factors affecting discrimination, such as color and level of illumination, sample size, sample texture, sample separations, and so on (CIE 1993) were assumed to have a negligible effect on this correlation. Ideally, samples were compared if and only if their physical properties were identical and illuminated and viewed identically. Complexity was also reduced by assuming that lightness and chromaticness (i.e. hue and chromatic intensity) were independent perceptually. Each could be modeled separately and then combined into a single three-dimensional space. CIELAB and CIELUV are examples of this approach.

Toward the end of the twentieth century, emphasis switched from developing improved color spaces to developing different ways to measure distance. A color difference became a function of the color coordinates of either the average of the pair or the sample identified as the standard. Formulas such as CMC and CIEDE2000 are examples.

Moving into the twenty-first century, color-appearance spaces have developed. These are spaces that predict color based on knowledge of viewing and illuminating conditions. CIECAM02 is an example (CIE 2004b, 2018).

L^* Lightness

The achromatic property of a color is one of the most important color attributes. Accordingly, scales that relate physical measurements with our perceptions of lightness, blackness, whiteness, etc. have received great attention over the years. As we described in Chapter 3, the Munsell value scale was the first achromatic scale to have both careful visual and instrumental definitions. Accordingly, it became the basis for a CIE lightness scale. When the Munsell system was published as colorimetric data (Newhall, Nickerson, and Judd 1943), luminance factor was a function of value, the function a fifth-order polynomial. Although this was useful for producing color chips with specific value, the inverse transformation, used to relate luminance factor and lightness, required the use of a precalculated published table (Nickerson 1950).

Glasser et al. (1958) determined that the relationship between luminance factor and value was well modeled using a cube-root psychometric function plus an offset. This led to the CIE L^* formula, given in Eqs. (4.50) and (4.51) (CIE 2018):

$$L^* = 116f\left({}^{Y}/_{Y_n}\right) - 16 \tag{4.50}$$

where

$$f(x) = \begin{cases} x^{1/3} & x > ({}^{24}/_{116})^3 \\ ({}^{841}/_{108})\,x + {}^{16}/_{116} & x \le ({}^{24}/_{116})^3 \end{cases} \tag{4.51}$$

The relationship between luminance factor and L^* is plotted in Figure 4.34.

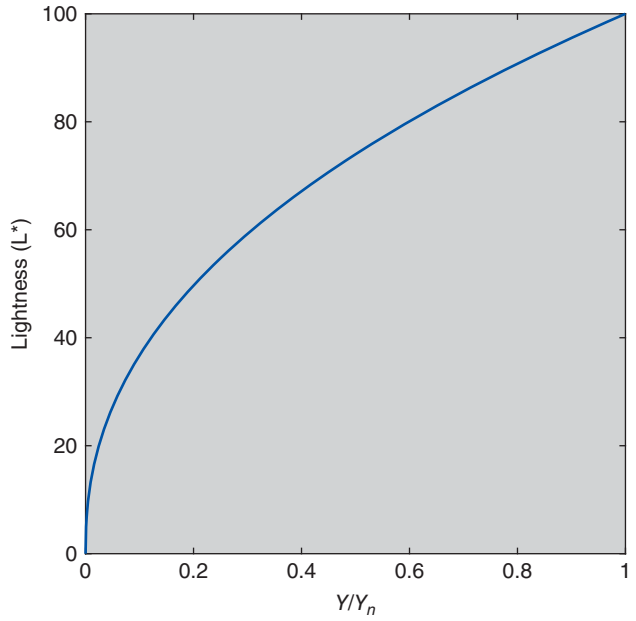

Figure 4.34 Relationship between luminance factor and CIE L^*.

Approximately uniform color-difference spaces recommended by the CIE use an asterisk to differentiate them from other formulas that use the same letters. Robertson (1990) describes the derivation of L^* and Berns (2000) provides a historical review of lightness formulas. Because of the −16 offset, black colors (i.e. luminance factor less than about 0.009) could lead to negative lightness values. As a consequence, a straight line from zero to the tangent of the cube-root function was used to avoid negative values (Pauli 1976) and as a result, a logical operator is necessary when calculating L^*.

The need for an offset resulted from defining the psychometric function as a cube root. By fitting an exponential psychometric function, the Munsell value scale can be predicted equally well without an offset, shown in Eq. (4.52) (Fairchild 1995)

$$V = 10\left({}^{Y}/_{Y_n}\right)^{1/2.3} \tag{4.52}$$

By replacing 10 with 100, a lightness function results that could be used instead of Eqs. (4.50) and (4.51).

$u'v'$ Uniform-Chromaticity Scale Diagram

The lighting and display industries have used the xy chromaticity diagram since its inception in 1931. This enabled the specification of color that was independent of luminance. Regions in chromaticity space were defined for signal lights. Broadcasting defined the colors of the red, green, and blue primaries and white point of televisions using chromaticities. The need to specify acceptable ranges in chromaticities quickly led to improved projections that had better visual uniformity. Rather than projecting tristimulus values onto a unit plane, shown in Figure 4.24, tristimulus values were projected obliquely. The geometry was determined by using color-discrimination data where observers scaled differences in chromaticities (Judd 1935; MacAdam 1937).

As an example, two lines are drawn in $\mathcal{X}\mathcal{Y}\mathcal{Z}$ space, one about four times longer than the other, shown in Figure 4.35. The endpoints represent a color-difference pair. Each pair has the same perceived color difference. Depending on our viewing direction, the differences in line length vary considerably. The optimal viewing direction, equivalent to a specific oblique projection, occurs such that the two lines are equal in length. At this projection, the calculated distance predicts the perceived distance.

Projections with improved visual spacing are known as *uniform chromaticity scale* (*UCS*) *diagrams*. The current CIE recommendation is u' ("u-prime"), v', the formulas shown in Eqs. (4.53) and (4.54). See Berns (2000) for its historical development

$$u' = \frac{4X}{X + 15Y + 3Z} \tag{4.53}$$

$$v' = \frac{9Y}{X + 15Y + 3Z} \tag{4.54}$$

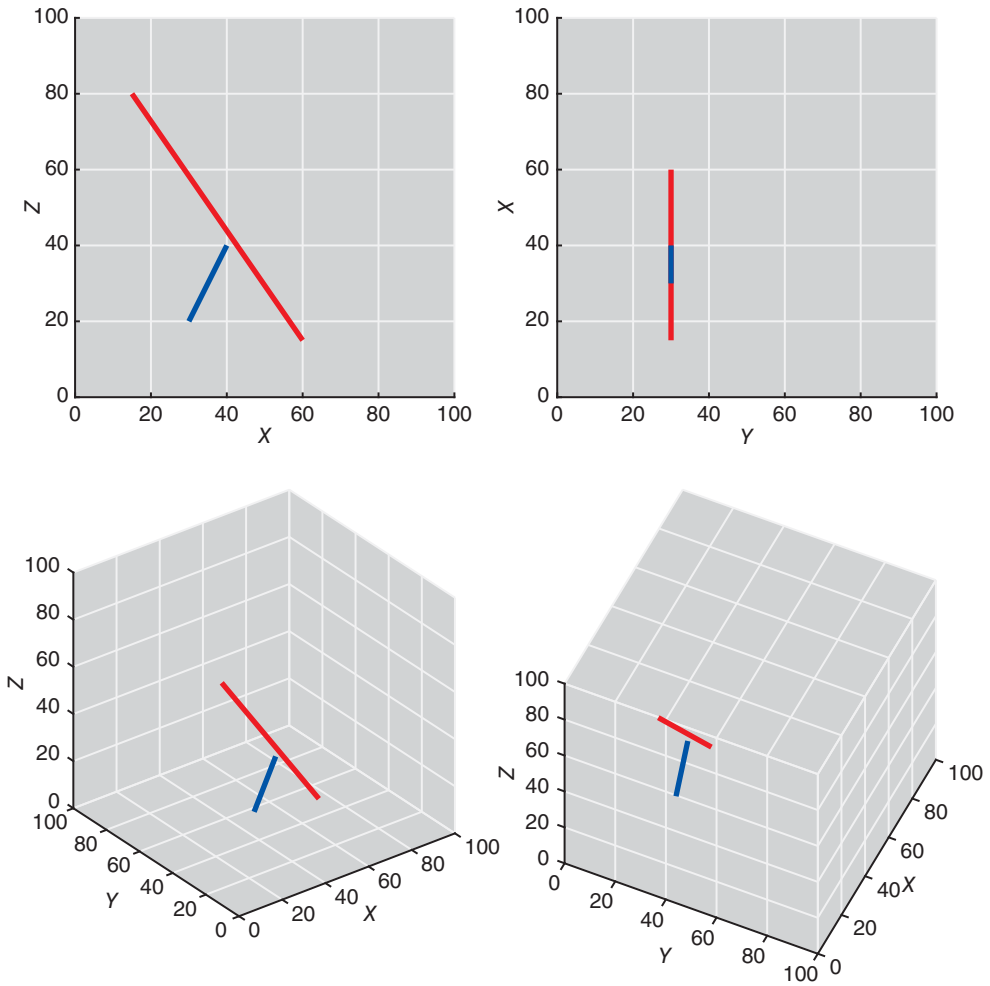

Figure 4.35 Two lines of unequal length, shown from different viewpoints.

It is also possible to calculate u' and v' from x and y and its inverse, shown in Eqs. (4.55)–(4.59). The third coordinate is w', calculated in similar fashion to z

$$u' = \frac{4x}{-2x + 12y + 3} \tag{4.55}$$

$$v' = \frac{9y}{-2x + 12y + 3} \tag{4.56}$$

$$w' = 1 - u' - v' \tag{4.57}$$

$$x = \frac{9u'}{6u' - 16v' + 12} \tag{4.58}$$

$$y = \frac{4v'}{6u' - 16v' + 12} \tag{4.59}$$

Plots similar to those shown in Figure 4.26 are shown for $u'v'Y$ in Figure 4.36. There is clear improvement compared with xyY.

CIELUV

The volume of nonfluorescent reflecting colors in xyY, shown in Figure 4.28, or $u'v'Y$, shown in Figure 4.36, has a somewhat conical shape with its apex at $Y = 100$. As a consequence, two color-difference pairs, each pair having the same chromaticity difference but dissimiliar average luminance factor, will appear unequal in color-difference magnitude. This can be corrected by scaling the chromaticity diagram as a function of luminance factor such that the cone becomes a cylinder. Hunter (1942) used this approach in the design of a tristimulus colorimeter and corresponding color space.

The $u'v'$ UCS and L^* were combined, resulting in *CIELUV* (Robertson 1990), having rectangular coordinates of L^*, u^*, and v^*. The formulas for L^*, u^*, and v^* are shown in Eqs. (4.60)–(4.63) (CIE 2018):

$$L^* = 116f\left({}^{Y}/_{Y_n}\right) - 16 \tag{4.60}$$

$$u^* = 13L^*(u' - u'_n) \tag{4.61}$$

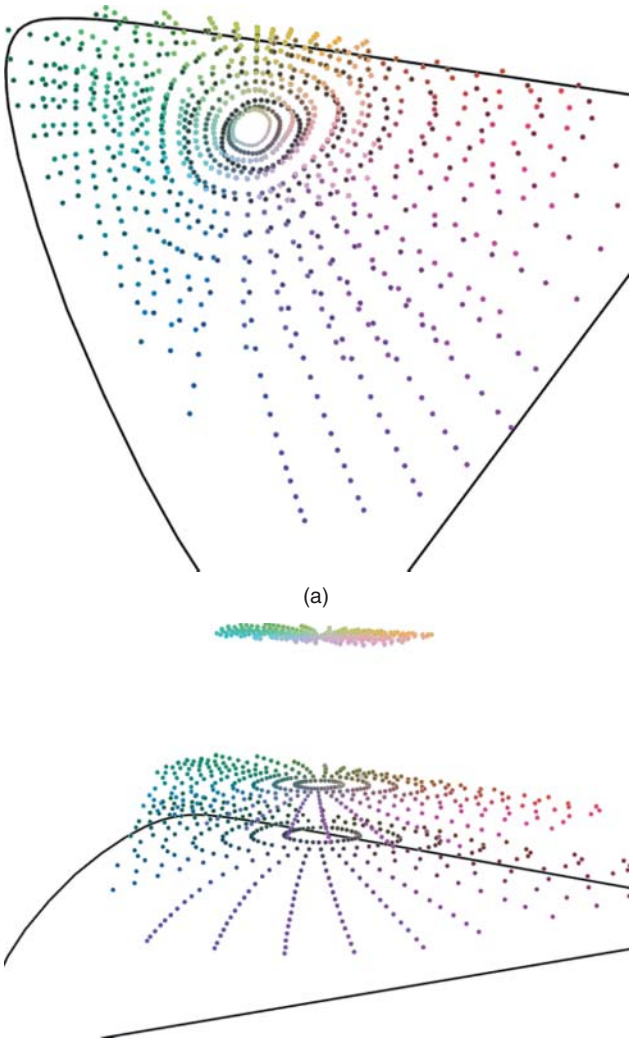

Figure 4.36 Munsell colors at value 3, 5, and 8 plotted in $u'v'Y$ at different orientations.

where se 4.76,77

$$v^* = 13L^*(v' - v'_n) \tag{4.62}$$

$$f(x) = \begin{cases} x^{1/3} & x > (24/116)^3 \\ (841/108)\,x + 16/116 & x \le (24/116)^3 \end{cases} \tag{4.63}$$

Because a white point can have a wide range of coordinates within $u'v'$, u^* and v^* result from a translation about the reference white, notated as u'_n and v'_n. This results in coordinates that are positive and negative and neutrals with $u^* = v^* = 0$. The Munsell colors at value 3, 5, and 8 are plotted in Figure 4.37.

Historically, CIELUV was used when both a UCS diagram and corresponding color-difference space were desired. Because of improvements in color-difference formulas that are not based on CIELUV, as we explain below, maintaining correspondence is not seen as advantageous and the use of CIELUV had diminished appreciably.

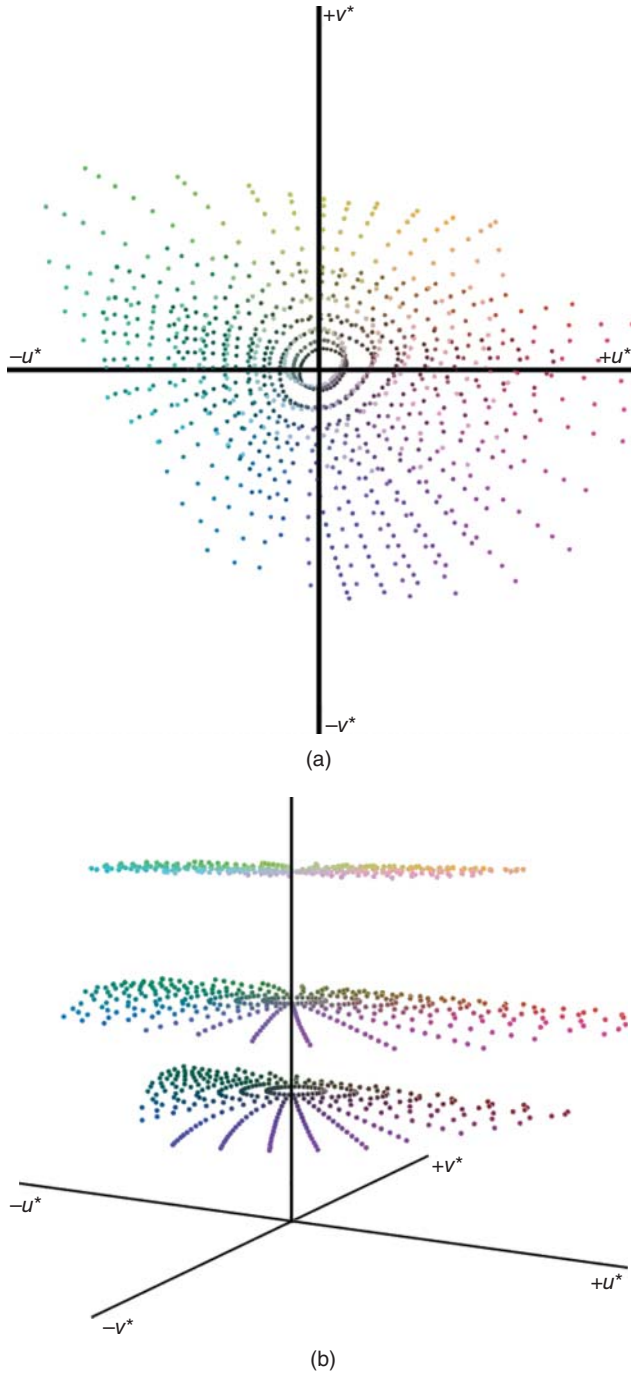

Figure 4.37 Munsell colors at value 3, 5, and 8 plotted in CIELUV at different orientations.

CIELAB

A second approach was taken to develop an approximately uniform color-difference space, also during the early 1940s.

Adams's (1942) approach was to transform tristimulus values directly without the intermediate step of a UCS. He used *XYZ* data for the Munsell system to develop and evaluate his new color space. Adams first rescaled the tristimulus values so that neutral colors would have equal tristimulus values, shown in Eqs. (4.64)–(4.66) (We introduce the prime superscript as a teaching aid.)

$$X' = \left(\frac{X}{X_n}\right) \tag{4.64}$$

$$Y' = \left(\frac{Y}{Y_n}\right) \tag{4.65}$$

$$Z' = \left(\frac{Z}{Z_n}\right) \tag{4.66}$$

Since neutrals colors have $X' = Y' = Z'$, then $(X' - Y')$ and $(Z' - Y')$ are zero. Plotting colors this way would result in coordinates that are both positive and negative, in a similar fashion to Hunter (1942). Adams reasoned that the nonlinearity between Munsell value and luminance factor should be applied to all the tristimulus values, finally resulting in his *chromatic value space*.

Nickerson and Stultz (1944) modified Adam's space by optimizing constants using their color-difference data. With the suggestion by Glasser and Troy (1952) to rearrange one of the chromatic axes to result in opponent properties similar to those of Hunter, ANLAB resulted, shown in Eqs. (4.67)–(4.69):

$$L = 9.2 f_V(Y') \tag{4.67}$$

$$a = 40[f_V(X') - f_V(Y')] \tag{4.68}$$

$$b = 16[f_V(Y') - f_V(Z')] \tag{4.69}$$

where $f_V(x)$ is the nonlinear relationship requiring table lookup.

The CIE Colorimetry Committee met in 1973 and by combining ANLAB and the Glasser et al. (1958) cube-root psychometric function, CIELAB was "born," shown in Figure 4.38. Following the meeting, the final coefficients were determined (Robertson 1990). The new color space was named CIELAB with rectangular coordinates of L^*, a^*, and b^*. The formula is shown in Eqs. (4.70)–(4.73):

$$L^* = 116 f\left({}^{Y}/_{Y_n}\right) - 16 \tag{4.70}$$

$$a^* = 500\left[f\left({}^{X}/_{X_n}\right) - f\left({}^{Y}/_{Y_n}\right)\right] \tag{4.71}$$

$$b^* = 200\left[f\left({}^{Y}/_{Y_n}\right) - f\left({}^{Z}/_{Z_n}\right)\right] \tag{4.72}$$

where

$$f(x) = \begin{Bmatrix} x^{1/3} & x > ({}^{24}/_{116})^3 \\ ({}^{841}/_{108})\, x + {}^{16}/_{116} & x \le ({}^{24}/_{116})^3 \end{Bmatrix} \tag{4.73}$$

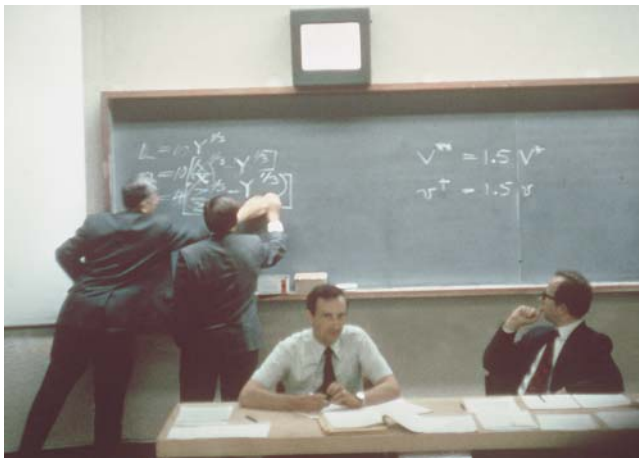

Figure 4.38 The "birth" of CIELAB during the colorimetry subcommittee meeting of the CIE, held at the City University, London. From left to right: E. Ganz, D. MacAdam, A. Robertson, and G. Wyszecki.
Source: Courtesy of F. W. Billmeyer.

Inverting CIELAB to tristimulus values is shown in Eqs. (4.74)–(4.77):

$$X = X_n f^{-1}\left(\frac{L^* + 16}{116} + \frac{a^*}{500}\right) \tag{4.74}$$

$$Y = Y_n f^{-1}\left(\frac{L^* + 16}{116}\right) \tag{4.75}$$

$$Z = Z_n f^{-1}\left(\frac{L^* + 16}{116} - \frac{b^*}{200}\right) \tag{4.76}$$

where

$$f^{-1}(x) = \begin{Bmatrix} x^3 & x > ({}^{24}/_{116}) \\ \frac{108}{841}(x - {}^{16}/_{116}) & x \le ({}^{24}/_{116}) \end{Bmatrix} \tag{4.77}$$

The Munsell renotation colors at value 3, 5, and 8 are plotted in Figure 4.39. The circularity is excellent and the hue lines are well spaced. However, the blue and purple lines are quite curved. Because the Munsell system has five principal hues, they do not line up with the a^* and b^* axes. Therefore, the color names red, green, yellow, and blue should not be associated with $+a^*$, $-a^*$, $+b^*$, and $-b^*$, respectively. In fact, the CIE documentation defining both CIELAB and CIELUV never refers to the chromatic axes with color names (CIE 2018).

Rotation of CIELAB Coordinates

Although CIELAB (and CIELUV) are rectangular systems, it is straightforward to define positions using polar-cylindrical coordinates. In this manner, there are approximate correlates of hue, h_{ab}, lightness, L^*, and

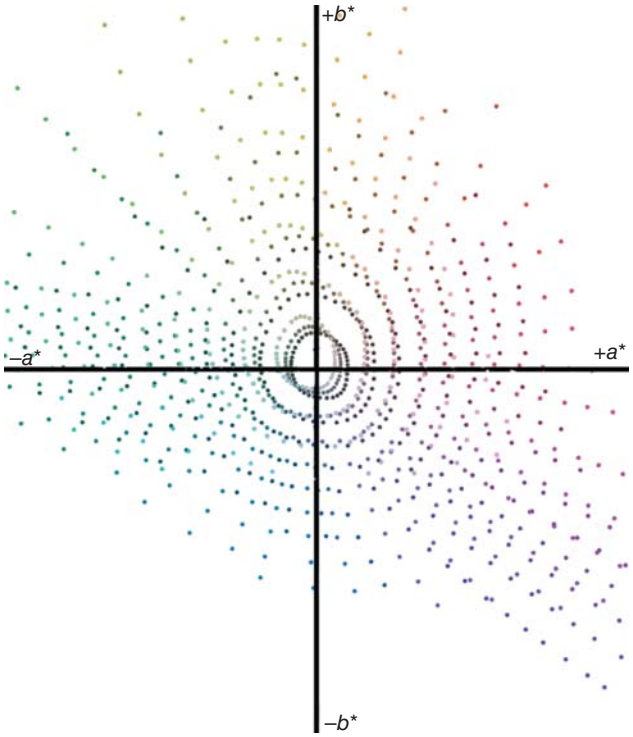

Figure 4.39 Munsell colors at value 3, 5, and 8 plotted in CIELAB at different orientations.

chroma, C^*_{ab}. The forward and reverse formulas for CIELAB hue and chroma are shown in Eqs. (4.78)–(4.82)

$$h_{ab} = \arctan\left({}^{b^*}\!/_{a^*}\right) \tag{4.78}$$

$$h_{ab} = \begin{cases} \frac{180}{\pi}\text{ATAN2}(b^*, a^*) & \text{ATAN2}(b^*, a^*) \geq 0 \\ \frac{180}{\pi}\text{ATAN2}(b^*, a^*) + 360 & \text{ATAN2}(b^*, a^*) < 0 \end{cases} \tag{4.79}$$

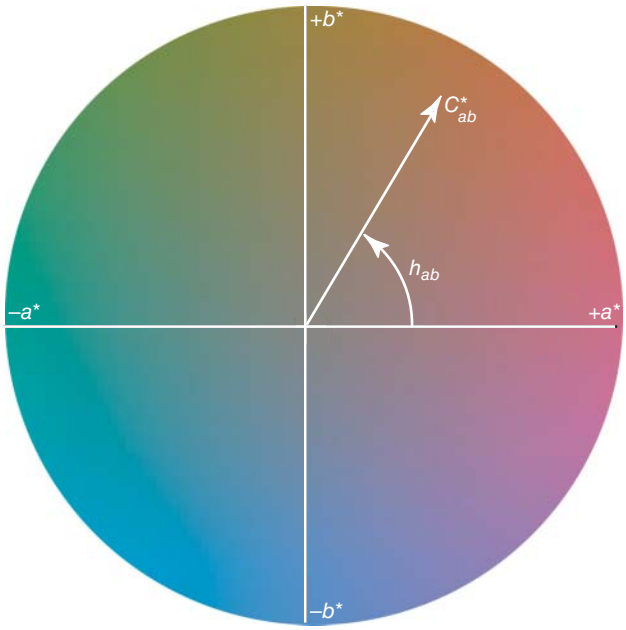

Figure 4.40 CIE 1976 a^*b^* projection at a constant lightness, $L^* = 50$. CIELAB hue is measured in degrees starting with $h_{ab} = 0°$ in the $+a^*$ direction and increasing counterclockwise. CIELAB chroma is measured as the length of the line from the neutral point ($a^* = b^* = 0$) to the sample point.

$$C^*_{ab} = \sqrt{(a^*)^2 + (b^*)^2} \tag{4.80}$$

$$a^* = C^*_{ab} \cos\left(\frac{\pi}{180} h_{ab}\right) \tag{4.81}$$

$$b^* = C^*_{ab} \sin\left(\frac{\pi}{180} h_{ab}\right) \tag{4.82}$$

CIELAB hue angle and chroma are shown in Figure 4.40. By convention, CIELAB hue angle is defined in degrees with the following values for each semiaxis: $+a^* = 0°$ (360°), $+b^* = 90°$, $-a^* = 180°$, and $-b^* = 270°$. The same caution about color names applies to h_{ab}. The NCS elementary hues red, yellow, green, and blue have h_{ab} values of approximately 25°, 90°, 165°, and 260°, respectively. Chroma is the distance from the neutral point ($a^* = b^* = 0$) to the sample. We prefer the use of a^*b^* for near neutrals and h_{ab} C^*_{ab} for chromatic colors.

Thus far, we have considered lightness and chromaticness independently. However, colors in mixture vary in both dimensions simultaneously. Billmeyer and Saltzman (1966) described terms used by textile dyers and paint formulators, shown in Figure 4.41. There is a rotation within a plane of constant hue.

We pointed out in Chapter 3 that NCS is arranged as a double cone. For some hues, this geometry is evident when the colors of constant nuance are plotted in CIELAB chroma versus lightness, for example, in Figure 4.42 for NCS R10B.

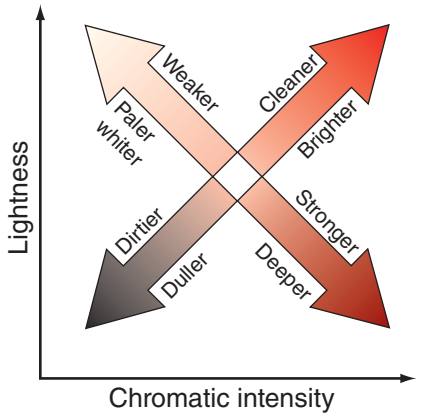

Figure 4.41 Terminology sometimes used by colorists.

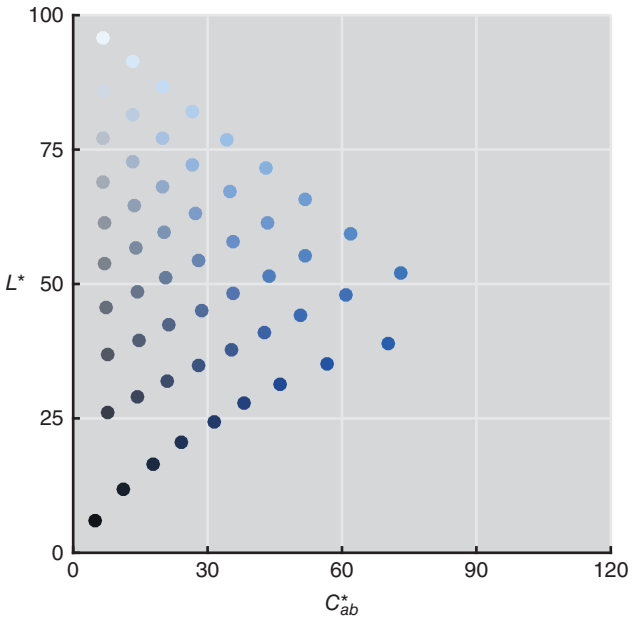

Figure 4.42 NCS colors of constant nuance plotted in CIELAB for NCS hue R10B.

- *Chroma:* An attribute of color used to indicate the degree of departure of the color from a neutral color of the same lightness.
- *Vividness:* An attribute of color used to indicate the degree of departure of the color from a neutral black color.
- *Depth:* An attribute of color used to indicate the degree of departure of the color from a neutral white color.
- *Clarity:* An attribute of color used to indicate the degree of departure of the color from its background color.

Berns (2014a) introduced two CIELAB variables, vividness, V^*_{ab}, and depth, D^*_{ab}, in order to increase the utility of CIELAB in relating coordinates with perception. Their formulas, both forward and inverse, are shown in Eqs. (4.83)–(4.88)

$$C^*_{ab} = \sqrt{(a^*)^2 + (b^*)^2} \tag{4.83}$$

$$V^*_{ab} = \sqrt{(L^*)^2 + (a^*)^2 + (b^*)^2} = \sqrt{(L^*)^2 + (C^*_{ab})^2} \tag{4.84}$$

$$\begin{aligned} D^*_{ab} &= \sqrt{(100 - L^*)^2 + (a^*)^2 + (b^*)^2} \\ &= \sqrt{(100 - L^*)^2 + (C^*_{ab})^2} \end{aligned} \tag{4.85}$$

$$C^*_{ab} = \sqrt{(D^*_{ab})^2 - (100 - L^*)^2} \tag{4.86}$$

$$C^*_{ab} = \sqrt{(V^*_{ab})^2 - (L^*)^2} \tag{4.87}$$

$$L^* = \frac{50 + (V^*_{ab})^2 - (D^*_{ab})^2}{200} \tag{4.88}$$

The inverse formulas are based on triangular coordinates where the third coordinate is calculated by knowing the coordinates of two other coordinates from among L^*, C^*_{ab}, V^*_{ab}, and D^*_{ab}. Their geometric meanings are diagrammed in Figure 4.43. Colors that become "cleaner" or "brighter" increase in CIELAB vividness. Colors that become "deeper" or "stronger" increase in CIELAB depth. The words "vivid" and "deep" have been used as adjectives to identify regions of the Munsell system (Kelly and Judd 1976). In the textiles industry, depth or depth of shade is a metric to aid in determining whether a batch of dyestuff has similar money value to previous batches (Smith 1997). Dye concentration is well correlated with D^*_{ab} (Berns 2014a).

When Berns was preparing visualizations of chroma, he noticed that if a color had the same lightness as the background, it became less distinct, seeming to fade away. This effect resulted irrespective of the starting color at maximum chroma or the color of the background, whether achromatic or colored. This led to a third dimension, clarity, T^*_{ab}, defined in Eq. (4.89) and its reverse defined in Eqs. (4.90) and (4.91)

$$T^*_{ab} = \sqrt{(L^*_{\text{background}} - L^*)^2 + (a^*_{\text{background}} - a^*)^2 + (b^*_{\text{background}} - b^*)^2} \tag{4.89}$$

$$C^*_{ab} = \sqrt{(T^*_{ab})^2 - (50 - L^*)^2} \tag{4.90}$$

$$L^* = \frac{25 + (V^*_{ab})^2 - (T^*_{ab})^2}{100} \tag{4.91}$$

An orange color is reduced in depth, clarity, chroma, and vividness in Figure 4.44 as an example. The background for the clarity calculation is the gray background used in the graph.

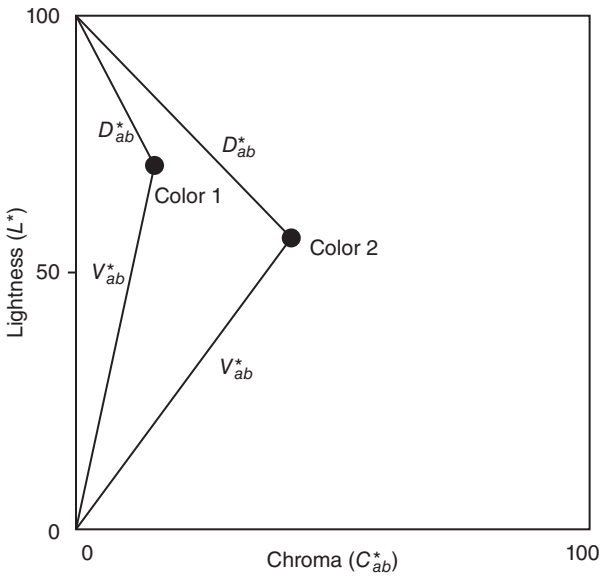

Figure 4.43 Dimensions of vividness, V^*_{ab}, and depth, D^*_{ab}, for colors 1 and 2. Line lengths define each attribute.

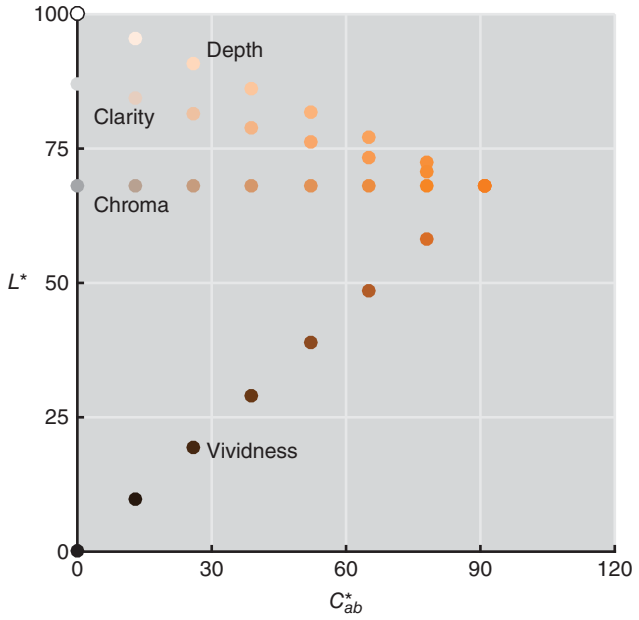

Figure 4.44 Orange color reducing in depth, clarity, chroma, and vividness.

The NCS eight principal hues at maximum chromaticness are reduced in CIELAB chroma, depth, vividness, and clarity, shown in Figure 4.45. In a recent experiment, over 100 naïve observers assessed about 120 samples using the words "saturation," "vividness," "blackness," and "whiteness." There was high correlation between CIELAB depth and "saturation," CIELAB clarity and "vividness," CIELAB vividness and "blackness," and CIELAB lightness and "whiteness" (Cho, Ou, and Luo 2017). CIELAB chroma had poorer correlation with "saturation" and "vividness," indicating the importance of having CIELAB variables that vary in both lightness and chroma.

H. COLOR-APPEARANCE MODELS

For many industries, CIELAB and CIELUV are sufficient for color specification. If two physical samples have the same CIELAB coordinates, then they match each other in color. (We devote an entire chapter to handling the more common case of having dissimilar coordinates: Chapter 5.) There is an expectation that both samples are illuminated identically, placed on the same surface in edge contact, and viewed by a single observer. In most cases, the samples have similar physical characteristics, such as size and texture.

In color imaging, the expectation is that the illuminating and viewing conditions are often dissimilar and the physical characteristics are usually different, for example, display and print. In such situations, CIELAB and CIELUV may be inadequate. A *color-appearance model* or *CAM*, by design, accounts for these differences.

As an example, an animator makes a movie. The movie has been created and viewed on a computer display in a dimly lit room, known as a *dim surround*. The movie will be shown using a digital projector and projected onto a large screen in a darkened room (*dark surround*). If the computer file is used directly as input to the digital projector, the movie will appear different compared with its appearance when created. By using a CAM, the data will be changed such that the projected movie matches the *color appearance* of the movie when seen on the computer display.

CAMs are used as shown in Figure 4.46. There are three sets of viewing conditions: source, reference, and destination. A forward model transforms source data to the reference condition. A reverse model transforms reference data to the destination condition. Quite often the two steps are concatenated, resulting in a single transformation from source condition to destination condition.

CAMs used today account for differences in light and chromatic adaptation, background lightness, and surround. The appearance attributes of lightness, brightness, chroma, colorfulness, saturation, and hue are predicted, described in Chapter 3. The greatest challenge was adaptation, and extensive research by Nayatani and by Hunt during the 1980s became the backbone for CAMs (Fairchild 2013). Research by Fairchild (1996) on the degree of chromatic adaptation added another component. Earlier research by Hunt (1952) and Stevens and Stevens (1963) was used to enable the estimation of colorfulness and brightness. Research by Bartleson and Breneman (1967) was used to estimate effects due to different surround. In 1998, the CIE recommended its first color-appearance space, CIECAM97s

Figure 4.45 Eight principal hues of the NCS system at maximum NCS chromaticness are reduced in (a) chroma, (b) depth, (c) vividness, and (d) clarity.

(1998). It was published as an "interim" space to be tested by both academia and the imaging industry. The results of these tests revealed shortcomings and in 2004, the CIE recommended a new CAM, CIECAM02, with better performance in predicting visual data and invertible mathematics, critical for use in imaging when needing to invert the model to transform between reference and destination viewing conditions (CIE 2004b).

Since 2002, mathematical inconsistencies in CIECAM02 have been uncovered (Brill and Mahy 2013; Li, Luo, and Wang 2014) and a CIE technical committee will likely be updating this model based on research by Li et al. (2017). Because of the complexity of the mathematics and the research nature of CAMs, we have decided to focus on deriving CAMs in general rather than provide formulas for CIECAM02 that will change in the near future. We

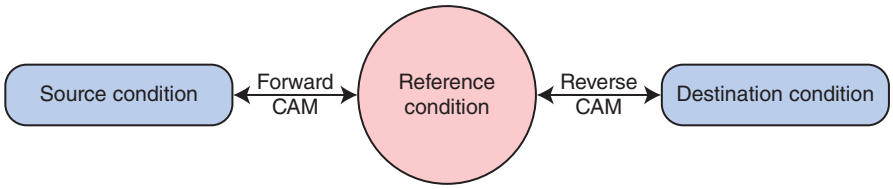

Figure 4.46 Use of color-appearance models (CAMs) in color reproduction where the source and destination conditions are dissimilar.

encourage readers requiring the use of CAMs to read the book on the same subject by Fairchild (2013).

Our color-appearance space has coordinates of $L^{\mathrm{PCT}}a^{\mathrm{PCT}}b^{\mathrm{PCT}}$, retaining the familiar L, a, and b variables and the superscript PCT are the initials for Principles of Color Technology. We begin by defining reference conditions—the 1964 standard observer, CIE illuminant D65, an adapting illuminance of 1000 lx, and an *average surround* (e.g. light booth or fully lit room). Illuminant D65 was selected because chromatic adaptation is always complete, irrespective of adapting illuminance.

The four stages of color vision described in Chapter 2—trichromacy, adaptation, compression, and opponency—are defined. The CAM will use cone fundamentals; thus, the first step is to transform *XYZ* to *LMS*. The CIE 2006 physiological observer for 32 years of age and the 10° field of view is used, equivalent to the 1964 standard observer (CIE 2006a). The matrix shown in Eq. (4.18) was inverted and rescaled to a D65 white point ($X_n = 0.94811$, $Y_n = 1$, $Z_n = 1.0734$) using Eqs. (4.43)–(4.46), the result shown in Eq. (4.92)

$$\begin{pmatrix} L \\ M \\ S \end{pmatrix} = \begin{pmatrix} 0.2181 & 0.8401 & -0.0437 \\ -0.4838 & 1.3546 & 0.0970 \\ 0 & 0 & 0.9316 \end{pmatrix}_{\mathrm{LMS}} \begin{pmatrix} X \\ Y \\ Z \end{pmatrix} \tag{4.92}$$

The chromatic adaptation transformation (CAT) introduced in Chapter 2 will be used, the formula shown again in Eq. (4.93):

$$\begin{pmatrix} L_{\mathrm{ref}} \\ M_{\mathrm{ref}} \\ S_{\mathrm{ref}} \end{pmatrix} = \begin{pmatrix} \frac{DL_{n,\mathrm{ref}}+(1-D)L_{n,s}}{L_{n,s}} & 0 & 0 \\ 0 & \frac{DM_{n,\mathrm{ref}}+(1-D)M_{n,s}}{M_{n,s}} & 0 \\ 0 & 0 & \frac{DS_{n,\mathrm{ref}}+(1-D)S_{n,s}}{S_{n,s}} \end{pmatrix}_{\nu\mathrm{KD}} \begin{pmatrix} L \\ M \\ S \end{pmatrix} \tag{4.93}$$

where subscript *s* indicates the source condition and subscript ref indicates the reference condition. This transform is based on the von Kries model and includes incomplete adaptation. The degree of adaptation, D, is defined by the user and typically ranges between 0.6 and 1.0.

The exponential psychometric function is used for the compression stage, shown in Eqs. (4.94)–(4.96). For the reference viewing condition, $\gamma = 2.3$ (Fairchild 1995)

$$L' = L^{\left(\frac{1}{\gamma}\right)} \tag{4.94}$$

$$M' = M^{\left(\frac{1}{\gamma}\right)} \tag{4.95}$$

$$S' = S^{\left(\frac{1}{\gamma}\right)} \tag{4.96}$$

The last required transform converts $L'M'S'$ to opponent channels, $L^{\mathrm{PCT}}a^{\mathrm{PCT}}b^{\mathrm{PCT}}$, the form of the transform shown in Eqs. (4.97)–(4.100):

$$\begin{pmatrix} L^{\mathrm{PCT}} \\ a^{\mathrm{PCT}} \\ b^{\mathrm{PCT}} \end{pmatrix} = \begin{pmatrix} e_1 & e_2 & e_3 \\ e_4 & e_5 & e_6 \\ e_7 & e_8 & e_9 \end{pmatrix} \begin{pmatrix} L' \\ M' \\ S' \end{pmatrix} \tag{4.97}$$

where

$$\sum_{i=1}^{i=3} e_i = 100 \tag{4.98}$$

$$\sum_{i=4}^{i=6} e_i = 0 \tag{4.99}$$

$$\sum_{i=7}^{i=9} e_i = 0 \tag{4.100}$$

The constraints are added such that the perfect reflecting diffuser has coordinates of $L^{\mathrm{PCT}} = 100$ and $a^{\mathrm{PCT}} = b^{\mathrm{PCT}} = 0$.

The Munsell colorimetric data for the 10 principal hues, 5R, 5YR, …, 5PR, sampling value 3, 5, and 8 at all chroma levels were used as aim data. Ideally, the data should be plotted as shown in Figure 4.47 where the hue angles are equally spaced and samples of constant hue plot as straight lines.

In order to use the colorimetric data, defined for the 1931 standard observer and illuminant C, the transformation developed by Derhak and Berns (2015a,b), known as a material adjustment transform, was used to transform the data for the 1964 standard observer and illuminant D65. This type of transform is required when converting between observers. The matrix coefficients, e_1–e_9, shown in Eq. (4.97), were determined using optimization where the average of the distance between each aim coordinate and its estimated value was minimized. The resulting matrix is shown in Eq. (4.101)

$$\begin{pmatrix} L^{\mathrm{PCT}} \\ a^{\mathrm{PCT}} \\ b^{\mathrm{PCT}} \end{pmatrix} = \begin{pmatrix} 70 & 30 & 0 \\ 580 & -630 & 50 \\ -70 & 290 & -220 \end{pmatrix} \begin{pmatrix} L' \\ M' \\ S' \end{pmatrix} \tag{4.101}$$

The Munsell colors are plotted in Figure 4.48. The performance is similar to CIELAB, plotted in Figure 4.49 for comparison.

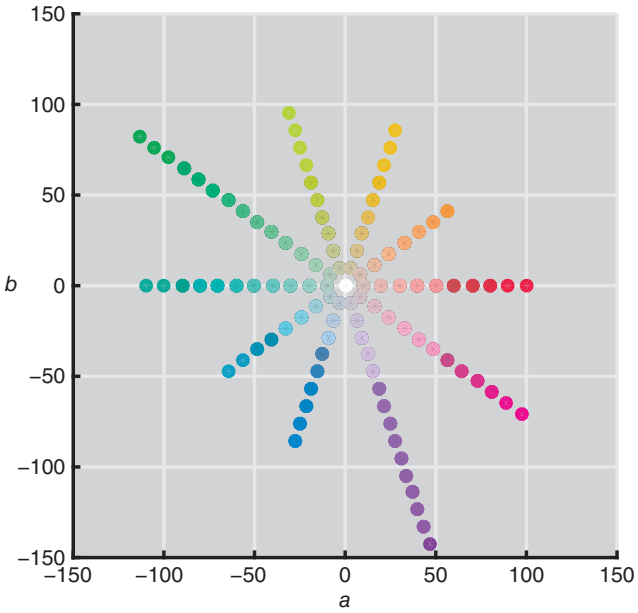

Figure 4.47 Spacing of the Munsell renotation data plotted in an ideal Lab system looking down the L axis.

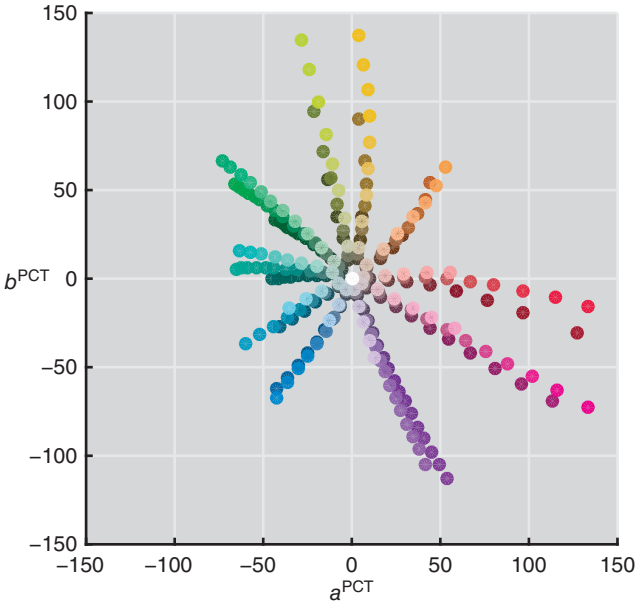

Figure 4.48 The Munsell renotation data plotted in $L^{PCT}a^{PCT}b^{PCT}$ looking down the L^{PCT} axis.

Chroma and hue angle are calculated in the usual manner, shown in Eqs. (4.102) and (4.103)

$$C^{PCT} = \sqrt{(a^{PCT})^2 + (b^{PCT})^2} \tag{4.102}$$

$$h^{PCT} = \arctan\left({}^{b^{PCT}}/_{a^{PCT}}\right) \tag{4.103}$$

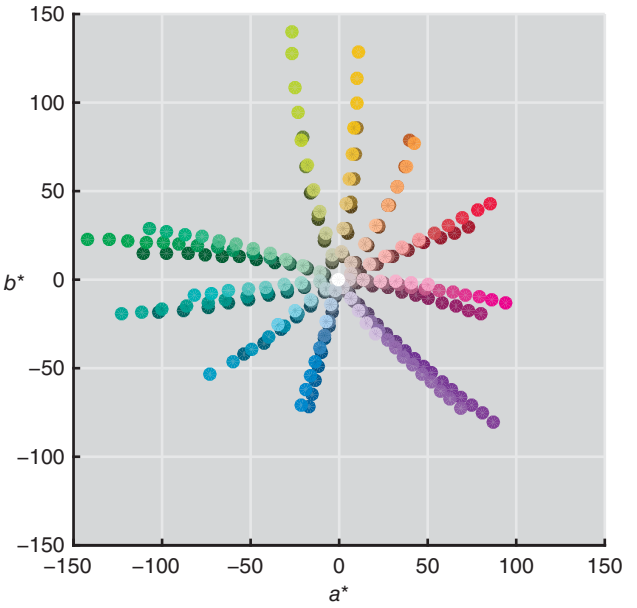

Figure 4.49 The Munsell renotation data plotted in $L^*a^*b^*$ looking down the L^* axis.

Saturation is calculated from lightness and chroma, shown in Eq. (4.104)

$$S^{PCT} = {}^{C^{PCT}}/_{L^{PCT}} \tag{4.104}$$

An important feature of CAMs is the prediction of brightness and colorfulness, defined in Chapter 3. This requires knowing the adapting illuminance, E_A. Hunt (1952) performed an experiment with chromatic stimuli and found that colorfulness increased with an increase in adapting illuminance and that high chroma samples increased at a faster rate than low chroma samples, known as the *Hunt effect*. The general trend is modeled using Eq. (4.105):

$$M^{PCT} = C^{PCT} \times 1.25^{\log_{10}\left(\frac{E_A}{1000}\right)} \tag{4.105}$$

where M refers to colorfulness and E_A is the adapting illuminance in units of lux. The value of 1000 in the denominator corresponds to the reference illuminance of 1000 lx. Enumerating Eq. (4.105) was used to visualize the relationship between illuminance and colorfulness and is plotted in Figure 4.50.

Stevens and Stevens (1963) performed an experiment where neutral samples were scaled for brightness with changes in adapting illuminance. Their results were similar to those of Hunt (1952). In this case, brightness increased with increases in illuminance. The increase depended on the lightness of the sample. Light samples increased in brightness at a faster rate than dark samples. The same model used to predict colorfulness was used to predict brightness, Q, the

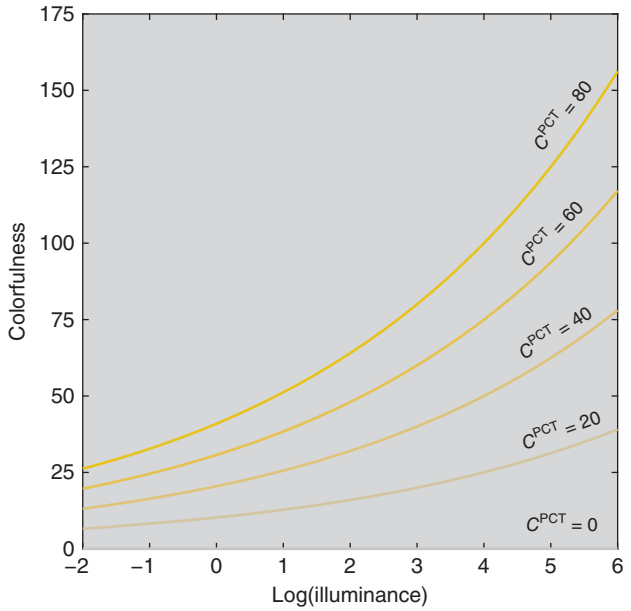

Figure 4.50 The *Hunt effect* where colorfulness increases with increasing adapting illuminance. Each line corresponds to a sample with chroma as indicated.

formula shown in Eq. (4.106)

$$Q^{\mathrm{PCT}} = L^{\mathrm{PCT}} \times 1.75^{\log_{10}\left(\frac{E_A}{1000}\right)} \tag{4.106}$$

The relationship between illuminance and brightness, known as the *Stevens effect*, is plotted in Figure 4.51, based on enumerating Eq. (4.106).

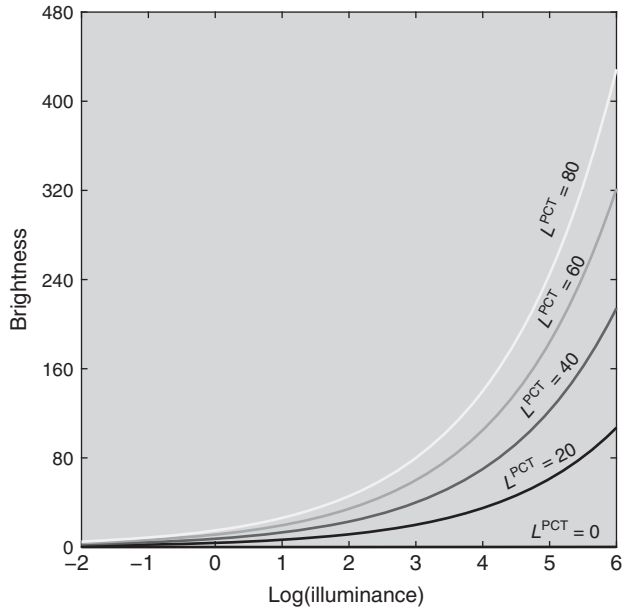

Figure 4.51 The *Stevens effect* where brightness increases with increasing adapting illuminance. Each line corresponds to a sample with lightness as indicated.

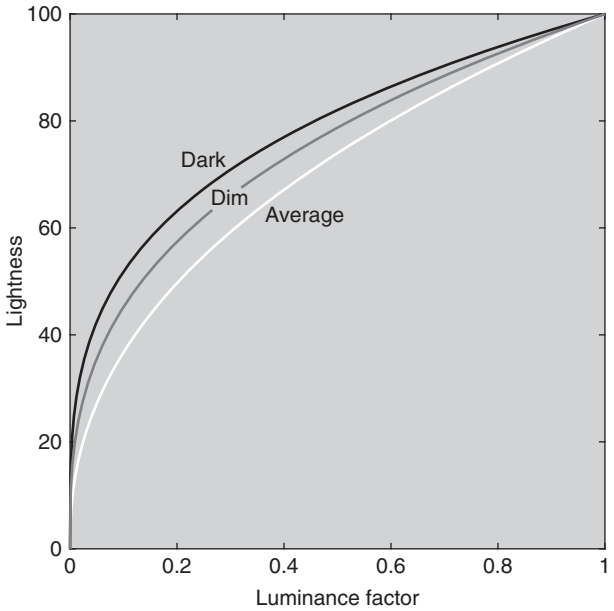

Figure 4.52 The *Bartleson–Breneman effect* where the relationship between luminance factor and lightness is changed to compensate for the effects of surround.

Recalling the example of the animator, he or she would have noticed that the lightness of the projected movie was incorrect where midtones looked somewhat washed out. Viewing the movie in the dark rather than in dim conditions caused this change in appearance. Bartleson and Breneman (1967) performed experiments to quantify the effect of surround on lightness. Fairchild (1995) modeled this surround effect by changing the γ in the psychometric function. Average conditions have $\gamma = 2.3$, dim conditions have $\gamma = (2.3 \times 1.25) = 2.9$, and dark conditions have $\gamma = (2.3 \times 1.5) = 3.5$. In imaging, this change is often called a change in contrast. The relations between luminance factor and lightness for these three surrounds, known as the *Bartleson–Breneman effect*, are plotted in Figure 4.52.

Although $L^{\mathrm{PCT}}a^{\mathrm{PCT}}b^{\mathrm{PCT}}$ was optimized using Munsell renotation data, Munsell hue was not well predicted, seen by comparing the hue spacing in Figure 4.48 with Figure 4.47. Furthermore, relating Munsell designations with appearance requires training. NCS hue is more intuitive, relying on our ability to imagine unique red, yellow, green, and blue. The samples at maximum chromaticness for the 24 hues of the NCS system were used as aim data to transform h^{PCT} to U^{PCT}. ("H" was not used to avoid confusion with a hue-difference calculation, described in Chapter 5.) Nonlinear optimization was used to fit a parabola for each quadrant where NCS R was defined at $U^{\mathrm{PCT}} = 0$. The optimization was constrained to avoid discontinuities between quadrants. Hue is assigned in which red, yellow, green, and blue have $U^{\mathrm{PCT}}$of 0 (or 400), 100, 200, and 300. For example, a color

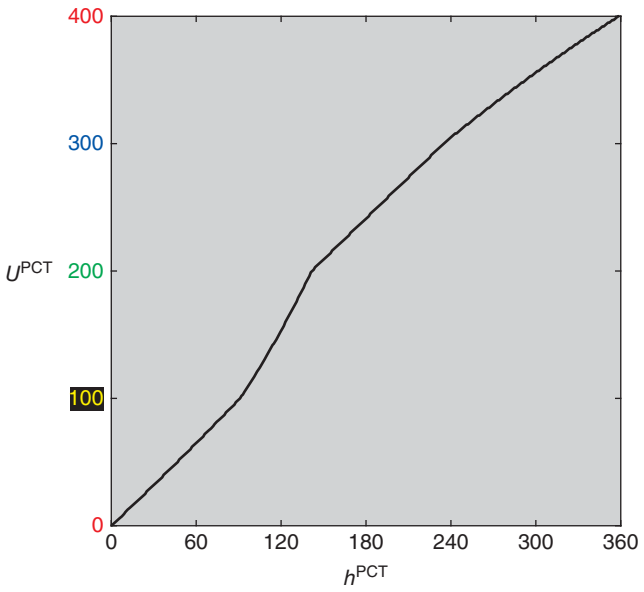

Figure 4.53 The conversion from h^{PCT} to U^{PCT} based on enumerating Eq. (4.107).

with $U^{PCT} = 50$ would appear orangish. The conversion from h^{PCT} to U^{PCT} is plotted in Figure 4.53, the formula shown in Eq. (4.107)

$$U^{PCT} = \begin{cases} 0.0114 + 1.0474h^{PCT} + 0.0006(h^{PCT})^2 & 0 \le h^{PCT} \le 91 \\ 0.1010 + 0.5335h^{PCT} + 0.0062(h^{PCT})^2 & 92 \le h^{PCT} \le 141 \\ 44.4724 + 1.1135h^{PCT} + 0.0001(h^{PCT})^2 & 142 \le h^{PCT} \le 234 \\ 44.4472 + 1.2747h^{PCT} + 0.0008(h^{PCT})^2 & 235 \le h^{PCT} \le 359 \end{cases} \tag{4.107}$$

Our textbook example of "PCT-CAM," while capturing many of the features of a CAM, does not account for all the effects modeled in CIECAM02 and more comprehensive models such as CIECAM97s and accordingly, we are not advocating its use. CAMs are an important advancement in color technology and are indispensable in cases where it is critical to account for differences in viewing conditions such as chromatic adaptation, adapting illuminance, background luminance factor, and surround.

I. WHITENESS AND YELLOWNESS

- *Whiteness:* Attribute of color perception by which a color is judged to approach a preferred white.
- *Yellowness:* Attribute of color perception by which an object color is judged to depart from colorless or a preferred white toward yellow.

Whiteness

Whiteness is associated with a region in color space within which objects are recognized as white; degree of whiteness is, in principle, measured by the degree of departure of the object from a "perfect" white. Unfortunately, there are strong prejudices associated with industrial and national preferences which have prevented agreement on exactly what the "perfect" white is, and which directions of departure from it (toward blue, yellow, red, or green) are preferred or avoided. One consistent trend is that bluish whites appear whiter than neutral whites for samples having identical lightness. This is observed in Figure 4.54. In some circumstances, increasing blueness at the expense of reducing lightness increases whiteness.

With the introduction of fluorescent whitening agents (FWAs), it became possible to increase blueness without a reduction in lightness. FWAs absorb UV radiation and emit bluish light. These are used extensively, for example, in paper products, detergents, and plastics to increase whiteness. As fluorescent materials, the spectral properties of the illumination strongly affect the material's whiteness. This occurs for both visual evaluations and instrumental measurements.

Methods exist to evaluate whiteness using visual and instrumental measurements. See Smith (1997) for a historical review. Instrumentally, either spectral or colorimetric data can be analyzed. The CIE method uses colorimetric data (CIE 2018). It is also an ISO standard (2004). Research by Ganz (1976, 1979) and Griesser (1994) are the basis for a CIE whiteness index W—or commonly WI—where both luminance factor and hue are used in the calculation, shown in Eqs. (4.108) and (4.109) for the 1931 and 1964 standard observers, respectively

$$W = Y + 800(x_n - x) + 1700(y_n - y) \quad 40 < W < 5Y - 280 \tag{4.108}$$

$$W_{10} = Y_{10} + 800(x_{n,10} - x_{10}) + 1700(y_{n,10} - y_{10}) \quad 40 < W_{10} < 5Y - 280 \tag{4.109}$$

The illuminant in both cases is illuminant D65. These formulas assume that luminance factor for the perfect reflecting diffuser is 100.

The index is based on luminance factor, dominant wavelength, and purity, shown in Figure 4.25. With an increase in purity, a correlate of chromatic intensity, whiteness decreases. Depending on the dominant wavelength, a correlate of hue, whiteness will either increase or decrease. The hue weighting is along a blue-yellow axis where blue is favored over yellow. Ganz and Pauli (1995) derived an approximate whiteness index in CIELAB based on the CIE WI; whiteness was a function of only L^* and b^*. The CIE whiteness index for the five colors is listed in Figure 4.53.

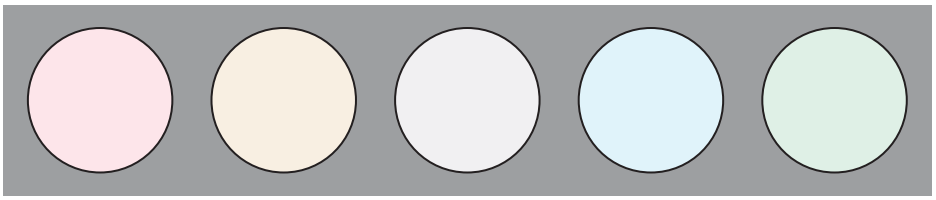

Figure 4.54 CIE whiteness, W, and tint, T_w, of five samples. The samples all have the same lightness.

The central color is neutral. The bluish sample has a higher whiteness than the neutral while the other colors have lower values. The yellow sample has the lowest whiteness.

The CIE method also includes the calculation of tint, T_W, shown in Eqs. (4.110) and (4.111)

$$T_W = 1000(x_n - x) - 650(y_n - y) \tag{4.110}$$

$$T_{W,10} = 900(x_{n,10} - x_{10}) - 650(y_{n,10} - y_{10}) \tag{4.111}$$

When T_W is positive, the sample is greenish; when T_W is negative, the sample is reddish.

For materials suspected of being fluorescent, the spectrophotometer's light source must closely approximate D65 in both the UV and visible regions of the spectrum (Bristow 1994; Lin, Shamey, and Hinks 2012). We describe the measurement of fluorescent materials in detail in Chapter 6.

There are two obvious limitations of the CIE whiteness index. The first is the limitation to a single illuminant — D65. The use of a chromatic adaptation transform overcomes this limitation (Wei et al. 2017). The second limitation is the use of a color space with poor visual uniformity — xyY. However, since the region of color space is quite limited, a uniform color space is unlikely to lead to marked improvement.

Yellowness

The presence of small amounts of yellowness in nearly white (or nearly colorless) samples is both common and, usually, objectionable; therefore, considerable attention has been paid to devising uniform yellowness scales. The ASTM (2015b) has adopted a yellowness index, YI, for both standard observers and illuminants C and D65 that is based on CIE tristimulus values, the formula shown in Eq. (4.112)

$$YI = 100\frac{(C_X X - C_Z Z)}{Y} \tag{4.112}$$

There are two constants, C_X and C_Z. Their values depend on the illuminant and observer combination, listed in Table 4.2. These scales correlate with visual perception only for colors seen as yellow or blue; in the latter case, the yellowness index is a negative number. They should never be used to describe colors that are visibly reddish or greenish.

Table 4.2 Coefficients for yellowness index formula shown in Eq. (4.108).

	1931 standard observer		1964 standard observer	
	Illuminant C	Illuminant D65	Illuminant C	Illuminant D65
C_X	1.2769	1.2985	1.2871	1.3013
C_Z	1.0592	1.1335	1.0781	1.1498

J. SUMMARY

Numerical color specification relies on the principle of metamerism in which two colors producing the same trichromatic response match in color. At first, a reference device that is able to produce all colors is standardized. If each color matches the reference device, then the two colors match each other. The reference device for CIE colorimetry has primaries of $\mathscr{X}$, $\mathscr{Y}$, and $\mathscr{Z}$ with amounts specified using tristimulus values, X, Y, and Z. This is referred to as the XYZ system. Any device that is related linearly to XYZ, that is, a linear transformation, can be used equivalently. Most RGB systems have this property. There are also reference observers that are surrogates for individual observers: the 1931 standard observer, the 1964 standard observer, and the 2006 cone-fundamental-based colorimetric observers. Soon after colorimetry was defined, it was apparent that this matching system was inadequate for quantifying color differences and relating numerical values to perceptual attributes. This led to approximately uniform color spaces such as CIELUV and CIELAB. By considering coordinates simultaneously, there are correlates of lightness, hue, chroma, saturation, vividness, depth, and clarity. Both CIELUV and CIELAB are designed for color specification under a single set of viewing and illuminating conditions. When it is necessary to compare colors under dissimilar conditions, CAMs may be required. These include the additional correlates of brightness and colorfulness. Whiteness and yellowness also require numerical specification and specific formulas have been developed for this purpose. In the next chapter, we will use numerical specification for defining color quality and setting color tolerances.

Chapter 5

Color-Quality Specification

Much of color technology is concerned with decisions about quality. Does this batch of material match the standard? Is this print a close reproduction of an original object? Does this process produce consistent color? If not, is the lack of color consistency acceptable? Can this new part be used interchangeably with parts made last month, or last year? All of these questions relate to *quality*. We believe that a quality product should minimize detrimental effects to our society. In addition to the usual goal of producing a product that meets or exceeds customer expectations, quality relates to productivity, worker job satisfaction, and minimizing waste and pollution. In this chapter, we describe types of visual judgments and various approaches to predict these judgments using color measurement, colorimetry, and color-difference formulas.

A. PERCEPTIBILITY AND ACCEPTABILITY VISUAL JUDGMENTS

- *Perceptibility:* "Can I see a difference in color?" "Is this difference in color greater than or less than the difference in color between members of a standard pair?"
- *Acceptability:* "Is this difference in color acceptable?"

The first step in measuring *color quality* is recognizing that there are two types of visual assessments, *perceptibility* and *acceptability*. Let's imagine the use of a visual colorimeter. Rather than performing color matches, as described in Chapter 4, the visual colorimeter is used to measure color differences. Monochromatic light is presented in each field. This experiment begins with the two halves of the bipartite field adjusted to the identical wavelength; by definition, the two fields match in color. An observer is asked to change the wavelength of one of the fields until a difference is first noticed. This is known as a *just-noticeable difference*, or *JND*. In the field of psychophysics, a *threshold* has been measured and there are many techniques used with much higher precision than this simple experiment (Bartleson and Grum 1984; Gescheider 1997; Engeldrum 1999; ASTM 2015c).

In our opinion, measuring a JND is solely a measurement of physiology. The observer is not interpreting the importance of this difference, simply judging whether a difference exists. A visual judgment made without interpreting its importance is known as a *perceptibility judgment*.

One of the limitations of developing a quality metric that is based on JND measurements is that the visual differences are too small compared to the typical variability of most industrial processes. It would seem that this problem could be overcome by increasing the size of the tolerance. This increase is known as a *commercial factor*. Just-noticeable difference data expanded by a commercial factor would be used to set a manufacturing color tolerance.

Billmeyer and Saltzman's Principles of Color Technology, Fourth Edition. Roy S. Berns.

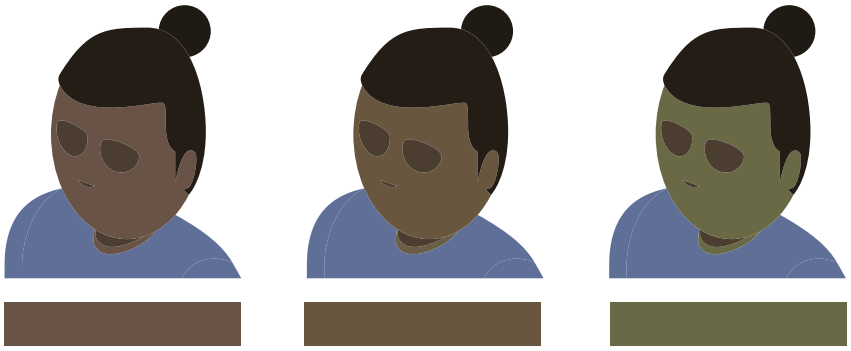

Figure 5.1 The faces and corresponding squares have the same color. If the standard is in the center, do the color differences have the same meaning when comparing the faces as they do comparing the squares?

However, there are many visual judgments to which meaning is assigned. The reproduction of skin color serves as an example, shown in Figure 5.1. Two color reproductions can be made, one slightly greenish and the other slightly reddish. Based on perceptibility data, they both have the same magnitude of hue difference from that of the reference skin color. However, most observers would find the greenish reproduction objectionable. They have interpreted the color differences. As another example, a plastic injection-molding machine has poor temperature control. This results in parts varying in yellowness. Over time, the production manager becomes more tolerant of yellowness changes. These are judgments of *acceptability* and the list of examples is endless. As soon as a batch of material is either "passed" or "failed," or "accepted" or "rejected," an acceptability decision has been made.

Our experience is that when color differences are slightly above threshold—*suprathreshold*—perceptibility and acceptability judgments are identical, validated by Na et al. (2013). As the size of the color difference increases, acceptability judgments are made, which are often different than the corresponding perceptibility judgment enlarged by a commercial factor. Many factors influence acceptability besides the similarity or dissimilarity of color. Although the visual difference between a batch of material and its standard is very large, it may become acceptable if its cost is severely reduced!

When instrumental measurements are made, the numbers should predict what observers see. The calculated color differences should predict visual color differences. Developing color-difference formulas that predict perceptibility judgments seems doable. However, how can we predict acceptability? Can an acceptability judgment ever be repeatable and reproducible? Can acceptability judgments from one industry be applied to another? Color-difference formulas are derived using visual data. It is important to know whether the visual data are perceptibility or acceptability judgments.

B. COLOR-DIFFERENCE GEOMETRY

CIELAB (and CIELUV) is a rectangular three-dimensional color space having axes of L^*, a^*, and b^*. Suppose that

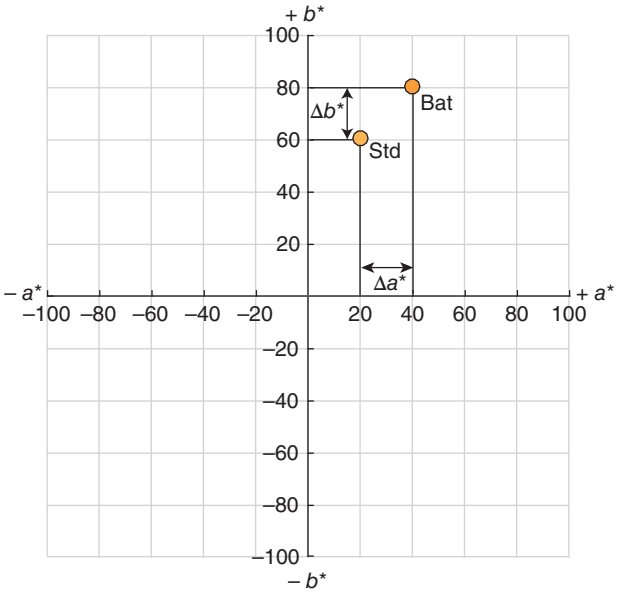

Figure 5.2 Standard (Std) and batch (Bat) plotted in CIELAB looking down the L^* axis. Projecting each point onto the a^* and b^* axes indicates Δa^* and Δb^*.

a color standard (or reference color) has coordinates of $L^* = 80$, $a^* = 20$, $b^* = 60$, and the comparison sample (or test color, trial, batch, or reproduction) has coordinates of $L^* = 80$, $a^* = 40$, $b^* = 80$, both plotted in Figure 5.2. The differences in coordinates are shown by projecting each color onto the a^* and b^* axes. The formulas are shown in Eqs. (5.1)–(5.3) where the Greek symbol, Δ *(delta)*, represents difference. In a similar fashion to the third edition of this book, the terms standard (Std) and batch (Bat) will be used

$$\Delta L^* = L^*_{\text{Bat}} - L^*_{\text{Std}} \tag{5.1}$$

$$\Delta a^* = a^*_{\text{Bat}} - a^*_{\text{Std}} \tag{5.2}$$

$$\Delta b^* = b^*_{\text{Bat}} - b^*_{\text{Std}} \tag{5.3}$$

By convention, positive differences mean that the batch has more of that variable than the standard. For example, a lightness difference greater than zero ($\Delta L^* > 0$) means

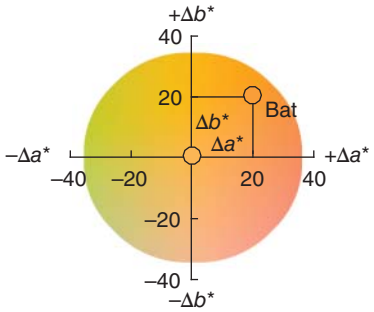

Figure 5.3 Standard and batch plotted in $\Delta a^* \Delta b^*$ looking down the ΔL^* axis. The standard is always plotted at the origin.

that the batch is lighter than the standard. A lightness difference less than zero ($\Delta L^* < 0$) means that the batch is darker than the standard. (A lightness difference equal to zero—$\Delta L^* = 0$—means that the batch and standard have the same lightness.)

In practice, the difference in color between a standard and batch is much smaller than shown in Figure 5.2. By translating the axes about the standard, as shown in Figure 5.3, these small differences are more readily seen.

In Chapter 4, we introduced the concept of a linear transformation, for example, transforming between *RGB* and *XYZ* and its interpretation as a rotation from one set of axes to another. This is shown in Figure 5.4 where colors at constant $L^* = 70$ are plotted. Any color can be defined by rectangular coordinates of a^* and b^* or d and e. Neither has a decided geometric advantage. Suppose that the rotation coincides with a standard's hue angle. In this case, batches having coordinates on the coincident axis correspond to differences in chroma while batches with coordinates on

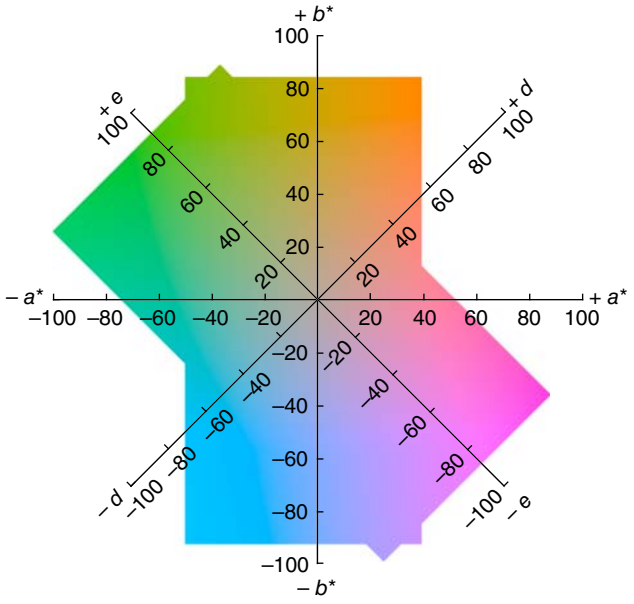

Figure 5.4 Colors at constant L^* of 70 defined by two sets of coordinates: a^* and b^* or d and e.

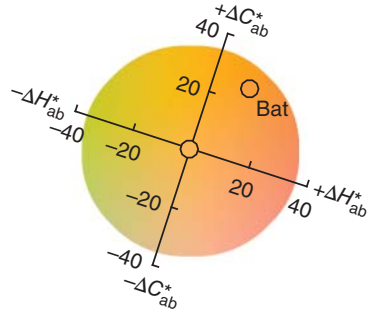

(a)

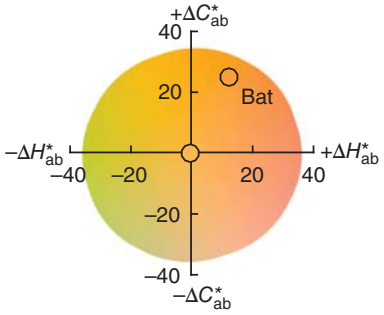

(b)

Figure 5.5 Standard and batch plotted in $\Delta C^*_{ab} \Delta H^*_{ab}$ looking down the L^* axis. The standard is always plotted at the origin. (a) Rotated axes maintaining $\Delta a^* \Delta b^*$ orientation. (b) Rotated axes with ΔC^*_{ab} in the vertical direction and ΔH^*_{ab} in the horizontal direction.

the perpendicular axis correspond to differences in hue. The rotation enables direct interpretation from coordinate differences to hue and chroma differences. Axes rotated in this fashion lead to coordinates having a clear advantage when the standard is not located near $a^* = b^* = 0$.

The Figure 5.3 $\Delta a^* \Delta b^*$ plot can be rotated about the standard's hue angle, the result shown in Figure 5.5. The rotation has axes of chroma difference, ΔC^*_{ab}, and hue difference, ΔH^*_{ab}. Such plots are commonly shown with ΔC^*_{ab} in the vertical direction and ΔH^*_{ab} in the horizontal direction. The rotation matrix from $\Delta L^* \Delta a^* \Delta b^*$ to $\Delta L^* \Delta C^*_{ab} \Delta H^*_{ab}$ is shown in Eq. (5.4). The term $\sqrt{h_{ab,\mathrm{Std}} h_{ab,\mathrm{Bat}}}$ defines the geometric mean hue angle of the color-difference pair

$$\begin{pmatrix} \Delta L^* \\ \Delta C^*_{ab} \\ \Delta H^*_{ab} \end{pmatrix} = \begin{bmatrix} 1 & 0 & 0 \\ 0 & \cos\left(\pi/180 \sqrt{h_{ab,\mathrm{Std}} h_{ab,\mathrm{Bat}}}\right) & \sin\left(\pi/180 \sqrt{h_{ab,\mathrm{Std}} h_{ab,\mathrm{Bat}}}\right) \\ 0 & -\sin\left(\pi/180 \sqrt{h_{ab,\mathrm{Std}} h_{ab,\mathrm{Bat}}}\right) & \cos\left(\pi/180 \sqrt{h_{ab,\mathrm{Std}} h_{ab,\mathrm{Bat}}}\right) \end{bmatrix} \begin{pmatrix} \Delta L^* \\ \Delta a^* \\ \Delta b^* \end{pmatrix} \tag{5.4}$$

Why not just use changes in chroma, ΔC^*_{ab}, and changes in hue angle, Δh_{ab}, the formulas shown in Eqs. (5.5) and (5.6)? After all, both coordinates were derived as correlates of Munsell chroma and hue. The answer is visualized in Figure 5.6. Because C^*_{ab} and h_{ab} are polar cylindrical coordinates, the distance between colors having the same Δh_{ab} depends on C^*_{ab}. As the chroma of the color-difference pair increases, the distance between them also increases. This

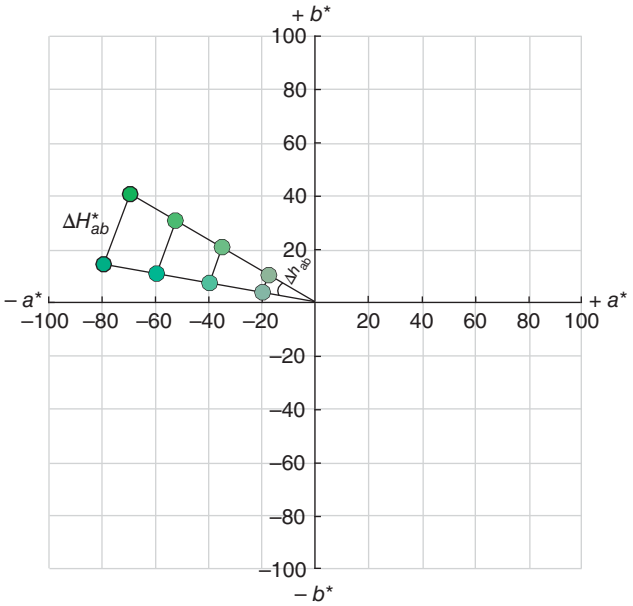

Figure 5.6 Each color-difference pair has the same chroma, C^*_{ab}, and constant hue-angle difference, Δh_{ab}. The distance between the color-difference pair samples is defined by hue difference, ΔH^*_{ab}. Hue difference increases with increases in the pair's chroma.

distance is a measure of ΔH^*_{ab}. The relationship between C^*_{ab} and ΔH^*_{ab} is shown in Eq. (5.7), one of several formulas for ΔH^*_{ab}. The difference in hue angle is scaled by the geometric mean chroma of the color-difference pair. In some applications, it is advantageous to calculate hue difference without first calculating hue angle difference (Stokes and Brill 1992; Séve 1996). The Séve formula is shown in Eq. (5.8)

$$\Delta C^*_{ab} = C^*_{ab,\text{Bat}} - C^*_{ab,\text{Std}} \tag{5.5}$$

$$\Delta h_{ab} = h_{ab,\text{Bat}} - h_{ab,\text{Std}} \tag{5.6}$$

$$\Delta H^*_{ab} = 2\sqrt{C^*_{ab,\text{Bat}} C^*_{ab,\text{Std}}} \cdot \sin\left(\frac{\pi}{180} \cdot \frac{\Delta h_{ab}}{2}\right) \tag{5.7}$$

$$\Delta H^*_{ab} = \frac{(a^*_{\text{Bat}} b^*_{\text{Std}} - a^*_{\text{Std}} b^*_{\text{Bat}})}{[0.5(C^*_{ab,\text{Bat}} C^*_{ab,\text{Std}} + a^*_{\text{Bat}} a^*_{\text{Std}} + b^*_{\text{Bat}} b^*_{\text{Std}})]^{1/2}} \tag{5.8}$$

When showing these delta-plots, we include a colored background for the colors surrounding the standard with lightness equal to the standard as a visual method of relating position with color. Words can be used in place of, or in addition to, the colored background and we recommend the terms redder, yellower, greener, bluer, higher chroma, and lower chroma. The hue modifiers change in each a^*b^* quadrant, shown in Figure 5.7.

Orange and green colors were used in explaining Δa^*, Δb^*, ΔC^*_{ab}, and ΔH^*_{ab}. Chroma and hue differences were the more useful metrics. For colors close to the L^* axis, these metrics lose their usefulness and Δa^* and Δb^* are much more useful. When looking at numerical data, we suggest calculating all the difference metrics and evaluate those that are most useful.

We are now ready to consider all three changes simultaneously, either $\Delta L^* \Delta a^* \Delta b^*$, or $\Delta L^* \Delta C^*_{ab} \Delta H^*_{ab}$. We are interested in defining a *total color difference* metric, that is, the summation of all three changes in color. Consider again the orange pair, replotted in Figure 5.8. For some of us, we would add each change in lightness, chroma, and hue successively. Numerically, the absolute values are added. In Figure 5.8, line segments a and b are summed. This type of distance measurement is called *city block* or *taxicab*. For others, the slant distance between colors defines the total color difference, referred to as a *Euclidean distance*. Numerically, the squares of the distances are added, followed by a square root, line segment c.

A Euclidean distance is "as the crow flies," not bounded by a street grid. Pythagoras' theorem refers to this two-dimensional example.

Let's explore this distinction further. A standard and three batches—matching in lightness but mismatching in chroma and hue—are shown in Figure 5.9. Their ΔC^*_{ab} and ΔH^*_{ab} differences get geometrically smaller from top to bottom. The equivalent lightness difference of each batch based on Euclidean and city block distances is also shown. The visual task is to decide which distance measurement correlates best with the total color difference between standard and batch. You might find that the best distance measurement changes with color-difference magnitude. This distinction is important because it is one reason for low correlation between visual and calculated color differences. That is, the magnitude of color difference impacts how distance should be measured.

The CIELAB Euclidean distance between two colors is defined as ΔE^*_{ab}, shown in Figure 5.10. The formulas are given in Eqs. (5.9) and (5.10)

$$\Delta E^*_{ab} = \sqrt{(\Delta L^*)^2 + (\Delta a^*)^2 + (\Delta b^*)^2} \tag{5.9}$$

$$\Delta E^*_{ab} = \sqrt{(\Delta L^*)^2 + (\Delta C^*_{ab})^2 + (\Delta H^*_{ab})^2} \tag{5.10}$$

The term "ΔE" does not refer to Euclidean difference; rather it was coined by Judd (1932) meaning the difference in sensation, based on the German word, *Empfindung*.

Finally, from Eq. (5.10), there is another way to calculate ΔH^*_{ab}, shown in Eq. (5.11). Hue difference is calculated as what is "left over" once the lightness and chroma differences are subtracted from the total color difference. ΔH^*_{ab} is assigned a positive value when Δh_{ab} is positive and assigned a negative value when Δh_{ab} is negative

$$\Delta H^*_{ab} = \sqrt{(\Delta E^*)^2 - (\Delta L^*)^2 - (\Delta C^*_{ab})^2} \tag{5.11}$$

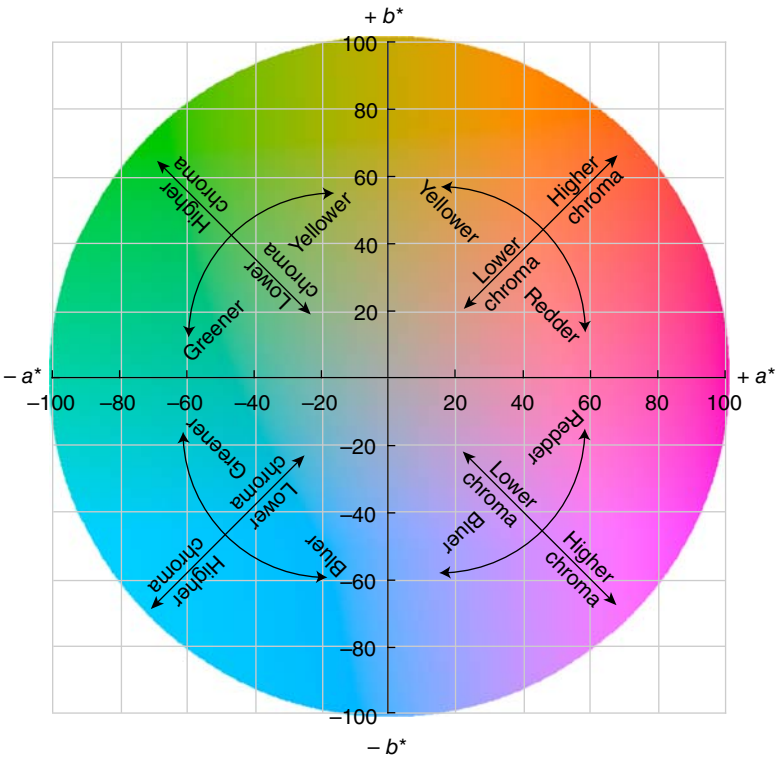

Figure 5.7 Color descriptors for changes in hue and chroma. Colored background has constant $L^* = 70$.

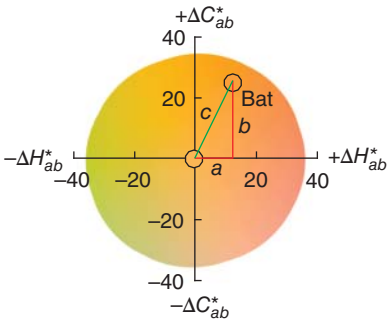

Figure 5.8 Standard and batch plotted in $\Delta C^*_{ab}\Delta H^*_{ab}$ looking down the L^* axis. The summation of line segments *a* and *b* is a city block distance. Line segment *c* is a Euclidean distance.

C. ELLIPSES AND ELLIPSOIDS

We will soon show that CIELAB has poor correlation with perceived color differences in the range of 0.5–5 ΔE^*_{ab}, a range often found in manufactured colored materials comparing a batch and standard. Perceptibility and acceptability ellipses and ellipsoids are often shown as evidence, for example, Figure 5.11. If ΔE^*_{ab} predicted the visual data perfectly, the plot would show circles with the same radius. But what, exactly, are ellipses and ellipsoids?

Suppose that we are manufacturing a part painted green. We select 100 parts at random and measure their color. We also judge whether the parts match the standard making pass or fail judgments. The standard is $L^* = 50$, $a^* = -50$, and $b^* = 0$. A $\Delta L^*\Delta a^*\Delta b^*$ plot is made, shown in Figure 5.12.

The ΔL^* data are used to make a histogram, shown in Figure 5.13. The lightness data are reasonably random. A plot of the standard deviation is overlaid.

Plotting the $\Delta L^*\Delta a^*\Delta b^*$ data projected onto the $\Delta a^*\Delta b^*$ plane is shown in Figure 5.14. Although a standard deviation can be calculated for both Δa^* and Δb^*, the values would be misleading because of the interaction between Δa^* and Δb^*. A standard deviation is required that is based on Δa^*, Δb^*, and their interaction, $\Delta a^*\Delta b^*$.

A *variance–covariance matrix*, **S**, defines variability in two or more dimensions, defined for CIELAB in Eq. (5.12):

$$\mathbf{S} = \begin{pmatrix} \sigma_{\Delta L^*}{}^2 & \sigma_{\Delta L^*}\sigma_{\Delta a^*} & \sigma_{\Delta L^*}\sigma_{\Delta b^*} \\ \sigma_{\Delta a^*}\sigma_{\Delta L^*} & \sigma_{\Delta a^*}{}^2 & \sigma_{\Delta a^*}\sigma_{\Delta b^*} \\ \sigma_{\Delta b^*}\sigma_{\Delta L^*} & \sigma_{\Delta b^*}\sigma_{\Delta a^*} & \sigma_{\Delta b^*}{}^2 \end{pmatrix} \tag{5.12}$$

where σ is a variable's standard deviation (Wyszecki and Stiles 1982; Tzeng and Berns 2005; Manly and Alberto 2017). Variance, σ^2, is the square of a standard deviation. The diagonal coefficients (top left to bottom right) are the variances for each axis and the off-diagonal coefficients represent interaction, that is, covariance between pairs of axes.

The variance–covariance matrix for the green data is shown in Eq. (5.13)

$$\mathbf{S} = \begin{pmatrix} 66.55 & -0.97 & -1.84 \\ -0.97 & 11.99 & 11.16 \\ -1.84 & 11.16 & 12.67 \end{pmatrix} \tag{5.13}$$

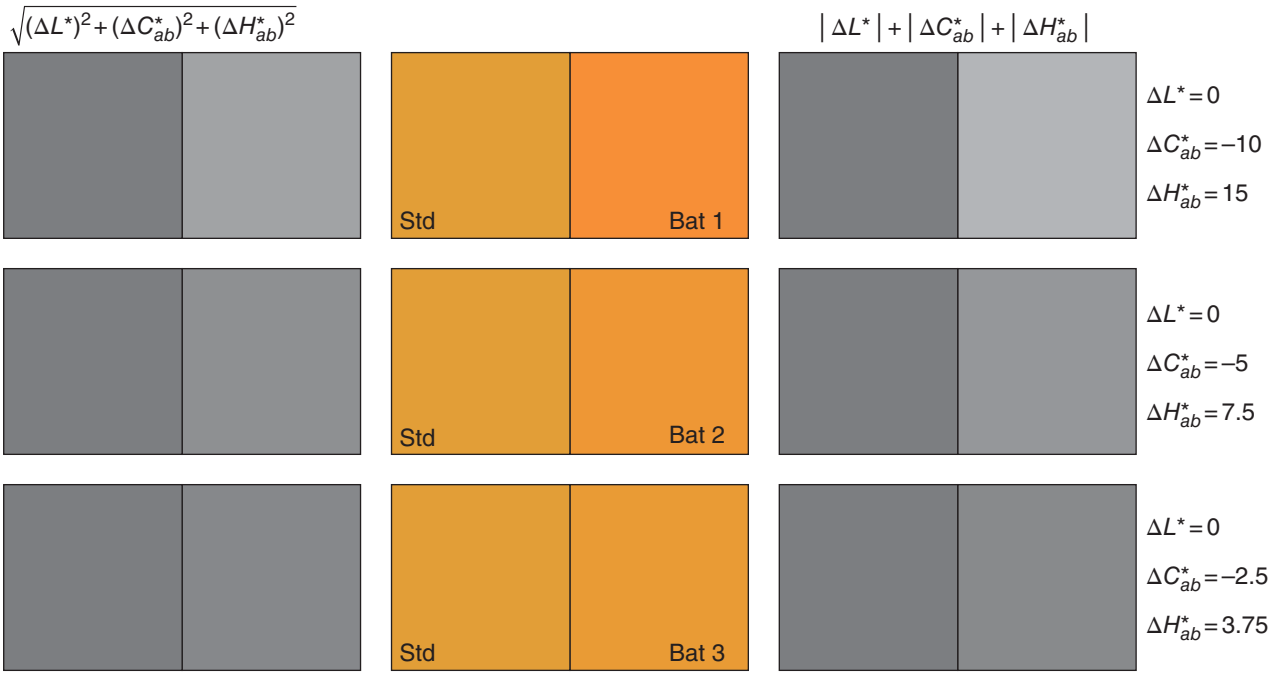

Figure 5.9 Color-difference pairs and their corresponding lightness differences for Euclidean (left) and city block (right) geometries.

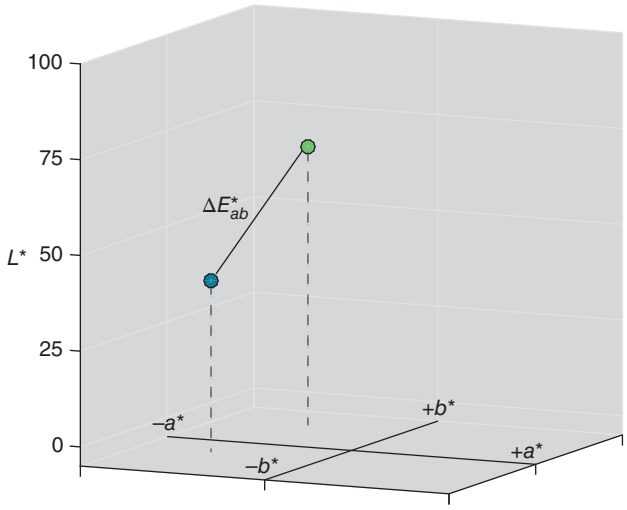

Figure 5.10 The difference in color between two stimuli can be quantified by plotting their coordinates in CIELAB. The distance between the two positions is defined by ΔE^*_{ab}.

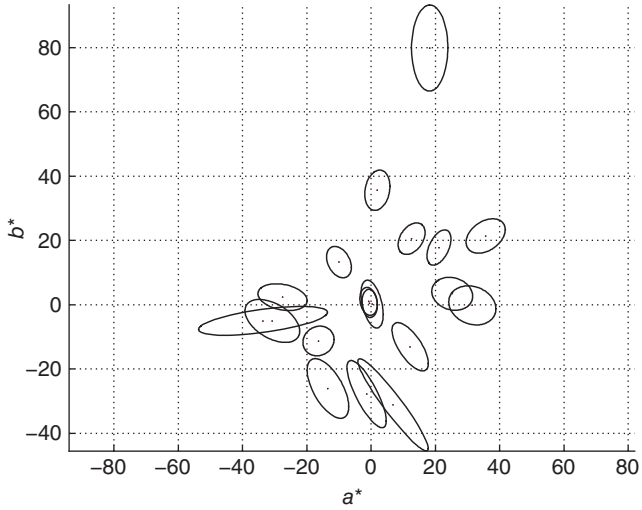

Figure 5.11 *RIT-DuPont dataset* plotted as perceptibility ellipsoids, magnified three times, projected onto the a^*b^* plane (Alman et al. 1989; Berns et al. 1991). Each ellipsoid represents the same visual color difference.

Lightness has the largest variance (65.55 compared with 11.99 and 12.67). The similar variances and covariances for Δa^* and Δb^* indicate the rotation of the data (11.99, 11.16, and 12.67). Notice that there are six unique values.

The coefficients of the variance–covariance matrix are used to derive an ellipsoid about the mean data (Tzeng and Berns 2005; Manly and Alberto 2017). Looking down the L^* axis results in an ellipse, also shown in Figure 5.14. The ellipsoid is plotted in Figure 5.15. The size of the ellipsoid can be changed to encompass a percentage of the total variance, to produce a confidence limit, or to correspond to a particular total color difference.

An optimized ΔE formula can be derived from the variance–covariance matrix, shown in Eqs. (5.14) and (5.15)

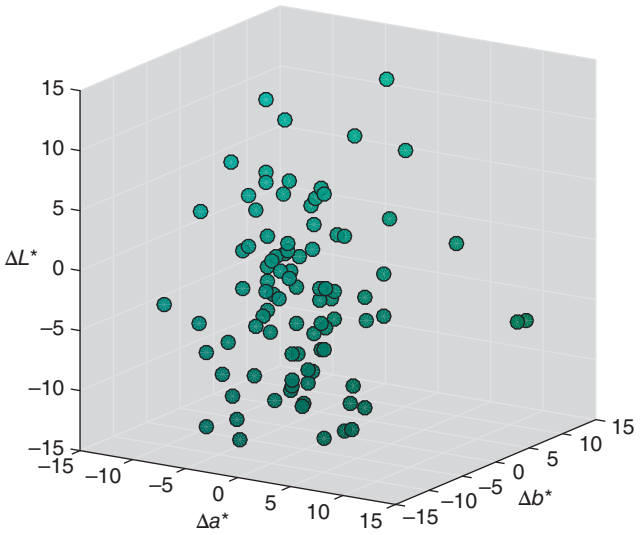

Figure 5.12 The $\Delta L^* \Delta a^* \Delta b^*$ coordinates of 100 random parts.

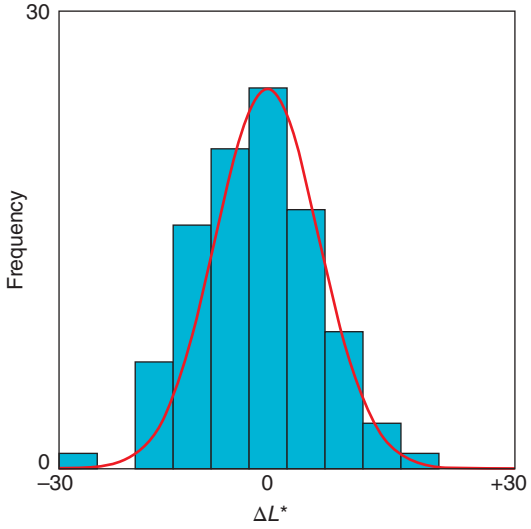

Figure 5.13 Histogram of the ΔL^* coordinates of the 100 random parts. Each vertical bar corresponds to 5 ΔL^*.

(Wyszecki and Stiles 1982; Tzeng and Berns 2005)

$$\mathbf{G} = \begin{pmatrix} g_{11} & g_{12} & g_{13} \\ g_{21} & g_{22} & g_{23} \\ a_{31} & a_{32} & g_{33} \end{pmatrix} = \mathbf{S}^{-1} \tag{5.14}$$

$$\Delta E_{\text{optimized}} = \sqrt{\begin{matrix} g_{11}(\Delta L^*)^2 + 2g_{12}(\Delta L^*)(\Delta a^*) + 2g_{13}(\Delta L^*)(\Delta b^*) \\ + g_{22}(\Delta a^*)^2 + 2g_{23}(\Delta a^*)(\Delta b^*) + g_{33}(\Delta b^*)^2 \end{matrix}} \tag{5.15}$$

Because the tilt about the L^* axis is slight, the formula can be simplified by removing the lightness covariance

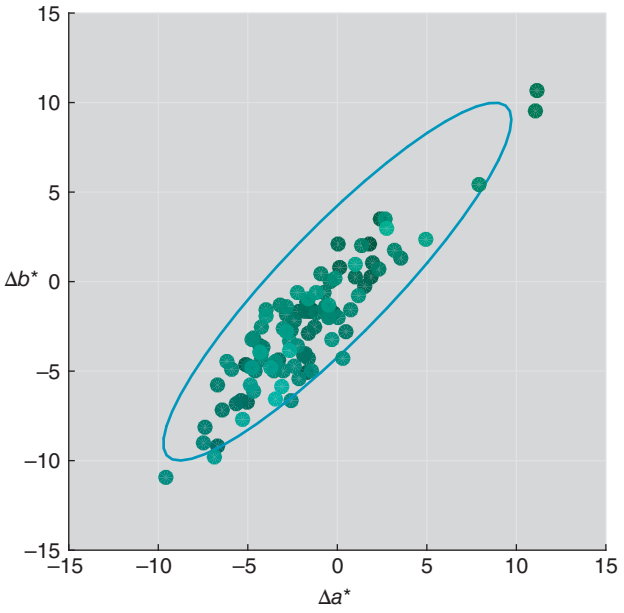

Figure 5.14 $\Delta L^* \Delta a^* \Delta b^*$ data for the green part projected onto the $\Delta a^* \Delta b^*$ plane. The cyan line is the 95% confidence ellipse.

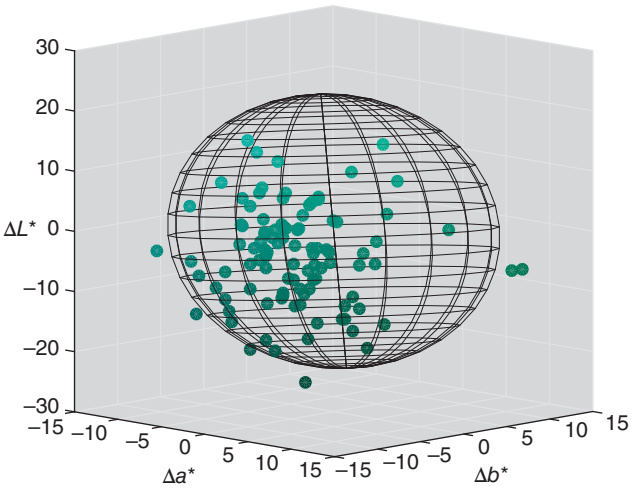

Figure 5.15 $\Delta L^* \Delta a^* \Delta b^*$ data for the 100 green parts along with a 95% confidence ellipsoid.

coefficients, resulting in the $\Delta E_{\text{optimized}}$ formula shown in Eq. (5.16)

$$\Delta E_{\text{optimized}} = \sqrt{\begin{matrix} 0.015(\Delta L^*)^2 + 0.464(\Delta a^*)^2 \\ - 0.820(\Delta a^*)(\Delta b^*) + 0.441(\Delta b^*)^2 \end{matrix}} \tag{5.16}$$

For the 100 parts, the total color difference ranges between 0.3 and 3.3 $\Delta E_{\text{optimized}}$. We might decide to set a tolerance limit to improve color consistency. Parts greater than the limit are rejected.

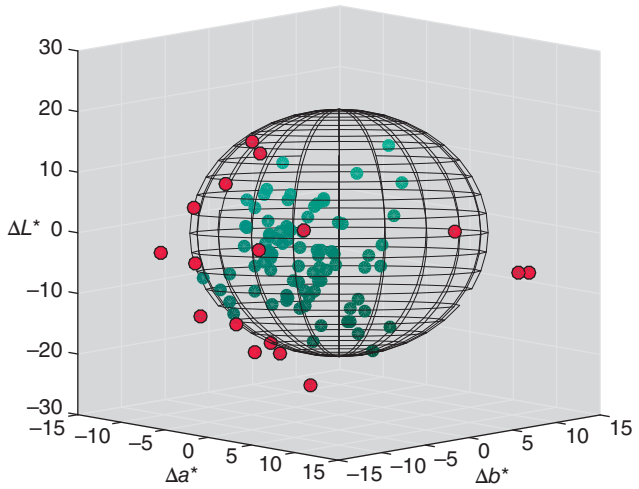

Figure 5.16 $\Delta L^* \Delta a^* \Delta b^*$ data for the 100 green parts along with an ellipsoid scaled to 2.5 $\Delta E_{\text{optimized}}$. Parts having $\Delta E_{\text{optimized}} > 2.5$ are shown in red.

The visual data are used to set the tolerance limit (Brown and MacAdam 1949; Allen and Yuhas 1984; Indow and Morrison 1991; Berns 1996a). This is shown in Figure 5.16 where coordinates in red correspond to parts with a total color difference greater than 2.5.

When the assessment is part of a laboratory experiment, the visual data may have numerical values and the ellipsoid and corresponding color-difference formula are derived that best predict the visual data. In many cases, the colorimetric data are not well distributed about the standard and there may be an insufficient number of data points to reliably estimate an ellipsoid. Depending on the experimental design and number of observers, the visual data may have low precision. This also affects reliability. As an example, 14 color-difference pairs from the RIT-DuPont datset (Alman et al. 1989; Berns et al. 1991) were used to estimate a color-difference ellipsoid where each pair had the same visual difference. Fifty observers performed the experiment and visual uncertainty was calculated for each pair. A Monte-Carlo technique was used to estimate 5000 ellipsoids using the uncertainty data (Shen and Berns 2009). Fifty randomly selected ellipsoids are plotted in Figure 5.17. This particular combination of data placement, number of data points, and visual uncertainty resulted in large changes in ellipsoid volume, but stable orientation. We will use ellipses, ellipsoids, and covariance matrices to define both color tolerances and instrumental measurement precision (described in Chapter 6).

D. THE COLOR-DIFFERENCE PROBLEM

"Pending the development of an improved coordinate system, the use of one of the following coordinate systems is recommended whenever a three-dimensional spacing perceptually more nearly uniform than that provided by the

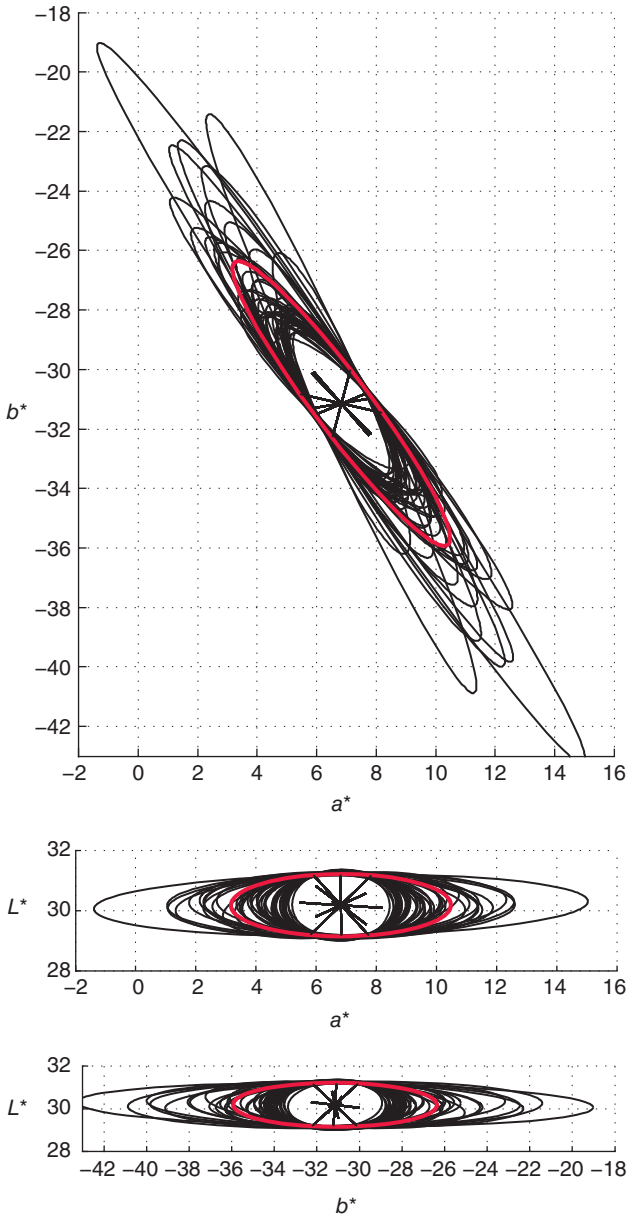

Figure 5.17 The effects of data placement, number of data points, and visual uncertainty on fitting ellipsoids. The red ellipsoid was based on the average visual data. The endpoints of each color-difference vector defined the positions of the colorimetric data. All plotted data are magnified three times.
Source: Adapted from Shen and Berns (2009).

XYZ system is desired" (CIE 2018). This one sentence paragraph precedes the description of CIELAB and CIELUV. This is not a strong endorsement of these "approximately uniform color spaces."

Luo and Rigg (1986) at the University of Bradford developed a single dataset combining the results from 13 different experiments, resulting in over 120 discrimination ellipses, known as the *BFD dataset*. By performing their own experiment where 20 observers scaled the color differences

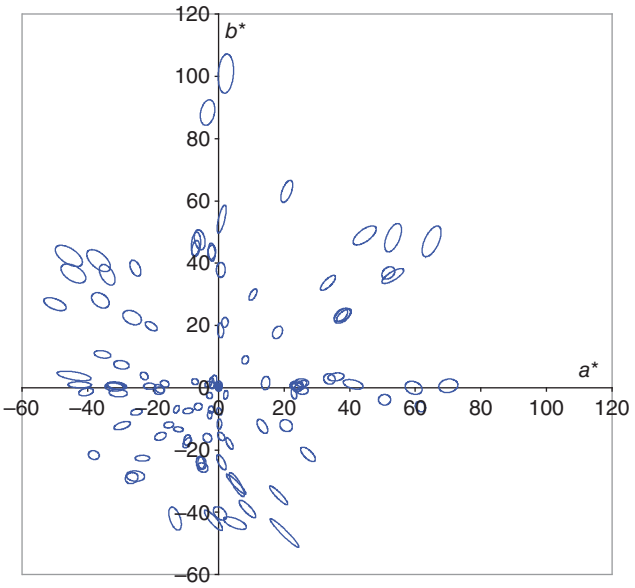

Figure 5.18 BFD ellipses plotted in CIELAB (Luo and Rigg 1986).

Table 5.1 Color discrimination parametric effects.

Magnitude of total color difference
Perceptibility or acceptability judgments
Texture
Sample edge and separation
Lightness of background
Sample size
Duration of observation
Observer variability
Psychophysical technique

of 600 pairs of wool samples, they were able to adjust the sizes of the ellipses to have a consistent visual difference. These ellipses are plotted in Figure 5.18. If CIELAB well predicted the visual data, the ellipses would be circular with similar radii.

The effects normalized by Luo and Rigg are known as *parametric factors* and several are listed in Table 5.1 (Robertson 1978; CIE 1993). The word "parametric" stems from the root word parameter and in this context, refers to effects influencing color-difference judgments. These are worth exploring in detail.

We have already demonstrated that the size of the total color difference is a parametric factor because it affects how distance is measured, shown in Figure 5.9.

Texture has a marked effect (Montag and Berns 2000; Xin, Shen, and Lam 2005), shown in Figure 5.19 where the average total color difference between each pair is the same, about 3 ΔE^*_{ab}.

Sample separation and the sharpness of the edge between two samples are also parametric effects (Witt 1990), shown in Figure 5.20. The top sample pair has been blurred. The second pair from the top is not outlined in black. As samples increase in separation, eye movements are required, resulting

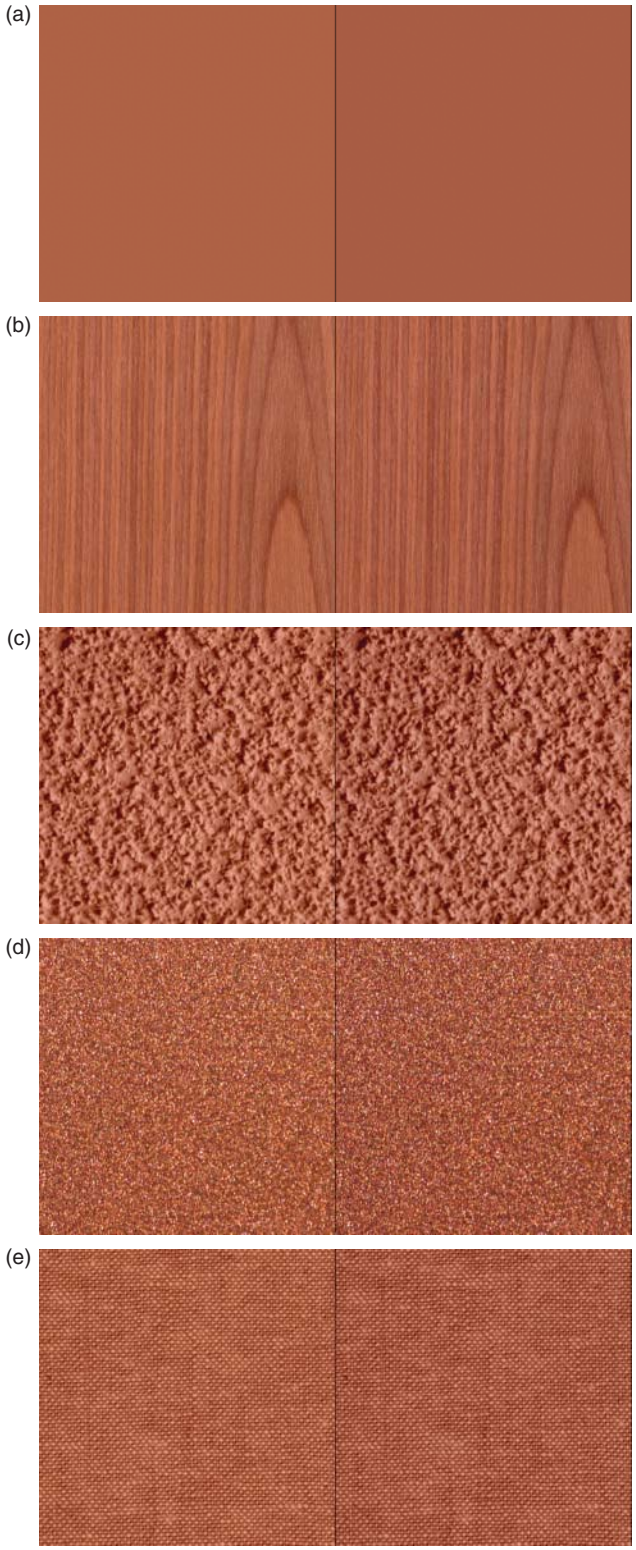

Figure 5.19 Samples of differing texture having the same average color difference. (a) solid, (b) wood laminate, (c) popcorn ceiling, (d) metallic coating, and (e) linen.

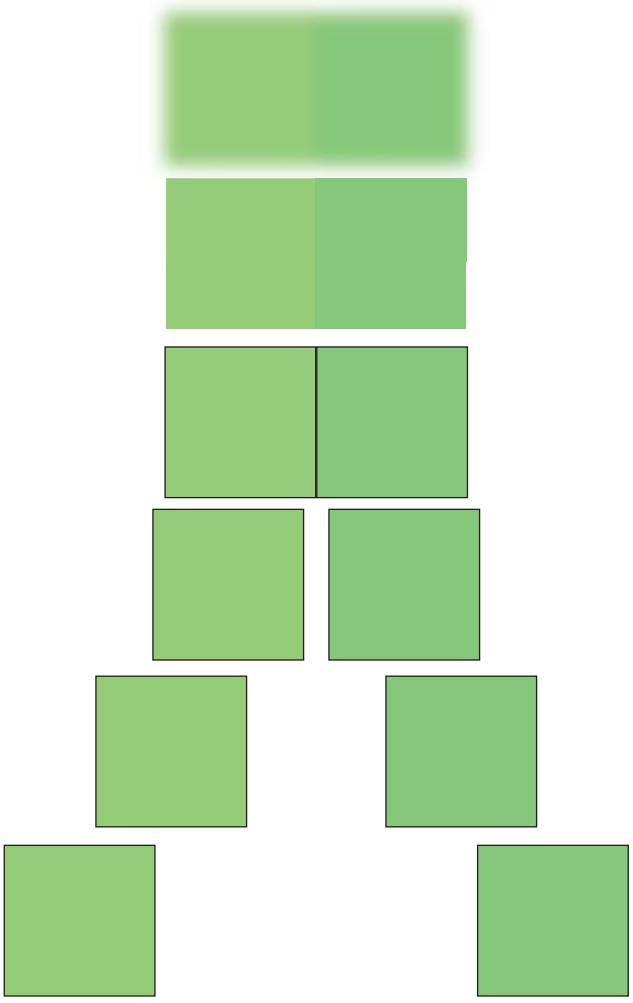

Figure 5.20 The effects of edge sharpness and sample separation on color discrimination.

in a short-term memory match. Such matches are less precise than simultaneous viewing (Newhall, Burnham, and Clark 1957; de Fez et al. 2001).

Background color and lightness affect perceived color differences (Guan and Luo 1999a,b; Xin, Lam, and Luo 2001). In Figure 5.21, a dark-brown color-difference pair has a white and black background. The visual difference is larger when this pair is viewed against the black background. The black background has a similar lightness to the average lightness of the pair. This results in "*crispening*" where the lightness difference is amplified (Takasaki 1966; Semmelroth 1970; Whittle 1992; Xin, Lam, and Luo 2004).

Sample size also affects visual differences, shown in Figure 5.22. We have already described how cone fundaments are a function of the field of view. In addition, effects caused by the color and lightness of the background diminish as samples increase in size (Brown 1952).

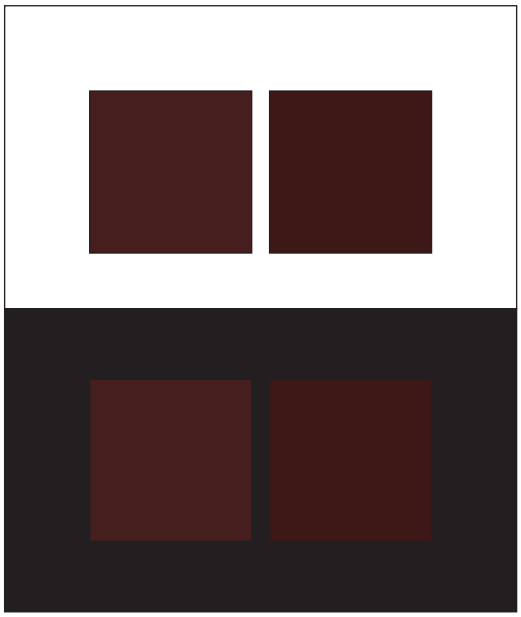

Figure 5.21 Brown color-difference pair viewed against white and black backgrounds. The black background has a similar lightness to the average lightness of the pair.

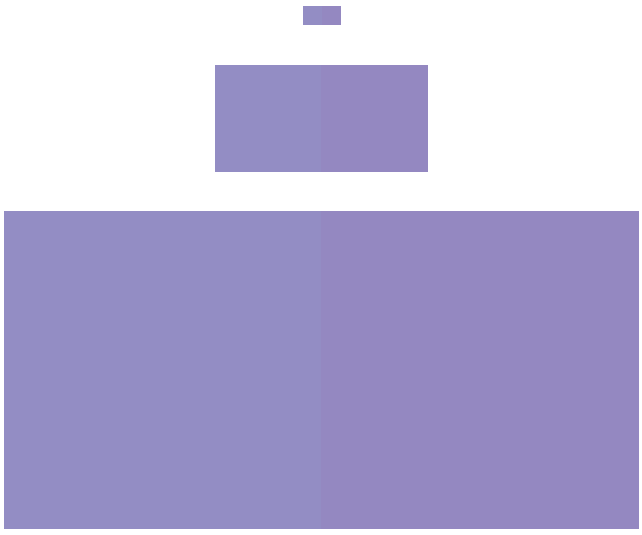

Figure 5.22 A color-difference pair shown at different sizes.

Increased observation time reduces the visual difference due to local adaptation to the samples. New colorists may experience this effect when staring at the batch and deciding how to adjust the recipe to improve the match to the standard. It is better to look at the pair for a brief time period and then look at neutral surfaces such as the walls of a light booth while making decisions.

Visual uncertainty has an enormous impact when defining color tolerances and developing color-difference formulas based on visual judgments. Berns (1996a) had 22 observers from various color industries perform a

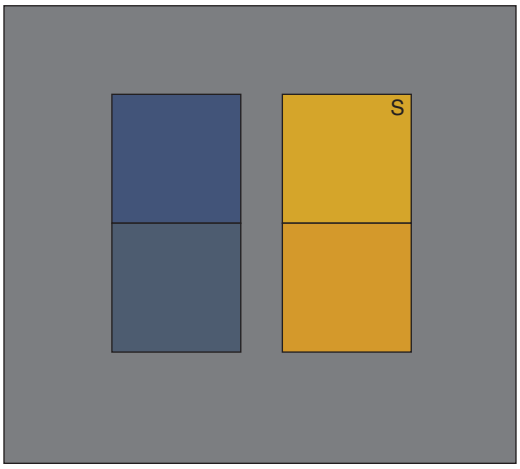

Figure 5.23 Color-difference experimental design. Color-difference pairs (right) are compared with a near-neutral anchor pair. The visual task is to decide if the pair's total color difference is smaller or larger than the anchor pair's total color difference.

color-difference experiment, shown in Figure 5.23, in which a gray color-difference pair was used to define each observer's quality criterion, known as an *anchor pair* (Alman et al. 1989). Thirty-two yellow samples representing batches were compared to a standard. 95% confidence ellipsoids were fit to samples that were passed, shown for three observers in Figure 5.24. Despite the use of an anchor pair, the differences between individual observers were striking. Conversely, Witt (1987) found considerably better observer reproducibility when measuring thresholds. We suspect that despite the presence of the anchor pair, some of the Berns observers were basing their judgments on their personal experiences. That is, acceptability rather than perceptibility judgments had been made.

The experimental configuration shown in Figure 5.23 was designed to eliminate acceptability judgments by using an anchor pair. However, having a single sample identified as the standard confounded the experiment leading some observers to perform acceptability judgments. A way to avoid this confound is to use color-difference pairs without an identified standard. This approach is used in laboratory experiments designed to measure perceptibility. When using a single anchor pair, the psychophysical technique known as the *method of constant stimuli* is used (Bartleson and Grum 1984; Gescheider 1997), designed to determine the magnitude of color difference where 50% of the observers would judge the color difference larger than the anchor pair and 50% would judge the color difference smaller, called T50 (tolerance at 50%) (Alman et al. 1989). This results in a series of estimated color differences all having the identical visual difference. An alternate technique is to produce a gray scale with samples varying in lightness, shown in Figure 5.25. One sample is fixed and the observer

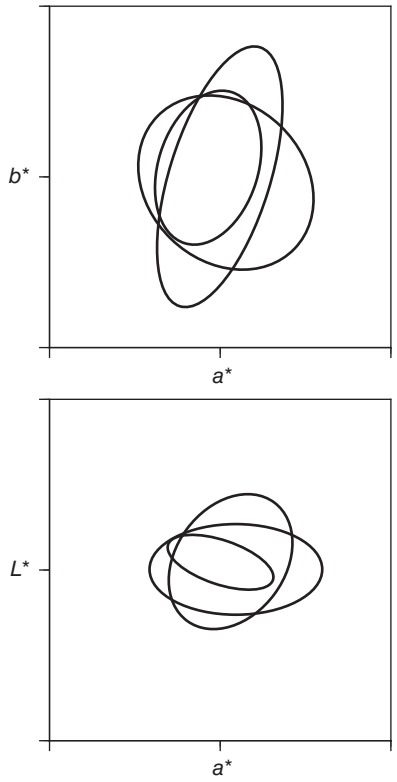

Figure 5.24 Tolerance ellipsoids for three different observers performing the same experiment.
Source: Berns (1996a). Reproduced with permission of John Wiley & Sons.

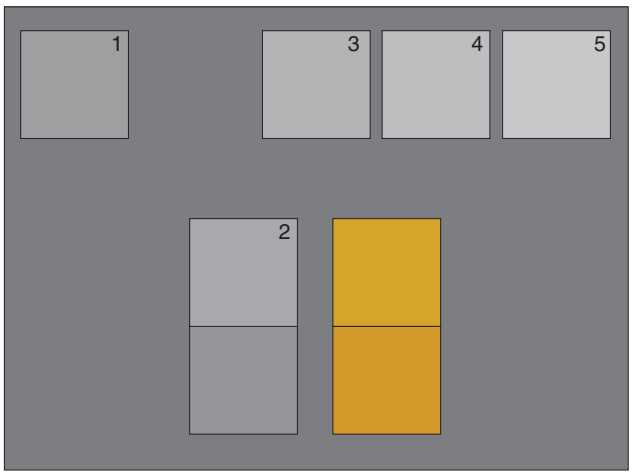

Figure 5.25 Gray scale (GS) method of determining the perceived total color difference of a color pair. A gray is selected resulting in the most similar visual difference followed by visual interpolation. This yellow pair might be judged equivalent to a gray difference of 2.3.

selects a second gray producing a lightness difference most similar to the total color difference of the test pair. Visual interpolation is encouraged and a gray-scale difference is estimated for the color-difference pair. This results in a series

of color-difference pairs with varying visual difference. The two techniques may produce different results and lead to different uncertainties (Montag and Wilber 2003).

E. WEIGHTED COLOR-DIFFERENCE FORMULAS

Having determined that Euclidean distances in CIELAB do not predict visual differences, we might take two approaches to improve prediction accuracy. The first would be to develop a new color space. The second would be to use CIELAB and develop an empirically derived color-difference formula. The new formula would produce total color differences that are ellipsoids rather than spheres. We will first consider the second approach.

Our first decision is the form of the color-difference formula. Will it be $\Delta L^* \Delta a^* \Delta b^*$ or $\Delta L^* \Delta C^*_{ab} \Delta H^*_{ab}$? This is visualized in Figure 5.26 where visual tolerances, shown as ellipses, can be approximated by $\Delta a^* \Delta b^*$ tolerances or $\Delta C^*_{ab} \Delta H^*_{ab}$ tolerances. The difference in area between each rectangle and corresponding ellipse is smaller when $\Delta C^*_{ab} \Delta H^*_{ab}$ tolerances are used. This trend is seen in Figure 5.18 for the BFD dataset. Thus, in general, a $\Delta C^*_{ab} \Delta H^*_{ab}$ tolerance is a closer approximation to the visual data.

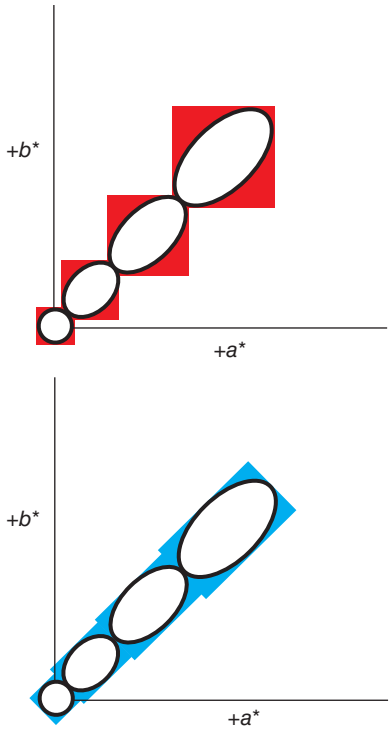

Figure 5.26 Visual tolerances, shown as ellipses, can be approximated by $\Delta a^* \Delta b^*$ tolerances, shown in the upper figure as the red rectangles, or $\Delta C^*_{ab} \Delta H^*_{ab}$ tolerances, shown in the lower figure as the cyan rectangles.

The second decision is choosing a performance metric. If we plot ΔE versus ΔV and fit a line, a correlation coefficient would be a simple metric. Over the years, a number of metrics have been proposed and used to quantify performance (García et al. 2007). We recommend *STRESS*, derived by Kruskal (1964), as it enables statistical significance testing. It is described in detail in a nearby sidebar and García et al. (2007). Formulas with poor performance have STRESS near 50. The best that can be achieved given visual uncertainty is about five (Shen and Berns 2009).

The third decision is choosing which datasets to use. For our purpose of explaining how color-difference formulas are derived, we will use the *RIT-DuPont data* (Alman et al. 1989; Berns et al. 1991), which is most familiar to the author. The method of constant stimuli, shown above in Figure 5.23, was used where 50 observers judged 875 color-difference pairs, about 44 000 observations. Each color pair was compared with a near neutral anchor pair with a $\Delta E^*_{ab} = 1$. Nineteen regions in CIELAB, referred to as *color centers*, were studied. At each center, glossy paint samples were prepared in a single vector direction in CIELAB. Between five and seven color-difference pairs were produced in a given direction. The vector directions were selected to determine the size and orientation of fitted ellipsoids for each color center. Using a technique known as *probit analysis* (Finney 1971), the T50 was determined for the 156 vector directions. These color tolerance vectors are plotted in Figure 5.27. The T50 dataset is one of several datasets used to derive the current CIE and ISO recommended color-difference formula, CIE2000 (CIE 2001, 2018; ISO/CIE 2014).

Figure 5.27 The RIT-DuPont data are a set of color-difference vectors, corresponding to a single visual difference. The differences in vector length reveal CIELAB's lack of visual uniformity. (The strong-orange-yellow color center is not shown.).
Source: Berns et al. (1991). Reproduced with permission of John Wiley & Sons.

Most color-difference datasets have a range of visual differences. The method of constant stimuli, used in the RIT-DuPont experiment, results in a single visual difference, defined as $\Delta V = 1$. An optimal formula for this dataset results in color differences near 1.0 and STRESS near 5. The performance of ΔE^*_{ab} is plotted in Figure 5.28a. The color differences were normalized to $\overline{\Delta E^*_{ab}} = 1.0$. Color differences range from 0.8 to 4.4 ΔE^*_{ab}. The *STRESS* for ΔE^*_{ab} is 33.42.

We can now begin to propose a color-difference formula, optimize its constants by minimizing STRESS, and compare its performance to CIELAB and other commonly used formulas by performing an *F*-test.

One way to weight a color-difference formula is to change the relative importance of lightness, chroma, and hue differences. This might be due to a parametric effect, differences in acceptability criteria, or CIELAB visual nonuniformity. The formula is shown in Eq. (5.17):

$$\Delta E_k = \frac{1}{k_E}\sqrt{\left(\frac{\Delta L^*}{k_L}\right)^2 + \left(\frac{\Delta C^*_{ab}}{k_C}\right)^2 + \left(\frac{\Delta H^*_{ab}}{k_H}\right)^2} \quad (5.17)$$

where k is a reciprocal weight. Optimization was used to estimate k_E, k_L, and k_C minimizing STRESS. The optimization was constrained where $\overline{\Delta E_k} = 1.0$, hence the need for $1/k_E$. The hue weighting, k_H, is defined as unity, resulting in weights relative to hue difference. The optimized formula, color-difference plot, and STRESS are shown in Figure 5.28b. The chroma weight, k_C, is about twice the magnitude of the other weights. Weights greater than unity reduce the contribution of the particular difference toward the total color difference.

The BFD ellipses and RIT-DuPont ellipsoids enlarge with increases in chroma. This results in a weighting that changes with CIELAB position. This was first recognized by McDonald (1974) and eventually led to the CMC(l:c) formula, developed by the Colour Measurement Committee of the Society of Dyers and Colourists, described below (Clarke, McDonald, and Rigg 1984). We will perform a similar analysis with the RIT-DuPont data.

Evaluating positional dependencies requires data with color differences varying in a single dimension. The 156 difference vectors were sorted by $\Delta L^*/\Delta E^*_{ab}$, $\Delta C^*_{ab}/\Delta E^*_{ab}$, and $\Delta H^*_{ab}/\Delta E^*_{ab}$. Those with ratios greater than 90% are plotted against position in Figure 5.29. There is considerable dispersion even though this dataset has high precision compared with other datasets (Shen and Berns 2009). The lightness data have curvature and were fit with a parabolic function. The chroma and hue data were fit with linear functions and show the expected increase with chroma position. These positional functions are referred to as S_L, S_C, and S_H, the general formula shown in Eq. (5.18)

$$\Delta E_{\text{graph}} = \frac{1}{k_E}\sqrt{\left(\frac{\Delta L^*}{S_L}\right)^2 + \left(\frac{\Delta C^*_{ab}}{S_C}\right)^2 + \left(\frac{\Delta H^*_{ab}}{S_H}\right)^2} \quad (5.18)$$

The formula using the line fit data, color-difference plot, and STRESS are shown in Figure 5.28c.

One limitation in using such line fits is the differing offsets. Each offset defines a reciprocal weight, k, which may not be appropriate when all three line-fits are used in a single formula. Using the line-fit coefficients as starting values, all of the formula coefficients were optimized simultaneously with the offsets defined as unity. The simultaneous optimization enables the inclusion of all of the visual data without the need to sort. The final formula, color-difference plot, and STRESS are shown in Figure 5.28d. As shown in the STRESS sidebar, the graph and optimized formulas had equal performance. Both were superior to the *k*-type formula, and all three formulas were superior to ΔE^*_{ab}.

The two weights are combined into a single formula, shown in Eq. (5.19) (CIE 1993)

$$\Delta V = \Delta E = \frac{1}{k_E}\sqrt{\left(\frac{\Delta L^*}{k_L S_L}\right)^2 + \left(\frac{\Delta C^*_{ab}}{k_C S_C}\right)^2 + \left(\frac{\Delta H^*_{ab}}{k_H S_H}\right)^2} \quad (5.19)$$

This formula is the basis for the CMC(l:c) and CIE94 formulas, described below.

Statistical Evaluation of Color-Difference Formula Performance Using STRESS

Over the years, a variety of metrics have been used to both optimize and evaluate color-difference formulas. Basically, calculated color differences are compared with visual color differences and correlation is measured. One important requirement is statistical significance testing. This is a similar problem in multidimensional scaling where the observational data are evaluated to determine the number of dimensions required to best fit the data. Kruskal (1964) developed a *standardized residual sum of squares metric*, or *STRESS*. This accounts for scale differences in each dimension. STRESS values can be used to perform an *F*-test where variability is tested for statistical significance. García et al. (2007) described the use of STRESS for comparing the performance of color-difference formulas. The formulas to calculate STRESS are shown in Eq. (5.20):

$$STRESS = 100\left(\frac{\sum_i (\Delta E_i - F\Delta V_i)^2}{\sum_i F^2 \Delta V_i^2}\right)^{1/2} \quad (5.20)$$

where i defines the number of color-difference pairs, ΔE is the formula being evaluated, and ΔV is visual difference. F is the scaling factor, shown in Eq. (5.21)

$$F = \frac{\sum_i \Delta E_i^2}{\sum_i \Delta E_i \Delta V_i} \quad (5.21)$$

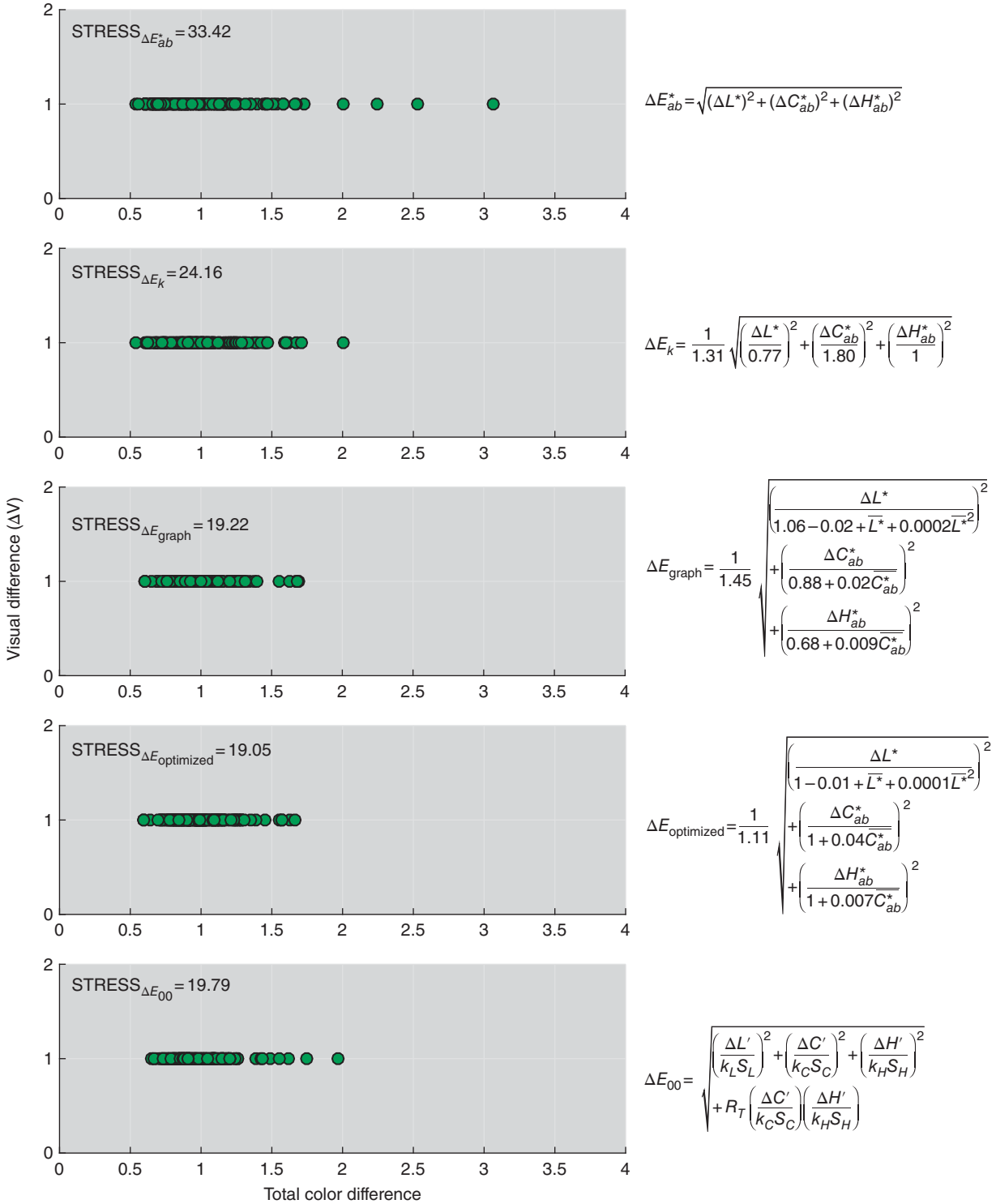

Figure 5.28 The performance of each listed total color-difference formula in predicting the RIT-DuPont visual data.

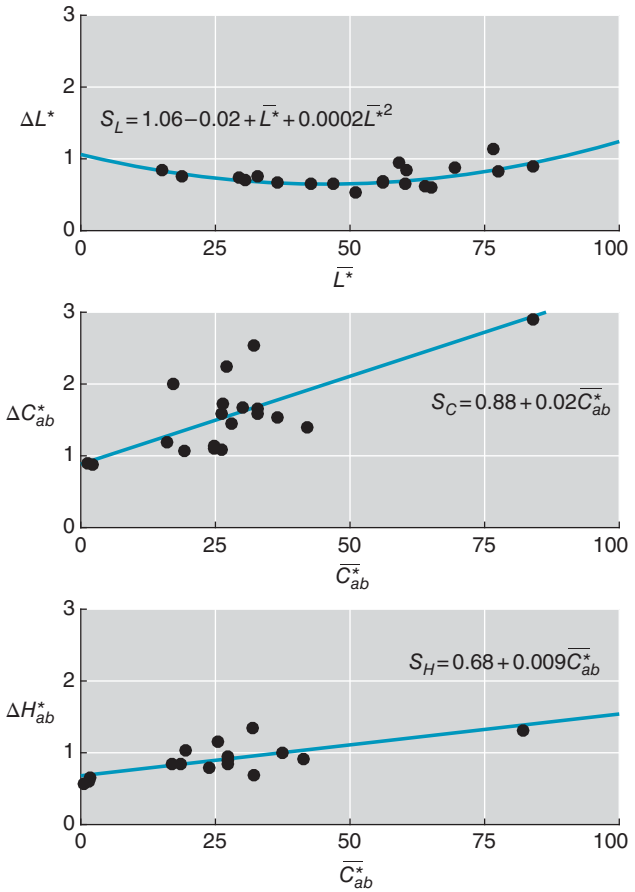

Figure 5.29 RIT-DuPont data sorted into pairs varying predominantly in CIELAB lightness, chroma, and hue.

When uncertainties are known for each ΔV, a weighted normalized STRESS can be used, shown in Eq. (5.19) where w defines the weight

$$WSTRESS = 100\left(\frac{\sum_i w_i(\Delta E_i - F\Delta V_i)^2}{\sum_i w_i F^2 \Delta V_i^2}\right)^{1/2} \quad (5.22)$$

Data having higher precision (i.e. lower uncertainty) have higher weighting.

When a color-difference formula predicts visual differences perfectly, STRESS equals zero.

An F-test is used to determine whether two formulas are statistically significantly the same or different. The F value is calculated as shown in Eq. (5.23):

$$F = \frac{(STRESS_{\Delta E_A})^2}{(STRESS_{\Delta E_B})^2} \quad (5.23)$$

where the two formulas are ΔE_A and ΔE_B. The two formulas are different when $F < F_C$ or $F > 1/F_C$, where F_C is the critical value of the two-tailed F distribution with 95% confidence level and $(N-1, N-1)$ degrees of freedom. N is the number of observations. In Microsoft Excel, F_C is calculated as FINV(0.975, $N-1$, $N-1$). The value 0.975 is used rather than 0.95 because this is a two-tailed test. A numerical example is shown in Table 5.2 using the RIT-DuPont data. For significance testing, the ±T50 data are used to calculate two color differences about a color center, resulting in 312 color differences and 311 degrees of freedom.

Table 5.2 Significance testing of each listed color-difference formula.

Formula A	Formula B	Stress A	Stress B	F	Significantly different
ΔE^*_{ab}	ΔE_k	33.42	24.16	1.80	Yes
ΔE^*_{ab}	ΔE_{graph}	33.42	19.22	3.02	Yes
ΔE_{graph}	$\Delta E_{\text{optimized}}$	19.22	19.05	1.02	No
ΔE_{00}	$\Delta E_{\text{optimized}}$	19.79	19.05	1.08	No

The degrees of freedom equaled 311. The critical values are 0.80 and 1.25.

F. CMC(L:C) COLOR-DIFFERENCE FORMULA

The United Kingdom's Society of Dyers and Colourists' Colour Measurement Committee (CMC) pioneered developing weighted color-difference formulas that predicted perceptibility and acceptability data. Dyeing textiles is a batch process where dye transfers from an aqueous solution to the textile. Once the dye has transferred, a sample is taken, washed, dried, cooled, measured with a spectrophotometer, and compared visually to a standard. If the match is unacceptable, the dyer will add more dye to the solution and repeat the procedure. Over time, a database is developed with standards, batches, and acceptable and unacceptable visual decisions.

The CMC evaluated various datasets and models and a formula was published in 1984, known as the *CMC* formula (Clarke, McDonald, and Rigg 1984), shown in Eqs. (5.24)–(5.29)

$$\Delta E_{\text{CMC}} = \sqrt{\left(\frac{\Delta L^*}{l\,S_L}\right)^2 + \left(\frac{\Delta C^*_{ab}}{c\,S_C}\right)^2 + \left(\frac{\Delta H^*_{ab}}{S_H}\right)^2} \quad (5.24)$$

$$S_L = \begin{cases} \dfrac{0.040\,975\,L^*_{\text{Std}}}{1+0.017\,65\,L^*_{\text{Std}}} & L^*_{\text{Std}} \geq 16 \\ 0.511 & L^*_{\text{Std}} < 16 \end{cases} \quad (5.25)$$

$$S_C = \frac{0.0638 C^*_{ab,\mathrm{Std}}}{1 + 0.0131 C^*_{ab,\mathrm{Std}}} + 0.638 \tag{5.26}$$

$$S_H = S_C(Tf + 1 - f) \tag{5.27}$$

$$f = \sqrt{\frac{(C^*_{ab,\mathrm{Std}})^4}{(C^*_{ab,\mathrm{Std}})^4 + 1900}} \tag{5.28}$$

$$T = \begin{cases} 0.56 + |0.2\cos(h_{ab,\mathrm{Std}} + 168°)| & 164° \le h_{ab,\mathrm{Std}} \le 345° \\ 0.36 + |0.4\cos(h_{ab,\mathrm{Std}} + 35°)| & \text{otherwise} \end{cases} \tag{5.29}$$

This is a weighted color-difference formula of the form shown in Eq. (5.19) and variables l and c are parametric factors, equivalent to k_L, and k_C. The optimization used to estimate the model coefficients minimized *instrumental-wrong decisions*, that is, minimized the number of cases where a formula predicted an acceptable match although the visual decision was unacceptable, and vice versa.

Its large number of significant figures suggests a level of precision and accuracy that cannot be supported on statistical grounds, given typical visual uncertainties judging color differences. Nevertheless, it corrects the major deficiency in CIELAB, that of chroma position dependency, and has provided significant improvement in comparison to CIELAB and CIELUV.

The color-tolerances ellipsoids (shown as projections) derived from the CMC formula are shown in Figure 5.30. Chroma differences are weighted by chroma position. Hue differences are weighted by both chroma position *and* hue angle. McDonald (1980a,b,c) found that if uniform weighting was applied for all hues, there were systematic instrumental-wrong decisions for brown and turquoise colors. By introducing a hue-angle-dependent weighting function, this could be corrected. However, this weighting applies to many colors, not just these two, e.g. brown, tan, and orange. Thus, the ellipses are narrower around CIELAB hue angles of 60° and 270°. Also, lightness differences are weighted by lightness position, where ellipses increase in radius with increasing lightness.

The CMC formula incorporates parametric factors, l and c, assuming that the hue factor is always unity. The Colour Measurement Committee found that a ratio of 2:1, that is, reducing the weighting of differences in lightness, better correlated with acceptability decisions when judging textiles. The formula is notated as ΔE_{cmc} (2:1). Many users of this formula maintain the 2:1 ratio without determining whether it is appropriate for their specific application. The formula remains in widespread use and is recommended by the ISO for quantifying the colorfastness of textiles (ISO 2009a), and the BSI (1988) and the AATCC (2015) for calculating small color differences.

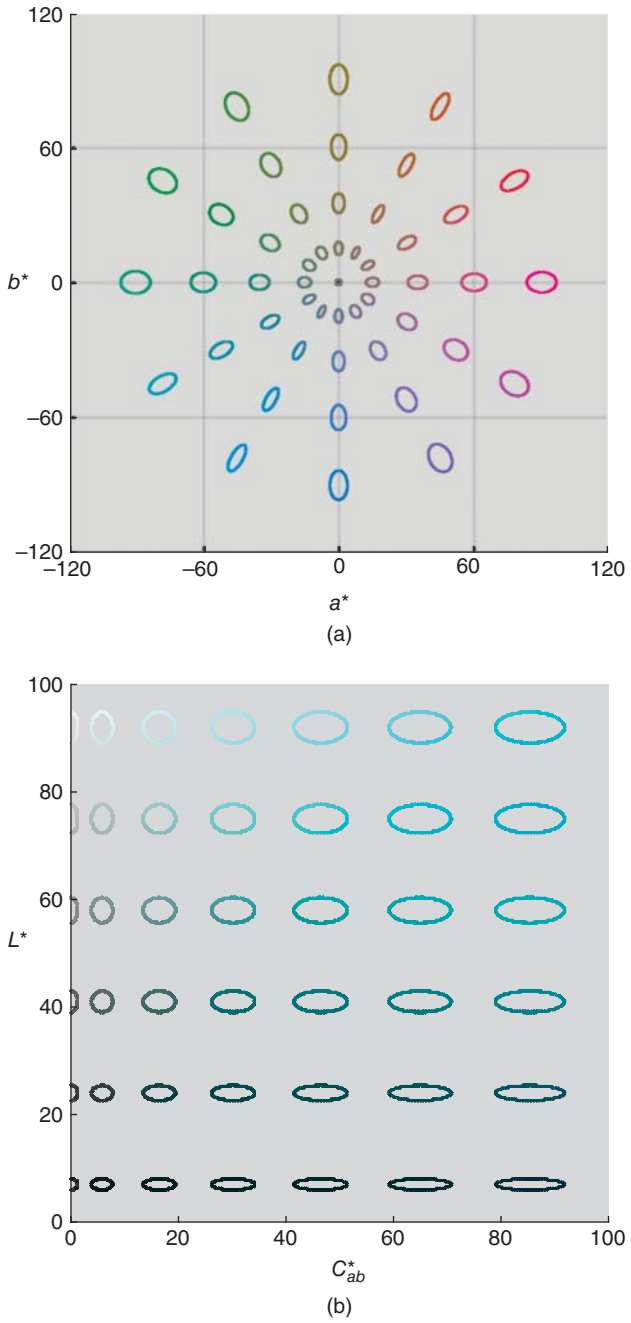

Figure 5.30 The CMC ΔE_{cmc} formula can be used to derive corresponding color-tolerance ellipsoids shown here for (a) color centers at a constant 50 L^*, two times magnification, and projected onto a a^*b^* diagram and (b) color centers at constant 200 h_{ab}, two times magnification, and projected onto a $L^*C^*_{ab}$ diagram.

G. CIEDE2000 COLOR-DIFFERENCE FORMULA

Until the 1990s, the CIE had taken the approach that color-difference spaces should be derived such that Euclidean distances could be used for assessing color

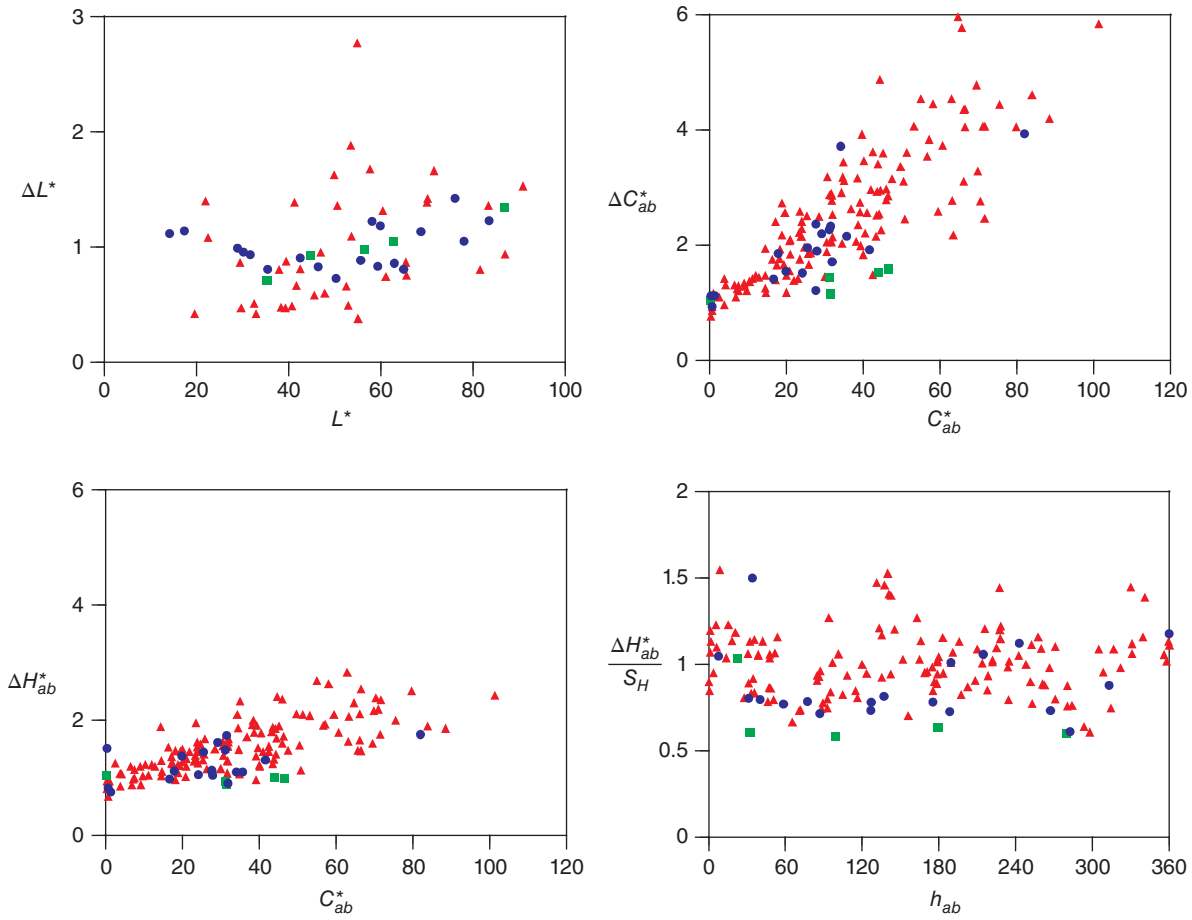

Figure 5.31 Three datasets were evaluated by the CIE technical committee that derived CIE94: BFD shown as red triangles, BAM shown as green squares, and RIT-DuPont shown as blue dots.
Source: Adapted from Berns (1993a).

quality. In other words, the transformation from *XYZ* to the uniform color space could be as complex as necessary. The formulas that calculated color differences would be simple. In this approach, the CIE would be recommending a new color space and as a consequence, CIELAB and CIELUV would become deprecated. Color-difference experts recognized that this approach would not be timely and that it would be very difficult to eliminate the use of CIELAB and CIELUV. Instead, the CIE also developed weighted color-difference formulas based on CIELAB: CIE94 (CIE 1995a) and CIEDE2000 (CIE 2001, 2018; ISO/CIE 2014).

Datasets were compiled meeting several criteria. The stimuli had to be physical samples such as painted panels, fabrics, or thread wound on cards—computer-controlled displays were specifically excluded. The experimental procedure and conditions had to be controlled and well documented. At least 20 observers must have participated in the experiment and uncertainty included in the reported visual data. Three datasets met these criteria: BFD (Luo and Rigg 1986), RIT-DuPont (Alman et al. 1989; Berns et al. 1991), and *BAM* (Witt and Döring 1983; Witt 1987). Each dataset was processed to extract color-difference pairs varying in only lightness, or chroma, or hue, enabling trend plots to be drawn. The trend plots evaluated by the CIE to determine the form of the color-difference formula are shown in Figure 5.31 (Berns 1993a). Each dataset had a unique trend in lightness difference. The chroma difference and hue difference trends were consistent. Finally, hue angle dependencies were evaluated, as included in the CMC formula. No trend was evident. Because of the dispersion of the data, only linear terms were used, the final formula shown in Eqs. (5.30)–(5.34)

$$\Delta E^*_{94} = \sqrt{\left(\frac{\Delta L^*}{k_L S_L}\right)^2 + \left(\frac{\Delta C^*_{ab}}{k_C S_C}\right)^2 + \left(\frac{\Delta H^*_{ab}}{k_H S_H}\right)^2} \tag{5.30}$$

$$S_L = 1 \tag{5.31}$$

$$S_C = 1 + 0.045 C^*_{ab} \tag{5.32}$$

$$S_H = 1 + 0.015C^*_{ab} \tag{5.33}$$

$$C^*_{ab} = \left\{ \begin{array}{c} C^*_{ab,\mathrm{Std}} \\ \sqrt{C^*_{ab,1} C^*_{ab,2}} \end{array} \right\} \tag{5.34}$$

The color-tolerance ellipsoids derived from the CIE94 formula are shown in Figure 5.32. Ellipsoids do not change with lightness nor with hue.

A set of reference parametric factors were defined when using CIE94 (CIE 1995a), shown in Table 5.3. Matching these factors will result in the best performance. Values for k_L, k_C, and k_H have been suggested for reference conditions dissimilar to the CIE conditions (CIE 1993).

As the 1990s progressed, additional datasets were identified that met the CIE criteria. The University of Leeds produced a new dataset that addressed lightness, chroma, and hue dependencies (Kim 1997; Kim and Nobbs 1997). Experiments concentrating on lightness dependencies were carried out at the University of Derby and the University of Keele (Chou et al. 2001). An experiment focusing on hue-angle dependencies was carried out at Rochester Institute of Technology (Qiao 1996; Qiao et al. 1998). These datasets and further inspection of the BFD, RIT-DuPont, and BAM datasets resulted in an improvement to CIE94 known as CIEDE2000 or ΔE_{00} (CIE 2001, 2018). Its development is described by Luo, Cui, and Rigg (2001). The formulas to calculate CIEDE2000 are shown in Eqs. (5.35)–(5.48). Parametric factors can also be used with CIEDE2000, notated, for example, as $\Delta E_{00}(2{:}1{:}1)$ when used for textile applications.

$$\Delta E_{00} = \sqrt{\left(\frac{\Delta L'}{k_L S_L}\right)^2 + \left(\frac{\Delta C'}{k_C S_C}\right)^2 + \left(\frac{\Delta H'}{k_H S_H}\right)^2 + R_T \left(\frac{\Delta C'}{k_C S_C}\right)\left(\frac{\Delta H'}{k_H S_H}\right)} \tag{5.35}$$

$$G = 0.5\left(1 - \sqrt{\frac{\overline{C}^{*7}_{ab}}{\overline{C}^{*7}_{ab} + 25^7}}\right) \tag{5.36}$$

$$L' = L^* \tag{5.37}$$

$$a' = (1 + G)a^* \tag{5.38}$$

$$b' = b^* \tag{5.39}$$

$$C' = \sqrt{a'^2 + b'^2} \tag{5.40}$$

$$h' = \left\{ \begin{array}{l} \arctan\left(b'/a'\right) \ \text{ if } \ C' \neq 0 \\ 0 \ \text{ if } \ C' = 0 \end{array} \right\} \tag{5.41}$$

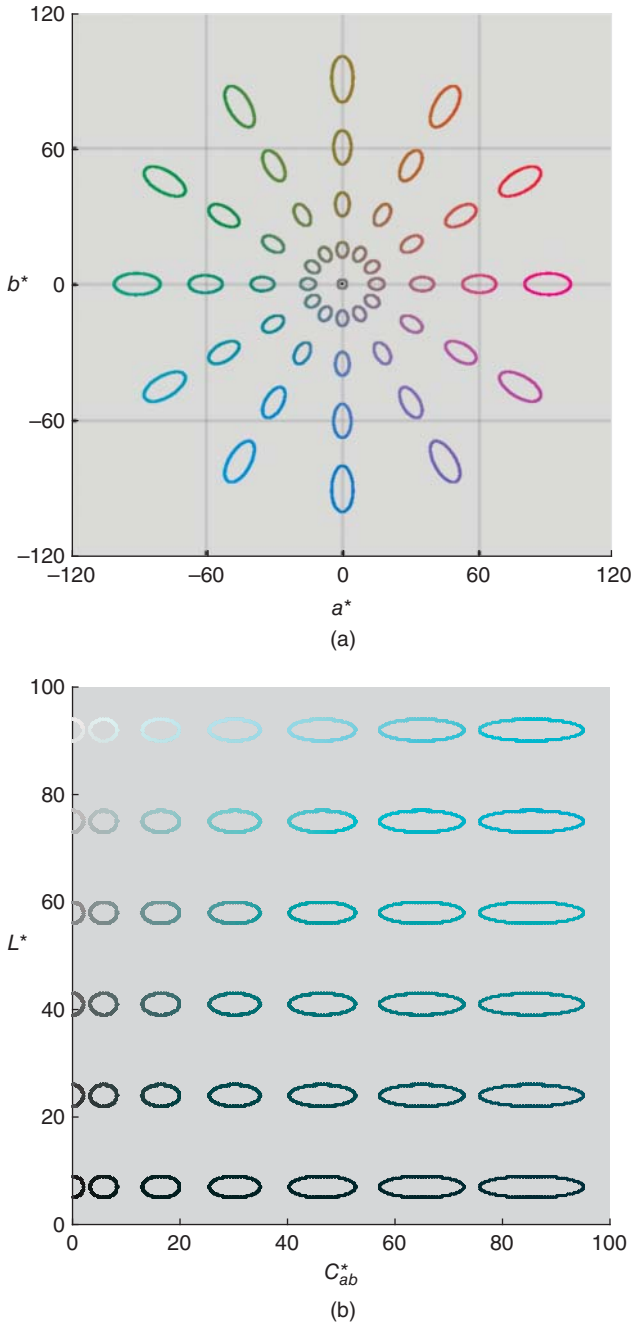

Figure 5.32 CIE94(1 : 1 : 1) formula can be used to derive corresponding color-tolerance ellipsoids, shown here for (a) color centers at a constant 50 L^*, two times magnification, and projected onto a a^*b^* diagram and (b) color centers at constant 200 h_{ab}, two times magnification, and projected onto a $L^*C^*_{ab}$ diagram.

$$S_L = 1 + \frac{0.015(\overline{L}' - 50)^2}{\sqrt{20 + (\overline{L}' - 50)^2}} \tag{5.42}$$

$$S_C = 1 + 0.045\overline{C}' \tag{5.43}$$

Table 5.3 The CIE reference conditions corresponding to the CIE generalized color-difference equation.

Illumination	D65 simulation
Illuminance	1000 lx
Surround field	Uniform, neutral gray with $L^* = 50$
Viewing mode	Object
Sample size	Greater than 4°
Sample separation	Minimum, in edge contact
Sample color-difference magnitude	0–5 ΔE^*_{ab}
Sample structure	Homogeneous, without visual non-uniformities

Source: Data from CIE (1995a).

$$T = 1 - 0.17\cos(\bar{h}' - 30^\circ) + 0.24\cos(2\bar{h}') + 0.32\cos(3\bar{h}' + 6^\circ) - 0.20\cos(4\bar{h}' - 63^\circ) \tag{5.44}$$

$$S_H = 1 + 0.015\bar{C}'T \tag{5.45}$$

$$R_T = -\sin(2\Delta\theta)R_C \tag{5.46}$$

$$\Delta\theta = 30\exp\{-[(\bar{h}' - 275^\circ)/25]^2\} \tag{5.47}$$

$$R_C = 2\sqrt{\frac{\bar{C}'^7}{\bar{C}'^7 + 25^7}} \tag{5.48}$$

The first improvement addressed near-neutral tolerances that projected onto the a^*b^* plane as ellipses rather than circles. A sigmoidal function, G, was derived to stretch the a^* axis for neutrals by 50% and taper off gradually. The function is given in Eq. (5.36) and plotted in Figure 5.33. The stretch results in a set of intermediate coordinates, L', a', b', C', and h', shown in Eqs. (5.37)–(5.41).

The second improvement was introducing an S_L function other than unity. The RIT-DuPont dataset had lightness dependencies as shown in Figure 5.30 where ΔL^* increased slightly for both light and dark colors. The Derby and Keele datasets had similar trends but of greater magnitude. The Witt and Leeds datasets had dependencies where ΔL^* increased with an increase in L^*. A "V" function was derived by Nobbs using the Derby and Keele datasets, the formula shown in Eq. (5.42) and plotted in Figure 5.34. The function minimum is at 50 L^*, the CIE reference background (CIE 1995a).

The third improvement was adding a hue-angle dependent function to S_H. The data used to derive the hue-angle dependent function, T, included the new Rochester Institute of Technology hue-difference data, the hue-difference data from Luo's visual experiments used to combine the 13 datasets forming the BFD dataset, and hue-difference data from the RIT-DuPont, BFD, and BAM datasets (Berns 2001), the formula is shown in Eq. (5.44) and plotted in Figure 5.35. The S_H function is shown in Eq. (5.45).

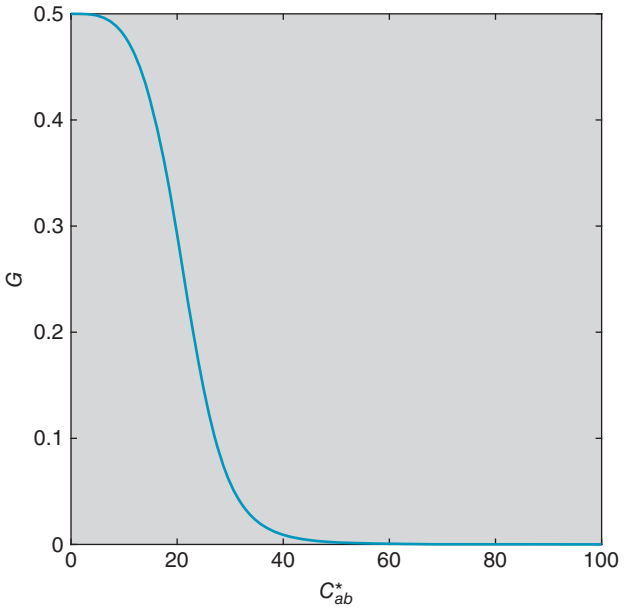

Figure 5.33 CIEDE2000 G function.

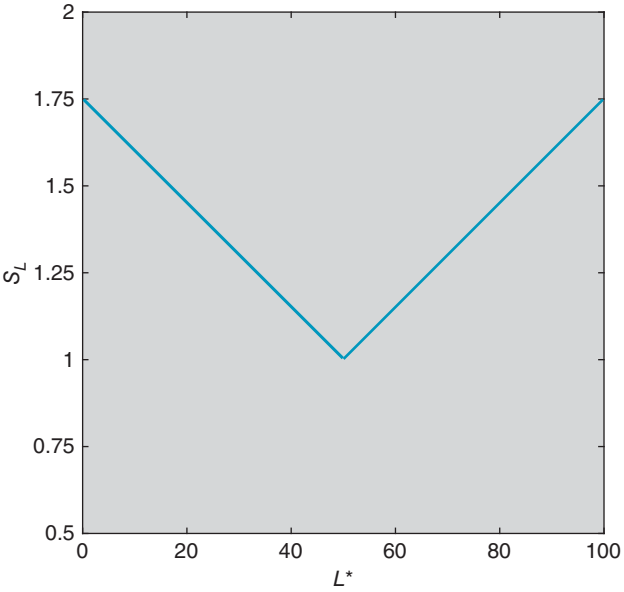

Figure 5.34 CIEDE2000 S_L function.

A limitation of CIELAB is poor correlation between h_{ab} and perceived hue for blue colors, seen in Figure 4.39 for Munsell colors of constant hue. As a consequence, ellipsoids in this region of CIELAB do not point toward neutral but toward $-a^*$ coordinates, seen in Figure 5.18 for the BFD dataset. This was modeled by introducing a covariance term between ΔC^*_{ab} and ΔH^*_{ab}, and a hue-angle dependent

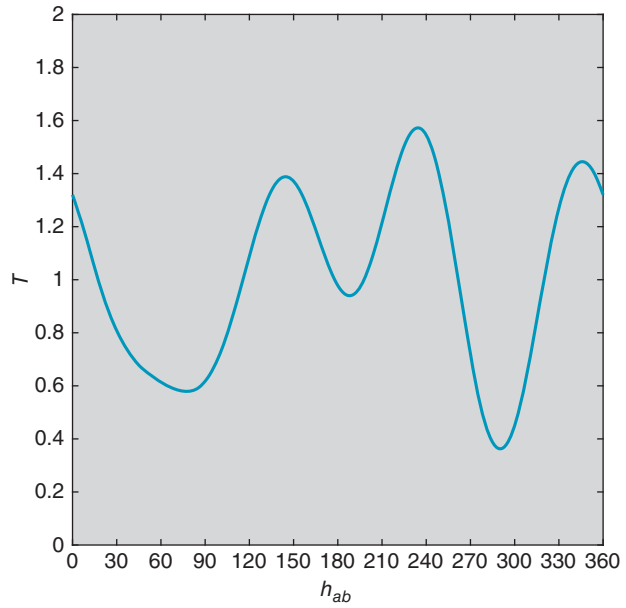

Figure 5.35 CIEDE2000 T function.

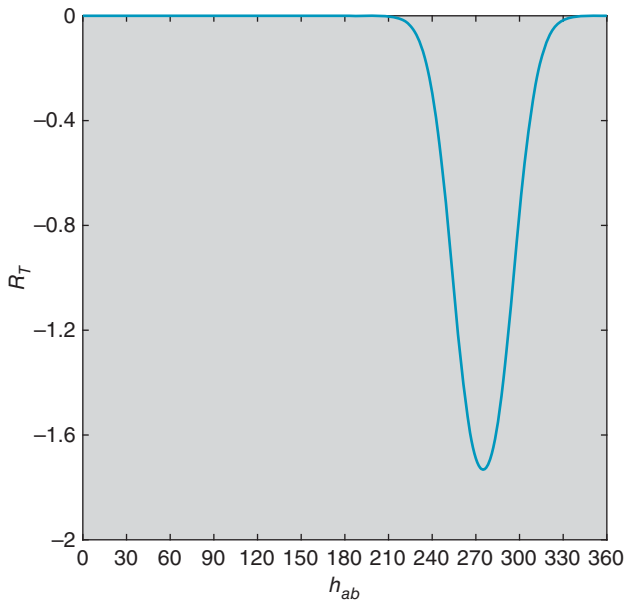

Figure 5.36 CIEDE2000 R_T function at 100 C'.

function that adds covariance for blue colors. A blue dataset was produced by sorting data from the BFD, RIT-DuPont, and BAM datasets having h_{ab} between 230° and 320° and differences primarily in ΔC^*_{ab}, and ΔH^*_{ab}. This blue dataset was used to derive a rotation function (Luo, Cui, and Rigg 2001), the formulas shown in Eqs. (5.46)–(5.48) and plotted in Figure 5.36.

The color-tolerances ellipsoids derived from the CIEDE2000 formula are shown in Figure 5.37. The

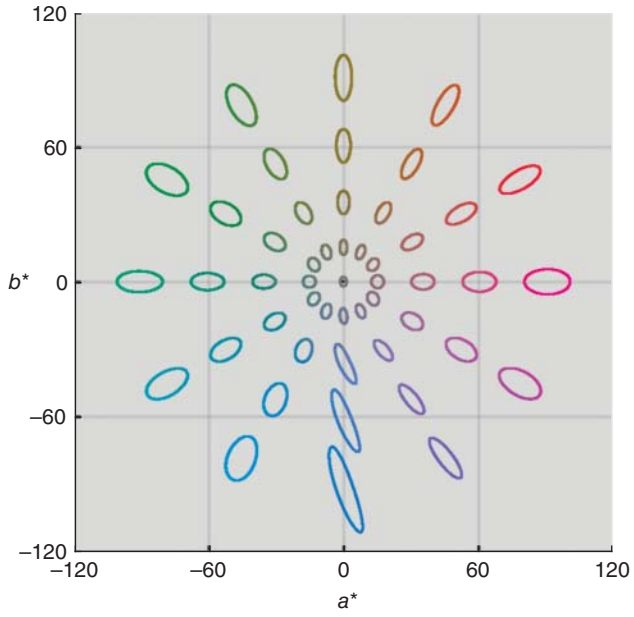

(a)

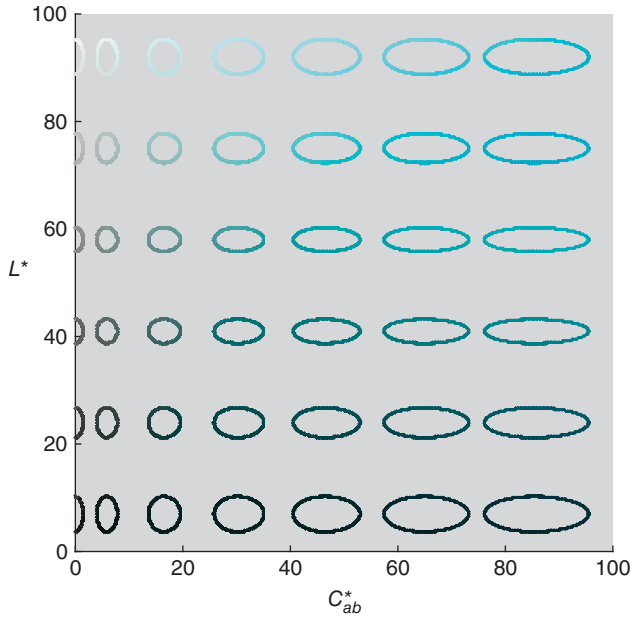

(b)

Figure 5.37 The CIEDE2000 formula can be used to derive corresponding color-tolerance ellipsoids, shown here for (a) color centers at a constant 50 L^*, two times magnification, and projected onto a a^*b^* diagram and (b) color centers at constant 200 h_{ab}, two times magnification, and projected onto a $L^*C^*_{ab}$ diagram.

ellipsoids projected onto the a^*b^* plane are narrow at 80°, 190° and 290° and rotate around 270°. The ellipsoids projected onto the $L^*C^*_{ab}$ diagram increase in height for both light and dark colors.

One-dimensional Lightness, Chroma, and Hue Difference Metrics

The total color difference between two colors is a measure of magnitude, not direction. As shown in Figure 5.1, a skin tone becoming greenish is unacceptable. The same magnitude of difference may be acceptable when the change is reddish. In many cases, it is important to evaluate the direction of change in addition to the magnitude, referred to as *lightness, chroma, and hue difference splitting* (CIE 2001; Nobbs 2002; CIE 2018). Using CIELAB, we would evaluate ΔL^*, ΔC^*_{ab}, and ΔH^*_{ab}. However, CIELAB is nonuniform with respect to industrial-sized color differences. If CMC(l:c) is used as the color-difference formula, we would evaluate $(\Delta L^*/lS_L)$, $(\Delta C^*_{ab}/cS_C)$, and $(\Delta H^*_{ab}/S_H)$. For CIE94, we would evaluate $(\Delta L^*/k_L S_L)$, $(\Delta C^*_{ab}/k_C S_C)$, and $(\Delta H^*_{ab}/k_H S_H)$. Nobbs (2002) derived formulas to calculate the equivalent metrics for CIEDE2000. The covariance term of CIEDE2000 necessitates calculations that include rotating $\Delta L'$, $\Delta C'$, and $\Delta H'$ to new coordinates $\Delta L''$, $\Delta C''$, and $\Delta H''$, the amount of rotation calculated by the CIEDE2000 R_T term, shown in Eqs. (5.49)–(5.52). The rotation is also used to recalculate the positional functions, shown in Eqs. (5.53)–(5.55). The final directional terms and the total color-difference formula are shown in Eqs. (5.56)–(5.59)

$$\Delta L'' = \Delta L' \tag{5.49}$$

$$\Delta C'' = \Delta C' \cos(\phi) + \Delta H' \sin(\phi) \tag{5.50}$$

$$\Delta H'' = \Delta H' \cos(\phi) - \Delta C' \sin(\phi) \tag{5.51}$$

$$\tan(2\phi) = R_T \frac{(k_C S_C)(k_H S_H)}{(k_H S_H)^2 - (k_C S_C)^2} \tag{5.52}$$

$$S''_L = (k_L S_L) \tag{5.53}$$

$$S''_C = (k_C S_C)\sqrt{\frac{2(k_H S_H)}{2(k_H S_H) + R_T(k_C S_C)\tan(\phi)}} \tag{5.54}$$

$$S''_H = (k_H S_H)\sqrt{\frac{2(k_C S_C)}{2(k_C S_C) + R_T(k_H S_H)\tan(\phi)}} \tag{5.55}$$

$$\Delta L_{00} = \frac{\Delta L''}{S''_L} \tag{5.56}$$

$$\Delta C_{00} = \frac{\Delta C''}{S''_C} \tag{5.57}$$

$$\Delta H_{00} = \frac{\Delta H''}{S''_H} \tag{5.58}$$

$$\Delta E_{00} = \sqrt{(\Delta L_{00})^2 + (\Delta C_{00})^2 + (\Delta H_{00})^2} \tag{5.59}$$

An example calculation is shown in Table 5.4. Additional examples can be found in Nobbs (2002).

Table 5.4 Test data for CIEDE2000 and difference splitting.

	Standard	Batch
L^*	61.43	61.29
a^*	2.25	3.72
b^*	−4.96	−5.39
C^*_{ab}	5.45	6.55
h_{ab}	294.37	304.61
ΔL^*	−0.14	
ΔC^*_{ab}	1.10	
ΔH^*_{ab}	1.06	
ΔE^*_{ab}	1.5	
$\overline{C^*_{ab}}$	6.00	
G	0.5	
L'	61.43	61.29
a'	3.36	5.57
b'	−4.96	−5.39
C'	6.00	7.75
h'	304.14	315.92
T	0.70	
$k_L S_L$	1.16	
$k_C S_C$	1.31	
$k_H S_H$	1.07	
R_T	−0.0032	
$\Delta\theta$	4.21	
R_C	0.02	
ΔE_{00}	1.9	
$\tan(2\phi)$	0.0079	
$\phi(^\circ)$	0.23	
$\Delta C''$	1.76	
$\Delta H''$	1.39	
$S''C'$	1.31	
S''_H	1.07	
ΔL_{00}	−0.12	
ΔC_{00}	1.34	
ΔH_{00}	1.3	

H. UNIFORM COLOR-DIFFERENCE SPACES

Earlier in the chapter, we introduced city block and Euclidean geometries as two approaches to measuring distance. We now introduce a third approach, that of a curve, referred to as Riemannian geometry. On a map, we can crudely judge the time required to travel between two cities by their Euclidean distance. However, if the road has lots of curves and a mountain between the two cities, the true distance is

longer. Integration is used to calculate the distance along the road. This concept can be applied to color-difference formulas. The most significant limitation of CIELAB when predicting industrial color tolerances is the need to correct for the average chroma of the color-difference pair using the S_C positional function (Melgosa, Huertas, and Berns 2004). This S_C function can be integrated, shown in Eqs. (5.60)–(5.61)

$$\int \left(\frac{1}{1 + 0.045x} \right) dx = \frac{1}{0.045} \ln|0.045x + 1| \tag{5.60}$$

$$C = \frac{1}{0.045} \ln(0.045C^*_{ab} + 1) \tag{5.61}$$

Applying the integration to C^*_{ab}, shown in Eq. (5.61), transforms chroma from a Euclidean to a Riemannian geometry. CIELAB chroma is compressed where equal differences in C result from small changes in C^*_{ab} for dark colors and large changes in C^*_{ab} for light colors, plotted in Figure 5.38.

The compression results in a large reduction in the range of values where $100C^*_{ab}$ equals $37.9C$. The compressed values can be scaled to equal C^*_{ab} at a single value, such as 100, and a uniform color-difference space is derived, shown in Eqs. (5.62)–(5.65) where the subscript ucd stands for uniform color difference. The compressed space results in a Euclidean color-difference formula, shown in Eq. (5.66). Equal CIEDE2000 color-difference ellipsoids are plotted in Figure 5.39 and the improvement in circularity is evident compared with Figure 5.37a. This simple space cannot correct for the other limitations in CIELAB that are modeled using CIEDE2000

$$L_{\text{ucd}} = L^* \tag{5.62}$$

$$C_{\text{ucd}} = 58.65 \ln(0.045C^*_{ab} + 1) \tag{5.63}$$

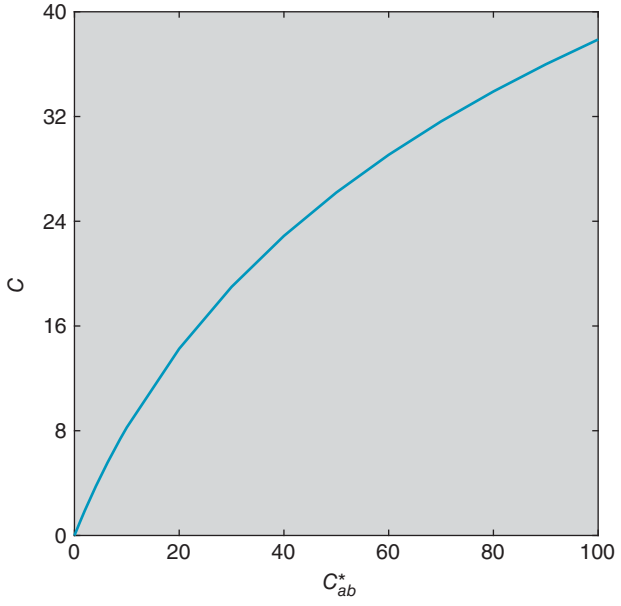

Figure 5.38 Nonlinear transformation from C^*_{ab} to C.

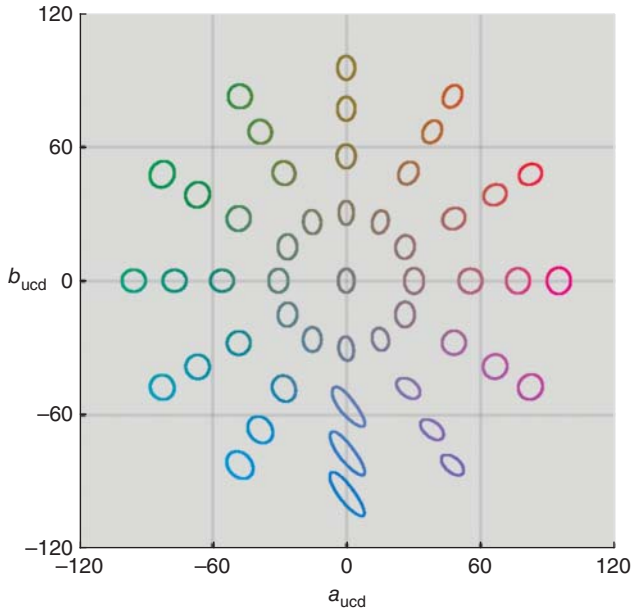

Figure 5.39 The CIEDE2000 formula can be used to derive corresponding color-tolerance ellipsoids, shown here for color centers at a constant 50 L^*, two times magnification, and projected onto the $a_{\text{ucd}}b_{\text{ucd}}$ diagram.

$$a_{\text{ucd}} = C_{\text{ucd}} \cos(h_{ab}) \tag{5.64}$$

$$b_{\text{ucd}} = C_{\text{ucd}} \sin(h_{ab}) \tag{5.65}$$

$$\Delta E_{\text{ucd}} = \sqrt{(\Delta L_{\text{ucd}})^2 + (\Delta C_{\text{ucd}})^2 + (\Delta H_{\text{ucd}})^2} \tag{5.66}$$

This approach to developing a uniform color-difference space with a Euclidean color-difference metric was derived by Rohner and Rich (1996) for Datacolor International, called DCI-95. Their goals were to calculate tolerances of the same magnitude as CMC(2:1), achieve equivalent performance to CMC(2:1) for textiles applications, have similar units to CIELAB, improve the spacing of the Munsell system compared with CIELAB, and use straightforward mathematics. This formula was quite successful and the concept of converting from a Euclidean to a Riemannian geometry has been incorporated into a number of color-difference spaces such as LABmg (Colli, Gremmo, and Moniga 1989), DIN99 (DIN 2001), DIN99o (Cui et al. 2002), CAM02-UCS (Luo, Cui, and Li 2006), and WLab (Derhak and Berns 2015b).

I. DETERMINING COLOR-TOLERANCE MAGNITUDE

Suppose that an employee has just been transferred to the color laboratory following the retirement of the company's color expert. She has been asked by management to develop an instrumental-based procedure for evaluating color quality.

Her company produces a variety of colored vinyls, each with a corresponding color standard. The laboratory has a spectrophotometer, a light booth, and extensive color files.

Our budding color scientist sits at her new desk and starts opening drawers. She finds a standard procedure for instrumental measurement including geometry, standard illumination, standard observer, sampling, sample presentation, and averaging. These are integrating sphere with specular component excluded, illuminant D65, 1964 10° observer, five samples per batch, and each sample measured three times with replacement and averaged. There is also a procedure for visual evaluation where the light booth's "Daylight" source is used, samples are cut into three-inch squares, placed in the light booth in edge contact, and viewed to exclude gloss. The procedures were developed by a color consultant.

Next, she walks over to the color files and starts opening up folders. In each folder, there are numbered color swatches and a log sheet with the standard stapled at the top. The log sheet lists each batch of material, comments about the production run, and an acceptability decision. There is no indication of instrumental measurements. Phoning her predecessor, she discovers that the instrumental data were never used for color control. The spectrophotometer was purchased based on a recommendation by the consultant. The retiree did not believe that the instrumental data could predict visual decisions.

Our new colorist returns to her desk and looks again at the report written by the color consultant. There are a number of references to ASTM test methods and color science textbooks. Following many weeks of study, she performs the following evaluations.

For each standard, she sorts the swatches into "pass" and "fail." She also reads the log sheet carefully ensuring that the acceptability decisions were based on a batch's color, not other attributes. Any ambiguous samples are excluded.

She looks at the light booth's manual to determine exactly what "Daylight" means. Then she selects an illuminant in the color system's software that is closest in spectral power distribution and correlated color temperature. Since her light booth uses fluorescent lamps to achieve "Daylight," she uses illuminant FL3.15 rather than D65. (FL3.15 replaces F7, described in Chapter 7.) The samples are three inches square. Thus, the 1964 10° observer is the appropriate observer. She sets the spectrophotometer to its largest aperture in order to spatially average the largest area.

Following sufficient warm-up time, she calibrates the instrument and measures the average spectral reflectance factor of the standard and each swatch. The instrument's software calculates CIELAB coordinates for the standard and each swatch and difference coordinates between each swatch and the standard.

Looking at the data for one of the standards, variability in L^* is small while a^* and b^* have a much larger range of values. She plots both the pass and fail batches on a $\Delta a^* \Delta b^*$ plot, shown in Figure 5.40a. She is quite surprised to find that the data are inconsistent. Some samples very close in color space location have different visual judgments. Some samples with large differences are passed while others with small color differences are failed. She finds similar plots for each standard.

The instrument software has the capability of fitting a tolerance ellipsoid around all of the passed data points, shown in Figure 5.40b. Samples inside the ellipsoid are passed while those outside the ellipsoid are failed. She is unsure whether this is the correct approach. The ellipsoid shape and orientation are very sensitive to the particular samples that have been measured. One acceptable sample seems to have a large influence on the orientation of the ellipsoid. She tests this by removing the sample from the dataset, shown in Figure 5.40c. The change in shape is astounding.

Based on her studies, it seems more prudent to use a color-difference formula based on judgments from multiple observers and materials with similar characteristics to the vinyls. She selects CIEDE2000 with its parametric factors set to unity. The CIEDE2000 reference conditions are quite close to hers. The software plots an ellipsoid based on the position of the standard. She can vary the total color difference to either enlarge or shrink the size of the ellipsoid without changing either its orientation or shape. She finds a total color difference that minimizes the number of instrumental wrong decisions, shown in Figure 5.40d. If only "pass" data are available, the total color difference is set to encompass 80% of the pass data (Berns 1996a).

She repeats this for every color standard. The average total color difference is used to define her instrumental-tolerance limit.

The color scientist has taken a conservative approach to defining an instrumental tolerance limit. Rather than optimizing tolerances about each standard, she has used a color-difference formula and optimized its magnitude. The assumption is that the color-difference formula is correcting CIELAB's lack of visual uniformity. The S_L, S_C, and S_H functions correct CIELAB to a more visually uniform color-difference space. She has relied on her predecessor to determine the color-quality criterion based on years of visual judgments.

There are three limitations to the approach used by our color scientist we wish to point out. The first limitation is treating tolerances in an "either or" fashion: batches with color differences less than or equal to the tolerance limit are acceptable while those with color differences greater than the tolerance limit are unacceptable. Any set of measurements, whether visual or instrumental, is a statistical sampling. In a color tolerance ellipsoid, data points closer to the ellipsoid surface have greater uncertainty. The second concern is treating any color-difference formula as if it correlates perfectly with visual judgments. The best formulas have STRESS values around 20, far from perfect correlation. Both limitations are remedied by having a region defined near the ellipsoid

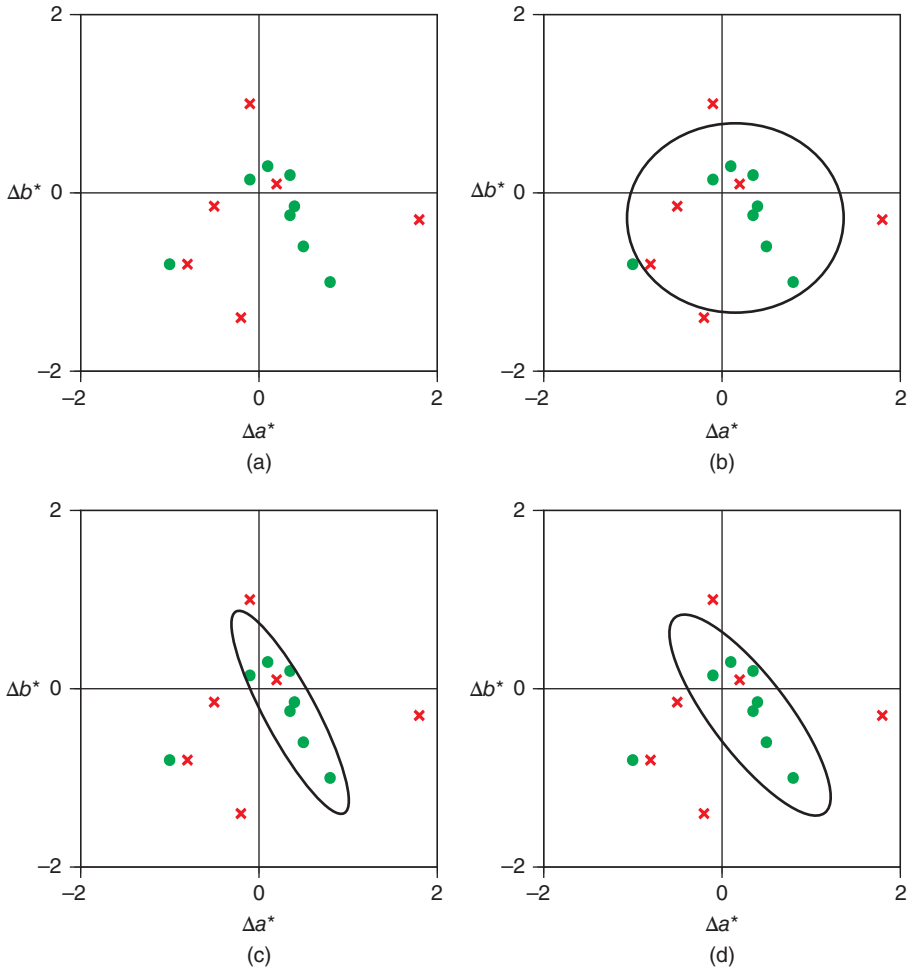

Figure 5.40 (a) Batches having similar L^* but dissimilar a^* and b^* projected onto a $\Delta a^*\Delta b^*$ diagram where the green dots are "accept" responses and the red crosses are "reject" responses, (b) fitted tolerance ellipsoid optimized to include 80% of the acceptable batches, (c) fitted tolerance ellipsoid optimized to include 80% of the acceptable batches after discarding the left-most acceptable batch from the optimization, and (d) fitted tolerance ellipsoid based on minimizing instrumental wrong decisions using CIEDE2000 with its parametric factors set to unity.

surface that indicates the need for a visual validation. Third, a color tolerance based on a weighted color-difference formula is asymmetric in chroma and symmetric in hue. At the beginning of this chapter, we showed an example of skin color reproduction. Hue error was clearly asymmetric. One solution is to change the colorimetric coordinates of the standard so the acceptable and unacceptable data are correctly distributed about the tolerance ellipsoid. A second approach is to fit an ellipsoid to the acceptability data having verified the reliability of the visual data. A third approach is to use difference splitting and define asymmetric ranges, for example, $-5 \geq \Delta H_{00} \leq +2$.

Setting an Instrumental Color Tolerance from Instrumental and Visual Historical Data

Determining an acceptability limit about a color standard requires a bit more effort than the quip, "Any batch with a ΔE greater than 1 is unacceptable!" In this example, we will assume that the color measurement device and the act of measuring samples have high precision and accuracy. We will also assume that visual judgments have been made under controlled illumination and viewing, are repeatable, and that the judgments are only based on color difference. More details about measuring color visually are described in Chapter 6. Ideally there are color measurements of batches that are both acceptable and unacceptable, though we will also show how to set a tolerance using only acceptability data.

For a given standard, visual and instrumental data are collected. In this example, colorimetric data are based on D65, the 1964 10° observer, 45°c:0° geometry, and an average of three measurements for each sample. Two-inch square samples were placed in edge contact and evaluated in a light booth with a filtered-tungsten daylight simulator. Perceptibility judgments relative to a near-gray anchor pair were made in which observers judged whether the color difference between a sample and standard was smaller than or greater than the color difference of the anchor pair. For simplicity, we will call the visual judgments in which the color difference was smaller than the anchor pair a "pass" judgment and visual judgments in which the color difference was greater than the anchor pair a "fail" judgment (Berns 1996a). Each

Table 5.5 Visual and colorimetric data for 32 batches compared with a standard.

Sample	ΔL^*	Δa^*	Δb^*	Visual decision
1	–2.73	–0.80	–2.53	Pass
2	0.82	2.78	–0.73	Pass
3	–3.91	0.52	–4.12	Fail
4	–1.74	5.73	–0.37	Fail
5	–3.58	–10.31	–3.70	Fail
6	0.76	3.06	–1.65	Pass
7	–1.58	–1.29	1.62	Fail
8	–2.32	–4.92	0.78	Fail
9	0.49	3.52	5.07	Fail
10	1.38	–0.43	–0.23	Pass
11	3.31	0.09	2.55	Fail
12	–0.84	2.41	–4.68	Pass
13	–0.07	3.87	–2.82	Pass
14	–2.29	–1.56	–6.57	Fail
15	0.81	2.63	3.23	Pass
16	1.62	1.58	5.02	Pass
17	0.91	0.09	3.48	Pass
18	–1.36	–2.87	0.05	Pass
19	0.14	1.10	2.03	Pass
20	–2.61	–4.98	–7.66	Fail
21	–2.05	4.37	1.30	Fail
22	1.37	–0.07	2.88	Pass
23	–3.38	–4.10	–8.75	Fail
24	–2.28	3.96	–6.50	Fail
25	–2.40	–0.49	0.38	Pass
26	–0.26	4.39	3.90	Fail
27	–1.48	5.92	1.88	Fail
28	–0.68	–3.75	1.09	Pass
29	2.00	–0.92	4.63	Fail
30	–1.49	5.58	–4.69	Fail
31	–2.01	–4.88	–1.83	Fail
32	2.68	0.76	5.95	Fail

sample's ΔL^*, Δa^*, Δb^*, and visual decision is shown in Table 5.5.

The samples are sorted in pass and fail, and listed in ascending order as shown in Table 5.6. Cumulative percentages are calculated for each group, $C_{\text{Pass},\,i}$ and $C_{\text{Fail},\,i}$, shown in Eqs. (5.67) and (5.68):

$$C_{\text{pass},i} = 100\frac{i}{n_p} \tag{5.67}$$

$$C_{\text{fail},i} = 100 - 100\frac{i}{n_f} \tag{5.68}$$

where n_p represents the number of samples that were passed, n_f represents the number of samples that were failed, and i represents sample 1, 2, …, n_p or n_f. Finally, the cumulative percentages versus ordered color difference are plotted, shown in Figure 5.41. The intersection of the two sets of data defines the optimized tolerance. For these data, the color difference that minimized the number of instrumental wrong decisions is 1.9 ΔE_{00}. There are five instrumental wrong decisions.

Table 5.6 Data from Table 5.5 listed in ascending color difference along with cumulative percentages for "pass" and "fail" visual data.

Pass	Pass cumulative percentage	CIEDE2000	Fail	Fail cumulative percentage	DE2000
1	7.1	0.6	1	94.4	1.7
2	14.3	1.1	2	88.9	1.7
3	21.4	1.4	3	83.3	1.9
4	28.6	1.4	4	77.8	2.3
5	35.7	1.5	5	72.2	2.7
6	42.9	1.5	6	66.7	2.7
7	50.0	1.6	7	61.1	2.9
8	57.1	1.8	8	55.6	2.9
9	64.3	1.8	9	50.0	2.9
10	71.4	1.8	10	44.4	3.0
11	78.6	1.9	11	38.9	3.1
12	85.7	2.0	12	33.3	3.1
13	92.9	2.4	13	27.8	3.3
14	100	2.8	14	22.2	3.3
			15	16.7	3.6
			16	11.1	4.0
			17	5.6	4.1
			18	0	5.7

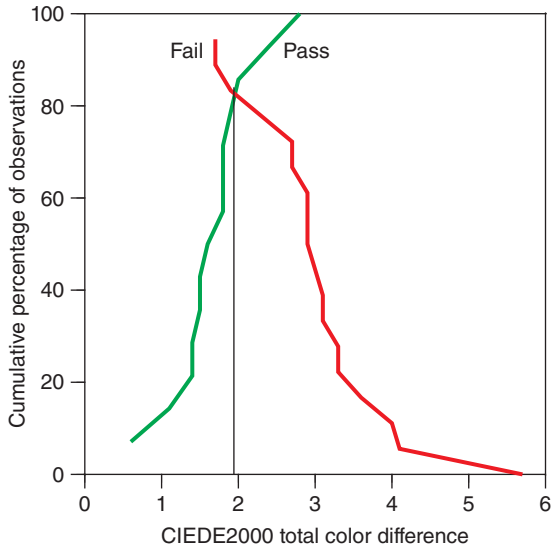

Figure 5.41 Cumulative percentage of pass and fail samples along with each sample's CIEDE2000. The intersection of the two lines defines the tolerance that minimizes instrumental wrong decisions. Samples with percentages greater than the intersection are wrong decisions.

The CIEDE2000 tolerance ellipsoid and all the samples are plotted in Figure 5.42. Many of the failed

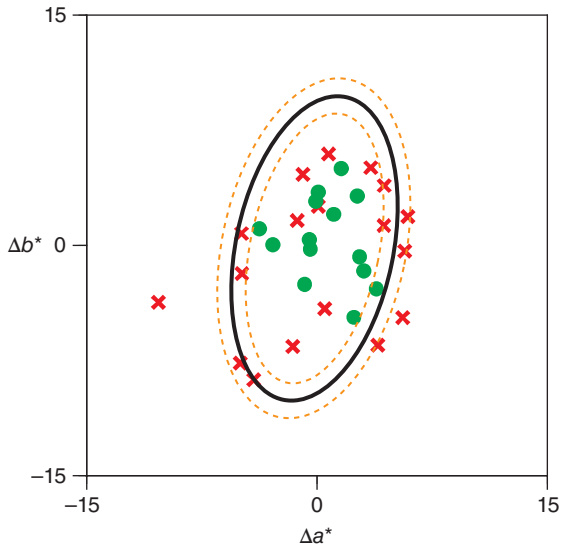

Figure 5.42 CIEDE2000 optimized color tolerance ellipsoid (black line) and $\pm 0.2\Delta E_{00}$ ellipsoids (dashed orange line) projected onto the $\Delta a^* \Delta b^*$ plane. Samples shown as green dots are pass samples while those shown as red *x*'s are fail samples.

samples appear within the tolerance. This is because the three-dimensional positions are projected onto the $\Delta a^* \Delta b^*$ plane. Only two of the failed samples are, in fact, within the tolerance ellipsoid. Similarly, two of the passed samples are outside the tolerance ellipsoid. We have added ellipsoids that are $\pm 0.2\ \Delta E_{00}$, shown as dashed orange lines in Figure 5.42. This is a region of uncertainty where visual validation is required.

Suppose that only pass data are retained. In this case, the color-difference data are ordered, pass cumulative percentages calculated, and the proper tolerance is at 80%, also 1.9 for this example. This process can be repeated for a number of standards throughout color space. The average optimized color-difference magnitude defines the final color-tolerance limit.

J. SUMMARY

We have described an approach to specifying color quality based on visual and color measurements, the validity dependent on the reliability of the measurements. Visual assessments must be performed in a standardized fashion including sample size, sample separation, viewing distance and geometry, and lighting. Color measurements are also standardized including sampling, sample preparation, number of measurements, instrument geometry, standard observer, and standard illuminant. From these data, tolerances can be defined using difference coordinates such as ΔH^*_{ab} or ΔH_{00}, a color-difference formula such as CIEDE2000, or fitting a tolerance ellipsoid.

Even using best practices, there is still a need for visual validation for colors close to the tolerance. There are many reasons. Statistically, uncertainty is greatest at the tolerance boundary. The visual data used to derive and optimize a color-difference formula are imprecise. Individuals probably have different color-matching functions than a standard observer. A real light source will be different than a standard illuminant. The first edition of this book had a recurring figure that stated, "Think! Look!" This advice is particularly relevant when defining color quality.

Chapter 6

Color and Material-Appearance Measurement

We have seen—several times by now—that three components are needed for the production of most colors: a light source, an object to be illuminated, and an observer who both detects the light and converts the detected signal into a response that the human brain recognizes as color, shown in Figure 6.1. For colored lights, the three components reduce to two—the light and the observer. We have seen also that, for many reasons, it is useful to assign numbers to this response called color so that it can be described accurately to someone else, somewhere else, and at some other time. Now we come to the question of how this can be done, the subject of color measurement, also shown in Figure 6.1.

- *Body color*: Color produced by absorption and scattering of light by colorants within a colored material, characterized by diffuse reflectance factor after accounting for any refractive index discontinuity at the material's surface.
- *Microscopic material appearance*: Surface structure that varies at a microscopic size, characterized by a bidirectional reflectance distribution function (BRDF) or similar function.
- *Macroscopic material appearance*: Surface structure that varies at a macroscopic size, characterized by the spatial frequency of an image of the surface, a height map, or a surface-normal map.

A. BASIC PRINCIPLES OF MEASURING COLOR AND MATERIAL APPEARANCE

An injection-molded plastic was produced having different surface properties, shown in Figure 6.2. Its backside matches the smooth surface. There is only a single *body color* (Shafer 1985). The different surfaces have changed the plastic's *material appearance*. The change from smooth to rough occurs at a *microscopic* level. The change from flat to textured occurs at a *macroscopic* level. The plastic can be reproduced by quantifying its body color, microscopic properties, and macroscopic properties. These properties are used in computer graphics to render objects.

Before pressing "measure," we must first answer the question, "Why are we making the measurement?" This question is most important because it guides us in selecting the appropriate instruments and their measurement parameters. The more important answers when measuring a sample include:

Billmeyer and Saltzman's Principles of Color Technology, Fourth Edition. Roy S. Berns.

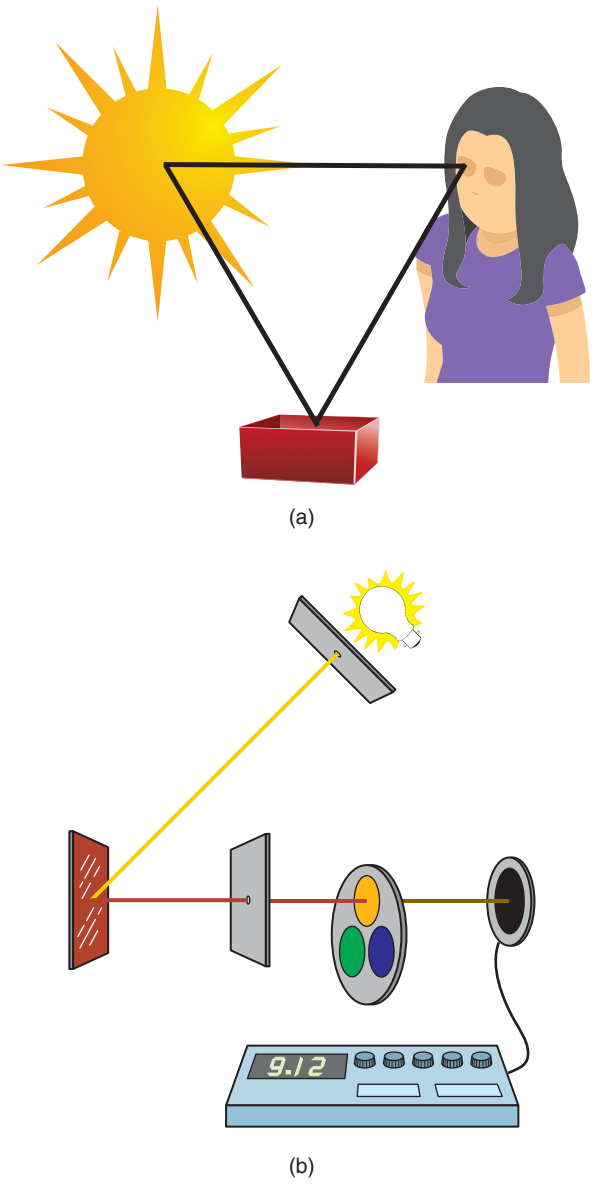

(a)

(b)

Figure 6.1 (a) "Color" results from the interaction of a light source, an object, and the eye and brain, or visual system. (b) "Color" also results from the interaction of a light source, an object, a detector, and signal processor.

"I am measuring this sample in order to define its color for a specific set of illuminating and viewing conditions."

"I am measuring this sample in order to determine if it matches the color of another sample for one or more sets of illuminating and viewing conditions."

"I am measuring this sample in order to determine its composition."

"I am measuring this sample to order to determine whether a coloration process is in control."

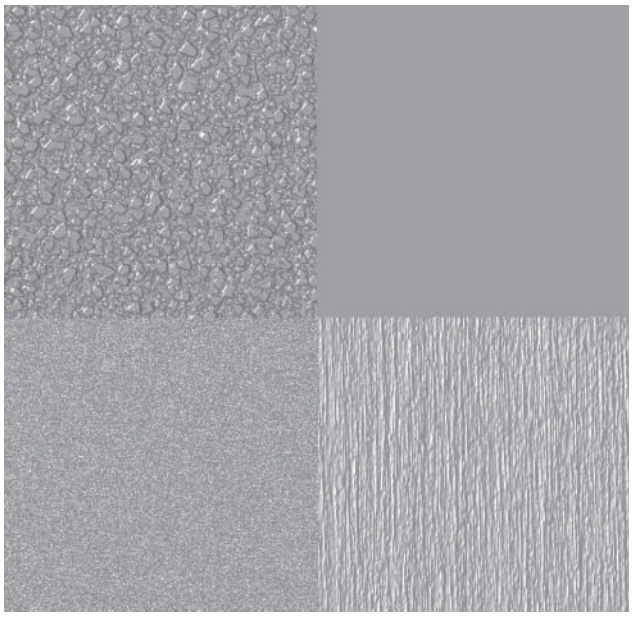

Figure 6.2 Injection molded plastic with different surfaces.

"I am measuring this sample in order to characterize its gloss."

"I am measuring this sample in order to characterize its sparkle."

"I am measuring this sample in order to characterize its texture."

B. THE SAMPLE

As we start our consideration of the steps involved in color and material-appearance measurement, we come first to the origin and preparation of the sample. We believe that these points should be considered in some detail.

One thing that we in the business of coloring frequently forget is that color measurement is nothing more than a special technique of analysis. As such, it shares with all other analytical techniques the fundamental problem of obtaining a representative sample (Deming 1950; Montgomery 2013). Care must be taken in the way in which the sample for analysis is selected, regardless of the means to be used for examining and evaluating the sample. If a decision is to be made, on the basis of color measurement, about a run of molded-plastic articles, painted parts, or bolts of dyed cloth, we must be certain that the sample to be examined truly represents the material being considered.

Our justification in mentioning this fact, which seems so obvious, lies in our experience that the question of sampling for color measurement is so often ignored. Laboratories, in which standard products such as hydrochloric acid are carefully sampled according to statistical plans, and in which the results of replicate analyses must agree within previously

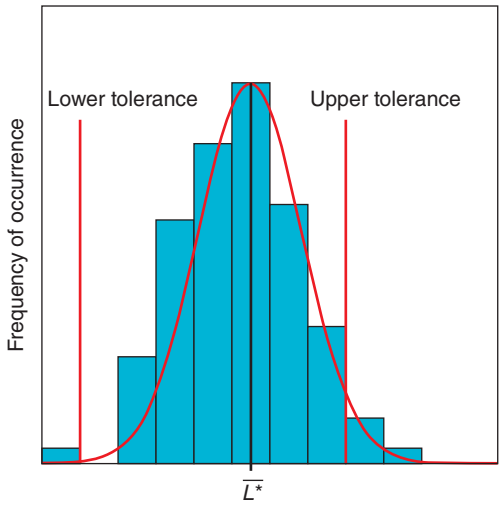

Figure 6.3 A lightness histogram of 100 specimens taken from of a batch of material along with the standard's upper and lower tolerances.

stated tolerances, frequently make their color judgments on the basis of a single measurement on a single specimen obtained in some fashion unknown to the analyst. Why this should be so we cannot say, except that there is a general aura of mystery and confusion surrounding the question of color measurement in many laboratories.

In Chapter 5, we learn about random distributions. Variability in lightness for the process described in that chapter is shown in Figure 6.3. Upper and lower tolerances have been added. Imagine the danger of using one specimen to determine if the batch of material is within tolerance. Without using good statistical practices, you run the risk of making bad decisions. In this case, there are several individual specimens out of tolerance. If one of these is used to determine whether the batch is within tolerance, the incorrect decision is made. Sampling by measuring multiple specimens leads to the correct answer that the process is within tolerance.

Whether sampling truly represents the material being examined is the first question to be asked before undertaking any color measurement, visual or instrumental. This question includes both selecting specimens and the further step of converting them into a form suitable for inspection. While there are a few cases in which a finished article is already in a form suitable for either visual or instrumental examination, most materials require that the specimen be handled in some special way. For example, a sample of fabric must be folded so that a standard number of layers is presented for examination. Sewing thread is wound on a flat card. Roofing granules are placed in a cup such that all the granules have the same orientation on the top-most layer.

In the case of colorants, the problems are much more difficult, for it is not possible to make a suitable judgment of the performance of the colorant on the basis of its appearance as a dry powder. There is no substitute for the conversion of the

Figure 6.4 Cadmium red light (PR 108) dispersed in four different media.

colorant to the final form in which it is to be used. This is shown in Figure 6.4 where the same cadmium red pigment was dispersed in four different paint media and applied at the same film thickness.

The conversion of any sample of colored material into a form suitable for examination requires a standardized procedure that is both repeatable (by the same person in the same laboratory) and reproducible (by different people in different laboratories at different times). Only after this ability is acquired and reliable data are available as to the repeatability of the test can one begin to discuss a comparison of a batch of material with any accepted standard. We cannot emphasize too strongly the need to examine every sample-preparation procedure, by statistical means, to ensure that precise knowledge of its repeatability has been obtained. As we see in the remainder of this chapter, color-measuring instruments have become so precise in recent years that all too often the ability to prepare suitable samples is the weakest link in the measurement chain.

The question of converting a colorant into a form suitable for inspection assumes greater importance when the measurement of color is done by instruments. When, for example, a paint panel is being looked at and compared to a standard, a trained observer can notice whether or not the sample and standard are in good condition, or whether the coating has been applied correctly. A spectrophotometer cannot determine the condition of a specimen. Although imaging systems can quantify spatial variability, most color measurements are performed using spectrophotometers.

C. VISUAL COLOR MEASUREMENT

We are strong advocates for using color measurement to define colors and setting tolerances. In fact, much of the book is devoted to the proper use of instrumentation and numerical-color specification. Even so, visual standards can be effective tools for color specification provided that certain procedures are followed. We will consider a scenario where a corporation has a corporate color, possibly trademarked, and where a variety of products are sold having the corporate color. Each product is made by a different manufacturer.

The corporation needs to provide a color standard. Chances are, this color achieved distinction for a particular product and coloration system. Examples include Owens-Corning pink (colored fiberglass insulation), John

Deere green (painted farm machinery), and 3M canary yellow (repositionable note pads of dyed paper). The standard should be produced in the same material and using the same colorants in order to ensure that the standard is not metameric. These are sent to the various manufacturers.

Because visual assessment is being used, there needs to be consistent lighting and viewing, most easily achieved using the same brand and model light booth. As booths have multiple light types, the particular type (or types rank ordered) is specified.

The manufacturer produces samples in their material that match the corporate standard. Hopefully, the specimen is not metameric to the standard. This can be tested visually by changing light type and evaluating whether the match changes. A highly metameric specimen will only match under one type of illumination and for one observer. The changes are often in hue. How the standard and test specimens are placed in the booth, viewing distance, and viewing position need to be defined, shown in Figure 6.5. Many factors in addition to the materials' color affect the magnitude of visual difference, called parametric factors and discussed in Chapter 5. These factors need to be consistent. Hopefully, there is sufficient consistency such that judgments are repeatable.

The next step is the most important, selecting the specimen that will become the manufacturer's standard. An exact match may not be possible. The new material may have different microscopic and macroscopic material appearance. The color may be less chromatic because the coloration system has a smaller range of producible colors. It is critical to come to an agreement on the new color.

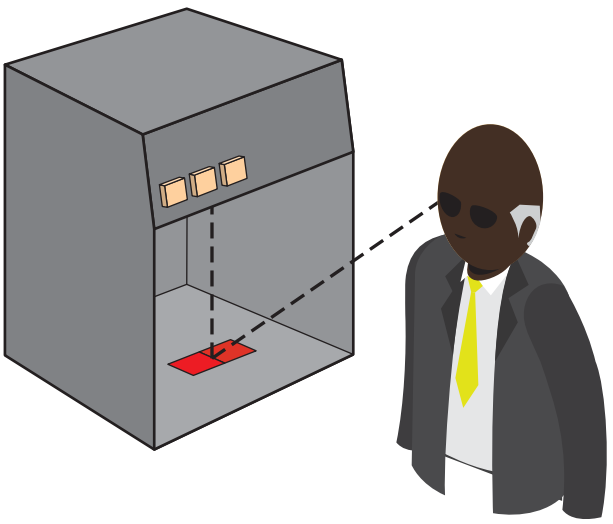

Figure 6.5 When judging samples visually, specimen placement, viewing distance and geometry, and the specific properties of the light booth need to be recorded and kept consistent.

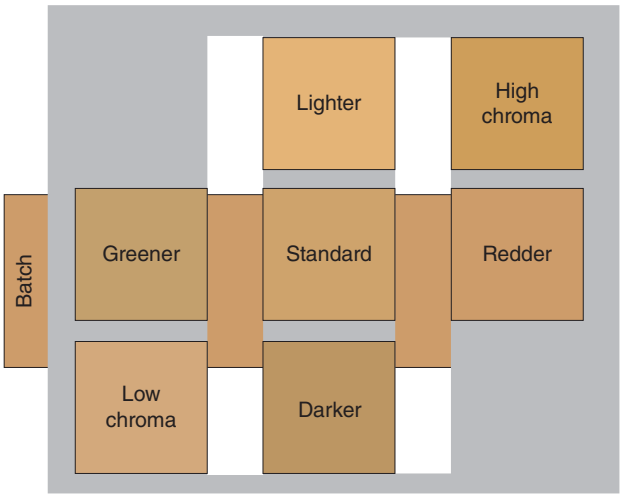

Figure 6.6 A visual color-tolerance chart with hue, lightness, and chroma limits.

The final step is defining a tolerance about the standard. Samples should be produced that represent the limits in hue, lightness, and chromatic intensity, shown in Figure 6.6. We are excellent at judging whether a color is within a set of limits. Without such limits, we are inconsistent.

There is another common scenario where the color requiring matching is a Pantone swatch, or a color affixed to a storyboard. The same procedure is followed where the key step is defining a manufacturing standard and limits.

The advantage of this approach is that the manufacturing standard can be matched without metamerism and with the same microscopic and macroscopic material appearance. Eliminating metamerism is crucial when making visual measurements.

We want to point out that metamerism can still occur at the manufacturing stage if different colorants are used, perhaps to reduce cost, or if the colorants are off shade.

D. MEASUREMENT GEOMETRIES

In Chapter 1, we learn that light interacting with a material can result in specular and diffuse reflection, regular and diffuse transmission, and absorption, shown in Figure 6.7. The particular combination of each component depends on body color and material appearance. The distribution of light reflection for different materials is shown in Figure 6.8, known as a goniophotometric plot or indicatrix. As materials increase in gloss, the distribution of light about the specular angle narrows and the amount of diffuse reflection decreases. Computer graphics software was used to render three bowls with the same body color but having different gloss, shown in Figure 6.9. The indicatrices shown in Figure 6.8 correlate with the changes in appearance.

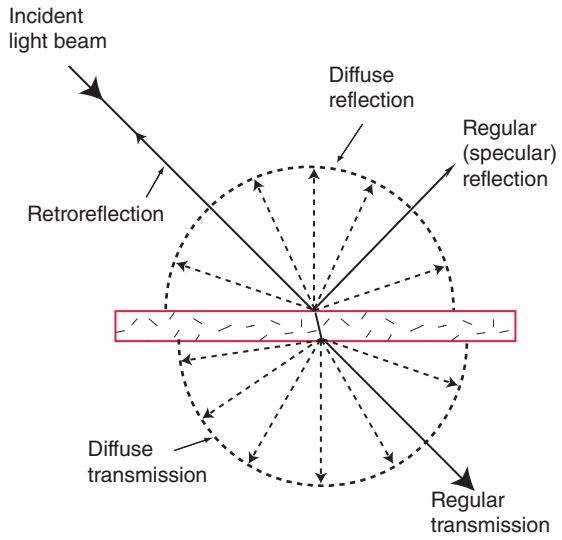

Figure 6.7 A ray of light striking a translucent material. Light not reflected or transmitted is absorbed.

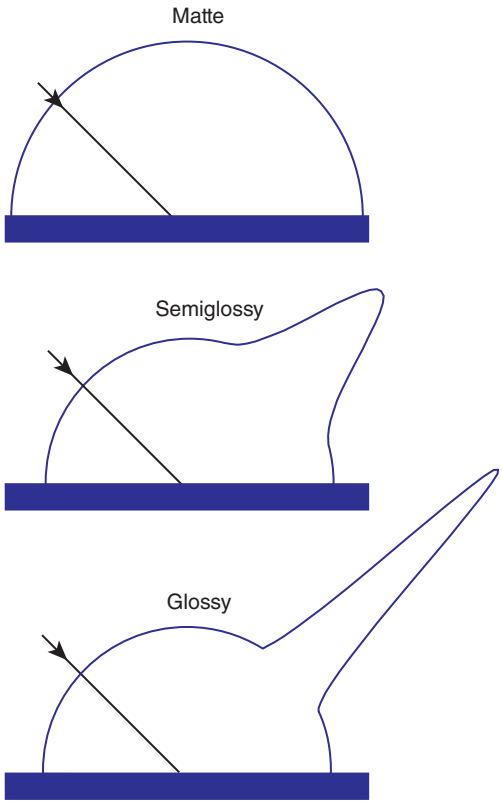

Figure 6.8 Indicatrices of three opaque materials.

Bidirectional Reflectance Distribution Function

A *bidirectional reflectance distribution function* (*BRDF*), defines a material's reflectance at all influx and efflux geometries relative to the sample's *surface normal* (Nicodemus et al. 1977). The *normal angle*, *n*, is the angle perpendicular to the tangent of a surface. This is shown in Figure 6.10 where the normal angle changes with the curvature of the semicircle.

Two angles are required to define a position in three-dimensional space, shown in Figure 6.11. The direction of a ray with a given solid angle, which forms the yellow cone, is defined by its *polar angle* (θ), and its *azimuthal angle* (ϕ). A complete geometric specification requires four angles, two to define influx and two to define efflux. Dimension *Z* is coincident with the normal angle.

CIE Recommended Geometries for Measuring Spectral Reflectance Factor

During 1931, when the CIE was defining the standard observer, standard sources, and standard illuminants, a standard geometry of 45° illumination from the normal angle and viewing along the normal angle was proposed. Since an object's "color" is largely defined by its diffuse reflection, an instrument with this geometry would directly measure diffuse reflectance. However, the General Electric-Hardy Recording Spectrophotometer, developed at this time period, had a geometry of approximately 0° illumination and diffuse viewing. Except for very matte surfaces, these two geometries are not equivalent (Billmeyer and Marcus 1969). Because of the projected importance of this instrument, both geometries were recommended in 1931. In fact, four geometries are specified by the CIE (2018) for reflectance measurements because light is reversible through any optical system, known as the *Helmholtz reciprocity law* (von Helmholtz 1866). These are shown in Figure 6.12.

The first pair of geometries are labeled as *45°:0°* and *0°:45°*, known as *bidirectional* geometries. The designation corresponds to *influx:efflux* (illumination:viewing) angles. The simplest way to build an instrument meeting this standard is to have a collimated beam of light illuminate a specimen at a single azimuthal angle. However, this results in insufficient amounts of light and directionality problems where samples rotated in their own plane lead to very different measured quantities. The solution is shown in Figure 6.13a where light is incident at all azimuthal angles, *annularly*, notated as *45°a:0°*. In some bidirectional instruments, the annular geometry is approximated where fiber optic bundles are placed at a number of azimuthal angles. This is known as circumferential geometry, notated as *45°c:0°*.

The second pair of geometries are labeled as *d:0°* and *0°:d* and refer to the use of *integrating spheres*. An integrating sphere is a hollow metal sphere several inches or more in diameter coated with a highly reflecting diffuse material such as barium sulfate or polytetrafluoroethylene. An integrating sphere collects all the light reflected from the surface of a sample placed against an opening into the sphere (called

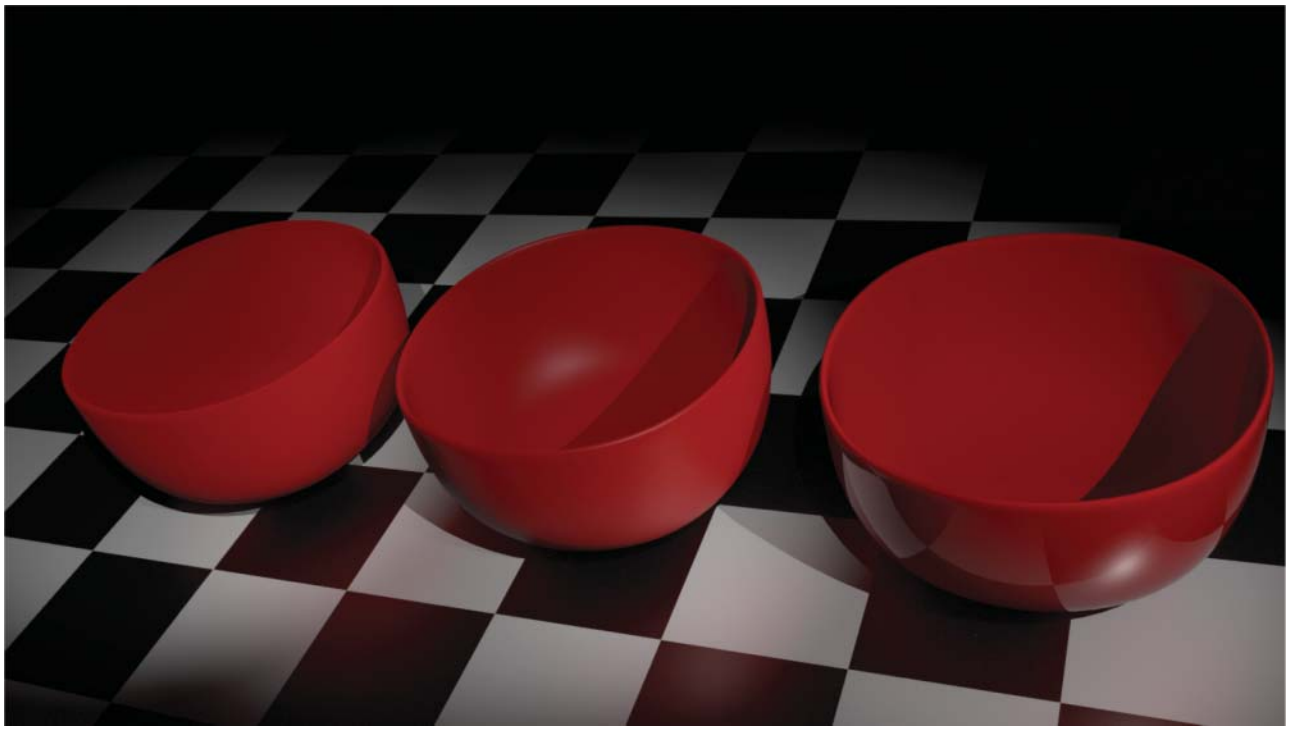

Figure 6.9 Red bowls with (left) matte, (center) semiglossy, and (right) glossy surfaces illuminated by several spotlights. The three bowls have the same body color.

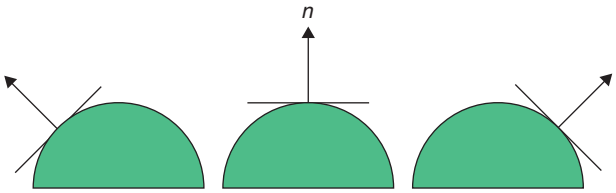

Figure 6.10 The normal angle, *n*, is perpendicular to the tangent at a point on a surface.

- *di:8°*: Diffuse influx and 8° efflux with the specular component included.
- *de:8°*: Diffuse influx and 8° efflux with the specular component excluded.
- *45°a:0°*: Annular 45° influx and normal efflux.
- *45°c:0°*: Circumferential 45° influx and normal efflux.
- *0°:0°*: Normal influx and normal efflux.
- *d:d*: Diffuse influx and diffuse efflux.

a port). If the normal angle is maintained when building the instrument, any specular reflection exits through either the source or detector port. However, integrating spheres designed for color measurement offset the normal angle between about 6° and 8°. By placing a *specular port* at the

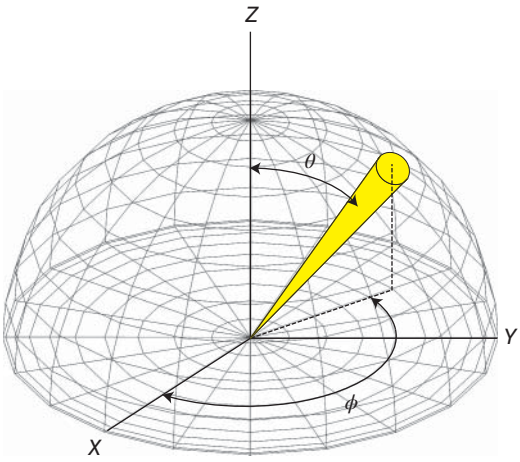

Figure 6.11 Defining an influx or efflux geometry requires polar, θ, and azimuthal, ϕ, angles.

opposite angle, the specular reflection can be either included or excluded from the measurement by placing material identical to the sphere's interior or a black trap, respectively, at the specular port, shown in Figure 6.13b. This design was first implemented by Hardy (1935, 1936, 1938). He noted that when observers look at glossy samples, they always rotate them to eliminate any specular reflections. By excluding this light from a color measurement, the result would have better correlation to visual measurements.

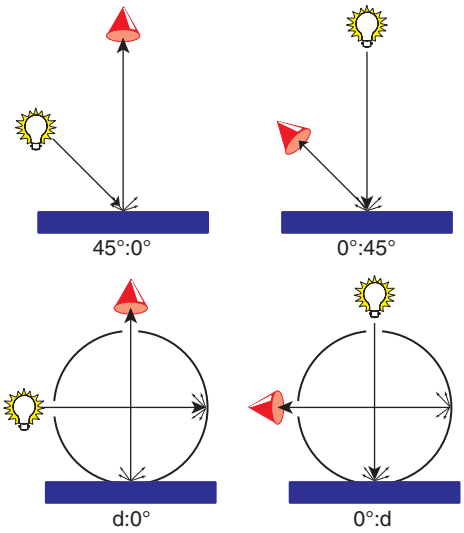

Figure 6.12 Simplified diagrams of the four CIE recommended geometries for color measurement.

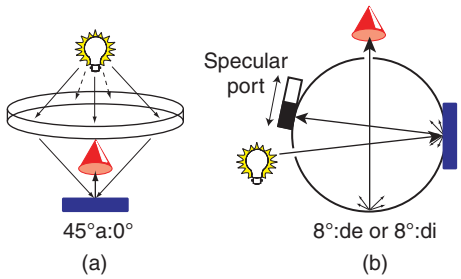

Figure 6.13 (a) Bidirectional annular geometry and (b) integrating sphere geometry where the specular component can be included or excluded (as shown).

Although the CIE specifies that the total area of all ports must not exceed 10% of the internal area, the *size* of the specular port relative to the illumination area is not standardized. As a consequence, a material of intermediate specular gloss will often have different measured values depending on the particular instrument (CIE 2006b), shown in Figure 6.14. In this example, neither port completely excludes the specular gloss. A semiglossy tile was measured with 45°a:0°, de:8°, and di:8°, the reflectance spectra shown in Figure 6.15. Colorimetric comparisons are listed in Table 6.1. The choice of geometry affects the sample's measured color. The correct measurement depends on the answer to "Why am I measuring this sample?"

Some industries have standardized geometries. In other cases, there can be a choice, and it is important to understand the equivalent illuminating and viewing environment for the three geometries. (These descriptions also apply to each corresponding reverse geometry.)

The di:8° geometry corresponds to completely diffuse illumination in which any specular reflection and texture

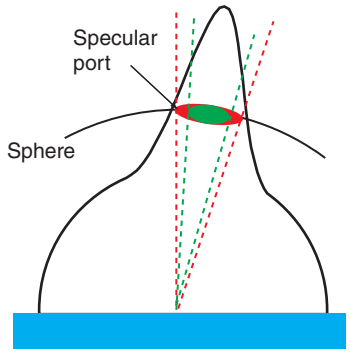

Figure 6.14 An indicatrix for a semiglossy material is superimposed on an integrating sphere with two possible port diameters.

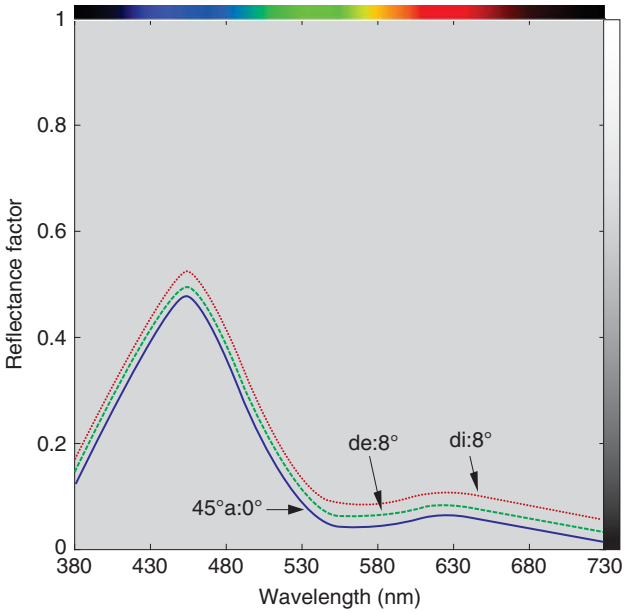

Figure 6.15 Spectral reflectance of a semiglossy tile measured with each listed geometry.

Table 6.1 Colorimetric data of a semiglossy tile measured with each listed geometry.

	L^*	C^*_{ab}	h_{ab}	ΔE_{00} di:8°	ΔE_{00} 45°a:0°
di:8°	51.1	41.5	269		
45°a:0°	44.8	46.9	268	6.6	
de:8°	47.5	44.6	268	3.9	2.7

would not be observable. That is, we would never notice a mirror image in a glossy specimen. The specular reflection would consist of uniform white light added to our visual evaluation of the specimen, regardless of how we rotate it. Although there are many environments that are quite diffuse, such as cloudy skies and uniform artificial illumination, it is rare that our viewing geometry subtends a small enough

field of view that we wouldn't receive any specular or textural information (particularly since there are objects in our visual field that obscure the lighting enabling us to sense a specimen's specular properties).

The de:8° geometry also corresponds to completely diffuse illumination, but here specular reflection is excluded (but not necessarily all its first-surface reflections). In most lighting conditions, we can see specular reflections and the sample must be rotated in order to exclude them from our visual evaluation. Texture would not be observable.

The 45°a:0° geometry does not have a real-world equivalent. If we reverse the geometry to 0°:45°a, this corresponds to a sample being directionally illuminated and viewed off axis, thus excluding specular reflections. If the sample is spun quickly in its own plane and viewed, this would be equivalent to the annular geometry. Texture would not be observable.

There are two striking discrepancies between the implied illuminating and viewing conditions of the CIE geometries and what we see when we look at materials, either in the real world or in a light booth. First, all three of these geometries average out texture, yet texture is very much a part of a specimen's appearance and has a large effect on color tolerances as we discuss in Chapter 5. It is unlikely that the manner in which we account for texture is equivalent to an instrument's spatial averaging. Second, most lighting is a combination of directional *and* diffuse components whereas a CIE geometry provides either directional *or* diffuse components.

Fortunately, this significant problem can be reduced in scope. Diffuse materials look approximately the same whether they are illuminated with directional or diffuse illumination since the first-surface reflection is uniformly spread out over all viewing angles. Thus, when one is measuring diffuse materials, the choice of geometry has little importance; all three geometries will give nearly identical results and correlate closely with visual measurements. For highly glossy materials, the first surface forms a well-defined specular reflection. Observers always rotate samples to exclude specular reflections. If the sample is placed on the floor of the booth and viewed at 45°, the back of the booth should be lined with black velvet. Thus, when one is measuring glossy materials, either 45°a:0° or de:8° should be used; they will give nearly identical results and correlate closely with visual measurements since the first-surface reflection is excluded in both cases.

The color appearance of specimens with first-surface reflection properties intermediate between highly glossy and highly diffuse is very dependent on lighting geometry. If we imagine having the ability to change the proportions of directional and diffuse components while maintaining the color and the level of the illumination, we would see the lightness and chroma of these materials change. If we were limited to choosing only one CIE geometry, we would choose 45°a:0°. Because the port sizes in integrating spheres are not standardized, de:8° measurements suffer from a lack of interinstrument agreement. This is less of a problem for bidirectional instruments. However, if minimizing directional sensitivity is critical (e.g. when measuring fabrics and granules), an experiment should be performed in which the measurement variation as a function of rotation is compared between candidate 45°a:0° and de:8° instruments. It may be more important to reduce directional sensitivity than to have good interinstrument agreement. Because circumferential geometry is sampling rather than continuously measuring at all azimuthal angles, a circumferential instrument may suffer from significant directional sensitivity.

Some integrating sphere instruments measure both specular included and excluded automatically. The difference in reflectance can be used as a measure of specular gloss.

We began this chapter with defining body color and microscopic and macroscopic material appearance. Body color is calculated from internal reflectance. From knowledge of a material's refractive index and the specific measurement geometry, internal reflectance is calculated from measured reflectance using the Fresnel equations, introduced in Chapter 1 for transparent materials. The specific formulas for reflecting materials are known as the Saunderson equations (1942) that we describe in Chapter 9. The preferred geometry is integrating sphere with specular component included. However, the calculation can be made for any of the CIE geometries.

CIE Recommended Geometries for Measuring Spectral Transmittance Factor

The CIE recommends the integrating sphere geometries of di:0°, 0°:di, de:0°, 0°:de as well as the two limiting cases of 0°:0° and d:d. For completely transparent specimens, all of these geometries would yield identical results. However, if any scattering is present, measured values can be quite different (except between reverse geometries which, by definition, are identical). An integrating sphere instrument offers the most flexibility enabling regular and diffuse transmittance to be measured, shown in Figure 6.16. This is particularly useful when characterizing transmission haze, essentially diffuse transmission (Billmeyer and Chen 1985; ASTM 2013b).

Multiangle Geometries

We describe in Chapter 1 that many coatings containing gonioapparent materials have appearances that change with changes in illumination or viewing angle, requiring measurements at multiple angles. The ASTM (2017c) defines nine geometries for interference pigments, shown in Figure 6.17. When the influx angle was always 45°, aspecular angles were sufficient to define geometry.

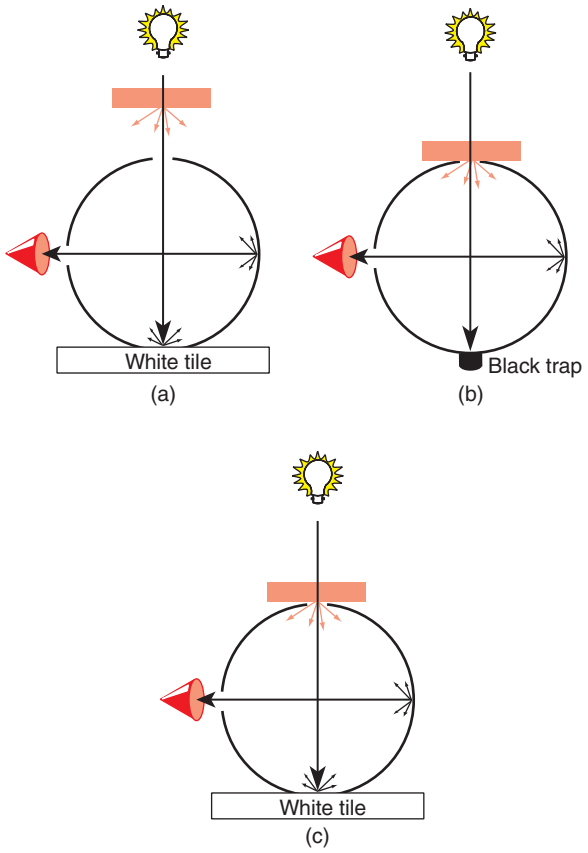

Figure 6.16 (a) Regular, (b) diffuse, and (c) total transmittance can be measured with an integrating sphere depending on the use of a white tile or black trap and the placement of the sample.

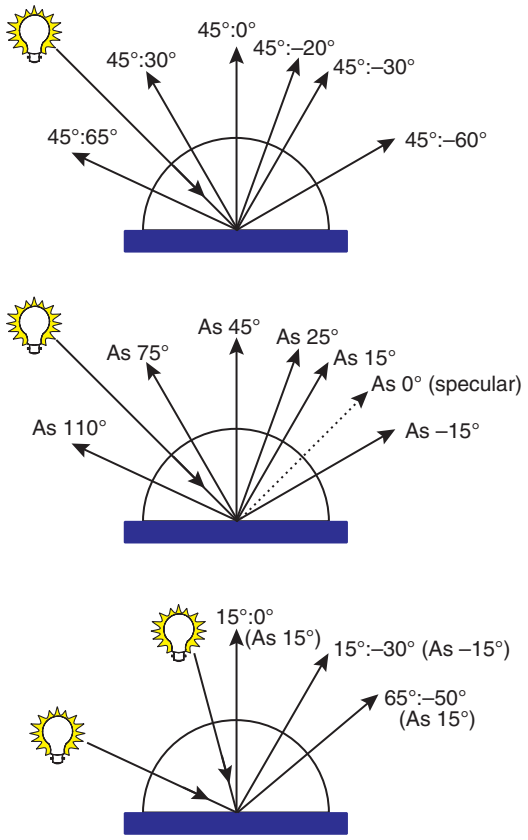

Figure 6.17 Geometries recommended by ASTM to characterize interference pigments. Angles defined from the specular angle, the aspecular angle, are notated by "As."

Additional influx angles require the CIE nomenclature. Coatings with metal flake pigments can be characterized with geometries of 45°: –30°, 45°:0°, and 45°:65° (ASTM 2017a).

E. SPECTROPHOTOMETRY

Spectrophotometers are instruments that measure the reflectance from or the transmittance through materials as a function of wavelength. The name for this instrument is misleading because it includes "photometer," implying that the detector has spectral sensitivity equal to the luminous efficiency function. The first such instruments used the human visual system as the detector (Gibson 1934) and spectrophotometer is an accurate description. Today, photosensitive detectors are used and the wavelength range can extend beyond the visible spectrum. The United States National Institute of Standards and Technology (NIST) uses the term *reflectometer* (Nadal et al. 2008), which would expand to *spectroreflectometer*. We will use the more familiar term, spectrophotometer.

The main components of all spectrophotometers for color measurement are a source of optical radiation with defined geometric conditions of illumination, a reflecting or transmitting specimen, some means of dispersing light, a detector, and a signal processing system that converts light into signals suitable for analysis, shown in Figure 6.18.

Physical properties of the specimens to be measured ultimately determine instrument design. In particular, materials may contain fluorescent colorants or fluorescent whitening agents; this affects the design of the illumination system. The absorption and scattering characteristics of colorants lead to slowly varying reflectance and transmittance as a function of wavelength in the visible spectrum; this affects the design of the dispersing element and the detector. Furthermore, because our visual system is such an excellent detector for observing differences, signal-processing requirements are stringent. That is, the instrument should be at least as sensitive in detecting small differences in color as an observer.

Those familiar with analytical spectrophotometers will notice that color-measurement spectrophotometers place the specimen between illumination and dispersion, whereas analytical spectrophotometers place the specimen between

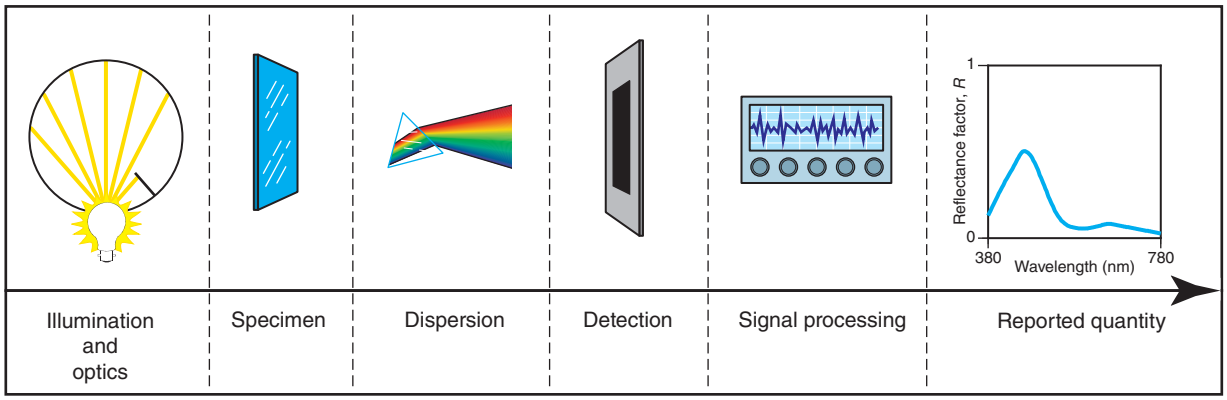

Figure 6.18 Block diagram of the subsystems comprising a spectrophotometer designed for color measurement.

dispersion and detection. Because light in an optical system is reversible, the two configurations are identical. The exception is fluorescent materials, described below. Placing the specimen between the illumination and dispersion results in a measurement that correlates with viewing a fluorescent specimen illuminated by white light. The reverse geometry does not.

- *Reflection*: The process by which radiant energy is returned from a material or object.
- *Reflectance factor*: The ratio of the flux reflected from the specimen to the flux reflected from the perfect reflecting diffuser under the same geometric and spectral conditions of measurement.
- *Transmission*: The process whereby radiant energy passes through a material or object.
- *Transmittance*: The ratio of transmitted flux to incident flux, under specified geometric and spectral conditions.

Reflectance and transmittance are both ratios in comparison to influx optical radiation. Accordingly, any light source with sufficient power over the wavelength range of interest can be used for spectrophotometry. However, when a specimen is fluorescent, the spectral properties of the light source affect the final measured value as we describe in Chapter 1 and below. Therefore, the light source in a spectrophotometer ideally should be identical to the light of the viewing environment. Because this ideal is impractical, most instruments use sources that attempt to match the spectral characteristics of D65 between 300 and 780 nm (ASTM 2016c). The ultraviolet region is important to match because this is the region of excitation for fluorescent whitening agents. Common sources when measuring fluorescent materials include incandescent plus a UV emitting LED and pulsed Xenon. Glass filters can be added to adjust their spectral properties to simulate those of D65.

Using one of the CIE geometries, light interacts with a specimen leading to reflectance or transmittance that is, in turn, dispersed. The first dispersing elements were prisms, known as *monochromators*, where a scanning mechanism isolated a single wavelength (or group of wavelengths). Today, *spectrographs* are used that are comprised of a diffraction grating and detector array. By passing a slit of light through glass with many narrowly spaced ruled lines, often hundreds of lines per millimeter, light is diffracted, by an amount that depends on its wavelength. The slit is spread into a spectrum and a detector array measures the light simultaneously. Many instruments use reflection-type *concave holographic diffraction gratings* that both disperse and focus the incident light, shown in Figure 6.19. The number of array elements can vary from 16 to several thousand. Increasing the number of elements leads to higher wavelength resolution and simpler techniques to calibrate the wavelength scale.

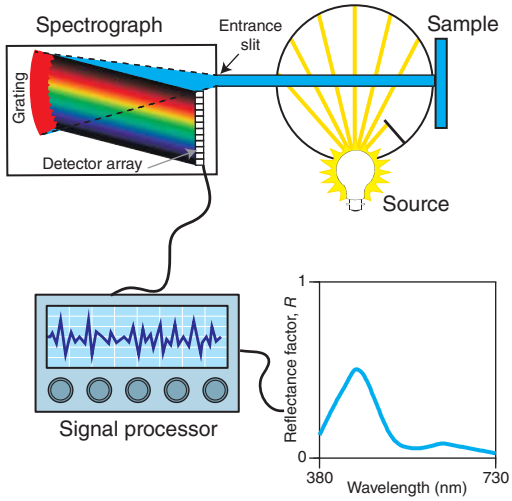

Figure 6.19 Spectrophotometer design using an integrating sphere, spectrograph, and signal processor.

The spreading of the spectrum by the grating is continuous while each detector in an array has a fixed size. A detector does not collect one wavelength but a range of wavelengths. The dispersion properties of the grating and the sizes of the entrance slit and each individual detector determine the weighting of each wavelength, called the *instrument passband*. When the sizes match, the shape is triangular. When they are different, the shape is trapezoidal. The width of the shape at one half its height is defined as *bandwidth*. Ideally, the reported wavelength increment and bandwidth should be equal. Typically, bandwidth exceeds the wavelength increment. When the number of detectors exceeds the number of reported wavelengths, the sensor data can be corrected to achieve a triangular passband with equal bandwidth and increment (Woolliams et al. 2011).

The electrical signal is amplified, digitized, and numerically processed yielding either spectral reflectance factor or spectral transmittance. For most applications, a 5 nm sampling and bandwidth are sufficient to analyze spectral information given the inherent absorption and scattering properties of natural and man-made colorants in the visible region. The spectral data are used to calculate tristimulus values, described in Chapter 4. The particular light source in a spectrophotometer does not limit the calculation of colorimetric coordinates to a single source. Reflectance and transmittance are *ratios*. By definition, the power distribution of the spectrophotometer's light source is factored out. Thus, we can calculate X, Y, Z or L^*, a^*, b^* coordinates for each CIE illuminant and CIE standard observer of interest from the same reflectance or transmittance curve. There are many CIE illuminants that, hopefully, can be selected that well approximate the lighting used to evaluate color visually. CIE illuminants are described in Chapter 7. In the specific case of fluorescent specimens, the spectral data will be somewhat in error in comparison to data resulting from the actual spectral radiance. For most applications, it is more important to have a consistent measurement and calculation procedure than to accurately account for fluorescence. Accurate methods for characterizing fluorescent materials are described below.

All measuring instruments require calibration. Calibrating the *wavelength and radiometric scales* (often referred to as the photometric scale) are the most important in spectrophotometers designed for color measurement. Instruments are calibrated by the manufacturer. Users *standardize* their instrument by measuring a white tile supplied with the instrument, the formulas shown in Eqs. (6.1) and (6.2) for spectral reflectance factor and spectral transmittance, respectively, where d defines the detector signal

$$R_{\lambda,\text{sample}} = \frac{d_{\lambda,\text{sample}} - d_{\lambda,\text{black}}}{d_{\lambda,\text{white}} - d_{\lambda,\text{black}}} R_{\lambda,\text{white}} \tag{6.1}$$

$$T_{\lambda,\text{sample}} = \frac{d_{\lambda,\text{sample}} - d_{\lambda,\text{black}}}{d_{\lambda,\text{no sample}} - d_{\lambda,\text{black}}} \tag{6.2}$$

The measurement of the white tile is used to transfer the scale of reflectance factor or transmittance. Each specific white tile has been calibrated by the instrument manufacturer and its data, $R_{\lambda,\text{white}}$, are stored in the instrument. It is important to keep this tile clean and if damaged, replaced by the manufacturer along with new calibration data. Using clothing to clean the white tile is discouraged since most detergents have optical brighteners that can transfer to the tile, affecting accuracy (Pons and Campos 2004). The black measurement varies with manufacturer. It can be a measurement with the light source turned off, an open sample port measurement with the instrument aimed at a location where light from the instrument will not be reflected back into the instrument, or a black trap, a device that collects all light. When measuring total transmittance, the standard is usually air and the calibration white tile or a diffuse white is placed at the sample port. We describe methods of validating accuracy later in this chapter.

F. SPECTRORADIOMETRY

Spectroradiometers measure light, whether it is a source, display, or light reflecting from a material. The specific units of measurement depend on the entrance optics. One measured quantity is *irradiance*, the amount of light received on a surface per unit area, often defined by watts per unit area expressed in meters squared (W/m^2) and the letter "E." Devices can use a flat round diffuser, or a diffuse half hemisphere, called a *cosine diffuser*, shown in Figure 6.20a. The cosine diffuser produces measurements that are equivalent to a spatially uniform diffuse light. Without the cosine diffuser, handheld measurements are highly variable.

A second measured quantity is *radiance*, the amount of light emanating from or falling on a surface per unit projected area, often defined by watts per unit area per solid angle expressed in meters squared steradians (W/m^2 Sr) and the letter "L." We can think of solid angle as a measure of the size of an object relative to a fixed position. An object that is close to us subtends a larger solid angle than the same object viewed from a distance. Instruments that measure irradiance have diffusers while instruments that measure radiance have lenses. A specific solid angle can be achieved using a lens and a Pritchard aperture, shown in Figure 6.20b. The image through the lens is projected onto a mirror with a hole in it. The lens and the diameter of the hole determine the solid angle. The light passing through the hole is measured. Looking through the eyepiece, an image is seen reflected from a second mirror where the aperture appears as a black dot, enabling precise aiming.

Instrument calibration is mostly done by the manufacturer. The number of elements in the detector array tends to range from 128 to 3648, giving excellent wavelength resolution. Calibrating the wavelength scale involves measuring line sources such as mercury–cadmium or

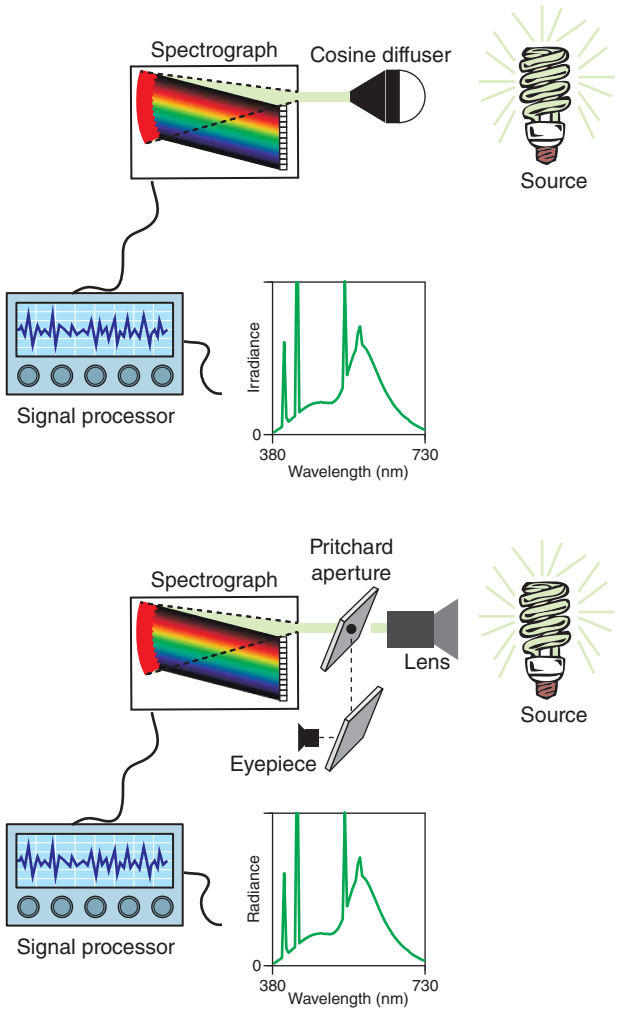

Figure 6.20 Spectroradiometer design using a (a) cosine diffuser or (b) lens and Pritchard aperture.

- *Radiant flux*: The time rate of flow of radiant energy. "Power" and "flux" are synonymous.
- *Irradiance*: The radiant flux incident per unit area.
- *Radiance*: Radiant flux in a beam, emanating from a surface, or falling on a surface, in a given direction, per unit of projected area of the surface as viewed from that direction, per unit of solid angle.

mercury–argon. Each peak is evaluated and the corresponding detector-element number recorded. Regression is used to fit a cubic polynomial where the detector number is the independent variable and the peak wavelength is the dependent variable. The fitted polynomial is used to convert from detector number to wavelength. There are two ways to transfer the radiometric scale. The first is using a calibrated light source, typically an incandescent lamp. The second is measuring an incandescent lamp simultaneously with both a calibrated detector and the spectroradiometer. The lamp is being calibrated at the time of measurement. The second approach is preferred because a calibrated detector has lower uncertainty than a calibrated source.

Many spectroradiometers are auto-ranging where integration time varies depending on the amount of radiant flux. Following this measurement, a second measurement of the same time duration is made with the light blocked. This is a measure of the sensor's *dark current*, the signal that occurs without incident light. These measurements and the stored data from the calibrated lamp are used to calculate spectral irradiance or radiance, shown in Eq. (6.3) for spectral radiance. This is the same as the formula for calibrating a spectrophotometer with the addition of an integration-time correction, $t_{\text{integration}}$

$$L_{\lambda,\text{light}} = \frac{d_{\lambda,\text{light}} - d_{\lambda,\text{light}}^{\text{dark current}}}{d_{\lambda,\text{reference}} - d_{\lambda,\text{reference}}^{\text{dark current}}} t_{\text{integration}} L_{\lambda,\text{reference}} \quad (6.3)$$

G. FLUORESCENCE MEASUREMENTS

We introduce photoluminescence in Chapter 1 where light is absorbed in one spectral region, the *excitation range*, and a portion is emitted in a different spectral region, the *emission range*. Phosphorescence continues after excitation ceases, whereas fluorescence ceases when excitation ceases. Mielenz (1982) and Zwinkels, DeRose, and Leland (2014) provide details about fluorescence and its measurement.

The colors we see when looking at fluorescent materials result from a combination of the nonfluorescent reflection, known as the *reflected spectral radiance factor*, $\beta_{\lambda,r}$, and the fluorescent emission, known as the *luminescent spectral radiance factor*, $\beta_{\lambda,l}$. The combination of both components is known as the *total spectral radiance factor*, $\beta_{\lambda,t}$, shown in Eq. (6.4)

$$\beta_{\lambda,t} = \beta_{\lambda,r} + \beta_{\lambda,l} \quad (6.4)$$

The luminescent spectral radiance factor is a function of both the excitation spectrum and the light source spectral power distribution. Colorimetric calculations will not predict visual evaluation when the light source in a spectrophotometer does not well simulate the calculation illuminant, for example, Lin, Shamey, and Hinks (2012), and Gu et al. (2016). This includes both the UV and visible regions of the spectrum. This has often been a problem when measuring materials containing fluorescent whitening agents such as paper.

The CIE D-series illuminants are defined from 300 to 830 nm. Because this range includes UV, D65 and D50

are often used when measuring and specifying fluorescent materials. Light booth and instrument manufacturers may use a combination of lights and filters to simulate these illuminants. We describe simulating and assessing daylight illuminants in Chapter 7.

Spectrophotometers used to measure fluorescent materials must have the dispersing element between the sample and the detector. The preferred geometry is bidirectional (Alman and Billmeyer 1976; Gundlach and Terstiege 1994). This is known as the *one-monochromator method* (ASTM 2016c), and total radiance factor is measured directly. Tristimulus values are calculated in the usual fashion where total spectral radiance factor is used in place of spectral reflectance factor.

Bispectrometers (Donaldson 1954) are instruments designed to measure fluorescent materials, shown in Figure 6.21. The instrument has two dispersing elements, one between the source and sample (excitation), and the second between the sample and detector (emission). The excitation dispersing element is fixed at a specific wavelength, and this monochromatic light is incident on the sample. The reflected light enters a spectrograph where the entire spectrum is recorded, simultaneously. This is repeated for each excitation wavelength.

Since two variables are changing, the data form a matrix, known as the *Donaldson matrix*, plotted in Figure 6.22 for a fluorescent yellow paint. Diagonal matrix elements are reflected radiance factor and off-diagonal elements are luminescent radiance factor. The excitation region spans between 320 and 520 nm. The emission region spans between 460 and 630 nm.

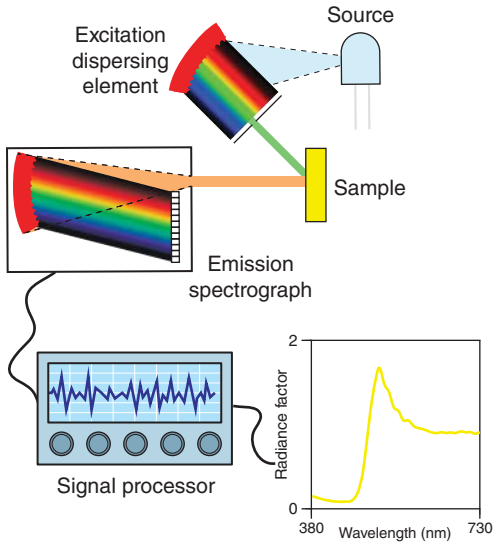

Figure 6.21 Bispectrometer used to measure fluorescent materials.

The Donaldson matrix is used to calculate the reflected, luminescent, and total spectral radiance factor for any illuminant of interest (Leland, Johnson, and Arecchi 1997; Zwinkels, DeRose, and Leland 2014; ASTM 2017a), shown in Figure 6.23 for a fluorescent yellow paint illuminated by D65. The magnitude of the excitation and emission spectra depend on the relative spectral power distribution of the illuminant. The absolute spectral radiance is not required because the measurement is relative to a perfect

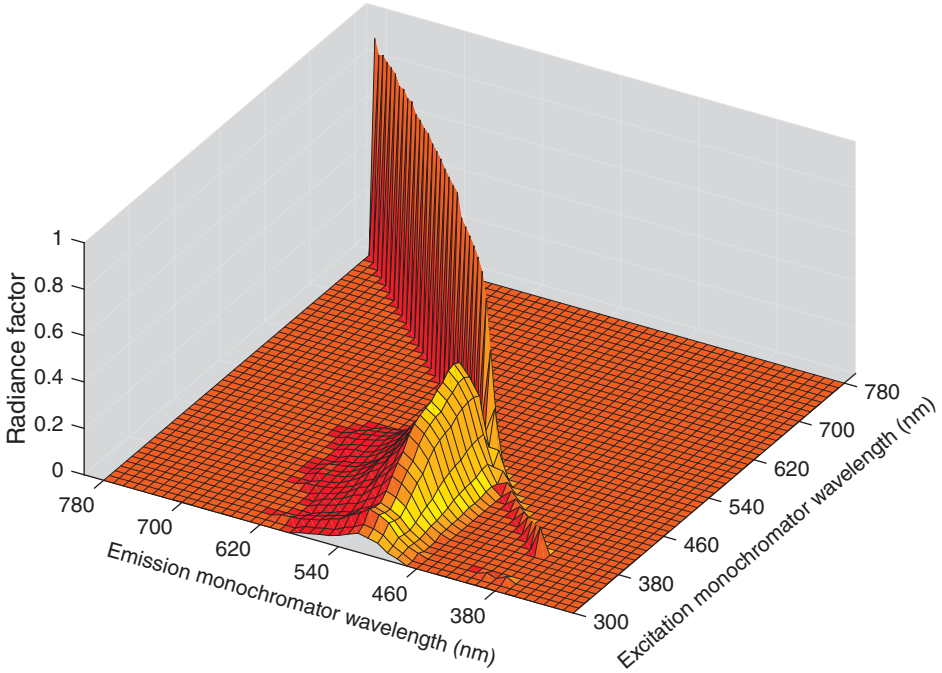

Figure 6.22 False color surface map of Donaldson matrix for a fluorescent yellow paint. Off-diagonal elements have been multiplied by five.

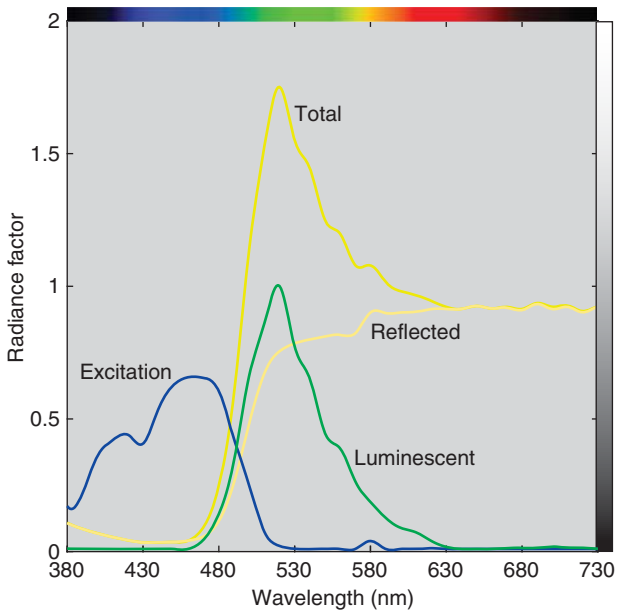

Figure 6.23 Excitation, luminescent, reflected, and total radiance factor of a fluorescent yellow paint illuminated by D65.

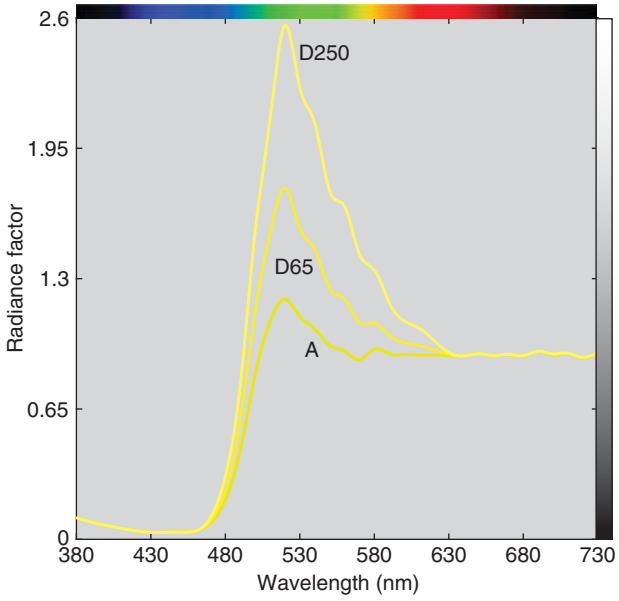

Figure 6.24 Total radiance factor spectra of a fluorescent yellow paint illuminated by CIE illuminants D65, D250 (25 000 K), and A.

reflecting diffuser. The total radiance factor of the fluorescent yellow paint illuminated by CIE illuminants D65, D250 (25 000 K), and A are shown in Figure 6.24. Total radiance factor increases as the amount of short wavelength light increases.

H. PRECISION AND ACCURACY MEASUREMENTS

We have described a number of instruments used in color technology, for example, spectrophotometers, spectroradiometers, and bispectrometers. Following calibration, each instrument is reproducing a standardized scale, for example, spectral reflectance factor and spectral radiance. All these scales are defined internationally, and methodologies have been developed to transfer these scales with a minimum of *measurement uncertainty*, for example, Early and Nadal (2004, 2008).

Uncertainty is divided two categories, *precision* and *accuracy*. Throwing darts at a target is a convenient tool for explaining precision and accuracy, shown in Figure 6.25. The dispersion of the darts about the target describes *precision*. As the grouping gets smaller, precision improves. The average of the grouping compared with the center of the target describes *accuracy*. The closer the grouping is to the center of the target, the better the accuracy. As you might imagine, it is often easier to improve accuracy than to improve precision. A slight adjustment can correct accuracy. A different form of throwing or more practice may be required to improve precision. A great deal of analysis may be required to determine the cause for the lack of precision. Instruments exhibit all four combinations of precision and accuracy. Statistically, a lack of precision is mainly due to *random* errors and a lack of accuracy is mainly due to *systematic* errors, sometimes called *bias* errors.

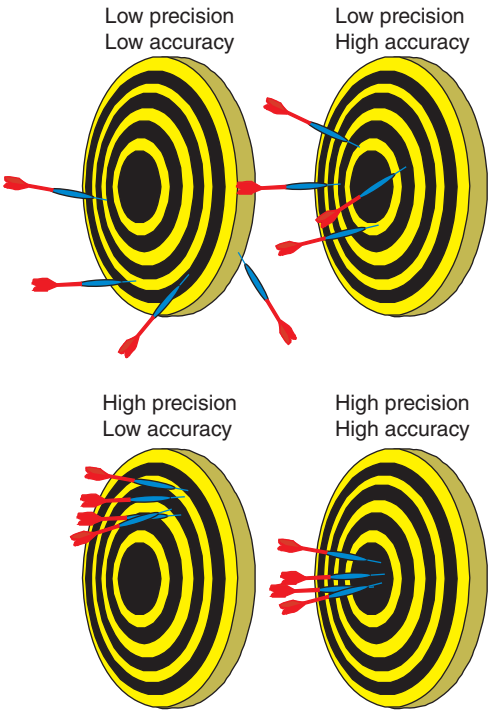

Figure 6.25 Throwing darts at a target and each combination of high and low precision and accuracy.

- *Precision*: The closeness of agreement between test results obtained under prescribed conditions.
- *Accuracy*: The closeness of agreement between a test result and an accepted reference value.

Color measurement instrumentation is evaluated for *repeatability*, *reproducibility*, *interinstrument* and *intermodel reproducibility*, and *accuracy* (ASTM 2016e). Wyble and Rich (2007a,2007b) have clearly explained these differences, which we repeat here.

- *Repeatability*: Repeatability is how well an instrument can repeat identical measurements. Repeatability can be quantified in terms of short, medium, and long times between measurements. These types of repeatability are taken over seconds or minutes (short); hours (medium); and days, weeks, or longer (long). Intuitively, repeatability can be thought of as the degree to which an instrument makes self-consistent measurements.
- *Reproducibility*: Reproducibility is similar to repeatability except that some aspect of the measurement conditions has changed. This might be the operator, the instrument, or some other condition. The intuitive understanding of reproducibility is the degree to which an instrument makes consistent measurements even when conditions are slightly changed. Consider the reliability of an operator to consistently replace a sample for replicate measurements. The ability of the operator is an important factor, but so is the mechanical configuration of the instrument, in the sense that some instruments' sample positioning hardware will better facilitate consistent replacement.
- *Interinstrument and intermodel reproducibility*: These are special cases of repeatability where instruments of identical design (interinstrument) or different design (intermodel) are compared.
- *Accuracy*: Accuracy is how closely an instrument can conform to the accepted value for a given sample. "Accepted" values accompany specific samples and are usually provided by a high-accuracy laboratory, such as a national metrological institute. From these samples, accuracy is independently determined for the wavelength scale and the radiometric scale.

Repeatability

We were asked to investigate a quality control problem for a red-powder-coated part. In the last two months, the number of parts out of tolerance had increased substantially. The company used an integrating-sphere spectrophotometer and measurements were made with the specular component included: di:8°. The spectrophotometer was on the production floor and serviced regularly. The color of the standard was $L^* = 40$, $a^* = 60$, and $b^* = 35$, calculated for illuminant D65 and the 1964 standard observer. The tolerance was 2.5 ΔE_{00}.

ASTM (2016e) recommends 30 measurements when characterizing precision. During a production run, 30 parts were measured by the spectrophotometer operator and set aside. At a later time, we measured these same parts. We also measured one part 30 times with replacement. We describe in Chapter 5 that a confidence limit for three-dimensional data is an ellipsoid. The colorimetric data along with their 95% confidence limits for these three cases are shown in Figure 6.26. Our first observation was the extreme difference in the variability of the production measurements compared with ours. The orientations were similar while the volumes were very different. The measurements of the single part resulted in a typical amount of variability.

The next day, we watched the operator and noticed that some of the parts were warm to the touch during measurement and that measurement temperature was not controlled. We suspected thermochromism as the source of variability, and we ran a simple experiment where measurements were performed while a part was heated. These data are plotted in Figure 6.26d. The orientation is similar to the production measurements. It turned out that the operator had been making color measurements for two months with a minimum of training. Following more training and an explanation about thermochromism, the measurement temperature was controlled and the number of parts out of tolerance returned to their historical values.

The confidence ellipsoid is useful to visualize variability. It may also be useful to quantify the variability. One approach is to calculate the volume of the confidence ellipsoid, known as the *generalized sample variance* (Johnson and Wichern 2007). It is the determinant of the variance–covariance matrix and can be scaled for a given confidence percentage. The determinants for the three cases are listed in Table 6.2.

Most of us are much more familiar with a total color difference. The *mean color difference from the mean*, *MCDM*, is used as an approximation to the ellipsoid volume, calculated as shown in Eq. (6.5) using the CIELAB color-difference formula (Billmeyer and Alessi 1981). The MCDM is the radius of a sphere and the 95% confidence limit (i.e. the sphere) is the MCDM plus 1.645 times the standard deviation (Nadal, Miller, and Fairman 2011). Any color difference formula can be used such as CIEDE2000. The standard is the mean $L^*a^*b^*$ coordinates. MCDMs are reported typically without scaling to a percentage confidence limit

$$\mathrm{MCDM} = \frac{\sum_{i=1,n} \sqrt{\left(L_i^* - \overline{L}^*\right)^2 + \left(a_i^* - \overline{a}^*\right)^2 + \left(b_i^* - \overline{b}^*\right)^2}}{n} \tag{6.5}$$

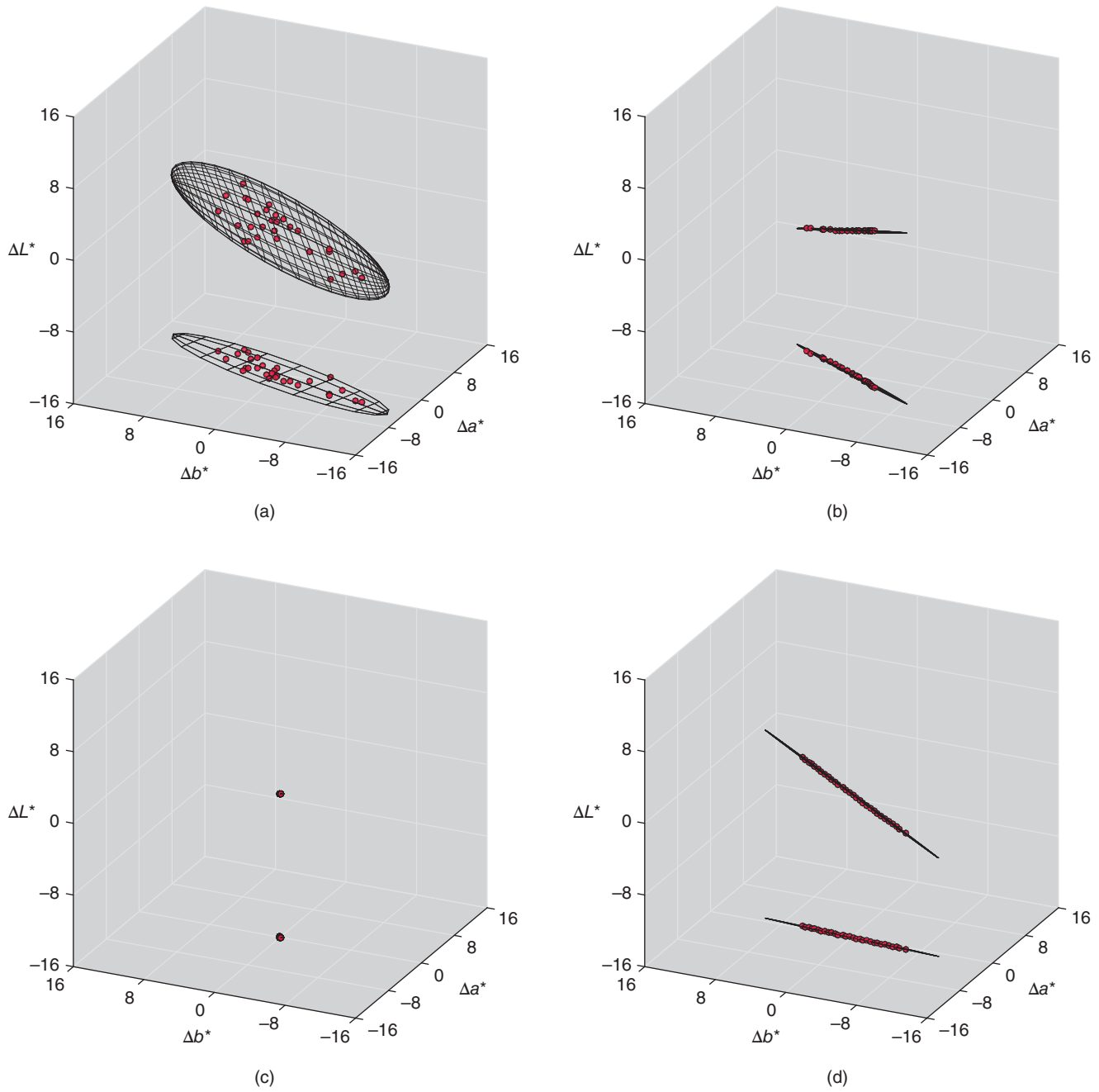

Figure 6.26 $\Delta L^*\Delta a^*\Delta b^*$ 95% confidence ellipsoids and their projection onto the $\Delta a^*\Delta b^*$ plane for (a) 30 parts measured during production, (b) the same 30 parts at a later time, (c) one part measured 30 times with replacement, and (d) during a heating experiment.

There are two limitations using an MCDM as a measure of variability. MCDM is a poor approximation to an elongated ellipsoid, shown in Figure 6.27 using the controlled temperature production data where a confidence ellipsoid and MCDM sphere have the same generalized sample variance. The second limitation is more fundamental. Color differences are not normally distributed, but skewed because color differences are only positive, shown in Figure 6.28 for 1000 CIELAB total color differences calculated from normally distributed random ΔL^*, Δa^*, and Δb^* values. The validity of a mean requires normally distributed data. Other techniques can be used to calculate a confidence ellipsoid from color-difference data (Nadal, Miller, and Fairman 2011). Despite these limitations, we still believe it is reasonable to use MCDM because of our familiarity with relating the magnitude

Table 6.2 Generalized sample variance, CIELAB, and CIEDE2000 mean color difference from the mean (MCDM) of each listed data set.

Measurements $n = 30$	Generalized sample variance	CIELAB MCDM	CIEDE2000 MCDM
Uncontrolled temperature	6.92	5.3	2.8
Controlled temperature	1.02E−05	3.0	1.3
Repeatability	2.88E−11	0.1	0.0

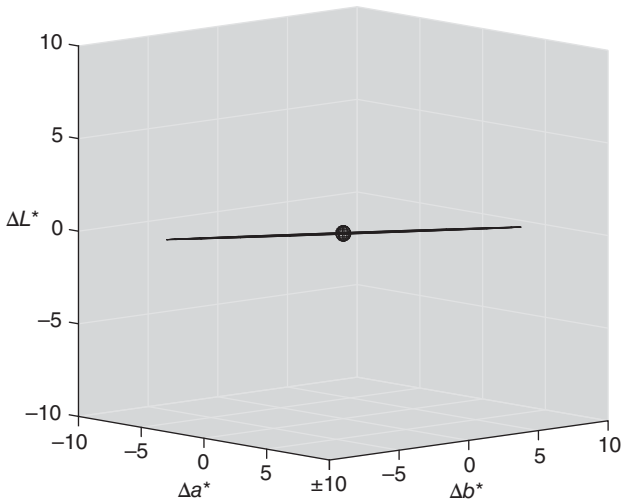

Figure 6.27 $\Delta L^*\Delta a^*\Delta b^*$ 95% confidence ellipsoid for 30 parts measured under controlled temperature and the corresponding ΔE^*_{ab} MCDM. Both have the same generalized sample variance.

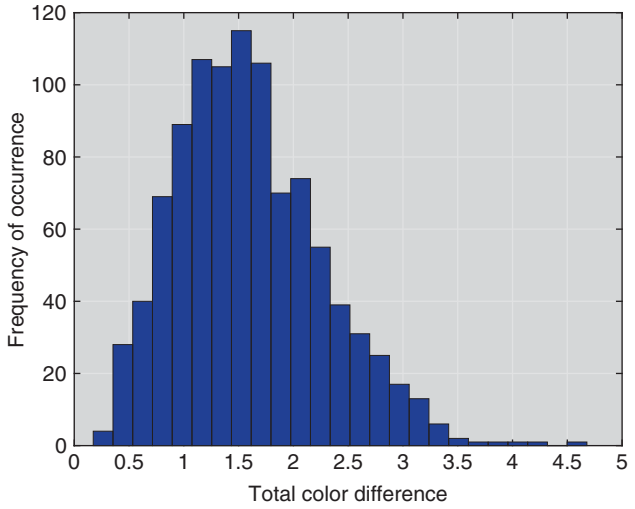

Figure 6.28 CIELAB total color difference histogram for 1000 normally distributed random ΔL^*, Δa^*, and Δb^* values.

of a color difference with our experiences looking at color-difference pairs.

Intramodel Reproducibility

Two spectrophotometers of the same make and model were evaluated for reproducibility. These instruments have 45°a:0° geometry and an incandescent source that is pulsed for each measurement. The manufacturer specifications are as follows: repeatability of 0.1 ΔE^*_{94} (D50, 1931 standard observer, mean of 10 measurements every three seconds), intramodel reproducibility of 0.4 ΔE^*_{94} average, 1.0 ΔE^*_{94} maximum (deviation from manufacturing standard at a temperature of 73.4 °F on 12 Lucideon tiles, D50, and the 1931 standard observer). *Lucideon tiles*, often referred to as CERAM or BCRA Series II tiles, are a set of 12 ceramic tiles that are used extensively to analyze color measurement precision and accuracy (Rich et al. 1995; Fairman and Hemmendinger 1998). Their reflectance spectra are shown below.

The Lucideon white tile was measured 150 times without replacement using software that triggered a measurement every three seconds. Every 10 successive measurements were averaged and a CIE94 total color difference calculated comparing the first set and each successive set. The results for Instruments 1 and 2 are plotted in Figure 6.29. Instrument 1 is out of specification since all the color differences are greater than 0.1 ΔE^*_{94}. Instrument 2 is within specification. However, both instruments are increasing in total color difference indicating a systematic error. Each of the

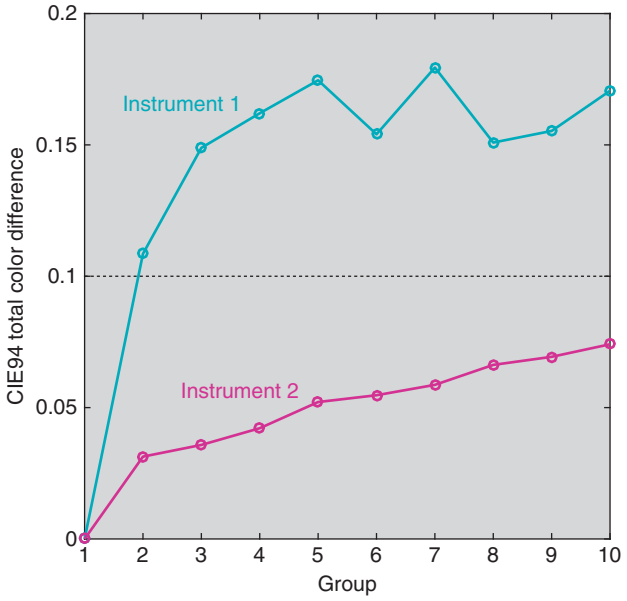

Figure 6.29 Short-term repeatability of Instrument 1 (cyan line) and Instrument 2 (magenta line) where averages of 10 successive measurements were compared with the first set of average measurements.

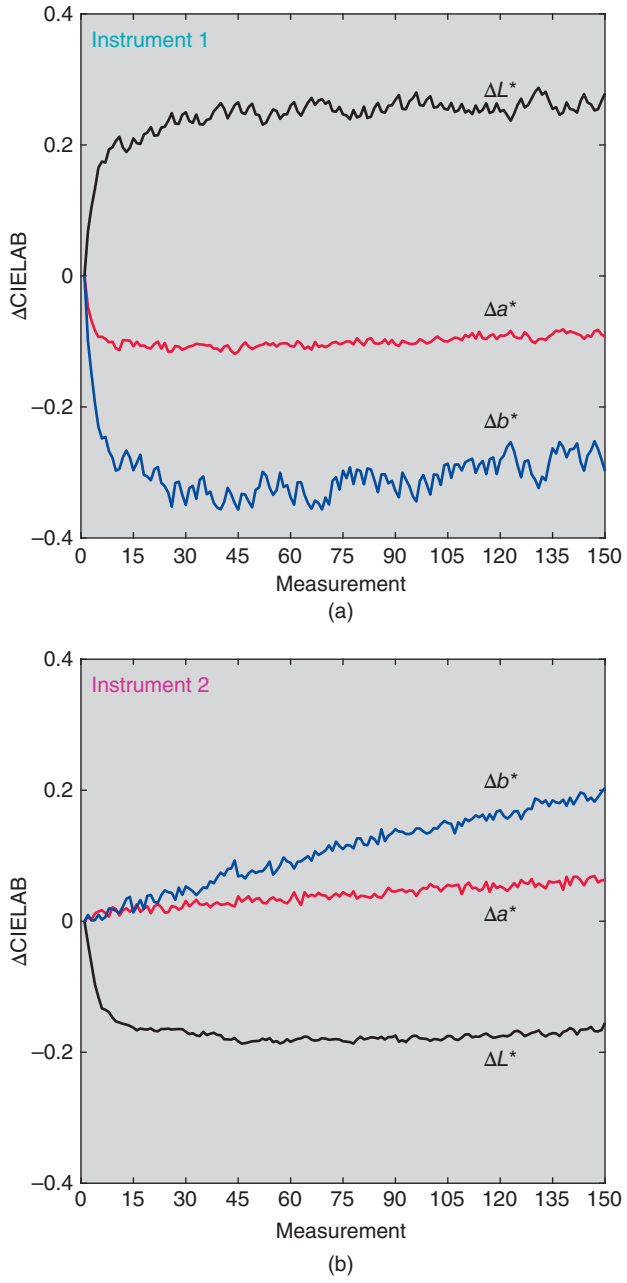

Figure 6.30 CIELAB $\Delta L^*\Delta a^*\Delta b^*$ coordinates of 150 repeat measurements of the Lucideon white tile for (a) Instrument 1 and (b) Instrument 2. Each measurement is compared with the first measurement.

150 CIELAB values was compared with the first measurement, shown in Figure 6.30. Instrument 1 stabilizes by the 30th measurement while Instrument 2 continues to increase. Neither instrument has acceptable repeatability, despite Instrument 2 meeting the manufacturer's specification.

The colorimetric data and 95% confidence limit for Instrument 2 are shown in Figure 6.31. Because of the systematic increase in CIELAB values, the data are not

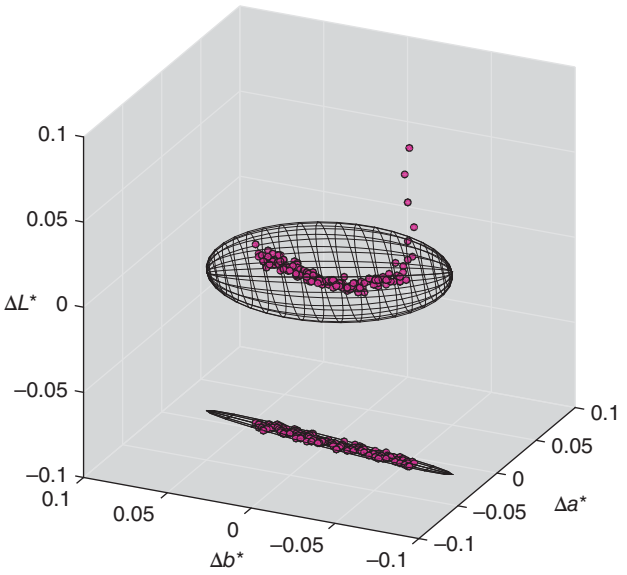

Figure 6.31 $\Delta L^*\Delta a^*\Delta b^*$ 95% confidence ellipsoid and its projection onto the $\Delta a^*\Delta b^*$ plane for 150 repeat measurements of the Lucideon white tile for Instrument 2.

random and a confidence limit is not meaningful. For random data, the ellipsoid is spherical. The measurement range was reduced to measurements 50–99 and confidence limits were calculated, shown in Figure 6.32. The measurement variability of Instrument 1 is larger than Instrument 2. The generalized sample variances for Instruments 1 and 2 are 1.13×10^{-13} and 1.16×10^{-15}, respectively.

Intrainstrument reproducibility answers the question, "Are the mean values from the same or different populations?" Another way to ask the question is, "Are the mean values statistically significantly different?" For univariate data, the Student's *t*-test is used. For multivariate data, *Hotelling's T-squared* (T^2) *test* is used (Johnson and Wichern 2007; Manly and Alberto 2017; ASTM 2016e). Details of the calculation are shown in the nearby sidebar. For these two sets of measurements, they are not from the same population; that is, they are statistically significantly different at a 95% confidence limit. This can be performed for all 12 Lucideon tiles (Wyble and Rich 2007b).

Accuracy

An accurate measurement has a minimum of systematic (bias) error. Recalling our example of throwing darts at a target, the closer the grouping is to the center of the target, the more accurate is the group of throws. The position of the grouping is defined by its average.

Commercial spectrophotometers are *traceable* to a national standards laboratory. The national laboratory realizes a radiometric scale as a function of wavelength, such as spectral reflectance factor. The scale has *uncertainty*, and national laboratories well document these uncertainties,

Hotelling's *T*-squared Test

Hotelling's T^2 test is a generalization of the Student's *t*-test for multivariate data (Johnson and Wichern 2007; Manly and Alberto 2017). Ideally, the two populations should have the same variability. When they do not, it is important that the sample number is the same, otherwise the test requires modification.

The first step is to calculate the mean vector, $\overline{\mathbf{x}}$, and the variance–covariance matrix, $\mathbf{S}$, shown in Eqs. (6.6) and (6.7)

$$\overline{\mathbf{x}} = \begin{pmatrix} \overline{L^*} \\ \overline{a^*} \\ \overline{b^*} \end{pmatrix} \tag{6.6}$$

$$\mathbf{S} = \begin{pmatrix} \sigma_{L^*}^2 & \sigma_{L^*}\sigma_{a^*} & \sigma_{L^*}\sigma_{b^*} \\ \sigma_{a^*}\sigma_{L^*} & \sigma_{a^*}^2 & \sigma_{a^*}\sigma_{b^*} \\ \sigma_{b^*}\sigma_{L^*} & \sigma_{b^*}\sigma_{a^*} & \sigma_{b^*}^2 \end{pmatrix} \tag{6.7}$$

Next, the pooled variance–covariance matrix is calculated, $\mathbf{S}_{\text{pooled}}$, using Eq. (6.8) where n is the number of measurements

$$\mathbf{S}_{\text{pooled}} = \frac{(n_1 - 1)\mathbf{S}_1 + (n_2 - 1)\mathbf{S}_2}{n_1 + n_2 - 2} \tag{6.8}$$

The T^2 statistic is calculated using Eq. (6.9). Note that this is a matrix formula

$$T^2 = \frac{n_1 n_2}{n_1 + n_2}(\overline{\mathbf{x}}_1 - \overline{\mathbf{x}}_2)'\mathbf{S}_{\text{pooled}}^{-1}(\overline{\mathbf{x}}_1 - \overline{\mathbf{x}}_2) \tag{6.9}$$

Statistical significance is evaluated by comparison to an F distribution, shown in Eq. (6.10). When T^2 is larger than the critical value, the two instruments are from different populations. That is, the mean values are statistically significantly different at a 95% confidence level

$$T^2 > \frac{3(n_1 + n_2 - 2)}{n_1 + n_2 - 4} F_{0.05}(3, n_1 + n_2 - 4) \tag{6.10}$$

For example, the 50 repeat measurements of the Lucideon white tile from Instruments 1 and 2, plotted in Figure 6.32, are tested using Hotelling's T^2. The values are given in Eqs. (6.11)–(6.19)

$$\overline{\mathbf{x}}_1 = \begin{pmatrix} 96.24 \\ -0.52 \\ 1.66 \end{pmatrix} \tag{6.11}$$

$$\mathbf{S}_1 = \begin{pmatrix} 0.1406 & -0.0176 & 0.1566 \\ -0.0176 & 0.0140 & 0.0416 \\ -0.1566 & 0.0416 & 0.2832 \end{pmatrix} \cdot 10^{-3} \tag{6.12}$$

$$\overline{\mathbf{x}}_2 = \begin{pmatrix} 95.98 \\ -0.53 \\ 1.62 \end{pmatrix} \tag{6.13}$$

$$\mathbf{S}_2 = \begin{pmatrix} 0.0019 & -0.0005 & 0.0021 \\ -0.0005 & 0.0068 & 0.0115 \\ 0.0021 & 0.0115 & 0.1125 \end{pmatrix} \cdot 10^{-3} \tag{6.14}$$

$$\mathbf{S}_{\text{pooled}} = \begin{pmatrix} 0.0713 & -0.0091 & -0.0773 \\ -0.0091 & 0.0104 & 0.0265 \\ -0.0773 & 0.0265 & 0.1978 \end{pmatrix} \cdot 10^{-3} \tag{6.15}$$

$$\mathbf{S}_{\text{pooled}}^{-1} = \begin{pmatrix} 0.2449 & -0.0464 & 0.1019 \\ -0.0464 & 1.4637 & -0.2146 \\ 0.1019 & -0.2146 & 0.1192 \end{pmatrix} \cdot 10^{5} \tag{6.16}$$

$$T^2 = 1.4810 \times 10^5 \tag{6.17}$$

$$F_{0.05}(3, 96) = 2.699 \tag{6.18}$$

$$\frac{3(n_1 + n_2 - 2)}{n_1 + n_2 - 4} F_{0.05}(3, n_1 + n_2 - 4) = 8.1517 \tag{6.19}$$

For this example, $1.4810 \times 10^5 > 8.1517$. The two instruments are from different populations.

for example, Early and Nadal (2004). National laboratories sell *standard reference materials* (*SRMs*) that enable an instrument manufacturer to transfer a scale to their reference instrument. Nadal et al. (2008) describe how NIST calibrates Lucideon tiles for 0°:45° geometry. Their goal is to have the uncertainty of each tile less than $0.5\,\Delta E_{ab}^*$. An instrument manufacturer purchases a set of calibrated tiles and uses them to transfer a scale to their reference instrument. This instrument is used to calibrate other sets of tiles known as *working standards* that are used to calibrate and verify instruments for purchase. These uncertainties propagate and commercial instruments cannot achieve the same level of accuracy as a national laboratory. What manufacturers strive for is excellent intrainstrument and interinstrument reproducibility for a specific CIE geometry.

There are many sources of systematic errors leading to a lack of accuracy (Zwinkels 1989; Early and Nadal 2004, 2008; Germer, Zwinkels, and Tsai 2014). Spectrophotometer errors include radiometric scale, wavelength scale, stray light, bandwidth, polarization, and geometry. These can lead to large colorimetric errors (Robertson 1967; Kishner 1977; Raggi and Barbiroli 1993; Berns and Reniff 1997; Wyble and Rich 2007a). We describe three systematic spectrophotometric errors: *reference white*, *reference black*, and *wavelength*.

Reference white errors occur primarily when the white calibration plaque provided with the instrument changes due

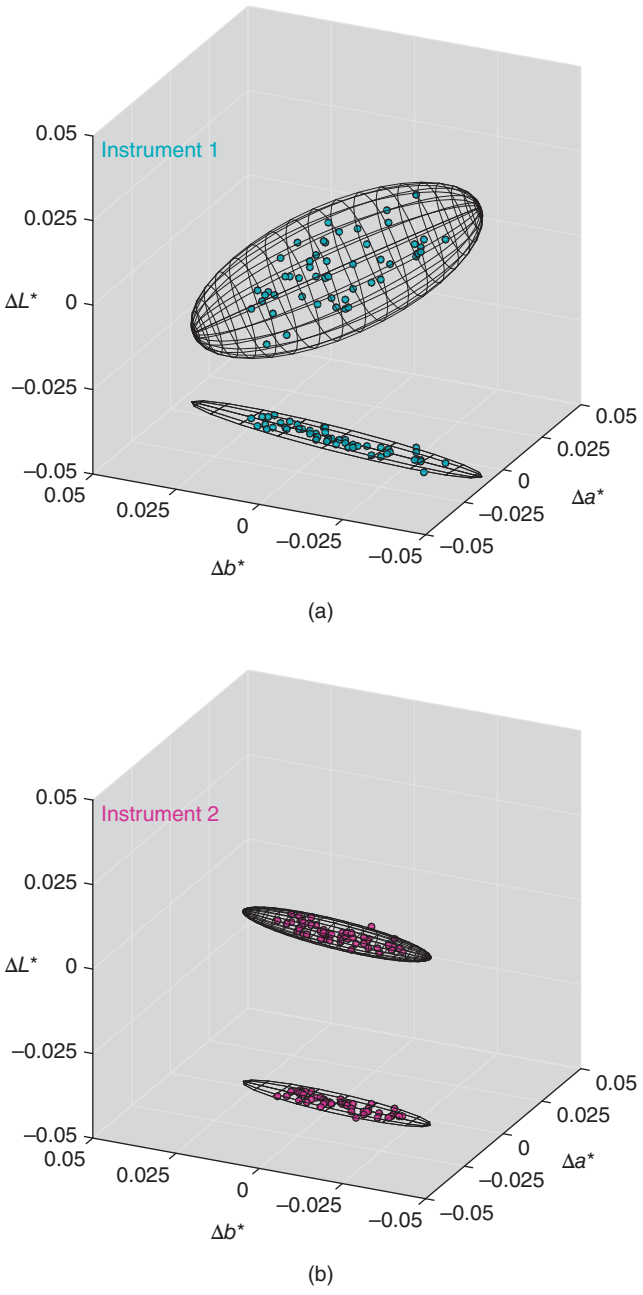

Figure 6.32 $\Delta L^*\Delta a^*\Delta b^*$ 95% confidence ellipsoids and their projection onto the $\Delta a^*\Delta b^*$ plane for 50 repeat measurements (50–59) of the Lucideon white tile for (a) Instrument 1 and (b) Instrument 2.

to age, usage, and dirt. *Reference black errors* occur by ambient light entering the instrument in measurable quantities, by the use of a black calibration plaque or black trap with increased reflectance factor caused by age, usage, and dirt, and by changes in electronics such as the analog-to-digital conversion process. *Wavelength errors* can occur in scanning instruments due to mechanical wear of the drive mechanism, or in instruments using interference filter wheels due

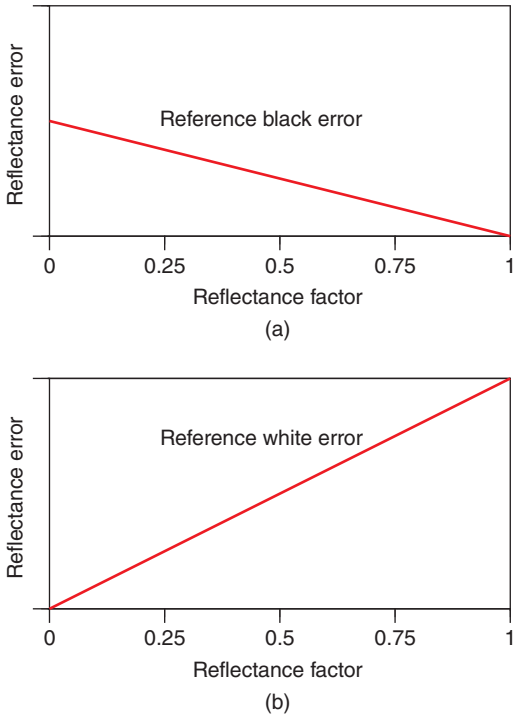

Figure 6.33 The effect of (a) reference black and (b) reference white errors on spectral reflectance factor.

to delamination of the filters. The alignment of the grating in a scanning or array instrument can change if the instrument is subjected to a shock. The effect of these errors is shown in Figures 6.33 and 6.34. Reference white errors affect the upper portion of the radiometric scale more than the lower portion. Reference black errors affect the lower portion of the radiometric scale. These two errors together are analogous to the equation defining a straight line. The reference white affects the slope while the reference black affects the intercept. Wavelength errors affect the portion of the reflectance curve where there is the greatest rate of change (i.e. first derivative). In regions where the spectral curve is flat, there would be no error; small errors occur where the curve has little slope; large errors occur where the curve is steep.

Because these errors affect measured reflectance differently, their influence on colorimetric accuracy depends on the spectral properties of the material being measured. The Lucideon tiles are commonly used to evaluate accuracy, their spectral reflectances shown in Figure 6.35. The five gray tiles are used to analyze radiometric errors while the chromatic tiles are used to evaluate wavelength and bandwidth errors. Berns and Reniff (1997) calculated the effects on colorimetric accuracy due to typical reference white, reference black, and wavelength errors using this set of tiles. CIELAB color differences were as large as about 9 ΔE^*_{ab}.

Many of the techniques that are routinely used by standardizing laboratories and instrument manufacturers to diagnose and correct these and other systematic errors are impractical for most users. Robertson (1987) recognized

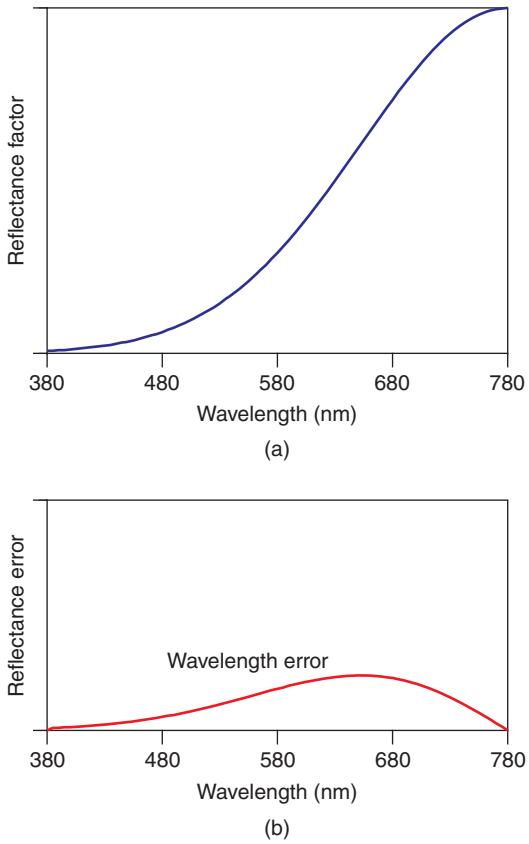

Figure 6.34 The effect of wavelength scale error on spectral reflectance factor.

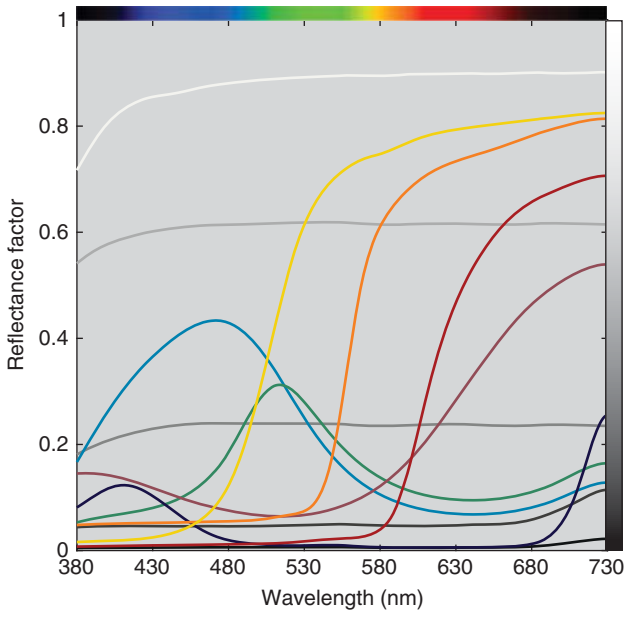

Figure 6.35 Spectral reflectance factor measurements of Lucideon ceramic tiles measured with a reference bidirectional spectrophotometer.

that plotting the difference in spectral reflectance between data collected on test and reference instruments could be used to diagnose systematic errors. He noted that errors in wavelength and bandwidth produced difference-spectra similar to first and second derivatives, respectively. Berns and Petersen (1988) expanded on this idea in consultation with Robertson and developed a statistical method to both diagnose and correct systematic-spectrophotometric errors using multiple-linear regression. The difference between measured (subscript m) and reference data is modeled as shown in Eq. (6.20) where $\partial R_{\lambda,m}/\partial\lambda$ is the first derivative, $\partial^2 R_{\lambda,m}/\partial\lambda^2$ is the second derivative, and ε_λ is error not accounted for by the model. This model diagnoses reference black, reference white, wavelength, and bandwidth errors, respectively. One or more reference tiles are measured and linear regression is used to estimate the model coefficients, β_0–β_3. The coefficients are used to both diagnose and correct the measured data, the latter shown in Eq. (6.21). Berns and Petersen (1988) also described various nonlinear radiometric and wavelength errors, and model coefficients that were functions of wavelength, shown in Eq. (6.22). Wavelength-dependent coefficients are important when optical components have systematic errors as a function of wavelength, such as the use of interference-based dispersing elements (Rich and Martin 1999)

$$R_{\lambda,\text{reference}} - R_{\lambda,m} = \beta_0 + \beta_1 R_{\lambda,m} + \beta_2 \frac{\partial R_{\lambda,m}}{\partial\lambda} + \beta_3 \frac{\partial^2 R_{\lambda,m}}{\partial\lambda^2} + \varepsilon_\lambda \tag{6.20}$$

$$R_{\lambda,\text{corrected}} = R_{\lambda,m} + \beta_0 + \beta_1 R_{\lambda,m} + \beta_2 \frac{\partial R_{\lambda,m}}{\partial\lambda} + \beta_3 \frac{\partial^2 R_{\lambda,m}}{\partial\lambda^2} \tag{6.21}$$

$$R_{\lambda,\text{corrected}} = R_{\lambda,m} + \beta_{0,\lambda} + \beta_{1,\lambda} R_{\lambda,m} + \beta_{2,\lambda} \frac{\partial R_{\lambda,m}}{\partial\lambda} + \beta_{3,\lambda} \frac{\partial^2 R_{\lambda,m}}{\partial\lambda^2} \tag{6.22}$$

As an example, the full set of Lucideon tiles was measured using Instruments 1 and 2 described above. Each tile was measured six times with replacement and the tiles and instruments were at a temperature between 68 and 69 °F. The average spectral reflectance of the second through sixth measurements from the two instruments is shown in Figure 6.36a. Color differences ranged from 0.08 to 1.4 ΔE^*_{ab} (0.07 to 0.69 ΔE_{00}). The average CIE94 color difference for the 12 tiles was 0.40 and the maximum difference was 0.87. These two instruments meet the manufacturer's stated intrainstrument reproducibility of average and maximum values of 0.4 and 1.0 ΔE^*_{94}.

Although these instruments are within specification for reproducibility, their spectral differences are systematic enabling correction using this statistical approach. We

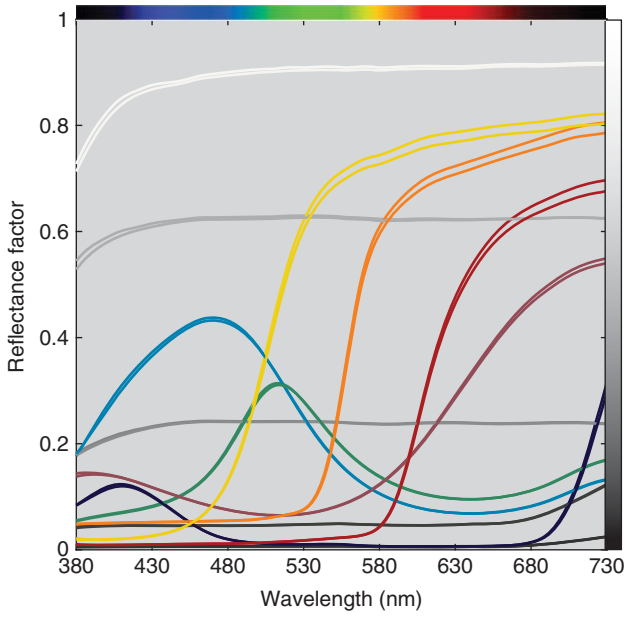

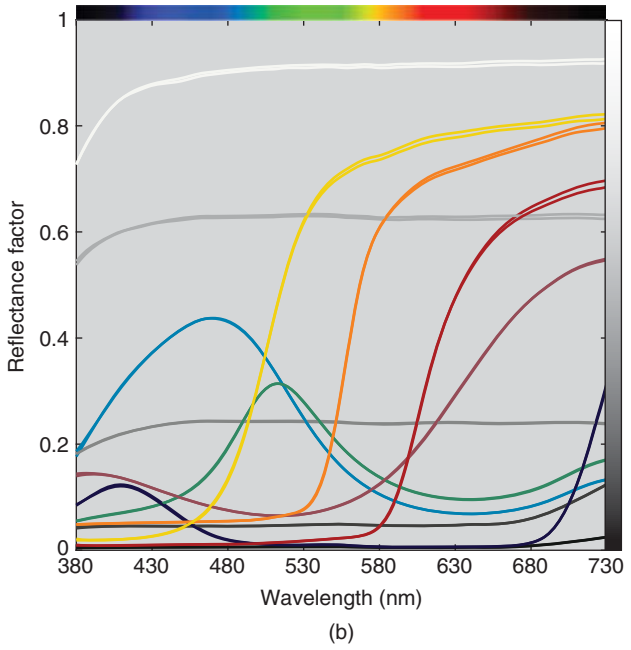

Figure 6.36 Spectral reflectance factor measurements of the Lucideon tiles from two spectrophotometers of the same make and model (a) before and (b) following correction of Instrument 2 using Eq. (6.23).

hypothesized that the differences in spectral reflectance were caused by reference black, reference white, and wavelength systematic errors. Instrument 1 was defined as the reference instrument and model coefficients were estimated using linear regression minimizing spectral reflectance RMS difference. The correction formula using the estimated model parameters is shown in Eq. (6.23)

$$R_{\lambda,\text{corrected}} = -0.0006 + 1.0123R_{\lambda,m} + 0.48\frac{\partial R_{\lambda,m}}{\partial \lambda} \quad (6.23)$$

There was a 1.23% radiometric scale difference and 0.48 nm wavelength difference. The spectra following correction are shown in Figure 6.36b; the spectra are more coincident. Color differences ranged from 0.09 to 1.03 ΔE^*_{ab} (0.04 to 0.51 ΔE_{00}). The average and maximum CIE94 color differences following correction were 0.23 and 0.65, respectively. Further improvement would require wavelength dependent coefficients and nonlinear radiometric terms.

This approach is used by color measurement instrument manufacturers to evaluate and improve spectral accuracy and instrument reproducibility, known as *instrument profiling*.

The specific tile set used in the above example had been calibrated by a standards laboratory. We could have done the analysis to evaluate each instrument's accuracy relative to a standards laboratory. We chose not to do this because our laboratory temperature was different than the reported calibration temperature. All chromatic materials exhibit thermochromism and the red, orange, and yellow tiles are very problematic (Fairchild and Grum 1985; Malkin et al. 1997). Our preference is to use only the white and cyan tiles to evaluate accuracy. The cyan tile is the least thermochromic of the chromatic tiles and has sensitivity to reference black and wavelength errors (Berns and Reniff 1997). The second derivative of the cyan tile is plotted in Figure 6.37. An *inflection point* is identified where the curve crosses zero, describing a change in direction of a curve. Inflection points are preferred to reflectance maxima and

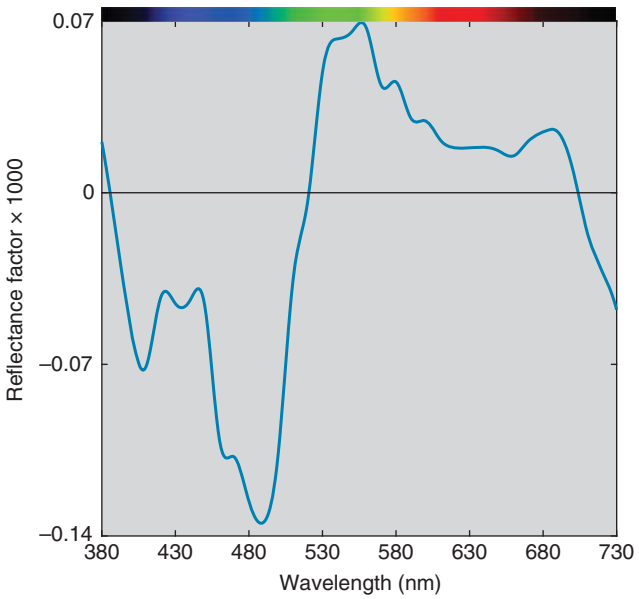

Figure 6.37 Second derivative of reflectance factor for the Lucideon cyan tile.

minima because inflection points are invariant to differences in bandwidth. The cyan Lucideon tile has three inflection points that are well spaced across the visible spectrum, making it an ideal sample to diagnose wavelength-related errors. An abridged technique to analyze systematic errors using only the cyan tile is shown in the nearby sidebar.

Abridged Method to Analyze Systematic Spectrophotometric Errors

Hemmendinger (1979) and Berns and Reniff (1997) found that typical amounts of systematic error encountered in color-measuring spectrophotometers were directly proportional to colorimetric differences. For example, wavelength errors distribute in a straight line when plotted on a $\Delta a^* \Delta b^*$ diagram for the Lucideon cyan tile, shown in Figure 6.38. Straight lines also result when evaluating reference white and black errors.

These linear relationships suggest that simple formulas can be derived to relate spectrophotometric errors and colorimetric differences. Only the measurement of a single calibrated tile is needed. CIELAB differences in L^*, a^*, and b^* calculated between the calibration and measured spectral data are used to predict reference white, reference black, and wavelength errors. From a detailed analysis of all of the Lucideon tiles, Berns and Reniff concluded that the cyan tile was the best tile among the set. The formulas to transform between colorimetric data and systematic errors are shown in Eq. (6.24) for integrating sphere specular included and in Eq. (6.25) for bidirectional geometries. Colorimetric data are calculated for illuminant D65 and the 1964 standard observer. These formulas are only expected to work for the Lucideon cyan tile. It is straightforward to derive formulas for different samples (Berns and Reniff 1997).

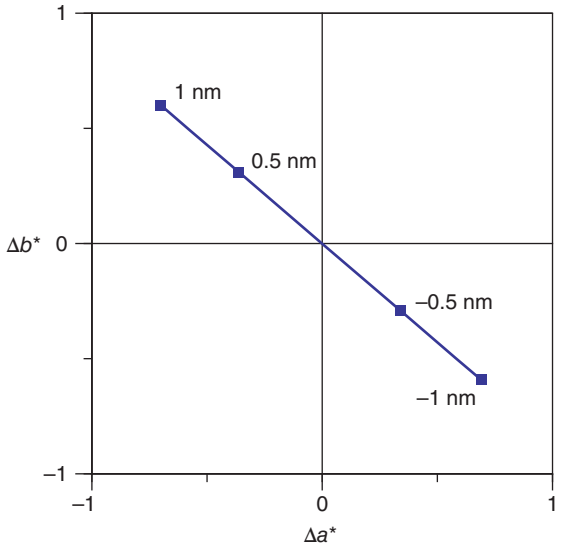

Figure 6.38 The relationship between wavelength error and Δa^* and Δb^* is shown for the cyan Lucideon tile. Source: Adapted from Berns and Reniff (1997).

$$\begin{pmatrix} E_{\text{reference white}} \\ E_{\text{reference black}} \\ E_{\text{wavelength}} \end{pmatrix} = \begin{pmatrix} -2.58 & 1.79 & 3.04 \\ -0.36 & -0.62 & -0.54 \\ -0.05 & -0.95 & 0.77 \end{pmatrix}_{\text{di:8°}} \begin{pmatrix} \Delta L^* \\ \Delta a^* \\ \Delta b^* \end{pmatrix} \tag{6.24}$$

$$\begin{pmatrix} E_{\text{reference white}} \\ E_{\text{reference black}} \\ E_{\text{wavelength}} \end{pmatrix} = \begin{pmatrix} -2.79 & 1.50 & 2.96 \\ -0.32 & -0.48 & -0.42 \\ 0.08 & -0.82 & 0.67 \end{pmatrix}_{\text{45°c:0°}} \begin{pmatrix} \Delta L^* \\ \Delta a^* \\ \Delta b^* \end{pmatrix} \tag{6.25}$$

The following are the step-by-step instructions:

1. Warm up the instrument and perform a calibration.
2. Measure the spectral reflectance factor of the cyan tile at least 30 times with replacement. Record the average L^*, a^*, b^* coordinates for CIE illuminant D65 and the 10° observer. Use either integrating sphere with the specular component included (e.g. di:8°) or bidirectional (e.g. 45°c:0°) geometry.
3. Calculate ΔL^*, Δa^*, Δb^* where Δ = (measured data − reference data).
4. Calculate spectrophotometric errors, E, using the appropriate set of equations. Note that the reference white and reference black errors have units of percent reflectance factor; wavelength error has units of nanometer.
5. Record the errors.

For example, below is a table showing the error analysis of the two 45°c:0° spectrophotometers:

	Instrument 1	Instrument 2
Reference data		
L^*	51.44	51.44
a^*	−18.41	−18.41
b^*	−30.21	−30.21
Measured data		
L^*	51.06	51.64
a^*	−18.25	−18.93
b^*	−30.03	−29.32
Differences		
ΔL^*	−0.38	0.20
Δa^*	0.16	−0.52
Δb^*	0.18	0.90
Spectrophotometric error estimates		
Reference white	1.83	1.33
Reference black	−0.03	−0.19
Wavelength	−0.04	1.04

This technique can be used to track repeatability, reproducibility, and accuracy. Changes in the error coefficients over time indicate a change in repeatability. Differences in the error coefficients among a group of instruments indicate a lack of reproducibility. Slight nonzero coefficients indicate uncertainties and differences in traceability between the instrument manufacturer and the supplier of the calibrated tile set. (The equations we show are for tiles traceable to the United States' NIST.) Appreciable nonzero coefficients indicate a lack of accuracy. By frequently measuring the Cyan tile and tracking systematic spectrophotometer errors using established statistical-process-control techniques, the operator can quickly diagnose whether the spectrophotometer was miscalibrated, requires further analyses such as an evaluation using the complete set of tiles, or requires service. Recognize that this abridged method is not a substitute for a detailed spectral analysis of all types of spectrophotometric errors. It does provide a very convenient method of indicating the most likely spectrophotometric errors.

I. SPECTRAL IMAGING

We have described instrumentation that average reflectance or transmittance over a specified solid angle, corresponding to sample diameters of several millimeters to several inches. There are many industries requiring measurements in the micrometer range. Digital cameras can measure millions of locations, their size determined by the sensor, optics, and distance from the object. We describe digital cameras in detail in Chapter 10 where the goal is to measure tristimulus values as a function of spatial position. Devices built to measure colorimetry without the intermediate step of measuring spectra are known as *colorimeters*. Nonimaging colorimeters are still used in the lighting and display industries. The majority of color-measuring instrumentation is spectral. We focus on spectral imaging.

Spectral imaging results in a data cube having dimensions of X, Y, and λ, shown in Figure 6.39. *Multispectral systems* collect x and y data for each image capture. Multiple channels result from using narrow-band LED illumination or placing colored filters between the object and sensor. Both approaches can be used together, further expanding the number of channels. The camera often has a monochrome sensor. Filters are absorption filters, interference filters, or liquid-crystal tunable filters. Multispectral systems have high spatial resolution and low wavelength resolution.

Hyperspectral systems collect X (or Y) and λ data for each image capture. A diffraction grating is used to disperse the spectrum across one dimension of the sensor. The camera

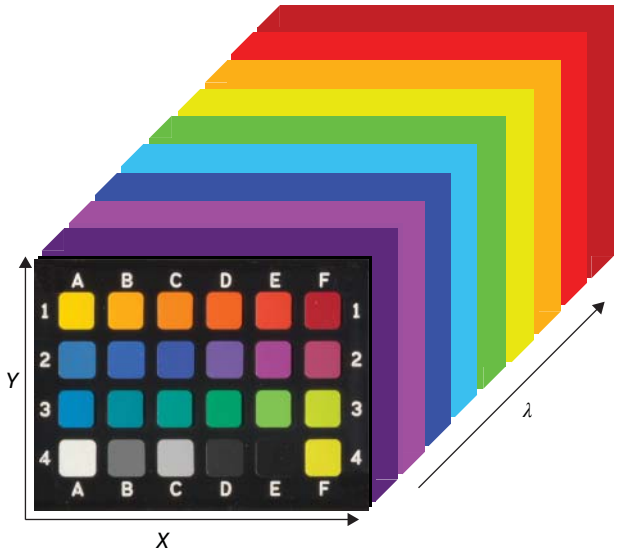

Figure 6.39 Multispectral data cube of spectral calibration target.

or object is stepped in the direction of the other position. Hyperspectral systems have low spatial resolution and high wavelength resolution. Resolution can be increased by moving either the camera or object in a grid. Calibrating these systems is identical to calibrating a spectrophotometer.

Multispectral systems that use narrow-band (i.e. 10–20 nm bandwidth) interference filters measure spectral reflectance with similar spectral resolution to a spectrophotometer designed for color measurement. Calibrating these systems is more complex than a hyperspectral system because interference filters change their peak wavelength with influx angle necessitating a correction as a function of X and Y position. Berns, Cox, and Abed (2015) used the Robertson (1987) and Berns and Petersen (1988) statistical technique to correct a liquid-crystal tunable filter spectrally and spatially.

The use of colored LED lights or colored absorption filters under-samples the spectrum. Transforming these signals to evenly sampled data is an *inverse mapping* problem because we are mapping from a few dimensions to many. Typical techniques are summarized by Ribés and Schmitt (2008). An effective approach is to use a camera calibration target as training data. A mapping is derived from camera signals to spectral reflectance factor. The scale of spectral reflectance factor is transferred to the multispectral system. This approach assumes that the spectral and material appearance properties of the imaged object are well represented by the calibration target.

As an example, Berns (2018) designed and built a multispectral imaging system that used seven glass absorption filters and a 50-megapixel monochrome sensor. The camera spectral sensitivities are shown in Figure 6.40. The filters were first designed for colorimetric accuracy,

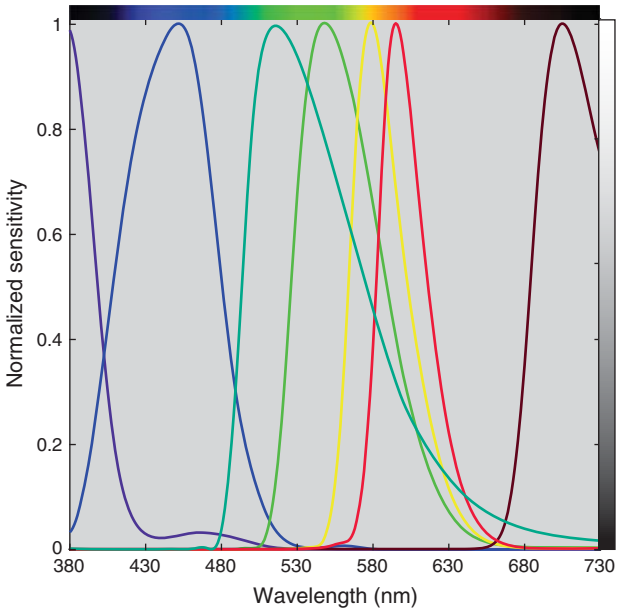

Figure 6.40 Normalized spectral sensitivities (filter transmittance multiplied with the sensor quantum efficiency) for a seven-channel multispectral camera. The peak wavelengths occur at 370, 450, 520, 550, 580, 600, and 710 nm.

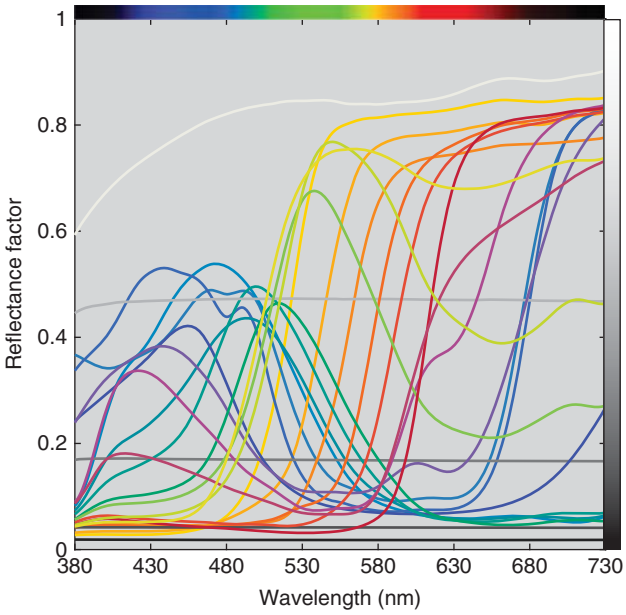

Figure 6.41 Spectral reflectance factor measurements of the custom multispectral imaging target shown in Figure 6.39.

spectral accuracy, and low image noise (Wang and Berns 2017). Berns (2018) changed the shortest and longest wavelength filters to facilitate UV and UV-fluorescence imaging and improve spectral estimation accuracy for colorants with long-wavelength inflection points. Because of the three quality criteria, the spectrum is not evenly sampled. The peak wavelengths were 370, 450, 520, 550, 580, 600, and 710 nm.

The calibration target, shown in Figure 6.39, has 24 patches and was made using a variety of matte acrylic-dispersion artist paints. Five of the samples are neutral. The remaining 19 samples hue at high vividness. The white pigment was lead white, selected because it does not have strong absorption at short wavelengths, important when calibrating the 370 nm channel. The target's reflectance spectra are shown in Figure 6.41.

A linear model was used to transform from camera signals corrected for dark noise and lighting spatial nonuniformity (described in Chapter 10), C, to spectral reflectance, shown in Eq. (6.26)

$$\begin{pmatrix} R_{\lambda=380\text{ nm}} \\ \vdots \\ R_{\lambda=730\text{ nm}} \end{pmatrix} = \mathbf{M} \begin{pmatrix} C_{370\text{ nm}} \\ C_{450\text{ nm}} \\ C_{520\text{ nm}} \\ C_{550\text{ nm}} \\ C_{580\text{ nm}} \\ C_{600\text{ nm}} \\ C_{710\text{ nm}} \end{pmatrix} \tag{6.26}$$

A pseudo-inverse was used to derive the transformation matrix, **M**, shown in Eq. (6.27):

$$\mathbf{M} = \begin{pmatrix} R_{\lambda=380\text{ nm},1} & \cdots & R_{\lambda=380\text{ nm},24} \\ \vdots & \cdots & \vdots \\ R_{\lambda=730\text{ nm},1} & \cdots & R_{\lambda=730\text{ nm},24} \end{pmatrix} \begin{pmatrix} C_{370\text{ nm},1} & \cdots & C_{370\text{ nm},24} \\ C_{450\text{ nm},1} & \cdots & C_{450\text{ nm},24} \\ C_{520\text{ nm},1} & \cdots & C_{520\text{ nm},24} \\ C_{550\text{ nm},1} & \cdots & C_{550\text{ nm},24} \\ C_{580\text{ nm},1} & \cdots & C_{580\text{ nm},24} \\ C_{600\text{ nm},1} & \cdots & C_{600\text{ nm},24} \\ C_{710\text{ nm},1} & \cdots & C_{710\text{ nm},24} \end{pmatrix}^{+} \tag{6.27}$$

where the superscript "+" notates pseudo-inverse. The pseudo-inverse is equivalent to multiple linear regression where spectral reflectance RMS error is minimized. When pixel data are not averaged for each patch, there are at least 60 000 data points and an intrinsic function is more efficient than using statistics software.

The number of matrix rows in **M** equals the total number of wavelengths and the number of matrix columns equals the total number of camera channels. In this example, **M** is a (36×7) matrix.

The matrix is visualized by plotting the normalized coefficients for each channel as a function of wavelength, shown in Figure 6.42. Ideally, each channel has a single positive peak located near the peak spectral sensitivity without large negative peaks. This was achieved for the channels with peak sensitivities at 370, 450, 520, 600, and 710 nm. The channels with peak sensitivities at 550 and 580 nm had multiple positive and negative peaks. The ideal coefficients can only be attained by increasing the number of channels and optimizing the filters for only spectral accuracy.

The spectral accuracy of the calibration target is shown in Figure 6.43. The general shapes are well estimated although

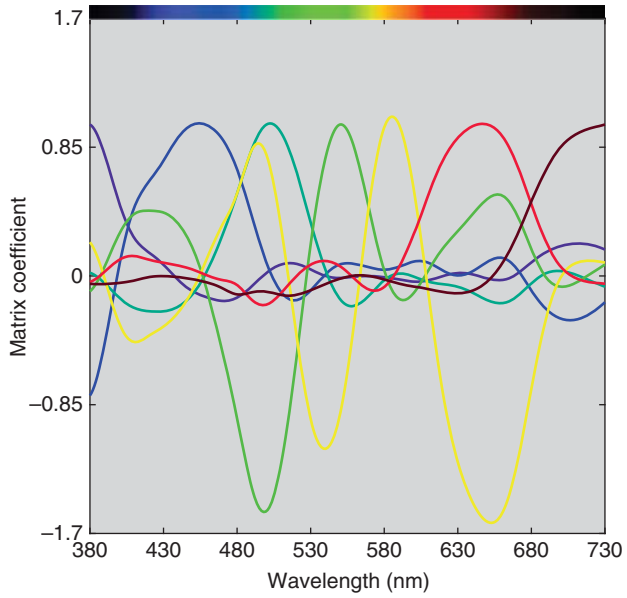

Figure 6.42 Matrix coefficients as a function of wavelength that transform camera signals to spectral reflectance. The color-coding matches Figure 6.40.

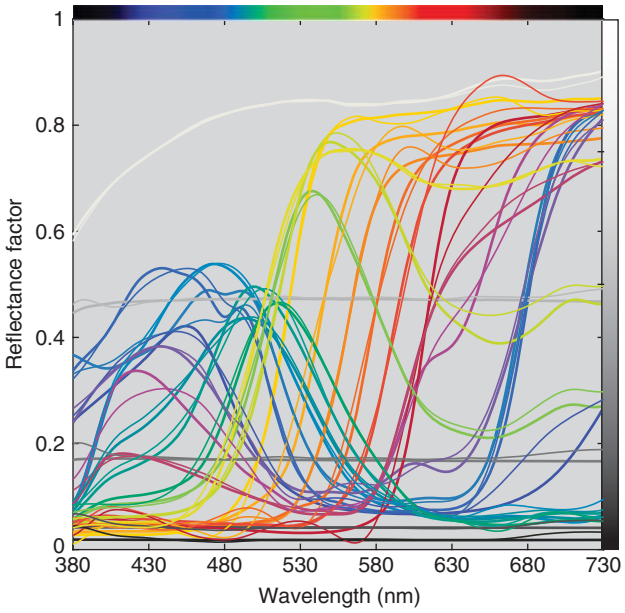

Figure 6.43 Measured (thick lines) and estimated (thin lines) spectral reflectance factor of the calibration target.

the camera spectra are more undulating. These estimated spectra are linear combinations of the spectra plotted in Figure 6.42. That is, the matrix coefficients as a function of wavelength are camera-based "colorants." These spectra are very sensitive to the calibration samples (Berns 2018). More optimal results might be obtained by weighting some samples more than others. Weighting the neutral scale would reduce the amount of undulation in the spectrally flat regions of the chromatic samples. Other inverse-mapping functions could be more effective.

The multispectral image can be transformed to an *RGB*-encoded image, shown in Figure 6.44. Each spectral channel is also shown where black and white areas correspond to zero and unity reflectance factor, respectively. The changes in gray-scale value track the spectral reflectance data plotted in Figure 6.41.

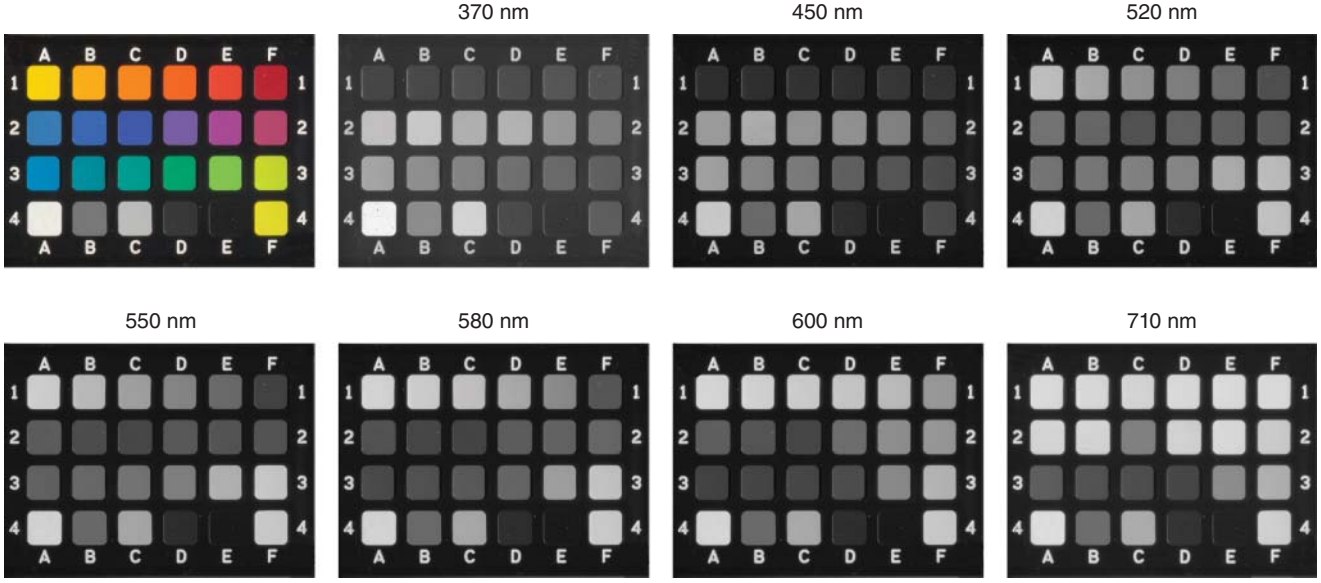

Figure 6.44 (Top left) RGB image calculated from the camera-estimated spectral-reflectance factor. The gray-scale images correspond to the 370, 450, 520, 550, 580, 600, and 710 nm channels. They have been nonlinearly encoded to better differentiate the changes in gray level.

J. MATERIAL-APPEARANCE MEASUREMENTS

Gloss

We describe in Chapter 1 that Hunter (1937) identified six types of gloss: specular gloss, sheen, contrast gloss, absence-of-bloom gloss, distinctness-of-reflected-image gloss, and absence-of-surface-texture gloss. These and other types of gloss relate to illuminating and viewing geometries and a material's BRDF. A generalized glossmeter at a single influx angle is shown in Figure 6.45 where a detector array is used to measure reflected light at different near-specular angles. The detector signals can be used to estimate the material's indicatrix that, in turn, can be used to calculate various types of gloss. Two common types are specular and distinctness-of-image (DOI) gloss, determined by the height and width of the specular component, respectively. An example of DOI gloss is shown in Figure 6.46 where a grid is projected onto a coating. The grid becomes blurry and lower in contrast when the coating has poor DOI gloss.

Glossmeters measure specular gloss and common angles are 20°:−20°, 60°:−60°, 75°:−75°, and 85°:−85°. They are calibrated relative to a highly polished black glass that is assigned 100 *gloss units* (*GUs*). Because first surface reflection increases with influx angle, described in Chapter 1, materials with low gloss are measured at high influx angles. A piece of paper that is matte has observable gloss when illuminated and viewed at grazing angles. The paper industry often uses 75°:−75° (ISO 2009c). The paint industry uses 20°, 60°, and 85° instruments (ASTM 2014). A measurement is first made at 60°. If the GU is greater than 70, the angle is reduced to 20°. If the GU is less than 10, the angle is increased to 85°.

- *Gloss*: Angular selectivity of reflectance, involving surface-reflected light, responsible for the degree to which reflected highlights or images of objects may be seen as superimposed on a surface.
- *Specular gloss*: Ratio of flux reflected in the specular direction to incident flux for a specified influx angle and illumination and detection solid angles.
- *Distinctness-of-image gloss*: Aspect of gloss characterized by the sharpness of images of objects produced by reflection at a surface.

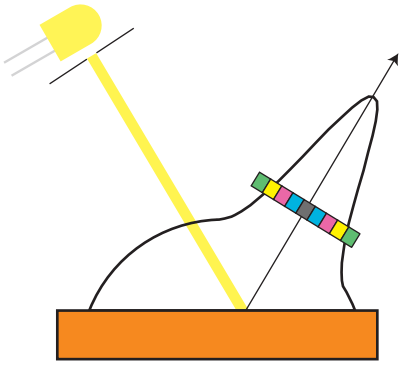

Figure 6.45 Generalization of gloss measurements relative to the specular angle. Color coding differentiates geometry differences from the specular angle.

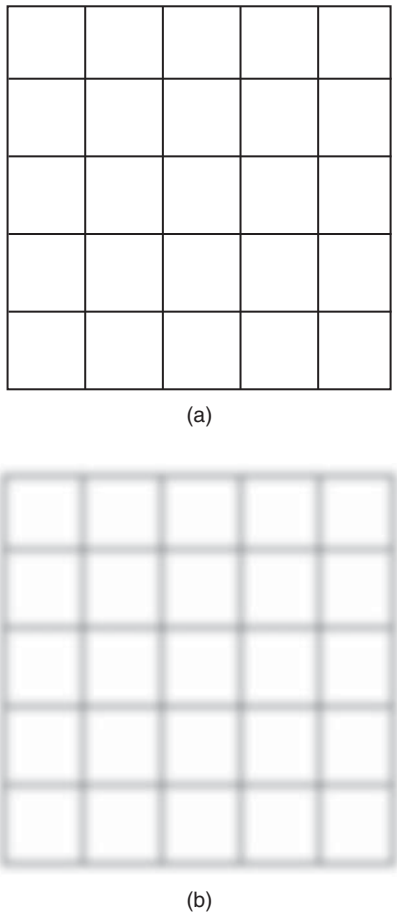

(a)

(b)

Figure 6.46 (a) An image of a grid is projected onto a surface with poor distinctness-of-image gloss, resulting in (b) a low contrast and blurry grid.

Microstructure – Bidirectional Reflectance Distribution Function

Microstructure is characterized by measuring a material's BRDF, a four-dimensional function where illumination and detection are each described by polar and azimuthal coordinates, defined in Figure 6.11. Sampling at every degree would require about 200 million measurements! Many materials have BRDFs that do not change with rotations about the surface normal, reducing the BRDF to a three-dimensional function requiring less than 2 million measurements at 1° sampling. The use of a camera speeds measurement time since multiple geometries are captured simultaneously. The range of geometries can be expanded by wrapping materials around cylinders (Lu, Koenderink, and Kappers 1998,

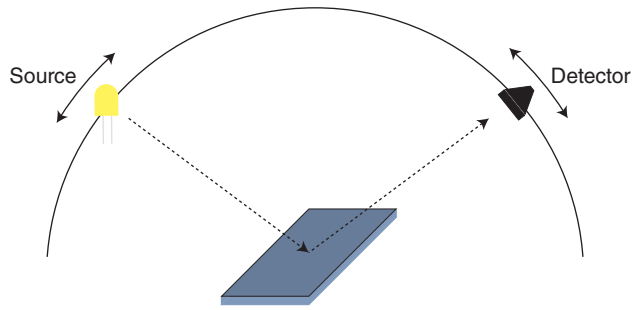

Figure 6.47 Measurements in a single plane where azimuthal angle is fixed and the polar angle varies for influx and efflux.

Table 6.3 Specular gloss measurements for each listed coating and geometry.

Sample	20°	60°	85°
Conventional pigments	2.3	3.0	4.0
Mica particles and carbon black	9.5	32.8	33.0
Interference pigment	1.9	18.7	26.1

2000; Marschner et al. 2000) or coating spheres (Marschner et al. 2000; Matusik et al. 2003).

For some applications, the BRDF is reduced to a two-dimensional function where the azimuthal angle is fixed and the polar angle varies, shown in Figure 6.47. This is a common configuration for *goniospectrophotometers*.

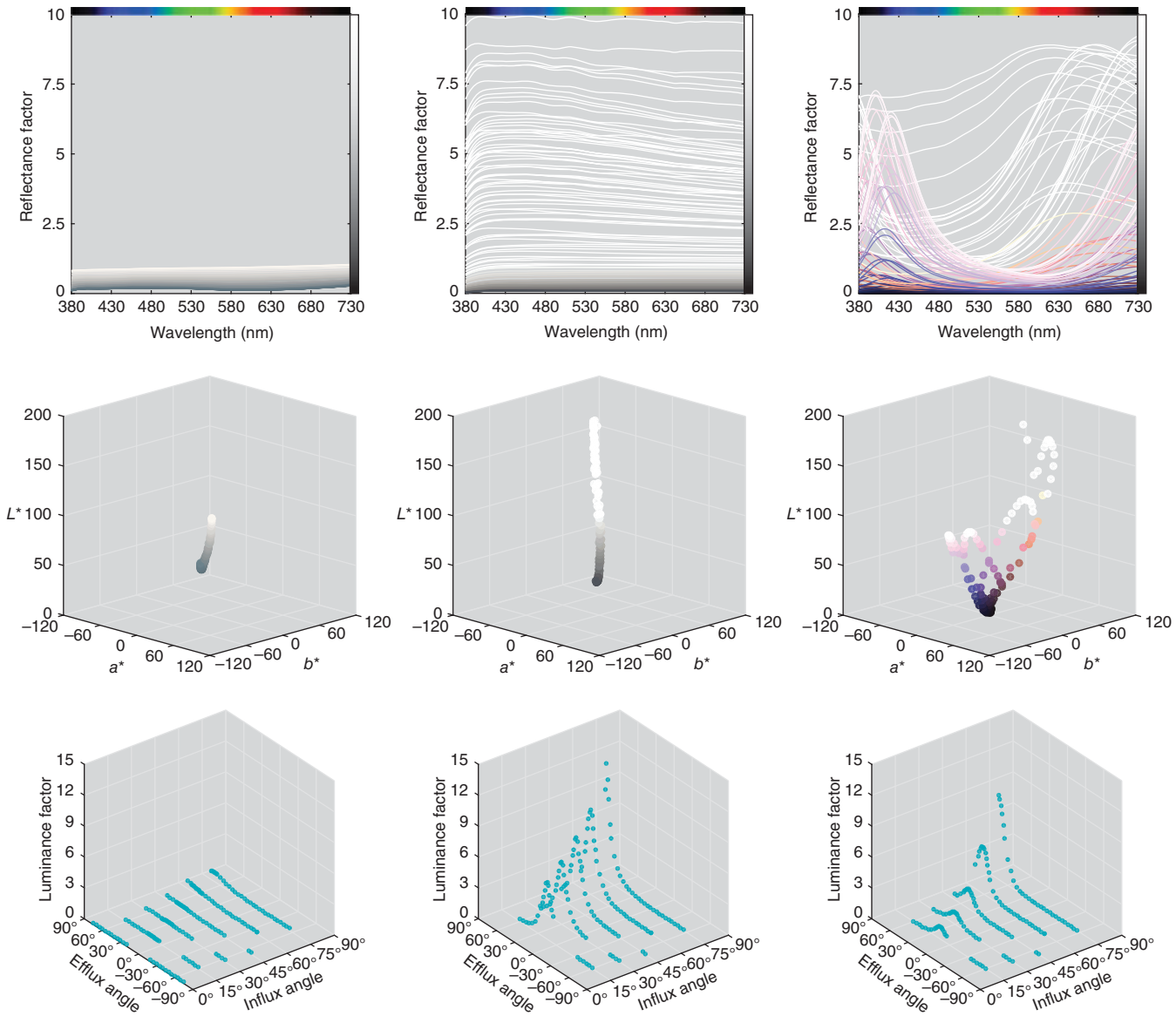

Figure 6.48 Spectral reflectance factor (first row), CIELAB (second row), and goniophotometric (third row) plots of coatings containing (left) conventional pigments, (center) titanium-dioxide-coated mica particles and carbon black, and (right) interference pigment.

As an example, three opaque coatings were applied to a paper substrate. The coatings contained either a mixture of conventional pigments, titanium-dioxide-coated mica particles and carbon black, or an interference pigment. The samples had a range of specular gloss, shown in Table 6.3.

A goniospectrophotometer was used to measure each sample at influx angles of 15°, 30°, 45°, 60°, and 75° and a range of efflux angles. The system was calibrated relative to a perfect reflecting diffuser. The spectral data were used to calculate luminance factor (Y/Y_n) and CIELAB coordinates for the 1964 standard observer and illuminant D65. The data for the three coatings are shown in Figure 6.48. The spectra for the conventional pigment and mica samples are nearly flat without any strong absorption. The spectra for the interference-pigment coating change dramatically. The mica and interference-pigment coatings have reflectances that far exceed unity. The CIELAB data track the spectral characteristics. The interference-pigment coating has five loci corresponding to the five influx angles. The data for 45° influx is plotted separately in Figure 6.49. The dramatic color changes for this pigment are clearly seen. The goniophotometric data are calculated relative to a perfect reflecting diffuser. Diffuse materials are flat lines and highly glossy materials have very sharp peaks about the specular angle. The conventional-pigment coating is matte; the luminance factor profiles are featureless. For the other coatings, there is the expected increase in luminance factor with increasing influx angle. The mica sample has a sharper specular profile than the interference coating, consistent with the specular gloss measurements.

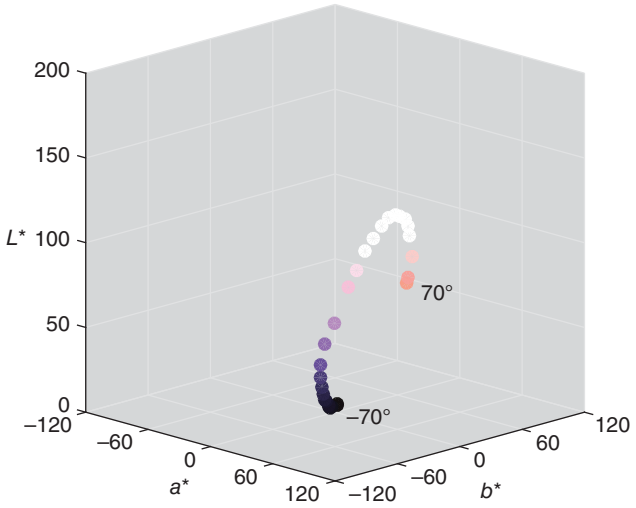

Figure 6.49 CIELAB data for the interference-pigment coating with 45° influx and efflux angles ranging from −70° to 70°.

Principal Component Analysis

Principal component analysis (*PCA*), is a statistical technique with a variety of color-technology applications (Tzeng and Berns 2005). PCA is used to reduce the dimensionality of data containing a large number of interrelated variables to a new set of variables that are uncorrelated and are ordered so that the first few variables retain most of the variation in all of the original variables (Jolliffe 2002). Suppose that we measure 1000 colors displayed on an LCD using a spectroradiometer. Each wavelength is a variable. PCA should reduce the data to three dimensions, that is, three principal components. Each dimension is a spectrum. We recommend the books by Jolliffe (2002), Bajorski (2012), and Manly and Alberto (2017) for details. We are describing PCA in this chapter because two of the data sets will aid in understanding this important statistical tool.

The production measurements of the red-powder-coated part were expanded in chroma and used to create two additional groups of colors by changing CIELAB hue angle, shown in Figure 6.50. We want to add trendlines. Regression can be used to fit a line for the red data where a^*, *the independent variable*, predicts b^*, the *dependent variable*. The correlation coefficient, R^2, is 0.96. When the same approach is taken for the green and yellow data, R^2 for the green data is nearly zero, and undefined for the yellow data. The problem is that b^* is not a dependent variable. Both a^* and b^* are independent variables. PCA is used to describe the variability of independent variables. For the three hues, most of the variability is in a single dimension.

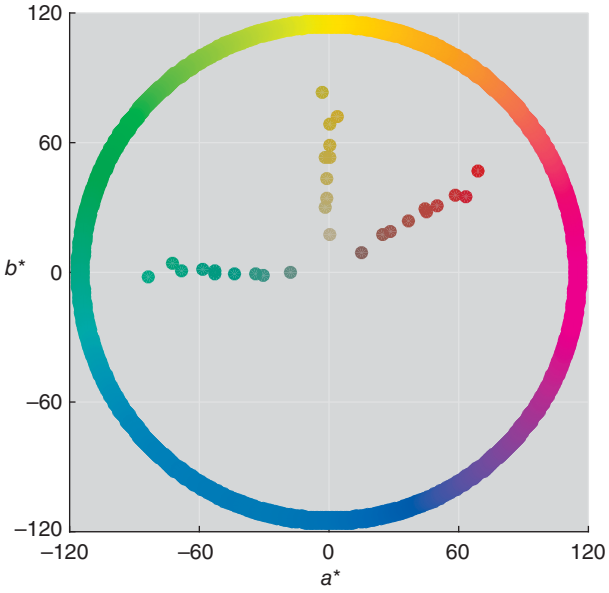

Figure 6.50 CIELAB coordinates projected onto the a^*b^* plane for three datasets with identical variability and chroma but having average CIELAB hue angles of 33°, 90°, and 180°.

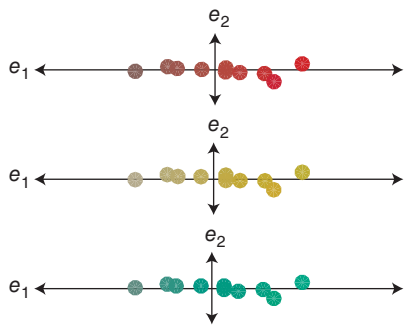

Figure 6.51 Results of principal component analysis where each dataset shown in Figure 6.50 has been rotated to new coordinates, e_1 and e_2. The intersection of the two axes defines the mean location.

PCA will rotate the three datasets to new coordinates where one axis, e_1, describes the principal variability and the second axis, e_2, describes the remaining variability, shown in Figure 6.51. The three datasets and eigenvectors (described below) are identical because the same data were used in all three cases except rotated to different average CIELAB hue angle. The mean is located where the two axes cross.

Knowing that the second dimension is process variability that will always be present, the colors can be defined by their position along the principal axis. The data have been reduced from two dimensions to a single dimension. The axes are called *eigenvectors*. *Eigen* is a German word meaning characteristic. *Principal components* refer to the coordinates of the new axes.

The interference pigment spectral data are the second dataset analyzed using PCA, shown in Figure 6.48. Looking at the spectra, the number of eigenvectors necessary to describe the spectral variability is not obvious. By definition, each successive eigenvectors accounts for a smaller percentage of the variability in the dataset.

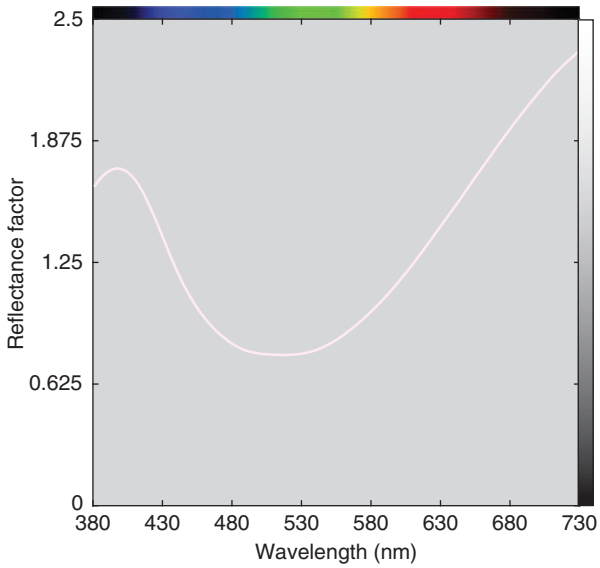

Figure 6.53 Mean spectral reflectance factor of the interference-pigment dataset.

Rather than plotting this percentage, the cumulative variance is plotted, shown in Figure 6.52. The first, the first two, the first three, the first four, and the first five eigenvectors account for 84.19%, 93.58%, 99.50%, 99.87%, and 99.99%, of the total variance, respectively. Based on our experience, we expect that three to five eigenvectors will be adequate to reconstruct the spectral data. We use cumulative variance as a guideline and indices of metamerism as a quantitative metric (Tzeng and Berns 2005; Berns 2008b). We describe metameric indices in detail in Chapter 8.

The mean and first five eigenvectors are plotted in Figures 6.53 and 6.54, respectively. The mean has appreciable absorption in the middle of the visible spectrum.

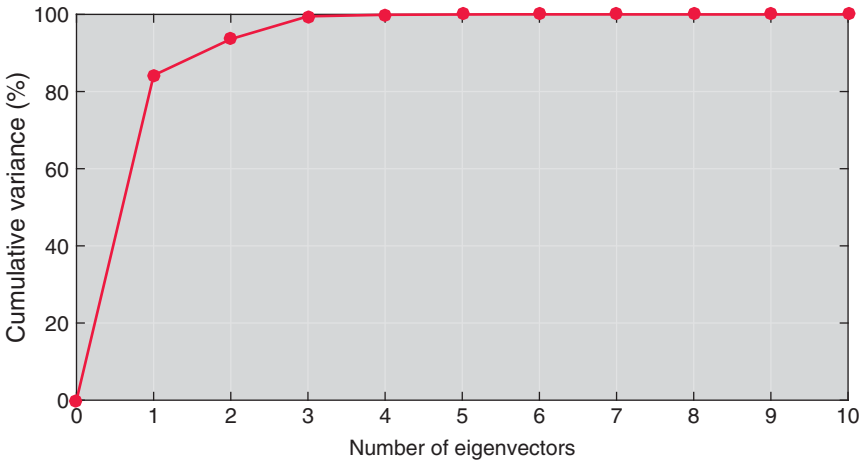

Figure 6.52 Percent variance explained by each listed number of eigenvectors.

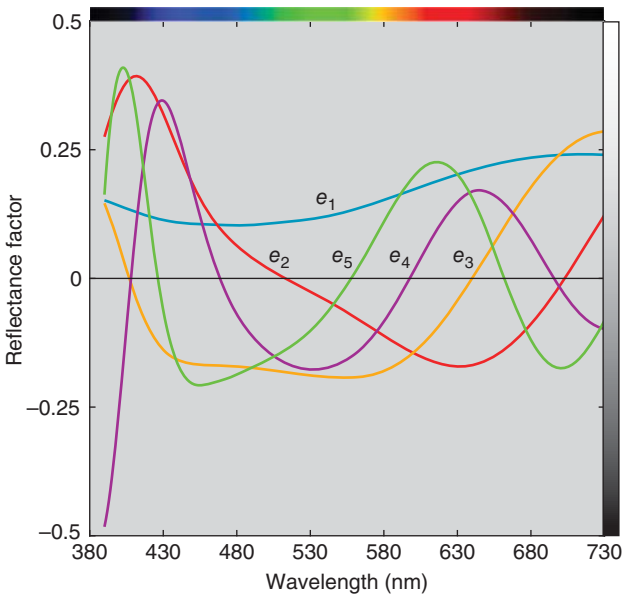

Figure 6.54 First five eigenvectors of the interference-pigment dataset. Color-coding is arbitrary.

Because each successive eigenvector explains less of the total variance, the spectra increase in the number of oscillations with each additional eigenvector. It can be difficult to relate the shapes of eigenvectors to changes in reflectance for a dataset for three reasons. First, eigenvectors can be positive and negative because they describe variance about the mean. Second, the coordinates can also be positive and negative. Third, the eigenvectors account for different amounts of total variance. The *spectral reconstructions* are often a better method to determine how a specific eigenvector contributes to the spectral characteristics of the dataset. This is shown in Figure 6.55 where the mean and one to five eigenvectors were used to reconstruct the measured data. Both four and five eigenvectors appear sufficient. A metameric analysis would be necessary for a definitive decision.

A reasonable question is whether PCA adds value? If the influx and efflux geometries can predict the eigenvector scalars, it should be possible to reduce the number of measurements necessary for quality control or modeling the behavior of similar pigments.

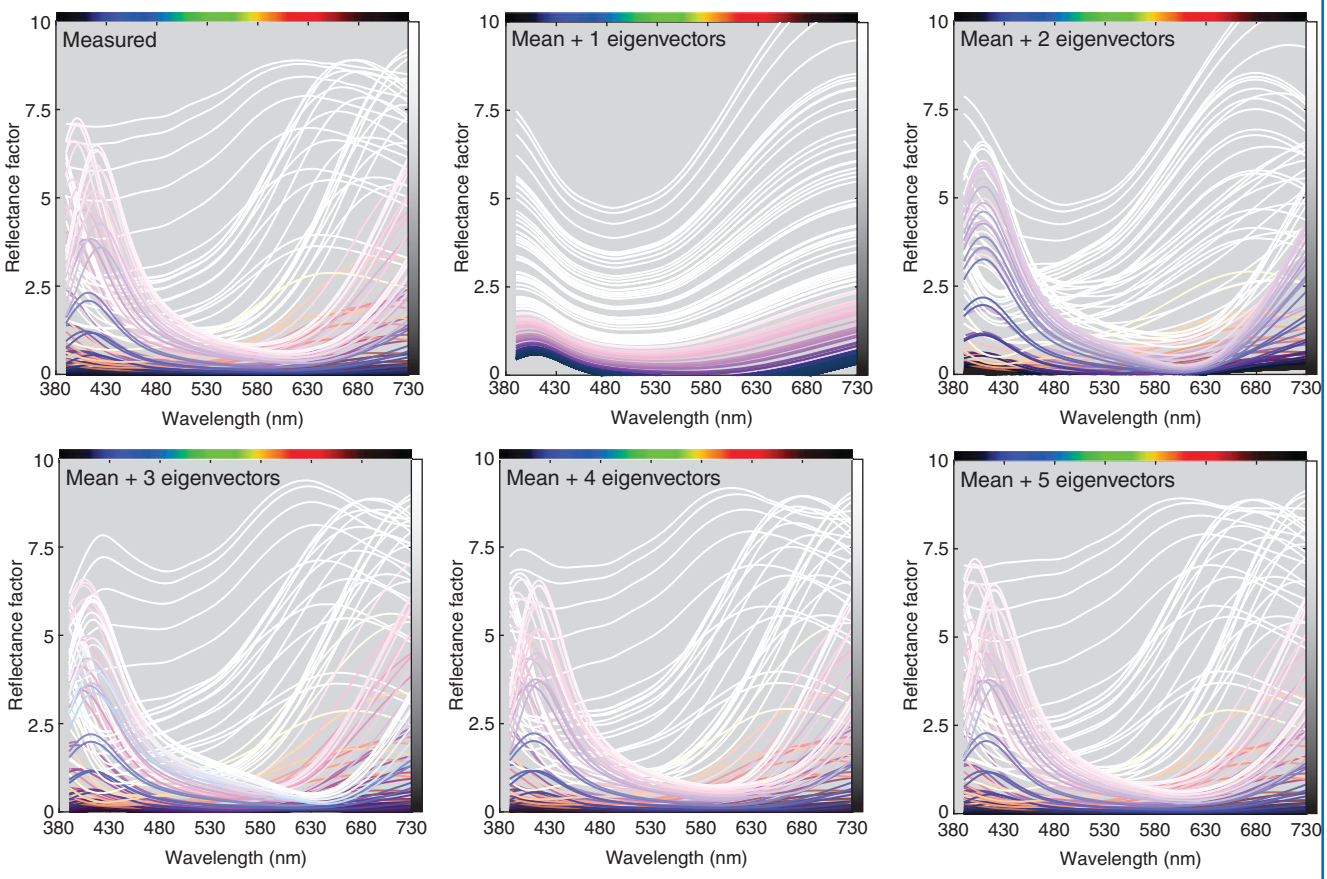

Figure 6.55 Measured spectral reflectance factor of the interference-pigment coating and spectral reconstructions using the mean and each listed number of eigenvectors.

Macrostructure

Macrostructure refers to three-dimensional features such as texture, brushstrokes, grooves, and pits. Computational approaches include spatial frequency and texture analyses of an image of the surface (Gonzalez and Woods 2018). However, the results may be dependent on lighting.

There are two approaches to measuring macrostructure. The first is a direct measurement of the surface's height, Z, as a function of position X and Y, known as a *height map*. Profilometry is often used to measure a height map over small areas and there are many approaches to profilometry that are both contact and noncontact. The second approach is to measure the surface's normal angle, n, as a function of position x and y, known as a *surface normal map*.

Photometric stereo (Woodham 1980) is often used to measure a surface normal map. It is based on the principle of Lambert's cosine law (1760) where the reflected light from a diffuse material is proportional to the cosine of the angle between the influx angle and the surface normal, shown in Eq. (6.28):

$$I_{\lambda,d} = k_{\lambda,d} I_{\text{influx}} \cos(\theta) \tag{6.28}$$

where $I_{\lambda,d}$ is the intensity of the reflected light, $k_{\lambda,d}$ is the diffuse material's body color, also called the *diffuse albedo*, I_{influx} is the intensity of the incident light, and θ, is the angle. For example, at 60° influx, the reflectance is one half of the reflectance at 0° influx.

Lambert's law is visualized in Figure 6.56 where the intensity of the reflected light reduces as the angle increases. Suppose that we have a measurement system with 45°:0° geometry and a diffuse sample can be rotated as shown in Figure 6.57. From the change in reflectance, the normal angle can be calculated by rearranging Eq. (6.28).

Equation (6.28) and Figures 6.56 and 6.57 describe Lambert's cosine law in a single plane. In three dimensions, Eqs. (6.29)–(6.31) are used where the position of the light source, $\mathbf{L}$, and the surface normal, $\mathbf{n}$, are defined in three-dimensional coordinates, shown in Figure 6.58

$$I_{\lambda,d} = k_{\lambda,d} I_{\text{influx}} (\mathbf{Ln}) \tag{6.29}$$

$$\mathbf{n} = \begin{pmatrix} n_X \\ n_Y \\ n_Z \end{pmatrix} \tag{6.30}$$

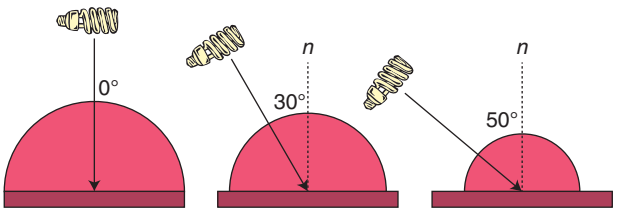

Figure 6.56 Visualization of Lambert's cosine law. The radius of the hemisphere is proportional to the cosine of the influx angle and the surface normal, fixed in this case.

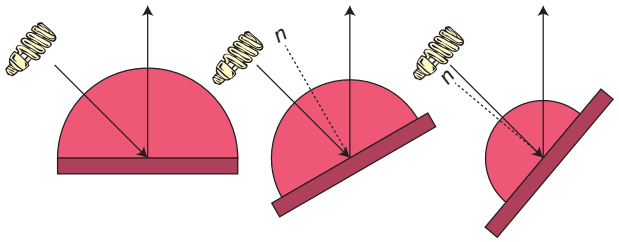

Figure 6.57 For a fixed geometry of 45°:0°, the change in the amount of reflected light, that is, the change in the radius of the hemisphere, can be used to calculate the normal angle.

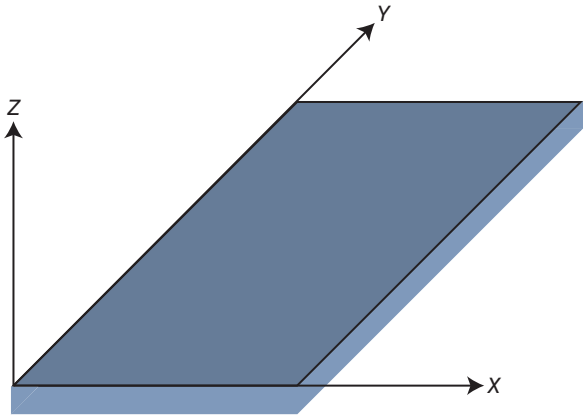

Figure 6.58 Three-dimensional coordinates X, Y, and Z.

$$\mathbf{L} = (L_X \;\; L_Y \;\; L_Z) \tag{6.31}$$

The surface normal map is encoded as a false-color RGB image where red defines X, green defines Y, and blue defines Z. The geometry is based on the viewpoint in the Z direction relative to the XY plane. A normal vector pointing toward the viewer has *RGB* coordinates of 128, 128, and 255 for an 8-bit encoded image. Because many of the normal vectors are not too different than the vector pointing toward the viewer, normal maps have this reddish-blue color, seen in Figure 6.59 for the normal map of a hemisphere.

Woodham (1980) recognized that the normal vector could be determined by measuring intensity from multiple light directions. In theory, only two directions are required, leading to the use of "stereo" in photometric stereo. In practice, a minimum of three directions are used. As an example, an RGB camera is positioned along the Z axis. Three collimated lights are positioned at polar angles of 45° and uniformly spaced in azimuthal angle, that is, 120° apart from each other, shown in Figure 6.60. Images are taken, sequentially, of a diffuse white board and the object. Intensity, I, is calculated at each pixel using Eqs. (6.32)–(6.35) where the *RGB* camera signals are linear radiometrically

$$R = \frac{R_{\text{object}} - R_{\text{dark current}}}{R_{\text{diffuse white}} - R_{\text{dark current}}} \tag{6.32}$$

$$G = \frac{G_{\text{object}} - G_{\text{dark current}}}{G_{\text{diffuse white}} - G_{\text{dark current}}} \tag{6.33}$$

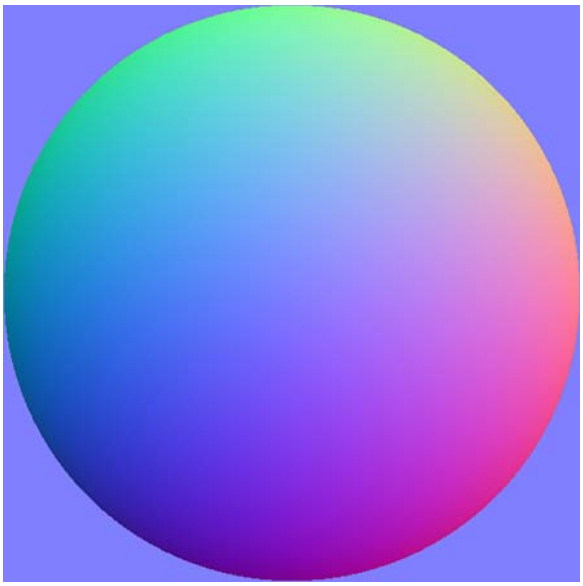

Figure 6.59 Surface normal mapping of a hemisphere.

$$B = \frac{B_{\text{object}} - B_{\text{dark current}}}{B_{\text{diffuse white}} - B_{\text{dark current}}} \tag{6.34}$$

$$I = R + G + B \tag{6.35}$$

The three intensities and corresponding light directions are combined into a matrix formula, shown in Eqs. (6.36)–(6.38):

$$\mathbf{I} = \mathbf{Ln} \tag{6.36}$$

where

$$\mathbf{I} = \begin{pmatrix} I_1 \\ I_2 \\ I_3 \end{pmatrix} \tag{6.37}$$

$$\mathbf{L} = \begin{pmatrix} L_{X_1} & L_{Y_1} & L_{Z_1} \\ L_{X_2} & L_{Y_2} & L_{Z_2} \\ L_{X_3} & L_{Y_3} & L_{Z_3} \end{pmatrix} \tag{6.38}$$

The normal vector is solved by inverting Eq. (6.36), shown in Eq. (6.39)

$$\mathbf{n} = \mathbf{L}^{-1}\mathbf{I} \tag{6.39}$$

The normal map for the object shown in Figure 6.60 is shown in Figure 6.61.

Photometric stereo is based on Lambert's cosine law and materials should be diffuse. The technique can be used with glossy materials by adding additional lights and removing data that correspond to specular highlights (Rushmeier, Taubin, and Guéziec 1997; Sun et al. 2007; Cox and Berns 2015). The polar angles for the set of lights are usually the same. The polar angle is determined experimentally in order to minimize both shadows and specular highlights.

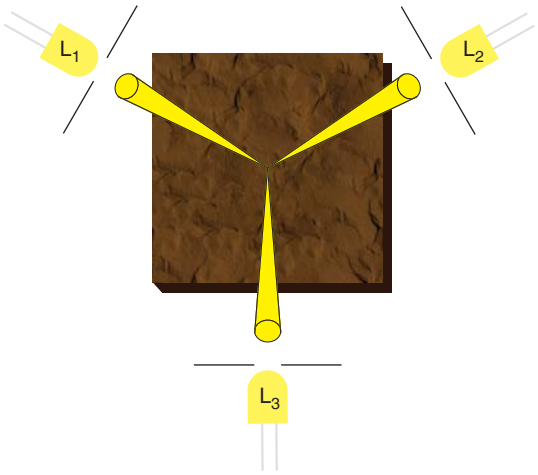

Figure 6.60 Three collimated lights are positioned at polar angles of 45° and uniformly spaced in azimuthal angle, that is, 120° apart from each other.

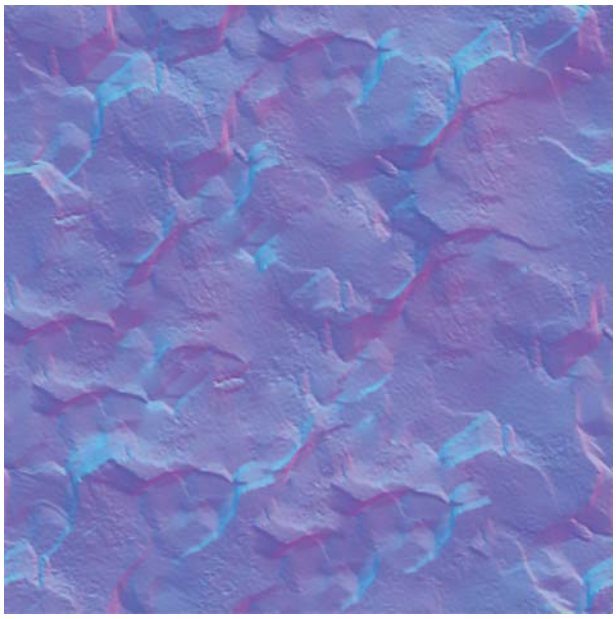

Figure 6.61 Normal map of the textured object shown in Figure 6.60.

Sparkle and Graininess

Coating industries have developed specialized material-appearance attributes, known as *visual texture* (McCamy 1996, 1998; Kirchner et al. 2007). Two attributes are particularly important in automotive coatings containing metallic flakes. One is *sparkle*, also called *glint impression*. It is seen under collimated illumination as tiny bright points of light. The second is *graininess*, sometimes called *diffuse coarseness*. It is seen under diffuse illumination as an irregular pattern of light and dark areas. Examples of materials

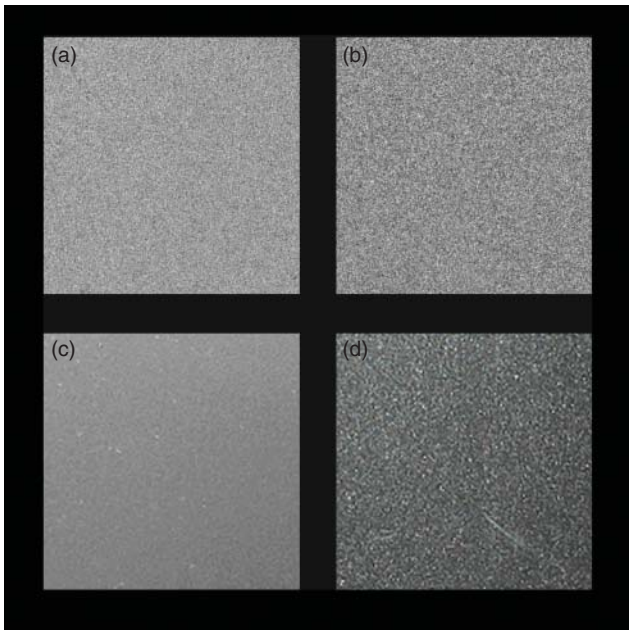

Figure 6.62 Coatings with metallic flakes exhibiting (a) low level of graininess, (b) high level of graininess, (c) low level of sparkle, and (d) high level of sparkle.
Source: Courtesy of AkzoNobel.

with large and small amounts of sparkle and graininess are shown in Figure 6.62.

- *Sparkle*: The aspect of the appearance of a material that seems to emit or reveal tiny bright points of light that are strikingly brighter than their immediate surround and are made more apparent when a minimum of one of the contributors (observer, specimen, light source) is moved.
- *Graininess*: (For gonioapparent coatings) the perceived contrast of the light/dark irregular pattern exhibited when viewed under diffuse illumination, scale typically <100 µm.

Instrumentation that measure sparkle and graininess are camera-based having three collimated sources and one diffuse source, shown in Figure 6.63. The collimated sources at 15°:0°, −45°:0°, and −75°:0° are used to characterize sparkle. The diffuse illumination is used to characterize graininess. Only polar angles are shown in Figure 6.63. An instrument could contain multiple sources sampling the azimuth. Images are takes sequentially using each source individually. The camera is calibrated to measure luminance, and the image statistics are used to calculate metrics that correlate with perceived sparkle and graininess. Sparkle is characterized by the density of sparkles and their luminance. These values can be used to define different flake types and concentration levels (Weixel 2016). Comparisons between

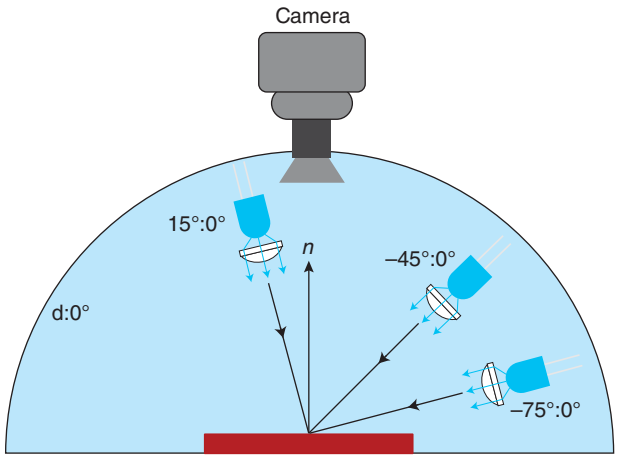

Figure 6.63 The geometry of measuring sparkle and graininess.

the three geometries indicate flake orientation. Graininess is characterized by a luminance or lightness histogram.

The metrics used in commercial instrumentation are proprietary. Even so, there have been visual experiments measuring perceived sparkle and graininess and predictive models based on the proprietary metrics (Wang and Luo 2016). A CIE technical committee is developing standardized methods of measurement, visual assessment, and metrics for both sparkle and graininess.

K. SUMMARY

A variety of instrumentation has been described to measure color and material appearance. An instrument we all have is our visual system, which can be effective under controlled conditions of illumination and viewing and used to distinguish differences. Spectrophotometers are used to measure spectral reflectance factor and spectral transmittance averaged over an area. Spectral imaging is equivalent to spectrophotometry where a camera replaces the single detector, resulting in millions of measurements. Spectroradiometers are used to measure spectral irradiance and spectral radiance. Bispectrometers measure both the luminescent and reflectance properties of fluorescent materials. All of these instruments have measurement uncertainty, and it is important to characterize repeatability, intrainstrument and interinstrument reproducibility, and accuracy. Material appearance is characterized using glossmeters, multiangle spectrophotometers, goniospectrophotometers, and imaging techniques that measure BRDF, surface normal, sparkle, and graininess. Having such an array of instruments reinforces asking and answering the question, "Why are we making the measurement?" We also believe that the simplest approach should be the first approach to evaluate.

Chapter 7
Lighting

We have stated, and will continue to state, that color depends on the light source, object, and the observer, shown in Figure 7.1. Chapter 1 is focused on the object while Chapter 2 considers the observer. We focus on the light source in this chapter. Many color tolerances are defined using standard illuminants such as D65. We describe how CIE daylight was derived as well as other standard illuminants. All viewing booths have lights that simulate CIE daylight. How well is daylight simulated? The luminous efficiency function, V_λ, is used to calculate luminance, illuminance, luminous efficacy of a source, and luminous efficacy of radiation (LER). These metrics are used to specify the amount of light necessary for a given task and to quantify energy efficiency. The color of a light source is defined by its chromaticity coordinates. However, it is difficult to infer hue from chromaticities. Instead correlated color temperature (CCT) is used. A wide variety of electric lighting is in use today including incandescent, fluorescent, metal halide, and solid state. These lights can have the same CCT, but because their spectral properties are vastly different, colored objects appear differently. The objects have been rendered differently and color rendering indices are used to quantify these differences compared with lights that are assumed to render an object's true color.

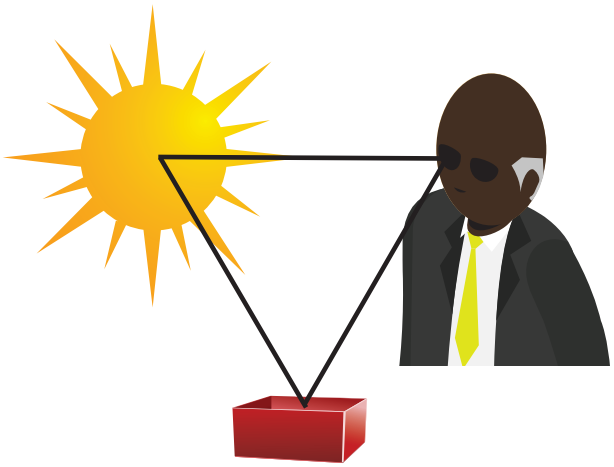

Figure 7.1 "*Color*" results from the interaction of a light source, an object, and the eye and brain, or visual system.

A. STANDARD ILLUMINANTS

We have been describing *light sources* and *illuminants* throughout the book. Light sources are physical and their spectral measurements correspond to a specific source, reported in units of irradiance, E_λ, or radiance, L_λ. Illuminants are standardized tabulated data that are based on physical measurements. CIE standard illuminants do not have absolute radiometric units. Instead, they are defined as relative spectral power distributions, notated S_λ (CIE 2018). For some illuminants, the spectra are normalized to 100 at 560 nm. An important distinction is that most sources have equivalent illuminants whereas not all illuminants have equivalent sources. This is an acute problem for the CIE daylight series illuminants, described below.

One type of standard illuminant is a *blackbody radiator,* also called a *Planckian radiator*. Blackbody radiators are materials that absorb all incident radiation, so called because at room temperature they appear black. The absorption heats the blackbody, which in turn causes it to emit its own radiation. The relationship between

Billmeyer and Saltzman's Principles of Color Technology, Fourth Edition. Roy S. Berns.

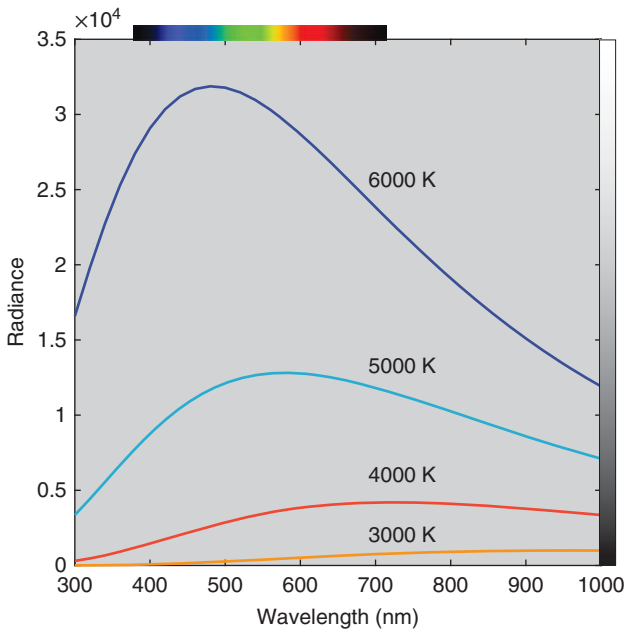

Figure 7.2 Enumeration of Planck's formula using Eq. (7.1). (Note extended wavelength scale.)

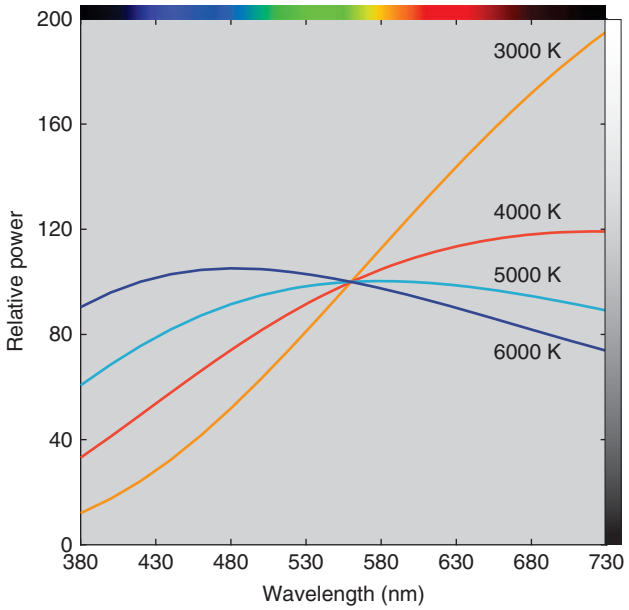

Figure 7.3 Enumeration of Planck's formula using Eq. (7.1) and normalized to 100 at 560 nm.

a blackbody's temperature and radiation is determinate (Planck 1901), and at extremely high temperatures, the radiation produces light. *Planck's formula* is shown in Eq. (7.1) where $c_{1L} = 3.741\,774\,9 \times 10^{-16}$ W/m^2-sr-m, $c_2 = 0.014\,387\,69$ m-K, λ is defined in meters (560 nm $= 5.6 \times 10^{-7}$ m), and temperature, T, is defined in kelvins

$$L_\lambda = \frac{c_{1,L}}{\lambda^5}\left(\frac{1}{e^{\frac{c_2}{\lambda T}} - 1}\right) \tag{7.1}$$

Equation (7.1) was enumerated for temperatures of 3000–6000 K, shown in Figure 7.2. The maximum radiance occurs at shorter wavelengths as temperature increases. These spectra are normalized to 100 at 560 nm and plotted in Figure 7.3. An increase in temperature increases the amount of short-wavelength light and decreases the amount of long-wavelength light. The color of the light becomes bluer with an increase in temperature and more orange with a decrease in temperature, and consequently, the term *color temperature* is used when referring to blackbody radiators.

The $u'v'$ chromaticities for blackbody radiators are shown in Figure 7.4. The chromaticities lie on a smooth contour, referred to as the *blackbody* or *Planckian locus*.

The CIE, in 1931, used Planck's formula to calculate a spectral power distribution that represented typical incandescent lighting during the early twentieth century, defined as *CIE standard illuminant A* (CIE 1931). The specific formula is shown in Eq. (7.2) where λ has units of nanometer. The relationship between Eqs. (7.1) and (7.2) is described in CIE (2018). Illuminant A has a CCT (defined below) of 2856 K

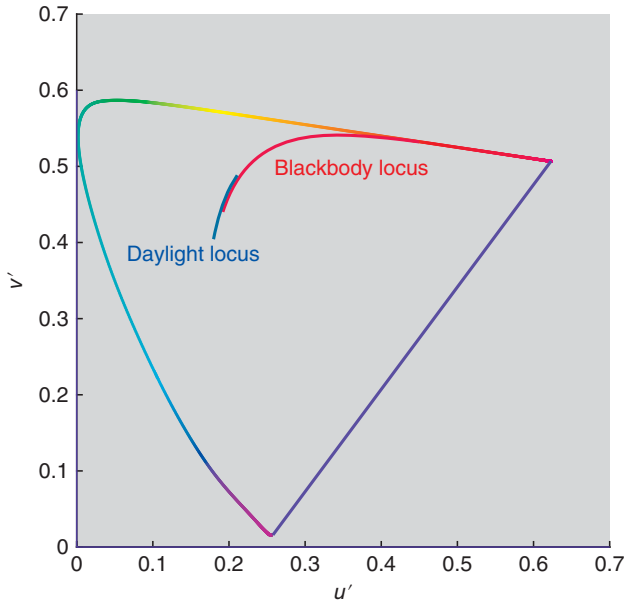

Figure 7.4 Blackbody and CIE daylight loci plotted in the $u'v'$ uniform chromaticity scale diagram. The blackbody locus ranges between 1000 and 10 000 K. The daylight locus ranges between 5000 and 50 000 K.

$$S_\lambda = 100\left(\frac{560}{\lambda}\right)^5\left(\frac{e^{\frac{1.435\times10^7}{2848\times560}} - 1}{e^{\frac{1.435\times10^7}{2848\,\lambda}} - 1}\right) \tag{7.2}$$

(The CIE also established sources and illuminants B and C, now obsolete and replaced with the CIE daylight series.)

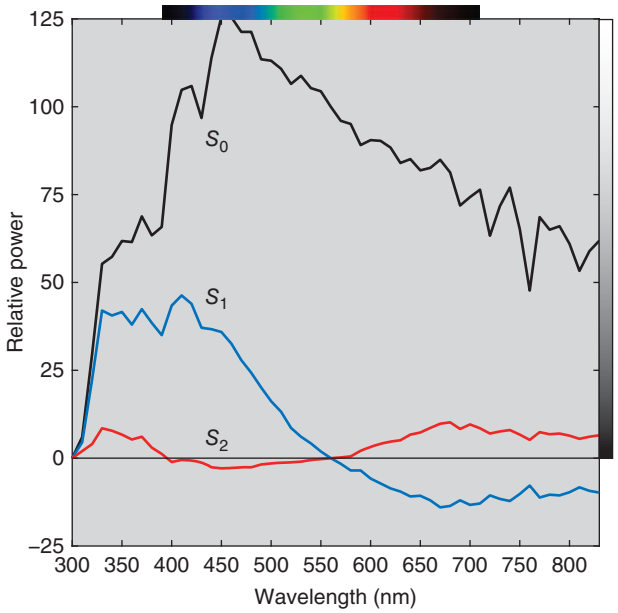

Figure 7.5 Mean, $S_{\lambda,0}$, and eigenvectors, $S_{\lambda,1}$ and $S_{\lambda,2}$, defining CIE daylight. (Note extended wavelength scale and relative power having both positive and negative values.)

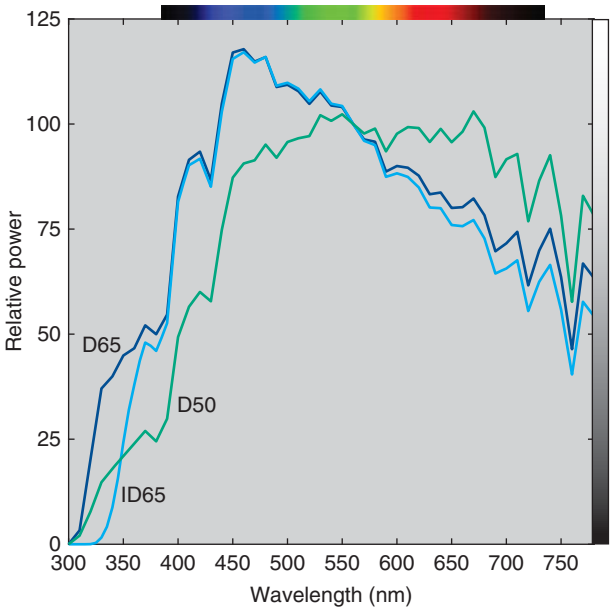

Figure 7.6 CIE illuminants D65, ID65, and D50. (Note the extended wavelength range.)

CIE Illuminant E is another standard having a spectral power distribution that is 100 at all wavelengths.

During the 1960s, over 600 measurements were made of natural daylight during different times of day, different sky conditions, and in three locations: Rochester, New York, United States; Ottawa, Canada; and Enfield, England (Judd et al. 1964). The data were normalized at 560 nm and principal component analysis (PCA) was used (Simonds 1963) to reduce the many spectra to three: an average, $S_{\lambda,0}$, and two eigenvectors, $S_{\lambda,1}$ and $S_{\lambda,2}$, shown in Figure 7.5. PCA is described in Chapter 6. The first eigenvector corresponds to "the presence or absence of clouds in the sky, and to the inclusion or exclusion of direct sunlight" while the second eigenvector may correspond to "the presence of little or much water in the form of vapor and haze" (Judd et al. 1964). A daylight distribution is determined by adding or subtracting the two eigenvectors to the mean. The most commonly used CIE daylight spectral power distributions have CCTs of 5000 K (D50) and 6500 K (D65), shown in Figure 7.6. Indoors, window glass absorbs UV radiation changing daylight's spectral power distribution. The CIE has defined the transmittance of window glass and used it to specify indoor D65 and D50, referred to as ID65 and ID50 (CIE 2018). The spectrum for indoors D65 (ID65) is also shown in Figure 7.6. ID65 and ID50 were developed so that colorimetric calculations would better correlate with the appearance of materials containing fluorescent whitening agents viewed indoors.

Light booth manufacturers and, to a lesser extent, color measurement instrumentation manufacturers, have always had difficulty producing a source with the same spectral power distribution as CIE daylight, particularly in the ultraviolet (UV) region (McCamy 1994). The CIE has a test method to evaluate the quality of a daylight simulator using metameric pairs that are sensitive to differences in spectral power distributions simulating daylight (ISO/CIE 2005). There are metamers for both the visible and UV regions of the electromagnetic spectrum. Depending on the magnitude of color difference, sources are rated on an alphabetic scale where category A is the best simulation and category E is the worst simulation. Categories are assigned for each spectral region, for example, BD where the first letter is the visible-region category and the second letter is the UV-region category. For critical visual evaluation, daylight simulators must be BC or better (ASTM 2016a). Light booths using fluorescent lamps tend to have ratings of BC while booths using filtered tungsten have ratings of BE (Lin, Shamey, and Hinks 2012; Wei and Chen 2018). Both lights can be improved to a BB rating with the addition of a separate UV source. Well simulating CIE daylight is very important when correlating whiteness indices with perceived whiteness (Lin, Shamey, and Hinks 2012) and evaluating color differences of metameric samples (Gu et al. 2016). Light booths are available that have multiple solid-state sources that can simulate daylight to a category AD, shown in Figure 7.7.

The CIE first published illuminant data for 12 types of fluorescent sources during the 1980s, notated F1–F12. Today's fluorescent sources are slightly different and the CIE has published 15 additional spectra (FL3.1–FL3.15). There are also five high-pressure discharge lamps (HP1–HP5), five phosphor-type solid-state lamps (LED-B1–LED-B5), a hybrid-type solid-state lamp (LED-BH1), two RGB-type

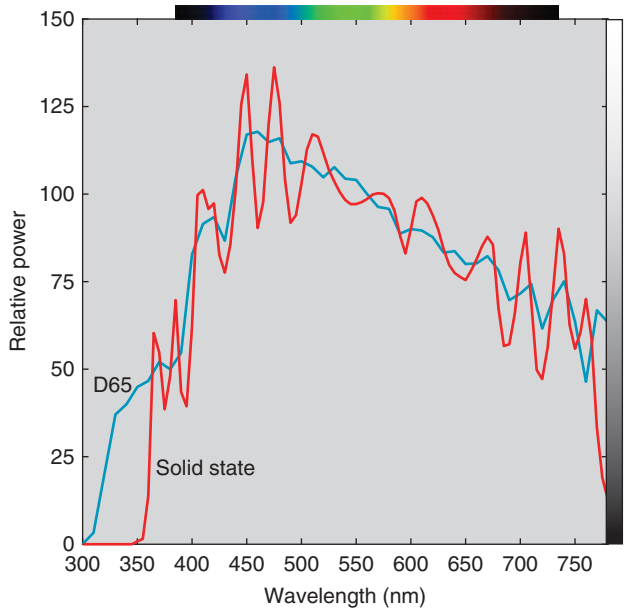

Figure 7.7 Spectral power distributions of multi-solid-state D65 simulator and CIE illuminant D65. (Note the extended wavelength range.)

solid-state lamps (LED-RGB1 and LED-RGB2), and two violet-pumped phosphor-type solid-state lamps (LEDV1 and LEDV2). The intent of these many illuminants is to improve correlation between colorimetry and color appearance. Common F-series illuminants are F2, F7, F8, and F11, corresponding to cool-white, 6500 K daylight, 5000 K daylight, and narrow-band fluorescent, respectively. The equivalent illuminants from the FL series are FL3.2, FL3.15, FL3.6, and FL3.8. These spectra are plotted in Figure 7.8.

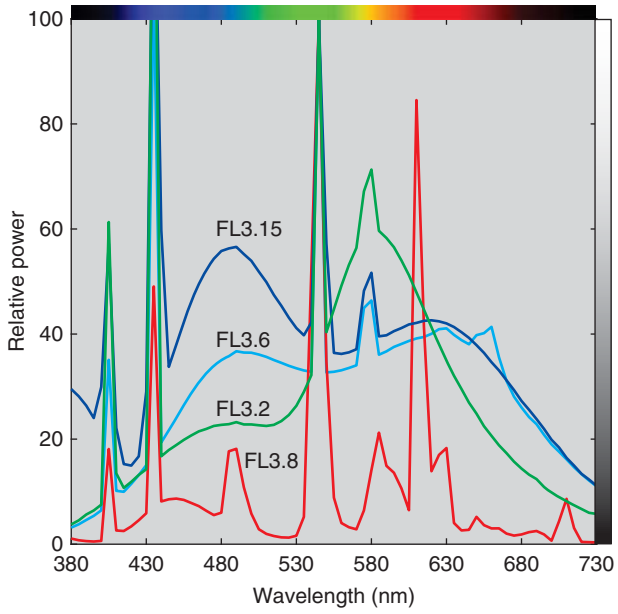

Figure 7.8 Spectral power distributions of selected CIE FL-series illuminants.

Calculating a Daylight Spectral Power Distribution from Correlated Color Temperature

Calculation of a daylight spectral power distribution, $S_{D,\lambda}$, is shown in Eq. (7.3):

$$S_{\lambda,D} = S_{\lambda,0} + M_1 S_{\lambda,1} + M_2 S_{\lambda,2} \tag{7.3}$$

where M_1 and M_2 are scalars that determine the magnitude of the two eigenvectors that either add to or subtract from the mean, $S_{\lambda,0}$.

The daylight measurements compiled by Judd et al. (1964) were used to calculate chromaticities. They found that the chromaticities plotted along a locus that was similar in shape but located slightly above the Planckian locus. Since chromaticities and the eigenvector scalars both are two dimensional, relationships were derived where the eigenvector scalars were calculated as a function of chromaticities, which were derived as a function of CCT. The daylight locus is shown in Figure 7.4.

The first step is to account for the change in the first radiation constant, c_1, that occurred in 1968 by multiplying the desired CCT by 1.4388/1.4380 (CIE 2018). Second, calculate x_D and y_D, shown in Eqs. (7.4) and (7.5) where T_{cp} is the corrected CCT

$$x_D = \begin{cases} \dfrac{-4.6070\times10^9}{T_{cp}^{\,3}} + \dfrac{2.9678\times10^6}{T_{cp}^{\,2}} + \dfrac{0.09911\times10^3}{T_{cp}} + 0.244063 & 4000 \le K \le 7000 \\ \dfrac{-2.0064\times10^9}{T_{cp}^{\,3}} + \dfrac{1.9018\times10^6}{T_{cp}^{\,2}} + \dfrac{0.24748\times10^3}{T_{cp}} + 0.237040 & 7000 < K \le 25\,000 \end{cases} \tag{7.4}$$

$$y_D = -3.000x_D^2 + 2.870x_D - 0.275 \tag{7.5}$$

Third, calculate M_1 and M_2 using Eqs. (7.6) and (7.7)

$$M_1 = \frac{-1.3515 - 1.7703x_D + 5.9114y_D}{0.0241 + 0.2562x_D - 0.7341y_D} \tag{7.6}$$

$$M_2 = \frac{0.0300 - 31.4424x_D + 30.0717y_D}{0.0241 + 0.2562x_D - 0.7341y_D} \tag{7.7}$$

Fourth, round M_1 and M_2 to three decimal places. Fifth, calculate the spectral power distribution using Eq. (7.3). For illuminant D65, $M_1 = -0.293$ and $M_2 = -0.689$.

B. LUMINANCE, ILLUMINANCE, AND LUMINOUS EFFICACY

Luminance and illuminance were defined in Chapter 4. For convenience, the formulas are shown again in Eqs. (7.8) and (7.9):

$$L = K_m \int_\lambda L_\lambda V_\lambda \, d\lambda \tag{7.8}$$

$$E = K_m \int_\lambda E_\lambda V_\lambda \, d\lambda \tag{7.9}$$

where L defines luminance and E defines illuminance. The normalizing constant, K_m, equals 683 lm/W, known as the *maximum luminous efficacy*. A *lumen* is a quantity that weights light by the luminous efficiency function, V_λ. When a light source's spectral irradiance, E_λ, is measured, illuminance, E, has units of lumens per square meter, abbreviated lux or lx. When spectral radiance, L_λ, is measured, luminance, L, has units of candelas per square meter, or lumens per square meter per steradian. A candela is a unit of luminous intensity defined as 1/683 W/Sr. Illuminance is used to define the amount of light falling on a surface expressed as lx or foot-candles (fc, lumens per square foot). Foot-candles multiplied by 10.76 equals lx. Luminance is used to define the amount of light generated by a source. Essentially, luminance measurements are not dependent on distance; illuminance measurements are. See Wyszecki and Stiles (1982) and McCluney (2014) for greater details on photometry and radiometry.

There are two additional metrics used in lighting engineering that are also based on the luminous efficiency function. The first is the *luminous efficacy of a source*. It is the luminous flux emitted by a source divided by the input electrical power. Because of consumer familiarity with incandescent lighting for about 100 years, bulbs are rated by wattage, not luminous efficacy. It is understood that a 75 W bulb is brighter than a 60 W bulb. Today, there is a large range in luminous efficacy and consumers should evaluate both lumens and wattage. For example, a 60 W incandescent bulb produces about 700 lm. A solid-state bulb requires about 10 W to produce the same number of lumens. The solid-state bulb may be marketed as "60 W equivalent."

The second metric is the *luminous efficacy of radiation*, abbreviated as LER and notated as K, the formula shown in Eq. (7.10)

$$K = \frac{K_m \int_\lambda V_\lambda S_\lambda \, d\lambda}{\int_\lambda S_\lambda \, d\lambda} \tag{7.10}$$

This is a measure of the ability of a light source to produce a visual sensation. Ideally, radiation should only occur in the visual spectrum. Incandescent lighting is being phased out because it has poor luminous efficacy of a source and poor LER.

C. CORRELATED COLOR TEMPERATURE

- *Color temperature:* Temperature, usually expressed in kelvins, of a blackbody radiator.
- *Correlated color temperature (CCT):* Temperature, usually expressed in kelvins, of a blackbody radiator that most closely resembles the color of a light source.

Many non-blackbody light sources can be described by the color temperature of the blackbody that they most resemble visually. This is called their *correlated color temperature*, abbreviated as CCT and notated at T_{cp}. Similarity is based on colorimetry. When an exact colorimetric match occurs, the blackbody radiator is metameric to the non-blackbody light source. When an exact match is not possible, the blackbody radiator that leads to the minimum distance in the now obsolete CIE 1960 *uv* uniform chromaticity scale diagram defines the CCT of the non-blackbody light source. The method described by Robertson (1968) is most often used for calculating CCT though other methods have been developed, summarized by Li et al. (2016).

Not all sources can be assigned a CCT. A difference metric, D_{uv}, is calculated, shown in Eqs. (7.11)–(7.13):

$$D_{uv} = \sqrt{(u'_t - u'_b)^2 + 4/9(v'_t - v'_b)^2} \cdot \mathrm{sgn}(v'_t - v'_b) \tag{7.11}$$

$$\mathrm{sgn}(x) = 1 \qquad x \geq 0 \tag{7.12}$$

$$\mathrm{sgn}(x) = -1 \qquad x < 0 \tag{7.13}$$

where subscript t refers to the test source and subscript b refers to the blackbody source. The source must have a $|D_{uv}| \leq 0.05$ in order to assign a CCT. A source's CCT is determined by minimizing $|D_{uv}|$. A positive D_{uv} can indicate a greenish white while a negative D_{uv} can indicate a pinkish white. The sign and magnitude of D_{uv} are useful for determining whether a source appears white or tinted (Ohno and Fein 2014; Smet, Deconinck, and Hanselaer 2015) and can also be correlated with preferred color (Bodrogi et al. 2018).

CCT has always been an important property of lighting and today's solid-state lights for consumer use are designed for four different CCTs: 2700 K, the nominal value of incandescent lights; 3000 K, the nominal value of tungsten-halogen lights; 4000 K, the nominal value of cool-white fluorescent lights, and 5000 K. The adjectives "soft," "bright," and "cool," have been used for 2700, 3000, and 4000 K. Lights that are 5000 K and above tend to be labeled as "daylight."

The effects of changing a light's CCT are shown in Figure 7.9 where a museum gallery space is lit identically except CCT. The common change from orange (warm) to blue (cool) as CCT increases is evident. A number of preference experiments have been performed, the goal of which is to determine an optimal CCT for viewing artwork (Scuello et al. 2004; Pinto, Linhares, and Nascimento 2008; Liu et al. 2013; Nascimento and Masuda 2014; Zhai, Luo, and Liu 2015). Unfortunately, the results depend on the experimental conditions and can be inconclusive due to large variability among observers and object-specific results. Furthermore, studies involving museum professionals have shown strong prejudices toward specific CCTs irrespective of experimental evidence (Miller and Rosenfeld 2012).

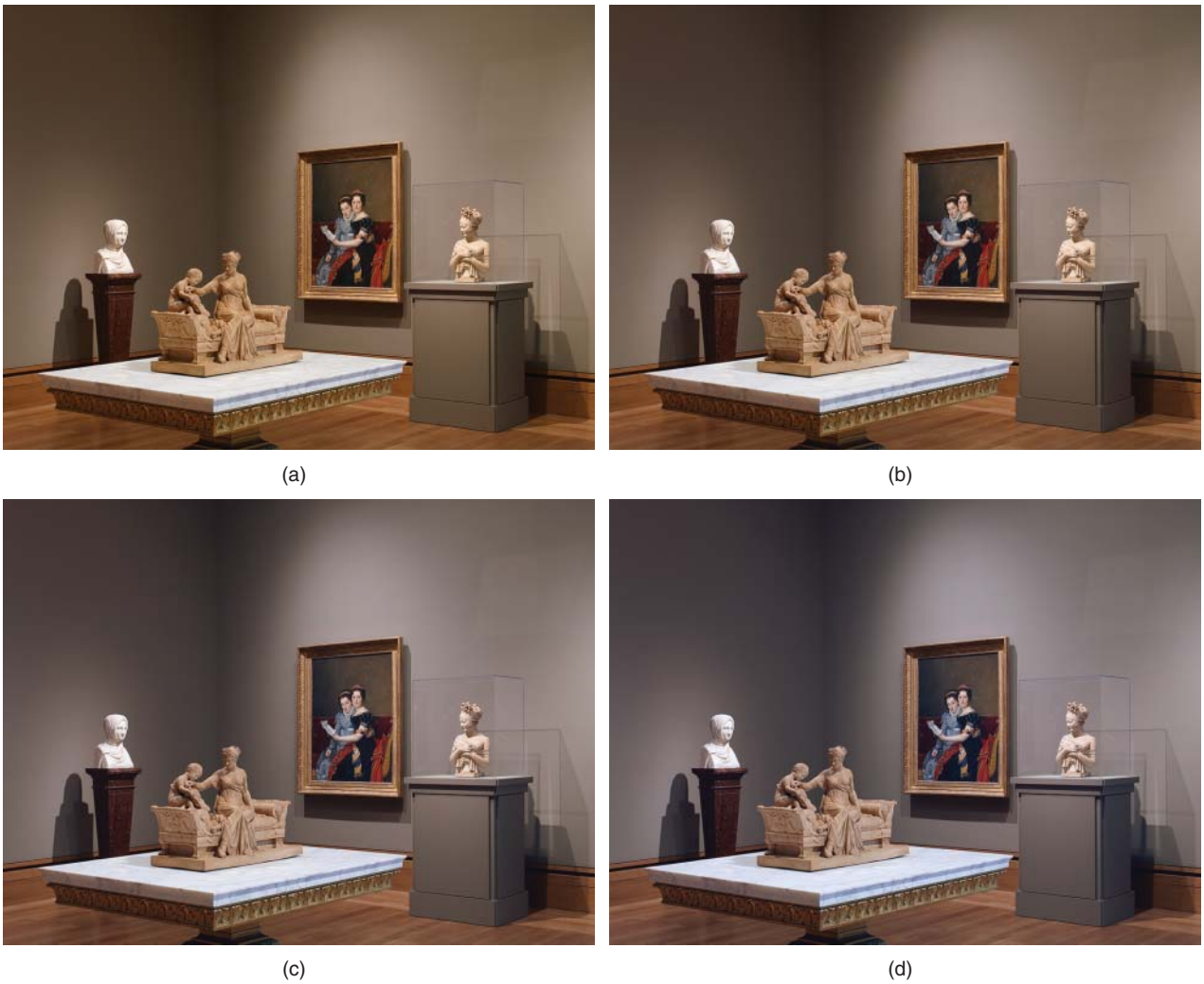

Figure 7.9 Gallery of late Neoclassicism in European art and design at the Getty Museum, Los Angeles. Lighting varies between (a) soft, (b) bright, (c) cool, and (d) daylight.
Source: Digital image courtesy of the Getty's Open Content Program.

D. COLOR RENDITION

Lights can be designed to have the same CCT and luminance such as soft-white light made using incandescent and solid-state technologies. Different technologies lead to different spectral radiances and as a consequence, colored objects can appear different. As an example, a sofa was illuminated by three sources with matching CCT and luminance and dissimilar spectral radiance, shown in Figure 7.10. Which color is the "true" or "natural" color of the sofa? For many people, they would want to see the sofa lit with natural daylight during the day and by incandescent during the night. In fact, one of the lights is D65 and the other two are theoretical RGB-type solid-state lights designed to distort colors (Berns 2011). The spectra of the three lights are plotted in Figure 7.11. Changing the wavelength location of the green primary changed the hue from cyan to purple. The sofa has been rendered differently and the lights are said to have different *color rendition* or *color rendering*.

The need for a color rendering metric arose with the use of fluorescent lighting during the mid-twentieth century. Warm-white fluorescent lighting with a CCT near 2900 K rendered colors very poorly compared with incandescent lighting with the same CCT. Cool-white fluorescent lighting, used extensively in offices and warehouses, also had poor color rendition. Research began in the 1950s (Nickerson 1960), and in 1965, the CIE recommended a method and index to quantify the color rendering of lighting (CIE 1995b). The index, known as the *color rendering index*, abbreviated as CRI and notated as R_a, is used universally within the lighting industry. Many of today's solid-state lights list CRI along with wattage, lumens, and CCT on their packaging.

Figure 7.10 Visualization of sofa lit by (a) SS-1, (b) D65, and (c) SS-2.

The key aspect of quantifying color rendering is its relative nature where a test light is compared with a reference light, the reference being either a blackbody radiator below a CCT of 5000 K or CIE daylight having a CCT of 5000 K and above. These reference illuminants are assumed to match our expectations of defining a colored object's "true color." The reference illuminant is selected based on the test source's CCT. The colorimetric coordinates are calculated for a set of reference colors for both the test source and reference illuminant using the 1931 standard observer. A scaled total color difference between the pair of coordinates quantifies rendering accuracy and the average is used as the index, the

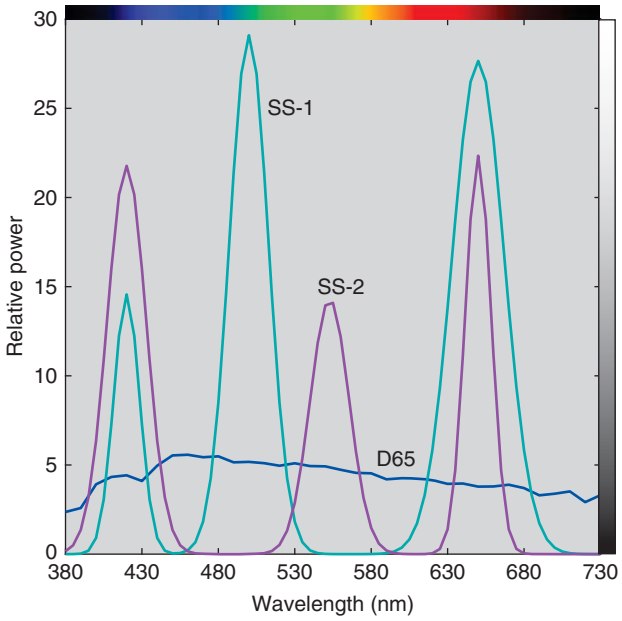

Figure 7.11 Spectral power distributions of D65, SS-1, and SS-2.

scaling resulting in warm-white fluorescent lighting having a $R_a = 50$ and the reference illuminant having a $R_a = 100$. There is not a lower bound. When the test source and reference illuminant have a D_{uv} other than zero, a chromatic adaptation transformation is used to calculate corresponding colors for the reference colors transforming from the test source to reference illuminant. Details about the use of corresponding colors in a color difference calculation are given in Chapter 8. There are 14 reference colors, defined spectrally, the first eight of which are used to calculate R_a where subscript a denotes average. The eight were selected from the Munsell Book of Color equally sampling hue at a similar lightness and chroma (Nickerson 1960). This sampling scheme resulted in low chroma colors, problematic because low chroma samples are somewhat insensitive to lighting differences. To remedy this limitation, six more Munsell samples were selected. The 14 samples are notated as TCS1–TCS14 (test color sample) and their rendering values notated as R_1–R_{14}. TCS9 is a vivid red color and R_9 is often listed in addition to R_a because many solid-state lights render red colors poorly with a noticeable dulling.

Cubes were rendered, each having a spectral reflectance equal to the 14 samples and an additional spectrally nonselective gray, where the cubes were lit from the top by D65 and by the left and right sides by SS-1 and SS-2, respectively, shown in Figure 7.12. Many colors are distorted. The high chroma yellow and blue cubes, TCS10 and TCS12, resulted in quite dramatic changes when lit by these theoretical sources.

The cubes were again rendered, this time using CIE LED B-5 and CIE FL 3.15, both representing commercial lights. The rendering is shown in Figure 7.13 and their spectral

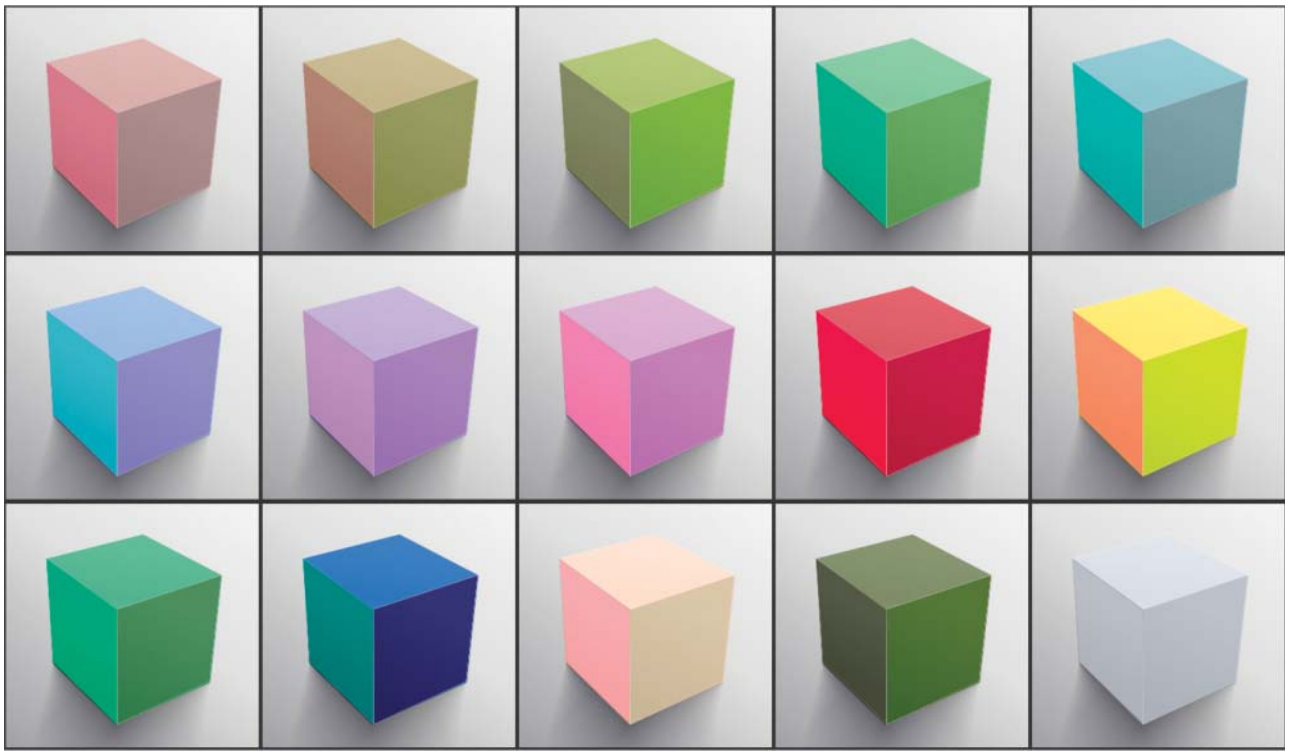

Figure 7.12 Rendered cubes where the top is illuminated by D65, the left-facing side is illuminated by SS-1, and the right-facing side is illuminated by SS-2.

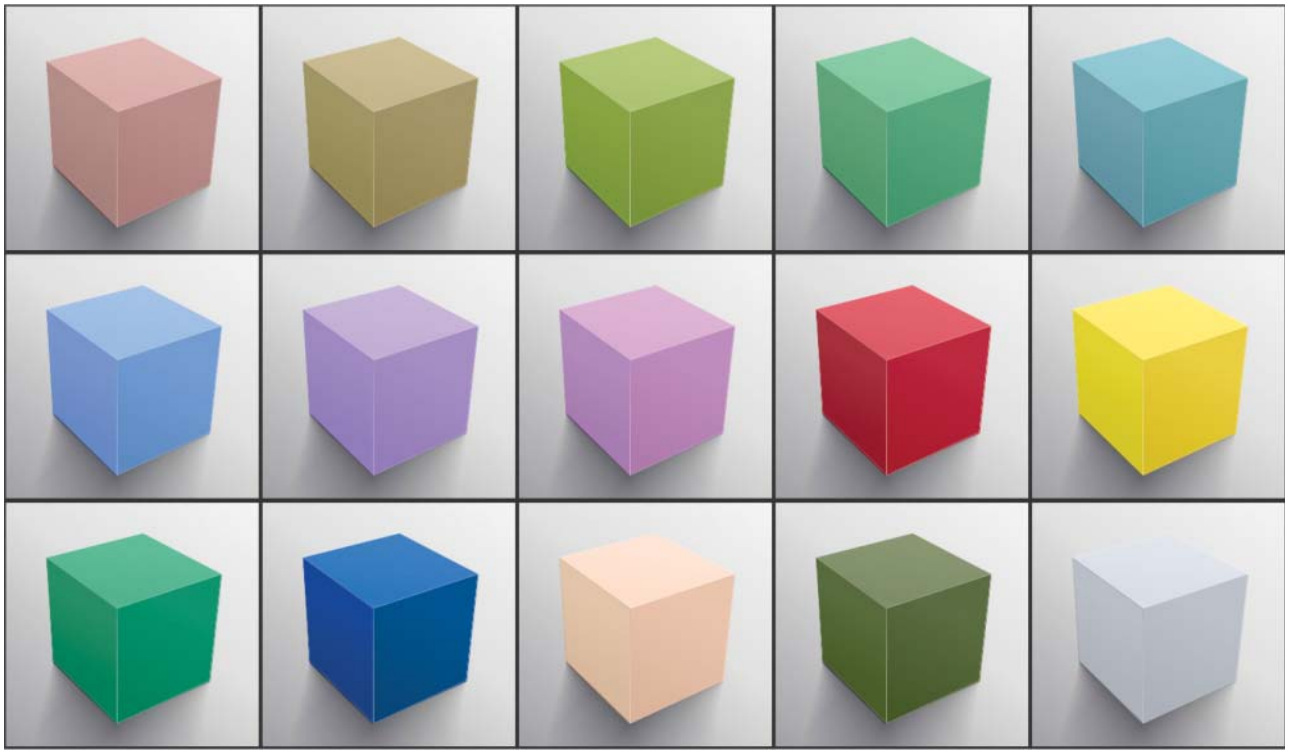

Figure 7.13 Rendered cubes where the top is illuminated by D65, the left-facing side is illuminated by LED B-5, and the right-facing side is illuminated by FL 3.15.

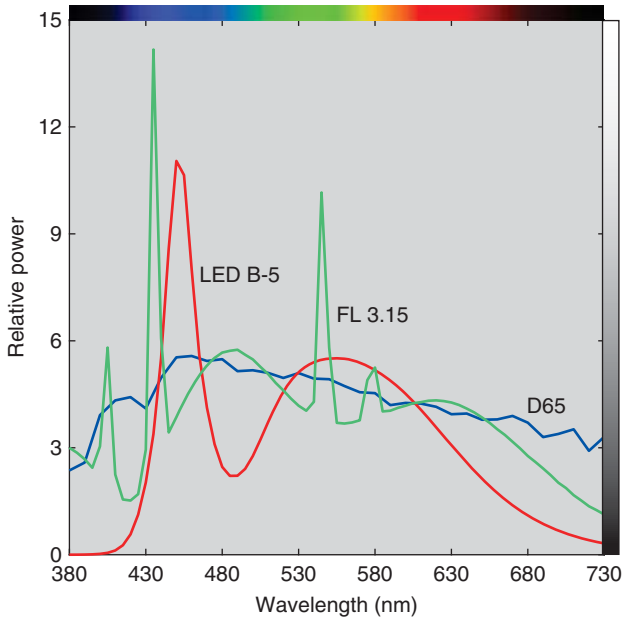

Figure 7.14 Spectral power distributions of D65, LED B-5, and FL 3.15.

power distributions are shown in Figure 7.14. The changes in rendering are less severe than SS-1 and SS-2 but still noticeable. The three CIE illuminants, D65, LED B-5, and FL 3.15 were used to render a steak, shown in Figure 7.15, illustrating the importance of excellent rendition of red colors. The dulling of the steak's color when illuminated by LED B-5 demonstrates the problem with some solid-state lights. The R_a and R_9 for the five illuminants are listed in Table 7.1. The values for SS-1 and SS-2 are extremely low. The lack of long-wavelength radiance of LED B-5 results in $R_a = 80$ and $R_9 = 7$. The fluorescent lamp has excellent color rendering with values near 100.

The CIE method of quantifying color rendering has long been criticized, summarized by Houser et al. (2013). The eight samples are a particular problem because of their low chroma and as a consequence, the index has low sensitivity. The color-difference calculation is based on an obsolete color space with poor correlation to perceived color differences and as a consequence, there is an imbalance between hues. These deficiencies have resulted in poor correlation when CRI is used to predict visual judgments of fidelity, particularly for narrow-band fluorescent and solid-state lights. CRI is a scaled total color difference, and all the limitations of ΔE apply to CRI. A total color difference discards the direction of difference and whether the difference is attributed to hue, lightness, or chroma. These limitations can be easily remedied and the published literature has many examples, also summarized by Houser et al. (2013). Unfortunately, the CIE has been unsuccessful in updating its method.

Reproducing the color rendering of a reference illuminant does not lead to preferred color rendition. Consumers tend to prefer sources that slightly increase vividness (Ohno, Miller, and Fein 2015; Khanh et al. 2017). Judd (1967) and later Thornton (1974) modified CRI so that the test colors' reference chromaticities were changed corresponding to an increase in vividness. A light source that increased vividness would have a preference index greater than the reference source and a rendering index less than the reference source. Unfortunately, neither index was adopted by the lighting industry and the CIE did not pursue a CPI (color preference index) as a companion to CRI.

Preferred color rendition and the need for two indices were revived by Rea and Freyssinier-Nova (2008, 2010). The area of the bounding octahedron defined by the chromaticities of the eight test color samples was calculated for the test source. Rather than comparing this area to the area calculated for the reference illuminant, they compared the test source area to a single reference illuminant, the equal energy spectrum. They called this the *gamut area index*, abbreviated as GAI. The authors found that both CRI and GAI were important to predict the color rendering properties of electric lighting.

The Illuminating Engineering Society of North America (IESNA), in 2015, developed a new method to evaluate color rendering (David et al. 2015; IESNA 2015). There are three significant differences compared with the CIE method. First, there are 99 reflectance spectra, selected based on their spectral characteristics and their color. Second, a color appearance space is used. Third, two indices are reported. One index quantifies color fidelity, notated as R_f. It is an updated R_a. The second index quantifies gamut area, notated as R_g. It is an updated GAI. The IES indices for the five sources are also listed in Table 7.1. R_f led to the same ranking as R_a though the values are very different. SS-1, SS-2, and LED B-5 have very similar R_g values, and these values below 100 indicate

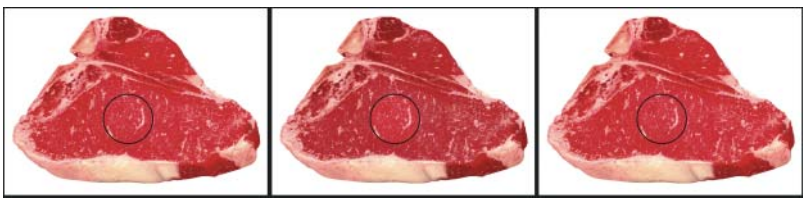

Figure 7.15 Color rendering of a steak using CIE illuminants D65 (a), LED B-5 (b), and FL3.15 (c). The circular cutout is the steak's color illuminated by D65. For this simulation, the average spectral reflectance of the muscle equaled the spectral reflectance of TCS9.

Table 7.1 Lighting metrics for each listed illuminant.

Metric	D65	SS-1	SS-2	LED B-5	FL3.15
CCT	6503	6503	6503	6598	6508
D_{uv}	0.0032	0.0032	0.0032	0.0009	0.0031
LER	204	141	210	305	235
CIE R_a	100	−45	32	80	98
CIE R_9	100	−463	−11	7	96
IES R_f	100	5	19	77	99
IES R_g	100	93	95	94	101

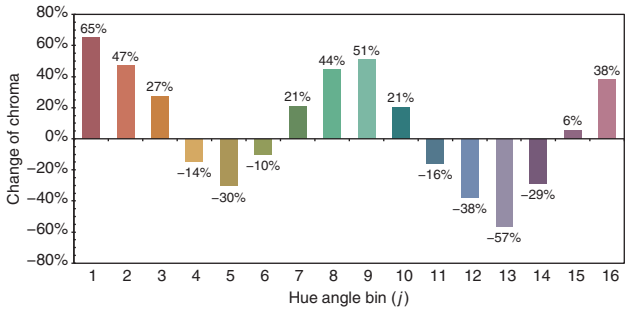

Figure 7.16 Percentage change of chroma as a function of hue angle region for solid-state light SS-1.

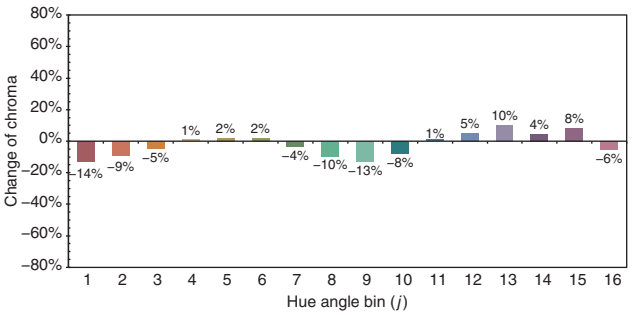

Figure 7.17 Percentage change of chroma as a function of hue angle region for solid-state light LED B-5.

that all three sources reduce vividness, clearly not the case when evaluating the rendered cubes. This limitation is typical of indices based on averages. For color-critical applications, each hue region needs to be evaluated individually. This is shown in Figures 7.16 and 7.17 comparing SS-1 and LED B-5 using software provided by IESNA.

The CIE recently issued a technical report describing a color fidelity index, R_f, "for accurate scientific use" (CIE 2017). This index is very similar to the index developed by IESNA. The report notes that the CIE R_f is not a replacement for CRI and that replacing CRI "will be a matter of future study . . ." As consumers, we hope that one day, CRI will be replaced with one or more indices that will enable us to make more informed purchase decisions.

Creating Visualizations

It is very difficult to mentally visualize an object's color based on its spectral reflectance, the spectral power distribution of a light source, and the color matching functions of an observer. The vastly different hues of the sofa shown in Figure 7.10 are an example. These visualizations were produced computationally.

The first step is to calculate tristimulus values for a reflectance spectrum for a specific source and observer, shown in Eqs. (7.14)–(7.17):

$$\begin{pmatrix} X \\ Y \\ Z \end{pmatrix} = \mathbf{TSR} \tag{7.14}$$

where

$$\mathbf{T} = \begin{pmatrix} \bar{x}_\lambda & \dots & \bar{x}_\lambda \\ \bar{y}_\lambda & \dots & \bar{y}_\lambda \\ \bar{z}_\lambda & \dots & \bar{z}_\lambda \end{pmatrix} \tag{7.15}$$

$$\mathbf{S} = \begin{pmatrix} S_\lambda & 0 & 0 \\ 0 & \ddots & 0 \\ 0 & 0 & S_\lambda \end{pmatrix} \tag{7.16}$$

$$\mathbf{R} = \begin{pmatrix} R_\lambda \\ \vdots \\ R_\lambda \end{pmatrix} \tag{7.17}$$

Second, the *RGB* encoding is defined in order to know the reference white point and observer. For this book, 16-bit ProPhoto RGB was used having a D50 white point for the 1931 standard observer (see Chapter 10).

The third step is to use a chromatic adaptation transform (CAT) to convert from the specific source and observer to the reference condition. The CAT embedded in CIECAM16 was used (Li et al. 2017), shown in Eqs. (7.18)–(7.20):

$$\begin{pmatrix} R \\ G \\ B \end{pmatrix} = \begin{pmatrix} 0.401288 & 0.650173 & -0.051461 \\ -0.250268 & 1.204414 & 0.045854 \\ -0.002079 & 0.048952 & 0.953127 \end{pmatrix}_{CAT16} \begin{pmatrix} X \\ Y \\ Z \end{pmatrix} \tag{7.18}$$

$$\begin{pmatrix} R_{D50} \\ G_{D50} \\ B_{D50} \end{pmatrix} = \begin{pmatrix} \frac{DR_{n,D50}+(1-D)R_{n,s}}{R_{n,s}} & 0 & 0 \\ 0 & \frac{DG_{n,D50}+(1-D)G_{n,s}}{G_{n,s}} & 0 \\ 0 & 0 & \frac{DB_{n,D50}+(1-D)B_{n,s}}{B_{n,s}} \end{pmatrix}_{\text{vKD}} \begin{pmatrix} R \\ G \\ B \end{pmatrix} \tag{7.19}$$

$$\begin{pmatrix} X_{D50} \\ Y_{D50} \\ Z_{D50} \end{pmatrix} = \begin{pmatrix} 0.401288 & 0.650173 & -0.051461 \\ -0.250268 & 1.204414 & 0.045854 \\ -0.002079 & 0.048952 & 0.953127 \end{pmatrix}^{-1}_{CAT16} \begin{pmatrix} R_{D50} \\ G_{D50} \\ B_{D50} \end{pmatrix} \tag{7.20}$$

where R, G, and B are pseudo-cone fundamentals and D defines the degree of adaptation. (Strictly, a CAT should not be used to convert between observers. Derhak and Berns (2015a) describe a method that could be used. For simplicity, this was not implemented.)

The fourth step is to calculate ProPhoto RGB, also known as Reference Output Medium Metric (ROMM) RGB (ISO 2013), from *XYZ*, shown in Eqs. (7.21)–(7.23)

$$\begin{pmatrix} R_{\text{linear}} \\ G_{\text{linear}} \\ B_{\text{linear}} \end{pmatrix} = \begin{pmatrix} 1.3460 & -0.2556 & -0.0511 \\ -0.5446 & 1.5082 & 0.0205 \\ 0.0000 & 0.0000 & 1.2123 \end{pmatrix}_{\substack{\text{ProPhoto} \\ \text{RGB}}} \begin{pmatrix} X_{D50} \\ Y_{D50} \\ Z_{D50} \end{pmatrix} \tag{7.21}$$

$$R, G, B = f(R_{\text{linear}}, G_{\text{linear}}, B_{\text{linear}}) \tag{7.22}$$

$$f(x) = \begin{Bmatrix} 0; & x < 0 \\ 16x; & 0 \le x < 0.001953 \\ x^{1/1.8}; & 0.001953 \le x < 1.0 \\ 1; & x \ge 1.00 \end{Bmatrix} \tag{7.23}$$

An image is created defining the object to be recolored. In this chapter, images of a sofa, a steak, and a cube were used. The image should have an average color close to the ProPhoto *RGB* values. If this isn't possible, middle gray is the next choice. An alpha channel mask of the object is made; this will be the image area that is recolored. The image is encoded in 16-bit ProPhoto RGB.

The fifth step is to calculate the average *RGB* values of the image mask, calculate the *RGB* difference between the visualized color and the average, and translate each pixel within the mask, shown in Eqs. (7.24)–(7.26)

$$R_{\text{Translated pixel}} = R_{\text{pixel}} + \left(R - R_{\substack{\text{mask} \\ \text{average}}} \right) \tag{7.24}$$

$$G_{\text{Translated pixel}} = G_{\text{pixel}} + \left(G - G_{\substack{\text{mask} \\ \text{average}}} \right) \tag{7.25}$$

$$B_{\text{Translated pixel}} = B_{\text{pixel}} + \left(B - B_{\substack{\text{mask} \\ \text{average}}} \right) \tag{7.26}$$

This approach assumes that the variability in pixel values does not change with changes in color. Because the color gamut of any set of colorants forms an irregular shape in CIELAB, as seen in Figure 8.4, this assumption is false. The middle gray is used to minimize this error. Despite this limitation, the visualizations appear realistic.

For the visualizations in this book, Matlab was used. It is also possible to use Photoshop by making custom adjustment curves (Berns et al. 2006).

As a final consideration, when using the *D* factor, this should also be applied to the background.

E. SUMMARY

A light source can be defined in a number of ways. In many cases, it can be represented by a CIE standard illuminant of which there are many to choose from. CIE illuminants are used when defining colors colorimetrically and when setting tolerances. If we are producing a material to match a colorimetric specification, visual validation may be necessary. It is important that the lighting well represents the illuminant. This has always been a challenge when the standard illuminant is D50 or D65. There is a standard for defining the quality of a CIE daylight simulator in both the visible and UV wavelength regions. General purpose white lighting is defined by lumens, energy efficiency, correlated color temperature (CCT), and color rendering. Lumens correlate with brightness based on our experiences with incandescent lighting. Light sources are now manufactured with high energy efficiency and incandescent lighting is being phased out because of its poor energy efficiency. CCT indicates whether the white light appears soft, bright, cool, daylight, or other similar terminology. Color rendering is a measure of a light's naturalness. The CIE color rendering index (CRI) indicates whether a source renders familiar colors in the same way as daylight or incandescent lighting. It is a measure of total color difference and for some applications, the direction of change is also important. There is a preference for sources that increase vividness and indices have been derived that improve upon CRI and measure the change in vividness.

Chapter 8

Metamerism and Color Inconstancy

We hope our readers recognize that the single most important aspect of color vision, particularly from the standpoint of color technology, is metamerism. Because of the trichromatic nature of our color vision, spectrally dissimilar stimuli can produce the same visual response. As a consequence, it is possible to produce color matches without using the identical materials. Metamerism has enabled many different color technologies to flourish. Most color reproduction systems including television, photography, movies, and printing rely on three or four primaries to represent our chromatic world. Colorants found to be toxic can be replaced with more benign ones. Colorants can also be replaced in order to reduce cost. Because of metamerism, it is possible to reformulate a color recipe using different colorants. Designers can coordinate the colored items in a room to match one another despite being made using dissimilar colorants. For these examples, metamerism is a blessing. It is also a curse because these matches are often *conditional*, matching for only one observer, and if the metamers are samples, for only one light source. When the change in lighting leads to a large color mismatch, one of the samples changes color dramatically, that is, it exhibits color inconstancy. If either sample can be the standard, the most color constant is a better choice.

A. METAMERISM TERMINOLOGY

In Chapter 2, we define metamerism as the phenomenon in which spectrally different stimuli match to a given observer. We showed an example of a woman standing outdoors and her reproduction on a liquid crystal display. In this chapter, we will focus on physical samples, requiring additional definitions.

- *Metameric:* (i) Pertaining to spectrally different objects or color stimuli that have the same colorimetric coordinates. (ii) Pertaining to objects, having different spectrophotometric curves, that match when illuminated by at least one specific spectral composition and observed by a specific observer.
- *Parameric:* Pertaining to specimens having different spectrophotometric curves that produce approximately the same color sensation under the same illuminating and viewing conditions.
- *Illuminant metamerism:* The property of specimens having different spectral characteristics and having the same color when viewed by a normal observer under a given illuminant, but different colors when viewed under a different illuminant, other conditions remaining the same.
- *Observer metamerism:* The property of specimens having different spectral characteristics and having the same color when viewed by one observer, but different colors when viewed by a different observer under the same conditions.

Billmeyer and Saltzman's Principles of Color Technology, Fourth Edition. Roy S. Berns.

It is a common (and sometimes unpleasant) fact that pairs of colors with different spectral reflectance curves can match under one set of viewing and illuminating conditions but fail to match under another. They are called *metameric pairs* or *metamers*. When the mismatch occurs due to a change in illumination, the phenomenon is called *illuminant metamerism*, shown in Figure 8.1. When the mismatch occurs due to a change in observer, the phenomenon is called *observer metamerism*, shown in Figure 8.2. Strictly, metamers match exactly, having identical colorimetric coordinates for a specific illuminant and observer, that is, a total color difference of zero. In practice, color pairs rarely have a total color difference of zero. In this case, they are called *parameric pairs* or *paramers*.

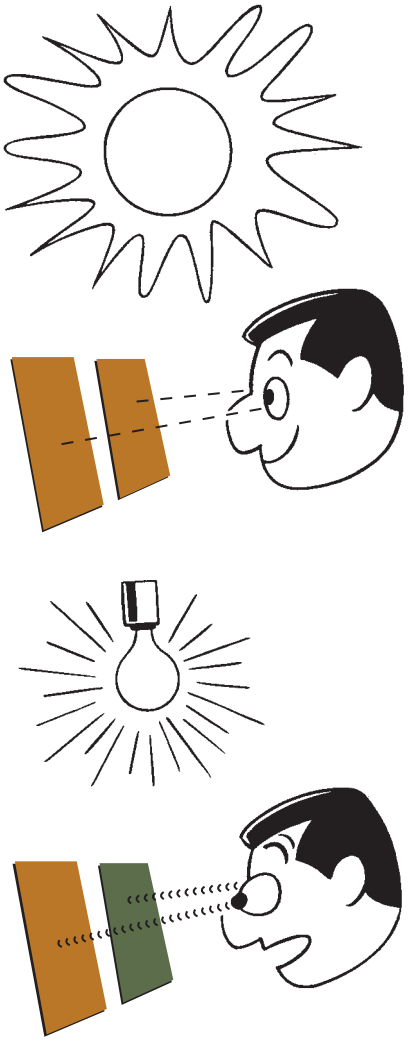

Figure 8.1 Illuminant metamerism.
Source: Courtesy of P. Miller.

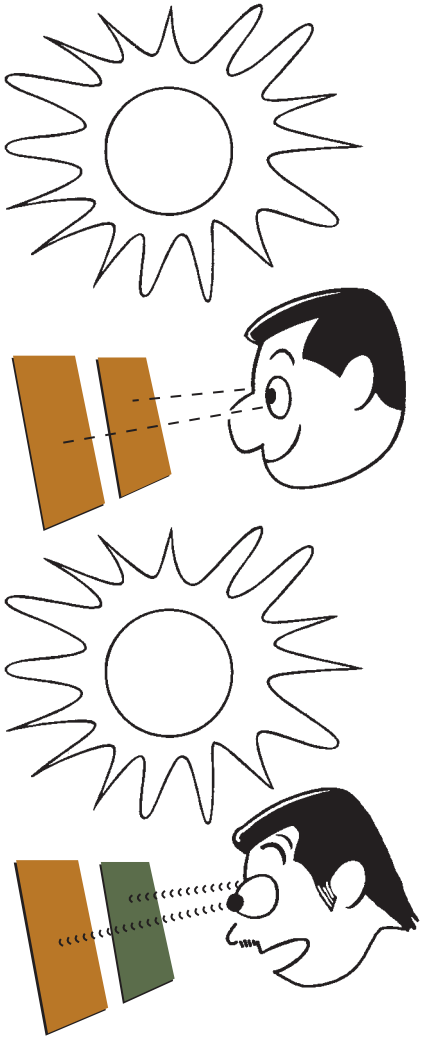

Figure 8.2 Observer metamerism.
Source: Modified drawing by P. Miller.

B. PRODUCING METAMERS

Red, orange, yellow, green, cyan, blue, magenta, black, and white artist acrylic-dispersion paints were used to produce color mixtures. The reflectance spectra of the nine paints are shown in Figure 8.3. Each chromatic paint has a unique shape and cannot be matched spectrally by intermixing any of the other paints. Thus, they are defined as *primaries*. Their color gamut is shown in Figure 8.4, calculated for illuminant D50 and the 1931 standard observer. This set of paints is capable of matching a large range of colors.

A neutral color having 0.2 reflectance factor across wavelength was defined as a standard. Matches were formulated using all the combinations of three paints plus white. For these eight paints, there are 56 possible combinations (e.g. red, yellow, blue; red, yellow, green; red, yellow, black).

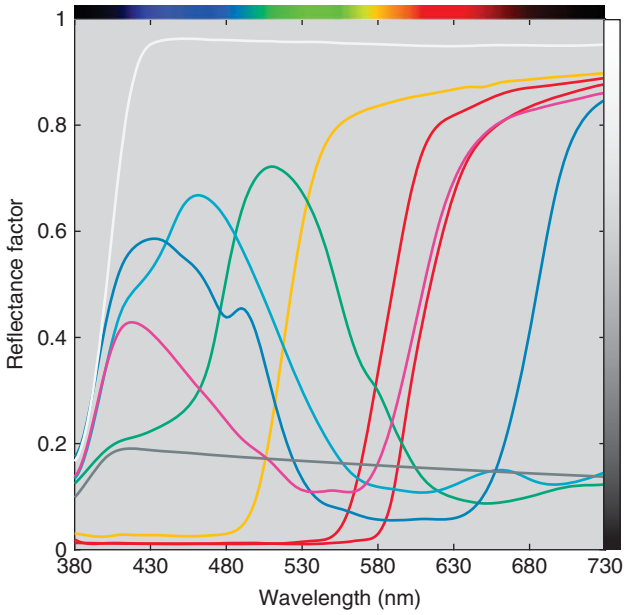

Figure 8.3 Spectral reflectance factor of red, orange, yellow, green, cyan, blue, magenta, black, and white artist acrylic dispersion paints. The green, cyan, blue, magenta, and black paints were mixed with the white paint to better reveal their spectral shapes.

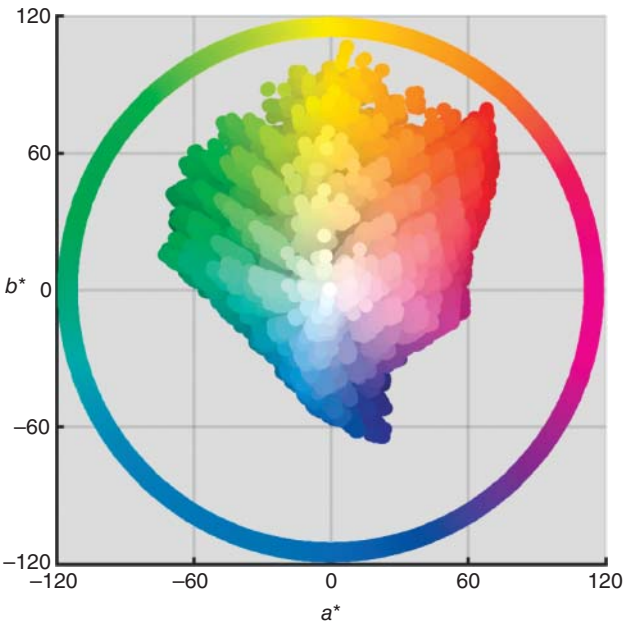

Figure 8.4 Color gamut achieved by intermixing red, orange, yellow, green, cyan, blue, magenta, black, and white artist paints. CIELAB calculated using illuminant D50 and the 1931 standard observer.

Each combination matched the standard as closely as possible when viewed by the 1964 standard observer under illuminant D65. (The mixing was computational, the subject of Chapter 9.) Color differences ranged between 0 and 25 ΔE_{00}. Mixtures with color differences greater than 0 were combinations that could not match the standard, for example, red, yellow, and orange. The standard and the 16 combinations matching the standard are plotted in Figure 8.5. There is a wide range of spectral shapes, particularly at longer wavelengths. The metamers are similar in reflectance below 500 nm. This occurred because all of the matches contained either red, yellow, or orange, all of which absorb light below 500 nm, as seen in Figure 8.3. Across all the wavelengths beyond 400 nm, the metamers crossed the standard between three and six times. Multiple crossovers are a good indicator of a metameric match. The number of crossovers and their locations depend on the absorption and scattering properties of the primaries (Berns and Kuehni 1990).

We describe in Chapter 7 that most light booths having a "daylight" or "D65" button do not reproduce the spectrum of illuminant D65. As an example, a controllable lighting system containing red, green, and blue LEDs produced a source matching the chromaticities of D65. The metamers' spectra were used to produce visualizations illuminated by D65, the RGB simulated D65, and a blackbody radiator at 2000 K (equivalent to a dimmed 60 W incandescent lightbulb), shown in Figure 8.6. The RGB daylight caused some of the metamers to become bluish or greenish. When illuminated by incandescent light, some of the metamers

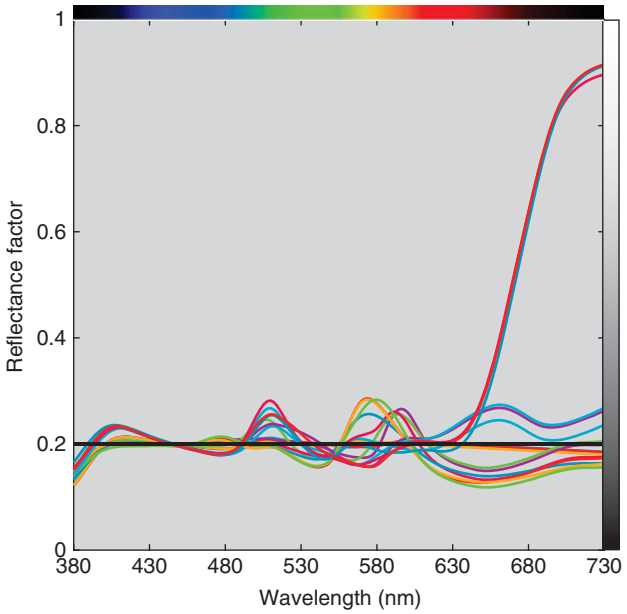

Figure 8.5 Spectral reflectance factor of the standard (bold black line) and the 16 metamers matching the standard under D65 for the 1964 standard observer. (Color coding is arbitrary.)

became noticeably greenish or reddish. The observer was changed from the 1964 standard observer to the "uncommon observer" (Berns 2016), corresponding to a color-normal observer very different from the 1931 standard observer (Fairchild and Heckaman 2013), and illuminated by D65. The color changes are similar to those occurring for the

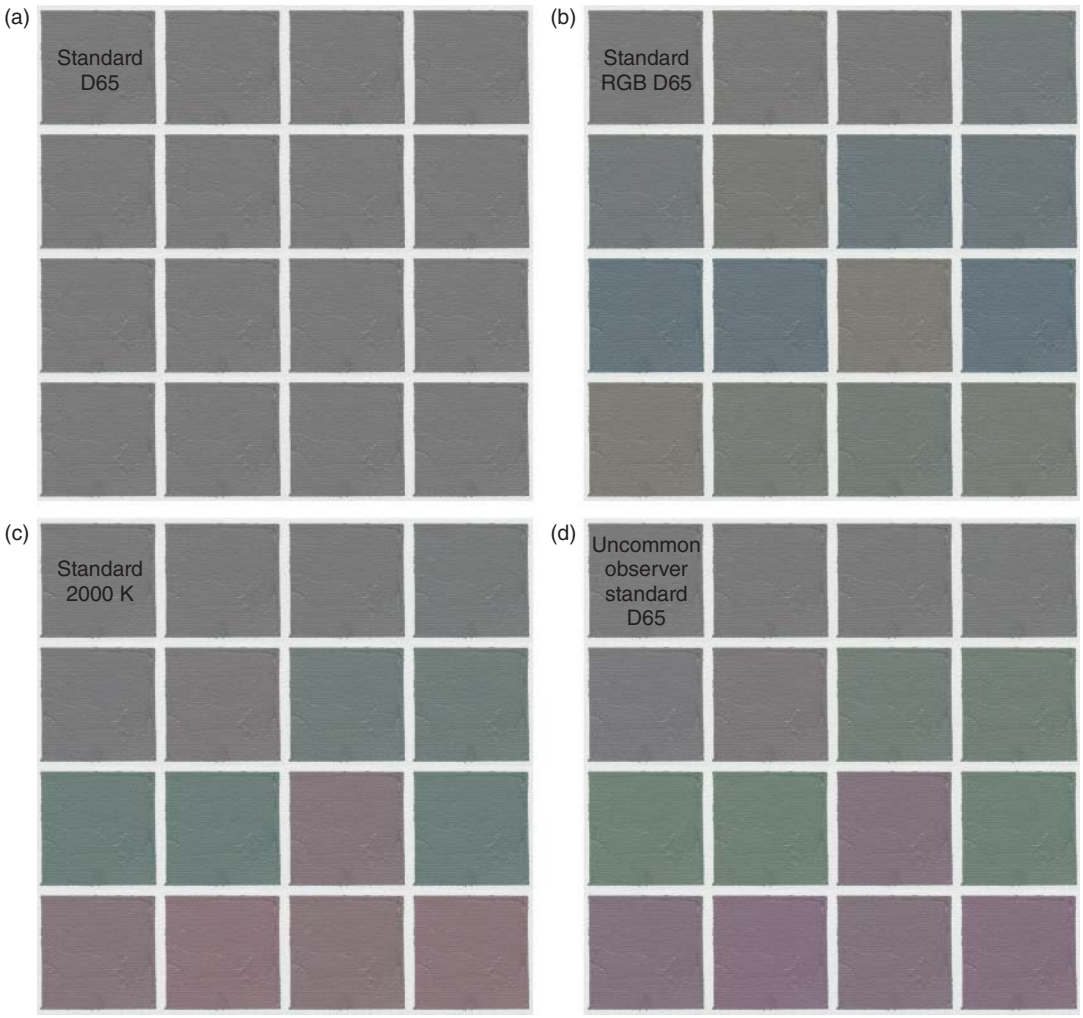

Figure 8.6 Visualization of the standard (top left) and 15 metamers when viewed by the CIE 1964 standard observer under (a) illuminant D65, (b) RGB LED simulating D65, (c) blackbody radiator at 2000 K, and (d) viewed by the uncommon observer under D65.

1964 standard observer and incandescent illumination. This correlation was found previously by Billmeyer and Saltzman (1980) and Nardi (1980).

The metamers, visualized in Figure 8.6, were ordered from left to right and from top to bottom in increasing spectral reflectance RMS difference from the standard. For this set of metamers, spectral differences and color differences were somewhat correlated. Even so, it would be challenging to predict these color changes from spectral differences, or, that these spectra can produce a match.

C. INDICES OF METAMERISM

The most important engineering property when developing a color recipe is for the formulation to be minimally metameric to the standard. Color-formulation software, described in Chapter 9, are used to calculate a number of potential recipes, each with a different degree of metamerism to the standard, such as shown above. We need a metric to help select the best recipe. For this, *indices of metamerism* are used.

Special Index of Metamerism

The most common indices are based on colorimetric coordinates. We define a *reference condition*, in which the metameric pair match, and a *test condition*, for evaluating the degree of metamerism. For example, the reference condition is CIE illuminant D65 and the 1964 10° standard observer and the test condition is illuminant A and the 1964 10° standard observer. Illuminant D65 is called the *primary illuminant* and illuminant A is called the *secondary illuminant*. An index of metamerism is the color difference

between a recipe (or corresponding batch) and the standard for the test condition. CIEDE2000 would be used to calculate the color difference. This is known as a *special index of metamerism, change in illuminant* (CIE 2018).

Before the prevalence of fluorescent sources, illuminant metamerism was evaluated under illuminant A for samples matching under D65. If a pair of metameric samples matched for both illuminants, it was assumed that metamerism would not be a problem under various real sources (e.g. Billmeyer 1963). This practice was abandoned as fluorescent illumination became commonplace, particularly narrow-band types. This has resulted in the notion of secondary, tertiary, quaternary, and so on illuminants and the need to rank order illumination. For example, Berns, Fairchild, and Beering (1988) found that for standards that required matching under illuminants D65, A, F2, and F11, the assignment of primary, secondary, tertiary, and quaternary illuminants had a significant effect on match quality. Having rank ordered the test conditions, a metameric index (MI) can be a weighted average of each color difference, shown in Eq. (8.1) where w defines a weight and n is the specific illuminant. Another approach is to calculate the maximum color difference, shown in Eq. (8.2). This eliminates the need to rank order. Any statistical metric can be used such as the mean or a given percentile. Our preference is either Eq. (8.1) or (8.2)

$$\mathrm{MI}_{\mathrm{weighted}} = \frac{\sum_n w_n \Delta E_{\mathrm{oo},n}}{\sum_n w_n} \tag{8.1}$$

$$\mathrm{MI}_{\mathrm{maximum}} = \max(\Delta E_{\mathrm{oo},n}) \tag{8.2}$$

Most color-matching software requires a reference condition. There might be cases where a reference condition is undefined: "I want the batch to match under all lighting, of course." Any formulator would agree; unfortunately, this may not be possible. An interesting approach is to formulate where each illuminant is the reference illuminant, calculate a MI using Eq. (8.2) for each test condition, and use the formulation with the smallest MI (Ruiz 2002). There is not a standardized index for evaluating illuminant metamerism. Choudhury and Chatterjee (1996) and Kuo and Luo (1996a,b) have compared the performance of several indices.

A *special index of metamerism, change in observer* (CIE 2018) can also be calculated. The Asano, Fairchild, and Blondé (2016) model described in Chapter 2 can be used to calculate cone fundamentals for specific parameters of interest. These can be transformed to color-matching functions using least squares and an index of metamerism calculated. As shown in Figure 8.6, illuminant and observer metamerism are correlated. Thus, minimizing illuminant metamerism minimizes observer metamerism simultaneously and as a consequence, an index of observer metamerism is largely unnecessary.

Quite often, a pair of samples will appear as metamers, that is, closely match under a reference condition and mismatch under a test condition, but not have colorimetric equality under any illuminant. Such samples form a *parameric pair*. In order to calculate a special index of metamerism, the batch's colorimetric coordinates for the test condition are corrected to minimize the effect caused by the small color difference under the reference condition. The method recommended by the CIE (2018) is shown in Eqs. (8.3)–(8.5):

$$X'_{\mathrm{Bat,test}} = X_{\mathrm{Bat,test}} \frac{X_{\mathrm{Std,reference}}}{X_{\mathrm{Bat,reference}}} \tag{8.3}$$

$$Y'_{\mathrm{Bat,test}} = Y_{\mathrm{Bat,test}} \frac{Y_{\mathrm{Std,reference}}}{Y_{\mathrm{Bat,reference}}} \tag{8.4}$$

$$Z'_{\mathrm{Bat,test}} = Z_{\mathrm{Bat,test}} \frac{Z_{\mathrm{Std,reference}}}{Z_{\mathrm{Bat,reference}}} \tag{8.5}$$

where the tristimulus values of the batch calculated for the test illuminant are scaled by the ratio of the tristimulus values calculated for the reference condition. The corrected tristimulus values, notated by the prime superscript, are used to calculate a MI. The batch can also be corrected spectrally, shown in the nearby sidebar.

Spectral Correction for Paramers

The multiplicative correction recommended by the CIE, unfortunately, has poor performance (Li and Berns 2007) and we do not advocate its use. When the colorants are known, their concentrations are adjusted until a tristimulus match is achieved. This is *batch correction*, a common feature of color-formulation software. When the colorants are unknown, batch correction is approximated.

One aspect of the approximation is assuming a linear relationship between concentration and spectral reflectance for colorants that both scatter and absorb. (We describe in Chapter 9 that this relationship is nonlinear.) These *pseudo-colorants*, which function as primaries, can be statistical, based on principal or independent component analysis of a set of physical samples (Li and Berns 2007), color matching functions (Fairman 1987), or subtractive primary spectra (Berns 1994; Attarchi and Amirshahi 2009). Only three primaries are required because the correction is for three tristimulus values. The relationship between primary spectra, R_λ, concentration, c, and their mixture, $R_{\lambda,\mathrm{mixture}}$, is shown in either Eq. (8.6) or Eqs. (8.7)–(8.10):

$$R_{\lambda,\mathrm{mixture}} = c_1 R_{\lambda,1} + c_2 R_{\lambda,2} + c_3 R_{\lambda,3} \tag{8.6}$$

$$\mathbf{R} = \mathbf{PC} \tag{8.7}$$

where

$$\mathbf{R} = \begin{pmatrix} R_{\lambda,\text{mixture}} \\ \vdots \\ R_{\lambda,\text{mixture}} \end{pmatrix} \tag{8.8}$$

$$\mathbf{P} = \begin{pmatrix} R_{\lambda,1} & R_{\lambda,2} & R_{\lambda,3} \\ \vdots & \vdots & \vdots \\ R_{\lambda,1} & R_{\lambda,2} & R_{\lambda,3} \end{pmatrix} \tag{8.9}$$

$$\mathbf{C} = \begin{pmatrix} c_1 \\ c_2 \\ c_3 \end{pmatrix} \tag{8.10}$$

We define a ($\lambda \times 3$) matrix, **A**, composed of either ASTM tristimulus weights or calculated from the product of the reference illuminant, **S**, and reference observer, **T**, shown in Eq. (8.11):

$$\mathbf{A} = \mathbf{S}\mathbf{T}' \tag{8.11}$$

where **T** and **S** are defined in Eqs. (2.8) and (2.9) (Chapter 2).

The tristimulus matrix, **M**, for the three primaries at unit concentration is calculated using Eq. (8.12)

$$\mathbf{M} = \mathbf{A}'\mathbf{P} \tag{8.12}$$

The relationship between concentration and the tristimulus values of a mixture is shown in Eq. (8.13)

$$\begin{pmatrix} X_{\text{mixture}} \\ Y_{\text{mixture}} \\ Z_{\text{mixture}} \end{pmatrix} = \mathbf{M}\mathbf{C} \tag{8.13}$$

The difference in tristimulus values between the standard and batch can be used to calculate concentration, shown in Eq. (8.14)

$$\mathbf{C} = \mathbf{M}^{-1} \begin{pmatrix} X_{\text{Std}} - X_{\text{Bat}} \\ Y_{\text{Std}} - Y_{\text{Bat}} \\ Z_{\text{Std}} - Z_{\text{Bat}} \end{pmatrix} \tag{8.14}$$

These concentrations are used to calculate a reflectance spectrum using Eq. (8.7). This reflectance spectrum and the reflectance of the batch are added together wavelength by wavelength. This corrects the batch to have tristimulus values equal to the standard. This reflectance spectrum can be both positive and negative depending on the tristimulus differences. Equations (8.6)–(8.14) can be combined into a single formula, shown in Eq. (8.15) (Li and Berns 2007).

Following spectral correction, a MI is calculated. There is a limit to the effectiveness of correcting paramers, whether using a colorimetric or spectral correction. As a rule of thumb, the color difference of a pair of paramers should not exceed $5\Delta E^*_{ab}$ for the reference condition (Berns 2008b)

$$\underset{\text{corrected}}{\mathbf{R}_{\text{Bat}}} = \mathbf{R}_{\text{Bat}} + \mathbf{P}(\mathbf{A}\prime\mathbf{P})^{-1}\mathbf{A}'(\mathbf{R}_{\text{Std}} - \mathbf{R}_{\text{Bat}}) \tag{8.15}$$

General Index of Metamerism

Metamerism, by definition, occurs because of spectral differences between samples. The RMS spectral difference could define an index, shown in Eq. (8.16)

$$\text{MI}_{\text{RMS}} = \sqrt{\frac{\sum_{\lambda=1}^{n} \Delta R_\lambda^2}{n}} \tag{8.16}$$

A spectral-based index is sometimes called a *general index of metamerism*. Each wavelength has equal weighting. Given that our sensitivities to wavelength are unequal, it makes sense to weight each wavelength differently, shown in Eq. (8.17):

$$\text{MI}_{w\ \text{RMS}} = \sqrt{\frac{\sum_{\lambda=1}^{n} (w_\lambda \Delta R_\lambda)^2}{n}} \tag{8.17}$$

where w_λ defines the weight.

Two weighting functions might be V_λ or the sum of a set of color-matching functions, shown in Eqs. (8.18) and (8.19)

$$w_\lambda = V_\lambda \tag{8.18}$$

$$w_\lambda = (\bar{x} + \bar{y} + \bar{z})_\lambda \tag{8.19}$$

V_λ is problematic because our response to chromaticness is ignored. Summing the color-matching functions ignores their linear independence, which was recognized and corrected by Nimeroff and Yurow (1965), shown in Eq. (8.20)

$$w_\lambda = \left(\sqrt{\bar{x}^2 + \bar{y}^2 + \bar{z}^2}\right)_\lambda \tag{8.20}$$

The weighting function we prefer to was derived by Viggiano (1990, 2001) and described in a nearby sidebar.

Viggiano Spectral-Weighting Function

Viggiano (1990, 2001) recognized that color matching functions (or any transformation such as cone fundamentals) do not correlate exactly with perceived color differences because spectral differences are not linearly related to color differences. The cube-root function of CIELAB is evidence of a lack of linearity. He also recognized that the weighting should depend on the standard's color. Viggiano calculated how the change in a single wavelength affected a CIELAB total color difference for a given standard, shown in Eqs. (8.21)–(8.24):

$$w_\lambda = \sqrt{\left(\frac{\partial L^*}{\partial R_\lambda}\right)^2 + \left(\frac{\partial a^*}{\partial R_\lambda}\right)^2 + \left(\frac{\partial b^*}{\partial R_\lambda}\right)^2} \tag{8.21}$$

$$\frac{\partial L^*}{\partial R_\lambda} = 116 a_{\lambda,y} \frac{1}{3Y}\left(\frac{Y}{Y_n}\right)^{\frac{1}{3}} \tag{8.22}$$

$$\frac{\partial a^*}{\partial R_\lambda} = 500\left[a_{\lambda,\bar{x}} \frac{1}{3X}\left(\frac{X}{X_n}\right)^{\frac{1}{3}} - a_{\lambda,\bar{y}} \frac{1}{3Y}\left(\frac{Y}{Y_n}\right)^{\frac{1}{3}}\right] \tag{8.23}$$

$$\frac{\partial b^*}{\partial R_\lambda} = 200\left[a_{\lambda,\bar{y}} \frac{1}{3Y}\left(\frac{Y}{Y_n}\right)^{\frac{1}{3}} - a_{\lambda,\bar{z}} \frac{1}{3Y}\left(\frac{Z}{Z_n}\right)^{\frac{1}{3}}\right] \tag{8.24}$$

where a_λ is an ASTM tristimulus weight or the product of the reference illuminant and color matching function (Eq. (8.11)).

Spectral weights were calculated for a spectrally non-selective sample with $L^* = 50$ for illuminant E and the 1964 standard observer using Eqs. (8.20) and (8.21), the results shown in Figure 8.7. The Nimeroff and Yurow approach using color-matching functions resulted in a weight having two peaks. (Cone fundamentals produce the same result.) The Viggiano weight has three peaks, more in line with trichromatic vision. In applications where it is impractical to calculate a weight for each color, we recommend a weight based on a neutral gray with $L^* = 50$, as shown in Figure 8.7.

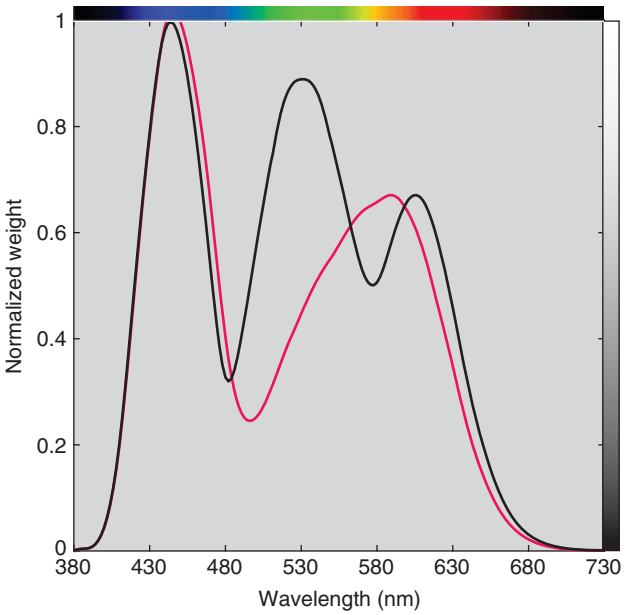

Figure 8.7 Normalized spectral weights for the 1964 standard observer, illuminant E, and a sample with $L^* = 50$, $a^* = b^* = 0$ using Eq. (8.20) (red line) and Eq. (8.21) (black line).

Using Indices of Metamerism

Evaluating the degree of metamerism between two stimuli requires some experience. Our advice is to first look at the spectra of the metameric pair. For samples, these are the reflectance curves. How similar are they to one another? If they are very different, metamerism will occur. If there is the opportunity to change colorants, do so. If there isn't, recognize that the match is conditional. There is no substitute for looking at spectral curves when metamerism is suspected. Second, calculate a special index of illuminant metamerism for each illuminant of interest. If some illuminants are known to be more important than others, a weighted average is useful. Finally, look at the individual colorimetric errors (e.g. ΔL^*, ΔC^*_{ab}, ΔH^*_{ab}). Depending on the application, error in one dimension and, possibly, one direction may be more important to evaluate than the total color difference.

As a final remark, it is imperative to use the actual light source spectral power distributions or a CIE illuminant closely matching the actual source when calculating colorimetric coordinates for use in indices of metamerism. Just as visual differences are dramatically affected by illumination, so are colorimetric differences. Calculations for D65 cannot be expected to correlate with visual evaluations under fluorescent daylight. Similar poor correlation will result when viewing samples under "horizon" light (incandescent with a correlated color temperature of around 2300 K) while performing colorimetric calculations for illuminant A (2856 K). Kuo and Luo (1996a,b) found a significant improvement in correlation between visual assessment and calculated indices of illuminant and observer metamerism when actual sources were used rather than CIE illuminants.

D. COLOR INCONSTANCY AND INDICES OF COLOR INCONSTANCY

We describe in Chapter 2 the concepts of incomplete chromatic adaptation, cognitive discounting of the color of the illumination, and as a consequence, the tendency for objects to appear color constant. This tendency is also aided by our poor color memory (Brady et al. 2013). When we look closely at colored objects under multiple lighting we observe hue shifts, shown in Figure 8.8. Color constancy has not occurred. These materials exhibit *color inconstancy*. Only materials having nonselective reflectances are color constant (Wright 1981a) such as the gray standard used above.

- *Color inconstancy:* A single object changing color with changes in the color of the illumination.
- *Metameric pair:* Two objects having dissimilar color inconstancy.

An index of color inconstancy is very useful for many applications. For example, safety colors should be color constant. Color-order systems are often viewed under nonstandard lighting and as a consequence, color constancy is an important engineering requirement (McCamy 1985). Colorants used in printing should lead to color constancy, again, because we view printed documents under a wide variety of illuminations.

Many color technologists ignore issues surrounding color inconstancy because their job is to match the standard. If the standard has significant color inconstancy, they will match it anyway. However, the customer may not be aware of their standard's engineering defect. If the degree of color inconstancy is large, the product's quality will certainly suffer. There may be long-term hidden costs if the product is rejected at a later time.

Colors can be defined solely by their colorimetric values and it may be necessary to produce materials matching such specifications. There can be many formulations depending on the number of primaries in the coloration system. We believe that the most color constant formulation would be the best formulation.

A *color-inconstancy index*, (*CII*), can be as simple as calculating the color difference between a sample's CIELAB coordinates under two different illuminants. However, correspondence between CIELAB and a sample's actual appearance worsens as an illuminant's CCT diverges from D65. Suppose that we could formulate a color constant Munsell Book of Color or Natural Colour System. We would find that the CIELAB coordinates for each sample would be changing with changes in illumination rather than remaining the same. The problem is that the chromatic adaptation transformation (CAT) embedded in CIELAB is inaccurate: X/X_n, Y/Y_n, and Z/Z_n. One of the reasons for developing color appearance models was to incorporate a more accurate CAT.

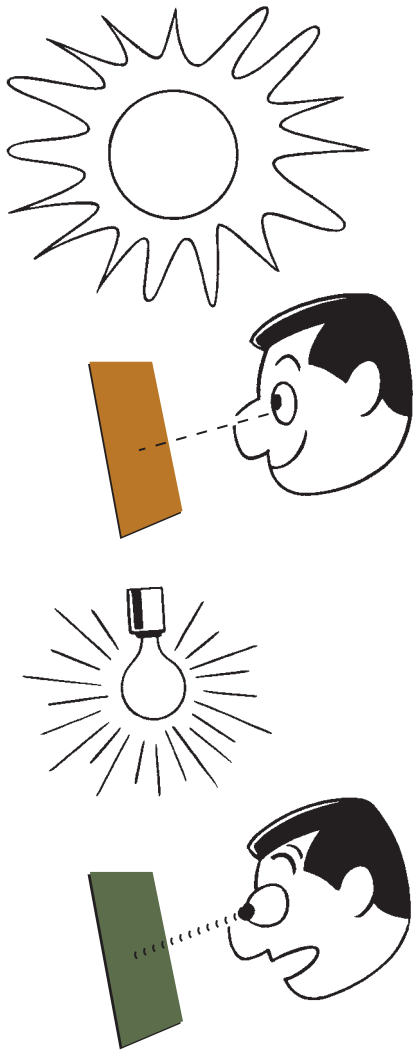

Figure 8.8 Color inconstancy.
Source: Modified drawing by P. Miller.

Berns and Billmeyer (1983) proposed a CII where a more accurate CAT was used to transform the tristimulus values calculated using any illuminant to D65. This included both reference and test illuminants. The transformed coordinates were used to calculate a CIELAB total color difference as an index of color inconstancy. The same approach was described by Luo and Hunt using a different CAT (1998). The Color Measurement Committee of the Society of Dyers and Colourists recommended the Luo and Hunt approach using CMC as the color difference formula (Luo et al. 1999). This was updated in 2002 using the chromatic adaptation transform embedded in CIECAM02 (CIE 2004b). The index is called *CMCCON02* (Luo et al. 2003). This became an ISO textiles standard in 2007 (ISO 2007b).

The general approach is shown in Eqs. (8.25)–(8.29) where a CAT, in this case based on cone fundamentals, is used to transform a sample's tristimulus values calculated

for a test illuminant to its corresponding tristimulus values for a reference illuminant, notated by the prime superscript

$$\begin{pmatrix} X'_{\text{Test}} \\ Y'_{\text{Test}} \\ Z'_{\text{Test}} \end{pmatrix} = \mathbf{M}_{\text{CAT}} \begin{pmatrix} X_{\text{Test}} \\ Y_{\text{Test}} \\ Z_{\text{Test}} \end{pmatrix} \tag{8.25}$$

$$\mathbf{M}_{\text{CAT}} = \mathbf{M}_{\text{LMS}}^{-1} \mathbf{M}_{\nu\text{KD}} \mathbf{M}_{\text{LMS}} \tag{8.26}$$

$$L^*_{\text{Test}} a^*_{\text{Test}} b^*_{\text{Test}} = f(X'_{\text{Test}}, Y'_{\text{Test}}, Z'_{\text{Test}}) \tag{8.27}$$

$$L^*_{\text{Ref}} a^*_{\text{Ref}} b^*_{\text{Ref}} = f(X_{\text{Ref}}, Y_{\text{Ref}}, Z_{\text{Ref}}) \tag{8.28}$$

$$\text{CII} = \Delta E(2{:}2{:}1) = f(L^*_{\text{Test}}, a^*_{\text{Test}}, b^*_{\text{Test}}; L^*_{\text{Ref}}, a^*_{\text{Ref}}, b^*_{\text{Ref}}) \tag{8.29}$$

The transformed tristimulus values and the sample's tristimulus values calculated for the reference illuminant are used to calculate a color difference. This color difference defines the CII. Lightness and chroma parametric factors, for example, l and c for CMC or K_L and K_C for CIEDE2000, are set to two in order to reduce the importance of lightness and chroma differences compared with hue differences, generally the most objectionable.

A total color difference, whether CIEDE2000 or CMC, is a measure of magnitude, not direction. Looking at the visualization shown in Figure 8.6, greenish changes might be more objectionable than red changes, or vice versa. This can be remedied by difference splitting (CIE 2001; Nobbs 2002) and calculating ΔH_{00} as a color inconstancy index, the formulas shown in Chapter 5. In this manner, direction is retained. This can be further simplified using Eqs. (8.30) and (8.31) with a small loss of accuracy. (C_{ucd} is described in Chapter 4.) We recommend using $|\Delta H_{00}|$ or $|\Delta H_{\text{ucd}}|$ as an index of color inconstancy rather than a total color difference:

$$\text{CII} = |\Delta H_{\text{ucd}}| = 2\sqrt{C_{\text{ucd,Test}} C_{\text{ucd,Ref}}} \times \sin\left(\frac{h_{ab,\text{Test}} - h_{ab,\text{Ref}}}{2}\right) \tag{8.30}$$

where

$$C_{\text{ucd}} = 58.65 \ln(0.045 C^*_{ab} + 1) \tag{8.31}$$

Some of our readers might notice an inconsistency in the procedures for calculating metamerism and color inconstancy indices. When calculating an MI, the CIELAB data for any illuminant is used whereas when calculating a CII, tristimulus data are transformed using a CAT to a single reference illuminant, such as D65, and then calculating CIELAB. When Berns and Billmeyer (1983) proposed using a more accurate CAT, they advocated its use for both an MI and CII using the phrase "*constant chromatic adaptation*." Choudhury and Chatterjee (1996) found improved correlation using this approach when comparing visual assessment with metameric indices. We were aware of this inconsistency when writing the third edition and chose to not address this directly. We believed that any distortions in CIELAB were negligible locally. That is, color differences would be similar for commonly used illuminants. The CIE did not address this at all, stating that CIELAB should only be used for illuminants "not too different from that of average daylight" (CIE 1986). Without an alternative, using CIELAB for non-daylight illuminants has been common practice since its inception. The current CIE recommendations require the use of a CAT and a color appearance model (CIE 2018) and excellent progress has been made, for example, CAM02-SCD (Luo, Cui, and Li 2006) and CAM16-UCS (Li et al. 2017). Another approach is to use a uniform material color equivalency space such as *WLab* (Derhak and Berns 2015a,b).

Despite such progress, we believe that CIELAB will continue as the most used color space, particularly as a legacy specification and its necessity for calculating CIEDE2000, the current internationally standardized color-difference formula for industrial applications (ISO/CIE 2014). Incorporating a more accurate CAT into CIELAB is shown in a nearby sidebar.

Improving CIELAB by Incorporating a More Accurate Chromatic-Adaptation Transformation

Berns and Billmeyer (1983) provided a step-by-step procedure for incorporating a CAT into CIELAB. Their updated procedure is the following using CAT16 (Li et al. 2017):

Step 1. Calculate tristimulus values for a perfect reflecting diffuser using both D65 (reference illuminant) and the non-daylight source (test illuminant) for a single observer using Eq. (8.32)

$$\begin{pmatrix} X_n \\ Y_n \\ Z_n \end{pmatrix}_{\text{Illuminant}} = \mathbf{TS} \begin{pmatrix} 1 \\ \vdots \\ 1 \end{pmatrix} \tag{8.32}$$

Step 2. Transform the Step 1 tristimulus values to pseudo-cone fundamentals using Eq. (8.33)

$$\begin{pmatrix} R \\ G \\ B \end{pmatrix} = \begin{pmatrix} 0.401288 & 0.650173 & -0.051461 \\ -0.250268 & 1.204414 & 0.045854 \\ -0.002079 & 0.048952 & 0.953127 \end{pmatrix}_{\text{CAT16}} \begin{pmatrix} X \\ Y \\ Z \end{pmatrix} \tag{8.33}$$

Step 3. Calculate the von Kries diagonal matrix for complete adaptation, shown in Eq. (8.34) using the Step 2 pseudo-cone fundamentals for D65 and the test illuminant.

$$\begin{pmatrix} R' \\ G' \\ B' \end{pmatrix} = \begin{pmatrix} \frac{R_{n,\mathrm{D65}}}{R_{n,\mathrm{Test}}} & 0 & 0 \\ 0 & \frac{G_{n,D65}}{G_{n,\mathrm{Test}}} & 0 \\ 0 & 0 & \frac{B_{n,D65}}{B_{n,\mathrm{Test}}} \end{pmatrix}_{vK} \begin{pmatrix} R \\ G \\ B \end{pmatrix} \tag{8.34}$$

Step 4. Calculate corresponding tristimulus values at a constant chromatic adaptation of D65 using Eq. (8.35)

$$\begin{pmatrix} X' \\ Y' \\ Z' \end{pmatrix} = \mathbf{M}_{\mathrm{CAT16}}^{-1} \mathbf{M}_{vK} \mathbf{M}_{\mathrm{CAT16}} \mathbf{T} \mathbf{S}_{\mathrm{Test}} \mathbf{R} \tag{8.35}$$

Step 5. Calculate CIELAB coordinates where X_n, Y_n, and Z_n are the tristimulus values for D65 and the selected observer. For the 1964 standard observer, L^*, a^*, and b^* are calculated using Eqs. (8.36)–(8.39)

$$L^* = 116 f\left({}^{Y}/_{100.00}\right) - 16 \tag{8.36}$$

$$a^* = 500\left[f\left({}^{X}/_{94.81}\right) - f\left({}^{Y}/_{100.00}\right)\right] \tag{8.37}$$

$$b^* = 200\left[f\left({}^{Y}/_{100.00}\right) - f\left({}^{Z}/_{107.32}\right)\right] \tag{8.38}$$

$$f(x) = \begin{cases} (x)^{1/3} & (x) > \left({}^{24}/_{116}\right)^3 \\ \left({}^{841}/_{108}\right) x + {}^{16}/_{116} & (x) \le \left({}^{24}/_{116}\right)^3 \end{cases} \tag{8.39}$$

Note that the values for the denominators in the CIELAB formulas change only with a change in observer. They remain constant for all non-daylight sources. We also recommend this procedure for any source or illuminant dissimilar to D65, even if it "is not too different from that of average daylight."

Concatenated (right-hand side of Eq. (8.35)) chromatic adaptation matrices for illuminant A and D50, both for the 1964 standard observer are shown in Eqs. (8.40) and (8.41), respectively

$$\underset{\substack{\text{ill } A \\ 1964}}{\mathbf{M}_{\mathrm{CAT}}} = \begin{pmatrix} 0.9482 & -0.1977 & 0.2614 \\ -0.0270 & 1.0339 & -0.0113 \\ -0.0027 & 0.0903 & 2.8008 \end{pmatrix} \tag{8.40}$$

$$\underset{\substack{D50 \\ 1964}}{\mathbf{M}_{\mathrm{CAT}}} = \begin{pmatrix} 0.9884 & -0.0436 & 0.0439 \\ -0.0059 & 1.0070 & -0.0017 \\ -0.0004 & 0.0149 & 1.3000 \end{pmatrix} \tag{8.41}$$

Metamer and Color Inconstancy Cartoons

The cartoons depicting metamerism and color inconstancy shown in Figures 8.1, 8.2, and 8.8 are based on two wool fabrics dyed by Dr. Roland Derby for an Inter-Society Color Council meeting. Under incandescent illumination, one sample appears green and the other, brown. Under daylight around 6500 K, they match. Under skylight with a CCT of 30 000 K, they again mismatch; however, the sample that appeared brown under incandescent now appears greenish and vice versa, first noted by Johnston (1973)! Their reflectance spectra are shown in Figure 8.9. The spectra were used to make visualizations, shown in Figure 8.10. The samples are, indeed, remarkable.

These samples were used to calculate various metameric and color constancy indices where Samples 1 and 2 were defined as the standard and batch, respectively. The 1964 standard observer was used for all the calculations. The reference illuminant was D65 and the test illuminant was a blackbody radiator with a color temperature of 2000 K. The colorimetric data are listed in Table 8.1 and the indices are listed in Table 8.2. The pair is a parameric pair with a ΔE_{00} of 0.2.

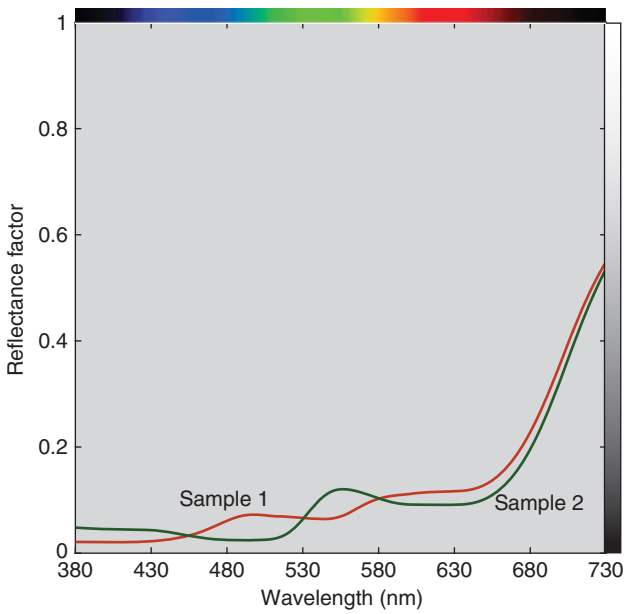

Figure 8.9 Two wool samples exhibiting metamerism.

Figure 8.10 Visualization of the spectra plotted in Figure 8.9 for each listed illuminant and the 1964 standard observer.

Equation (8.15) was used to correct the batch's spectrum where the spectra for red, yellow, and blue, plotted in Figure 8.3, were used as pseudo-colorants. Following correction, the degree of metamerism was 7.0 ΔE_{00}. Because the 2000 K illuminant is so different from D65, the tristimulus values for the standard and batch were transformed to D65 using Eqs. (8.32)–(8.39). This increased the MI to 11.5. The Viggiano weighting was used to calculate a general index of metamerism, Eqs. (8.17) and (8.21). Because this weighting changes with color, it is difficult to interpret the value. However, if a set of formulations are compared, only rank order is required. The degree of color inconstancy of the batch was 6.1 $\Delta E_{00\,(2:2:1)}$ and 9.9 ΔH_{ucd}.

Table 8.2 Indices of metamerism (MI) and color inconstancy (CII) using the data shown in Table 8.1.

Index	Metric	Formulas	Value
MI	ΔE_{00}	Equation (5.35)	7.0
MI′	ΔE_{00}	Equations (5.35) and (8.15)	11.5
MI	Viggiano	Equations (8.17) and (8.21)	7.99E−04
CII	$\Delta E_{00\,(2:2:1)}$	Equations (5.35) and (8.32)–(8.39)	6.3
CII	ΔH_{ucd}	Equations (8.32)–(8.39) and (8.30)	9.9

Table 8.1 Colorimetric values of Sample 1 (standard) and Sample 2 (batch) for each listed condition using the 1964 standard observer.

		X_n	Y_n	Z_n	L^*	a^*	b^*	C^*_{ab}	h_{ab}
Illuminant	D65	94.81	100.00	107.15	100.00	0.00	0.00	0.00	
Illuminant	2000 K	128.54	100.00	14.01	100.00	0.00	0.00	0.00	
		X	Y	Z	L^*	a^*	b^*	C^*_{ab}	h_{ab}
Standard	D65	8.42	8.19	3.86	34.38	5.95	20.79	21.62	74.03
Batch	D65	8.31	8.08	3.75	34.16	5.92	21.06	21.88	74.31
	Δ	−0.11	−0.11	−0.11	−0.23	−0.03	0.28	0.26	0.27
Corrected batch		8.42	8.19	3.86	34.38	5.95	20.79	21.62	74.03
	Δ	0.00	0.00	0.00	0.00	0.00	0.00	0.00	0.00
Standard	2000 K	14.39	9.81	0.61	37.49	10.41	21.77	24.13	64.44
Corrected batch	2000 K	13.09	9.66	0.48	37.22	4.08	27.01	27.32	81.42
	Δ	−1.30	−0.15	−0.14	−0.27	−6.34	5.24	3.18	16.98
Standard'	2000 K′	10.39	9.75	5.98	37.39	9.16	15.67	18.15	59.71
Corrected batch'	2000 K′	9.15	9.66	5.14	37.22	−0.06	19.15	19.15	90.18
	Δ	−1.24	−0.09	−0.84	−0.17	−9.22	3.48	1.00	30.48

E. SUMMARY

Metamerism occurs when materials matching in color have different spectral reflectances. Illuminant metamerism refers to a color mismatch caused by a change in lighting while observer metamerism refers to a color mismatch caused by a change in observer. Metamerism results from each of the material's colorants having different spectral absorption and scattering properties. Metamerism can only be minimized by selecting colorants with similar spectral properties. Metameric indices are an aid toward selection. However, even when using indices and looking at spectral plots, spectral matches are very difficult to achieve, and all the skill of the colorist is required to avoid metameric matches.

Metamerism can be recast in terms of color inconstancy where the samples forming a metameric pair have dissimilar color constancy. Typically, with a change in lighting, one of the samples changes color noticeably while the other appears color constant. Sometimes, we only notice poor color constancy in relation to a matching sample that is reasonably color constant. In similar fashion to a metameric batch having poor quality, a color inconstant standard also has poor quality. Color-inconstancy indices are very useful in validating the color constancy of a standard. They are indispensable when formulating to a standard with only a colorimetric specification.

The steps required to calculate a CII reveal one of the shortcomings of CIELAB, the accuracy of its chromatic-adaptation transform. These steps also reveal that the practice of calculating CIELAB for non-daylight illuminants is a poor one. Attempts by the CIE to replace CIELAB have been unsuccessful and it is unlikely manufacturing industries will switch to a color-appearance space, even those with similar performance to CIEDE2000. This is why we described how to incorporate an improved chromatic-adaptation transform into CIELAB.

Finally, we want to stress that color inconstancy applies to a *single sample* viewed under multiple illuminants. "Metamerism" should never be used when describing a single sample's change in color due to changes in illumination. Metamerism always describes the color relationships between a *pair of samples*, at minimum.

Chapter 9

Optical Modeling of Colored Materials

There are many applications where it is useful to know the relationship between colorants and their resulting color when mixed. For thousands of years, artisans have used their experiences to develop this relationship for ceramics, textiles, paints, and glass, to name a few. This experience was handed down to the next generation through apprenticeships. Trade guilds, developed during medieval times, exemplify the apprentice approach. The introduction of spectrophotometers capable of measuring opaque samples opened the possibility of using the spectral data to establish a relationship between the materials' spectral properties, concentrations, and the resulting spectra following mixing. Colorimetric coordinates were calculated from the mixture's spectrum, defining the mixture's color. Having established such a relationship, it should be possible to reverse the relationship. This facilitates answering the following questions. What are the concentrations necessary to produce a particular color, that is, predicting a color formula (or recipe)? Are the selected colorants the best colorants to use, either leading to the least amount of metamerism when matching a standard, or the least amount of color inconstancy when the standard is colorimetric? Do the selected colorants minimize color variability caused by process variability? When the batch does not match, how is the formula adjusted to improve the match?

There are several ways to establish the relationship between concentration and color. One way is to derive a spectral-based theoretical optical model and adjust the model coefficients empirically to maximize accuracy. In some cases, this approach is inadequate and modeling is abandoned. A database is created by producing mixtures where concentration is sampled systematically. The database is used to create a multidimensional lookup table and interpolation is used to calculate a formula for a specific color. The database can also be used as training data to create a neural network or other learning-based algorithms. In this chapter, we focus on the model-based approach.

A. GENERIC APPROACH TO COLOR MODELING

Berns (1997) found that many coloration systems could be modeled using a generic, two-step approach. The first step was discovering a model where the relationship between the color components and spectral data was linear. Discovery took the form of a literature search or a derivation based on first principles. The models we describe come from the literature.

A linear relationship has two requirements. The first is scalability. The spectral data for each colorant should be scalable. This is tested by producing a series of colors where the amount is varied between minimum and maximum. We use the example of a liquid crystal display where spectral radiance was measured of each primary at six different digital values (amounts), shown in Figure 9.1. Scalability is verified when the spectra are coincident following normalization to a single wavelength, shown in Figure 9.2. This means that all

Billmeyer and Saltzman's Principles of Color Technology, Fourth Edition. Roy S. Berns.

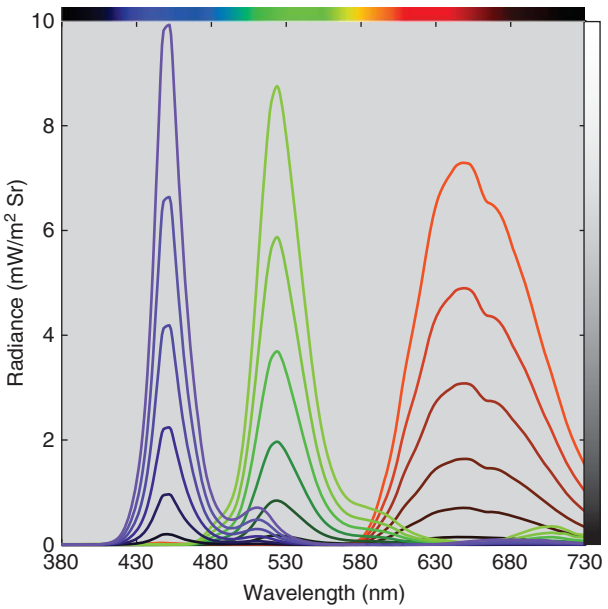

Figure 9.1 Spectral radiance measurements of red, green, and blue primary ramps for a liquid crystal display.

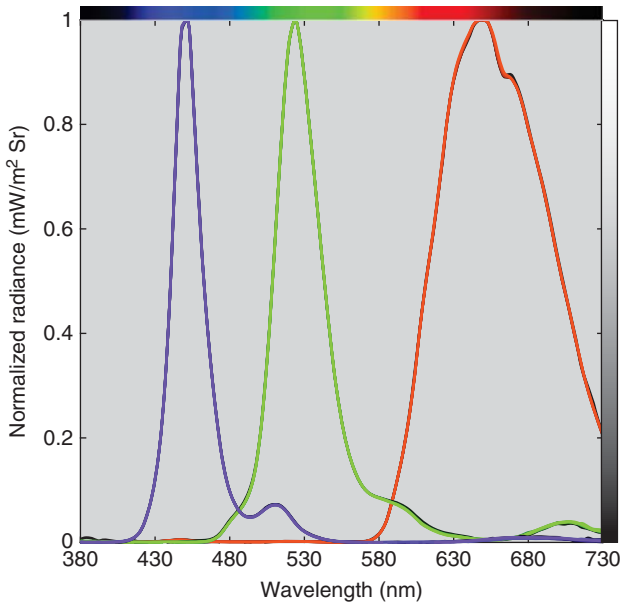

Figure 9.2 Spectral radiance measurements of red, green, and blue primary ramps normalized to each spectrum's peak radiance.

the spectra can be predicted by a single spectrum, usually the maximum for displays. This is shown in Eq. (9.1):

$$L_\lambda = c_e L_{\lambda,\max} \tag{9.1}$$

where spectral radiance, L_λ, is predicted from the colorant's maximum spectral radiance, $L_{\lambda,\,\max}$, and effective colorant amount, c_e, equivalent to a scalar in linear algebra. The direct measurement of spectral radiance defines the linear model. Scalar c_e can be calculated as a ratio at the peak wavelength, the ratio of the integration of the spectrum, or is estimated using least squares linear regression using all the wavelength data.

The second requirement is additivity where a mixture is predicted by the summation of each colorant, shown in Eq. (9.2)

$$L_\lambda = L_{\lambda,r} + L_{\lambda,g} + L_{\lambda,b} \tag{9.2}$$

This is verified by predicting mixtures from a linear combination of each colorant's maximum spectral radiance, shown in Eq. (9.3)

$$L_\lambda = c_{e,r}L_{\lambda,\max,r} + c_{e,g}L_{\lambda,\max,g} + c_{e,b}L_{\lambda,\max,b} \tag{9.3}$$

Regression is used to estimate effective colorant amount where spectral radiance RMS error is minimized. A comparison of the measured and estimated spectra is shown in Figure 9.3. The spectra are nearly coincident. Spectral differences can also be used as a measure of scalability.

The second step of Berns' generic approach was to discover the relationship between the *user controls,* digital counts (d) in this example, and effective colorant amount, shown in Eq. (9.4). Discovery took the form of a literature search, a derivation based on first principles, fitting measurement data, or building a one-dimensional lookup table. The relationship between digital counts and effective colorant amount for the measured liquid-crystal display is shown in Figure 9.4. This display-based relationship is referred to as an *optoelectronic conversion function*, *OECF*, or *tone-response curve, TRC*

$$c_e = f(d) \tag{9.4}$$

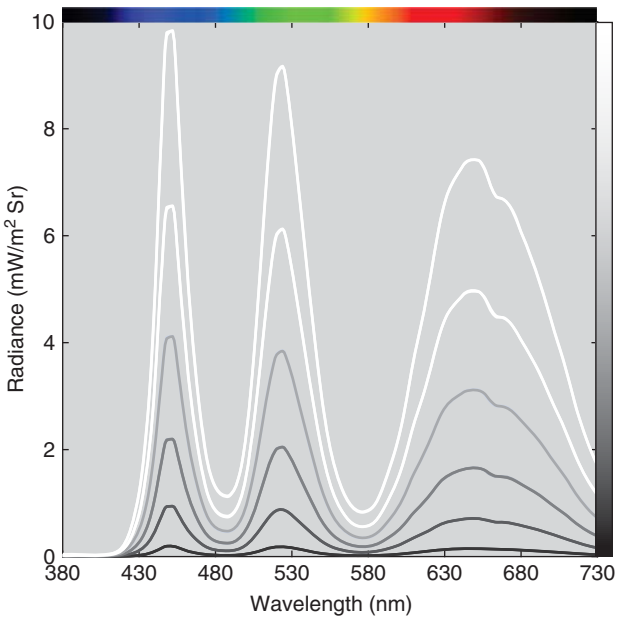

Figure 9.3 Measured (thick lines) and estimated (thin lines) spectral radiance of neutral colors based on Eq. (9.3).

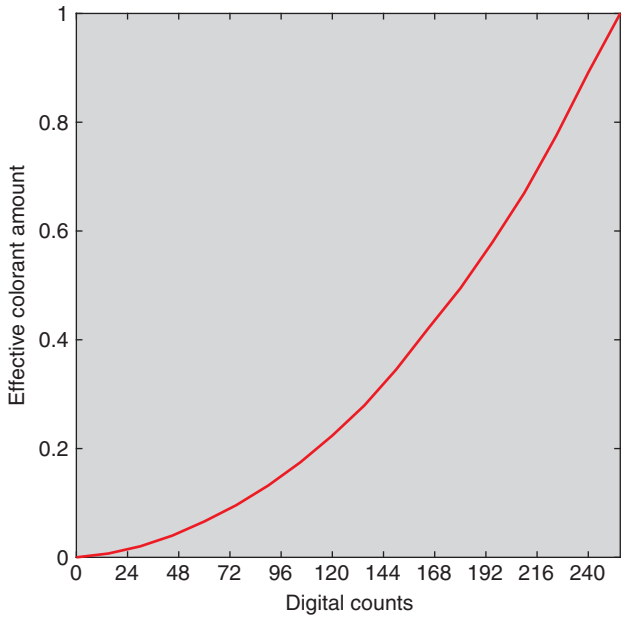

Figure 9.4 Nonlinear relationship between digital counts and effective colorant amount for the red primary of a liquid crystal display. Although not plotted, the blue and green primaries have similar relationships.

This generic approach will be used throughout this chapter.

B. MODELING TRANSPARENT MATERIALS

- *Transmission:* The process whereby radiant energy passes through a material or object.
- *Transmittance:* The ratio of the transmitted radiant flux to the incident radiant flux under specified geometric and spectral conditions.
- *Internal transmittance:* The ratio of radiant flux reaching the exit surface of a specimen to the radiant flux that penetrates the entry surface.
- *Absorption:* The transformation of radiant energy to a different form of energy by interaction with matter.
- *Absorptance:* The ratio of the absorbed radiant flux to the incident radiant flux.
- *Absorbance:* Logarithm to the base 10 of the reciprocal of the internal transmittance.
- *Absorptivity:* Measure of the absorption of radiant energy from an incident beam as it traverses an absorbing medium; synonymous with absorption coefficient or extinction coefficient.

The modeling of transparent materials is subtractive where colorants absorb light. Bouguer (1729) and later Lambert (1760) discovered that spectral transmittance could be transformed using logarithms to achieve a linear system. Experiments were performed using colored glass of different thickness, shown in Figure 9.5. Suppose that a 1 cm thick glass transmitted one half of the light incident upon it at some arbitrary wavelength. It would seem that if the glass was 2 cm thick, it would transmit no light. Each centimeter of material would subtract one half of the light (½–½). However, they instead found that the transmittance was one quarter of the light. If the glass thickness was increased to 3 cm, the transmittance was one eighth of the light. We see that each centimeter of material has an exponential rather than a subtractive effect [$¼ = (½)^2$; $⅛ = (½)^3$].

The measured transmittance of the three 1 cm glasses will be slightly less than the single 3 cm glass because there are three times the number of first-surface reflections at each air and glass interface. We have to account for this difference in order to correctly use the exponential relationship. As we learned in Chapter 1, the Fresnel formulas are used to "get inside" the glass, that is, calculate internal transmittance, $T_{\lambda,i}$. If we assume that the light strikes the glass along its normal angle, Eqs. (9.5)–(9.7) are used to transform between internal and measured transmittance, $T_{\lambda,m}$:

$$T_{\lambda,i} = \frac{-(1-K_1)^2 + \sqrt{(1-K_1)^4 + 4K_1^2 T_{\lambda,m}^2}}{2K_1^2 T_{\lambda,m}^2} \tag{9.5}$$

$$K_1 = \left(\frac{n_{\text{material}} - n_{\text{air}}}{n_{\text{material}} + n_{\text{air}}}\right) \tag{9.6}$$

$$T_{\lambda,m} = \frac{(1-K_1)^2 T_{\lambda,i}}{1 - K_1^2 T_{\lambda,i}^2} \tag{9.7}$$

where n is refractive index (Allen 1980). The n of air is 1. For different angles of incidence, Eqs. (1.1)–(1.3), shown in Chapter 1, are used.

The *Bouguer–Lambert law* is shown in Eq. (9.8):

$$T_{\lambda,i} = t_\lambda^b \tag{9.8}$$

where internal transmittance, $T_{\lambda,i,}$ depends on the glass' internal transmittance at unit thickness, t_λ, and its thickness, b. (Note the deliberate use of upper- and lower-case letters.)

When designing filters for cameras and colorimeters, multiple glasses are glued together. If the refractive index of the glue matches that of the glasses, the total transmittance is a product of the individual glasses, shown in Eq. (9.9) for two filters

$$T_{\lambda,i} = t_{\lambda,1}^{b_1} t_{\lambda,2}^{b_2} \tag{9.9}$$

About 100 years later, Beer found that the same principles that described the relationship between transmittance

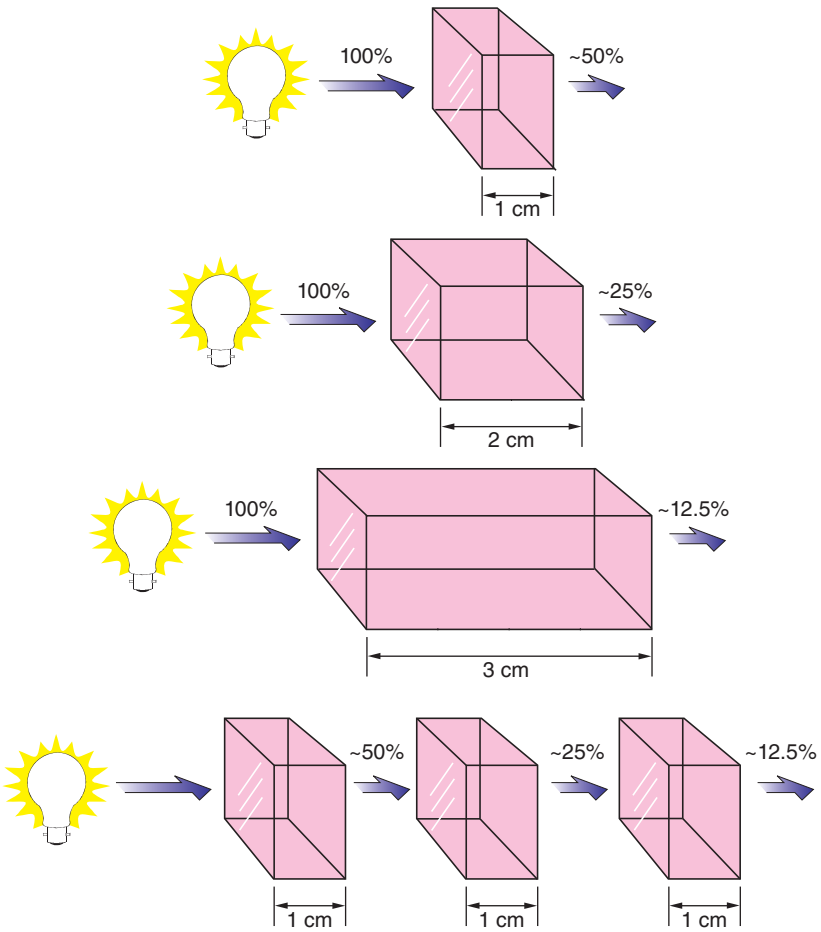

Figure 9.5 Bouguer and later Lambert discovered that there was an exponential relationship between thickness and spectral transmittance.

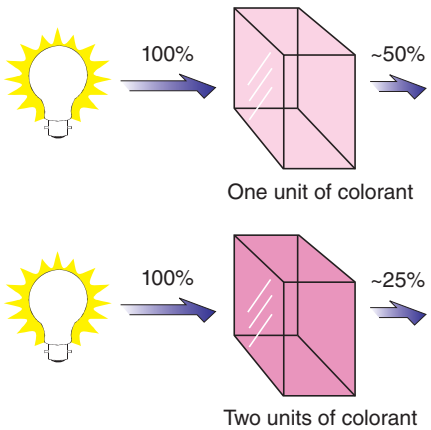

Figure 9.6 Beer discovered that there was an exponential relationship between concentration and spectral transmittance.

and thickness for transparent materials also applied to liquids of varying concentration (Beer 1852, 1854), shown in Figure 9.6. Thus, the linear mixing law for colored materials that do not scatter light is known as the *Bouguer–Beer law* or *Lambert–Beer law*.

The linear model is defined by a logarithmic transformation of internal transmittance, shown in Eq. (9.10):

$$A_\lambda = -\log_{10}(T_{\lambda,i}) = \log_{10}\left(\frac{1}{T_{\lambda,i}}\right) \tag{9.10}$$

where A defines absorbance. The absorbance of a transparent material depends on its unit absorptivity, a_λ, thickness, b, and concentration, c, shown in Eq. (9.11)

$$A_\lambda = a_\lambda bc = \varepsilon_\lambda bc = k_\lambda bc = \alpha_\lambda bc \tag{9.11}$$

Absorptivity is also called an absorption coefficient, k or α, or an extinction coefficient, ε.

A classic experiment in analytical chemistry is to verify Beer's law by dissolving a dye in a solvent at different concentrations and comparing absorbance, usually at the wavelength of maximum absorbance, and concentration. A pair of matched cuvettes is used where the solvent is in one cuvette ("*blank*") and the solvent and dye are in the other cuvette. A single-beam spectrophotometer is calibrated with the blank in the optical path. Cuvettes filled with solvent are placed in both positions when calibrating a double-beam spectrophotometer. Measurements are directly internal transmittance.

A line is fit where absorbance is predicted from concentration. Any deviation from linearity is known as Beer's law failure, reasons including experimental error, measurement imprecision, and changes in the electronic characteristics of the dye molecules at very low and high concentrations.

As an example, a purple polystyrene plastic was molded into sections ranging from 1.00 to 6.00 mm in 1 mm increments and measured with a spectrophotometer, the data shown in Figure 9.7. Transmittance decreases with an increase in thickness. The change, however, is not proportional with thickness.

Polystyrene has a refractive index that varies from 1.68 at 380 nm to 1.50 at 730 nm. The average, 1.60, was used to calculate a K_1 of 0.053 and used to transform to internal transmittance using Eqs. (9.5) and (9.6), the data plotted in Figure 9.8. Internal transmittance always increases compared with measured transmittance.

Absorbance was calculated from internal transmittance using Eq. (9.10), the spectra shown in Figure 9.9. Absorbance increases with a decrease in transmittance. Absorbance is proportional to thickness.

The absorbance at 1 mm was defined as the unit absorptivity. The simplest way to estimate thickness is by dividing the absorbance at 550 nm for each spectrum by the unit absorptivity, the results shown in Figure 9.10 and Table 9.1. There is a slight amount of error for the thickest sample, likely caused by measurement imprecision. Alternatively, least squares linear regression can be used to estimate thickness using all the wavelengths where spectral absorbance RMS error is minimized. This resulted in an accurate estimation of thickness.

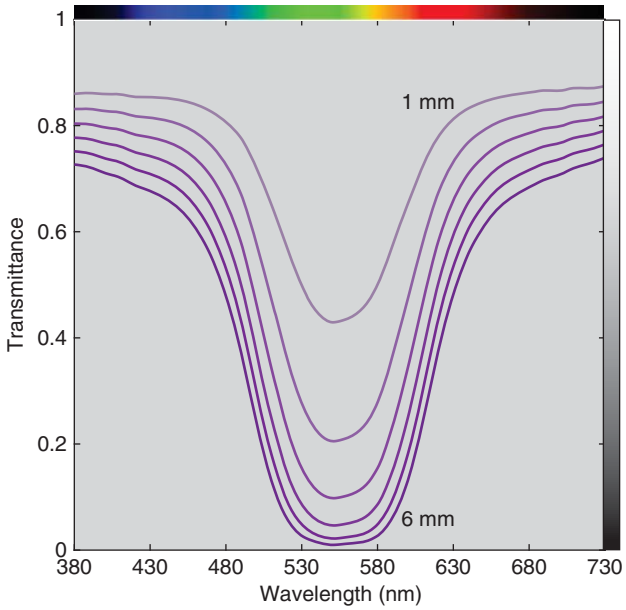

Figure 9.7 Spectral transmittance of polystyrene plastic at varying thickness in 1 mm increments.

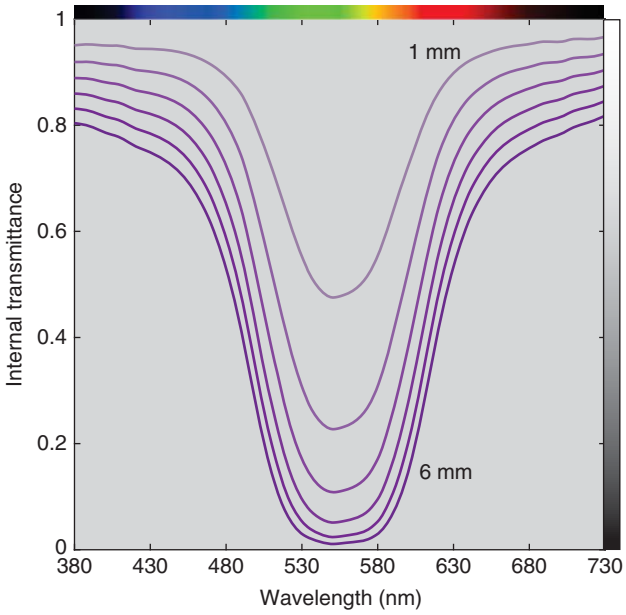

Figure 9.8 Spectral internal transmittance of polystyrene plastic at varying thickness.

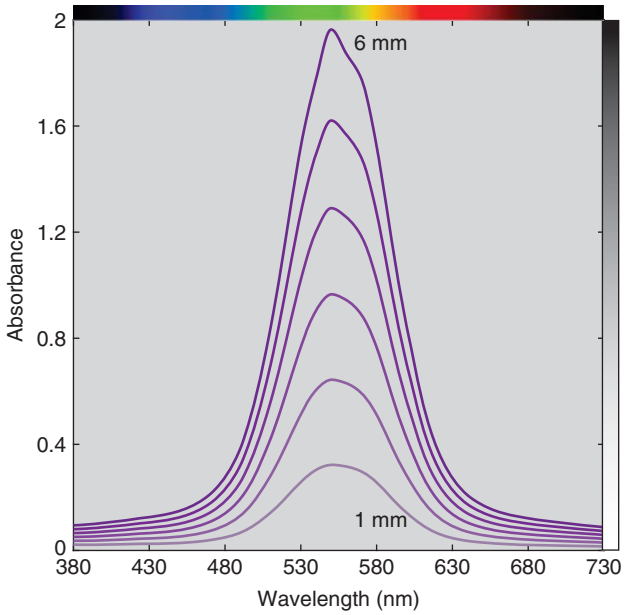

Figure 9.9 Spectral absorbance of polystyrene plastic at varying thickness.

It is appealing to ignore first surface reflections because Eq. (9.5) is complex (and much more difficult to memorize than the linear model, $A = abc$). The calculations were repeated where "absorbance" was calculated from measured transmittance rather than internal transmittance. Using either the wavelength data at 550 nm or the entire spectrum, error increased with increasing thickness where thickness was underestimated. This error was caused by a lack of

Table 9.1 Calculated values for polystyrene plastic having a refractive index of 1.60.

	550 nm	First surface correction				No first surface correction	
Thickness (b)	T_m	T_i	A	b_{estimate} 550 nm	b_{estimate} least squares	b_{estimate} 550 nm	b_{estimate} least squares
1.00	0.4292	0.4783	0.3203	1.00	1.00	1.00	1.00
2.00	0.2050	0.2285	0.6410	2.00	2.00	1.87	1.78
3.00	0.0977	0.1089	0.9630	3.01	3.00	2.75	2.56
4.00	0.0462	0.0516	1.2877	4.02	4.00	3.63	3.34
5.00	0.0216	0.0241	1.6181	5.05	5.00	4.53	4.12
6.00	0.0098	0.0109	1.9613	6.12	6.00	5.47	4.90

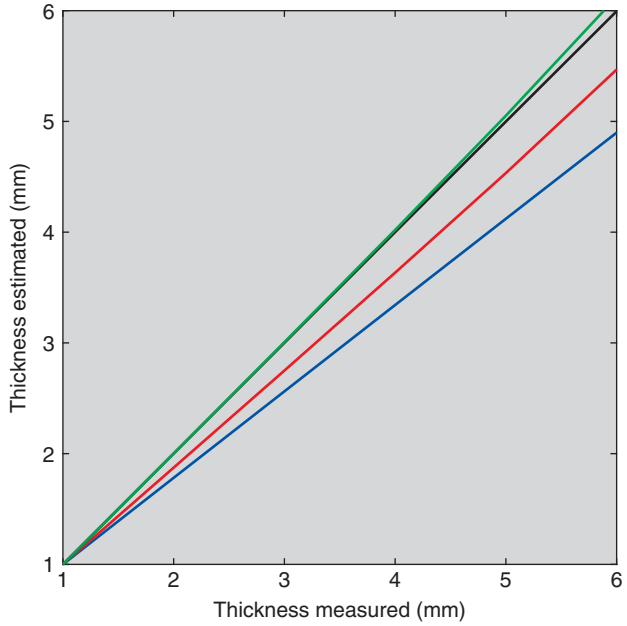

Figure 9.10 Measured and estimated thickness using absorbance at 550 nm (green line), absorbance using all wavelengths (black line), "absorbance" ignoring first surface reflections at 550 nm (red line), and "absorbance" ignoring first surface reflections using all wavelengths (blue line).

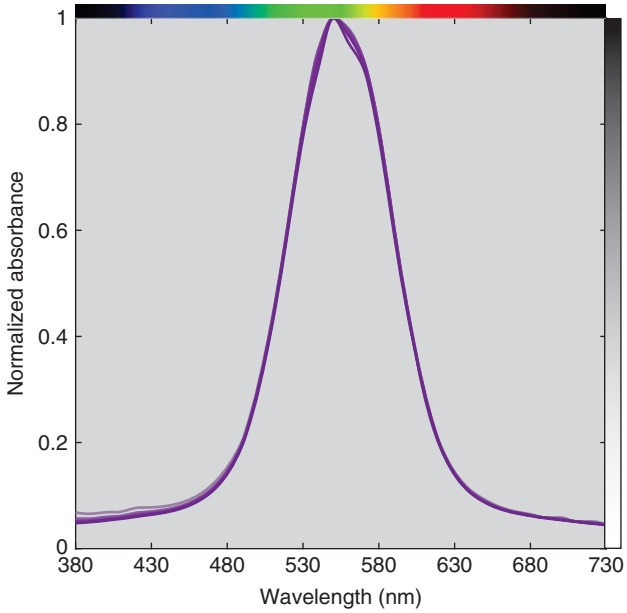

Figure 9.11 Normalized spectral absorbance of polystyrene plastic at varying thickness.

scalability, shown in Figures 9.11 and 9.12 where normalized absorbance is plotted as a function of wavelength. The correct absorbance data are nearly coincident, whereas the incorrect "absorbance" data vary. This reinforces the importance of plotting the normalized linear model spectral data in order to validate the model.

Predicting thickness from transmittance measurements can be interpreted in terms of the generic approach to color modeling. The first step, discovering the linear model, was the Bouguer–Beer model using internal transmittance. The second step, discovering the relationship between the user controls and effective colorant amount, was assumed to be one-to-one. That is, $c_e = b$. This assumption is often false when modeling opaque materials, described below.

A colorant's spectral properties can be used for identification. In this example all the plotted spectra are similar. However, decreases in thickness reduce the clarity of the spectral signature. In the same way that the base 10 logarithm of transmittance transformed an exponential relationship to a multiplicative relationship, the base 10 logarithm of absorbance transforms a multiplicative relationship to an additive relationship where the spectral signature is independent of thickness, shown in Figure 9.13. We recommend this practice when using visual methods for identification.

C. MODELING OPAQUE MATERIALS

Most colored materials are not transparent—they are either translucent or opaque, a result of internal scattering. An incident beam of light changes directions multiple times depending on the scattering properties of the colorants, their concentrations, their size and shape, how the colorants are dispersed within the material including orientation, and the thickness of the material. Determining the exact amount of reflection, absorption, and transmission is complex. Such calculations were first made in the field of astrophysics to understand how radiation is propagated through

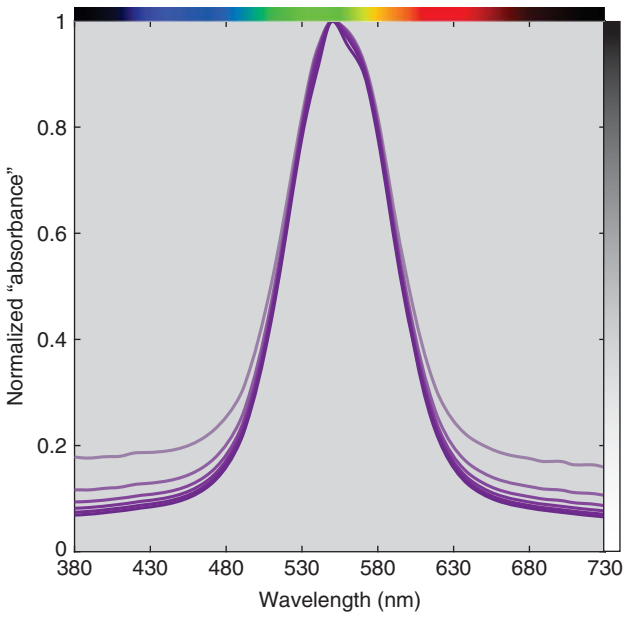

Figure 9.12 Normalized spectral "absorbance" of polystyrene plastic at varying thickness. First surface reflections were ignored in the calculation of absorbance.

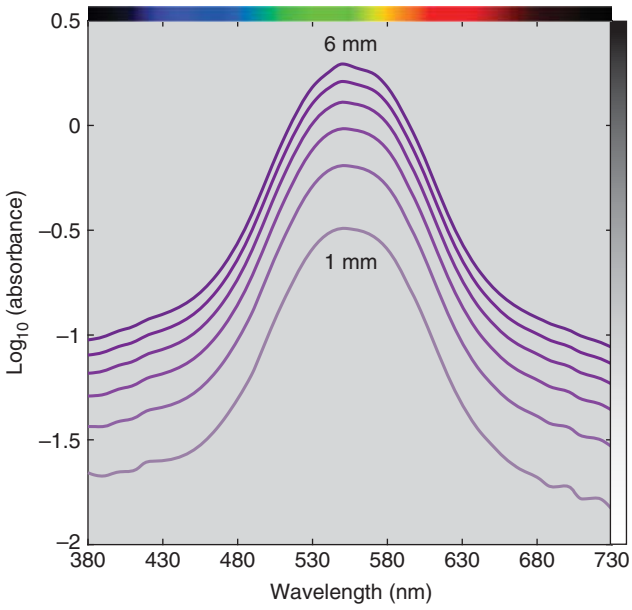

Figure 9.13 Base 10 logarithm of spectral absorbance of polystyrene plastic at varying thickness.

a foggy atmosphere (Schuster 1905). These calculations evolved tremendously throughout the twentieth century. See, for example, Rybicki and Lightman (2008). Beginning in the 1930s, Kubelka and Munk made a simplifying assumption that the light inside a scattering layer travels either up or down perpendicular to the plane of the sample nonpreferentially (Kubelka and Munk 1931; Kubelka 1948, 1954). This became known as the *two-flux model* and enabled the modeling of opaque paints, plastics, and textiles, launching color-formulation software in the middle of that century. Later developments included three- four- and many-flux models, summarized by Völz (2001) and Klein (2010). Statistical approaches have also been derived, for example, Wang, Jacques, and Zheng (1995) and Rogers (2016).

Today's formulation systems use *multiflux models*, a term that implies traditional two-flux modeling is not used, but little else because the specific mathematics are proprietary. Multiflux systems are used to model textiles, opaque and translucent paints and plastics, printing inks on a variety of substrates, multilayer materials, and to a limited extent, materials containing fluorescent and gonioapparent colorants. Because of the complexity of the mathematics, a thorough coverage of published models is beyond the scope of this book. However, the principles of using optical models to predict mixtures are the same irrespective of the model complexity, and we will use the two-flux approach to model opaque paints and textiles. For good summaries of the use of Kubelka–Munk theory in color technology, see Kortüm (1969), Johnston (1973), Judd and Wyszecki (1975), Kuehni (1975), Allen (1980), Nobbs (1985), Park (1994), McDonald (1997), Nobbs (1997), Zhao and Berns (2009), and Hébert and Emmel (2015).

Kubelka and Munk considered a translucent colorant layer on top of an opaque background, shown in Figure 9.14. The colorant layer and background are in optical contact; that is, there is not a change in refractive index at this boundary. Within the colorant layer, both absorption, K_λ, and scattering, S_λ, occur and light flux travels in many directions. This was simplified to two light directions, up or down, also shown in Figure 9.14, which resulted in a pair of differential equations, one for each direction, shown in Eqs. (9.12) and (9.13)

$$\frac{di}{-dx} = -(K_\lambda + S_\lambda)_i + S_{\lambda,j} \tag{9.12}$$

$$\frac{dj}{dx} = -(K_\lambda + S_\lambda)_j + S_{\lambda,i} \tag{9.13}$$

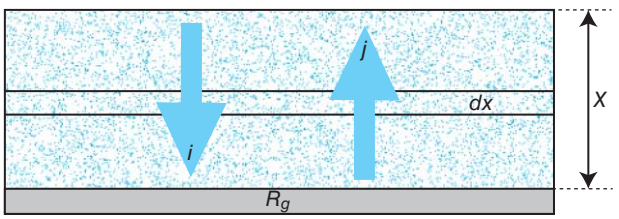

Figure 9.14 Kubelka–Munk theory assumes that the light flux within a translucent absorbing and scattering layer having a thickness X on top of an opaque support with reflectance of R_g travels either downward (direction i) or upward (direction j).

Light in the downward, i, direction is weakened due to absorption and scattering, $-(K_\lambda + S_\lambda)_i$, and strengthened by scattered light from the opposite direction, $+S_{\lambda,j}$. This also occurs in the upward direction. By convention, the downward direction is the negative direction, hence, $-dx$.

Solving the pair of differential equations (see Allen 1980; Haase and Meyer 1992; Hébert and Emmel 2015 for detailed descriptions of the calculus) results in Eqs. (9.14)–(9.17):

$$R_{\lambda,i} = \frac{1 - R_{\lambda,g}[a_\lambda - b_\lambda \text{Coth}(b_\lambda S_\lambda X)]}{a_\lambda - R_{\lambda,g} + b_\lambda \text{Coth}(b_\lambda S_\lambda X)} \tag{9.14}$$

$$a_\lambda = \left(\frac{K}{S}\right)_\lambda + 1 \tag{9.15}$$

$$b_\lambda = \sqrt{a_\lambda^2 - 1} \tag{9.16}$$

$$\text{Coth}(x) = \frac{e^x + e^{-x}}{e^x - e^{-x}} \tag{9.17}$$

where internal reflectance, $R_{\lambda,i}$, is calculated from knowledge of the background reflectance, $R_{\lambda,g}$, the absorption, K_λ, and scattering, S_λ, properties of the colorant layer, and its thickness, X. Coth refers to the hyperbolic cotangent.

The key assumption in applying Kubelka–Munk theory is that the light within the colorant layer is completely diffuse, that is, the material is isotropic. As a result, Kubelka–Munk theory does not apply to most gonioapparent pigments or to colorant layers that change the degree of polarization of the incident light significantly. Kubelka–Munk theory also does not apply to fluorescent colorants though it is used as a starting point for more elaborate approaches (see Bonham 1986; Simon, Funk, and Laidlow 1994; McDonald 1997; Shakespeare and Shakespeare 2003). Finally, Kubelka–Munk theory applies to a single wavelength at a time, necessitating the use of a spectrophotometer. Theoretically, the geometry should be diffuse illumination and diffuse collection, which does not occur in any spectrophotometer. Nonetheless, Kubelka–Munk theory has been used successfully to model a number of coloration systems.

Kubelka–Munk theory is used to develop mixing laws for three types of samples, shown in Figure 9.15. The first is translucent materials where the general form of Kubelka–Munk theory as shown in Eq. (9.14) is used. Zhao and Berns (2009) have reviewed common approaches to modeling translucent materials using the general form. Equation (9.14) can be rearranged algebraically to facilitate calculating reflectance, transmittance, scattering, and absorption for a number of practical applications (Kubelka 1948). (Care should be taken in using these formulas because typographical errors occur in a number of references; we use Wyszecki and Stiles 1982 and Hébert and Emmel 2015.) Judd and Wyszecki (1975) provide several numerical examples.

The second type of sample is one in which a transparent colorant layer is in optical contact with an opaque, diffusely

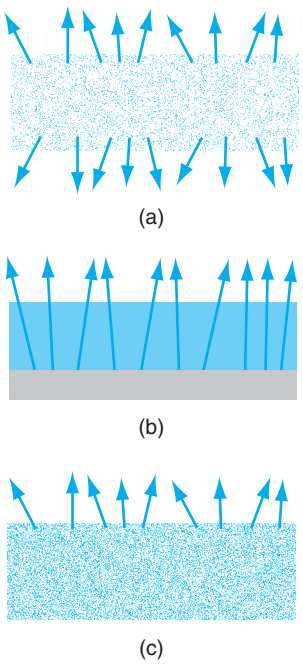

Figure 9.15 Kubelka–Munk theory is most often applied to (a) translucent materials, (b) transparent colored layers on an opaque, scattering support, and (c) opaque materials.

scattering support. As scattering of the colorant layer approaches zero, the general form reduces to Eq. (9.18)

$$R_{\lambda,i} = R_{\lambda,g} e^{-2K_\lambda X} \tag{9.18}$$

This formula has been used to model photographic paper and continuous-tone prints using thermal-transfer technologies (Berns 1993b; Kang 1997).

The third type of sample is opaque absorbing and scattering materials such as textiles, dyed paper, coatings, and plastics. At opacity, thickness is infinite, that is, an increase in thickness does not change reflectance, and the general form reduces to Eq. (9.19)

$$R_{\lambda,i} = 1 + \left(\frac{K}{S}\right)_\lambda - \sqrt{\left(\frac{K}{S}\right)_\lambda^2 + 2\left(\frac{K}{S}\right)_\lambda} \tag{9.19}$$

We will model opaque paints and textiles to illustrate the use of Kubelka–Munk theory.

Opaque Paints

Kubelka–Munk theory has been used to model opaque paint mixtures since the 1940s where each paint's absorption and scattering properties are used to define a linear model (Duncan 1940). This is shown in Eq. (9.20) for three colorants:

$$\left(\frac{K}{S}\right)_{\lambda,\text{mixture}} = \frac{c_{e,1}k_{\lambda,1} + c_{e,2}k_{\lambda,2} + c_{e,3}k_{\lambda,3}}{c_{e,1}s_{\lambda,1} + c_{e,2}s_{\lambda,2} + c_{e,3}s_{\lambda,3}} \tag{9.20}$$

where c_e denotes effective colorant amount and k_λ and s_λ are the absorption and scattering properties of a colorant at unit amount. This is often called *two-constant Kubelka–Munk theory* since each colorant has two independent spectra.

For this example, ultramarine blue (PB 29), red iron oxide (PR 101), and titanium white (PW 6) matte artist acrylic dispersion paints were used. Ultramarine blue is nearly transparent while red iron oxide is nearly opaque. Mixtures were made of blue and white and red and white at percentage weight ratios of 80:20, 60:40, 40:60, and 20:80. Mixtures were also made of blue, red, and white at weight ratios of 50:50:0, 45:45:10, 30:30:40, 20:20:60, 10:10:80, and 5:5:90. Because weight ratios are used, there are only two unknowns when determining effective colorant amounts, shown in Eq. (9.21)

$$\left(\frac{K}{S}\right)_{\lambda,\text{mixture}} = \frac{c_{e,\text{blue}}k_{\lambda,\text{blue}} + c_{e,\text{red}}k_{\lambda,\text{red}} + (1 - c_{e,\text{blue}} - c_{e,\text{red}})k_{\lambda,\text{white}}}{c_{e,\text{blue}}s_{\lambda,\text{blue}} + c_{e,\text{red}}s_{\lambda,\text{red}} + (1 - c_{e,\text{blue}} - c_{e,\text{red}})s_{\lambda,\text{white}}} \tag{9.21}$$

The mixtures were applied to contrast paper at a thickness of 0.006 in. (6 mil) using a drawdown bar. A drawdown of each paint at masstone (directly from the tube) was also made. The blue masstone drawdown was not opaque and the paint was reapplied on top of the first drawdown at 0.010 in. Example drawdowns are shown in Figure 9.16.

An integrating sphere spectrophotometer with the specular component included was used to measure each drawdown in four locations against the white and the black areas of the contrast paper. In all cases, the measurements were within the precision of the spectrophotometer, verifying opacity. The average of the eight measurements was used in all subsequent calculations. The spectral data for each paint are plotted in Figure 9.17. Because of the high tinting strength of ultramarine blue, there is a large change in reflectance between the masstone (100:0) and the 80:20 tint. For all the tints, the maximum reflectance is bounded by white.

Figure 9.16 Drawdowns of ultramarine blue and titanium white at percentage weight ratios of 100:0, 0:100, and 60:40 (left to right).

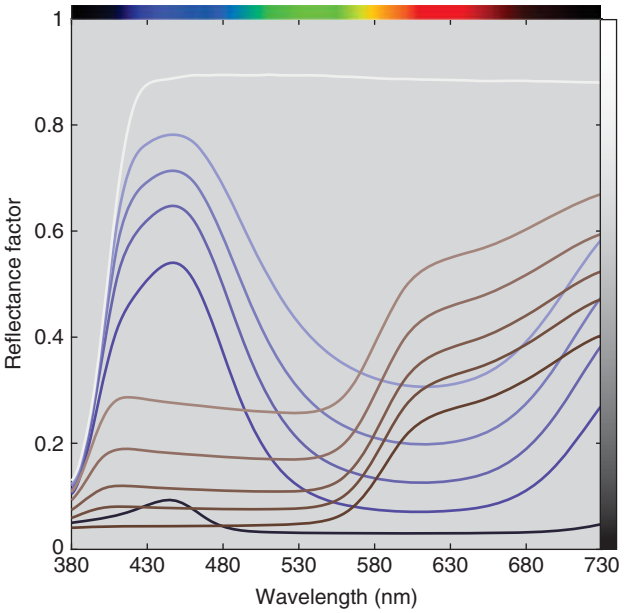

Figure 9.17 Spectral reflectance factor of ultramarine blue and red iron oxide tint ladders and masstones.

Kubelka–Munk theory predicts internal reflectance from colorant concentration and in similar fashion to modeling transparent materials, measured reflectance is converted to internal reflectance, in this case, using formulas first derived by Ryde (1931), Ryde and Cooper (1931), and later used by Saunderson (1942) when modeling pigmented plastics. The formulas can be generalized for both integrating sphere and bidirectional geometries, shown in Eqs. (9.22) and (9.23)

$$R_{\lambda,i} = \frac{R_{\lambda,m} - K_{\text{instrument}}K_1}{(1 - K_1)(1 - K_2) + K_2R_{\lambda,m} - K_{\text{instrument}}K_1K_2} \tag{9.22}$$

$$R_{\lambda,m} = \frac{(1 - K_1)(1 - K_2)R_{\lambda,i}}{1 - K_2R_{\lambda,i}} + K_{\text{instrument}}K_1 \tag{9.23}$$

Constant K_1 defines the amount of reflected collimated light at the boundary (i.e. surface of paint layer) and is calculated using the Fresnel formulas. Inside the paint layer, light is scattered equally in all directions and as a result, the light striking the boundary in the upward direction has a range of incident angles between 0° and 90° relative to the surface normal. Constant K_2 defines the integration of all the light reflecting at the boundary over this range of angles except the collimated angle. If the incident light is along the normal and the refractive index of the paint layer is 1.5, then $K_1 = 0.04$ and $K_2 = 0.6$ (Orchard 1969). Constant $K_{\text{instrument}}$ is the proportion of the collimated light reflecting from the surface that is included in the reflectance measurement. For an integrating sphere spectrophotometer with the specular component included, $K_{\text{instrument}} = 1$. When the geometry is bidirectional,

$K_{\text{instrument}} = 0$. For integrating spheres with the specular component excluded, $K_{\text{instrument}}$ depends on the material's gloss and the integrating sphere design, discussed in Chapter 6. The conversion from measured to internal reflectance and the reverse is known as the *Saunderson correction*.

The constants K_1 and K_2, by definition, are wavelength dependent since their values are based on the paint layer's refractive index, also wavelength dependent. When using Kubelka–Munk theory to model opaque materials, wavelength dependency is ignored. Furthermore, rather than define the values based on spectrophotometer geometry and average refractive index, they are determined empirically as we describe below. Optimizing the Saunderson constants has the effect of improving the linearity between measured weight and c_e.

Predicting the spectral reflectance of a paint mixture requires K_1, K_2, $K_{\text{instrument}}$, and each colorant's unit k_λ and s_λ. We use a two-step approach to determine these optical parameters (described in detail below). First, reasonable values for the Saunderson correction constants are defined and unit k_λ and s_λ are calculated directly. Second, nonlinear optimization is used where the first-step data become starting values. For both steps it is assumed that c_e equals measured weight.

Evaluating the minimum reflectance factor of all the measured samples, K_1 was defined as 0.03 and K_2 was defined as 0.5, the midpoint between the theoretical value of 0.6 and 0.4 as used by Saunderson (1942). $K_{\text{instrument}}$ was defined as 1.0. When the samples are opaque, it is common to define $s_{\lambda,\text{white}} = 1$ and $k_{\lambda,\text{white}} = (K/S)_{\lambda,\text{white}}$ where the transformation between $R_{\lambda,i}$ and $(K/S)_\lambda$ is shown in Eq. (9.24)

$$\left(\frac{K}{S}\right)_\lambda = \frac{(1 - R_{\lambda,\text{i}})^2}{2R_{\lambda,\text{i}}} \tag{9.24}$$

The spectra for the masstone (100:0), 20:80 tint, and white (0:100) were used to calculate k_λ and s_λ, the formulas shown in Eqs. (9.25)–(9.27) (Berns and Mohammadi 2007a; Zhao and Berns 2009)

$$k_{\lambda,\text{paint}} = \frac{1 - c_{\text{tint}}}{c_{\text{tint}}} s_{\lambda,0} \left(\frac{K}{S}\right)_{\lambda,\text{masstone}} \tag{9.25}$$

$$s_{\lambda,\text{paint}} = \frac{1 - c_{\text{tint}}}{c_{\text{tint}}} s_{\lambda,0} \tag{9.26}$$

$$s_{\lambda,0} \frac{s_{\lambda,\text{white}} \left(\frac{K}{S}\right)_{\lambda,\text{masstone}} - k_{\lambda,\text{white}}}{\left(\frac{K}{S}\right)_{\lambda,\text{masstone}} - \left(\frac{K}{S}\right)_{\lambda,\text{tint}}} \tag{9.27}$$

These were used as starting values for a nonlinear optimization estimating K_1, K_2, and k_λ and s_λ for blue and red where RMS spectral reflectance error was minimized. We prefer minimizing reflectance error rather than K/S to reduce the influence of dark colors such as masstones on estimating k and s. Nonlinear optimization requires reasonable starting values in order to converge to the minimum error, hence the need for the first step. The optimized K_1 and K_2 were 0.03 and 0.74, respectively. The unit data are plotted in Figure 9.18. As expected, the scattering of blue is nearly zero, whereas the scattering for red is quite large. There is an increase in k and s for both paints between 380 and 400 nm. This is an

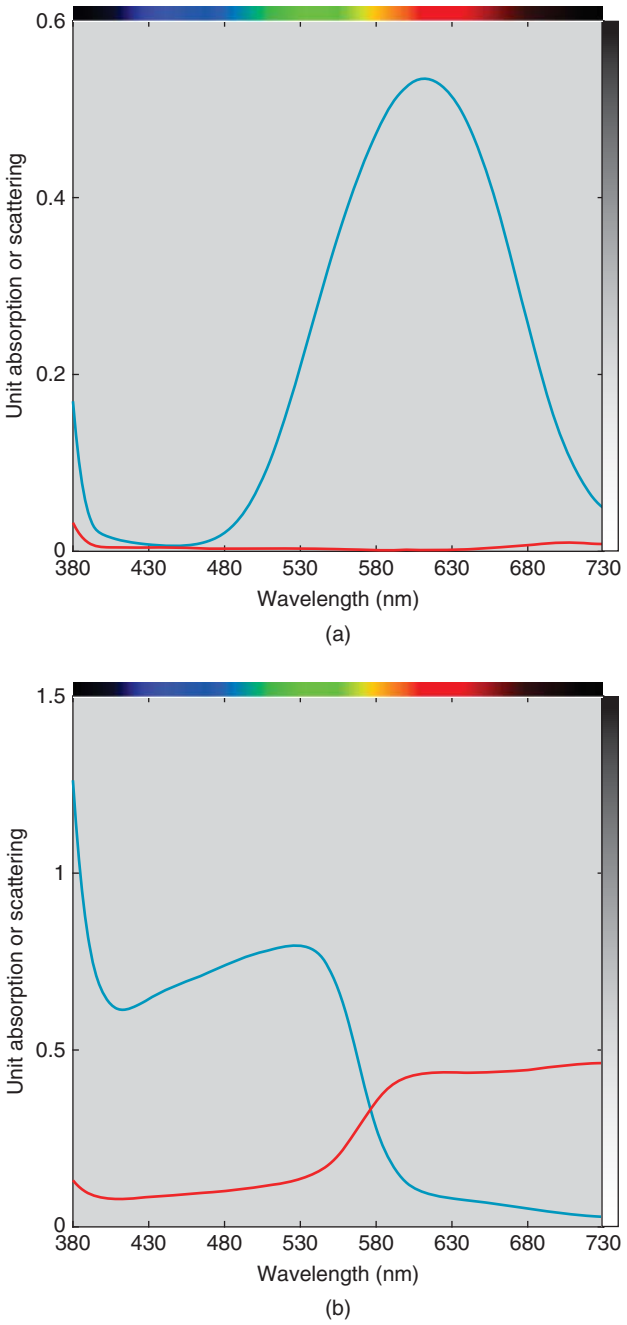

Figure 9.18 Unit k (blue line) and s (red line) for (a) ultramarine blue and (b) red iron oxide. Note the differences in the y-axis scales.

artifact of using a white paint with strong absorption in this region. Data for red at 450 nm are given in Table 9.2.

The model was evaluated several ways. Another optimization was performed to estimate c_e for each of the tints and masstones where RMS spectral reflectance error was minimized, the spectral results plotted in Figure 9.19. This is known as *spectral matching*, sometimes used in color formulation. This obviates assuming that c_e equals measured weight. The spectral similarity is a measure of scalability, which was reasonable for these paints. The effective and measured ratios were compared and differences were within the precision of the scale, that is, there was a linear relationship. This result is important because linearity was assumed when the optical parameters were estimated. Second, the c_e were estimated for the blue, red, and white mixtures where RMS spectral reflectance error was minimized, the spectral results plotted in Figure 9.20. Spectral accuracy was similar to the accuracy of the estimated tints. The effective and measured ratios were compared, the results plotted in Figure 9.21. There was a lack of linearity that exceeded scale imprecision, particularly for the mixture without white where the blue:red:white effective colorant amount ratio was 53:47:0 instead of the weighed ratio of 50:50:0. This discrepancy is typical for mixtures without white.

Table 9.2 Numerical data for red iron oxide at 450 nm for $K_1 = 0.03$ and $K_2 = 0.74$.

Sample	R_m	R_i	K/S
100:0 (masstone)	0.0438	0.0585	7.5766
80:20	0.0776	0.1694	2.0361
60:40	0.1141	0.2697	0.9888
40:60	0.1804	0.4143	0.4141
20:80	0.2749	0.5644	0.1681
0:100 (white)	0.8893	0.9673	0.0006

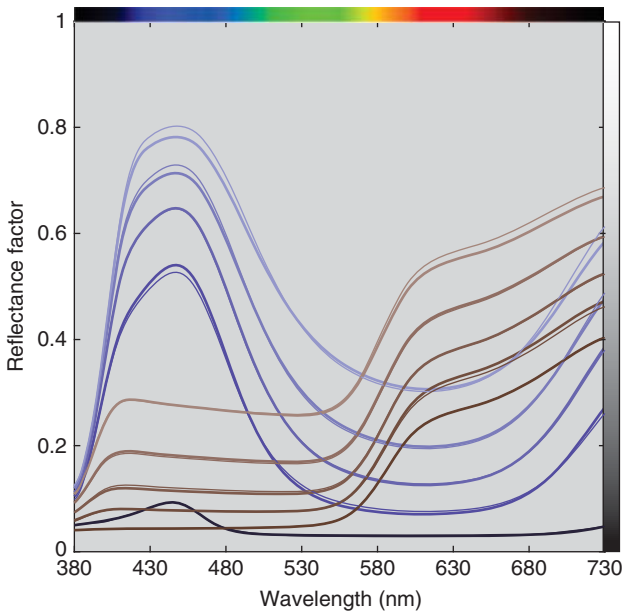

Figure 9.19 Measured (thick lines) and estimated (thin lines) spectral reflectance factor of ultramarine blue and red iron oxide tint ladders and masstones using two-constant Kubelka–Munk theory.

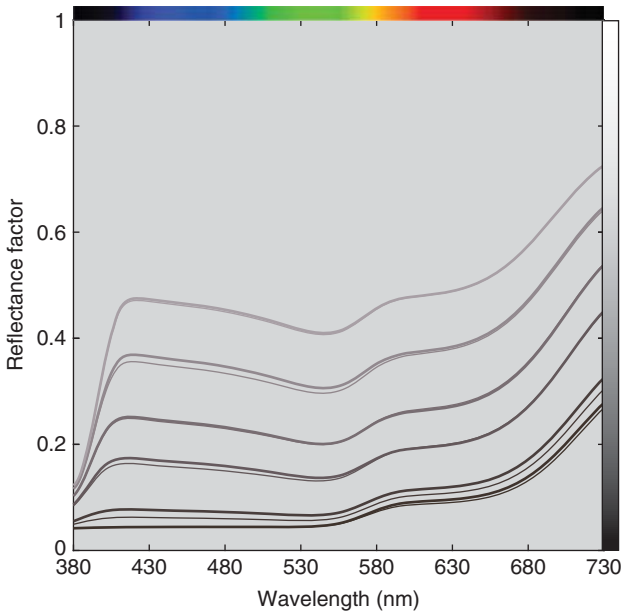

Figure 9.20 Measured (thick lines) and estimated (thin lines) spectral reflectance factor of 6 mixtures containing ultramarine blue, red iron oxide, and titanium white using two-constant Kubelka–Munk theory.

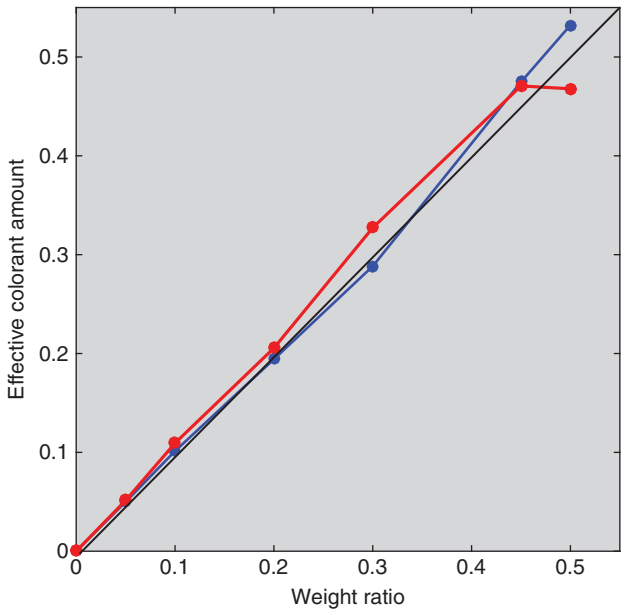

Figure 9.21 Relationship between actual weight and c_e of ultramarine blue (blue line) and red iron oxide (red line) for mixtures using two-constant Kubelka–Munk theory.

Two-constant Kubelka–Munk theory can be simplified for cases where scattering is dominated by white such as pastels (Billmeyer and Abrams 1973; Berns and Mohammadi 2007b). The Duncan formula, shown in Eq. (9.20), changes to Eq. (9.28), which can be rewritten as in Eqs. (9.29) and (9.30)

$$\left(\frac{K}{S}\right)_{\lambda,\text{mixture}} = \frac{C_{e,1}k_{\lambda,1} + c_{e,2}k_{\lambda,2} + \cdots + c_{\text{white}}k_{\lambda,\text{white}}}{c_{\text{white}}s_{\lambda,\text{white}}} \tag{9.28}$$

$$\left(\frac{K}{S}\right)_{\lambda,\text{mixture}} = \frac{c_{e,1}}{c_{\text{white}}}\left(\frac{k}{s}\right)_{\lambda,1} + \frac{c_{e,2}}{c_{\text{white}}}\left(\frac{k}{s}\right)_{\lambda,2} + \cdots + \frac{c_{\text{white}}}{c_{\text{white}}}\left(\frac{k}{s}\right)_{\lambda,\text{white}} \tag{9.29}$$

$$\left(\frac{k}{s}\right)_{\lambda,\text{paint}} = \left(\frac{k_{\text{paint}}}{s_{\text{white}}}\right)_{\lambda} \tag{9.30}$$

This simplification is known as *single-constant Kubelka–Munk theory*.

Unit $(k/s)_\lambda$ spectra were estimated for blue and red using the tints minimizing RMS spectral reflectance error. The 20:80 tint was used to calculate starting values where $(k/s)_\lambda = (K/S)_\lambda/0.2$. Then, c_e were estimated, also minimizing RMS spectral reflectance error. The predicted spectra are shown in Figure 9.22 and the effective and measured ratios are shown in Figure 9.23. The results for blue are similar to the two-constant model because ultramarine blue is a weak scatterer. For red, the single-constant simplification resulted in poor spectral accuracy and nonlinearity between weight and effective colorant amount because red oxide is a strong scatterer.

One limitation of the single-constant approach is that mixtures without white are undefined when $c_{\text{white}} = 0$. Abed and Berns (2017) modified single-constant Kubelka–Munk theory to overcome this limitation by assuming that the scattering of the nonwhite paint is a portion of the white's scattering. That is, $s_{\lambda,\text{paint}}$ becomes $p_{\text{paint}}s_{\lambda,\text{white}}$ where p is an *impurity index* where a nonwhite paint's scattering reduces the purity of the white. Rather than associating the impurity index with the white's unit scattering coefficient, it is associated with concentration, $c_{e,\text{paint}}p_{\text{paint}}$. Equation (9.29) becomes Eq. (9.31)

$$\left(\frac{K}{S}\right)_{\lambda,\text{mixture}} = \frac{c_{e,1}}{c_{\text{white}} + c_{e,1}p_1}\left(\frac{k}{s}\right)_{\lambda,1} + \frac{c_{e,2}}{c_{\text{white}} + c_{e,2}p_2}\left(\frac{k}{s}\right)_{\lambda,2} + \cdots + \frac{c_{\text{white}}}{c_{\text{white}} + c_{e,1}p_1 + c_{e,2}p_2 + \cdots}\left(\frac{k}{s}\right)_{\lambda,\text{white}} \tag{9.31}$$

The impurity index, p, and $(k/s)_\lambda$ were estimated for blue and red using the tints and masstones where RMS spectral reflectance error was minimized. The optimized unit $(k/s)_\lambda$ and $p = 0.5$ were used as starting values. The impurity indices for blue and red were 0.006 and 0.386, respectively. Then, c_e were estimated, also minimizing RMS spectral reflectance error. The predicted spectra are shown in Figure 9.24 and the effective and measured ratios are shown in Figure 9.25. The spectral estimation accuracy was

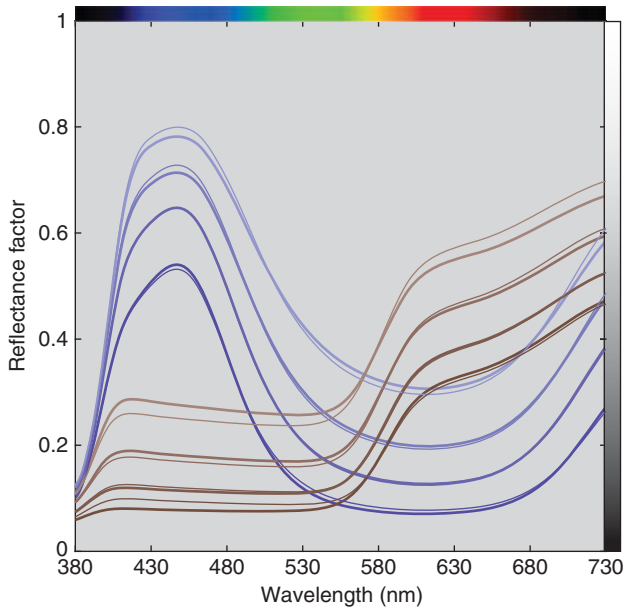

Figure 9.22 Measured (thick lines) and estimated (thin lines) spectral reflectance factor of ultramarine blue and red iron oxide tint ladders using single-constant Kubelka–Munk theory.

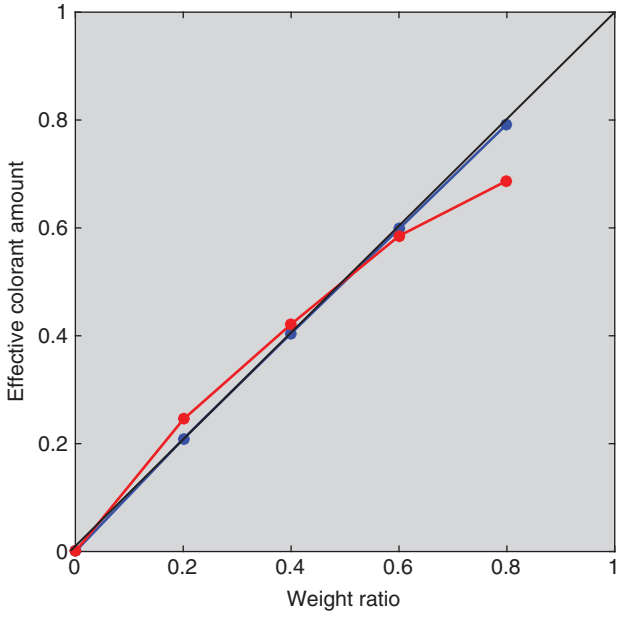

Figure 9.23 Relationship between actual weight and c_e of ultramarine blue (blue line) and red iron oxide (red line) tint ladders using single-constant Kubelka–Munk theory.

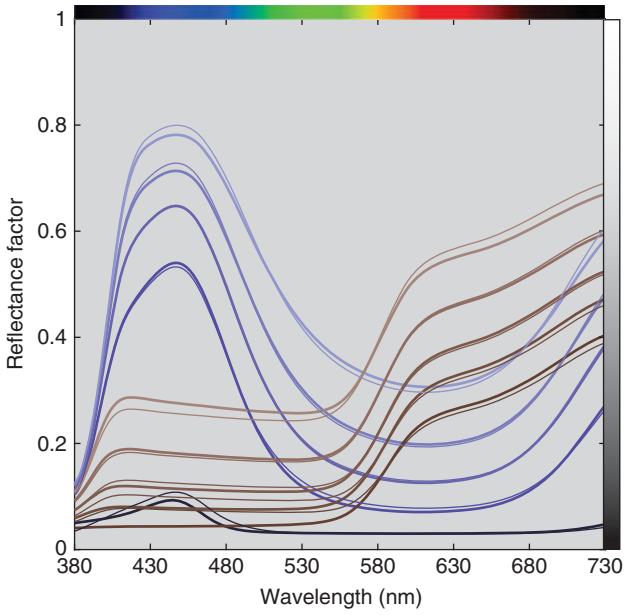

Figure 9.24 Measured (thick lines) and estimated (thin lines) spectral reflectance factor of ultramarine blue and red iron oxide tint ladders using single-constant Kubelka–Munk theory with an impurity index.

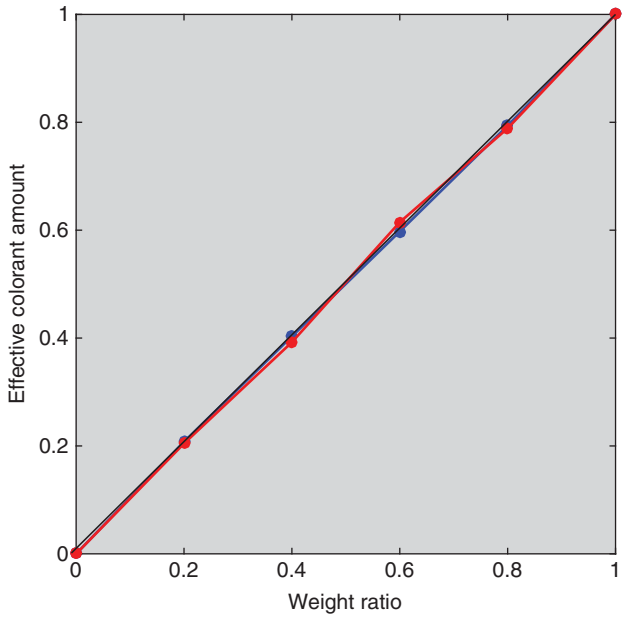

Figure 9.25 Relationship between actual weight and c_e of ultramarine blue (blue line) and red iron oxide (red line) tint ladders using single-constant Kubelka–Munk theory with an impurity index.

similar to the single-constant predictions. However, the relationships between weight and effective colorant amount had similar accuracy to the two-constant predictions, verifying the effectiveness of the impurity index.

c_e were optimized separately from the unit spectra and Saunderson constants for all three models. We have found that for the two-constant form of Kubelka–Munk theory, convergence is difficult as well as the results not improving significantly when all the optical parameters are optimized simultaneously. The same approach was used for the single-constant models for simplicity. Simultaneous optimization is used when modeling opaque textiles, described below.

Opaque Textiles

Textiles are opaque because the substrate scatters incident light, whether in fiber, yarn, or woven form. In most cases, the amount of scattering is large compared with scattering by colorants. This is also true for colored paper. When colorant scattering is negligible, single-constant Kubelka–Munk theory can be used, shown in Eqs. (9.32)–(9.35). The Saunderson correction is not required because the textile or paper fibers are immersed in air

$$\left(\frac{K}{S}\right)_\lambda = \frac{(1-R_{\lambda,m})^2}{2R_{\lambda,m}} \tag{9.32}$$

$$\left(\frac{K}{S}\right)_{\lambda,\text{mixture}} = c_{e,1}\left(\frac{k}{s}\right)_{\lambda,1} + c_{e,2}\left(\frac{k}{s}\right)_{\lambda,2} + \cdots + \left(\frac{k}{s}\right)_{\lambda,\text{substrate}} \tag{9.33}$$

$$\left(\frac{k}{s}\right)_{\lambda,\text{substrate}} = \left(\frac{K}{S}\right)_{\lambda,\text{substrate}} \tag{9.34}$$

$$R_{\lambda,m} = 1 + \left(\frac{K}{S}\right)_\lambda - \sqrt{\left(\frac{K}{S}\right)_\lambda^2 + 2\left(\frac{K}{S}\right)_\lambda} \tag{9.35}$$

As an example, polyester fabric was cold pad-batch dyed using red, yellow, and blue disperse dyes. Tint ladders were made where the fabric was dyed at concentrations of 0.0, 0.1, 0.5, 1.0, 2.0, and 5.0 grams per liter (g/l). Null concentration dyeings are called *blank dyeings*, important because the dyeing process can change the optical properties of the substrate. Fabrics were also dyed using two and three colorant combinations. Each dyed fabric was folded in half to achieve opacity and four measurements were taken, one at each rotation in four different locations, using an integrating sphere spectrophotometer with the specular component included. The four measurements were averaged and the spectra are shown in Figure 9.26. These spectra were transformed to *K/S* using Eq. (9.32), the results shown in Figure 9.27. Reflectance factor and *K/S* are inversely related, similar to the paint spectra shown above.

Equation (9.36) was used to normalize the spectra in order to evaluate scalability, the results shown in Figure 9.28

$$\left(\frac{K}{S}\right)_{\lambda,\text{normalized}} = \frac{\left(\frac{K}{S}\right)_{\lambda,\text{tint}} - \left(\frac{K}{S}\right)_{\lambda,\text{white}}}{\left[\left(\frac{K}{S}\right)_{\text{tint}} - \left(\frac{K}{S}\right)_{\text{white}}\right]_{\text{at }\lambda\text{ maximum}}} \tag{9.36}$$

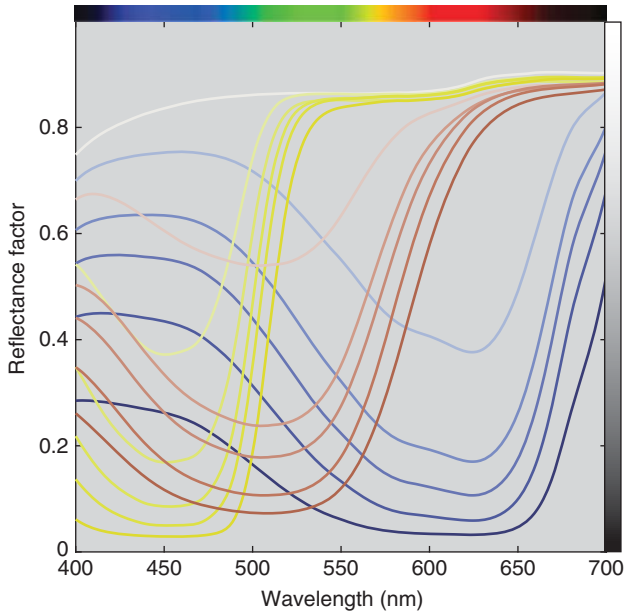

Figure 9.26 Spectral reflectance factor of polyester tints and blank-dyed fabric.

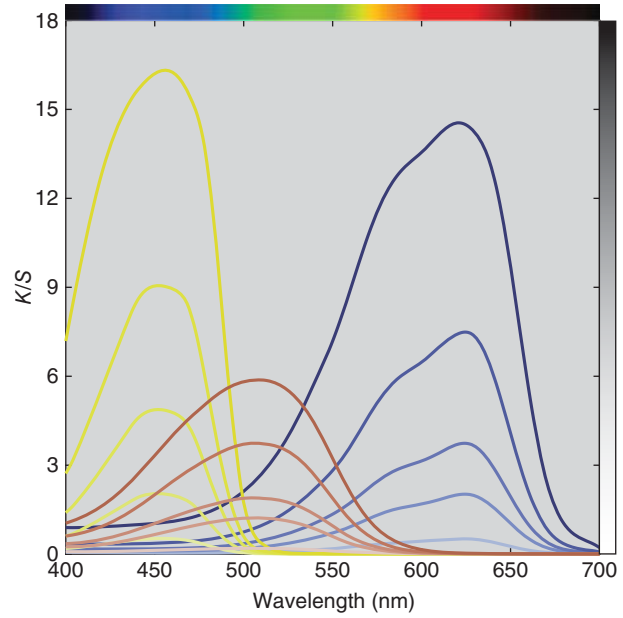

Figure 9.27 *K*/*S* spectra of polyester tints and blank-dyed fabric.

Scalability was reasonable for the three colorants between 0.0 and 2.0 g/l. The 5.0 g/l blue and yellow samples had spectra with wider bandwidth, indicating that single-constant theory is inadequate to model this coloration system at high concentrations. The 5.0 g/l samples for all three colorants were excluded limiting color matching to 2.0 g/l. The 0.5 g/l red sample also had a wider bandwidth, a result of poor dyeing uniformity of the fabric. Excluding

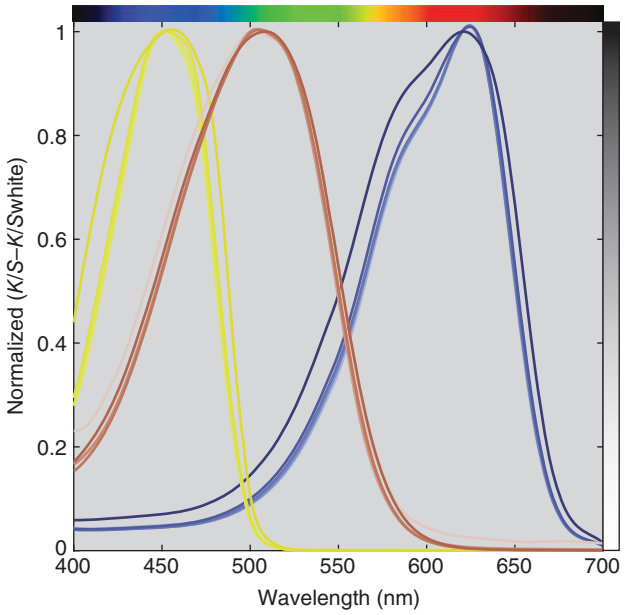

Figure 9.28 Normalized (*K*/*S*) spectra of polyester tints.

the 0.5 g/l red sample did not change the results and was retained for consistency.

Unit $(k/s)_\lambda$ were calculated using the 0.0 and 1.0 g/l samples, the formula shown in Eq. (9.37)

$$\left(\frac{k}{s}\right)_{\lambda,\text{colorant}} = \frac{\left(\frac{K}{S}\right)_{\lambda,\text{tint}} - \left(\frac{K}{S}\right)_{\lambda,\text{white}}}{c_{\text{tint}}} \tag{9.37}$$

These unit data and actual concentrations were used as starting values in an optimization that predicted $(k/s)_\lambda$ and c_e for all of the samples for each colorant where RMS spectral reflectance error was minimized. The resulting $(k/s)_\lambda$ for red, yellow, and blue are shown in Figure 9.29. Integrating $(k/s)_\lambda$ as a function of wavelength is sometimes used as a measure of tinting strength and depth of shade, useful when comparing batches of colorants that are priced according to their strength or depth (Smith 1997). For this example, the tinting strengths of red, yellow, and blue were 20.0, 34.4, and 35.3, respectively.

The optimization results in estimated reflectance spectra and c_e. Equations (9.38) and (9.35) are used to calculate estimated spectral reflectance

$$\left(\frac{K}{S}\right)_{\lambda,\text{estimated}} = c_e\left(\frac{k}{s}\right)_{\lambda,\text{colorant}} + \left(\frac{k}{s}\right)_{\lambda,\text{substrate}} \tag{9.38}$$

Comparison of the estimated and measured reflectance spectra was used to evaluate scalability in addition to Figure 9.28, shown in Figure 9.30. The blue sample matches were excellent; the yellow matches were reasonable; and the red matches were poor at long wavelengths. The relationship between concentration and c_e is shown in Figure 9.31. None

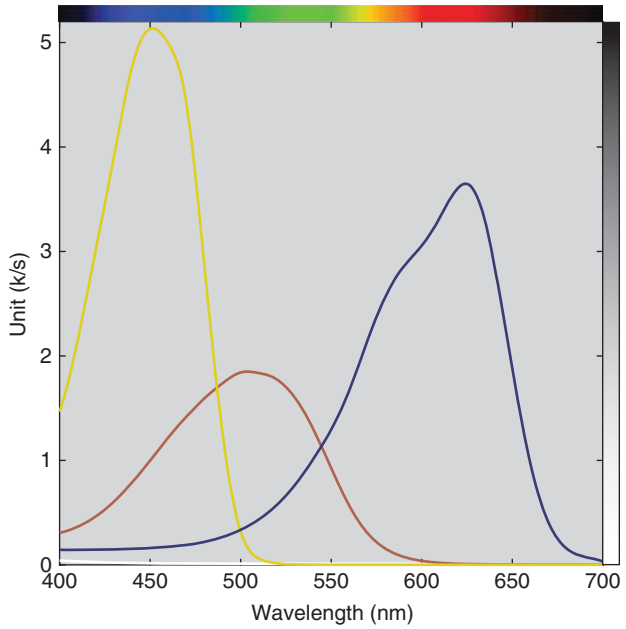

Figure 9.29 Unit $(k/s)_\lambda$ of red, yellow, and blue colorants.

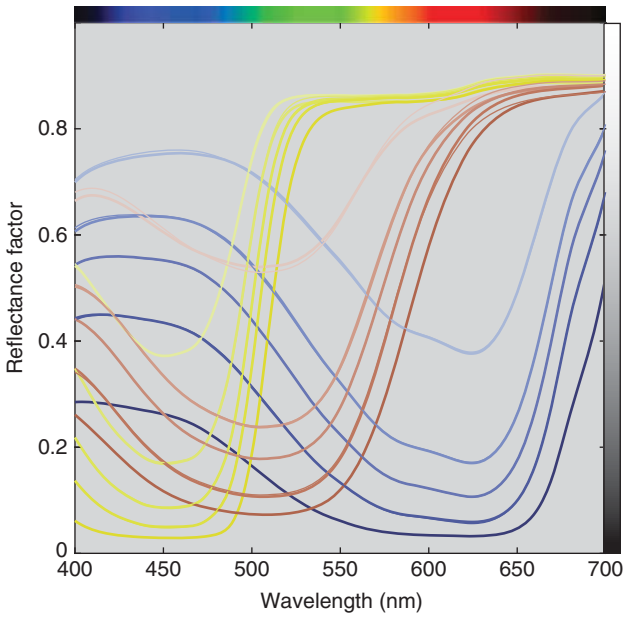

Figure 9.30 Measured (thick lines) and estimated (thin lines) spectral reflectance factor of the red, yellow, and blue tints using single-constant Kubelka–Munk theory.

of the colorants exhibited monotonicity, a result of poor process control. Exhaust dyeing would improve these results. Typically, c_e reduces as concentration increases because available dye sites are depleting. This was tested for the red colorant by adding back the 5.0 g/l tint and repeating the optimization, the results shown in Figure 9.32. (Recall that the red colorant was scalable at this high concentration, seen

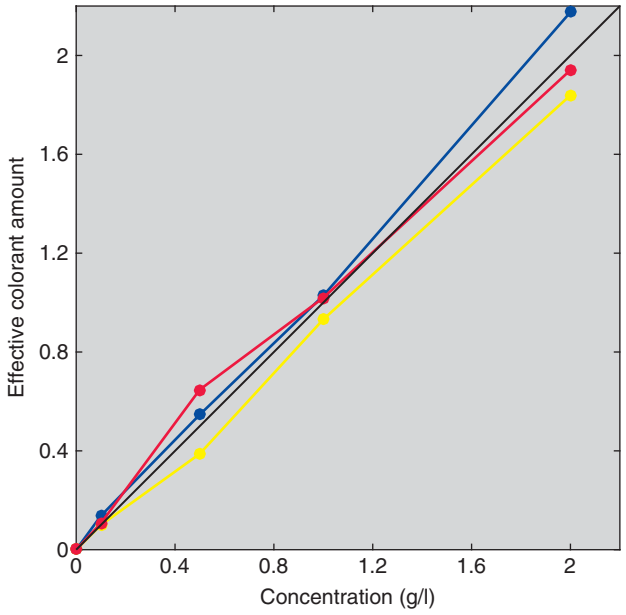

Figure 9.31 Relationships between concentration and c_e for the red, yellow, and blue tints.

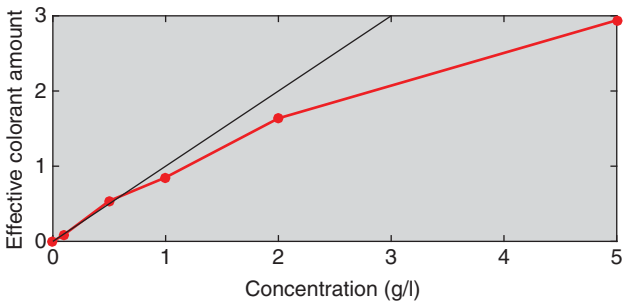

Figure 9.32 Relationship between concentration and c_e for red tints ranging between 0.0 and 5.0 g/l.

in Figure 9.28.) The reduction in effective colorant amount is evident. The data plotted in Figure 9.32 would be used to define the relationship between user controls, concentration, and c_e, the second step in the generic approach to color modeling.

Nine two-colorant dyeings were made for all combinations of 0.5, 1.0, and 2.0 g/l. Two three-colorant dyeings were also performed at concentrations of 0.1 and 1.0 g/l for each colorant. The $(k/s)_\lambda$ for each of the colorants were used to estimate c_e, minimizing RMS spectral reflectance error. The spectral fits are shown in Figure 9.33 for the 11 samples. The results were reasonable for mixtures with blue and yellow and blue and red. The results for mixtures with red and yellow were poor at long wavelengths.

The relationship between concentration and c_e for all of the samples is shown in Figure 9.34. We expected modest variability about the tint lines. This did not occur. Instead there was large variability as well as an increase in the range

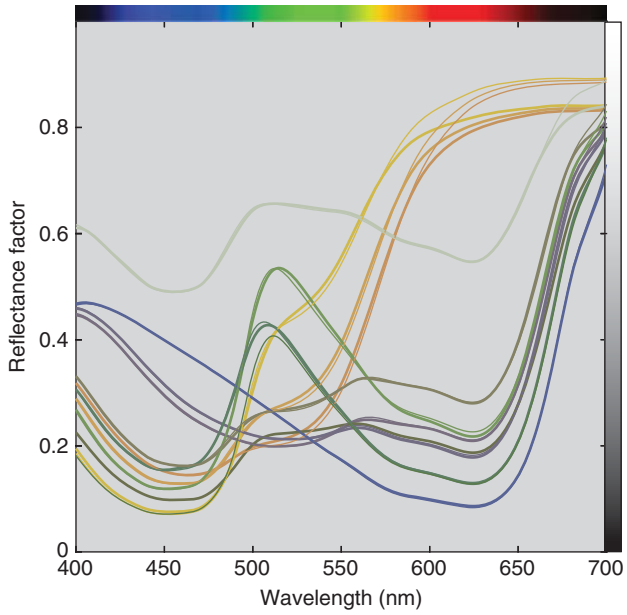

Figure 9.33 Measured (thick lines) and estimated (thin lines) spectral reflectance factor of 2 and 3 colorant mixtures using single-constant Kubelka–Munk theory.

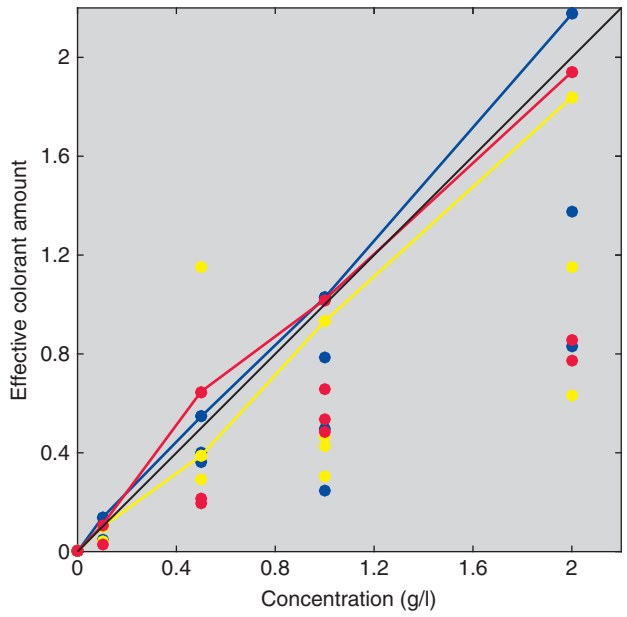

Figure 9.34 Relationships between concentration and c_e for all the samples.

of values with an increase in concentration. It is unclear whether this large variability is attributed mainly to poor process control or limitations in Kubelka–Munk theory. If the former, the process needs to be improved or replaced. If the latter, then a three-dimensional lookup table may be warranted.

D. MODELING GONIOAPPARENT MATERIALS

Gonioapparent materials change their appearance with changes in illuminating and viewing geometries, as described in Chapter 1. Gonioapparent materials include metallic flakes, pearlescent pigments, interference pigments, and diffraction pigments. These are used in addition to or in place of conventional absorbing and scattering colorants. Automotive coatings, printing inks, and cosmetics are examples of these materials. Models are used to predict spectral reflectance at geometries used by multiangle spectrophotometers and can be generalized to predict bidirectional reflectance distribution functions (BRDFs), required for computer graphics rendering. Researchers in computer graphics have been active in modeling many kinds of materials since the 1960s, summarized by Dorsey, Rushmeier, and Sillion (2008) and Montes and Ureña (2012). Models specific to coatings include Germer and Nadal (2001), Ďurikovič and Ágošton (2007), and Ferrero et al. (2016). Examples of using BRDF measurements for product design include Ďurikovič and Ágošton (2007), Kim and Lee (2011), Shimizu and Meyer (2015), and Musbach (2016). A simulation of an automotive coating containing aluminum flake is shown in Figure 9.35. Models that predict the optical behavior of gonioapparent materials are very complex and beyond the scope of this book. We suggest the books by Völz (2001), Klein (2010), and Kettler et al. (2016) as starting points.

E. COLOR-FORMULATION SOFTWARE

Color-formulation software, also known as *color-matching software*, is designed to aid a colorist in selecting colorants and determining their concentrations in order to match a color standard. The standard can be a physical sample, spectral data, or a colorimetric specification. Formulation software has three main components. The first is a database of the optical properties of the coloration materials. The second is the algorithms that select the colorants and predict a formulation (recipe). The third is the algorithms that correct the initial recipe when the match is not within tolerance, also known as *batch correction*.

Spectral-based algorithms require a spectrophotometer with high precision and accuracy. If numerical data are used to define the standard, intrainstrument and interinstrument reproducibility must also be excellent, considered in detail in Chapter 6.

The success of formulation software depends on a consistent and repeatable coloration process. The phrase “garbage in, garbage out” comes to mind. This is evaluated both in the color laboratory and in manufacturing. If the same recipe is used to make 10 samples, will the same color result? If the process variability and manufacturing tolerance are similar, producing an acceptable batch will only occur by chance.

Figure 9.35 Simulation of aluminum flake in a lacquer containing red dye, over gray primer (Musbach 2016).

Changing software will not improve the odds. It is absolutely essential to evaluate the process and make improvements if repeatability is poor.

The next step is to prepare samples that will be used to create the optical database. Different software requires different kinds and numbers of samples. Replicates are important in case there is a process error. A weighing error during database development will affect formulation accuracy.

Many matching algorithms are possible. For a spectral-based standard, the best formulation results in a spectral match. This eliminates metamerism. When a spectral match is not achievable, the least metameric formulation is the best. For a colorimetric standard, the best formulation is the most color constant. Indices of metamerism and color inconstancy are described in Chapter 8. These are used to rank order potential formulations. We have not listed cost in our definition of best. Any future issues with metamerism or color inconstancy will negate initial cost savings. For example, a commercial color order system was produced for a period of time where samples were replenished that had the lowest cost. The spectra from a constant-hue page are shown in Figure 9.36. Ideally, all the spectra should have similar shape so that the samples have similar color constancy. There are two types of spectra. Spectra having peak wavelengths at 560 nm were formulated for lowest cost. A visualization of the samples illuminated by illuminants D65 and A is shown in Figure 9.37. The samples formulated for least cost have very different color constancy where they become greenish under illuminant A. This difference in color constancy occurs for many illuminants. As a consequence, viewing this

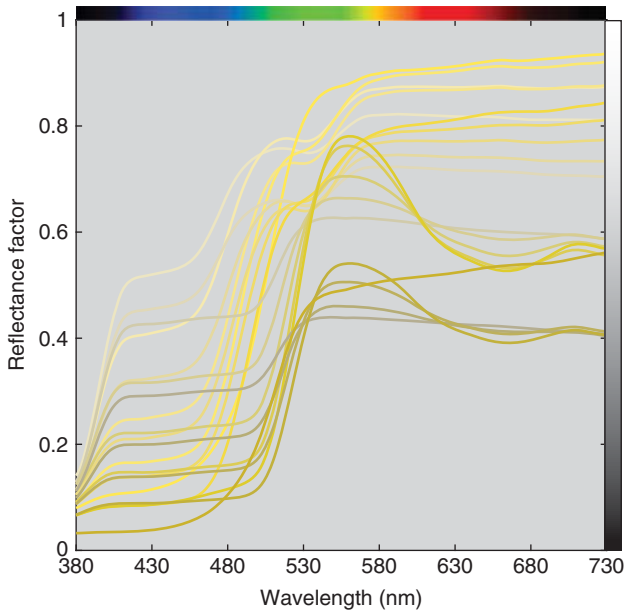

Figure 9.36 Spectral reflectance factor of samples at constant hue from a physical color order system.

page under nonstandard lighting greatly reduces the utility of a physical color order system.

The relationships between concentration and spectral reflectance and between concentration and colorimetry are nonlinear and accordingly, nonlinear optimization algorithms are required. These are constrained optimizations where concentration cannot be negative and in the case of paint, the sum of concentrations equals unity. Nonlinear

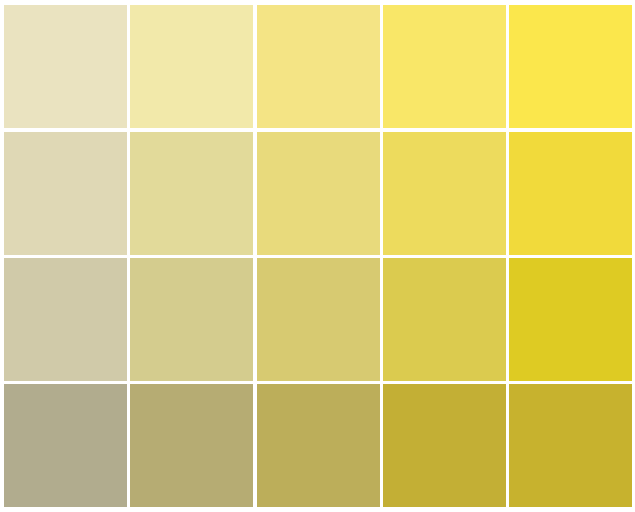

(a)

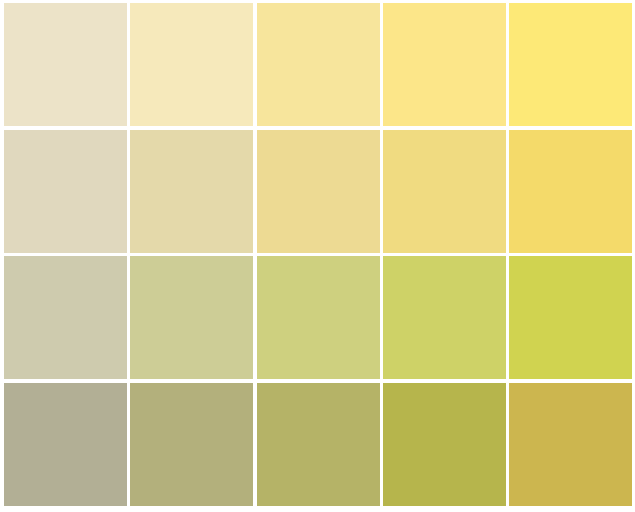

(b)

Figure 9.37 Visualization of the spectra shown in Figure 9.36 illuminated by (a) CIE illuminant D65 and (b) CIE illuminant A, viewed by the 1931 CIE standard observer.

optimization has the disadvantage of sometimes converging on a local minimum, resulting in a recipe that is correct, but not its best. This limitation is minimized by having reasonable starting values. For spectral algorithms, least squares linear regression can be used minimizing RMS *K*/*S* error (McGinnis 1967; Walowit, McCarthy, and Berns 1988). For colorimetric algorithms, pseudo-tristimulus values are calculated using *K*/*S* or weighted *K*/*S* in place of reflectance where the weighting improves linearity between concentration and pseudo-tristimulus values (Allen 1966, 1974, 1980). The pseudo-tristimulus values are used as additive primaries and concentration is estimated in the same manner as calculating *RGB* for a specific *XYZ*. See Berns (1997, 2000) for more details.

The second aspect of the matching algorithm is choosing the best colorants. Process variability is added to least metameric or least color inconstant when defining "best." There may be two formulations with similar color inconstancy. The formulation that leads to the smallest colorimetric variability is preferred. The optical model can be used to calculate the variability.

A third aspect is selecting the colorants to evaluate. Degrees of freedom come into play. Colorants were defined as ratios in the paint example and the white concentration was the remainder. If the formulation has four colorants, for example, three chromatic colorants and white, there are three degrees of freedom. There is always one less degree of freedom than the total number of colorants. When dispensing color concentrates into a base paint, such as retail paint and hardware stores, each concentrate has a single degree of freedom and the total degrees of freedom equal the number of concentrates. This is also true when dyeing textiles. Least-squares estimates have one degree of freedom less than the number of data points. For a wavelength range of 380–730 nm in 10 nm increments, there are $(36 - 1)$ degrees of freedom. In theory, the maximum number of colorants used in a formulation when spectral matching equals the number of degrees of freedom. It would seem that adding colorants will reduce metamerism—each additional colorant enables a match at an additional wavelength. This does not occur because absorption is across many wavelengths. Adding colorants rarely reduces metamerism. A colorimetric specification has three degrees of freedom, for example, *XYZ* or $L^*a^*b^*$. The degrees of freedom in a coloration system cannot exceed three.

Practically, the number of chromatic colorants in a formulation should not exceed four, that is, four degrees of freedom. Every combination of one, two, three, and four colorants should be evaluated. The number of combinations is calculated using Eq. (9.39):

$$\binom{N}{n} = \frac{N!}{(N-n)!n!} \tag{9.39}$$

where N defines the total number of colorants and n defines the number of colorants in a formulation. For 10 colorants, there are 10, 45, 120, and 210 one, two, three, and four colorant combinations, respectively. Equation (9.39) was enumerated for up to 25 colorants, shown in Figure 9.38. The total number of formulations for 25 colorants is 15 275. Limiting the formulation to three chromatic colorants reduces this number to 2625.

The approach we take when formulating is to test every combination. When the standard has spectral data, least squares linear regression minimizing *K*/*S* RMS error is used to obtain starting values. Then spectral reflectance RMS error is minimized. Finally, ΔE_{00} is minimized for a primary illuminant. Equation (8.2) is used as a special index of

metamerism or Eqs. (8.17) and (8.21) are used as a general index of metamerism. The effect of process variability is calculated by adding normally distributed random variability to each colorant in the formulation. Concentration defines the mean and the standard deviation is based on the process variability. The colorimetric data for the actual and perturbed formulations are compared and CIEDE2000 calculated for the primary illuminant. This is repeated 100 times. The average ΔE_{00} between the formulation and the 100 perturbations defines the process variability. The data are sorted first by metamerism and secondly by process variability and the best formulation selected. The approach we take when formulating to a colorimetric standard is to minimize ΔE_{00} and discard formulations that do not achieve a colorimetric match. The data are sorted first by color constancy and secondly by process variability.

For example, two-constant Kubelka–Munk theory was used to formulate the 16 gray metamers described in Chapter 8. Three were selected, their reflectance spectra shown in Figure 9.39 and their recipes and indices listed in Table 9.3. The first formulation is the closest spectral match. It is dominated by bone black and titanium white. The second formulation also contains bone black. However, its concentration is about half the amount of the first formulation, and as a consequence, the chromatic colorants have more of an influence on its spectral characteristics. The third formulation does not contain black but contains appreciable cobalt blue. This results in the large spectral mismatch at long wavelengths. All of the indices are correlated with each other and with the magnitude of spectral mismatch, quantified by reflectance RMS difference. Process variability was

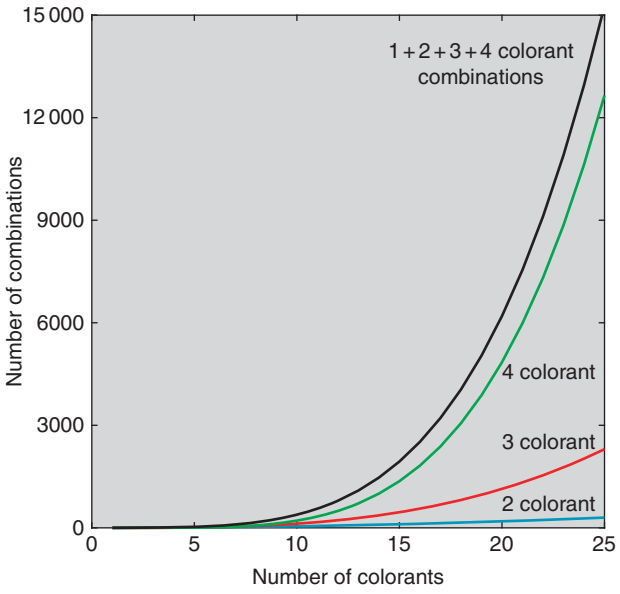

Figure 9.38 Number of combinations as a function of the total number of colorants, based on enumerating Eq. (9.39).

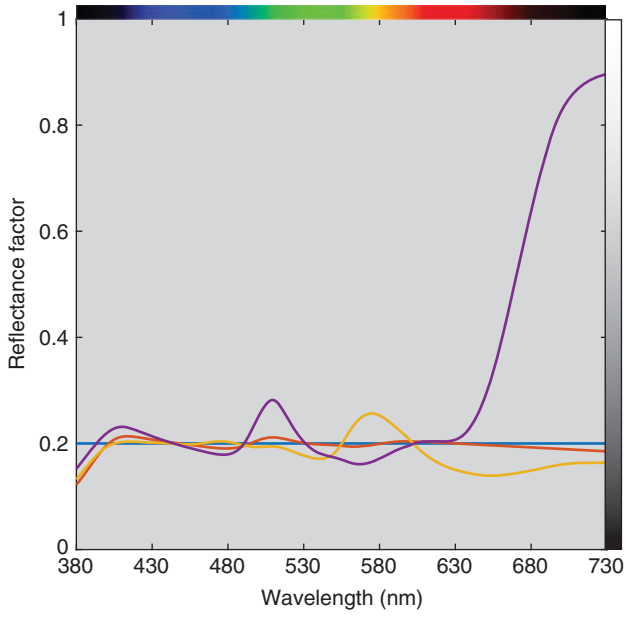

Figure 9.39 Spectral reflectance factor of standard (blue line), metamer 1 (red line), metamer 2 (orange line), and metamer 3 (purple line).

Table 9.3 Colorant amounts, metamerism indices, and process variability of three of the 16 metamers formulated for Chapter 8.

	Formulation 1	Formulation 2	Formulation 3
Colorant 1	Arylide yellow	Pyrrole orange	Arylide yellow
Colorant 2	Quinacridone magenta	Phthalocyanine green	Cobalt blue
Colorant 3	Bone black	Bone black	Quinacridone magenta
$c_{e,1}$	0.03	0.16	0.11
$c_{e,2}$	0.03	0.12	0.44
$c_{e,3}$	0.59	0.33	0.11
c_{white}	0.35	0.39	0.33
Reflectance RMS difference	0.016	0.034	0.301
Special metameric index, ΔE_{00}	0.1	3.5	5.4
General metameric index, Viggiano	0.0014	0.0058	0.0080
Process variability for primary illuminant, ΔE_{00}	0.6	2.0	3.5

assumed to result from weighing imprecision. For formulations summing to unity, the standard deviation was defined as 0.025. This uncertainty occurs for all four paints and is independent of weight ratio. This translates to $\pm 0.006c$. In this example, process variability correlated with the degree of metamerism. Clearly, Formulation 1 is the best formulation.

The third component, when required, is adjusting the initial formulation to more closely match the standard. Kubelka–Munk and possibly other optical models have limited accuracy, and as a result, either a second sample needs to be made in the laboratory or the production process adjusted. The measured spectral reflectance of the first sample is treated as a new standard and a formulation is determined. The differences between the initial and reformulated concentrations are used to create correction factors that adjust the relationship between weight and c_e. See McDonald (1997), Nobbs (1997), and Berns (2000) for more details. The adjustments are specific to the set of colorants. These corrections become part of the optical database and are used in future formulations when using the same colorants with similar concentrations.

Over time, a database is developed consisting of concentrations and colorimetric data. This is a multidimensional lookup table. The model can be replaced with the table and linear interpolation used to calculate a recipe for a specific color. The database can also be used as training data to create a neural network or other learning-based algorithm. The latter technique might lead to higher accuracy when the database is sparsely populated. These database approaches are very useful when an optical model cannot be developed with sufficient accuracy.

F. SUMMARY

Optical models of colored materials are used for both product development and color formulation. Modeling transparent materials, paints, and plastics requires calculating either internal transmittance or reflectance. The Fresnel and Saunderson formulas are used. Transparent materials such as glass and colorants dissolved in a solvent are modeled using the Bouguer–Beer law where transmittance is predicted from path length and concentration. Scattering materials such as coatings and textiles are modeled based on radiative transfer theory, pioneered by Shuster at the beginning of the twentieth century. Models used for predicting reflectance from colorant concentration simplify radiative transfer theory by assuming that light (flux) travels in only a specific number of directions. Examples include two-, three-, four-, many-, and multi-flux models. The two-flux model derived by Kubelka and Munk has been used extensively to model opaque materials and led to the development of colorant formulation software during the mid-twentieth century. The success of this software depends on process repeatability both in the laboratory and in production. Samples are prepared at various concentrations and when translucent, also at various thicknesses. They are measured with a spectrophotometer and used to develop an optical database. Formulations are predicted that match a standard using the colorants stored in the database. When the standard is spectral, the best match is the least metameric. When the standard is colorimetric, the best match is the most color constant. Formulations can also be evaluated for process variability and those leading to the smallest variability in total color difference are preferable. Selecting the best formulation is the most important feature of the software, particularly when the number of colorants in the database is large. Sometimes, materials, especially those containing gonioapparent pigments, cannot be modeled with sufficient accuracy and table lookup and learning-based algorithms are used.

Chapter 10
Color Imaging

The first color image, a tartan ribbon, was taken by Sutton in 1861 for a lecture given by Young (Cat 2013). The image was used to demonstrate trichromacy. Advances since that time have changed our cultural landscape including slide and print films, movie film, television, digital photography, digital printing, and digital cinema. Today, color imaging is ubiquitous where each cell phone contains a camera and display. Color consistency is excellent where images can be viewed on different phones, different computer displays, and printed on a variety of printers without large degradations in color quality. The consistency is a result of using colorimetry as a common language, developing transformations between device coordinates and colorimetry, and creating an imaging architecture to facilitate these transformations.

The Image

The properties of a digital image include dimensions, resolution, bit depth, file type, color mode, and color encoding (color management). We can think of a digital image as a piece of graph paper. Each square is called a pixel (a shortened form of "picture element"), and the number of squares on the sheet of paper defines the resolution, shown in Figure 10.1. Digital cameras are marketed according to their total number of pixels. A 24-megapixel (mpixel or MP or M) camera has 24 million pixels, usually arranged as 6000 pixels in one direction and 4000 pixels in the other direction: $6000 \times 4000 = 24\,000\,000$. Our numerical system is the decimal system, based on powers of 10 that are organized in ascending columns from right to left. Each column has 10 unique values: 0, 1, 2, ..., 9. Images use the binary system, based on powers of 2. Each position has two unique values: 0 and 1. Each column is called a bit. Most commonly, images use 8-bit encoding with values ranging from 00000000 to 11111111. There are 256 unique values: 0 to 255. The number of bits, called bit depth, determines numerical precision. In the past, most imaging hardware and software were limited to 8 bits. Recently, digital cameras have advanced to the point where their precision exceeds 12 bits, and improvements continue to be made. This has led to 16 and 32 bit-per channel images. Two common file types are TIFF and JPEG. TIFF files contain complete data, whereas JPEG files have reduced data that does not degrade image quality for many viewing applications. This is known as visually lossless file compression. The color mode defines the number of channels. Modes include grayscale (one channel), RGB (three channels: red, green, and blue), CMYK (four channels: cyan, magenta, yellow, and black), and Lab (three channels: L^*, a^*, and b^*). A color mode is underspecified until the color coordinates are assigned and related to a set of reference conditions. This process, called color encoding, is the domain of color management.

Billmeyer and Saltzman's Principles of Color Technology, Fourth Edition. Roy S. Berns.

Figure 10.1 Close up of Édouard Manet (French, 1832–1883), *Le Printemps (Jeanne Demarsy)*, 1881. Oil on canvas, 74 cm × 51.4 cm (29⅛ in. × 20¼ in.). At a distance, the pixels are not observed because the visual angle decreases.
Source: Digital image courtesy of the Getty's Open Content Program.

A. ANALYSIS AND SYNTHESIS

We learn in Chapter 2 that two stimuli match when an observer's *LMS* responses are equal. We learn in Chapter 4 that two stimuli match for a standard observer when colorimetric coordinates are equal. Let's consider Figure 10.2, first shown in Chapter 2. The displayed image implies that a camera was used to record the scene. This is shown in Figure 10.3 where the color cube represents a color transformation. The camera's *RGB* are transformed to the display's *RGB*.

The camera is *analyzing* the scene and the display is *synthesizing* the scene. The concept of analysis and synthesis was first described in the 1930s for color photography (Hardy and Wurzburg 1937; MacAdam 1938a,b) and was later used in the development of color television during the mid-twentieth century where the goal was to have the camera's linear *RGB* signals equal the display's linear *RGB* signals (Wintringham 1951; Epstein 1953). The chromaticities of a display were first defined. Color-matching functions were calculated for this display, the mathematics shown in a sidebar in Chapter 4. The color-matching functions were used as aim camera spectral sensitivities.

These calculations are repeated for an sRGB display, the results shown in Figure 10.4. There is a problem—sensors cannot have negative sensitivities. The practical solution

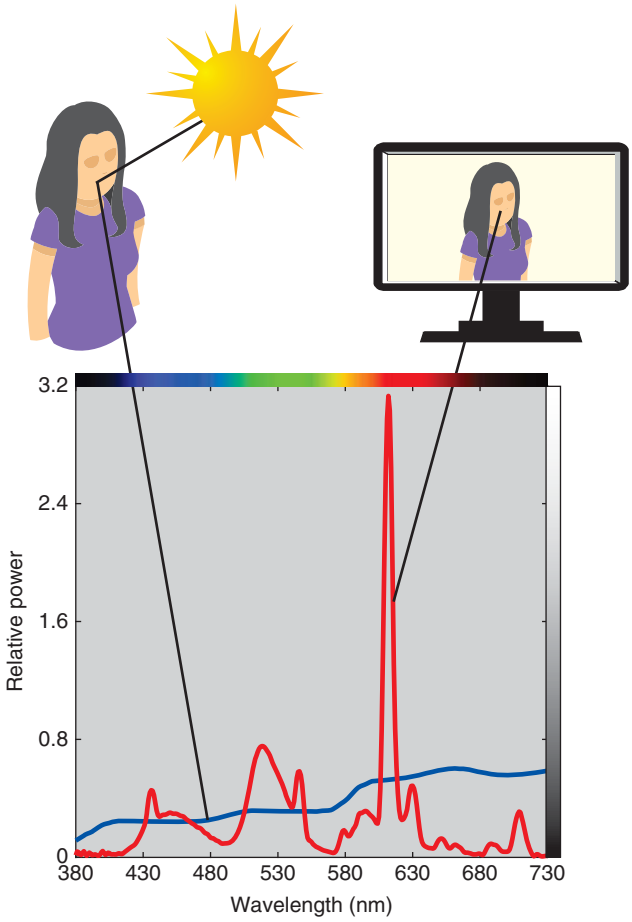

Figure 10.2 The sunlight reflecting from skin (blue line) and the light emitting from a liquid crystal display often used in color proofing (red line) result in a metameric match.

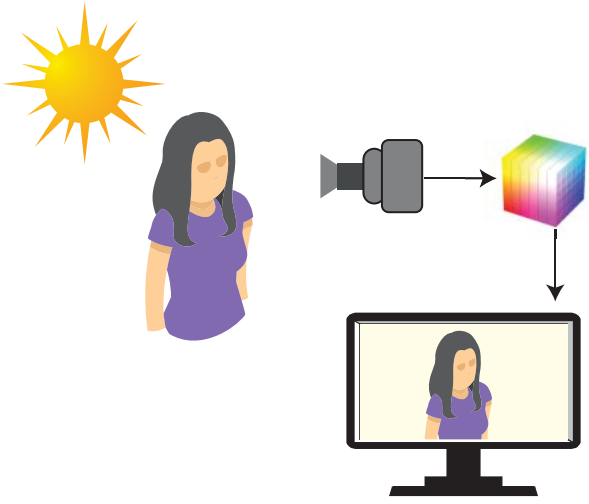

Figure 10.3 Imaging a scene and its reproduction on a display. The RGB color cube represents a color transformation.

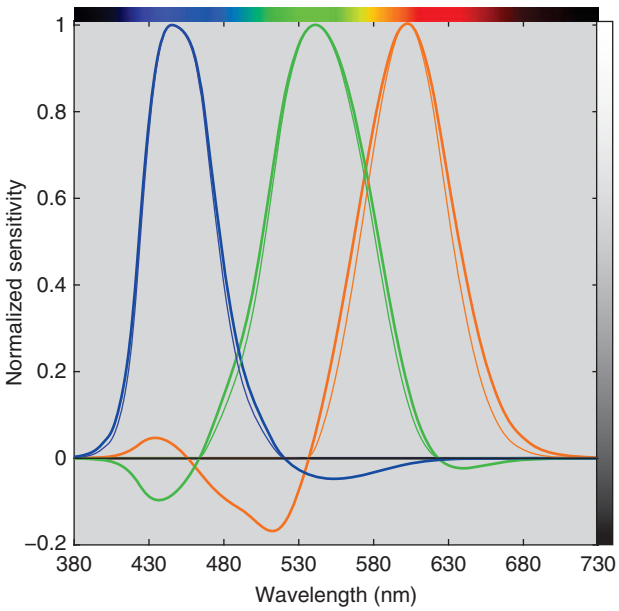

Figure 10.4 (Thick lines) Aim camera spectral sensitivities for an sRGB display based on methods used when standardizing broadcast television, (thin lines) all-positive approximations.

was to clip the color-matching functions, remove any secondary lobes, and reduce bandwidth resulting in integrated sensitivities equal to the aim color-matching functions, the results also shown in Figure 10.4. Cameras matching these ideal spectral sensitivities would have color accuracy below 1.5 ΔE_{00} on average with maximum errors less than 5.0 ΔE_{00} for colors within the display's color gamut.

B. COLOR MANAGEMENT

The broadcast television example is a single closed-loop system. Extending this approach to multiple imaging devices is shown in Figure 10.5 where a transformation is required between each input and output device. This approach quickly becomes unmanageable as devices are added. The use of a *reference color space* reduces the number of transformations from the product to the sum of the number of input and output devices, shown in Figure 10.6. This approach remains manageable.

Color management was formalized by the *International Color Consortium*, the *ICC*, in 1993 "by eight industry vendors for the purpose of creating, promoting and encouraging the standardization and evolution of an open, vendor-neutral, cross-platform color management system architecture and components. The outcome of this co-operation was the development of the ICC profile specification" (ICC 2018b). A *profile* defines the transformation linking a device with the reference color space, referred to as the *profile connection space* (*PCS*). The ICC profile specification was first published in 1994 that has evolved to become an ISO standard (ISO 2010) defining ICC.1 profiles. In 2015,

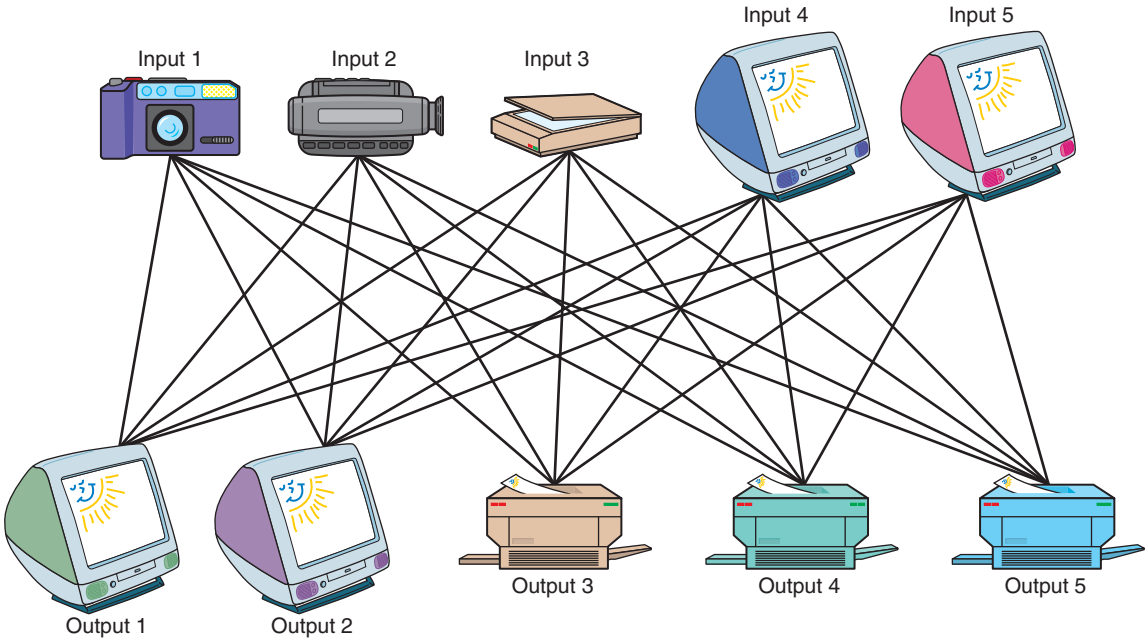

Figure 10.5 Each input device is connected to each output device. The total of the number of transformations is the number of input devices multiplied by the number of output devices. A display is an input device when used to create images.

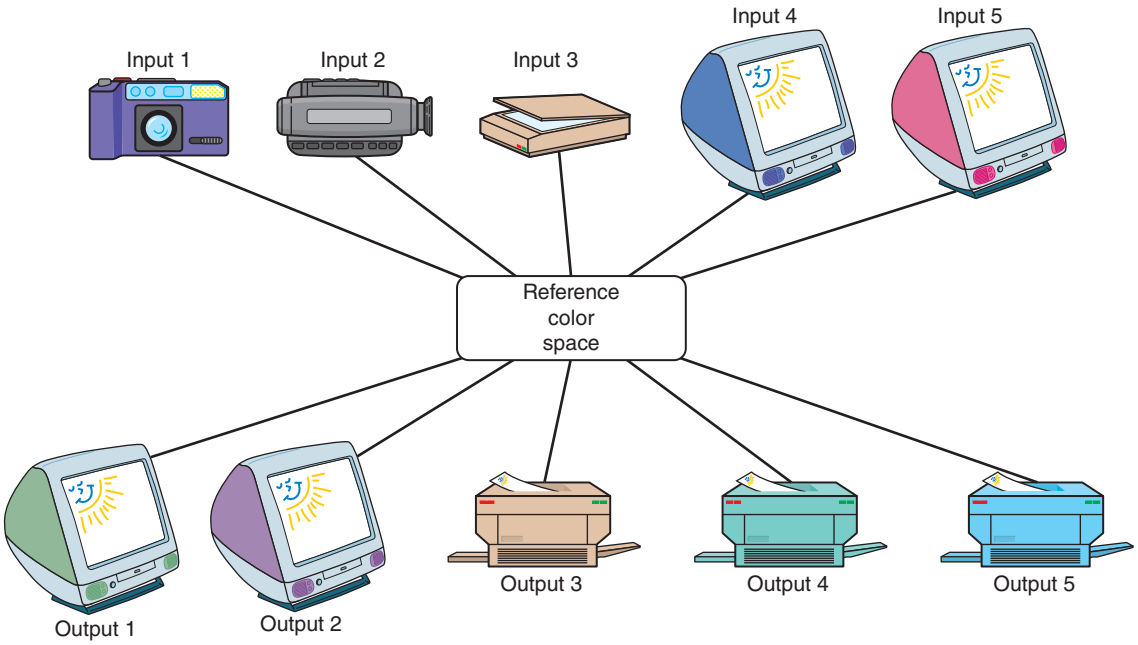

Figure 10.6 Each input and output device is connected to a reference color space.

the ICC published the ICC.2 (iccMAX) specification that defines extensions to ICC.1 profiles overcoming many of the limitations of ICC.1-based color management, described below (ICC 2018b).

The heart of ICC.1-based color management is the PCS. It has two embodiments. The first is colorimetric coordinates, either *XYZ* or $L^*a^*b^*$, defined for the 1931 standard observer and illuminant D50. Measurement geometry is bidirectional, for example, 45°a:0°. The second is a reference medium, a hypothetical print on a substrate with a spectrally nonselective reflectance factor of 0.81. The minimum reflectance is 0.11. It is viewed by the 1931 standard observer in an average surround against a gray background with a 0.2 reflectance factor. The illumination is CIE illuminant D50 at an illuminance of 500 lx. Chromatic adaptation is assumed to be complete. ICC color management, by design, is print-centric, a result of unacceptable color quality with the development of desktop publishing toward the end of the twentieth century. The requirements of the 1931 standard observer, illuminant D50, and bidirectional geometry stem from graphic-arts standards (ISO 2009b, 2017).

Profiles transform from device coordinates to *XYZ* or L^*a^*b and from a device's viewing conditions to the reference viewing conditions. They also handle situations where colors are out of gamut by performing *gamut mapping* of which there are many approaches (Morovič 2008). This is shown in Figure 10.7 for a sparsely sampled color gamut of 21 artist acrylic-dispersion paints with a glossy varnish compared with a CMYK offset print on smooth uncoated paper. The colors requiring mapping for this book's paper and ink are shown in gray.

The ICC has defined four types of mapping, known as *color-rendering intents*: *perceptual, saturation, media-relative colorimetric, and ICC-absolute colorimetric*. Perceptual mapping mimics chemical photographic systems from the twentieth century where the goal was to produce pleasing images. This mapping uses the reference medium as the PCS. Saturation mapping distorts colors to fully utilize a device's color gamut. Media-relative colorimetric rendering rescales the white point and clips out-of-gamut colors. This mapping uses colorimetric coordinates as the PCS. The rescaling assumes that each device's white defines the state of chromatic adaptation. The black point can also be rescaled, known as *black-point compensation*. Because of the rescaling of the white (and black) points, the amount of clipping caused by differences in color gamut is greatly reduced. The ICC-absolute colorimetric rendering clips out of gamut colors. Media-relative colorimetric rendering with black-point compensation was the rendering intent used for this book.

Profiles contain *metadata* in a specific file format that is used by the *color-management module*, also called the *color engine*, to transform between devices. The metadata for a display profile is listed in Table 10.1. Displays are defined by their white point, "wtpt," and the tristimulus values of each primary, "rXYZ," "gXYZ," and "bXYZ." The chromaticities for the primaries are plotted

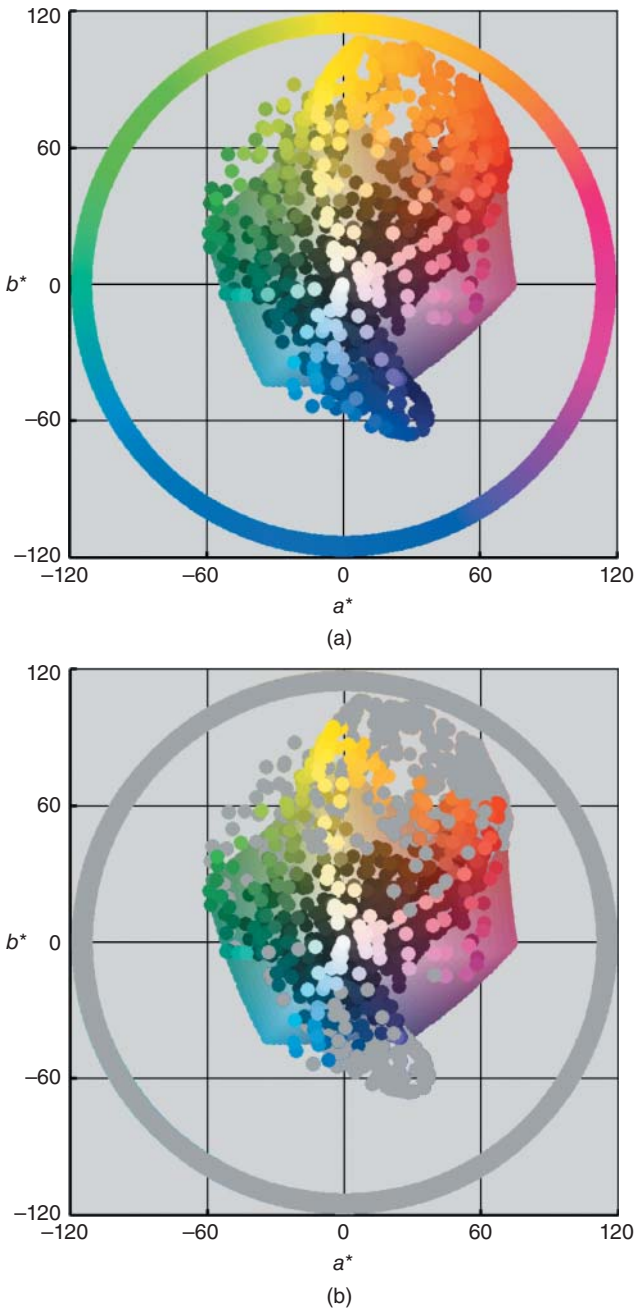

Figure 10.7 (a) Sparsely sampled CIELAB coordinates of mixtures of 21 artist acrylic dispersion paints with a glossy picture varnish overlaid on a CMYK offset print on smooth uncoated paper. (b) Areas in gray are out of gamut for the ink and paper used in this book (Printing gamut intentionally reduced in vividness).

in Figure 10.8. The nonlinear relationship between the user controls and the linear model (using terminology introduced in Chapter 9) is described by three 1024-point lookup tables, one for each primary: "rTRC," "gTRC," and "bTRC." The red primary lookup table, "rTRC," is plotted in Figure 10.9.

Table 10.1 ProPhoto RGB ICC v2 profile description.

No.	Tag	Data	Size	Description
3	"wtpt"	"XYZ"	20	Media white-point tristimulus
4	"rXYZ"	"XYZ"	20	Red colorant tristimulus
5	"gXYZ"	"XYZ"	20	Green colorant tristimulus
6	"bXYZ"	"XYZ"	20	Blue colorant tristimulus
7	"rTRC"	"curv"	2060	Red tone response curve
8	"gTRC"	"curv"	2061	Green tone response curve
9	"bTRC"	"curv"	2062	Blue tone response curve

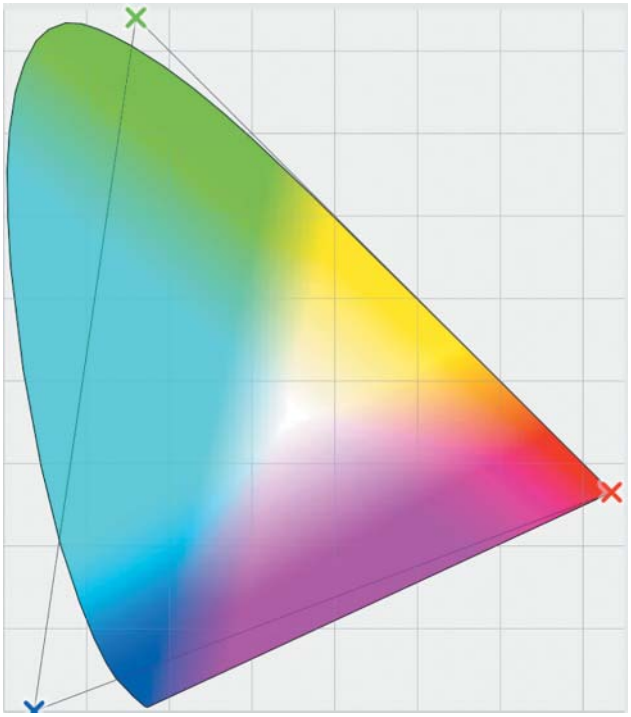

Figure 10.8 Screen capture using ColorSync Utility of the white point and colorant tags for the ProPhotoRGB ICC v2 profile plotted on a *xy* chromaticity diagram.

The metadata for a printer profile is listed in Table 10.2. Printer profiles contain multidimensional lookup tables to transform between device ("A") and PCS ("B") coordinates, usually CIELAB as shown in Figure 10.10. Interpolation is handled by the color-management module. There are three device-to-PCS and three PCS-to-device tables where the numerical designation identifies the rendering intent—0 for perceptual, 1 for media-relative colorimetric, and 2 for saturation. ICC-absolute data are calculated by rescaling the media-relative colorimetric data based on the media white-point tristimulus values. The "B2A" tables are large in order to achieve the highest colorimetric accuracy. "A2B" tables are smaller, seen by the smaller table size, because these tables are normally used to convert between different CMYK values where the mappings are similar.

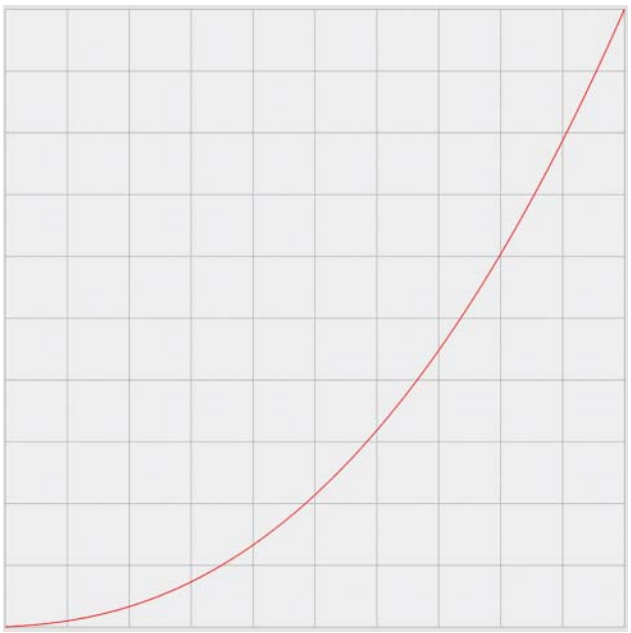

Figure 10.9 Screen capture using ColorSync Utility of the red tone response curve for the ProPhotoRGB ICC v2 profile.

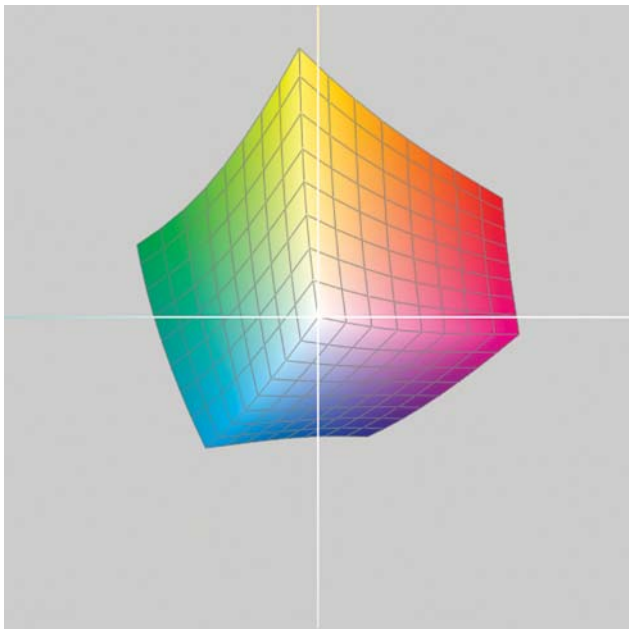

Figure 10.10 Screen capture using ColorSync Utility of the media-relative colorimetric A2B1 table for a US Web coated SWOP ICC v2 profile.

Table 10.2 US Web coated SWOP ICC v2 profile description.

No.	Tag	Data	Size	Description
3	"wtpt"	"XYZ"	20	Media white-point tristimulus
4	"A2BO"	"mft2"	41 478	Intent-0, 16-bit, device to PCS conversion table
5	"A2B1"	"mft2"	41 479	Intent-1, 16-bit, device to PCS conversion table
6	"A2B2"	"mft2"	41 480	Intent-2, 16-bit, device to PCS conversion table
7	"B2A0"	"mft1"	145 588	Intent-0, 16-bit, PCS to device conversion table
8	"B2A1"	"mft1"	145 588	Intent-1, 16-bit, PCS to device conversion table
9	"B2A2"	"mft1"	145 588	Intent-2, 16-bit, PCS to device conversion table
10	"gamt"	"mft1"	37 009	8-bit, PCS to gamut check table

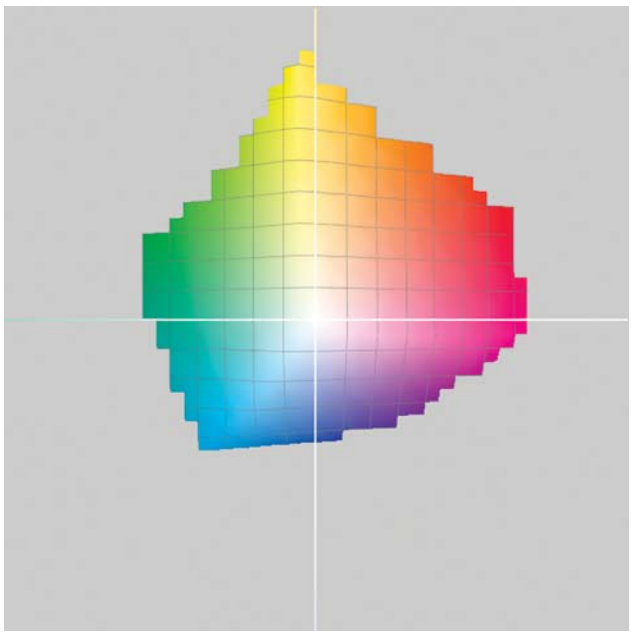

Figure 10.11 Screen capture using ColorSync Utility of the gamt table for a US Web coated SWOP ICC v2 profile.

A small lookup table is used, "gamt," to identify colors out of gamut. This was used in Figure 10.7b. The "gamt" table is shown in Figure 10.11 and when compared with Figure 10.10, indicates that identifying out-of-gamut colors is only approximate.

ICC.1-based color management has transformed printing and publishing. The images and graphs created for this book all have profiles that have resulted in reasonable color quality. Nonetheless, significant limitations remain. Foremost is metamerism. Spectral data are reduced to colorimetric data, eliminating the possibility of producing color reproductions that are not metameric. In Chapter 9, the best formulation to a colorimetric standard was the most color constant. Although it is possible to develop a printing transformation with this criterion (Chen 2006), it is rarely done. Most

colorants used in printing were designed for color gamut, not color constancy. The reference viewing illuminant is D50. We discussed in Chapter 7 the difficulty of simulating CIE daylight illuminants and potential problems when using simulated daylight to view materials that contain fluorescent whitening agents, such as many printing papers. There are also situations where the reference illuminant is not D50. Suppose that a painting and large-format print need to match each other under tungsten halogen lighting. Unless the camera and print profiles are created for this source, color errors will result caused by metamerism. Finally, gamut mapping is predefined. Output profiles have embedded transformations for the different rendering intents. More details about ICC.1 color management are found in Green (2010) and Sharma (2018).

C. ADDITIVE VERSUS SUBTRACTIVE MIXING

The terms *additive mixing* and *subtractive mixing* traditionally are used to differentiate between the mixing of colored lights and the mixing of colorants, shown in Figure 10.12. Mixing additive primaries produces white while mixing subtractive primaries produces black. Even when the individual primaries are separated spatially, such as displays and printing as shown in Figure 10.13, or temporally, such as projectors, the mixing behavior is still additive or subtractive because the eye cannot resolve the spatial pattern.

The relationship between additive and subtractive mixing is an important one and it is useful to describe this relationship using theoretical colorants. They can be either *theoretical additive primaries* or *theoretical subtractive primaries* (Hardy and Wurzburg 1937). The subtractive primaries are also known as *block dyes*. The visible spectrum is divided into thirds with divisions at 500 and 600 nm. Light below 500 nm is a *theoretical blue primary*; light between 500 and 600 nm is a *theoretical green primary*; light above 600 nm is a *theoretical red primary*. The theoretical red, green, and blue additive primaries produce light only in the spectral region corresponding to their color name. Outside of their respective wavelength regions, they do not produce any light. Adjusting the amount of a theoretical primary results in a different amount of light, but of the same spectral character, shown in Figure 10.14. As the amount of a primary increases from its minimum to its maximum, light is being added, hence the use of the term additive. Varying the amount of a theoretical additive primary results in colors varying between black and the particular primary. *Secondaries* are produced by combining pairs of primaries, shown in Figure 10.15. The combination of theoretical red and green produces a *theoretical yellow*. The combination of theoretical red and blue produces a *theoretical magenta*. The combination of theoretical blue and green produces a *theoretical cyan*. The combination of theoretical red, green, and blue produces a *theoretical white*. *Theoretical black* results when all three primaries are turned off. Again, light is being added or in the case of black, not added. This leads to two interlocking color triangles and a hue circle, shown in Figure 10.16. By definition, theoretical yellow is opposite theoretical blue, theoretical magenta is opposite theoretical green, and theoretical cyan is opposite theoretical red.

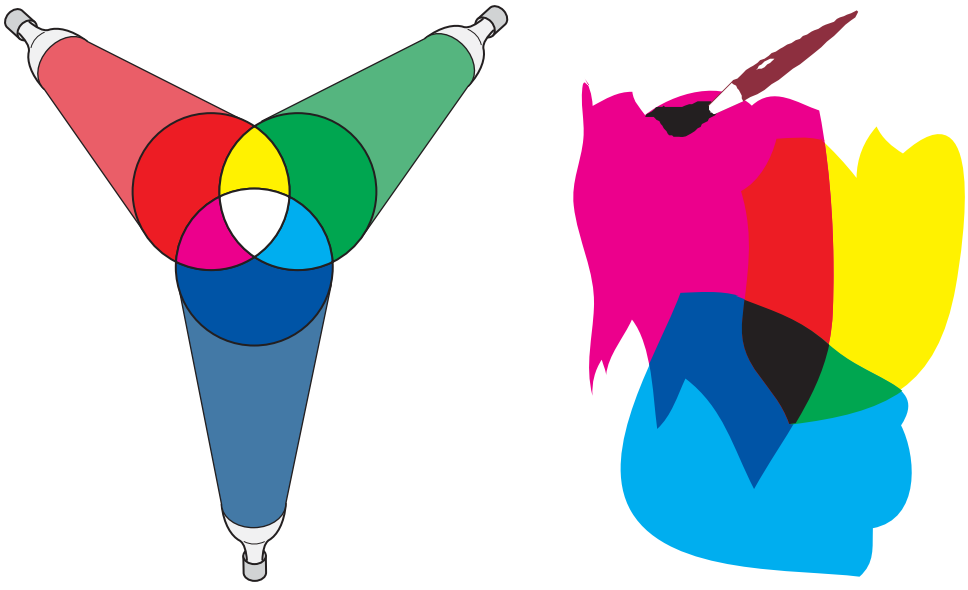

(a) (b)

Figure 10.12 The results of mixing (a) lights additively and (b) paints subtractively.

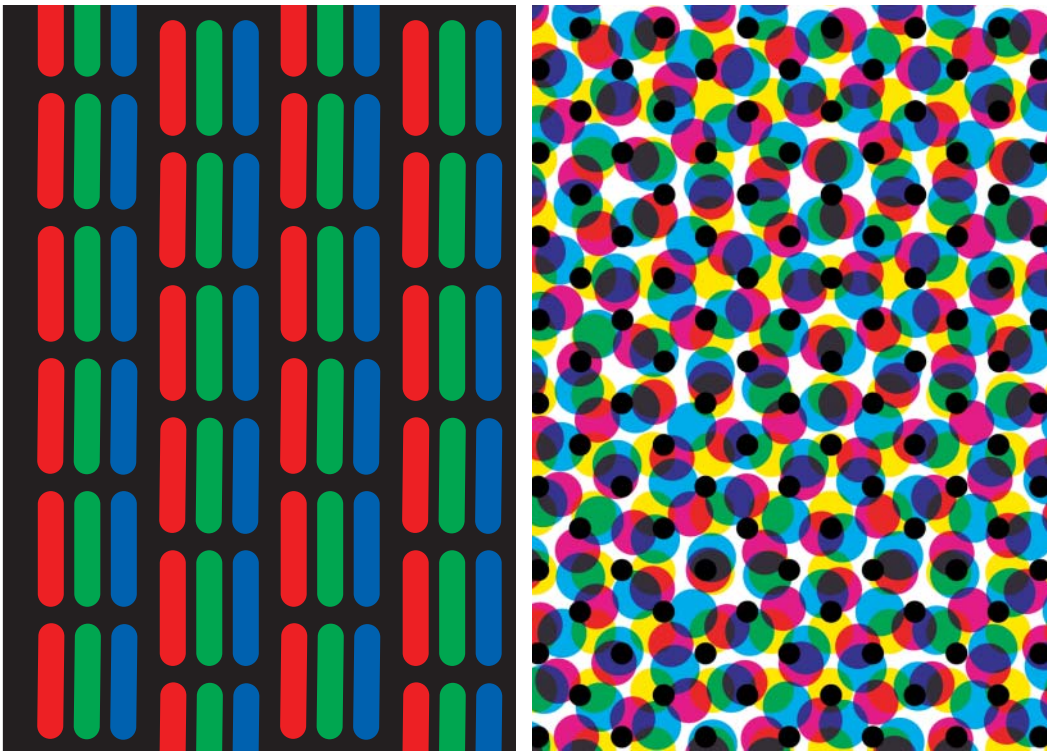

(a) (b)

Figure 10.13 Magnification of (a) an additive display and (b) a subtractive offset print.

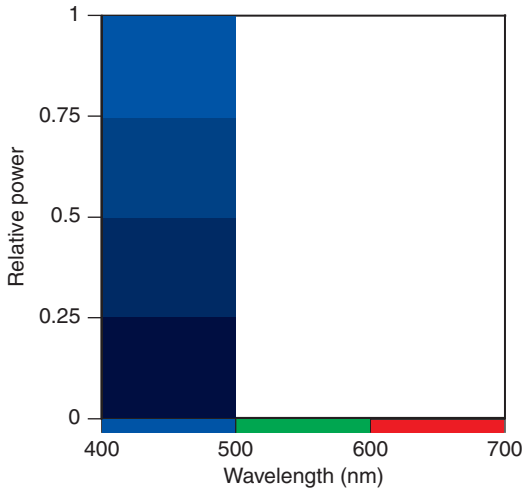

Figure 10.14 Theoretical blue additive primary. Light is only emitted between 400 and 500 nm. Varying the primary amount only affects the amount of output; its spectral shape is independent of intensity.

Theoretical red, green, blue, cyan, magenta, yellow, black, and white have specific definitions, based on their spectra.

The theoretical subtractive primaries are *cyan, magenta, and yellow*. Varying the amount of a theoretical subtractive primary from minimum to maximum results in colors varying between white and the particular primary. The term *subtractive* is used because light is subtracted through the process of selective absorption of light. A *theoretical cyan primary* subtracts red light, shown in Figure 10.17; a *theoretical magenta primary* subtracts green light; a *theoretical yellow primary* subtracts blue light. Combining theoretical cyan and yellow results in a *theoretical green* because the red and blue light have been subtracted, shown in Figure 10.18. Combining theoretical cyan and magenta results in a *theoretical blue* because the red and green light have been subtracted. Combining theoretical magenta and yellow results in a *theoretical red* because the green and blue light have been subtracted. Combining theoretical cyan, magenta, and yellow results in *theoretical black* because all of the light has been subtracted. We see that theoretical subtractive primaries control the amount of light that the visual system responds to in identical fashion to the theoretical additive primaries! In both cases, the amounts of red, green, and blue light are being controlled. This is why the theoretical subtractive primaries are opposite to the theoretical additive primaries when placed on a color wheel.

Many art educators continue to teach that red, yellow, and blue are the subtractive primaries. Many artist paint companies sell paints labeled primary red, yellow, and blue,

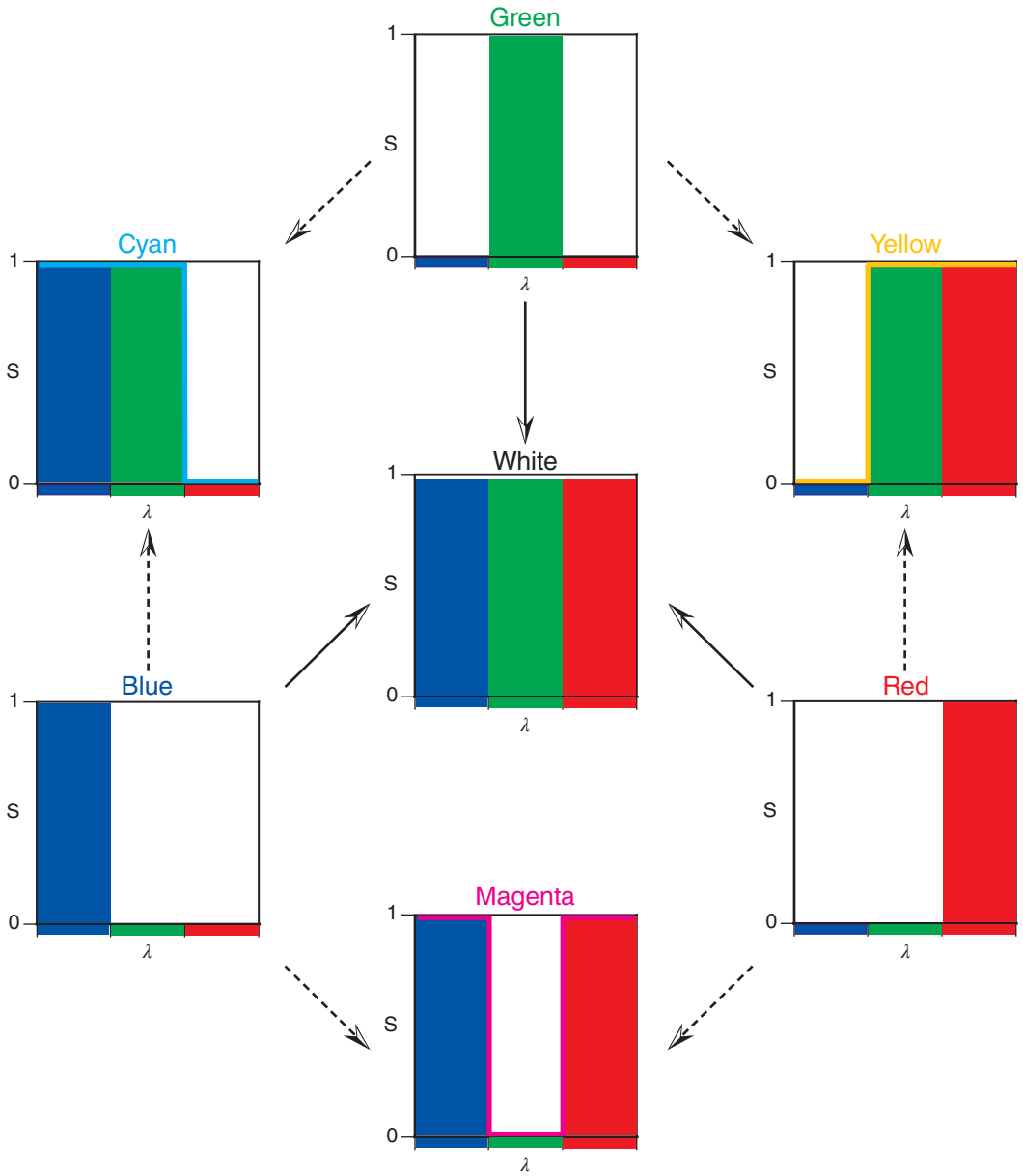

Figure 10.15 The theoretical additive primaries of red, green, and blue combine to produce white (shown by the solid arrows). When the additive primaries are combined pairwise, the secondaries of theoretical cyan, magenta, and yellow result (shown by the dashed arrows).

supporting this practice. The actual pigments have spectra similar to theoretical cyan, magenta, and yellow. Often quinacridone magenta, arylide yellow, and phthalocyanine blue (a cyan) are the colorants used to produce these primary red, yellow, and blue, respectively. What happens when we use the theoretical primaries of red, yellow, and blue in a subtractive process? Using a subtractive mixing model, a color gamut was calculated for these theoretical primaries, the results shown in Figure 10.19. There are not any greens nor magentas. Theoretical yellow absorbs all the blue light and theoretical blue absorbs all the green and red light; their mixture produces black, not green. Theoretical red absorbs all the blue and green light while theoretical blue absorbs all the green and red light; their mixture also produces black. Using the proper subtractive primaries, a full range of colors result, shown in Figure 10.20. Given that most of today's color systems are additive, such as cell phones, displays, and digital projectors, we hope this confusing practice discontinues.

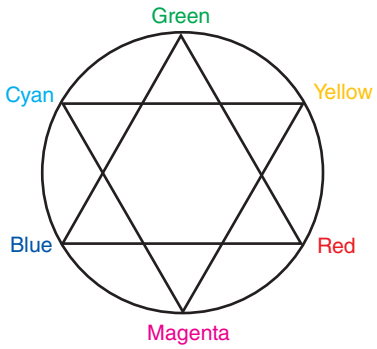

Figure 10.16 The relationship between the theoretical additive primaries and their secondaries, and between theoretical subtractive primaries and their secondaries, leads to a hue circle in which green and magenta, blue and yellow, and red and cyan are opposite one another.

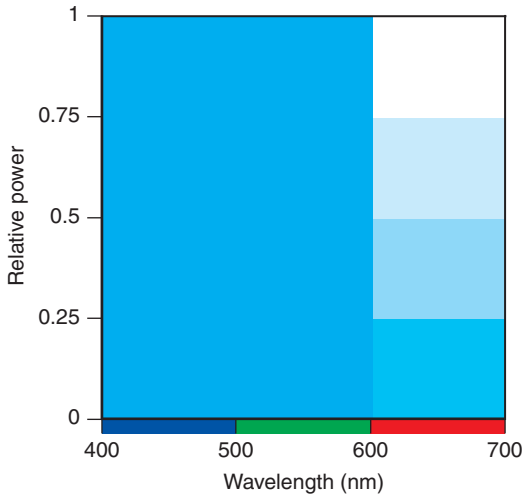

Figure 10.17 Theoretical cyan subtractive primary. Light is only absorbed above 600 nm. Varying the primary amount only affects the amount of absorption.

D. DISPLAYS AND ENCODING

The first color-managed displays were computer-controlled cathode ray tube (CRT) displays. Their colorimetry is shown in Eqs. (10.1)–(10.4) (IEC 2000a):

$$\begin{Bmatrix} R = \left[k_{g,r}\left(\frac{d_r}{2^N-1}\right) + k_{o,r}\right]^{\gamma_r} + R_o & k_{g,r}\left(\frac{d_r}{2^N-1}\right) + k_{o,r} \geq 0 \\ R = R_o & k_{g,r}\left(\frac{d_r}{2^N-1}\right) + k_{o,r} < 0 \end{Bmatrix} \tag{10.1}$$

$$\begin{Bmatrix} G = \left[k_{g,g}\left(\frac{d_g}{2^N-1}\right) + k_{o,g}\right]^{\gamma_g} + G_o & k_{g,g}\left(\frac{d_g}{2^N-1}\right) + k_{o,g} \geq 0 \\ G = G_o & k_{g,g}\left(\frac{d_g}{2^N-1}\right) + k_{o,g} < 0 \end{Bmatrix} \tag{10.2}$$

$$\begin{Bmatrix} B = \left[k_{g,b}\left(\frac{d_b}{2^N-1}\right) + k_{o,b}\right]^{\gamma_b} + B_o & k_{g,b}\left(\frac{d_b}{2^N-1}\right) + k_{o,b} \geq 0 \\ B = B_o & k_{g,b}\left(\frac{d_b}{2^N-1}\right) + k_{o,b} < 0 \end{Bmatrix} \tag{10.3}$$

$$\begin{pmatrix} X \\ Y \\ Z \end{pmatrix} = \begin{pmatrix} X_{r,\max} & X_{g,\max} & X_{b,\max} \\ Y_{r,\max} & Y_{g,\max} & Y_{b,\max} \\ Z_{r,\max} & Z_{g,\max} & Z_{b,\max} \end{pmatrix} \begin{pmatrix} R \\ G \\ B \end{pmatrix} \tag{10.4}$$

where N is the number of encoded bits, k_g and k_o are gun amplifier gain and offset, γ describes acceleration of an electron beam in a vacuum, and R_o, G_o, and B_o, account for ambient light, internal scattering, and light from other channels due to improper settings of the amplifier offsets. The nonlinear transformation between user controls and the linear model, that is, the *optoelectronic conversion function* (*OECF*) (*tone response curve* using ICC terminology) is analytical, its derivation described by Motta (1991), Berns (1996b), and Berns and Katoh (2002). Measurements of each primary sampling its digital range are used to estimate the model parameters k_g, k_o, γ, R_o, G_o, and B_o.

Today, most displays use back-lit liquid-crystal technology where the liquid crystal modulates the backlight at each pixel. Colored filters produce red, green, and blue channels. The backlight can be fluorescent or LED. Another technology is organic-based LED (OLED) that does not require backlight and colored filters. See Reinhard et al. (2008) for details of various display technologies. Fairchild and Wyble (1998) were the first to characterize the colorimetric properties of LCDs. See also IEC (2000b). By plotting the chromaticities of each primary's digital range, they observed that the chromaticities were converging to a single chromaticity, indicating light leakage at zero counts. Equation (10.4) was expanded to (10.5). The OECF could not be defined analytically and was replaced by three one-dimensional lookup tables, shown in Eqs. (10.6)–(10.8). Katoh, Deguchi, and Berns (2001a,b) derived how the CRT offsets, R_o, G_o, and B_o, could be combined into a single black-level term that would be subtracted from each measurement, also resulting in Eq. (10.5) and eliminating R_o, G_o, and B_o in Eqs. (10.1)–(10.3). We use Eq. (10.5) and an analytical or lookup table OECF when characterizing the colorimetry of all three-primary additive displays

$$\begin{pmatrix} X \\ Y \\ Z \end{pmatrix} = \begin{pmatrix} X_{r,\max} - X_{\text{black}} & X_{g,\max} - X_{\text{black}} & X_{b,\max} - X_{\text{black}} & X_{\text{black}} \\ Y_{r,\max} - Y_{\text{black}} & Y_{g,\max} - Y_{\text{black}} & Y_{b,\max} - Y_{\text{black}} & Y_{\text{black}} \\ Z_{r,\max} - Z_{\text{black}} & Z_{g,\max} - Z_{\text{black}} & Z_{b,\max} - Z_{\text{black}} & Z_{\text{black}} \end{pmatrix} \begin{pmatrix} R \\ G \\ B \\ 1 \end{pmatrix} \tag{10.5}$$

$$R = f(d_r) \tag{10.6}$$

$$G = f(d_g) \tag{10.7}$$

$$B = f(d_B) \tag{10.8}$$

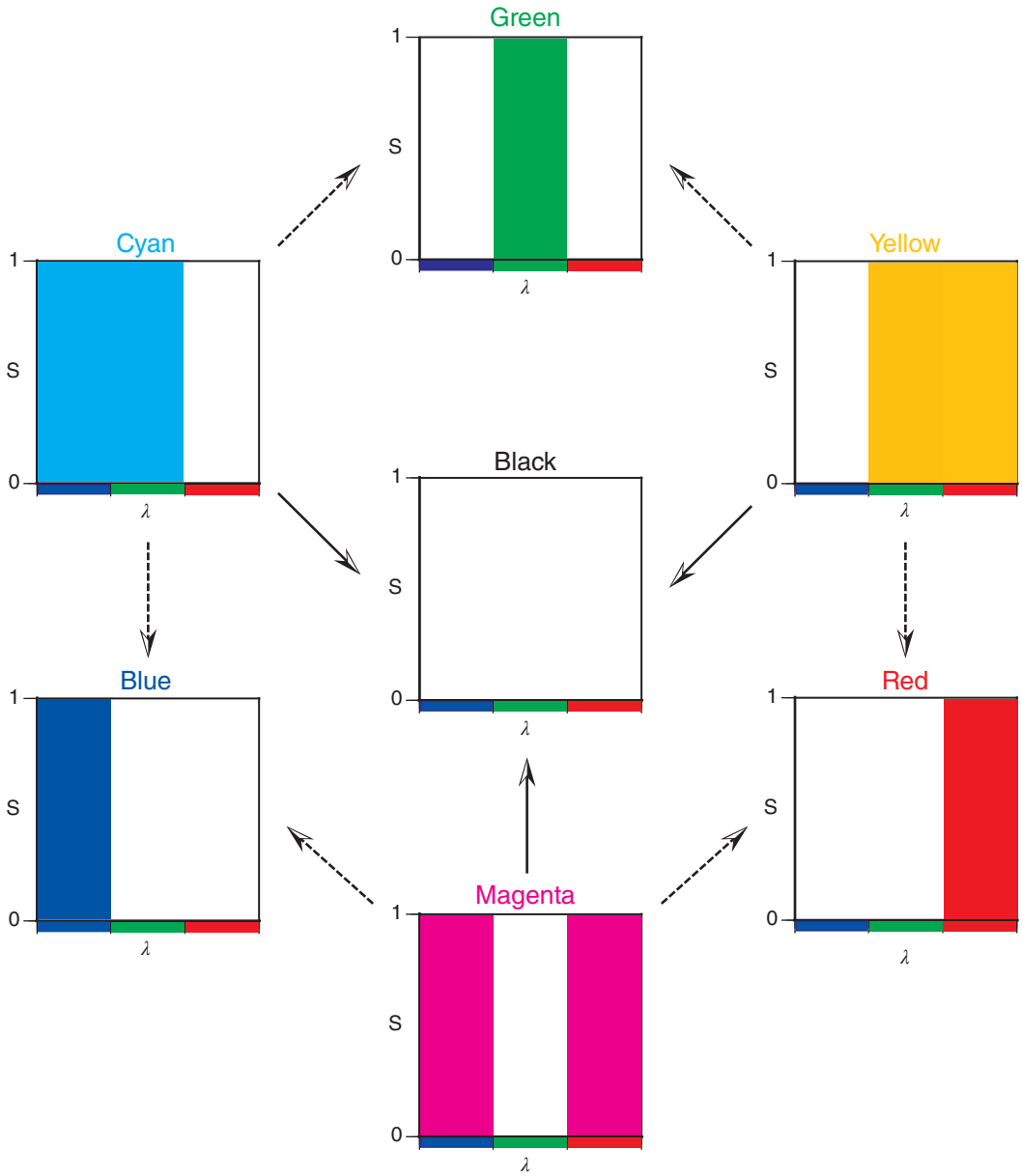

Figure 10.18 The theoretical subtractive primaries of cyan, magenta, and yellow combine to produce black (shown by the solid arrows). When combined pairwise, the secondaries of theoretical red, green, and blue result (shown by the dashed arrows).

As an example, an Apple operating-system-controlled liquid-crystal display was measured with a spectroradiometer where each primary and all three primaries combined (neutrals) were sampled between 0 and 255 counts at 5 count intervals. Measurements were also taken of every combination of d_r, d_g, and d_b at 33–238 counts with 50 count intervals and at 0–24 counts with 6 count intervals. The spectral data were used to calculate *XYZ* tristimulus values having units of cd/m^2. The data set is shown in Figure 10.21. Uniform sampling of digital counts does not result in uniform sampling in CIELAB.

The OECFs were first evaluated, shown in Figure 10.22 for the red primary where digital counts are plotted against the sum of tristimulus values. This display has been designed to emulate the OECF of a CRT. The line through the data points was calculated using Eq. (10.9)

$$R = \left[k_{g,r}\left(\frac{d_r}{2^N - 1}\right) + (1 - k_{g,r})\right]^{\gamma_r} \qquad (10.9)$$

where $k_g = 1$ and $\gamma = 2.2$ (CIE 1996).

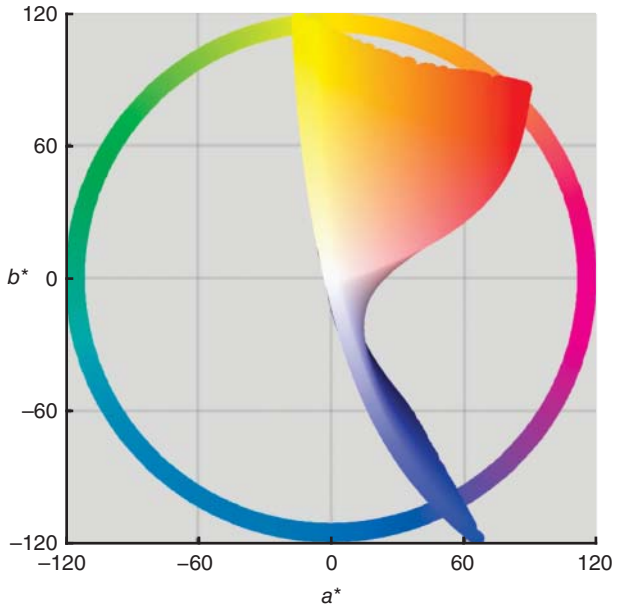

Figure 10.19 Color gamut resulting from the subtractive mixture of theoretical red, theoretical yellow, and theoretical blue primaries. (This viewpoint is looking down the L^* axis and as a consequence, the center appears white. Black is seen from the opposite viewpoint.)

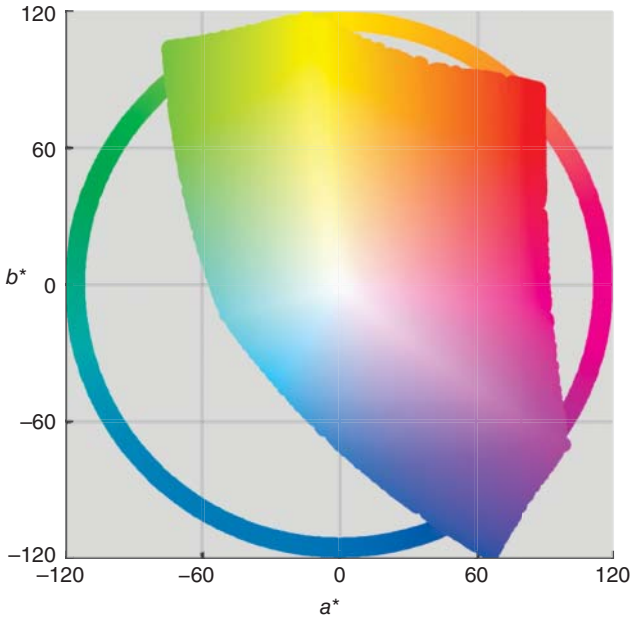

Figure 10.20 Color gamut resulting from the subtractive mixture of theoretical cyan, theoretical magenta, and theoretical yellow primaries.

The measurements of each primary were used to calculate $u'v'$ chromaticities, the results shown in Figure 10.23a. The convergence toward a single point indicates the presence of black-level light. This light does not equal the measured white point of the display.

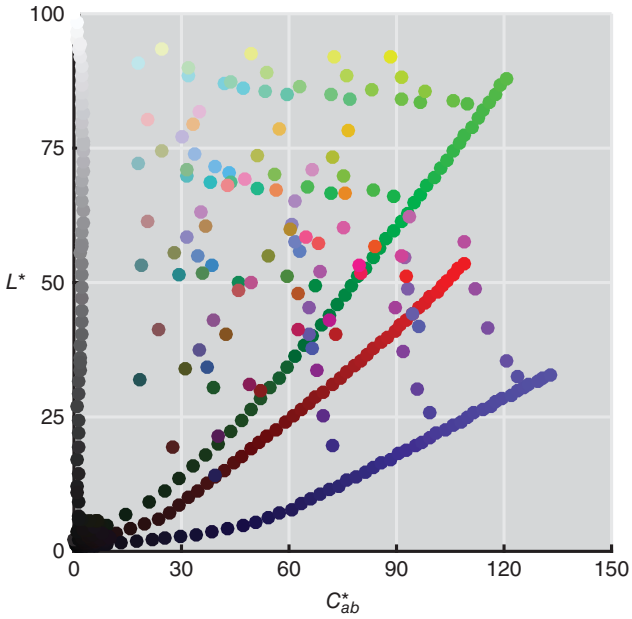

Figure 10.21 Dataset used to characterize the colorimetric properties of an LCD.

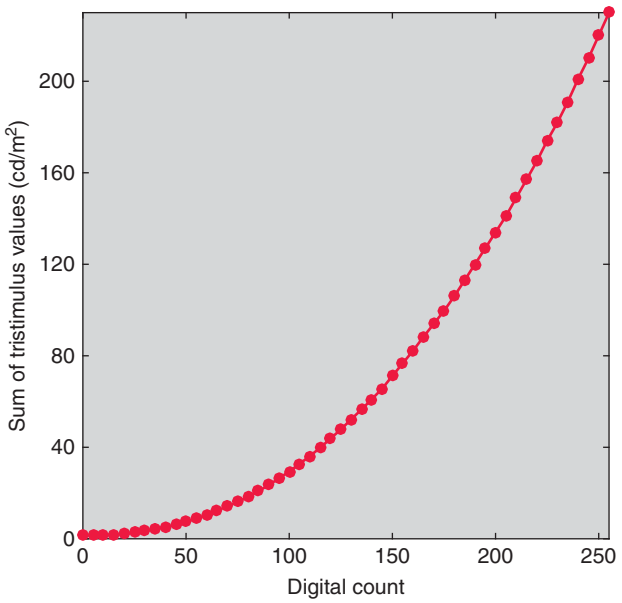

Figure 10.22 The optoelectronic conversion function for the red channel. Filled dots are measured values. The line was calculated using Eq. (10.9) where $k_g = 1$ and $\gamma = 2.2$.

Measurements of each primary at maximum and minimum were used as starting values for the Eq. (10.5) matrix where the average of the three minima defined the black level. Equation (10.9) was used as the OECF for each channel with starting values of $k_g = 1$ and $\gamma = 2.2$. Optimization was used to estimate the matrix and OECF coefficients where average CIEDE2000 was minimized. The optimization was constrained where the estimated white

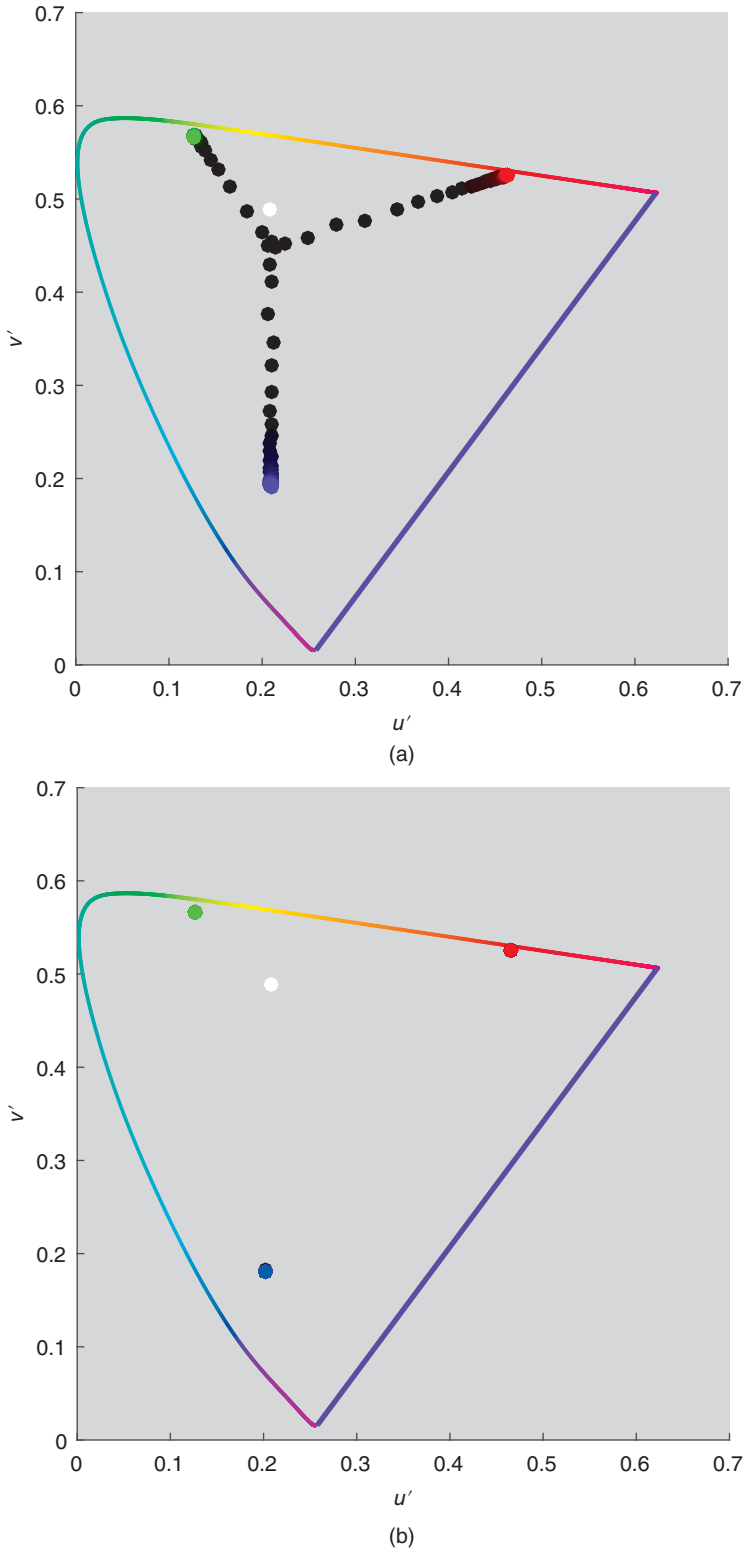

Figure 10.23 Chromaticities of the measurements of each primary between its minimum and maximum along with the display white point. (a) before and (b) after black level subtraction.

point equaled the measured white point. This constraint is important because the optimized matrix rarely predicts the measured white point since most displays do not exhibit perfect additivity. (Omitting this constraint resulted in a correlated color temperature error of about 500 K.) The chromaticities of the primary measurements following black level subtraction are shown in Figure 10.23b. The primaries remain nearly coincident. The OECF model coefficients

Table 10.3 Estimated optoelectronic conversion function model parameters.

	Red	Green	Blue
k_g	1.0000	1.0003	1.0089
γ	2.194	2.192	2.072

are listed in Table 10.3. The red and green channels well emulate a 2.2 gamma display, whereas the blue channel has a gamma of 2.072 and a gain of 1.009. The gamma and gain mismatches among the three channels led to a black level that is bluer than the measured white point and a neutral scale that is not achromatic throughout its digital range, seen in Figure 10.21 where the neutral scale does not maintain $0C^*_{ab}$. The characterization had excellent color accuracy with average and 90th percentile values of 0.5 and 0.9 CIEDE2000, respectively. (Our preference is to report the 90th percentile rather than the maximum error. Plotting a histogram is also useful.)

There is a distinction between characterization and calibration. This LCD display has been characterized and a profile can be made for the display at the time it was measured. It is also possible to calibrate this display to emulate an encoding standard such sRGB, described in a nearby sidebar. The process of characterization involves determining a device's behavior. The process of calibration involves changing a device's behavior to match a standard device.

Returning to the concept of analysis and synthesis, a camera can be calibrated such that the three channels define the scene colorimetry. The reverse of Eqs. (10.10)–(10.13) are used to define each pixel as *sRGB*. The image is said to be *encoded* as an sRGB image. We also use the term *color-gamut rendering* for the conversion from *XYZ* to a specific *RGB* (Berns 2007). The CIELAB color gamut of an sRGB display is shown in Figure 10.24. Scene colors outside the sRGB color gamut will be in error because image

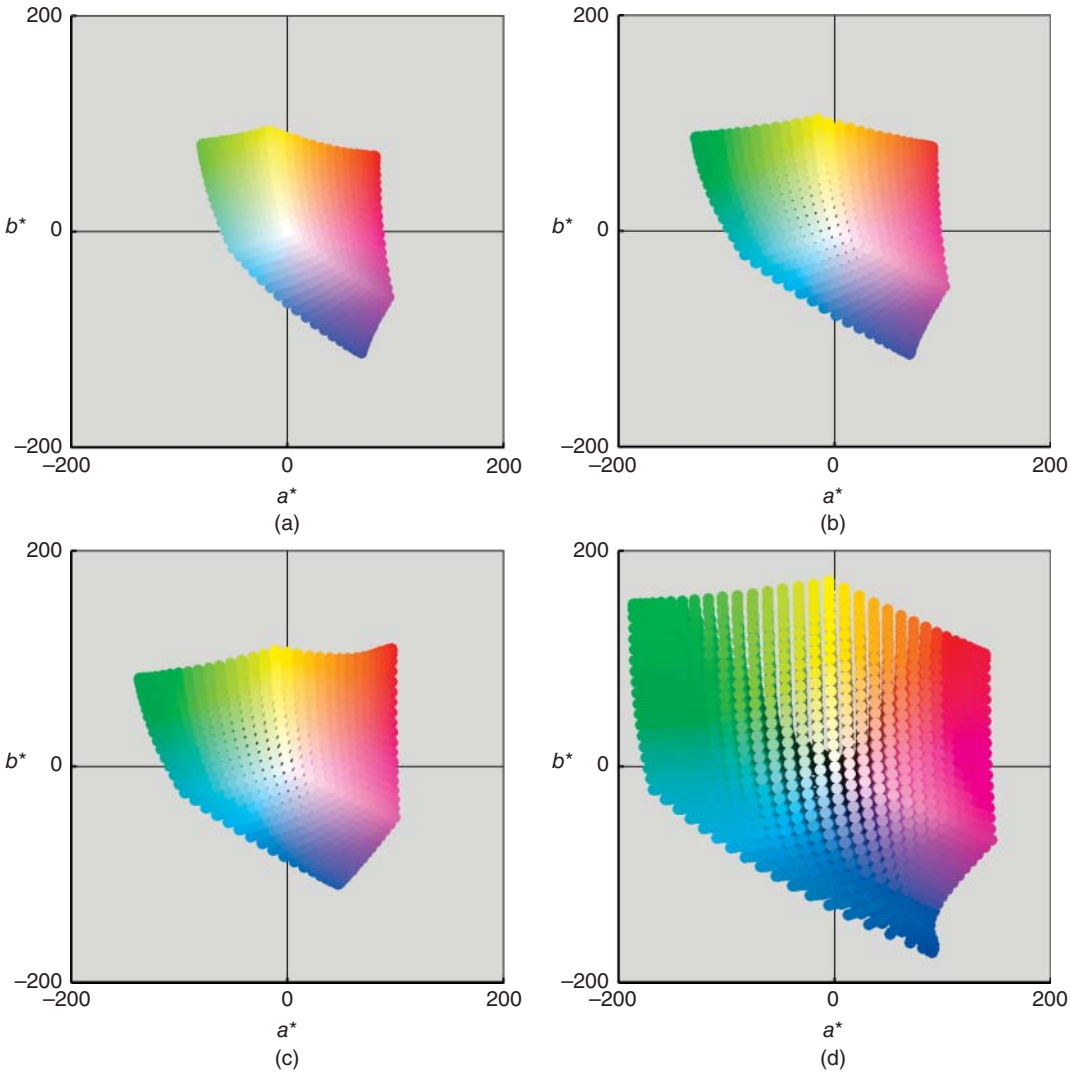

Figure 10.24 Color gamuts projected onto the a^*b^* plane of (a) sRGB, (b), AdobeRGB, (c) eciRGB_v2, and (d) ProPhotoRGB.

sRGB

The ICC selected a reference print as a component of the PCS early in the specification's development. Many color scientists without expertise in printing and publishing were surprised that the reference device was a printer. We expected the most common imaging device to be used, a CRT display. HP Inc. (Hewlett Packard) and Microsoft took this one step further—the most common computer-controlled CRT display ran the Microsoft operating system. HP and Microsoft worked jointly to define and standardize its colorimetric properties (Anderson et al. 1996). This was possible because the vast majority of CRT displays used the same phosphors (colorants), a set already standardized by the International Telecommunication Union (ITU) for high-definition broadcast television (ITU 1995). The ITU also standardized a white point equal to the chromaticities of CIE illuminant D65. The ITU specification was adopted for a new standardized display that became known as *sRGB* (IEC 1999). The last component to standardize was the optoelectronic conversion function. This has always been a source of confusion, not just for sRGB, but for CRT displays used in a variety of applications. Research by Motta (1991) and the description of the development of sRGB (Anderson et al. 1996) are recommended for further clarification. All CRT displays have controls to adjust the gun amplifier's gain and offset values using terms such as contrast and brightness. The optimal adjustment results in $k_g = 1$, $k_o = 0$, and $R_o = G_o = B_o = 0$, using the model described in Eqs. (10.1)–(10.3). In this case, the OECF is described as the normalized digital counts raised to the power of gamma, known as the *simple gamma model*. Many VGA CRT displays were measured and the average gamma was 2.2 with a standard deviation of about 0.2 (Anderson et al. 1996). This value was used to define the OECF. Requirements of integer mathematics necessitated an adjustment from the simple gamma model to Eqs. (10.10)–(10.12). The sRGB standard is shown in Table 10.4 and Eqs. (10.10)–(10.13)

$$R\begin{cases} \left(\frac{d_r}{2^N-1}\right)/12.92 & \left(\frac{d_r}{2^N-1}\right) \le 0.039\,28 \\ \left[\left(\frac{d_r}{2^N-1}\right)+0.055/1.055\right]^{2.4} & \left(\frac{d_r}{2^N-1}\right) > 0.039\,28 \end{cases} \tag{10.10}$$

$$G\begin{cases} \left(\frac{d_g}{2^N-1}\right)/12.92 & \left(\frac{d_g}{2^N-1}\right) \le 0.039\,28 \\ \left[\left(\frac{d_g}{2^N-1}\right)+0.055/1.055\right]^{2.4} & \left(\frac{d_g}{2^N-1}\right) > 0.039\,28 \end{cases} \tag{10.11}$$

$$B\begin{cases} \left(\frac{d_b}{2^N-1}\right)/12.92 & \left(\frac{d_b}{2^N-1}\right) \le 0.039\,28 \\ \left[\left(\frac{d_b}{2^N-1}\right)+0.055/1.055\right]^{2.4} & \left(\frac{d_b}{2^N-1}\right) > 0.039\,28 \end{cases} \tag{10.12}$$

$$\begin{pmatrix} X \\ Y \\ Z \end{pmatrix} = \begin{pmatrix} 0.4124 & 0.3576 & 0.1805 \\ 0.2126 & 0.7152 & 0.0722 \\ 0.0193 & 0.1192 & 0.9505 \end{pmatrix} \begin{pmatrix} R \\ G \\ B \end{pmatrix} \tag{10.13}$$

Table 10.4 The sRGB standard display chromaticities.

	Red	Green	Blue	White (D65)
x	0.6400	0.3000	0.1500	0.3127
y	0.3300	0.6000	0.0600	0.3290

The sRGB standard is THE profile connection space for consumer imaging. Cell phones, digital cameras, copiers, and ink-jet and laser printers use sRGB for both encoding and communication. Most desktop and office printers are sRGB devices where the transformation from sRGB to the printed page is part of the printer's internal processing. Cameras and phones can send images to be printed without using ICC color management. When an image is used from the Internet without an embedded ICC profile, it is safe to assume that the image is encoded as sRGB. When we embed images into presentations and documents, they are encoded as sRGB to ensure reasonable color regardless of computer operating system.

data are limited to 0 and $(2^N - 1)$. Colorimetric data beyond the sRGB color gamut are usually clipped.

A limitation of sRGB is that most CMYK printers have a larger color gamut. Once an image is sRGB encoded, scene colors outside the sRGB color gamut and inside a CMYK gamut are printed in error, a consequence of first mapping into a smaller color gamut. Adobe recognized this limitation and in 1998 defined a new *RGB* encoding specification that encompassed printer color gamuts, named *AdobeRGB (1998)* (Adobe Systems Incorporated 2005). It has the same D65 white point as sRGB. Its color-rendering gamut is shown in Figure 10.24 and the increase in volume compared with sRGB is appreciable. The European Color Initiative (ECI) in 1999 developed its own *RGB* encoding specification, *eciRGB* with the same goal as AdobeRGB. It has been updated to eciRGB_v2 where the OECF was changed from a 1.8 gamma to L^*. It uses a D50 white point and its color-rendering gamut is shown in Figure 10.24. The

Eastman Kodak Company in 2000 also developed an *RGB* specification, *ROMM RGB* (Reference Output Medium Metric RGB), usually referred to as *ProPhotoRGB* (Spaulding, Woolfe, and Giorgianni 2001). They were more concerned about encompassing all reflecting colors rather than only printed colors. ProPhotoRGB uses a D50 white point and its color-rendering gamut is plotted in Figure 10.24, much larger than any of the other *RGB* encodings. Because of this large gamut, images should be encoded in 16-bit rather than 8-bit in order to avoid errors caused by an insufficient number of levels, known as *quantization error* (Berns 2014b). Berns and Derhak (2015) developed an *RGB* specification, *ETRGB* (extended tristimulus RGB) that encompasses the spectrum locus and encodes colors up to $130L^*$ rather than the usual $100L^*$. It was designed to encompass metals, fluorescent colors, and modern materials containing iridescent and interference pigments. It has a D50 white point and must only be used in 16-bit encoding.

All of these encoding specifications are *RGB* and have corresponding chromaticities for their primaries. These are shown in Figure 10.25. sRGB, AdobeRGB (1998), and eciRGB_v2 primaries have a common origin from broadcast television (ITU 1995) and as a consequence, have some common vertices. ProPhotoRGB and ETRGB have primaries outside of the spectrum locus and displays with these chromaticities are not physically realizable. This is why we are minimizing the use of the word "display" when referring to these encoding specifications.

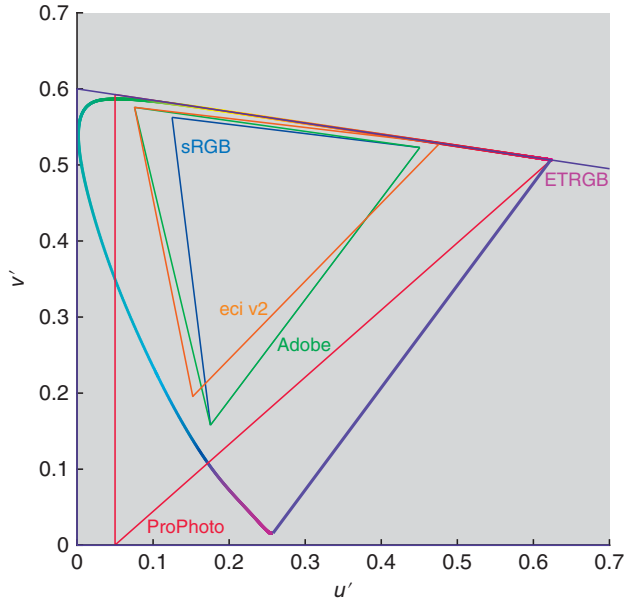

Figure 10.25 Chromaticities of the red, green, and blue primaries corresponding to sRGB, AdobeRGB (1998), eciRGB_v2, ProPhotoRGB, and ETRGB encoding specifications.

These *RGB* specifications have different white points. sRGB and AdobeRGB (1998) workflows are based on illuminant D65 and the 1931 standard observer. Because the ICC PCS uses illuminant D50, the tristimulus matrix, defined by the red, green, and blue colorant tristimulus values, incorporates a von Kries type chromatic adaptation transformation so that the matrix white point corresponds to illuminant D50 while the media white point corresponds to illuminant D65. eciRGB_v2 and ProPhotoRGB workflows are based on illuminant D50, eliminating the need for a chromatic adaptation transformation.

There are also displays that have more than three channels, known as *multiprimary displays*. The secondaries cyan, magenta, and yellow can be additional channels. Computer projectors often have the light source without a color filter as its fourth channel. The colorimetry is the same where the light from each primary is added together. Characterizing these displays can be challenging (Seime and Hardeberg 2003) because there are multiple combinations to match a specific color, similar to color formulation. The conversion from trichromatic signals to primary amounts is often proprietary.

E. PRINTING

Printing is a subtractive process where colorants absorb light. Different technologies have different approaches to modulating colorant amounts. The dyes in photographic print paper are modulated continuously, leading to the term *continuous tone* or *con-tone*. Strictly, each exposed film grain is a discrete step. Practically, the grain size is sufficiently small that changes in color appear continuous. Most printing systems cannot modulate colorant amounts continuously. At any position, there is either ink or no ink, leading to the term *halftone* (Talbot 1852). The number of tones can be increased by reducing resolution forming *halftone cells* and modulate the area within the cell. Suppose that a halftone cell is four pixels. The number of colors increases from two to five, shown in Figure 10.26. When the halftone cell is sufficiently small where we cannot resolve the individual pixels, the cell appears continuous tone.

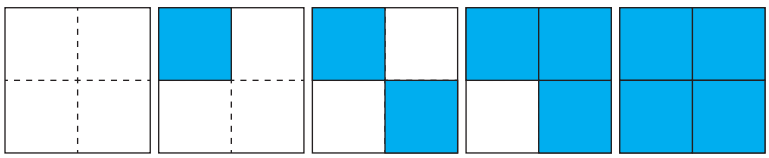

Figure 10.26 Four pixels combine forming a halftone cell, resulting in five unique tones when averaged.

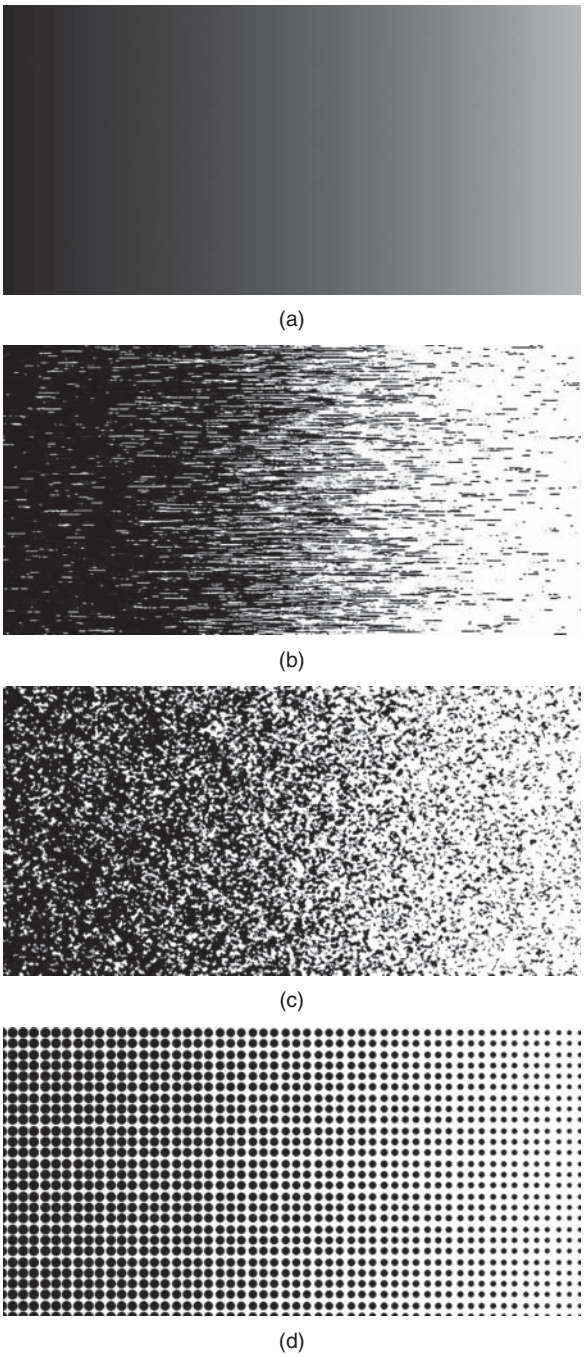

Figure 10.27 (a) Continuous tone gradient and simulation of (b) engraving, (c) mezzotint, and (d) screen.

The shape of a printed area depends on the printing technology. Engraving produces fine lines. Mezzotint, used in the first color printing processes, has a grainy structure. Offset lithography and gravure produce circles. These shapes are simulated in Figure 10.27 for a continuous tone gradient.

Color printing using three inks is attributed to Le Blon (1756) and there were a number of practitioners during the eighteenth century (Grasselli et al. 2003). Le Blon used the intaglio and mezzotint processes producing prints with the appearance of pastels. The color separations were performed visually where a line drawing was transferred to each plate to maintain registration. One of Le Blon's most famous prints was of Louis XV, the King of France, based on an engraving by Blakey. Interestingly, black, yellow, blue, carmine, brown, and white inks were used, dating multiink printing to the eighteenth century.

The term *halftoning* is used to convert from continuous tone to ink on paper and there are many approaches (Lau and Arce 2008). There is a trade-off between color and spatial image quality, shown in Figure 10.28 where the Manet painting can have either high spatial and low color resolution or high color and low spatial resolution. Today, printing systems can use inks at two or more different concentrations, fixed dot size, variable dot size, different shapes, and combinations of some or all of these variables. As a consequence, many print technologies produce images with both high color and high spatial quality.

The number of unique colors increases exponentially as the number of primary inks increases. For CMYK printing, there are 2^4 unique colors, that is, 16. For CMYKRGB printing, there are $2^N = 128$ unique colors where $N = 7$, the number of inks. The total percent area coverage of each unique color depends on the halftoning algorithm. The most common halftoning is rotated screen. The dot-on-dot halftoning shown in Figure 10.28 is equivalent to screen printing where all the angles are matched at 0°. The screen resolution is the number of dots across a specific length. The resolution and the periodic halftoning are easily seen. The size of the dot is modulated to increase the number of tones, known as *amplitude modulation* (*AM*) *screening*. Through experience and by studying the spatial properties of color vision, screens were rotated to specific angles for CMYK printing reducing the periodic appearance, shown in Figure 10.29 for a Claude Monet painting.

Many halftone algorithms are equivalent to a random printing process, either by design (Lau and Arce 2008), or as a consequence of their image statistics including rotated screen algorithms (Rogers 1998). Demichel (1924) and Neugebauer (1937; translated by Wyble and Kraushaar 2005) deduced the random nature of rotated screen halftones. As random variables, each unique color is calculated using probability theory, shown in Eqs. (10.14)–(10.29) for CMYK printing where P is the area of each unique color. We use "P" to reinforce that these are probabilities of occurrence for a given combination of cyan, magenta, yellow, and black ink. The subscripts for P identify the specific combinations of the four inks, often called *overprints*. Looking at the mathematical pattern, the equations can be extended to any number of inks. These equations can also be interpreted as weights for quadrilinear interpolation, diagrammed in

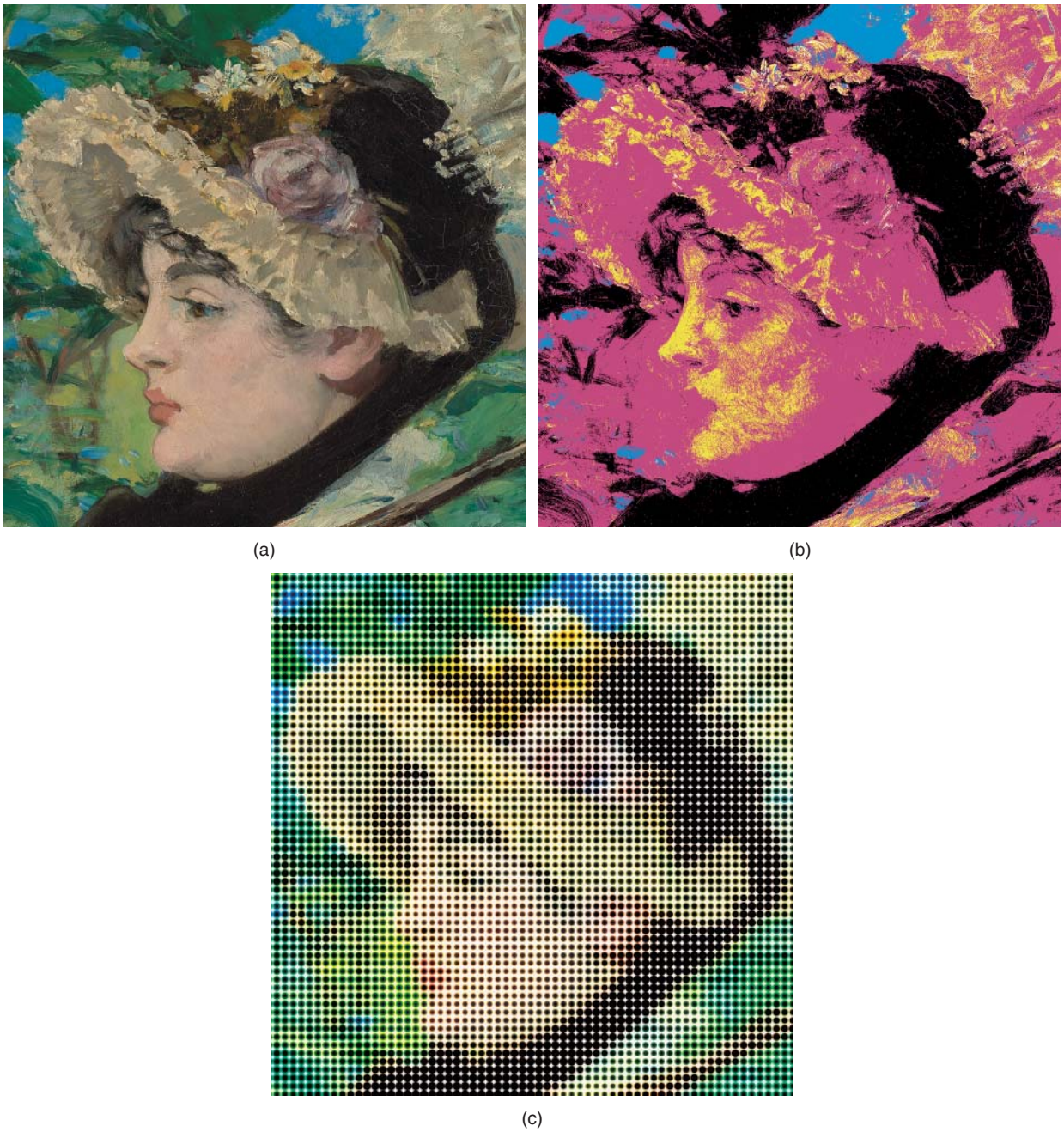

(a) (b)

(c)

Figure 10.28 (a) Closeup of Édouard Manet (French, 1832–1883), *Le Printemps (Jeanne Demarsy)*, 1881, Oil on canvas, 74 cm × 51.4 cm (29 1/8 in. × 20 1/4 in.), (b) full spatial resolution resulting in four unique colors – cyan, magenta, yellow, and black, and (c) dot-on-dot halftoning resulting in 16 unique colors.
Source: Digital image courtesy of the Getty's Open Content Program.

Figure 10.30 for an orange color printed using magenta and yellow inks

$$P_c = a_c(1 - a_m)(1 - a_y)(1 - a_k) \tag{10.14}$$

$$P_m = a_m(1 - a_c)(1 - a_y)(1 - a_k) \tag{10.15}$$

$$P_y = a_y(1 - a_c)(1 - a_m)(1 - a_k) \tag{10.16}$$

$$P_k = a_k(1 - a_c)(1 - a_m)(1 - a_y) \tag{10.17}$$

$$P_r = a_m a_y(1 - a_c)(1 - a_k) \tag{10.18}$$

$$P_g = a_c a_y(1 - a_m)(1 - a_k) \tag{10.19}$$

$$P_b = a_c a_m(1 - a_y)(1 - a_k) \tag{10.20}$$

Figure 10.29 Claude Monet (French, 1840–1926), *The Portal of Rouen Cathedral in Morning Light*, 1894, Oil on canvas, 100.3 cm × 65.1 cm (39½ in. × 25⅝ in.), Los Angeles, J. Paul Getty Museum 2001.33. Color separations and halftoning at CMYK angles of 15°, 75°, 0°, and 45°.

$$P_{cmy} = a_c a_m a_y (1 - a_k) \tag{10.21}$$

$$P_{ck} = a_c a_k (1 - a_m)(1 - a_y) \tag{10.22}$$

$$P_{mk} = a_m a_k (1 - a_c)(1 - a_y) \tag{10.23}$$

$$P_{yk} = a_y a_k (1 - a_c)(1 - a_m) \tag{10.24}$$

$$P_{rk} = a_m a_y a_k (1 - a_c) \tag{10.25}$$

$$P_{gk} = a_c a_y a_k (1 - a_m) \tag{10.26}$$

$$P_{bk} = a_c a_m a_k (1 - a_y) \tag{10.27}$$

$$P_{cmyk} = a_c a_m a_y a_k \tag{10.28}$$

$$P_w = (1 - a_c)(1 - a_m)(1 - a_y)(1 - a_k) \tag{10.29}$$

Let's consider a single ink with a known nominal area coverage, determined by the halftoning algorithm. "Nominal" is used to define user-controlled area coverage, sometimes referred to as *computer dots*. The average spectral reflectance of a printed area at any area coverage is calculated using Eq. (10.30):

$$R_\lambda = a_{\text{ink}} R_{\lambda,\text{ink}} + (1 - a_{\text{ink}}) R_{\lambda,\text{paper}} \tag{10.30}$$

where a defines effective area coverage and $R_{\lambda,\text{ ink}}$ is the measurement of the ink at 100% area coverage (Murray 1936).

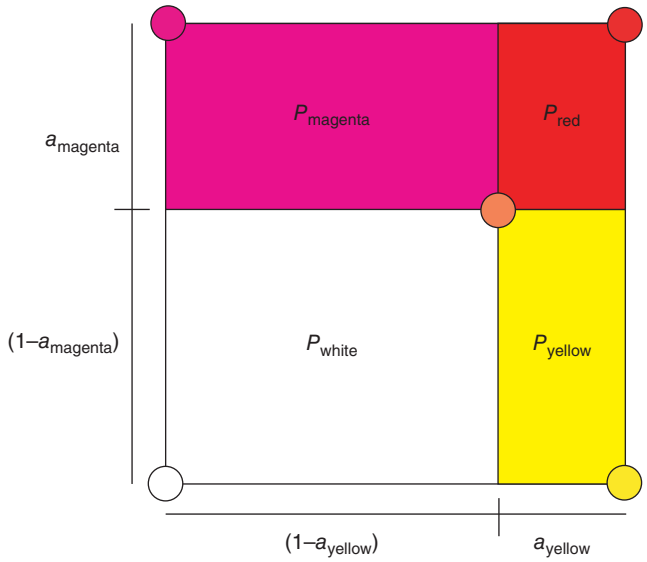

Figure 10.30 Probabilities can be interpreted as linear interpolation weights where each rectangle defines a weight.

The relationship between nominal and effective area coverages is determined experimentally for each ink, described below.

CMYK printing is modeled using Eq. (10.31):

$$R_\lambda = \sum_i P_i R_{\lambda,i} \tag{10.31}$$

where all null, single, double, triple, and quadruple combinations at 100% area coverage define spectral reflectance of the i unique colors. These colors are referred to as the *Neugebauer primaries*. The addition of the Neugebauer primaries scaled by their probability of occurrence defines the linear model.

Equations (10.14)–(10.29) and (10.31) can be used to estimate spectral reflectance for printed ink on paper. This was tested using a CMYK rotated-screen halftone print applied to a clay-coated paper with a fluorescent whitening agent. The digital color target is shown in Figure 10.31 (ISO 2006). It contains 1617 patches with a sampling scheme appropriate for producing color profiles. Each patch was measured with a 45a:0° spectrophotometer. Spectral measurements of the 16 Neugebauer primaries are shown in Figure 10.32. These 16 spectra and the nominal area coverages for each color patch were used to predict spectral reflectance. The results are shown in Figure 10.33a,b where the filled dot defines the measured color and the arrow head defines the predicted color. The average and 90th percentile color differences are shown in Table 10.5. This model has very poor performance with large systematic errors.

There are two possible reasons for the poor prediction accuracy. The first is the wrong linear model. The spectra for ramps of each individual ink are plotted in Figure 10.34. Scalability was evaluated by normalizing these spectra using Eq. (10.32), the resulting spectra plotted in Figure 10.35

$$R_{\lambda,\text{normalized}} = \frac{\left(R_{\lambda,\text{ink}}/R_{\lambda,\text{paper}}\right)}{\left(R_{\lambda,\text{ink}}/R_{\lambda,\text{paper}}\right)_{\text{at } \lambda \text{ minimum}}} \tag{10.32}$$

Magenta, yellow, and black have excellent scalability. Cyan has poor scalability. However, this lack of scalability cannot account for the large color differences.

The model was based on the assumption that the relationship between nominal and effective area coverages was linear. This assumption was tested by estimating

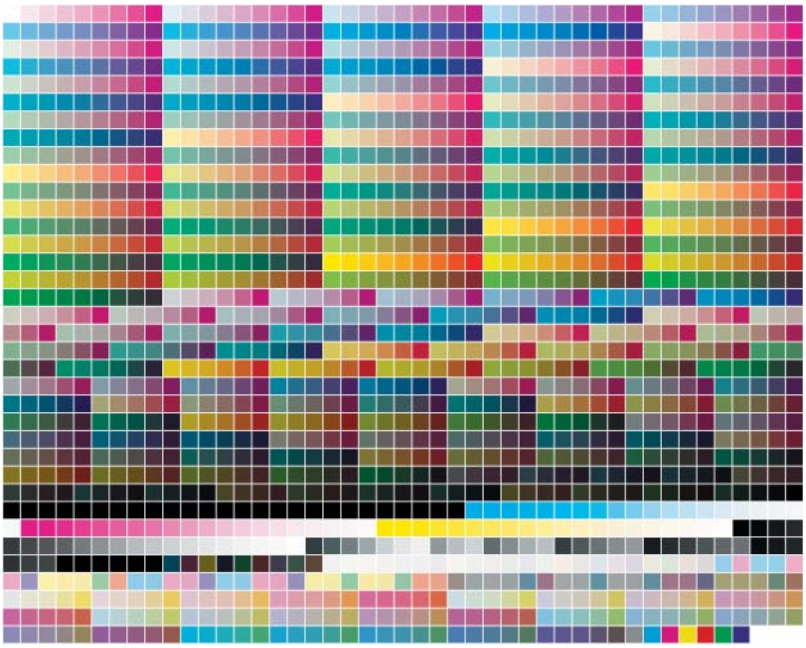

Figure 10.31 IT8.7/4 CMYK digital target.

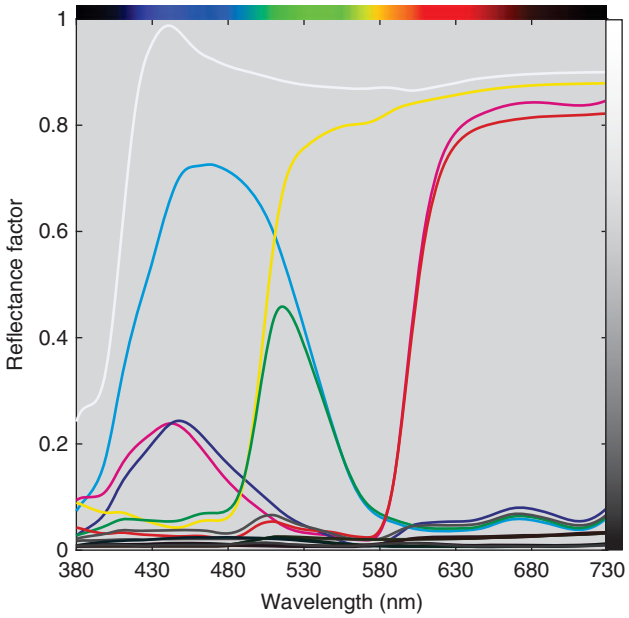

Figure 10.32 Spectral reflectance factor of the 16 Neugebauer primaries.

Table 10.5 CIEDE2000 statistics for each listed model predicting the target shown in Figure 10.31.

Model	Average	90th percentile
Spectral Neugebauer, $a = a_{\text{nominal}}$	7.3	11.2
Spectral Neugebauer, $a = f(a_{\text{nominal}})$	2.3	3.6
Yule–Nielsen-spectral–Neugebauer, $n = 2.15$, $a = f(a_{\text{nominal}})$	0.9	1.5

area coverages using linear regression where spectral reflectance RMS error was minimized (Wyble and Berns 2000). The results are plotted in Figure 10.36. There is a nonlinear relationship where effective area coverage is larger than nominal area coverage. Functions are required to transform from nominal to effective area coverage, shown in Eqs. (10.33)–(10.36). Quadratic functions well-fit the data. The model was tested with these additional functions, the results shown in Figure 10.33c,d and Table 10.5. The improvement in performance is dramatic

$$a_c = f(a_{\text{nominal},c}) \tag{10.33}$$

$$a_m = f(a_{\text{nominal},m}) \tag{10.34}$$

$$a_y = f(a_{\text{nominal},y}) \tag{10.35}$$

$$a_k = f(a_{\text{nominal},k}) \tag{10.36}$$

For this printing system, reflectance additivity led to reasonable results. In general, a nonlinear transformation from reflectance is required to achieve linearity, as we describe in Chapter 9 when using Kubelka–Munk theory to model paint and textile coloration systems. Yule and Nielsen (1951) derived an exponential transformation, shown in Eq. (10.37) where $1/n$ defines the exponent. The specific *n-value* depends principally on the halftoning algorithm, dot size, scattering properties of the substrate, ink scattering, and ink penetration into the substrate. Values range between about 1.5 and 20. Larger n-values occur for printing that appears continuous tone with high spatial image quality

$$R_\lambda = \left(\sum_i P_i R_{\lambda,i}^{1/n} \right)^n \tag{10.37}$$

An $n = 5$ was used to demonstrate the improvement in scalability. Normalized spectral reflectance plots using Eq. (10.38) are shown in Figure 10.35

$$R_{\lambda,\text{normalized}} = \frac{\left(R_{\lambda,\text{ink}} / R_{\lambda,\text{paper}} \right)^{1/n}}{\left(R_{\lambda,\text{ink}} / R_{\lambda,\text{paper}} \right)^{1/n}_{\text{at } \lambda \text{ minimum}}} \tag{10.38}$$

There is a 10-fold improvement in the scalability of cyan compared with reflectance additivity, that is, $n = 1$.

Effective area coverages of the primary ramps were estimated for an n-value of 5 using optimization where spectral reflectance RMS error was minimized, the results shown in Figure 10.36. The curvature has inverted indicating a lightening rather than darkening. Estimated effective area coverage depends on n, indicating that this model is not physically based. There are a number of approaches to model the spectral reflectance properties of ink on paper, many of which are more complex but without significant improvement compared with the Yule–Nielsen model. See summaries by Wyble and Berns (2000) and Hébert and Hersch (2015).

A global n-value and effective area coverages can be optimized simultaneously using all of the ramp data. Spectral reflectance RMS error or average CIEDE2000 can be minimized. In our experience, it is difficult to find the true minimum because n and effective area coverage are not independent. Instead, n is changed systematically, effective area coverages estimated, and error recorded as a function of n. The optimal n-value occurs where the error is at minimum. For this printing system, the optimal was $n = 2.15$. The results are shown in Figure 10.33e,f and Table 10.5. There was a twofold increase in accuracy compared with reflectance additivity.

The complete printing model is known as the *Yule–Nielsen-spectral–Neugebauer*, *YNSN*, model, first described by Viggiano (1985). The model consists of

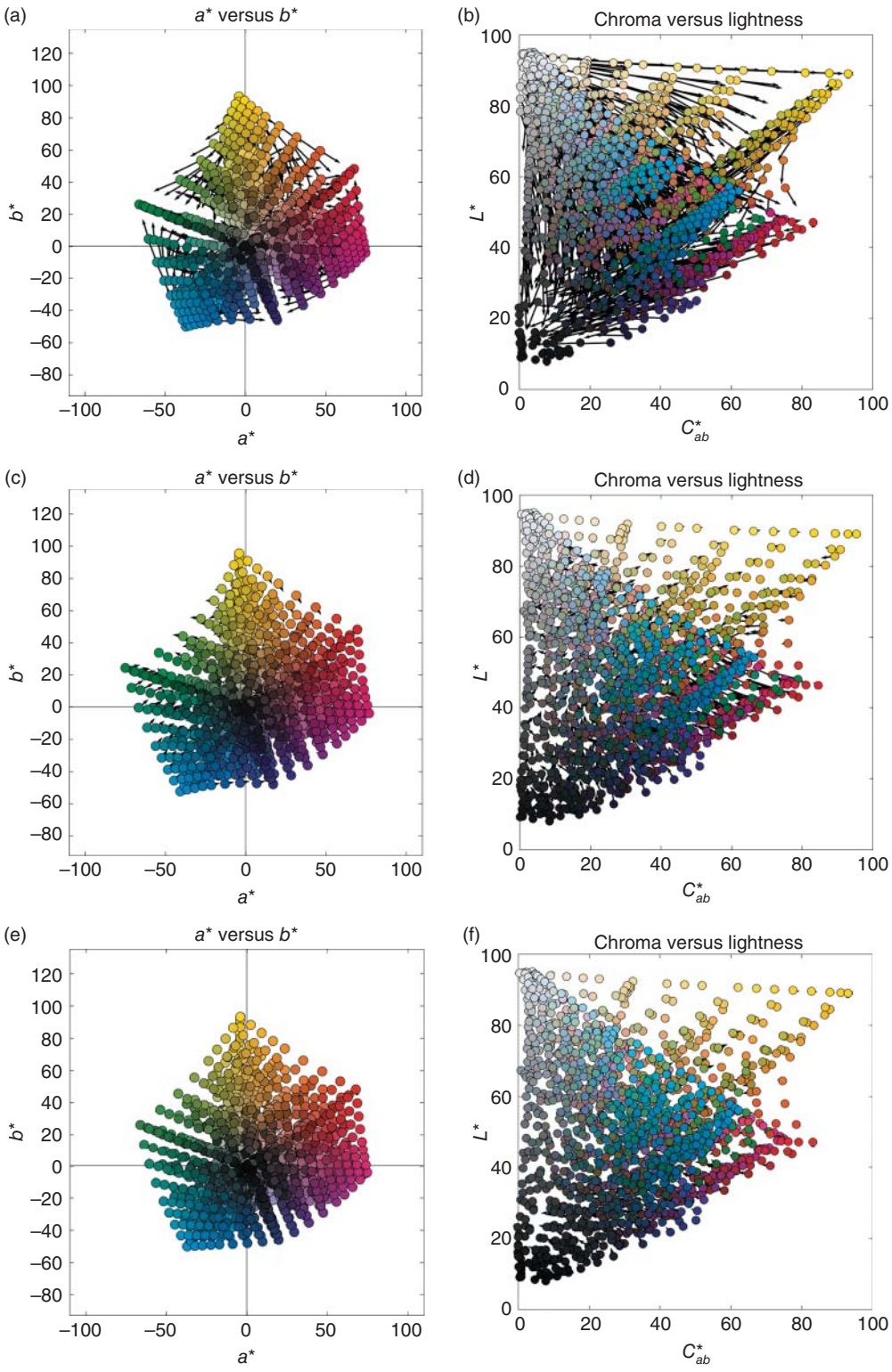

Figure 10.33 Color reproduction vector plots where the colored dot defines the coordinates of a measured color patch, while the arrowhead defines the coordinates of its estimate using (a and b) additivity in reflectance factor and linearity between nominal and effective area coverages, (c and d) additivity in reflectance factor and fitted nonlinearity between nominal and effective area coverages, and (e and f) *n*-value of 2.15 and fitted nonlinearity between nominal and effective area coverages.

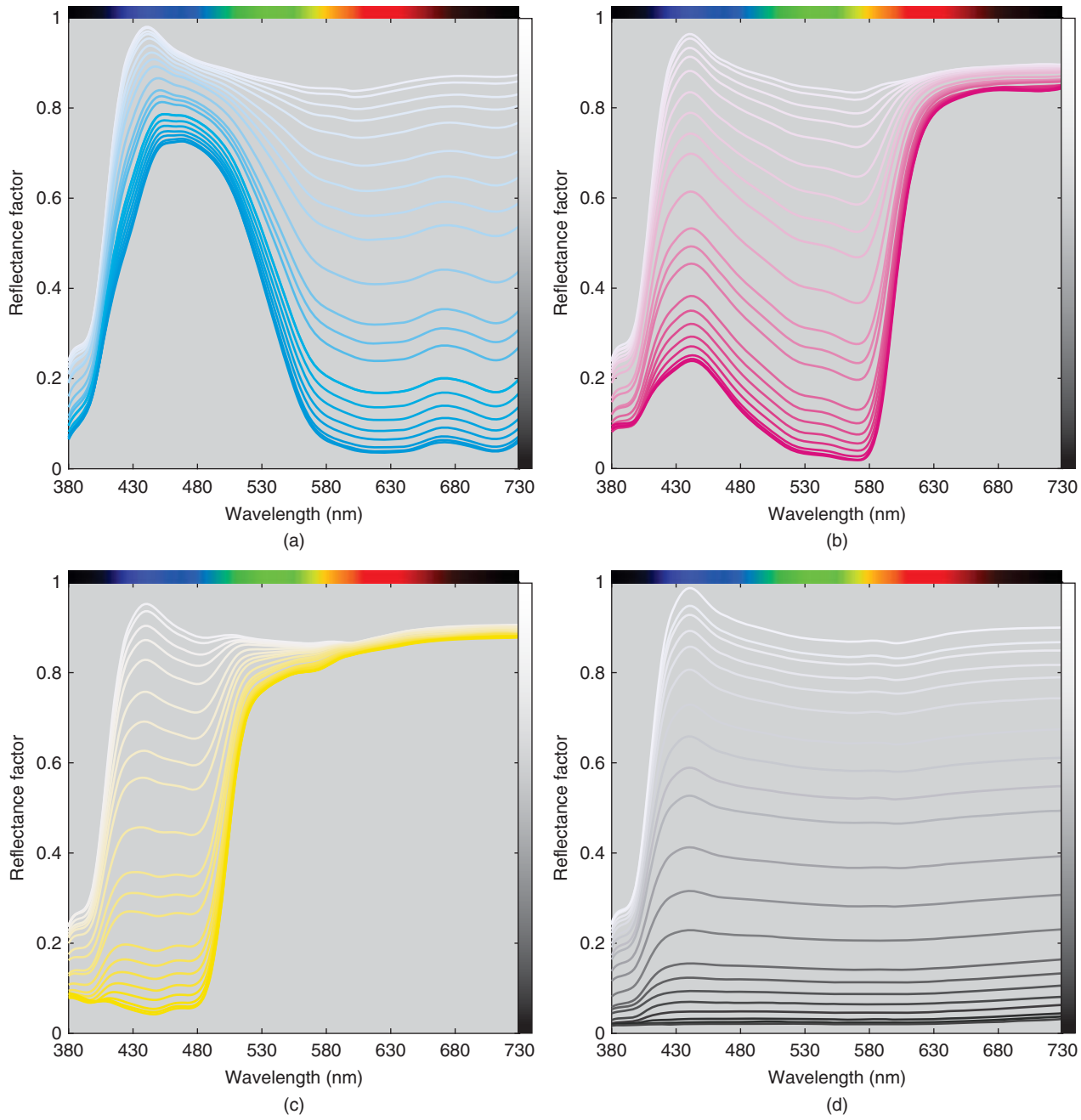

Figure 10.34 Spectral reflectance factor of (a) cyan, (b) magenta, (c) yellow, and (d) black ramps between 0 and 100% nominal area coverage. Plot (d) includes the paper substrate.

Eqs. (10.33)–(10.36) to calculate effective area coverages, Eqs. (10.14)–(10.29) to calculate probabilities, and Eq. (10.37) to calculate spectral reflectance factor. The model can be enhanced by dividing area coverages into cells to decrease the interpolation area and by calculating n-value as a function of wavelength (Heuberger, Jing, and Persiev 1992).

As a final note, the nonlinearity between nominal and effective area coverages is caused by the increase in size of a printed area compared with its nominal area, known as *mechanical dot gain*, and by subsurface scattering inside the paper where light passing through an ink is scattered laterally, in essence, reducing the reflectance of the paper, known as *optical dot gain*. The decrease in reflectance depends on ink absorption and scattering, paper scattering, and ink spreading and absorption into the paper. The effect of subsurface scattering is visualized in Figure 10.37. As scattering increases, the color between the printed areas darkens.

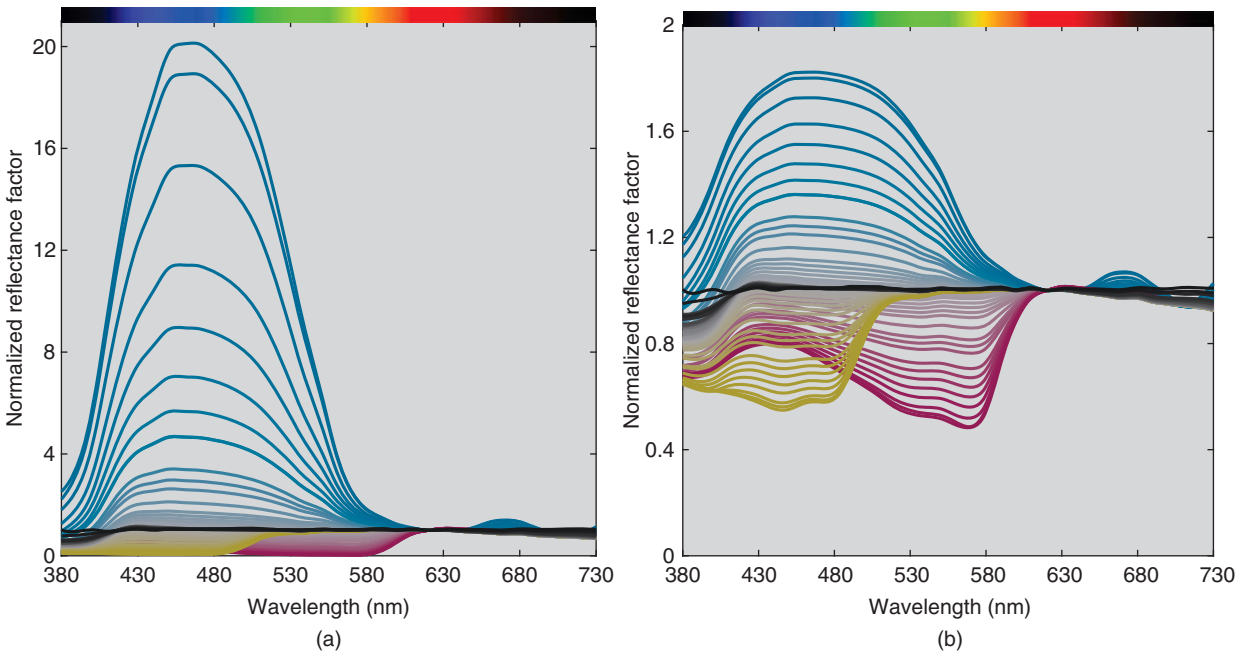

Figure 10.35 Normalized spectra for cyan, magenta, yellow, and black ramps for (a) spectral reflectance and (b) spectral reflectance with a Yule–Nielsen *n*-value of 5. All data are normalized at 620 nm, the peak absorption of cyan. Note the difference in scale between the figures.

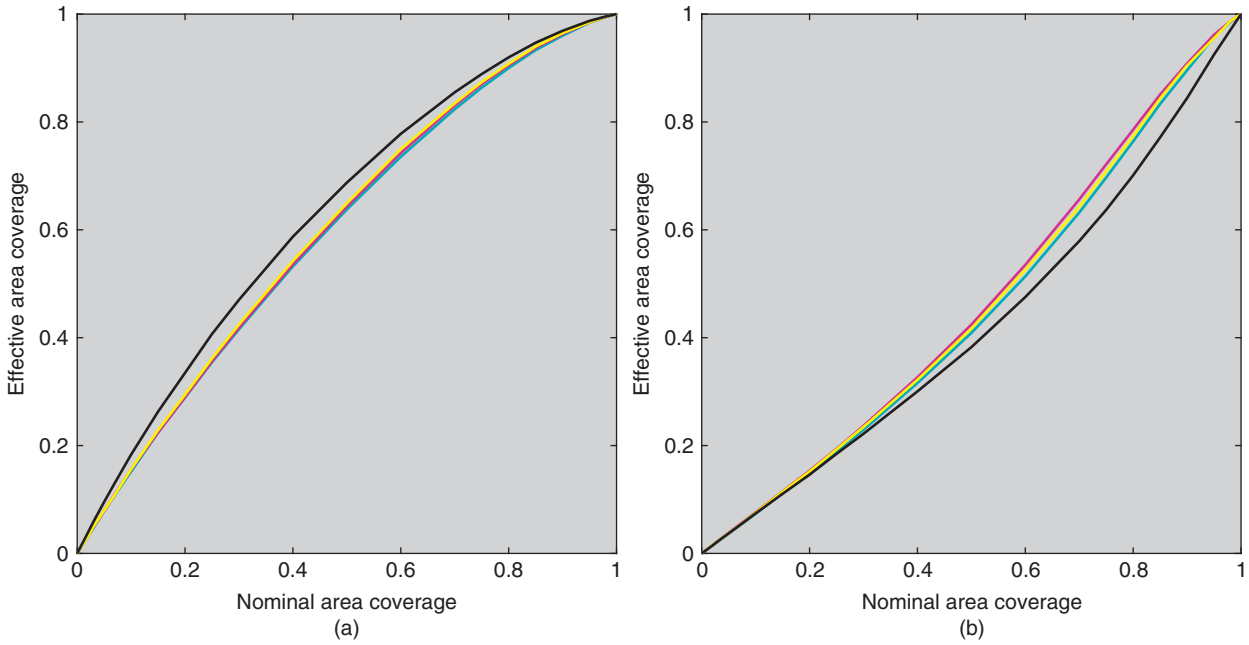

Figure 10.36 The relationship between nominal and effective area coverage for cyan, magenta, yellow, and black ramps for (a) spectral reflectance and (b) spectral reflectance with a Yule–Nielsen *n*-value of 5.

F. DIGITAL CAMERAS

Digital camera components include a lens, aperture, one or more filters, sensor, amplifier, analog-to-digital converter, and image processor. When we look at a properly focused and exposed image, image quality is primarily dependent on colorimetric accuracy and image noise, referred to as *color quality* and *spatial-image quality* (Phillips and Eliasson 2018), shown in Figure 10.38. How the image is used often influences which quality criterion is more important. There

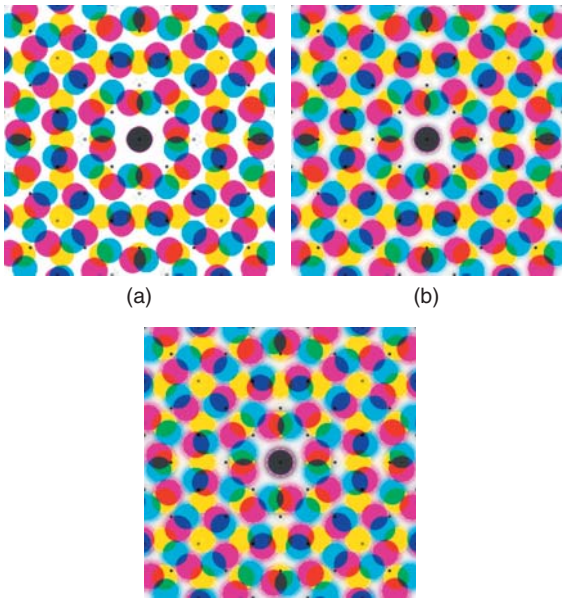

Figure 10.37 Printing on a substrate (a) without, (b) with moderate, and (c) with appreciable subsurface scattering.

is a trade-off between image noise and color accuracy when designing cameras and when deriving transformations from camera signals to colorimetry. See Burns and Berns (1997) and Kuniba and Berns (2008, 2009) for more details. See Gow et al. (2007), Reinhard et al. (2008), and Kuniba and Berns (2009) for reviews on camera-based image noise.

Colorimetric Accuracy

We are interested in using an RGB digital camera as a colorimetric instrument, an *imaging colorimeter*. The general requirement is that the camera can be operated manually where optimal aperture and exposure time are determined during setup and remain unchanged during imaging. Cameras have two file formats, JPEG with sRGB encoding and *camera raw*. These JPEG images are rendered to produce pleasing images, have low image noise, and have small file sizes. These images are not appropriate for colorimetric applications. Camera-raw images are unprocessed and software outside of the camera is used to render color-managed images.

As an example, a digital single-lens reflex (DSLR) camera having a 21-megapixel *CMOS* (complementary metal oxide semiconductor) sensor was used. Two *HMI* (hydrargyrum medium-arc iodide) lights having a correlated color temperature of 5600 K were placed on either side of an easel at 45° from the normal. The lights were adjusted to achieve spatial uniformity, verified by imaging a diffuse white board and evaluating the image data for consistency.

Images were taken of the diffuse white board, an Xrite ColorChecker® Digital SG (CCSG), and a Avian Rochester Next Generation Gloss Target (NGT) (Wyble 2017). The targets are shown in Figures 10.39 and 10.40, respectively

A common approach to convert from camera raw to color managed is using the *raw converter* accessed in Adobe Photoshop or similar editing software. The NGT image was converted to 16-bit ProPhotoRGB. The *RGB* data for the central 50% of each patch were averaged and transformed to CIELAB for illuminant D50 and the 1931 standard observer. These values were compared with the average of five measurements with replacement from a 45°a:0° spectrophotometer. Colorimetry was calculated for illuminant D50 and the 1931 standard observer. We analyze accuracy both graphically and statistically. Vector plots, shown in Figure 10.41, are used to evaluate the direction and magnitude of error. There are large errors for many colors, particularly yellows and greens where chroma increased significantly. The lightness reproduction is also in error where darker colors become darker and lighter colors become lighter. Statistically, we evaluate the average and 90th percentile CIEDE2000 total color differences, shown in Table 10.6. These are large color differences. For this particular example, the raw converter performed very poorly.

The second approach used the CCSG as a profiling (calibration) target. Each patch was measured five times with replacement using a 45°a:0° spectrophotometer. Colorimetry was defined for illuminant D50 and the 1931 standard observer.

The CCSG image was first divided by the white board image to correct any slight lighting nonuniformity and to compensate for differences in each pixel's radiometric response. The *RGB* values of the central 50% of each patch were averaged. The transformation from *RGB* to *XYZ* is shown in Eq. (10.39):

$$\begin{pmatrix} X \\ Y \\ Z \end{pmatrix} = \begin{pmatrix} a_{1,1} & a_{1,2} & a_{1,3} \\ a_{2,1} & a_{2,2} & a_{2,3} \\ a_{3,1} & a_{3,2} & a_{3,3} \end{pmatrix} \begin{pmatrix} R - R_o \\ G - G_o \\ B - B_o \end{pmatrix} \tag{10.39}$$

where the matrix coefficients, $a_{1,1}$–$a_{3,3}$, and R_o, G_o, and B_o were estimated minimizing average CIEDE2000 between the spectrophotometer and camera data. We have found a marked improvement adding the offsets, R_o, G_o, and B_o, as they compensate for differences in stray light between the spectrophotometer and the imaging system. The optimized model coefficients from the CCSG were used to transform the camera-raw signals to ProPhotoRGB for the NGT, the results shown in Figure 10.41 and Table 10.6. These results are very good demonstrating the effectiveness of building a profile for the actual imaging conditions. This level of accuracy is typical of commercial profiling systems. It is important to note that we are evaluating performance using a target different from the target used to profile the camera. Most commercial software report only the results for the calibration target, which overestimates accuracy.

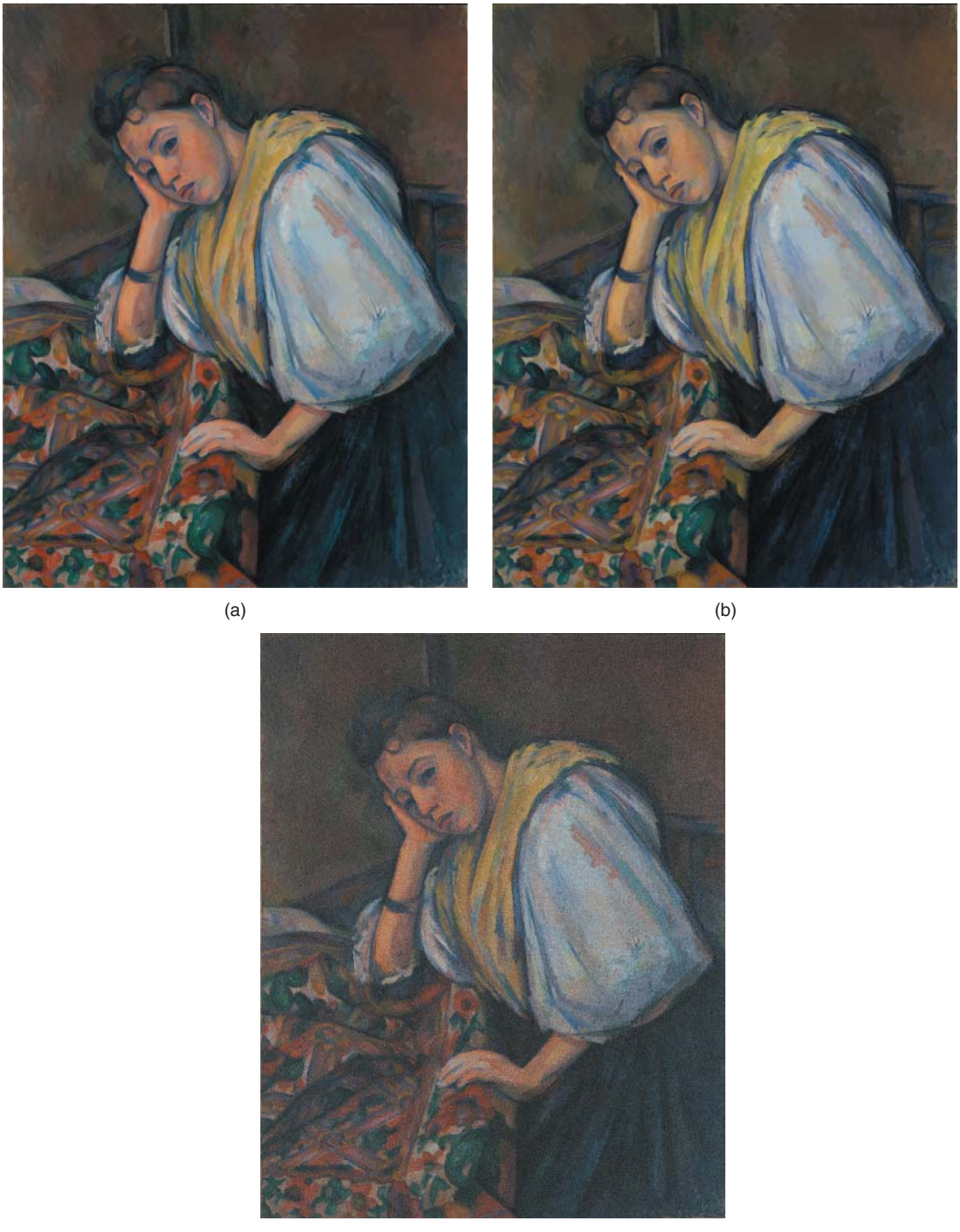

(a) (b)

(c)

Figure 10.38 Paul Cézanne (French, 1839–1906), *Young Italian Woman at a Table*, about 1895–1900, Oil on canvas, 92.1 cm × 73.5 cm (36 1/4 in. × 28 15/16 in.), (a) original image, (b) hue error, and (c) noise added.
Source: (a) Digital image courtesy of the Getty's Open Content Program.

Figure 10.39 Xrite ColorChecker® Digital SG (CCSG).

Figure 10.40 Avian Rochester Next Generation Gloss Target (NGT).

Color-critical observers quickly notice image areas with larger color errors. Nine-coefficient transformation matrices rarely result in sufficient color accuracy for all colors, particularly for applications such as image archiving. The 90th percentile, shown in Table 10.6, is a metric we believe correlates with this tendency to focus on larger errors. Maximum errors are misleading because it is a single sample that can be an outlier. Color-difference histograms are also useful.

One approach to improve accuracy is by adding terms to the transformation matrix, for example, Eq. (10.40) (Hong, Luo, and Rhodes 2001)

$$\begin{pmatrix} X \\ Y \\ Z \end{pmatrix} = \mathbf{M}(R \;\; G \;\; B \;\; RG \;\; RB \;\; GB \;\; RGB \;\; R^2 \;\; G^2 \;\; B^2 \;\; 1)' \tag{10.40}$$

Linear regression minimizing tristimulus value RMS error is used to calculate the coefficients. This approach is known as polynomial regression. It has the advantage of not requiring optimization. We do not advocate polynomial regression for two reasons. First, independent data with similar *RGB* are sometimes mapped to very different *XYZ* causing odd contouring of objects with smooth gradations. Polynomials often extrapolate data in unexpected ways, resulting in large errors in regions of *XYZ* undersampled by the calibration target.

A second approach is to build a multidimensional lookup table. It is critical that the target patches well-sample CIELAB and have a large color gamut.

A third approach to improve performance is to add channels beyond three, known as *multispectral imaging*. Imai and Berns (2009) developed a method where either multiple filters or multiple lights are used with an RGB camera. Each filter or light adds three additional channels. Berns implemented this approach by replacing the IR blocking filter, which all RGB cameras have, with clear glass extending the sensitivity of the camera to longer wavelengths (Berns et al. 2005). Cyan and yellow filters were fabricated that modulated the red and blue channels, resulting in narrow and wide-band blue and red channels and two greens that were nearly identical. The two-filter implementation is known as *dual-RGB*. The fabricated filters included a visible bandpass filter that absorbed optical radiation beyond 700 nm. The early implementation of this approach used linear regression between the camera signals and tristimulus values to estimate starting values for an optimization minimizing average CIEDE2000. Because the two green channels are highly correlated, the optimized matrix had large positive and negative coefficients for the two channels leading to unacceptable image noise. A second problem was a slight loss in sharpness when the registration between the two images was not perfect. These problems were minimized using Eq. (10.41) to estimate tristimulus values

$$\begin{pmatrix} X \\ Y \\ Z \end{pmatrix} = \begin{pmatrix} a_{1,1} & a_{1,2} & a_{1,3} & a_{1,4} & 0 & a_{1,6} \\ a_{2,1} & a_{2,2} & a_{2,3} & 0 & 0 & 0 \\ a_{3,1} & a_{3,2} & a_{3,3} & a_{3,4} & 0 & a_{3,6} \end{pmatrix} \begin{pmatrix} R_c - R_{c,o} \\ G_c - G_{c,o} \\ B_c - B_{c,o} \\ R_y - R_{y,o} \\ G_y - G_{y,o} \\ B_y - B_{y,o} \end{pmatrix} \tag{10.41}$$

Notice that the yellow-filtered green channel is not used and that only the cyan-filtered image is used when estimating tristimulus *Y*.

A dual-RGB system was used to capture images through cyan and yellow filters followed by dividing by the white-board image. The matrix coefficients and offsets were estimated that minimized average CIEDE2000 for the CCSG. The optimized model coefficients from the CCSG were used to transform the camera-raw signals to ProPhotoRGB for the NGT, the results shown in Figure 10.41

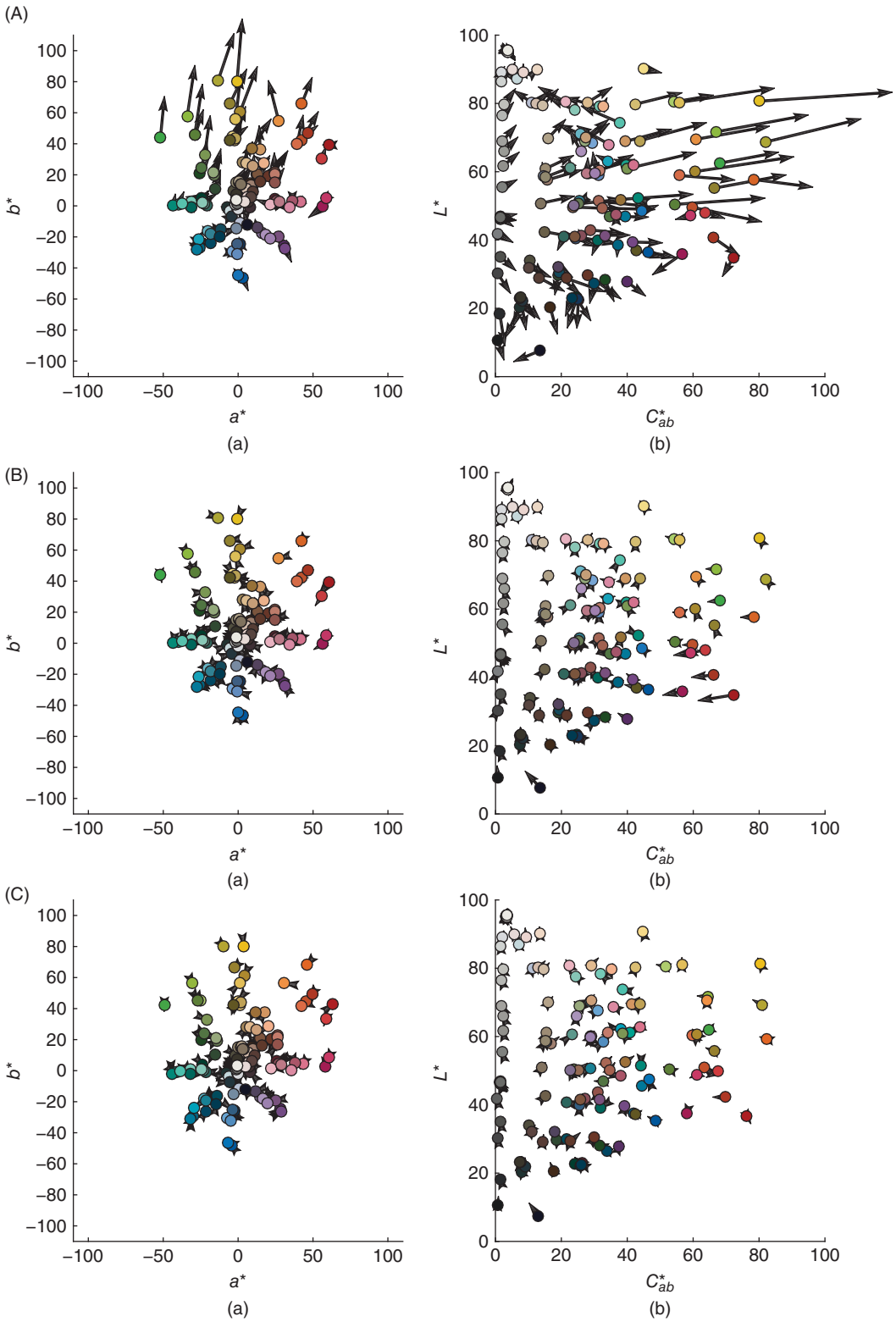

Figure 10.41 Color reproduction vector plots for the NGT where the colored dot defines the coordinates of a measured color patch, while the arrowhead defines the coordinates of its estimate using (A) Photoshop camera raw converter, and (B) profile using Eq. (10.39), and (C) dual-RGB profile using Eq. (10.41).

Table 10.6 Average and 90th percentile CIEDE2000 for the Next Generation Color Target for each listed workflow.

Workflow	Average	90th percentile
RGB camera raw to tiff using raw converter in Photoshop	5.7	8.9
RGB camera raw to tiff optimizing Eq. (10.39)	1.2	2.1
Dual-RGB camera raw to tiff optimizing Eq. (10.41)	1.0	1.1

and Table 10.6. There is a slight improvement in average performance compared with an RGB camera and a large improvement in the 90th percentile. This approach to colorimetric imaging is very effective for color-critical applications.

Spectral Accuracy

The similarity of camera spectral sensitivities to color-matching functions, that is, spectral accuracy, is another measure of color quality. Camera spectral sensitivities, s_λ, are a product of the lens spectral transmittance, $T_{\lambda,\,\text{lens}}$, color-filter spectral transmittances, $T_{\lambda,\,\text{filter}}$, and the sensor spectral quantum efficiency, Q_λ, shown in Eq. (10.42)

$$s_\lambda = T_{\lambda,\text{lens}} T_{\lambda,\text{filter}} Q_\lambda \tag{10.42}$$

Quantum efficiency is a measure of the number of signal-electrons per incident photon, plotted in Figure 10.42 for CMOS and *CCD* (charged-couple device) monochrome sensors. This CCD sensor is designed for scientific applications and was used in the seven-channel multispectral camera (Berns 2018) described in Chapter 6. The high quantum efficiency at short wavelengths makes this an excellent sensor when imaging in the UV region of the spectrum.

The normalized spectral sensitivities of the DSLR and dual-RGB cameras used above are shown in Figure 10.43.

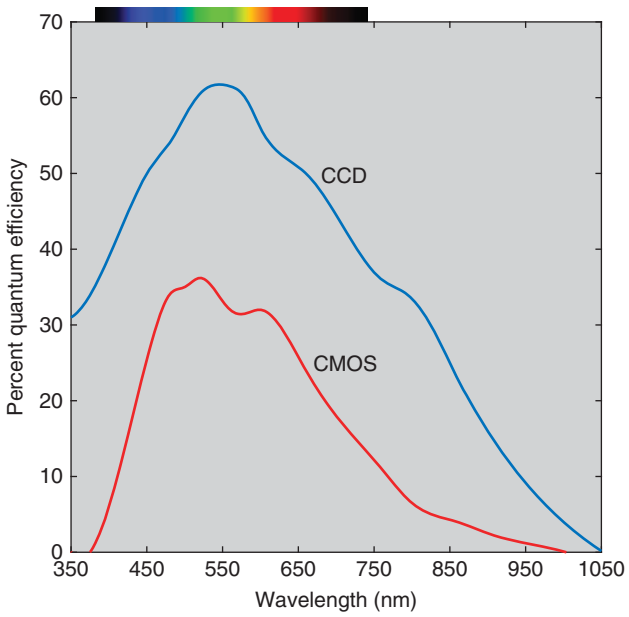

Figure 10.42 Percent quantum efficiency for CMOS (red line) and CCD (blue line) monochrome sensors. Note the extended wavelength range.

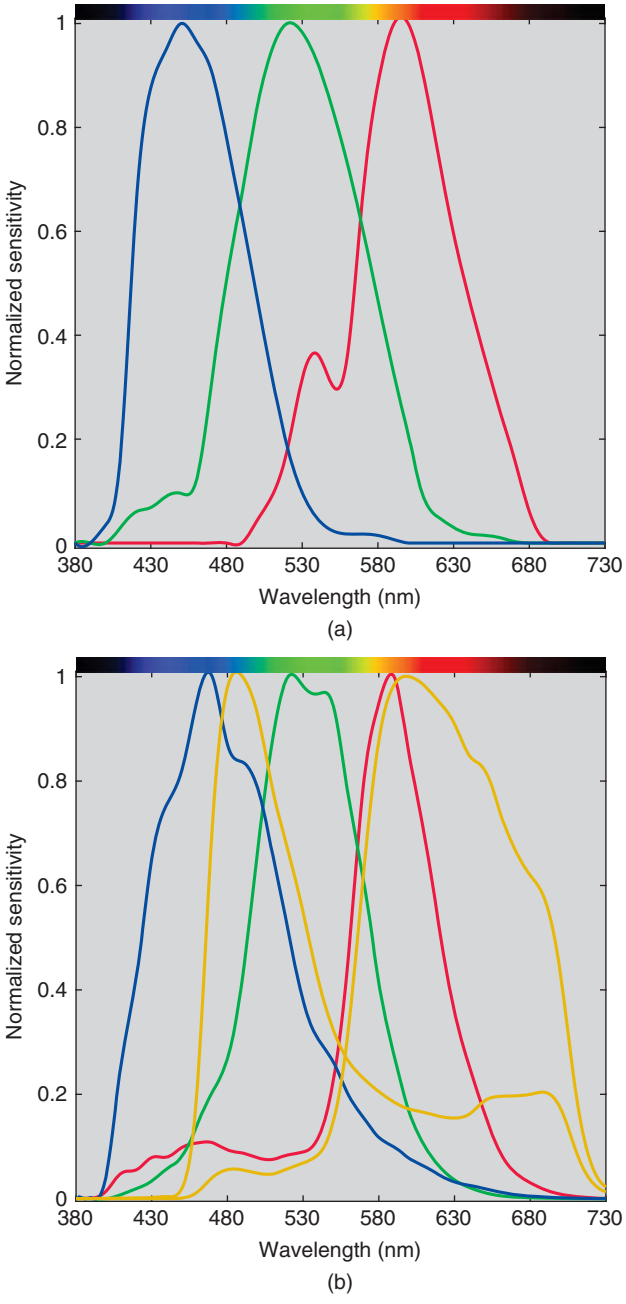

Figure 10.43 Normalized spectral sensitivities of (a) CMOS RGB DSLR camera and (b) CCD dual-*RGB* camera where sensitivities plotted in yellow correspond to the yellow filter.

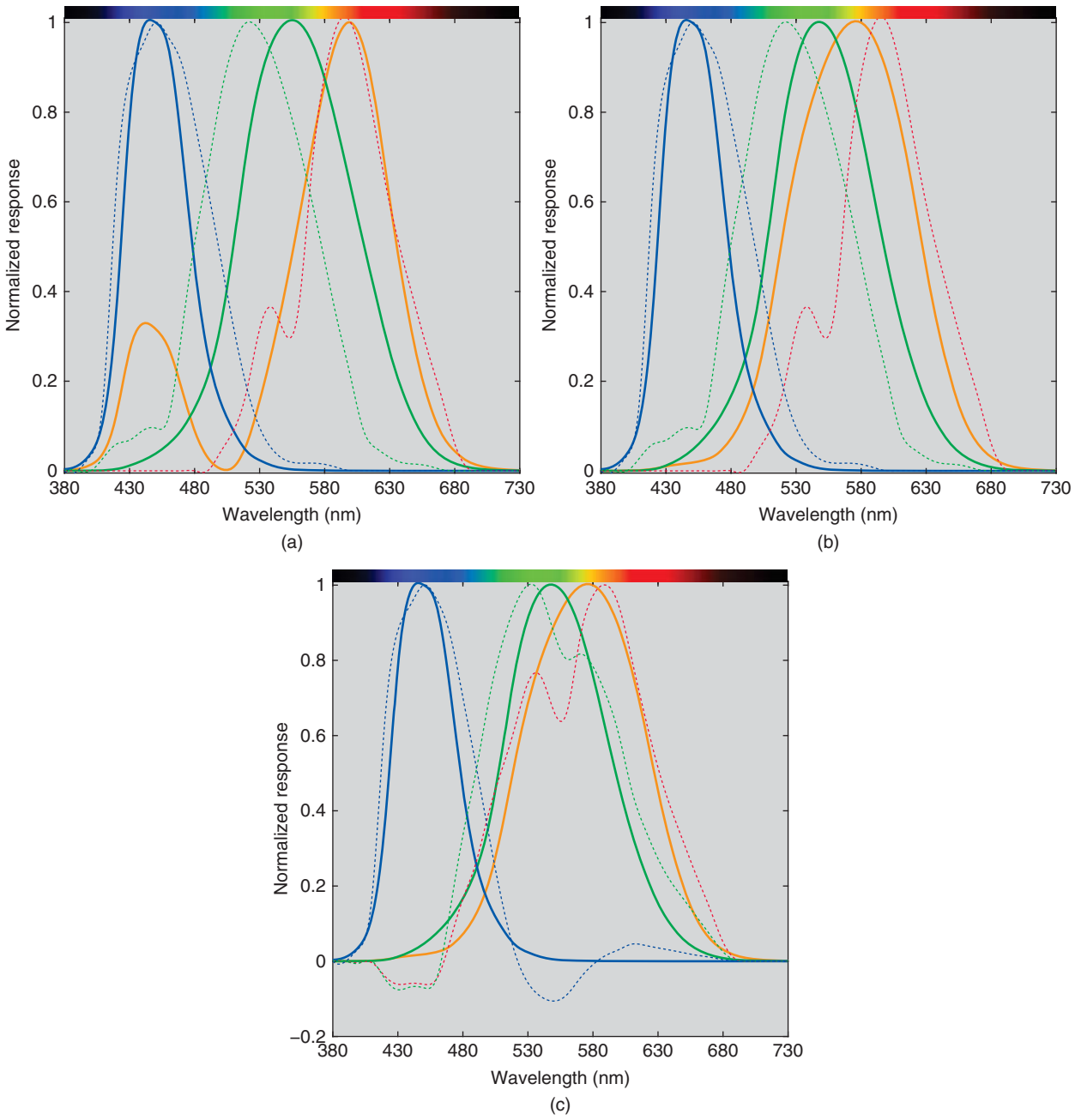

Figure 10.44 Normalized spectral responses of (a) CMOS sensor and the 1931 standard observer, (b) CMOS sensor and the HPE cone fundamentals, and (c) linear transformation of the CMOS spectral sensitivities and the HPE cone fundamentals.

The dual-RGB camera with the cyan filter is equivalent to a typical CCD camera.

Ideally, these spectral sensitivities should be equivalent to color-matching functions or cone responses. The CMOS spectral sensitivities are compared with the 1931 standard observer and the Hunter–Pointer–Estevez (HPE) cone fundamentals, shown in Figure 10.44. The red and blue channels reasonably match $\bar{x}_\lambda$ and $\bar{z}_\lambda$. The blue channel reasonably matches the S cone fundamental. The green channel is a poor match to $\bar{y}_\lambda$ and the M cone fundamental. Interpretation depends on the aim spectral sensitivities. It is more appropriate to compare responses following a linear transformation, derived by minimizing RMS spectral response error. This is shown in Figure 10.44c. The fits are reasonable. The same quality of fit would result for the standard observer.

Quantifying spectral goodness of fit was first explored by Neugebauer (1956) for a single sensor, known as q-factor (quality factor). This was extended by Vora and Trussell

Table 10.7 μ-Factor for each listed camera.

Camera system	μ-Factor
CMOS RGB	0.96
CCD dual-RGB	0.97
CCD RGB (cyan filter signals from dual-RGB)	0.92

The taking and reference illuminants are D50.

(1993) for any number of sensors, known as μ-factor. See Quan and Ohta (2002) for a comparison of the two metrics. Conceptually, μ-factor is the residual error following the linear transformation subtracted from unity. When $\mu = 1$, the camera and aim spectral sensitivities are linearly transformable. For example, the 1931 standard observer and HPE cone fundamentals result in $\mu = 1$.

The formula to calculate μ-factor when comparing an RGB camera to color-matching functions is shown in Eqs. (10.43)–(10.45):

$$\mu = \frac{\text{Trace}\{\mathbf{S}'\mathbf{A}(\mathbf{A}'\mathbf{A})^{-1}\mathbf{A}'\mathbf{S}(\mathbf{S}'\mathbf{S})^{-1}\}}{\alpha} \tag{10.43}$$

where

$$\mathbf{S} = \begin{pmatrix} I_{\lambda,\text{taking}} & 0 & 0 \\ 0 & \ddots & 0 \\ 0 & 0 & I_{\lambda,\text{taking}} \end{pmatrix} \begin{pmatrix} s_{\lambda,r} & s_{\lambda,g} & s_{\lambda,b} \\ \vdots & \vdots & \vdots \\ s_{\lambda,r} & s_{\lambda,g} & s_{\lambda,b} \end{pmatrix} \tag{10.44}$$

$$\mathbf{T} = \begin{pmatrix} I_{\lambda,\text{reference}} & 0 & 0 \\ 0 & \ddots & 0 \\ 0 & 0 & I_{\lambda,\text{reference}} \end{pmatrix} \begin{pmatrix} \bar{x}_\lambda & \bar{y}_\lambda & \bar{z}_\lambda \\ \vdots & \vdots & \vdots \\ \bar{x}_\lambda & \bar{y}_\lambda & \bar{z}_\lambda \end{pmatrix} \tag{10.45}$$

The constant α defines the number of visual channels, three in this case, s_λ, is defined in Eq. (10.42), $I_{\lambda,\text{taking}}$ is the spectral power distribution of the *taking illuminant*, and $I_{\lambda,\text{reference}}$ is the spectral power distribution of the reference illuminant. In the example above, the HMI sources are the taking illuminant and D50 is the reference illuminant.

μ-Factor for the CMOS camera, the dual-RGB camera, and the dual-RGB camera using only the cyan filter is shown in Table 10.7. The dual-RGB camera had the best spectral similarity and the single-filter dual-RGB camera had the poorest spectral similarity. We use a μ-factor as an indicator of color-accuracy potential where imaging systems with μ-factor less than 0.9 should not be used for colorimetric imaging.

G. SPECTRAL COLOR REPRODUCTION

ICC.1 color management is based on the principle of metamerism—two stimuli match when their colorimetric coordinates are equal. Because of the importance of metamerism and its associated problems and limitations, we devote a chapter to the subject, Chapter 8. A spectral workflow would eliminate a number of problems caused by a colorimetric-based profile-connection space, described earlier in this chapter. This idea can be further expanded where an image is defined by any number of channels. The channels could define, for example, ETRGB, spectral reflectance for a single geometry, spectral reflectance at multiple geometries using a multiangle spectrophotometer, spatially varying bidirectional reflectance distribution function (BRDF) model parameters, surface normal maps, and height maps. The image data would represent color and material appearance for samples containing conventional absorbing and scattering colorants, fluorescent colorants, and gonioapparent pigments. This would be a comprehensive approach for object documentation.

The ICC has recognized both the importance of adding a spectrally based PCS that is independent of the colorimetric-based PCS and the opportunity to encode material appearance attributes among others. This has culminated in a new ICC specification—ICC.2:2018, referred to as iccMAX (ICC 2018b). Spectra can be encoded of any wavelength range and increment. Spectra can be reflectance, transmittance, or a Donaldson matrix for luminescent materials. One of its intriguing features includes a programmable transform calculator that enables processing that is *late binding*. For example, colorimetric data can be calculated for any illuminant and observer combination. Nonlinear models can be directly encoded without using large multidimensional lookup tables. There are also possibilities of iterative calculations that could transform spectra into colorant maps for a known set of colorants and a linear color-mixing model (Bodner and Berns 2016). ETRGB, BRDF, and a height map could be used for 3d printing. iccMAX has tremendous flexibility with many opportunities to improve the current state of color management.

H. SUMMARY

Color imaging has its origins in trichromacy and metameric matching—an object or scene and its reproduction matches when colorimetric coordinates are equal. By first defining the colorimetric properties of an output system, input systems could be designed resulting in a direct mapping between devices, for example, broadcast color television. Changes in devices would require a new transformation. This became an acute problem with the introduction of desktop printing and publishing where having a direct transformation between each input and output device became impractical. The ICC developed a color management system where each device has a direct transformation to a reference color space, enabling an infinite number of devices to be interconnected. The reference color space is called the PCS having coordinates defined by tristimulus values or CIELAB. The transformation between device signals

and the PCS is called a color profile and matrices, multidimensional lookup tables, one-dimensional lookup tables, and analytical functions are used. Oftentimes, input colors cannot be reproduced on output devices due to color-gamut limitations and require re-rendering. The ICC has predefined four types of color rendering: perceptual, saturation, media-relative colorimetric, and ICC-absolute colorimetric. The transformations between devices is performed by a color management module—the color engine. Display profiles are often a combination of a matrix and either one-dimensional lookup tables or analytical functions. Printer profiles are multidimensional lookup tables. Camera profiles are a matrix or a multidimensional lookup table. Examples were shown for modeling a liquid crystal display, a rotated-screen halftone CMYK printer, a DSLR RGB camera, and a dual-RGB camera. This approach to color management has also been implemented using a reference display, the encoding known as sRGB, which greatly simplified color processing. Most consumer devices are sRGB devices, resulting in consistent color. Professional photographers and those involved in printing and publishing require the more comprehensive color management developed by the ICC. ICC color management continues to evolve. They have extended colorimetric profiles and the colorimetric profile connection space, and added a programmable transform calculator, all of which will facilitate spectral and multichannel profiles that will result in the documentation of color and material appearance. The new specification is called iccMAX and we anticipate tremendous growth in the archiving and reproduction of color and material appearance.

Bibliography

AATCC TM173-2015 (2015). *CMC: calculation of small color differences for acceptability*. Research Triangle Park, NC: American Association of Textile Chemists and Colorists.

Abed, F.M. and Berns, R.S. (2017). Linear modeling of modern artist paints using a modification of the opaque form of Kubelka-Munk turbid media theory. *Color Research & Application* 42: 308–315.

Adams, E.Q. (1942). X-Z planes in the 1931 I.C.I. (CIE) system of colorimetry. *Journal of the Optical Society of America* 32: 168–173.

Adobe Systems Incorporated (2005). Adobe® RGB (1998) Color Image Encoding. https://www.adobe.com/digitalimag/pdfs/AdobeRGB1998.pdf (accessed 17 October 2018).

Aitken, D., Burkinshaw, S.M., Griffiths, J., and Towns, A.D. (1996). Textile applications of thermochromic systems. *Review of Progress in Coloration and Related Topics* 26: 1–8.

Albers, J. (1963). *Interaction of Color*. New Haven, CT: Yale University Press.

Allen, E. (1966). Basic equations used in computer color matching. *Journal of the Optical Society of America* 56: 1256–1259.

Allen, E. (1974). Basic equations used in computer color matching, II. Tristimulus matching, two-constant theory. *Journal of the Optical Society of America* 64: 991–993.

Allen, E. (1980). Colorant formulation and shading. In: *Optical Radiation Measurements: Color Measurement*, vol. 2 (ed. F. Grum and C.J. Bartleson), 290–336. New York: Academic Press.

Allen, E. and Yuhas, B. (1984). Setting up acceptability tolerances: a case study. *Color Research & Application* 9: 37–48.

Alman, D.H. and Billmeyer, F.W. (1976). Integrating sphere errors in the colorimetry of fluorescent materials. *Color Research & Application* 1: 141–145.

Alman, D.H., Berns, R.S., Snyder, G.D., and Larsen, W.A. (1989). Performance testing of color-difference metrics using a color tolerance dataset. *Color Research & Application* 14: 139–151.

Anderson, M., Motta, R., Chandrasekar, S., and Stokes, M. (1996). Proposal for a standard default color space for the internet—sRGB. In: *IS&T 4th Color Imaging Conference*, 238–245. Scottsdale, AZ.

Asano, Y., Fairchild, M.D., Bondé, L., and Morvan, P. (2014). Observer variability in image color matching on an LCD monitor and a laser projector. In: *IS&T 22nd Color & Imaging Conference*, 1–6. Boston, MA.

Asano, Y., Fairchild, M.D., and Blondé, L. (2016). Individual colorimetric observer model. *PLoS ONE* 11 (2): e0145671. https://doi.org/10.1371/journal.pone.0145671.

ASTM E284 – 13b (2013a). *Standard terminology of appearance*. West Conshohocken, PA: ASTM International.

ASTM D1003 – 13 (2013b). *Standard test method for haze and luminous transmittance of transparent plastics*. West Conshohocken, PA: ASTM International.

ASTM E1345 – 14 (2014). *Standard practice for reducing the effect of variability of color measurement by use of multiple measurements*. West Conshohocken, PA: ASTM International.

ASTM E308 – 15 (2015a). *Standard practice for computing the colors of objects by using the CIE system*. West Conshohocken, PA: ASTM International.

ASTM E313 – 15 (2015b). *Standard practice for calculating yellowness and whiteness indices from instrumentally measured color coordinates*. West Conshohocken, PA: ASTM International.

ASTM E1808 – 96 (2015c). *Standard guide for designing and conducting visual experiments*. West Conshohocken, PA: ASTM International.

ASTM D1729 – 16 (2016a). *Standard practice for visual appraisal of colors and color differences of diffusely-illuminated opaque materials*. West Conshohocken, PA: ASTM International.

ASTM E178 – 16a (2016b). *Standard practice for dealing with outlying observations*. West Conshohocken, PA: ASTM International.

ASTM E991 – 16 (2016c). *Standard practice for color measurement of fluorescent specimens using the one-monochromator method*. West Conshohocken, PA: ASTM International.

ASTM E1499 – 16 (2016d). *Standard guide for selection, evaluation, and training of observers*. West Conshohocken, PA: ASTM International.

Billmeyer and Saltzman's Principles of Color Technology, Fourth Edition. Roy S. Berns.

ASTM 2214 – 16 (2016e). *Standard practice for specifying and verifying the performance of color-measuring instruments*. West Conshohocken, PA: ASTM International.

ASTM E2152 – 17 (2017a). *Standard practice for computing the colors of fluorescent objects from bispectral photometric data 1*. West Conshohocken, PA: ASTM International.

ASTM E2194 – 17 (2017b). *Standard test method for multiangle color measurement of metal flake pigmented materials*. West Conshohocken, PA: ASTM International.

ASTM E2539 – 17 (2017c). *Standard test method for multiangle color measurement of interference pigments*. West Conshohocken, PA: ASTM International.

Attarchi, N. and Amirshahi, S.H. (2009). Reconstruction of reflectance data by modification of Berns' Gaussian method. *Color Research & Application* 34: 26–32.

Backhaus, W.G.K., Kliegl, R., and Werner, J.S. (1998). *Color Vision Perspectives from Different Disciplines*. Berlin: Walter de Gruyter.

Bajorski, P. (2012). *Statistics for Imaging, Optics, and Photonics*, Wiley Series in Probability and Statistics. New York: Wiley.

Bartleson, C.J. and Breneman, E.J. (1967). Brightness perception in complex fields. *Journal of the Optical Society of America* 57: 953–957.

Bartleson, C.J. and Grum, F. (eds.) (1984). *Optical Radiation Measurements: Visual Measurements*, vol. 5. Orlando, FL: Academic Press.

van Beek, H.C.A. (1983). Light-induced colour changes in dyes and materials. *Color Research & Application* 8: 176–181.

Beer, A. (1852). Bestimmung der Absorption des rothen Lichts in farbigen Flüssigkeiten. *Annual Review of Physical Chemistry* 86 (2): 78–90.

Beer, A. (1854). *Grundriß des photometrischen Kalküls*. Branschweig.

Berlin, B. and Kay, P. (1969). *Basic Color Terms: Their Universality and Evolution*. Berkeley, CA: University of California Press.

Berns, R.S. (1993a). The mathematical development of CIE TC 1-29 proposed color difference equation: CIELCH. In: *7th Congress International Colour Association*, C19-1–C19-4. Budapest.

Berns, R.S. (1993b). Spectral modeling of a dye diffusion thermal transfer printer. *Journal of Electronic Imaging* 2: 359–370.

Berns, R.S. (1994). Synthetic reflectance curves. *Journal of the Society of Dyers and Colourists* 110: 386–388.

Berns, R.S. (1996a). Deriving instrumental tolerances from pass-fail and colorimetric data. *Color Research & Application* 21: 459–472.

Berns, R.S. (1996b). Methods for characterizing CRT displays. *Displays* 16: 173–182.

Berns, R.S. (1997). A generic approach to color modeling. *Color Research & Application* 22: 318–325.

Berns, R.S. (2000). *Billmeyer and Saltzman's Principles of Color Technology*. New York: Wiley.

Berns, R.S. (2001). Derivation of a hue-angle dependent, hue-difference weighting function for CIEDE2000. In: *AIC 2001—9th Congress of the International Colour Association*, 638–641. Rochester, NY.

Berns, R.S. (2007). Let's call it 'color-gamut rendering'. *Color Research & Application* 32: 334–335.

Berns, R.S. (2008a). Generalized industrial color-difference space based on multi-stage color vision and line-element integration. *Óptica Pura Y Aplicada* 41: 301–311.

Berns, R.S. (2008b). The proper use of indices of metamerism. *Color Research & Application* 33: 509–512.

Berns, R.S. (2011). Designing white LED lighting for the display of art: a feasibility study. *Color Research & Application* 36: 324–334.

Berns, R.S. (2014a). Extending CIELAB: vividness, V^*_{ab}, depth, D^*_{ab}, and clarity, T^*_{ab}. *Color Research & Application* 39: 322–330.

Berns, R.S. (2014b). *Camera Encoding Evaluation for Image Archiving of Cultural Heritage*. Rochester Institute of Technology Studio for Scientific Imaging and Archiving of Cultural Heritage http://www.rit-mcsl.org/Mellon/PDFs/CameraEncoding_TR_May_2014.pdf (accessed 16 October 2018).

Berns, R.S. (2016). *Color Science and the Visual Arts: A Guide for Conservators, Curators, and the Curious*. Los Angeles, CA: Getty Conservation Institute.

Berns, R.S. (2018). *Practical UV-VIS-NIR Multispectral Imaging*, 47–52. Washington, DC: IS&T Archiving Conference.

Berns, R.S. and Billmeyer, F.W. (1983). Proposed indices of metamerism with constant chromatic adaptation. *Color Research & Application* 8: 186–189.

Berns, R.S. and Billmeyer, F.W. (1985). Development of the 1929 Munsell book of color: a historical review. *Color Research & Application* 10: 246–250.

Berns, R.S. and de la Rie, E.R. (2003). Exploring the optical properties of picture varnishes using imaging techniques. *Studies in Conservation* 48: 73–82.

Berns, R.S. and Derhak, M. (2015). *ETRGB: An Encoding Space for Artwork Imaging*, 74–77. Los Angeles, CA: IS&T Archiving Conference.

Berns, R.S. and Katoh, N. (2002). Methods for characterizing displays. In: *Color Engineering: Achieving Device Independent Colour* (ed. P. Green and L.W. MacDonald), 127–164. Chichester: Wiley.

Berns, R.S. and Kuehni, R.G. (1990). What determines crossover wavelengths of metameric pairs with three crossovers? *Color Research & Application* 15: 23–28.

Berns, R.S. and Mohammadi, M. (2007a). Evaluating single- and two-constant Kubelka-Munk turbid media theory for instrumental-based inpainting. *Studies in Conservation* 32: 299–314.

Berns, R.S. and Mohammadi, M. (2007b). Single-constant simplification of Kubelka-Munk turbid-media theory for paint systems—a review. *Color Research & Application* 32: 201–207.

Berns, R.S. and Petersen, K.H. (1988). Empirical modeling of systematic spectrophotometric errors. *Color Research & Application* 13: 243–256.

Berns, R.S. and Reniff, L. (1997). An abridged technique to diagnose spectrophotometric errors. *Color Research & Application* 22: 51–60.

Berns, R.S., Fairchild, M.D., and Beering, M.M. (1988). Quantification of illuminant metamerism for four coloration systems via metameric mismatch gamuts. *Color Research & Application* 13: 346–357.

Berns, R.S., Alman, D.H., Reniff, L. et al. (1991). Visual determination of supra-threshold color-difference tolerances using probit analysis. *Color Research & Application* 16: 297–316.

Berns, R.S., Taplin, L.A., Nezamabadi, M., and Mohammadi, M. (2005). Spectral imaging using a commercial color-filter array digital camera. In: *ICOM 14th Triennial Meeting*, 743–750. The Hague.

Berns, R.S., Byrns, S., Casadio, F. et al. (2006). Rejuvenating the color palette of Georges Seurat's A Sunday on La Grande Jatte, 1884: a simulation. *Color Research & Application* 31 (4): 278–293.

Berns, R.S., Cox, B.D., and Abed, F.M. (2015). Wavelength-dependent spatial correction and spectral calibration of a liquid crystal tunable filter system. *Applied Optics* 54: 3687–3693.

Billmeyer, F.W. (1963). An objective approach to coloring. *Die Farbe* 12: 151–164.

Billmeyer, F.W. (1987). Survey of color order systems. *Color Research & Application* 12: 173–186.

Billmeyer, F.W. and Abrams, R.L. (1973). Predicting reflectance and color of paint films by Kubelka-Munk analysis. I. Turbid medium. *Journal of Paint Technology* 45: 23–30.

Billmeyer, F.W. and Alessi, P.J. (1981). Assessment of color-measuring instruments. *Color Research & Application* 6: 195–202.

Billmeyer, F.W. and Bencuya, A.K. (1987). Interrelation of the Natural Color System and the Munsell color order system. *Color Research & Application* 12: 243–255.

Billmeyer, F.W. and Chen, Y. (1985). On the measurement of haze. *Color Research & Application* 10: 219–224.

Billmeyer, F.W. and Marcus, R.T. (1969). Effect of illuminating and viewing geometry on the color coordinates of samples with various surface textures. *Applied Optics* 8: 763–768.

Billmeyer, F.W. and Saltzman, M. (1966). *Principles of Color Technology*. New York: Wiley.

Billmeyer, F.W. and Saltzman, M. (1980). Observer metamerism. *Color Research & Application* 5: 72.

Birch, J. (1993). *Diagnosis of Defective Colour Vision*. New York: Oxford University Press.

Birren, F. (1979). Chroma Cosmos 5000. *Color Research & Application* 4: 171–172.

Bodner, B. and Berns, R.S. (2016). An iccMAX material profile example: converting spectral images of artwork to paint-concentration images. In: *24th Color Imaging Conference*, 242–247. San Diego.

Bodrogi, P., Guo, X., Stojanovic, D. et al. (2018). Observer preference for perceived illumination chromaticity. *Color Research & Application* 43 (4): 506–516.

Bolomey, R.A. and Greenstein, L.M. (1972). Optical characteristics of iridescence and interference pigments. *Journal of Paint Technology* 44: 39–50.

Bonham, J.S. (1986). Fluorescence and Kubelka-Munk theory. *Color Research & Application* 11: 223–230.

Bouguer, P. (1729). *Essai d'optique sur la gradation de la lumière*. Paris: Claude Tombert.

Boyce, P.R. (2014). *Human Factors in Lighting*, 3e. Boca Raton, FL: CRC Press.

Brady, T.F., Konkle, T., Gill, J. et al. (2013). Visual long-term memory has the same limit on fidelity as visual working memory. *Psychological Science* 24: 981–990.

Brettel, H., Viénot, F., and Mollon, J.D. (1997). Computerized simulation of color appearance for dichromats. *Journal of the Optical Society of America A* 14: 2647–2655.

Brill, M.H. and Mahy, M. (2013). Visualization of mathematical inconsistencies in CIECAM02. *Color Research & Application* 38: 188–195.

Bristow, J.A. (1994). The calibration of instruments for the measurement of paper whiteness. *Color Research & Application* 19: 475–483.

Brown, W.R.J. (1952). The effect of field size and chromatic surroundings on color discrimination. *Journal of the Optical Society of America* 42: 837–844.

Brown, W.R.J. and MacAdam, D.L. (1949). Visual sensitivities to combined chromaticity and luminance differences. *Journal of the Optical Society of America* 39: 808–834.

BSI (1988). *Method for Calculation of Small Colour Differences*. London: British Standards Institution.

Burns, P.D. and Berns, R.S. (1997). Error propagation in color signal transformations. *Color Research & Application* 22: 280–289.

Cat, J. (2013). *Maxwell, Sutton, and the Birth of Color Photography: A Binocular Study*. New York: Palgrave Pivot.

Chen, Y. (2006). *Optimal Design of Ink Spectra for Multiple-Ink Color Reproduction*. Rochester Institute of Technology http://scholarworks.rit.edu/theses/7989/.

Chevreul, M.E. (1854). *The Principle of Harmony and Contrast of Colors* (based on the first English edition of 1854). New York: Reinhold Publishing Corporation.

Cho, Y.J., Ou, L.-C., and Luo, R. (2017). A cross-cultural comparison of saturation, vividness, blackness and whiteness scales. *Color Research & Application* 42: 203–215.

Chou, W., Lin, H., Luo, M.R. et al. (2001). Performance of lightness difference formulae. *Coloration Technology* 117: 19–29.

Choudhury, A.K.R. and Chatterjee, S.M. (1996). Evaluation of the performance of metameric indices. *Color Research & Application* 21: 26–34.

CIE (1926). *Proceedings 6th Session, International Commission on Illumination*. Cambridge: Cambridge University Press.

CIE (1931). *Proceedings of the 8th Session, Cambridge, England, International Commission on Illumination*. Paris: Bureau Central de la CIE.

CIE 15.2-1986 (1986). *Colorimetry*, 2e. Vienna: Commission Internationale de L'Éclairage.

CIE CIE No. 78 (1988). *Brightness-luminance relations: classified bibliography*. Vienna: Commission Internationale de L'Éclairage.

CIE 086-1990 (1990) *CIE 1988 2° Spectral luminous efficiency function for photopic vision*. Vienna: Commission Internationale de L'Éclairage.

CIE 101-1993 1993. *Parametric effects in colour-difference evaluation*. Vienna: Commission Internationale de L'Éclairage.

CIE 116-1995 (1995a). *Industrial colour-difference evaluation*. Vienna: Commission Internationale de L'Éclairage.

CIE 13.3-1995 (1995b). *Method of measuring and specifying colour rendering properties of light sources*. Vienna: Commission Internationale de L'Eclairage.

CIE 122:1996 (1996). *The relationship between digital and colorimetric data for computer-controlled CRT displays*. Vienna: Commission Internationale de L'Éclairage.

CIE 131-1998 (1998). *The CIE 1997 interim colour appearance model (Simple Version), CIECAM97s*. Vienna: Commission Internationale de L'Éclairage.

CIE 142:2001 (2001). *Improvement to industrial colour-difference evaluation*. Vienna: Commission Internationale de L'Eclairage.

CIE ISO 23539:2005(E)/CIE S 010/E:2004 (2004a). *Joint ISO/CIE standard: photometry—the CIE system of physical photometry*. Vienna: CIE Central Bureau.

CIE 159:2004 (2004b). *A colour appearance model for colour management systems: CIECAM02*. Vienna: Commission Internationale de L'Éclairage.

CIE 170-1:2006 (2006a). *Fundamental chromaticity diagram with physiological axes – Part 1*. Vienna: Commission Internationale de l'Éclairage.

CIE (2006b). *Geometric tolerances for colour measurements*. Vienna: Commission Internationale de l'Éclairage.

CIE Standard CIE S 017/E:2011 ILV (2011). *International lighting vocabulary*. Vienna: Commission Internationale de L'Éclairage.

CIE 224:2017 (2017). *Colour fidelity index for accurate scientific use*. Vienna: Commission Internationale de L'Eclairage.

CIE (2018). *Colorimetry*, 4e, Publication No. 15:2018. Vienna: Commission Internationale de L'Éclairage.

Clarke, F.J.J., McDonald, R., and Rigg, B. (1984). Modification to the JPC79 colour-difference formula. *Journal of the Society of Dyers and Colourists* 100: 128–132.

Cohen, J.B. (2000). *Visual Color and Color Mixture: The Fundamental Color Space*. Champaign, IL: University of Illinois Press.

Colli, A., Gremmo, E., and Moniga, P. (1989). Proposta per un nuovo spazio di colore (LABmg) lineare rispetto alle tolleranze CMC. *Unificazione & Certificazione* 33 (4): 33–42.

Corns, S.N., Partington, S.M., and Towns, A.D. (2009). Industrial organic photochromic dyes. *Coloration Technology* 125: 249–261.

Cox, B.D., and Berns, R.S. (2015). Imaging artwork in a studio environment for computer graphics rendering. *Proceedings Volume 9398, Measuring, Modeling, and Reproducing Material Appearance 2015*; 939803. SPIE/IS&T Electronic Imaging, San Francisco, CA, USA.

Cui, G., Luo, M.R., Rigg, B. et al. (2002). Uniform colour spaces based on the DIN99 colour-difference formula. *Color Research & Application* 27: 282–290.

David, A., Fini, P.T., Houser, K.W. et al. (2015). Development of the IES method for evaluating the color rendition of light sources. *Optics Express* 33: 15888–15906.

Daw, N. (2012). *How Vision Works: The Physiological Mechanisms Behind What We See*. New York: Oxford University Press.

De Valois, R.L., Smith, C.J., Kitai, S.T., and Karoly, S.J. (1958). Responses of single cells in different layers of the primate lateral geniculate nucleus to monochromatic light. *Science* 127: 238–239.

Demichel, M.E. (1924). *Procédé* 26: 17, 26–21, 27.

Deming, W.E. (1950). *Some Theory of Sampling*. New York: Wiley.

Derby, R.E. (1952). Applied spectrophotometry. I. Color matching with the aid of 'R' cam. *American Dyestuffs Reporter* 41: 550–557.

Derefeldt, G. (1991). Colour appearance systems. In: *The Perception of Colour* (ed. P. Gouras), 218–261. Boca Raton, FL: CRC Press.

Derhak, M.W. and Berns, R.S. (2015a). Introducing Wpt (Waypoint): a color equivalency representation for defining a material adjustment transform. *Color Research & Application* 40: 535–549.

Derhak, M.W. and Berns, R.S. (2015b). Introducing WLab—Going from Wpt (Waypoint) to a uniform material color equivalency space. *Color Research & Application* 40: 550–563.

DIN 6176:2001-03 (2001). *Farbmetrische Bestimmung von Farbabständen bei Körperfarben nach der DIN99-Formel*. Berlin: Deutsche Institut für Normung.

Donaldson, R. (1954). Spectrophotometry of fluorescent pigments. *British Journal of Applied Physics* 5: 210–214.

Dorsey, J., Rushmeier, H.E., and Sillion, F.X. (2008). *Digital Modeling of Material Appearance*, The Morgan Kaufmann Series in Computer Graphics. Amsterdam; Boston, MA: Morgan Kaufmann/Elsevier.

Duncan, D.R. (1940). The colour of pigment mixtures. *Proceedings of the Physical Society* 52: 390–400.

Ďurikovič, R. and Ágošton, T. (2007). Prediction of optical properties of paints. *Central European Journal of Physics* 5: 416–427.

Early, E.A. and Nadal, M.E. (2004). Uncertainty analysis for reflectance colorimetry. *Color Research & Application* 29: 205–216.

Early, E.A. and Nadal, M.E. (2008). Uncertainty analysis for the NIST 0:45 reflectometer. *Color Research & Application* 33: 100–107.

Ebner, F. and Fairchild, M.D. (1998). Development and testing of a color space (IPT) with improved hue uniformity. In: *6th IS&T Color and Imaging Conference*, 8–13. Scottsdale, AZ.

Engeldrum, P.G. (1999). *Psychometric Scaling: A Toolkit for Imaging Systems Engineers*. Winchester: Imcotek Press.

Epstein, D.W. (1953). Colorimetric analysis of RCA color television system. *RCA Review* 14: 227–258.

Exelby, R. (2008). A survey of photochromism. *Journal of the Society of Dyers and Colourists* 83: 450–452.

Fairchild, M.D. (1995). Considering the surround in device independent color imaging. *Color Research & Application* 20: 352–363.

Fairchild, M.D. (1996). Refinement of the RLAB color space. *Color Research & Application* 21: 338–346.

Fairchild, M.D. (2013). *Color Appearance Models*, Wiley-IS&T Series in Imaging Science and Technology, 3e (ed. M.A. Kriss). New York: Wiley.

Fairchild, M.D. and Grum, F. (1985). Thermochromism of ceramic reference tiles. *Applied Optics* 24: 3432–3433.

Fairchild, M.D. and Heckaman, R.L. (2013). Metameric observers: a Monte Carlo approach. In: *IS&T 21st Color and Imaging Conference*, 185–190. Albuquerque, NM.

Fairchild, M.D. and Heckaman, R.L. (2016). Measuring observer metamerism: the Nimeroff approach. *Color Research & Application* 41: 115–124.

Fairchild, M.D. and Johnson, G.M. (2004). METACOW: a public-domain, high-resolution, fully-digital, noise-free, metameric, extended dynamic- range, spectral test target for imaging system analysis and simulation. In: *12th Color Imaging Conference*, 239–245. Scottsdale, AZ.

Fairchild, M.D. and Wyble, D.R. (1998). Colorimetric Characterization of the Apple Studio Display (Flat Panel LCD). Munsell Color Science Laboratory Technical Report.

Fairchild, M.D. and Wyble, D.R. (2007). Mean observer metamerism and the selection of display primaries. In: *Final Program and Proceedings-IS&T/SID Color Imaging Conference. IS&T/SID 15th Color Imaging Conference*, 151–156. Albuquerque, NM.

Fairman, H.S. (1987). Metameric correction using parameric decomposition. *Color Research & Application* 12: 261–265.

Fairman, H.S. and Hemmendinger, H. (1998). Stability of ceramic color reflectance standards. *Color Research & Application* 23: 408–415.

Fairman, H.S., Brill, M.H., and Hemmendinger, H. (1997). How the CIE 1931 color-matching functions were derived from Wright-Guild data. *Color Research & Application* 22 (1): 11–23.

Fairman, H.S., Brill, M.H., and Hemmendinger, H. (1998). How the CIE 1931 color-matching functions were derived from Wright-Guild data. *Color Research & Application* 23 (4): 259.

Fechner, G.T. (1860). *Elemente der Psychophysik*, vol. 1. Leipzig: Elements of Psychophysics (trans. H.E. Adler). New York: Holt, Rinehart and Winston, 1966: Breitkopf & Härtel.

Ferrero, A., Bernad, B., Campos, J. et al. (2016). Color characterization of coatings with diffraction pigments. *Journal of the Optical Society of America A* 33: 1978–1988.

de Fez, M.D., Capilla, P., Luque, M.J. et al. (2001). Asymmetric colour matching: memory matching versus simultaneous matching. *Color Research & Application* 26: 458–468.

Finney, D.J. (1971). *Probit Analysis*, 3e. London: Cambridge University Press.

Gall, L. (1971). *The Colour Science of Pigments*. Ludwigshafen: Badische Anilin- & Soda-Fabrik AG.

Ganz, E. (1976). Whiteness: photometric specification and colorimetric evaluation. *Applied Optics* 15: 2039–2058.

Ganz, E. (1979). Whiteness perception: individual differences and common trends. *Applied Optics* 18: 2963–2970.

Ganz, E. and Pauli, H.K.A. (1995). Whiteness and tint formulas of the Commission Internationale de L'Éclairage: approximations in the $L^*a^*b^*$ color space. *Applied Optics* 34: 2998–2999.

García, P.A., Huertas, R., Melgosa, M., and Cui, G. (2007). Measurement of the relationship between perceived and computed color differences. *Journal of the Optical Society of America A* 24: 1823–1829.

Gegenfurtner, K.R. and Sharpe, L.T. (eds.) (1999). *Color Vision: From Genes to Perception*. Cambridge: Cambridge University Press.

Germer, T.A. and Nadal, M.E. (2001). Modeling the appearance of special effect pigment coatings. In: *Proceedings Volume 4447, Surface Scattering and Diffraction for Advanced Metrology*, 77–86.

Germer, T.A., Zwinkels, J.C., and Tsai, B.K. (2014). *Spectrophotometry: Accurate Measurement of Optical Properties of Materials*, Experimental Methods in the Physical Sciences (ed. T. Lucatorto, A.C. Parr and K. Baldwin). Amsterdam: Elsevier Inc.

Gescheider, G.A. (1997). *Psychophysics: The Fundamentals*, 3e. Mahwah, NJ: Lawrence Erlbaum Associates, Inc.

Gibson, K.S. (1934). Visual spectrophotometry. *Journal of the Optical Society of America* 24: 234–249.

Gibson, K.S. and Tyndall, E.P.T. (1923). The visibility of radiant energy. *Scientific Papers of the Bureau of Standards* 19: 156–159, 174.

Glasser, L.G. and Troy, D.J. (1952). A new high sensitivity differential colorimeter. *Journal of the Optical Society of America* 42: 652–660.

Glasser, L.G., McKinney, A.H., Reilly, C.D., and Schnelle, P.D. (1958). Cube-root color coordinate system. *Journal of the Optical Society of America* 48: 736–740.

Godlove, I.H. (1933). Neutral value scales. II. A comparison of results and equations describing value scales. *Journal of the Optical Society of America* 23: 419–425.

Gonzalez, R.C. and Woods, R.E. (2018). *Digital Image Processing*, 4e. London: Pearson.

Gow, R.D., Renshaw, D., Findlater, K. et al. (2007). A comprehensive tool for modeling CMOS image-sensor-noise performance. *IEEE Transactions on Electron Devices* 54: 1321–1329.

Grasselli, M.M., Phillips, I.E., Smentek, K., and Walsh, J.C. (2003). *Colorful Impressions: The Printmaking Revolution in Eighteenth-Century France*. Washington, DC: National Gallery of Art.

Grassmann, H. (1853). Zur Theorie der Farbenmischung. *Annalen der Physik* 165: 69–84.

Grassmann, H. (1854). On the theory of compound colors. *The London, Edinburgh, and Dublin Philosophical Magazine and Journal of Science* 7 (4): 254–264.

Green, P. (2010). *Color Management: Understanding and Using ICC Profiles*, The Wiley-IS&T Series in Imaging Science and Technology (ed. M. Kriss). New York: Wiley.

Greenstein, L.M. (1988). Nacreous (pearlescent) pigments and interference pigments. In: *Pigment Handbook: Properties and Economics*, vol. 1 (ed. P.A. Lewis), 829–858. New York: Wiley.

Griesser, R. (1994). Assessment of whiteness and tint of fluorescent substrates with good interinstrument correlation. *Color Research & Application* 19: 446–460.

Gu, H.T., Pointer, M.R., Liu, X.Y., and Luo, M.R. (2016). Quantifying the suitability of CIE D50 and A simulators based on LED light sources. *Color Research & Application* 42: 408–418.

Guan, S.S. and Luo, M.R. (1999a). Investigation of parametric effects using small colour differences. *Color Research & Application* 24: 331–343.

Guan, S.S. and Luo, M.R. (1999b). Investigation of parametric effects using large colour differences. *Color Research & Application* 24: 356–368.

Gueli, A.M., Bonfiglio, G., Pasquale, S., and Troja, S.O. (2017). Effect of particle size on pigments colour. *Color Research & Application* 42: 236–243.

Guild, J. (1931). The colorimetric properties of the spectrum. *Philosophical Transactions of the Royal Society of London* A230: 149–187.

Gundlach, D. and Terstiege, H. (1994). Problems in measurement of fluorescent materials. *Color Research & Application* 19: 427–436.

Haase, C.S. and Meyer, G.W. (1992). Modeling pigmented materials for realistic image synthesis. *ACM Transactions on Graphics* 11: 303–335.

Hård, A. and Sivik, L. (1981). NCS—Natural color system: a Swedish standard for color notation. *Color Research & Application* 6: 129–138.

Hård, A., Sivik, L., and Tonnquist, G. (1996a). NCS, natural color system—from concept to research and applications. Part I. *Color Research & Application* 21: 180–205.

Hård, A., Sivik, L., and Tonnquist, G. (1996b). NCS, natural color system—from concept to research and applications. Part II. *Color Research & Application* 21: 206–220.

Hardin, C.L. (1998). Basic color terms and basic color categories. In: *Color Vision Perspectives from Different Disciplines* (ed. W.G.K. Backhaus, R. Kliegl and J.S. Werner), 207–218. Berlin: Walter de Gruyter.

Hardy, A.C. (1929). A recording photoelectric color analyser. *Journal of the Optical Society of America* 18: 96–117.

Hardy, A.C. (1935). A new recording spectrophotometer. *Journal of the Optical Society of America* 25: 305–311.

Hardy, A.C. (1936). *Handbook of Colorimetry*. Cambridge: The Technology Press.

Hardy, A.C. (1938). History of the design of the recording spectrophotometer. *Journal of the Optical Society of America* 28: 360–364.

Hardy, A.C. and Wurzburg, F.L. (1937). The theory of three-color reproduction. *Journal of the Optical Society of America* 27: 227–240.

Hébert, M. and Emmel, P. (2015). Two-flux and multiflux matrix models for colored surfaces. In: *Handbook of Digital Imaging* (ed. M. Kriss), 1234–1278. New York: Wiley.

Hébert, M. and Hersch, R.D. (2015). Review of spectral reflectance models for halftone prints: principles, calibration, and prediction accuracy. *Color Research & Application* 40: 383–397.

von Helmholtz, H. (1866). *Treatise on Physiological Optics*, Translated from the 3rd edition (ed. J.P.C. Southall). Rochester, NY: Optical Society of America, 1924.

Hemmendinger, H. (1979). Colorimetric information and colorimetric errors. In: *Color Science in the Textile Industry*, 2–23. Research Triangle Park: American Association of Textile Chemists and Colorists.

Hering, E. (1878). *Zur Lehre vom Lichtsinne*. Vienna: Gerold & Sohn, translated by Hurvich, L.M. and Jameson, D. (1964). *Outlines of a Theory of the Light Sense*. Cambridge, MA: Harvard University Press.

Hesselgren, S. (1952). *Hesselgrens Färgatla med kortfattad färglära*. Stockholm: T. Palmer AB (in Swedish).

Heuberger, K.J., Jing, Z.M., and Persiev, S. (1992). Color transformations and lookup tables. In: *TAGA and ISCC Joint Annual Meeting*, 863–881. Williamsburg, VA.

Hofer, H., Carroll, J., Neitz, J. et al. (2005). Organization of the human trichromatic cone mosaic. *Journal of Neuroscience* 25: 9669–9679.

Holmes, J.G. (1981). Coloured light signals of the 1930's and 1980's. In: *Golden Jubilee of Colour in the CIE: Proceeding of a Symposium Held at Imperial College, London*, 78–97. Bradford: Society of Dyers and Colourists.

Hong, G., Luo, M.R., and Rhodes, P.A. (2001). A study of digital camera colorimetric characterization based on polynomial modeling. *Color Research & Application* 26: 76–84.

Houser, K.W., Wei, M., David, A. et al. (2013). Review of measures for light-source color rendition and considerations for a two-measure system for characterizing color rendition. *Optics Express* 21: 10393–10411.

Hunt, R.W.G. (1952). Light and dark adaptation and perception of color. *Journal of the Optical Society of America* 42: 190–199.

Hunt, R.W.G. (1976). Sky-blue pink. *Color Research & Application* 1: 11–16.

Hunt, T. (2000). Was Newton the first to show that visible light is polychromatic? *Engineering Science and Education Journal* 9 (4): 185–191.

Hunt, R.W.G. and Pointer, M.R. (1985). A colour-appearance transform for the CIE 1931 standard colorimetric observer. *Color Research & Application* (3): 165–179.

Hunt, R.W.G. and Pointer, M.R. (2011). *Measuring Colour*, 4e. Wiley-IS&T Series in Imaging Science and Technology (ed. M.A. Kriss). Chichester: Wiley.

Hunter, R.S. (1937). Methods of determining gloss, NBS research paper RP 958. *Journal of Research National Bureau of Standards* 18: 19–39.

Hunter, R.S. (1942). *Photoelectric Tristimulus Colorimetry with Three Filters*, NBS Circular 429. Washington, DC: U.S. Government Printing Office. Reprinted in (1942). *J. Opt. Soc. Am.* 32: 509–538.

Hurvich, L.M. (1981). *Color Vision*. Sunderland: Sinauer Assoc. Inc.

Hurvich, L.M. and Jameson, D. (1957). An opponent-process theory of color vision. *Psychological Review* 64: 384–404.

Hurvich, L.M. and Jameson, D. (1964). *Outlines of a Theory of the Light Sense*. (Translation of Hering 1878). Cambridge, MA: Harvard University Press.

ICC (2018a). Retreived from color.org (accessed 16 October 2018).

ICC ICC.2:2018 (2018b). *Image technology colour management—extensions to architecture, profile format, and data structure*. Reston, VA: International Color Consortium.

IEC 61966-2-1:1999 (1999). *Multimedia systems and equipment - colour measurement and management - Part 2-1: Colour management - default RGB colour space - sRGB*. Geneva: International Electrotechnical Commission.

IEC 61966-3:2000 (2000a). *Multimedia systems and equipment - colour measurement and management - Part 3: Equipment using cathode ray tubes*. Geneva: International Electrotechnical Commission.

IEC 61966-4:2000 (2000b). *Multimedia systems and equipment - colour measurement and management - Part 4: Equipment using liquid crystal display panels*. Geneva: International Electrotechnical Commission.

IESNA TM-30-15 IES (2015). *Method for evaluating light source color rendition*. New York: Illuminating Engineering Society of North America.

Imai, F.H. and Berns, R.S. (2009). System and method for scene image acquisition and spectral estimation using a wide-band multi-channel image capture. US Patent 7,554,586. Rochester, NY: Rochester Institute of Technology.

Indow, T. and Morrison, M.L. (1991). Construction of discrimination ellipsoids for surface colors by the method of constant stimuli. *Color Research & Application* 16: 42–56.

Ishihara, S. (1962). *Tests for Colour-Blindness 16 plates edition*. Tokyo: Kanehara Shuppan Co., Ltd.

ISO 11475:2004 (2004). *Paper and board – determination of CIE whiteness, D65/10 degrees (Outdoor Daylight)*. Geneva: International Organization for Standardization.

ISO 12642-2:2006 (2006). *Graphic technology—input data for characterization of 4-colour process printing—Part 2: Expanded data set*. Geneva: International Organization for Standardization.

ISO 11664-1:2007 (2007a). *(CIE S 014-1/E:2006) Colorimetry -- Part 2: CIE colorimetric observers*. Geneva: International Organization for Standardization.

ISO 105-J05:2007 (2007b). *Textiles – tests for colour fastness – Part J05: method for the instrumental assessment of the colour inconstancy of a specimen with change in illuminant (CMCCON02)*. Geneva: International Organization for Standardization.

ISO 105-J03:2009 (2009a). *Textiles—tests for colour fastness—Part J03: Calculation of colour differences*. Geneva: International Organization for Standardization.

ISO 3664:2009 (2009b). *Graphic technology and photography -- viewing conditions*. Geneva: International Organization for Standardization.

ISO 8254-1:2009 (2009c). *Paper and board—measurement of specular gloss—Part 1: 75 degree gloss with a converging beam, TAPPI method*. Geneva: International Organization for Standardization.

ISO 15076-1:2010 (2010). *Image technology colour management -- architecture, profile format and data structure -- Part 1: Based on ICC.1:2010*. Geneva: International Organization for Standardization.

ISO 22028-2:2013 (2013). *Preview photography and graphic technology—extended colour encodings for digital image storage, manipulation and interchange—Part 2: Reference output medium metric RGB colour image encoding (ROMM RGB)*. Geneva: International Organization for Standardization.

ISO 13655:2017 (2017). *Graphic technology -- spectral measurement and colorimetric computation for graphic arts images*. Geneva: International Organization for Standardization.

ISO/CIE ISO 23603:2005 (E)/CIE S 012/E:2004 (2005). Standard method of assessing the spectral quality of daylight simulators for visual appraisal and measurement of colour. Geneva: International Organization for Standardization.

ISO/CIE 11664-6:2014 (CIE S 014-6/E:2013) (2014). *Colorimetry -- Part 6: CIEDE2000 colour-difference formula*. Geneva: International Organization for Standardization.

ITU ITU-R BT.709-2 (1995). *Parameter values for the HDTV standards for production and international programme exchange*. Geneva: International Telecommunication Union.

Jameson, K.A. (2005). Why GRUE? An interpoint-distance model analysis of composite color categories. *Cross-Cultural Research* 39 (2): 159–204. https://doi.org/10.1177/1069397104273766.

Johansson, T. (1937). *Färg (Swedish)*. Stockholm: Lindfors Bokförlag, AB.

Johnson, R.A. and Wichern, D.W. (2007). *Applied Multivariate Statistical Analysis (Classic Version)*, Pearson Modern Classics for Advanced Statistics Series, 6e. London: Pearson.

Johnston, R.M. (1973). Color theory. In: *Pigments Handbook* (ed. T.C. Patton), 229–288. New York: Wiley.

Johnston-Feller, R. (2001). *Color Science in the Examination of Museum Objects: Nondestructive Procedures, Tools for Conservation*. Los Angeles, CA: Getty Conservation Institute.

Jolliffe, I.T. (2002). *Principal Component Analysis*, Springer Series in Statistics, 2e. London: Springer.

Judd, D.B. (1932). Chromaticity sensibility to stimulus differences. *Journal of the Optical Society of America* 22: 72–108.

Judd, D.B. (1933). The 1931 I.C.I. standard observer and coordinate system for colorimetry. *Journal of the Optical Society of America* 23: 359–374.

Judd, D.B. (1935). A Maxwell triangle yielding uniform chromaticity scales. *Journal of the Optical Society of America* 25: 24–35.

Judd, D.B. (1951). Basic correlates of the visual stimulus. In: *Handbook of Experimental Psychology* (ed. S.S. Stevens), 811–867. New York: Wiley.

Judd, D.B. (1967). A flattery index for artificial illuminants. *Illuminating Engineering* 62: 593–598.

Judd, D.B. and Wyszecki, G. (1975). *Color in Business, Science and Industry*, 3e. New York: Wiley.

Judd, D.B., MacAdam, D.L., Wyszecki, G. et al. (1964). Spectral distribution of typical daylight as a function of correlated color temperature. *Journal of the Optical Society of America* 54: 1031–1040, 1382.

Kaiser, P.K. (1981). Photopic and mesopic photometry: yesterday, today and tomorrow. In: *Golden Jubilee of Colour in the CIE: Proceeding of a Symposium Held at Imperial College, London*, 28–52. Bradford: Society of Dyers and Colourists.

Kang, H.R. (1997). *Color Technology for Electronic Imaging Devices*. Bellingham, WA: SPIE.

Katoh, N., Deguchi, T., and Berns, R.S. (2001a). An accurate characterization of CRT monitor (I) verification of past studies and clarifications of gamma. *Optical Review* 8: 205–314.

Katoh, N., Deguchi, T., and Berns, R.S. (2001b). An accurate characterization of CRT monitor (II) proposal for an extension to CIE method and its verification. *Optical Review* 8: 397–408.

Kay, P. and Regier, T. (2006). Language, thought and color: recent developments. *Trends in Cognitive Sciences* 10 (2): 51–54.

Kay, P., Berlin, B., Maffi, L. et al. (2010). *World Color Survey*. Stanford, CA: CSLI Publications.

Kelly, K.L. (1958). Centroid notations for the revised ISCC-NBS color-name blocks. *Journal of Research National Bureau of Standards* 61: 427–431.

Kelly, K.L. (1965). A universal color language. *Color Engineering* 3 (2): 16–21. Reprinted in Kelly and Judd 1976.

Kelly, K.L. and Judd, D.B. (1955). *The ISCC-NBS Method of Designating Colors and a Dictionary of Color Names, NBS Circular 553*. Washington, DC: U.S. Government Printing Office.

Kelly, K.L. and Judd, D.B. (1976). *Color: Universal Language and Dictionary of Names*, NBS Special Publication 440. Washington, DC: U.S. Government Printing Office.

Kettler, W., Binder, M., Franz, W. et al. (2016). *Colour Technology of Coatings*. Hanover: Vincentz Network.

Khanh, T.Q., Bodrogi, P., Guo, X. et al. (2017). Colour preference, naturalness, vividness and colour quality metrics, Part 5: A colour preference experiment at 2000 lx in a real room. *Lighting Research & Technology* http://journals.sagepub.com/doi/pdf/10.1177/1477153517737133.

Kim, D.-H. (1997). The influence of parametric effects on the appearance of small colour differences. PhD thesis. University of Leeds.

Kim, D.B. and Lee, K.H. (2011). Computer-aided appearance design based on BRDF measurement. *Computer-Aided Design* 43: 1181–1193.

Kim, D.-H. and Nobbs, J.H. (1997). New weighting functions for the weighted CIELAB colour difference formulae. In: *AIC Color 97—Proceedings of the 8th Congress of the International Colour Association*, 446–449. Kyoto.

Kirchner, E.J.J. and Houweling, J. (2009). Measuring flake orientation for metallic coatings. *Progress in Organic Coatings* 64: 287–293.

Kirchner, E., van den Kieboom, G.-J., Njo, L. et al. (2007). Observation of visual texture of metallic and pearlescent materials. *Color Research & Application* 32: 256–266.

Kishner, S.J. (1977). Effect of spectrophotometric errors on color difference. *Journal of the Optical Society of America* 67: 772–778.

Klein, G.A. (2010). *Industrial Color Physics*. New York: Springer.

Koenderink, J.J. (2010). *Color for the Sciences*. Cambridge: MIT Press.

Kortüm, G. (1969). *Reflectance Spectroscopy: Principles, Methods, Applications*. Berlin, Heidelberg: Springer-Verlag.

von Kries, J. (1882). *Die Gesich Empfindungen und ihre Analyse*. Leipzig: Veith & Co. (in German).

von Kries, L. (1902). *Chromatic Adaptation, Festchrift der Albrect-Ludwig-Universitat (Fribourg)* Translated in Macadam D.L. Sources of Color Science, 109–119. Cambridge, MA: MIT Press, 1970.

Kruskal, J.B. (1964). Multidimensional scaling by optimizing goodness of fit to a nonmetric hypothesis. *Pychometrika* 29: 1–27.

Kubelka, P. (1948). New contributions to the optics of intensely light-scattering materials. Part I. *Journal of the Optical Society of America* 38, 448–456, 1067.

Kubelka, P. (1954). New contributions to the optics of intensely light-scattering materials. Part II: Nonhomogeneous layers. *Journal of the Optical Society of America* 44: 330–355.

Kubelka, P. and Munk, F. (1931). Ein Beitrag zur Optik der Farbanstriche. *Zeitschrift fur Technische Physik* 12: 593–601. (in German).

Kuehni, R.G. (1975). *Computer Colorant Formulation*. Lexington, DC: Heath and Company.

Kuehni, R.G. (2002). The early development of the Munsell system. *Color Research & Application* 21: 20–27.

Kuehni, R.G. (2003). *Color Space and its Divisions: Color Order from Antiquity to the Present*. Hoboken, NJ: Wiley.

Kuehni, R.G. and Schwarz, A. (2008). *Color Ordered: A Survey of Color Order Systems from Antiquity to the Present*. Oxford: Oxford University Press.

Kuniba, H. and Berns, R.S. (2008). The trade-off between color reproduction accuracy and image sensor noise. In: *IS&T 16th Color and Imaging Conference*, 232–237. Portland.

Kuniba, H. and Berns, R.S. (2009). Spectral sensitivity optimization of color image sensors considering photon shot noise. *Journal of Electronic Imaging* 18: 023002-1–023002-14.

Kuo, W.G. and Luo, M.R. (1996a). Methods for quantifying metamerism. Part 1 – Visual assessment. *Journal of the Society of Dyers and Colourists* 112: 312–320.

Kuo, W.G. and Luo, M.R. (1996b). Methods for quantifying metamerism. Part 2 – Instrumental methods. *Journal of the Society of Dyers and Colourists* 112: 354–360.

Lambert, J.H. (1760). *Photometria sive de mensure et gradibus luminis colorum et umbrae (Latin: Photometry or on the Measurements and Grades (Degrees) of the Light of the Colors and the Shadow)*. Augsburg: Eberhard Klett.

Landa, E.R. and Fairchild, M.D. (2005). Charting color from the eye of the beholder. *American Scientist* 93: 436–443.

Lau, D. and Arce, G. (2008). *Modern Digital Halftoning*, 2e. Boca Raton, FL: CRC Press.

Le Blon, J.C. (1756). *Coloritto; Or the Harmony of Colouring in Painting: Reduced to Mechanical Practice, Under Early Precepts, and Infallible Rules: Together with Some Colour'd Figures, In Order to Render the Said Precepts and Rules Intelligible, Not Only to Painters, But Even to All Lovers of Painting*. London.

Leland, J.E., Johnson, N.L., and Arecchi, A.V. (1997). Principles of bispectral fluorescence colorimetry. In: *Optical Science, Engineering and Instrumentation '97*, 76–87. San Diego, CA.

Li, Z. and Berns, R.S. (2007). Comparison of methods of parameric correction for evaluating metamerism. *Color Research & Application* 32: 293–303.

Li, C., Luo, M.R., and Wang, Z. (2014). Different matrices for CIECAM02. *Color Research & Application* 39: 143–153.

Li, C., Cui, G., Melgosa, M. et al. (2016). Accurate method for computing correlated color temperature. *Optics Express* 24: 14066–14078.

Li, C., Li, Z., Wang, Z. et al. (2017). Comprehensive color solutions: CAM16, CAT16, and CAM16-UCS. *Color Research & Application* 42: 703–718.

Lin, J., Shamey, R., and Hinks, D. (2012). Factors affecting the whiteness of optically brightened material. *Journal of the Optical Society of America* 29: 2289–2300.

Liu, A., Tuzikas, A., Žukauskas, A. et al. (2013). Cultural preferences to color quality of illumination of different artwork objects revealed by a color rendition engine. *IEEE Photonics Journal* 5: 6801010.

Livingstone, M. (2014). *Vision and Art: The Biology of Seeing (Updated and Expanded Edition)*. New York: Harry N. Abrams.

Lovibond, J.W. (1887). The tintometer—a new instrument for the analysis, synthesis, matching, and measurement of colour. *Journal of the Society of Dyers and Colourists* 3: 186–193.

Lu, R., Koenderink, J.J., and Kappers, A.M.L. (1998). Optical properties (bidirectional reflection distribution functions) of velvet. *Applied Optics* 37: 5974–5984.

Lu, R., Koenderink, J.J., and Kappers, A.M.L. (2000). Optical properties (bidirectional reflectance distribution function) of shot fabric. *Applied Optics* 39: 5785–5795.

Luo, M.R. and Hunt, R.W.G. (1998). A chromatic adaptation transform and a colour inconstancy index. *Color Research & Application* 23: 154–158.

Luo, M.R. and Rigg, B. (1986). Chromaticity-discrimination ellipses for surface colors. *Color Research & Application* 11: 25–42.

Luo, M.R., Hunt, R.W.G., Rigg, B., and Smith, K.J. (1999). Recommended colour-inconstancy index. *Journal of the Society of Dyers and Colourists* 115: 183–188.

Luo, M.R., Cui, G., and Rigg, B. (2001). The development of the CIE 2000 colour-difference formula: CIEDE2000. *Color Research & Application* 26: 340–350.

Luo, M.R., Li, C.J., Hunt, R.W.G. et al. (2003). CMC 2002 colour inconstancy index: CMCCON02. *Coloration Technology* 119: 280–285.

Luo, M.R., Cui, G., and Li, C. (2006). Uniform colour spaces based on CIECAM02 colour appearance model. *Color Research & Application* 31: 320–330.

MacAdam, D.L. (1935). Maximum visual efficiency of colored materials. *Journal of the Optical Society of America* 25: 361–367.

MacAdam, D.L. (1937). Projective transformations of the I.C.I. color specifications. *Journal of the Optical Society of America* 27: 294–299.

MacAdam, D.L. (1938a). Photographic aspects of the theory of three-color reproduction. *Journal of the Optical Society of America* 28: 399–418.

MacAdam, D.L. (1938b). Subtractive color mixture and color reproduction. *Journal of the Optical Society of America* 28: 466–480.

MacAdam, D.L. (1974). Uniform color scales. *Journal of the Optical Society of America* 64: 1619–1702.

MacAdam, D.L. (1978). Colorimetric data for samples of OSA uniform color scales. *Journal of the Optical Society of America* 68: 121–130.

MacAdam, D.L. (1993). *Selected Papers on Colorimetry—Fundamentals*, SPIE Milestone Series, vol. MS 77. Bellingham, WA: International Society for Optical Engineering.

Maile, F.J., Pfaff, G., and Reynders, P. (2005). Effect pigments—past, present and future. *Progress in Organic Coatings* 54: 150–163.

Malkin, F., Larkin, J.A., Verrill, J.F., and Wardman, R.H. (1997). The BCRA-NPL ceramic colour standards, series II—master spectral reflectance and thermochromism data. *Journal of the Society of Dyers and Colourists* 113: 84–94.

Manly, B.F.J. and Alberto, J.A.N. (2017). *Multivariate Statistical Methods: A Primer*, 4e. Boca Raton, FL: CRC Press.

Marmor, M.F. (2006). Ophthalmology and art: simulation of Monet's cataracts and Degas' retinal disease. *Archives of Ophthalmology* 124: 1764–1769.

Marschner, S., Westin, S., Lafortune, E., and Torrance, K. (2000). Image-based measurement of the bidirectional reflectance distribution function. *Applied Optics* 39: 2592–2600.

Matusik, W., Pfister, H., Brand, M., and McMillan, L. (2003). Efficient isotropic BRDF measurement. In: *Proceedings of the 14th Eurographics Workshop on Rendering*, 241–247. Leuven, Belgium.

McCamy, C.S. (1985). Physical exemplifiction of color order systems. *Color Research & Application* 10: 20–25.

McCamy, C.S. (1994). Simulation of daylight for viewing and measuring color. *Color Research & Application* 19: 437–445.

McCamy, C.S. (1996). Observation and measurement of the appearance of metallic materials. I. Macro appearance. *Color Research & Application* 21: 292–304.

McCamy, C.S. (1998). Observation and measurement of the appearance of metallic materials. II. Micro appearance. *Color Research & Application* 23: 362–373.

McCluney, R. (2014). *Introduction to Radiometry and Photometry*, 2e. Boston, MA: Artech House.

McDonald, R. (1974). The effect on non-uniformity in the ANLAB color space on the interpretation of visual colour differences. *Journal of the Society of Dyers and Colourists* 90: 189–198.

McDonald, R. (1980a). Industrial pass/fail colour matching. Part I—Preparation of visual colour-matching data. *Journal of the Society of Dyers and Colourists* 96: 372–376.

McDonald, R. (1980b). Industrial pass/fail colour matching. Part II—Methods of fitting tolerance ellipsoids. *Journal of the Society of Dyers and Colourists* 96: 418–433.

McDonald, R. (1980c). Industrial pass/fail colour matching. Part III—Development of pass/fail formula for use with instrumental measurement of colour difference. *Journal of the Society of Dyers and Colourists* 96: 486–495.

McDonald, R. (1997). Recipe prediction for textiles. In: *Colour Physics for Industry* (ed. R. McDonald), 209–291. Bradford: Society of Dyers and Colourists.

McGinnis, P.H. (1967). Spectrophotometric color matching with the least squares technique. *Color Engineering* 5 (6): 22–27.

Melgosa, M., Huertas, R., and Berns, R.S. (2004). Relative significance of the terms in the CIEDE2000 and CIE94 color-difference formulas. *Journal of the Optical Society of America A* 21: 2269–2275.

Mielenz, K.D. (1982, 3). Photoluminescence spectrometry. In: *Optical Radiation Measurements* (ed. K.D. Mielenz). New York: Academic Press.

Miller, N.J. and Rosenfeld, S.M. (2012). Demonstration of LED Retrofit Lamps at the Smithsonian American Art Museum, Washington, DC: Final Report Prepared in Support of the U.S. DOE Solid-State Lighting Technology Demonstration GATEWAY Program. Richland, WA: Pacific Northwest National Laboratory.

Montag, E.D. and Berns, R.S. (2000). Lightness dependencies and the effect of texture on suprathreshold lightness tolerances. *Color Research & Application* 25: 241–249.

Montag, E.D. and Wilber, D.C. (2003). A comparison of constant stimuli and gray-scale methods of color difference scaling. *Color Research & Application* 28: 36–44.

Montes, R. and Ureña, C. (2012). An Overview of BRDF Models. Technical Report *LSI-2012-001*. University of Grenada.

Montgomery, D.C. (2013). *Statistical Quality Control*, 7e. New York: Wiley.

Morovič, J. (2008). *Color Gamut Mapping*, The Wiley-IS&T Series in Imaging Science and Technology (ed. M. Kriss). New York: Wiley.

Motta, R. (1991). *An Analytical Model for the Colorimetric Characterization of Color CRTs*. Rochester Institute of Technology http://scholarworks.rit.edu/theses/4553/.

Mullen, K.T. (1985). The contrast sensitivity of human colour vision red-green and blue-yellow chromatic gratings. *Journal of Physiology* 359: 381–400.

Müller, G.E. (1930). Über die Farben Empfindungen. *Zeitschrift für Psychologie* 17–18, pp. 46, 508.

Munsell, A.H. (1899–1918). Color diary. http://www.rit.edu/cos/colorscience/ab_munsell_diaries.php (accessed 17 October 2018).

Munsell, A.H. (1901). Photometer. US Patent 686,827 A.

Munsell, A.H. (1905). *A Color Notation*, 1e. Baltimore, MD: Munsell Color Company.

Munsell, A.H. (1915). *Atlas of the Munsell Color System*. Malden, MA: Wadsworth-Howland & Company.

Munsell (1929). *Munsell Book of Color*. Baltimore, MD: Munsell Color Company.

Munsell, A.E.O., Sloan, L.L., and Godlove, I.H. (1933). Neutral value scales. I. Munsell neutral value scale. *Journal of the Optical Society of America* 23: 394–411.

Murray, A. (1936). Monochrome reproduction in photoengraving. *Journal of the Franklin Institute* 221: 721–744.

Musbach, A. (2016). Wave-based computer graphic light modeling with applications to computer aided design. Dissertation. University of Minnesota.

Mylonas, D. and MacDonald, L. (2016). Augmenting basic colour terms in English. *Color Research & Application* 41: 32–42.

Na, N., Choi, K., Lee, J., and Suk, H.-J. (2013). Color tolerance study on white in practical aspect: perceptibility versus acceptability. *Color Research & Application* 39: 582–588.

Nadal, M.E., Early, E.A., Weber, W., and Bousquet, R. (2008). NIST 0:45 reflectometer. *Color Research & Application* 33: 94–99.

Nadal, M.E., Miller, C.C., and Fairman, H.S. (2011). Statistical methods for analyzing color difference distributions. *Color Research & Application* 36: 160–168.

Nardi, M.A. (1980). Observer metamerism in college-age observers. *Color Research & Application* 5: 73.

Nascimento, S.M.C. and Masuda, O. (2014). Best lighting for visual appreciation of artistic paintings—experiments with real paintings and real illumination. *Journal of the Optical Society of America A* 31: A214–A219.

Nassau, K. (2001). *The Physics and Chemistry of Color: The Fifteen Causes of Color*, 2e. New York: Wiley.

National Research Council (US) Committee on Vision (1981). Procedures for Testing Color Vision. *Report of Working Group 41*. Washington, DC: National Academy Press.

Nayatani, Y. (2005). Why two kinds of color order systems are necessary? *Color Research & Application* 30: 295–303.

Nemcsics, A. (1980). The Coloroid color system. *Color Research & Application* 5: 113–120.

Nemcsics, A. (1987). Color space of the Coloroid color system. *Color Research & Application* 12: 135–146.

Nemcsics, A. and Caivano, J.L. (2016). Color order systems. In: *Encyclopedia of Color Science and Technology* (ed. M.R. Luo), 329–343. Berlin, Heidelberg: Springer-Verlag.

Neugebauer, H.E.J. (1937). Die theoretischen Grundlagen des Mehrfarbendruckes. *Zeitscrift fur wissenschaftliche Photographie* 36: 73–89. Translated by Wyble and Kraushaar 2005.

Neugebauer, H.E.J. (1956). Quality factor for filters whose spectral transmittances are different from color mixture curves, and its application to color photography. *Journal of the Optical Society of America* 46: 821–824.

Newhall, S.M. (1940). Preliminary report of the O.S.A. subcommittee on the spacing of the Munsell colors. *Journal of the Optical Society of America* 30: 617–645.

Newhall, S.M., Nickerson, D., and Judd, D.B. (1943). Final report of the O.S.A. subcommittee on the spacing of the Munsell colors. *Journal of the Optical Society of America* 33: 385–418.

Newhall, S.M., Burnham, R.W., and Clark, J.R. (1957). Successive and simultaneous color matching. *Journal of the Optical Society of America* 47: 43–56.

Newton, I. (1730). *OPTICKS, or a Treatise of the Reflections, Refractions, Inflections & Colours of Light* (Reprint based on the 4th edition, London 1730). New York: Dover Publications.

Nickerson, D. (1940). History of the Munsell color system and its scientific application. *Journal of the Optical Society of America* 30: 575–580. Reprinted in *Color Research and Application* **1**, 69–77 (1976).

Nickerson, D. (1950). Tables for use in computing small color differences. *American Dyestuffs Reporter* 39: 541–549.

Nickerson, D. (1960). Light sources and color rendering. *Journal of the Optical Society of America* 50: 57–69.

Nickerson, D. (1963). History of the Munsell color system. *Color Engineering* 7 (5): 42–51. Reprinted in *Color Research and Application* **1**, 121–130 (1976).

Nickerson, D. (1978). Munsell renotations for samples of OSA uniform color scales. *Journal of the Optical Society of America* 68: 1343–1347.

Nickerson, D. (1981). OSA uniform color scales samples—a unique set. *Color Research & Application* 6: 7–33.

Nickerson, D. and Stultz, K.F. (1944). Color tolerance specification. *Journal of the Optical Society of America* 34: 550–570.

Nicodemus, F.E., Richmond, J.C., Hsia, J.J. et al. (1977). *Geometrical Considerations and Nomenclature for Reflectance*. Washington, DC: National Bureau of Standards, US Department of Commerce.

Nimeroff, I. and Yurow, J.A. (1965). Degree of metamerism. *Journal of the Optical Society of America* 55: 185–190.

Nobbs, J.H. (1985). Kubelka-Munk theory and the prediction of reflectance. *Review of Progress in Coloration and Related Topics* 15: 66–75.

Nobbs, J.H. (1997). Colour-match prediction for pigmented materials. In: *Colour Physics for Industry* (ed. R. McDonald), 292–372. Bradford: Society of Dyers and Colourists.

Nobbs, J.H. (2002). A lightness, chroma and hue splitting approach to CIEDE2000 color differences. *Advances in Colour Science and Technology* 5 (2): 46–53.

Ohno, Y. and Fein, M. (2014). Vision experiment on acceptable and preferred white light chromaticity for lighting. In: *CIE 2014 Lighting Quality and Energy Efficiency*, 192–199. Kuala Lumpur.

Ohno, Y., Miller, C.C., and Fein, M. (2015). Vision experiment on chroma saturation for color quality preference. The 28th Session of International Commission on Illumination, Manchester.

Oil (1929). The Hardy recording spectrophotometer: new electrically controlled instrument eliminates visual errors in colorimetry. *Oil & Fat Industries* 6 (9): 31–33.

Orchard, S.E. (1969). Reflection and transmission of light by diffusing suspensions. *Journal of the Optical Society of America* 59: 1584–1597.

Palmer, S.E. (1999). *Vision Science: Photons to Phenomenology*. Cambridge: MIT Press.

Park, M. (1994). *Instrumental Colour Formulation*. Bradford: Society of Dyers and Colourists.

Pattanaik, S.N., Ferwerda, J.A., Fairchild, M.D., and Greenberg, D.P. (1998). A multiscale model of adaptation and spatial vision for realistic imaging. In: *Proceedings of SIGGRAPH 98*, 287–298.

Pauli, H. (1976). Proposed extension of the CIE recommendation on uniform color spaces, color difference equations, and metric color terms. *Journal of the Optical Society of America* 66: 866–867.

Pellacini, F., Ferwerda, J.A., and Greenberg, D.P. (2000). Toward a psychophysically-based light reflection model for image synthesis. In: *Proceedings of the 27th Annual Conference on Computer Graphics and Interactive Techniques*, 55–64. New York: ACM Press/Addison-Wesley.

Pfaff, G. and Reynders, P. (1999). Angle-dependent optical effects deriving from submicron structures of films and pigments. *Chemical Review* 99: 1963–1981.

Phillips, J.B. and Eliasson, H. (2018). *Camera Image Quality Benchmarking*, The Wiley-IS&T Series in Imaging Science and Technology (ed. M. Kriss). New York: Wiley.

Pinto, P.D., Linhares, J.M.M., and Nascimento, S.M.C. (2008). Correlated color temperature preferred by observers for illumination of artistic paintings. *Journal of the Optical Society of America A* 25: 623–630.

Planck, M. (1901). Uber das Gesetz der Energieverteilung im Normalspectrum (German) On the law of distribution of energy in the normal spectrum (English). *Annalen der Physik* 4: 553–563.

Plateau, J.A.F. (1872). Sur le mesure des sensations physiques, et sur la loi qui lie l'intensité de ces sensations à l'intensité de la cause excitante. *Bulletin de l'Academie Royale de Belgique* 33 (Ser. 2): 376–388.

Pons, A. and Campos, J. (2004). Spectrophotometric error in colour coordinates introduced by fluorescence of white calibration tile. *Color Research & Application* 29: 111–114.

Qiao, Y. (1996). Visual determination of hue suprathreshold tolerances. MS thesis. Rochester Institute of Technology.

Qiao, Y., Berns, R.S., Reniff, L., and Montag, E. (1998). Visual determination of hue suprathreshold color-difference tolerances. *Color Research & Application* 23: 302–313.

Quan, S. and Ohta, N. (2002). Evaluating hypothetical spectral sensitivities with quality factors. *Journal of Imaging Science and Technology* 46: 8–14.

Raggi, A. and Barbiroli, G. (1993). Colour-difference measurement: the sensitivity of various instruments compared. *Color Research & Application* 18: 11–27.

Rea, M.S. and Freyssinier-Nova, J.P. (2008). Color rendering: a tale of two metrics. *Color Research & Application* 33: 192–202.

Rea, M.S. and Freyssinier-Nova, J.P. (2010). Color rendering: beyond pride and prejudice. *Color Research & Application* 35: 401–409.

Reinhard, E., Khan, E.A., Akyüz, A.O., and Johnson, G.M. (2008). *Color Imaging: Fundamentals and Applications*. Boca Raton: CRC Press.

Ribés, A. and Schmitt, F. (2008). Linear inverse problems in imaging: an introductory survey. *IEEE Signal Processing Magazine* 25 (4): 84–99.

Rich, D.C. and Martin, D. (1999). Improved model for improving the inter-instrument agreement of spectrocolorimeters. *Analytica Chimica Acta* 380: 263–276.

Rich, D.C., Battle, D.R., Ingleson, A. et al. (1995). Evaluation of the long term repeatability of reflectance spectrophotometers. In: *Spectrophotometry, Luminescence and Colour; Science & Compliance*: Papers presented at the second joint meeting of the UV Spectrometry Group of the UK and the Council for Optical Radiation Measurements of the USA (ed. C. Burgess and D.G. Jones), 137–153. Amsterdam: Elsevier.

Richter, M. (1952/53). Das System der DIN-Farbenkarte. *Farbe* 1: 85–98. (in German).

Richter, M. (1955). The official German standard color chart. *Journal of the Optical Society of America* 45: 223–226.

Richter, M. (1984). The development of color metrics. *Color Research & Application* 9: 69–83.

Richter, M. and Witt, K. (1986). The story of the DIN color system. *Color Research & Application* 11: 138–145.

Robertson, A.R. (1967). Colorimetric significance of spectrophotometric errors. *Journal of the Optical Society of America* 57: 691–698.

Robertson, A.R. (1968). Computation of correlated color temperature and distribution temperature. *Journal of the Optical Society of America* 58: 1528–1535.

Robertson, A.R. (1978). CIE guidelines for coordinated research on colour-difference evaluation. *Color Research & Application* 3: 149–151.

Robertson, A.R. (1987). Diagnostic performance evaluation of spectrophotometers. In: *Advances in Standards and Methodology in Spectrophotometry* (ed. C. Burgess and K.D. Mielenz), 277–286. Amsterdam: Elsevier.

Robertson, A.R. (1990). Historical development of CIE recommended color difference equations. *Color Research & Application* 15: 167–170.

Rogers, G.L. (1998). Neugebauer revisited: random dots in halftone screening. *Color Research & Application* 28: 104–113.

Rogers, G.L. (2016). Random walk analysis for reflection and transmission of turbid media. *Color Research & Application* 41: 580–584.

Rohner, E. and Rich, D.C. (1996). Eine angenähert gleichförmige metrik fur industrielle farbtoleranzen von körperfarben (An approximately uniform object color metric for industrial color tolerances). *Die Farbe* 42: 207–220.

Roorda, A., Mehta, A.B., Lennie, P., and Williams, D.R. (2001). Packing arrangement of the three cone classes in primate retina. *Vision Research* 41: 1291–1306.

Rösch, S. (1929). Darstellung der Farbenlehre für die Zwecke des Mineralogen. *Schweizerische Mineralogische und Petrographische Mitteilungen* 13: 73–234. (in German).

Ruiz, J.M.M. (2002). Proposed metameric indices for goniochromatic objects. *Color Research & Application* 27: 382–390.

Rushmeier, H., Taubin, G., and Guéziec, A. (1997). Applying shape from lighting variation to bump map capture. In: *8th Eurographics Rendering Workshop*, 35–44. Saint Etienne.

Rybicki, G.B. and Lightman, A.P. (2008). *Radiative Processes in Astrophysics*. Weinheim: Wiley-VCH.

Ryde, J. (1931). The scattering of light by turbid media. Part I. *Proceedings of the Royal Society of London A* 131: 451–464.

Ryde, J. and Cooper, B. (1931). The scattering of light by turbid media. Part II. *Proceedings of the Royal Society of London A* 131: 464–475.

Saunderson, J.L. (1942). Calculation of the color of pigmented plastics. *Journal of the Optical Society of America* 32: 727–736.

Schanda, J. (2007). *Colorimetry: Understanding the CIE System*. Hoboken, NJ: Wiley.

Schrödinger, E. (1920). Grundlinien einer Theorie der Farbenmetrik im Tagessehen. *Annalen der Physik* 63: 297–447. , 481–520. (Outline of a theory of color measurement for daylight vision.) Transl.: D.L. MacAdam, ed., *Sources of Color Science*. Cambridge: MIT Press, pp. 134–182.

Schuster, A. (1905). Radiation through a foggy atmosphere. *Astrophysical Journal* 21: 1–22.

Scuello, M., Abramov, I., Gordon, J., and Weintraub, S. (2004). Museum lighting: optimizing the illuminant. *Color Research & Application* 29: 121–127.

Seime, L. and Hardeberg, J.Y. (2003). Colorimetric characterization of LCD and DLP projection displays. *Displays* 11: 349–358.

Semmelroth, C.C. (1970). Prediction of lightness and brightness on different backgrounds. *Journal of the Optical Society of America* 60: 1685–1689.

Séve, R. (1996). Practical formula for the computation of CIE 1976 hue difference. *Color Research & Application* 21: 314.

Shafer, S. (1985). Using color to separate reflection components. *Color Research & Application* 10: 210–218.

Shakespeare, T. and Shakespeare, J. (2003). A fluorescent extension to the Kubelka-Munk model. *Color Research & Application* 28: 4–14.

Sharma, A. (2018). *Understanding Color Management*, The Wiley-IS&T Series in Imaging Science and Technology, 2e (ed. M. Kriss). New York: Wiley.

Shen, S. and Berns, R.S. (2009). Evaluating color difference equation performance incorporating visual uncertainty. *Color Research & Application* 34: 375–390.

Shevell, S.K., and Martin, P.R. (2017). Color opponency: tutorial. *Journal of the Optical Society of America A* 34: 1099–1108.

Shimizu, C. and Meyer, G.W. (2015). A computer aided color appearance design system for metallic car paint. *Journal of Imaging Science and Technology* 59: 030403-1–030403-10.

Simon, F.T. (1980). Color order. In: *Optical Radiation Measurements: Color Measurement*, vol. 2 (ed. F. Grum and C.J. Bartleson), 165–235. New York: Academic Press.

Simon, F.T. (1997). Color order. In: *Color Technology in the Textile Industry*, 2e, 153–187. Research Triangle Park, NC: American Association of Textile Chemists and Colorists.

Simon, F.T., Funk, R.A., and Laidlow, A.C. (1994). Match prediction of highly fluorescent colors. *Color Research & Application* 19: 461–474.

Simonds, J.L. (1963). Application of characteristic vector analysis to photographic and optical response data. *Journal of the Optical Society of America* 53: 968–974.

Sivik, L. (1994). Systems for descriptive colour notations—Implications of definitions and methodology. *Farbe* 40: 37–49.

Smet, K.A.G., Deconinck, G., and Hanselaer, P. (2015). Chromaticity of unique white in illumination mode. *Optics Express* 23: 12488–12495.

Smith, K.J. (1997). Colour-order systems, colour spaces, colour difference and colour scales. In: *Colour Physics for Industry* (ed. R. McDonald), 121–208. Bradford: Society of Dyers and Colourists.

Smith, V.C. and Pokorny, J. (1975). Spectral sensitivity of the foveal cone photopigments between 400 nm and 500 nm. *Vision Research* 15: 161–171.

Spaulding, K.E., Woolfe, G.J., and Giorgianni, E.J. (2001). Optimized extended gamut color encoding for scene-referred and output-referred image states. *Journal of Imaging Science and Technology* 45 (9): 418–426.

Speranskaya, N.I. (1959). Determination of spectrum color co-ordinates for twenty-seven normal observers. *Optics and Spectroscopy* 7: 424–428.

Stevens, S.S. (1957). On the psychophysical law. *Psychological Review* 64: 153–181.

Stevens, J.C. and Stevens, S.S. (1963). Brightness functions: effects of adaptation. *Journal of the Optical Society of America* 53: 375–385.

Stiles, W.S. and Burch, J.M. (1959). N.P.L. colour-matching investigation: final report (1958). *Optica Acta* 6: 1–26.

Stokes, M. and Brill, M.H. (1992). Efficient computation of ΔH^*_{ab}. *Color Research & Application* 17: 410–411.

Sun, J., Smith, M., Smith, L. et al. (2007). Object surface recovery using a multi-light photometric stereo technique for non-Lambertian surfaces subject to shadows and specularities. *Image and Vision Computing* 25: 1050–1057.

Svaetichin, G. (1956). Spectral response curves from single cones. *Acta Physiologica Supplement* 39 (134): 17–46.

Swedish Standards Institute (1979). SS 01 91 00, Colour Notation System.

Takasaki, H. (1966). Lightness change of grays induced by change in reflectance of gray background. *Journal of the Optical Society of America* 56: 504–509.

Talbot, W.H.F. (1852). Improvements in the art of engraving. British Patent Specification No. 565.

Thornton, W.A. (1974). A validation of the color-preference index. *Journal of the Illuminating Engineering Society* 4: 48–52.

Tilley, R.J.D. (2011). *Colour and the Optical Properties of Materials: An Exploration of the Relationship Between Light, the Optical Properties of Materials and Colour*, 2e. Chichester: Wiley.

Trezona, P.W. and Parkins, R.P. (1998). Derivation of the 1964 colorimetric standards. *Color Research & Application* 23: 221–225.

Troland, L.T. (1922). Report of the committee on colorimetry. *Journal of the Optical Society of America* 6: 527–595.

Tzeng, D.-Y. and Berns, R.S. (2005). A review of principal component analysis and its applications to color technology. *Color Research & Application* 30: 84–98.

Valberg, A. (2005). *Light Vision Color*. Chichester: Wiley.

Viggiano, J.A.S. (1985). The color of halftone tints. In: *TAGA Annual Meeting*, 647–661.

Viggiano, J.A.S. (1990). Comparison of radiance ratio spectra: assessing a model's goodness of fit. In: *SPSE's 43rd Annual Conference*, 222–225. Rochester, NY.

Viggiano, J.A.S. (2001). Perception-referenced method for comparison of radiance ratio spectra and its application as an index of metamerism. In: *9th Congress of the International Colour Association* (ed. R.Y. Chung and A.B.J. Rodrigues), 701–704. Rochester, NY.

Viková, M. and Vik, M. (2006). Colour shift photochromic pigments in colour space CIE $L^*a^*b^*$. *Molecular Crystals and Liquid Crystals* 431: 403–415.

Völz, H.G. (2001). *Industrial Color Testing: Fundamentals and Techniques*, 2e. Weinheim: Wiley-VCH.

Vora, P.L. and Trussell, H.J. (1993). Measure of goodness of a set of color-scanning filters. *Journal of the Optical Society of America A* 10: 1499–1508.

Walowit, E., McCarthy, C.J., and Berns, R.S. (1988). Spectrophotometric color matching based on two-constant Kubelka-Munk theory. *Color Research & Application* 13: 358–362.

Wang, Y. and Berns, R.S. (2017). Filter selection for multispectral imaging optimizing spectral, colorimetric and image quality. In: *IS&T International Symposium on Electronic Imaging: Image Sensors and Imaging Systems*, 25–32. Burlingame, CA.

Wang, Z.W. and Luo, M.R. (2016). Looking into special surface effects: diffuse coarseness and glint impression. *Coloration Technology* 132: 153–161.

Wang, L., Jacques, S.L., and Zheng, L. (1995). MCML—Monte Carlo modeling of light transport in multi-layered tissues. *Computer Methods and Programs in Biomedicine* 47: 131–146.

Ward, G.J. (1992). Measuring and modeling anisotropic reflection. In: *Proceedings of the 19th Annual Conference on Computer Graphics and Interactive Techniques*, 265–272. New York: ACM Press.

Weale, R.A. (1957). Trichromatic ideas in the seventeenth and eighteenth centuries. *Nature* 179: 648–651.

Weber, E.H. (1834). *De Pulsu, resorptione, auditu et tactu. Annotationes anatomicae et physiologicae*. Leipzig: C. F. Koehler.

Wei, M. and Chen, S. (2018). Impact of spectral power distribution of daylight simulators on whiteness specification for surface colors. *Color Research & Application* 43: 27–33.

Wei, M., Ma, S., Wang, Y., and Luo, M.R. (2017). Evaluation of whiteness formulas for FWA and non-FWA whites. *Journal of the Optical Society of America A* 34: 640–647.

Weixel, S. (2016). Measuring the texture of effect finishes. In: *Colour Technology of Coatings*, 172–179. Hanover: Vincentz Network.

Whittle, P. (1992). Brightness, discriminability and the "crispening effect". *Vision Research* 32: 1993–1507.

Wiesel, T.N. and Hubel, D.H. (1966). Spatial and chromatic interactions in the lateral geniculate body of the rhesus monkey. *The Journal of Physiology* 29: 1116–1156.

Wintringham, W.T. (1951). Color television and colorimetry. *Proceedings of the Institute of Radio Engineers* 39: 1135–1172.

Witt, K. (1987). Three-dimensional threshold color-difference perceptibility in painted samples: variability of observers in four CIE color regions. *Color Research & Application* 12: 128–134.

Witt, K. (1990). Parametric effects on surface color-difference evaluation at threshold. *Color Research & Application* 15: 189–199.

Witt, K. and Döring, G. (1983). Parametric variations in threshold color-difference ellipsoid for green painted samples. *Color Research & Application* 8: 153–163.

Woodham, R. (1980). Photometric method for determining surface orientation from multiple images. *Optical Engineering* 19: 139–144.

Woolliams, E.R., Baribeau, R., Bialek, A., and Cox, M.G. (2011). Spectrometer bandwidth correction for generalized bandpass functions. *Metrologia* 48: 164–172.

Wright, W.D. (1928–1929). A re-determination of the trichromatic coefficients of the spectral colours. *Transactions Optical Society of London* 30: 141–164.

Wright, W.D. (1929–1930). A re-determination of the mixture curves of the spectrum. *Transactions Optical Society of London* 31: 201–211.

Wright, W.D. (1981a). Why and how chromatic adaptation has been studied. *Color Research & Application* 6: 147–152.

Wright, W.D. (1981b). The historical and experimental background to the 1931 CIE system of colorimetry. In: *Golden Jubilee of Colour in the CIE: Proceeding of a Symposium Held at Imperial College, London*, 3–18. Bradford: Society of Dyers and Colourists.

Wright, W.D. (1981c). 50 years of the 1931 CIE standard observer for colorimetry. *Proceedings 4th Congress International Colour Association*, Paper A3.

Wyble, D.R. (2017). Next generation camera calibration target for archiving. In: *IS&T Archiving Conference*, 127–132. Washington, DC.

Wyble, D.R. and Berns, R.S. (2000). A critical review of spectral models applied to binary color printing. *Color Research & Application* 25: 4–19.

Wyble, D. and Kraushaar, A. (2005). The theoretical basis of multicolor letterpress printing: translation of H. E. J. Neugebauer 1937. *Color Research & Application* 30: 322–331.

Wyble, D.R. and Rich, D.C. (2007a). Evaluation of methods for verifying the performance of color-measuring instruments. Part I: Repeatability. *Color Research & Application* 32: 166–175.

Wyble, D.R. and Rich, D.C. (2007b). Evaluation of methods for verifying the performance of color-measuring instruments. Part II: Inter-instrument reproducibility. *Color Research & Application* 32: 176–194.

Wyszecki, G. and Stiles, W.S. (1982). *Color Science*, 2e. New York: Wiley.

Xin, J.H., Lam, C.C., and Luo, M.R. (2001). Investigation of parametric effects using medium colour-difference pairs. *Color Research & Application* 26: 376–383.

Xin, J.H., Lam, C.C., and Luo, M.R. (2004). Evaluation of the crispening effect using CRT-displayed colour samples. *Color Research & Application* 29: 374–380.

Xin, J.H., Shen, H.-L., and Lam, C.C. (2005). Investigation of texture effect on visual colour difference evaluation. *Color Research & Application* 30: 341–347.

Young, T. (1802). On the theory of light and colours. *Philosophical Transactions Royal Society of London* 92: 12–48.

Young, R.W. (1991). *Age-Related Cataract*. New York: Oxford University Press.

Yule, J.A.C. and Nielsen, W.J. (1951). The penetration of light into paper and its effect on halftone reproduction. In: *TAGA Annual Meeting*, 65–76.

Zhai, Q.Y., Luo, M.R., and Liu, X.Y. (2015). The impact of illuminance and colour temperature on viewing fine art paintings under LED lighting. *Lighting Research and Technology* 47: 795–809.

Zhang, H. and Montag, E.D. (2006). How well can people use different color attributes? *Color Research & Application* 31: 445–457.

Zhao, Y. and Berns, R.S. (2009). Predicting the spectral reflectance factor of translucent paints using Kubelka-Munk turbid media theory: review and evaluation. *Color Research & Application* 34: 417–431.

Zwinkels, J.C. (1989). Errors in colorimetry caused by the measuring instrument. *Textile Chemist and Colorist* 21: 23–29.

Zwinkels, J.C., DeRose, P.C., and Leland, J.E. (2014). Spectral fluorescence measurements. In: *Spectrophotometry: Accurate Measurement of Optical Properties of Materials* (ed. T.A. Germer, J.C. Zwinkels and B.K. Tsai), 221–290. Amsterdam: Elsevier Inc.

Annotated Bibliography

These citations are all excellent and recommended for more details than were possible to include in this book. Book recommendations forming a color-science library are listed separately.

Adams, E.Q. (1942). X-Z planes in the 1931 I.C.I. (CIE) system of colorimetry. *Journal of the Optical Society of America* 32: 168–173.

Adams was the first to derive an opponent-type color space from tristimulus values. This was the basis for later work with Nickerson, ultimately resulting in CIELAB.

Albers, J. (1963). *Interaction of Color*. New Haven, CT: Yale University Press.

The "Interaction of Color" is available in several forms including an interactive version where colors can be moved to demonstrate how the juxtaposition of colors affects perception. This and Itten's "Elements of Color" are considered landmarks in color design.

Allen, E. (1980). Colorant formulation and shading. In: *Optical Radiation Measurements: Color Measurement*, vol. 2 (ed. F. Grum and C.J. Bartleson), 290–336. New York: Academic Press.

Allen was the first to publish color-formulation algorithms using single- and two-constant Kubelka–Munk theory. The chapter summarizes these articles and explains Kubelka–Munk theory and Bouguer–Beer's law. The chapter is very well written and insightful.

Allen, E. and Yuhas, B. (1984). Setting up acceptability tolerances: a case study. *Color Research & Application* 9: 37–48.

This article describes how three-dimensional confidence ellipsoids are derived. This paper and the Indow and Morrison paper are excellent background reading for using visual data to develop colorimetric confidence ellipsoids.

Asano, Y., Fairchild, M.D., and Blondé, L. (2016). Individual colorimetric observer model. *PLoS ONE* 11 (2): e0145671. https://doi.org/10.1371/journal.pone.0145671.

The CIE physiological model predicts average color vision as a function of age and field size. This research extends the CIE model to incorporate individual variation about the average.

ASTM E284 – 13b (2013). Standard terminology of appearance. West Conshohocken, PA: ASTM International.

The ASTM is cited throughout this book and all the documents are useful. This is an excellent reference providing standard terminology.

Backhaus, W.G.K., Kliegl, R., and Werner, J.S. (1998). *Color Vision Perspectives from Different Disciplines*. Berlin: Walter de Gruyter.

A contributed-chapter text that is engaging and an interesting departure from typical color science texts. It is divided into four sections: color vision in art and science, physiology and neuroethology, psychology and philosophy, and color metrics and applications.

Berns, R.S. (1996a). Deriving instrumental tolerances from pass-fail and colorimetric data. *Color Research & Application* 21: 459–472.

Berns uses data collected in an industrial short course to demonstrate how to define a total color difference tolerance from visual assessments.

Berns, R.S. (1997). A generic approach to color modeling. *Color Research & Application* 22: 318–325.

Berns taught a graduate course on color modeling and over time, recognized generalities when modeling coloration systems such as displays and paints.

Berns, R.S. (2014a). Extending CIELAB: Vividness, V^*_{ab}, depth, D^*_{ab}, and clarity, T^*_{ab}. *Color Research & Application* 39: 322–330.

Color mixtures and colored shadows, among others, do not vary independently in CIELAB chroma, C^*_{ab}, but co-vary in chroma and lightness. Berns derived new coordinates that correlate with co-varying color changes.

Berns, R.S., Alman, D.H., Reniff, L. et al. (1991). Visual determination of supra-threshold color-difference tolerances using probit analysis. *Color Research & Application* 16: 297–316.

This is the RIT-DuPont color-tolerance dataset, one of the datasets used to derive CIEDE2000.

Berns, R.S. and Billmeyer, F.W. (1983). Proposed indices of metamerism with constant chromatic adaptation. *Color Research & Application* 8: 186–189.

Billmeyer and Saltzman's Principles of Color Technology, Fourth Edition. Roy S. Berns.

The authors recognized that the chromatic adaptation transformation (CAT) embedded in CIELAB is inaccurate and proposed metameric and color-inconstancy indices where a more accurate CAT is used.

Berns, R.S. and Petersen, K.H. (1988). Empirical modeling of systematic spectrophotometric errors. *Color Research & Application* 13: 243–256.

This describes how to implement Robertson's concept of diagnosing spectrophotometric errors by comparing spectra of ceramic colored tiles measured on reference and test instruments. This approach is known as instrument profiling.

Berns, R.S. and Reniff, L. (1997). An abridged technique to diagnose spectrophotometric errors. *Color Research & Application* 22: 51–60.

The cyan tile from the Lucideon ceramic tile set can be used to transform CIELAB $\Delta L^* \Delta a^* \Delta b^*$ to reference black, white, and wavelength errors. The differences can be calculated between reference and test instruments or for a single instrument, useful to track instrument accuracy over time.

Billmeyer, F.W. and Alessi, P.J. (1981). Assessment of color-measuring instruments. *Color Research & Application* 6: 195–202.

The concept of MCDM, the mean color difference from the mean, is introduced as a measure of instrument precision.

Billmeyer, F.W. and Bencuya, A.K. (1987). Interrelation of the natural color system and the Munsell color order system. *Color Research & Application* 12: 243–255.

The differences between the NCS and Munsell systems are evaluated by plotting the four elementary NCS hues in Munsell value-chroma and Munsell hue-chroma coordinates.

Fred, W., Billmeyer, J., and Saltzman, M. (1966). *Principles of Color Technology*. New York: Wiley.

This was written when Billmeyer and Saltzman were industrial scientists who well understood the importance of focusing on principles and the concept of thinking and looking before any action. This was written when industrial color measurement was still novel.

Brettel, H., Viénot, F., and Mollon, J.D. (1997). Computerized simulation of color appearance for dichromats. *Journal of the Optical Society of America A* 14: 2647–2655.

A technique to transform a color image as seen by a color-normal observer to images as seen by observers missing L, M, or S cones.

Brown, W.R.J. and MacAdam, D.L. (1949). Visual sensitivities to combined chromaticity and luminance differences. *Journal of the Optical Society of America* 39: 808–834.

One of the earliest discrimination experiments where stimuli varied in both chromaticity and luminance factor. The follow-on to MacAdam's experiments measuring discrimination at constant luminance factor, the "MacAdam ellipses": MacAdam, D.L. (1943). Specification of small chromaticity differences. *Journal of the Optical Society of America* 33: 18–26.

Burns, P.D. and Berns, R.S. (1997). Error propagation in color signal transformations. *Color Research & Application* 22: 280–289.

Color conversions from *RGB* to *XYZ* to $L^*a^*b^*$ propagate error caused by uncertainty in the original coordinate system. Formulas are derived to calculate this error.

Chevreul, M.E. (1967). *The Principle of Harmony and Contrast of Colors* (based on the first English edition of 1854). New York: Reinhold Publishing Corporation.

Chevreul was a dye chemist who discovered the law of simultaneous contrast and other perceptual effects. This was one of the books studied by the post-impressionists.

CIE 15:2018 (2018). *Colorimetry*, 4e. Vienna: Commission Internationale de L'Éclairage.

The International Commission on Illumination has defined colorimetry. This is the primary reference.

Clarke, F.J.J., McDonald, R., and Rigg, B. (1984). Modification to the JPC79 colour-difference formula. *Journal of the Society of Dyers and Colourists* 100: 128–132.

The CMC formula was based on an earlier formula used by J. P. Coates for quality control of textiles. This article describes the derivation of CMC.

Cui, G., Luo, M.R., Rigg, B. et al. (2002). Uniform colour spaces based on the DIN99 colour-difference formula. *Color Research & Application* 27: 282–290.

Color-appearance spaces do not predict visual color tolerance data. The spaces can be transformed using Riemannian geometry to uniform color-appearance spaces.

Derhak, M.W. and Berns, R.S. (2015). Introducing Wpt (Waypoint): a color equivalency representation for defining a material adjustment transform. *Color Research & Application* 40: 535–549.

Material adjustment transforms are used to convert the color of an object viewed under one lighting or observer condition to another lighting or observer condition. This is not a chromatic adaptation transform. It is used in place of having spectral data that are used to calculate colorimetry for any illuminant and observer.

Donaldson, R. (1954). Spectrophotometry of fluorescent pigments. *British Journal of Applied Physics* 5: 210–214.

Donaldson developed the use of a bispectrometer to characterize fluorescent materials, described in this article.

Duncan, D.R. (1940). The colour of pigment mixtures. *Proceedings of the Physical Society* 52: 390–400.

This is the first publication stating that absorption and scattering are considered a linear system in predicting colorant mixtures.

Early, E.A. and Nadal, M.E. (2004). Uncertainty analysis for reflectance colorimetry. *Color Research & Application* 29: 205–216.

Scientists from the U.S. National Institute of Standards and Technology describe various spectrophotometric errors and how they are propagated, resulting in measurement uncertainty.

Fairman, H.S., Brill, M.H., and Hemmendinger, H. (1997). How the CIE 1931 color-matching functions were derived from Wright-Guild data. *Color Research & Application 22* 22: 11–23.

Fairman, H.S., Brill, M.H., and Hemmendinger, H. (1998). How the CIE 1931 color-matching functions were derived from Wright-Guild data. *Color Research & Application 22* 23: 259.

The authors explain the various derivations and transformations beginning with the fundamental experiments of Wright and Guild and ending with the CIE 1931 standard observer.

Germer, T.A., Zwinkels, J.C., and Tsai, B.K. (2014). Spectrophotometry: accurate measurement of optical properties of materials. In: *Experimental Methods in the Physical Sciences* (ed. T. Lucatorto, A.C. Parr and K. Baldwin). Amsterdam: Elsevier Inc.

A contributed chapter book about spectrophotometry, written for the expert. Chapters include, introduction, theoretical concepts in spectrophotometric measurements, dispersive methods, Fourier transform methods, regular reflectance and transmittance, diffuse reflectance and transmittance, spectral fluorescence measurements, angle-resolved diffuse reflectance and transmittance, spectral emissivity measurements, color and appearance, the use of spectrophotometry in the pharmaceutical industry, spectrophotometry applications: remote sensing, and microspectrophotometry.

Gescheider, G.A. (1997). *Psychophysics: The Fundamentals*, 3e. Mahwah, NJ: Lawrence Erlbaum Associates, Inc.

Introduction to measuring the human response to external stimuli. Chapters include psychophysical measurement of thresholds: differential sensitivity, psychophysical measurement of thresholds: absolute sensitivity, the classical psychophysical methods, classical psychophysical theory, the theory of signal detection, further considerations of TSD, procedures of TSD, some applications of TSD, the measurement of sensory attributes and discrimination scales, partition scales, psychophysical ratio scaling, evaluation of ratio scaling methods, the psychophysical law, and some fundamental issues in psychophysical scaling.

Glasser, L.G., McKinney, A.H., Reilly, C.D., and Schnelle, P.D. (1958). Cube-root color coordinate system. *Journal of the Optical Society of America* 48: 736–740.

This is the origin of the cube-root used in L^*, a^*, and b^*.

Grasselli, M.M., Phillips, I.E., Smentek, K., and Walsh, J.C. (2003). *Colorful Impressions: The Printmaking Revolution in Eighteenth-Century France*. Washington, DC: National Gallery of Art.

A beautiful exhibition catalog describing the development of color printing. It is incredible to think that multi-ink printing was accomplished using only the eye and experience.

Hård, A., Sivik, L., and Tonnquist, G. (1996a). NCS, natural color system—from concept to research and applications. Part I. *Color Research & Application* 21: 180–205.

Hård, A., Sivik, L., and Tonnquist, G. (1996b). NCS, natural color system—from concept to research and applications. Part II. *Color Research & Application* 21: 206–220.

These scientists developed the NCS system and this pair of articles provides considerable insight into the system.

Hardy, A.C. and Wurzburg, F.L. (1937). The theory of three-color reproduction. *Journal of the Optical Society of America* 27: 227–240.

Colorimetric color reproduction did not begin with the ICC. It began in this article.

Hébert, M. and Emmel, P. (2015). Two-flux and multiflux matrix models for colored surfaces. In: *Handbook of Digital Imaging* (ed. M. Kriss), 1234–1278. New York: Wiley.

For those conversant in matrix algebra, this is an excellent description of the optical modeling of mixtures of absorbing and scattering colorants.

Hébert, M. and Hersch, R.D. (2015). Review of spectral reflectance models for halftone prints: principles, calibration, and prediction accuracy. *Color Research & Application* 40: 383–397.

An excellent and very readable review of modeling halftone printing. The follow-on to the Wyble and Berns review from 2000.

Hering, E. (1964). *Outlines of a Theory of the Light Sense*, translated by L.M Hurvich and D. Jameson (Zur Lehre vom Lichtsinne. Vienna, Austria: Druck und Verlag von Gerold's sohn, 1878). Cambridge, MA: Harvard University Press.

Primary reference for opponent color theory.

Hunt, R.W.G. (1976). Sky-blue pink. *Color Research & Application* 1: 11–16.

Hunt describes the problem of color specification that is independent of the adapting illuminant. A stimulus defined by only its chromaticities and luminance factor can appear either blue or pink depending on whether the adaptation is incandescent or daylight.

Hunter, R.S. (1937). Methods of determining gloss, NBS research paper RP 958. *Journal of Research National Bureau of Standards* 18: 19–39.

Hunter invented a variety of instruments to characterize gloss. Equally important, he defined six perceptual attributes of gloss: specular gloss, sheen, contrast gloss, absence-of-bloom gloss, distinctness-of-reflected-image gloss, and absence-of-surface-texture gloss.

Hunter, R.S. (1942). Photoelectric tristimulus colorimetry with three filters. NBS Circular 429, U.S. Government Printing Office, Washington, DC, Reprinted in. *Journal of the Optical Society of America* 32: 509–538.

Hunter invented filter colorimeters and went on to a develop color-difference meter and his own color space, HunterLab. HunterLab is a precursor to CIELUV. Hunter recognized that the filters did not need to match color-matching functions; rather, the combination of filters and signal processing would lead to the same result as using color-matching functions.

IESNA TM-30-15 (2015). *IES Method for Evaluating Light Source Color Rendition*. New York: Illuminating Engineering Society of North America.

This method was developed by a team of lighting scientists and engineers to replace the CIE color-rendering index. It will not, but can be used for more detailed analyses of white light and calculating preference.

Indow, T. and Morrison, M.L. (1991). Construction of discrimination ellipsoids for surface colors by the method of constant stimuli. *Color Research & Application* 16: 42–56.

Pass/fail visual data combined from many observers are used to calculate confidence ellipsoids. This paper and the Allen and Yuhas paper are excellent background reading for using visual data to develop colorimetric confidence ellipsoids.

Judd, D.B., MacAdam, D.L., Wyszecki, G. et al. (1964). Spectral distribution of typical daylight as a function of correlated

color temperature. *Journal of the Optical Society of America* 54: 1031–1040, 1382.

Detailed description of the derivation of the CIE D-series illuminants.

Kirchner, E., van den Kieboom, G.-J., Njo, L. et al. (2007). Observation of visual texture of metallic and pearlescent materials. *Color Research & Application* 32: 256–266.

Definitions, examples, visual experiments, and data analysis of sparkle and graininess.

Kubelka, P. (1948). New contributions to the optics of intensely light-scattering materials. Part I. *Journal of the Optical Society of America* 38: 448–456, 1067.

Kubelka, P. (1954). New contributions to the optics of intensely light-scattering materials. Part II: Nonhomogeneous layers. *Journal of the Optical Society of America* 44: 330–355.

Kubelka derives a number of formulas enabling the practical use of Kubelka–Munk theory.

Kuehni, R.G. (2002). The early development of the Munsell system. *Color Research & Application* 21: 20–27.

A summary of A. H. Munsell's diary providing insight into the Munsell system.

Leland, J.E., Johnson, N.L., and Arecchi, A.V. (1997). Principles of bispectral fluorescence colorimetry. In: *Optical Science, Engineering and Instrumentation '97*, 76–87. San Diego, CA.

Overview of measuring fluorescent materials with a bispectrometer and calculating colorimetric coordinates.

Luo, M.R., Cui, G., and Rigg, B. (2001). The development of the CIE 2000 colour-difference formula: CIEDE2000. *Color Research & Application* 26: 340–350.

CIEDE2000 was developed by CIE technical committee TC1-47, composed of experts from the United States, Japan, Switzerland, Great Britain, Spain, Canada, and Germany, the authors among them. The article includes a brief history of weighted color-tolerance formulas, the experiments used to create a dataset, and the various optimized functions.

Luo, M.R. and Rigg, B. (1986). Chromaticity-discrimination ellipses for surface colors. *Color Research & Application* 11: 25–42.

This is the Bradford color-tolerance dataset, one of the datasets used to derive CIEDE2000.

MacAdam, D.L. (1935). Maximum visual efficiency of colored materials. *Journal of the Optical Society of America* 25: 361–367.

Description of the "MacAdam limits" that were calculated to define the color gamut of nonfluorescent reflecting materials. A variety of computational methods have been published over the years. The displays community still uses this calculation as a comparative index where a given display encompasses some percentage of the MacAdam limits.

Maile, F.J., Pfaff, G., and Reynders, P. (2005). Effect pigments—past, present and future. *Progress in Organic Coatings* 54: 150–163.

Comprehensive overview of gonioapparent colorants.

McCamy, C.S. (1985). Physical exemplification of color order systems. *Color Research & Application* 10: 20–25.

In this time period, McCamy oversaw the manufacture of the Munsell Book of Color. His insights led to the "ten commandments" of producing color-order systems. It is important reading for those involved in producing visual standards.

McCamy, C.S. (1996). Observation and measurement of the appearance of metallic materials. I. Macro appearance. *Color Research & Application* 21: 292–304.

McCamy, C.S. (1998). Observation and measurement of the appearance of metallic materials. II. Micro appearance. *Color Research & Application* 23: 362–373.

The study of visual texture begins with these articles. A motivating factor for McCamy was the inadequate geometric descriptions and large tolerances of the CIE recommended geometries for spectrophotometry. McCamy defined the geometry of densitometers while working at the U.S. National Institute of Standards and Technology.

McDonald, R. (1997). Recipe prediction for textiles. In: *Colour Physics for Industry* (ed. R. McDonald), 209–291. Bradford: Society of Dyers and Colourists.

This is an excellent chapter on colorant formulation for textiles. It is authoritative and includes Kubelka–Munk theory and physical-chemistry approaches to color predictions.

Melgosa, M., Huertas, R., and Berns, R.S. (2004). Relative significance of the terms in the CIEDE2000 and CIE94 color-difference formulas. *Journal of the Optical Society of America A* 21: 2269–2275.

CIEDE2000 has a large number of coefficients and many nonlinear functions. The authors analyze the statistical significance of the positional functions: S_L, S_C, S_H, and T. The most important parameters in improving correlation between perceived and calculated color tolerances were S_C and S_H.

Munsell, A.H. (1899–1918). Color diary. http://www.rit.edu/cos/colorscience/ab_munsell_diaries.php (accessed 19 October 2018).

Transcription of his diaries during his invention of the Munsell system and products based on his system. His thinking is recorded in his drawings, traced from the original diaries.

Nayatani, Y. (2005). Why two kinds of color order systems are necessary? *Color Research & Application* 30: 295–303.

This article is very helpful to understand the differences between NCS and Munsell and why each is valuable.

Newhall, S.M., Nickerson, D., and Judd, D.B. (1943). Final report of the O.S.A. subcommittee on the spacing of the Munsell colors. *Journal of the Optical Society of America* 33: 385–418.

Visual experiments were performed to improve the spacing of the Munsell system. The results were published as a lookup table of Munsell coordinates and corresponding x, y, Y colorimetric coordinates. The data were extrapolated beyond the visual results to facilitate conversion programs that calculate Munsell coordinates from colorimetric data.

Nicodemus, F.E., Richmond, J.C., Hsia, J.J. et al. (1977). *Geometrical Considerations and Nomenclature for Reflectance*. Washington,

DC: National Bureau of Standards, US Department of Commerce http://physics.nist.gov/Divisions/Div844/.

The definitive description of the bidirectional reflectance distribution function, BRDF. Their nomenclature is still used and many articles that measure BRDF cite this reference.

Nobbs, J.H. (1985). Kubelka-Munk theory and the prediction of reflectance. *Review of Progress in Coloration and Related Topics* 15: 66–75.

An excellent review of Kubelka–Munk theory, written at an intermediate level.

Nobbs, J.H. (1997). Colour-match prediction for pigmented materials. In: *Colour Physics for Industry* (ed. R. McDonald), 292–372. Bradford: Society of Dyers and Colourists.

The companion chapter to McDonalds' chapter on color formulation of textiles. It is comprehensive but not written at an introductory level.

Nobbs, J.H. (2002). A lightness, chroma and hue splitting approach to CIEDE2000 color differences. *Advances in Colour Science and Technology* 5 (2): 46–53.

Nobbs derived "$\Delta L \Delta C \Delta H$" descriptions based on CIEDE2000.

Ribés, A. and Schmitt, F. (2008). Linear inverse problems in imaging: an introductory survey. *IEEE Signal Processing Magazine* 25 (4): 84–99.

A summary of methods to convert from camera signals to spectral reflectance factor. It is an inverse mapping problem because multispectral imaging systems have fewer channels than the number of wavelengths in a spectrophotometer.

Robertson, A.R. (1968). Computation of correlated color temperature and distribution temperature. *Journal of the Optical Society of America* 58: 1528–1535.

The most commonly used method to calculate correlated color temperature. Many other approaches have since been published.

Robertson, A.R. (1987). Diagnostic performance evaluation of spectrophotometers. In: *Advances in Standards and Methodology in Spectrophotometry* (ed. C. Burgess and K.D. Mielenz), 277–286. Amsterdam: Elsevier.

This is the origin of instrument profiling. Robertson spent his career at the National Research Council Canada and was very involved in color measurement and colorimetry.

Robertson, A.R. (1990). Historical development of CIE recommended color difference equations. *Color Research & Application* 15: 167–170.

Robertson was a member of the CIE subcommittee that developed CIELAB and CIELUV. In fact, he derived the constants 116, 16, 500, and 200 in CIELAB. He describes the committee work, voting, and corrects misconceptions about the differences between CIELAB and CIELUV.

Saunderson, J.L. (1942). Calculation of the color of pigmented plastics. *Journal of the Optical Society of America* 32: 727–736.

One of the important publications about color formulation. He introduces the use of correcting for refractive index discontinuities to convert from measured to internal spectral reflectance factor. Despite citing Ryde in 1931, who derived the formulas, the correction is known as the "Saunderson correction."

Shafer, S. (1985). Using color to separate reflection components. *Color Research & Application* 10: 210–218.

This article introduces the concept of body color as an inherent property of materials that is independent from material-appearance attributes. Body color takes on significance with the use of cameras to measure material appearance for color technology.

Simonds, J.L. (1963). Application of characteristic vector analysis to photographic and optical response data. *Journal of the Optical Society of America* 53: 968–974.

Principal component analysis (PCA) was used to define the CIE D-series illuminants. Simonds performed the analyses. This article explains the use of PCA to reduce the dimensionality of spectral data, then called characteristic vector analysis.

Stevens, S.S. (1957). On the psychophysical law. *Psychological Review* 64: 153–181.

Detailed description of using an exponential function ("power law") as a psychometric function to describe the relationship between a stimulus and the human response.

Tzeng, D.-Y. and Berns, R.S. (2005). A review of principal component analysis and its applications to color technology. *Color Research & Application* 30: 84–98.

This article explains PCA and how it is used in color technology including confidence ellipsoids, estimating the spectral properties of colorants from a dataset of mixtures, and spectral reconstruction using several principal components.

Wintringham, W.T. (1951). Color television and colorimetry. *Proceedings of the Institute of Radio Engineers* 39: 1135–1172.

This is a summary of colorimetry and its application to broadcast television. The article was very timely because color television signal processing was standardized in 1953.

Wright, W.D. (1981a). The historical and experimental background to the 1931 CIE system of colorimetry. In: *Golden Jubilee of Colour in the CIE: Proceeding of a Symposium Held at Imperial College, London*, 3–18. Bradford: Society of Dyers and Colourists.

The 1931 standard observer is based on experiments by Wright and Guild. This paper tells the story. This is required reading for anyone wanting a deeper understanding of CIE colorimetry.

Wyble, D.R. and Berns, R.S. (2000). A critical review of spectral models applied to binary color printing. *Color Research & Application* 25: 4–19.

Predicting spectral reflectance factor and color statistics from primary ink amounts has been a research topic for nearly 100 years. This article reviews empirical and first-principles models.

Wyble, D.R. and Rich, D.C. (2007a). Evaluation of methods for verifying the performance of color-measuring instruments. Part I: Repeatability. *Color Research & Application* 32: 166–175.

Wyble, D.R. and Rich, D.C. (2007b). Evaluation of methods for verifying the performance of color-measuring instruments. Part II: inter-instrument reproducibility. *Color Research & Application* 32: 176–194.

This pair of articles describes current practices to quantify precision using the Lucideon ceramic tiles. The authors describe both univariate and multivariate methods. Analyses are performed on both spectral and colorimetric data. Hotelling's *T*-squared

statistic is used to test statistical significance of interinstrument reproducibility.

Zhao, Y. and Berns, R.S. (2009). Predicting the spectral reflectance factor of translucent paints using Kubelka-Munk turbid media theory: review and evaluation. *Color Research & Application* 34: 417–431.

Before the use of multiflux optical models, Kubelka–Munk theory was used to model paints not at complete hiding. This article reviews the more popular approaches and includes experimental results.

Zwinkels, J.C. (1989). Errors in colorimetry caused by the measuring instrument. *Textile Chemist and Colorist* 21: 23–29.

A well-written summary article describing common sources of error in spectrophotometers. This is a good starting point to understand these errors.

Recommended Books

These books are recommended for those wanting to create a color-science library.

Bartleson, C.J. and Grum, F. (eds.) (1984). *Optical Radiation Measurements: Visual Measurements*, vol. 5. Orlando, FL: Academic Press.

This is a contributed chapter text about vision and psychophysics. The second part of the book covers psychophysics and its utility are the examples drawn from visual experiments quantifying how observers see images and how various factors affect the appearance of images. Chapters include introduction, the eye as an optical system, the eye as a detector, visual pigments and sensitivity, mechanisms of vision, psychophysics, thresholds and matching, measuring differences, direct ratio scaling, multidimensional scaling, photometric measurements, and colorimetric measurements.

Boyce, P.R. (2014). *Human Factors in Lighting*, 3e. Boca Raton, FL: CRC Press.

This is a comprehensive and authoritative book about lighting from a visual perspective. With the emergence of solid-state lighting, a deeper understanding of this subject is important. Chapters include fundamentals, visual system, non-image-forming system, lighting and work, lighting and visual discomfort, lighting and the perception of spaces and objects, lighting for offices, lighting for industry, escape lighting, lighting for driving, lighting for pedestrians, lighting and crime, lighting for the elderly, light and health, light pollution, lighting and electricity consumption, and the way ahead.

CIE (2018). *Colorimetry*, 4e, Publication No. 15:2018. Vienna: Commission Internationale de L'Éclairage.

The International Commission on Illumination has defined colorimetry. This is the primary reference.

Daw, N. (2012). *How Vision Works: The Physiological Mechanisms Behind What We See*. New York: Oxford University Press, Inc.

This is an introductory book about human vision with a focus on its physiology. There are 12 chapters: introduction, organization of the visual system, brightness and contrast, color vision, perception of motion, depth perception, objects and faces, control of eye movements, adaptation and aftereffects, attention, visual memory, and summary.

Dorsey, J., Rushmeier, H.E., and Sillion, F.X. (2008). *Digital Modeling of Material Appearance*, The Morgan Kaufmann Series in Computer Graphics. Amsterdam and Boston, MA: Morgan Kaufmann/Elsevier.

This book describes modeling material appearance for computer graphics applications. Chapters include introduction, background, observation and classification, mathematical terms, general material models, specialized material models, measurement, aging and weathering, specifying and encoding appearance descriptions, and rendering appearance.

Fairchild, M.D. (2013). *Color Appearance Models*, 3e. New York: Wiley.

Color appearance models extend spaces such as CIELAB. Fairchild has carried out a number of experiments defining the field. Chapters include human color vision, psychophysics, colorimetry, color appearance terminology, color order systems, color appearance phenomena, viewing conditions, chromatic adaptation, chromatic adaptation models, color appearance models, The Nayatani et al. model, the Hunt model, the RLAB model, other models, the CIE color appearance model (1997), CIECAM97s, CIECAM02, testing color appearance models, traditional colorimetric applications, device-independent color imaging, image appearance modeling and the future, and high-dynamic-range color space.

Hunt, R.W.G. and Pointer, M.R. (2011). *Measuring Colour*, Wiley-IS&T Series in Imaging Science and Technology (ed. M.A. Kriss). Chichester: Wiley.

This is an introductory book on color technology covering similar content to *Billmeyer and Saltzman's Principles of Color Technology*. Because the authors spent much of their careers performing research for photographic applications, the emphasis is different. Their introduction to colorimetry came from Wright, whose experimental results were used to define the 1931 standard observer. Chapters include color vision, spectral weighting functions, relations between color stimuli, light sources, obtaining spectral data and tristimulus values, metamerism and color constancy, color rendering by light sources, color order systems, precision and accuracy in colorimetry, fluorescent colors, RGB colorimetry, colormetry with digital cameras, colorant mixtures, factors affecting the appearance of colored objects, the CIE color appearance

Billmeyer and Saltzman's Principles of Color Technology, Fourth Edition. Roy S. Berns.

model CIECAM02, models of color appearance for stimuli of different sizes, and model of color appearance for unrelated colors in photopic and mesopic illuminances.

Kettler, W., Binder, M., Franz, W. et al. (2016). *Colour Technology of Coatings*. Hanover: Vincentz Network.

This is a contributed chapter book that reads as if written by a single author. It evolved from industrial education and focuses on the coatings industry, particularly automotive coatings. Chapters include fundamentals of color perception; color measurement, color measurement systems and visual color assessment; visual color assessment; color-order systems; instrumental color difference assessment; definition and applications of color tolerances; pigment optics—physical processes; practical applications; measuring the texture of effect finishes; characterization of pigments; and recipe prediction.

Klein, G.A. (2010). *Industrial Color Physics*, Springer Series in Optical Sciences (ed. W.T. Rhodes). Boca Raton, FL: Springer.

This book's strength is its coverage of the optical modeling of colorant mixtures. Readers should have a working knowledge of calculus for the maximum benefit. Chapters include light sources, types of colorants, observer; systems of standardized tristimulus values, color qualities, chroma of effect pigments; measuring colors; theories of radiative transfer, and recipe prediction.

Kruschwitz, J.D.T. (2018). *Field Guide to Colorimetry and Fundamental Color Modeling*, vol. FG42, SPIE Field Guides (ed. J.E. Greivenkamp). Belllingham, WA: SPIE Press.

The SPIE Field Guides are desk references designed for the practicing engineer or scientist. The author has distilled many of the key concepts in color technology into 126 well-organized pages. It is fully searchable as a PDF. Chapters include color matching experiments, 1931 CIE color space, color terminology, display color gamuts, color order systems, uniform color spaces, color difference equations, basic chromatic adaptation, color equivalency mapping, color measurement, color modeling, printing models, and color management.

Kuehni, R.G. and Schwarz, A. (2008). *Color Ordered: A Survey of Color Order Systems from Antiquity to the Present*. Oxford: Oxford University Press.

This is a summary of the development of logical arrangements of color. Chapters include the universe of human color experiences, linear systems, color diagrams and color circles, from two to three dimensions, psychological color order systems, psychophysical and neurobiological color diagrams and solids, connecting empirical perceptual data with psychophysical scales, physical order, technical color systems, miscellaneous systems I: psychophysical dis mixture, cube, and colorant mixture systems, miscellaneous systems II: incomplete and unconventional systems, color order systems: categorization, color mixture, and perceptual experience.

Livingstone, M. (2014). *Vision and Art: The Biology of Seeing* (Updated and Expanded Edition). New York: Harry N. Abrams.

This is an introductory book about vision using original and manipulated images of paintings as visual aids. Chapters include fiat lux: let there be light, the eye and color vision, luminance and night vision, the first stages of processing color and luminance: where and what, acuity and spatial resolution: central and peripheral vision, the next level of color processing: surround effects, from 3-d to 2-d: perspective, from 3-d to 2-d: shading and chiaroscuro, from 3-d to 2-d: stereopsis, illusions of motion, color mixing and color resolution, television, movies, and computer graphics, and epilogue: talent, music, and learning disabilities.

Manly, B.F.J. and Alberto, J.A.N. (2017). *Multivariate Statistical Methods: A Primer*, 4e. Boca Raton, FL: CRC Press.

Many multivariate-analysis books are written for statisticians, that is, many derivations and few examples. This book is the opposite. It is concise and contains many examples. The 4th edition includes examples using the software, R. Chapters include the material of multivariate analysis, matrix algebra, displaying multivariate data, tests of significance with multivariate data, measuring and testing multivariate distances, principal components analysis, factor analysis, discriminant function analysis, cluster analysis, canonical correlation analysis, multidimensional scaling, and ordination.

McDonald, R. (1997). *Colour Physics for Industry*, 2e. Bradford: Society of Dyers and Colourists.

This is a contributed chapter book and as a consequence, the depth and mathematical level are uneven. Being 20 years old, some of the content is outdated. Even so, there are several outstanding chapters, listed in the annotated bibliography. Chapters include light, light sources and light interactions; the measurement of color; colorimetry and the CIE system; color order systems, color spaces, color difference and color scales; recipe prediction for textiles; color-match prediction for pigmented materials; color in visual displays; and how we see color.

Reinhard, E., Khan, E.A., Akyüz, A.O., and Johnson, G.M. (2008). *Color Imaging: Fundamentals and Applications*. Boca Raton, FL: CRC Press.

This book has a wealth of information about creating, perceiving, capturing, processing, displaying, and managing color. The appendix includes a review of the necessary mathematics to understand the material. Chapters include introduction, physics of light, chemistry of matter, human vision, perception, radiometry and photometry, colorimetry, color spaces, illuminants, chromatic adaptation, color and image appearance models, image capture, high dynamic-range image capture, display technologies, image properties and image display, color management, and dynamic range reduction.

Tilley, R.J.D. (2011). *Colour and the Optical Properties of Materials: An Exploration of the Relationship Between Light, the Optical Properties of Materials and Colour*, 2e. Chichester: Wiley.

This book describes the physics of producing color. Chapters include light and color, colors due to refraction and dispersion, the production of color by reflection, polarization and crystals, color due to scattering, color due to diffraction, color from atoms and ions, color from molecules, luminescence, and color in metals, semiconductors, and insulators.

Tooms, M.S. (2016). *Colour Reproduction in Electronic Imaging Systems: Photography, Television, Cinematography*. Chichester: Wiley.

This introductory book concentrates on digital imaging including cameras, printed output, broadcast television, and digital cinema. It contains 34 chapters divided into seven sections: color – perception, characteristics, and definition; the measurement and generation of color, the concepts of color reproduction, the fundamentals of color

reproduction, color reproduction in television, color reproduction in photography, and color reproduction in digital cinematography. The book is more textual than mathematical.

Wyszecki, G. and Stiles, W.S. (1982). *Color Science*, 2e. New York: Wiley.

This book continues to be extremely useful, despite being over 30 years old. Part of its utility is the inclusion of experimental and physical data. The authors were among a handful of scientists that shaped colorimetry. Chapters include physical data, colorimetry, photometry, visual equivalence and visual matching, uniform color scales, visual thresholds, and theories and models of color vision.

Index

Billmeyer and Saltzman's Principles of Color Technology, Fourth Edition. Roy S. Berns.

WILEY END USER LICENSE AGREEMENT

Go to www.wiley.com/go/eula to access Wiley’s ebook EULA.